MATERIALS SCIENCE AND TECHNOLOGY

EDITORS

ALLEN M. ALPER
GTE Sylvania Inc.
Precision Materials Group
Chemical & Metallurgical Division
Towanda, Pennsylvania

A. S. NOWICK
Henry Krumb School of Mines
Columbia University
New York, New York

A. S. Nowick and B. S. Berry, ANELASTIC RELAXATION IN CRYSTALLINE SOLIDS, 1972

E. A. Nesbitt and J. H. Wernick, RARE EARTH PERMANENT MAGNETS, 1973

W. E. Wallace, RARE EARTH INTERMETALLICS, 1973

J. C. Phillips, BONDS AND BANDS IN SEMICONDUCTORS, 1973

J. H. Richardson and R. V. Peterson (editors), SYSTEMATIC MATERIALS ANALYSIS, VOLUMES I, II, AND III, 1974; IV, 1978

A. J. Freeman and J. B. Darby, Jr. (editors), THE ACTINIDES: ELECTRONIC STRUCTURE AND RELATED PROPERTIES, VOLUMES I AND II, 1974

A. S. Nowick and J. J. Burton (editors), DIFFUSION IN SOLIDS: RECENT DEVELOPMENTS, 1975

J. W. Matthews (editor), EPITAXIAL GROWTH, PARTS A AND B, 1975

J. M. Blakely (editor), SURFACE PHYSICS OF MATERIALS, VOLUMES I AND II, 1975

G. A. Chadwick and D. A. Smith (editors), GRAIN BOUNDARY STRUCTURE AND PROPERTIES, 1975

John W. Hastie, HIGH TEMPERATURE VAPORS: SCIENCE AND TECHNOLOGY, 1975

John K. Tien and George S. Ansell (editors), ALLOY AND MICROSTRUCTURAL DESIGN, 1976

M. T. Sprackling, THE PLASTIC DEFORMATION OF SIMPLE IONIC CRYSTALS, 1976

James J. Burton and Robert L. Garten (editors), ADVANCED MATERIALS IN CATALYSIS, 1977

Gerald Burns, INTRODUCTION TO GROUP THEORY WITH APPLICATIONS, 1977

L. H. Schwartz and J. B. Cohen, DIFFRACTION FROM MATERIALS, 1977

Paul Hagenmuller and W. van Gool, SOLID ELECTROLYTES: GENERAL PRINCIPLES, CHARACTERIZATION, MATERIALS, APPLICATIONS, 1978

Zenji Nishiyama, MARTENSITIC TRANSFORMATION, 1978

In preparation

G. G. Libowitz and M. S. Whittingham, MATERIALS SCIENCE IN ENERGY TECHNOLOGY

Martensitic Transformation

Zenji Nishiyama

Fundamental Research Laboratories
Nippon Steel Corporation
Kawasaki, Japan

Edited by

Morris E. Fine

Department of Materials Science and Engineering
Northwestern University
Evanston, Illinois

M. Meshii

Department of Materials Science and Engineering
Northwestern University
Evanston, Illinois

C. M. Wayman

Department of Metallurgy and Mining Engineering
University of Illinois at Urbana–Champaign
Urbana, Illinois

ACADEMIC PRESS New York San Francisco London 1978

A Subsidiary of Harcourt Brace Jovanovich, Publishers

COPYRIGHT © 1978, BY ACADEMIC PRESS, INC.
ALL RIGHTS RESERVED.
NO PART OF THIS PUBLICATION MAY BE REPRODUCED OR TRANSMITTED IN ANY FORM OR BY ANY MEANS, ELECTRONIC OR MECHANICAL, INCLUDING PHOTOCOPY, RECORDING, OR ANY INFORMATION STORAGE AND RETRIEVAL SYSTEM, WITHOUT PERMISSION IN WRITING FROM THE PUBLISHER.

ACADEMIC PRESS, INC.
111 Fifth Avenue, New York, New York 10003

United Kingdom Edition published by
ACADEMIC PRESS, INC. (LONDON) LTD.
24/28 Oval Road, London NW1

Library of Congress Cataloging in Publication Data

Main entry under title:

Martensitic transformation.

(Materials science and technology series)
Includes bibliographical references.
1. Martensitic transformations. 2. Crystallography.
I. Nishiyama, Zenji, Date
TN690.M2662 669'.94 77-24960
ISBN 0-12-519850-7

PRINTED IN THE UNITED STATES OF AMERICA

First original Japanese language edition published
by Maruzen Co., Ltd. Tokyo, 1971.

Preface to English Edition

The text of this edition has been revised somewhat to include new information which became available after the publication of the original book. When appropriate, some material has been deleted.

The translation was prepared by: Dr. S. Sato, Hokkaido University; Dr. I. Tamura, Kyoto University; Dr. S. Nenno, Dr. H. Fujita, Dr. K. Shimizu, Dr. K. Otsuka, Dr. H. Kubo, and Mr. T. Tadaki, Osaka University; Dr. M. Oka, Tottori University; Dr. S. Kajiwara, National Research Institute for Metals; Dr. T. Inoue, Dr. M. Matsuo, and Dr. I. Yoshida, Fundamental Research Institute, Nippon Steel Corporation.

The English translation was edited by Dr. Morris E. Fine and Dr. M. Meshii, Northwestern University and Dr. C. M. Wayman, University of Illinois.

The author would like to express his sincere appreciation to the translators and the technical editors.

Preface to Japanese Edition

The martensitic transformation is an important phenomenon which controls the mechanical properties of metallic materials and has been studied extensively in the past. At first, the studies were made mainly by optical microscopy, and the high degree of hardness of the martensite in steels was interpreted as being due to its fine microstructure. Without inquiry into its fundamental nature, the martensitic transformation was explained chiefly from the thermodynamical point of view, and it seemed in those days that the theory was reasonably well established. Subsequently, with advances in research techniques, e.g., x-ray diffraction and electron microscopy, the structures of various martensites were determined and the presence of substructures such as arrays of lattice defects was established. New views of martensitic transformation have been developed that consider the new experimental facts. The author considered it timely to summarize the more recent research results on martensite and undertook the writing of this book.

Because of the emphasis on phenomena, the presentation is based on the known crystallographical data and, accordingly, some readers may not be familiar with this approach. Therefore, an elementary description of the martensite transformation that may also be regarded as a summary is given in Chapter 1. This chapter is written in terms as elementary as possible and, though it lacks strictness, even the beginner or nonprofessional will be able to appreciate the organization of this book. The main thrust of the book begins with Chapters 2 and 3, in which crystallographic data are given in detail. Chapter 4 deals with thermodynamical problems and kinetics and Chapter 5 with conditions for the nucleation of martensite and problems concerning stabilization of austenite. The last chapter discusses the theory of the mechanism of the martensitic transformation.

The text is arranged according to phenomena; thus, data for a certain material are scattered throughout and may be difficult to locate. To overcome this inconvenience, the alloys are given in terms of element–element in the index.

The frank opinions of the author may, in some instances, be dogmatic or prejudiced. For the reader who may doubt the author's opinions or other descriptions and for the reader who may want to study the subject in more detail, all references known to the author are included. Nevertheless, some important papers may have been unintentionally omitted. The author would very much like to be informed of such papers.

The author is planning to write a second book concerning other problems associated with martensite, e.g., the massive transformation, the bainitic transformation, the tempering of martensite, and the hardening mechanism in martensite.

The author is indebted to the support given him by the Fundamental Research Laboratories, Nippon Steel Corporation, and especially for the encouragement of Academician S. Mizushima, Honorable Director, and Dr. T. Otake, Director of the Laboratories.

In preparing the manuscript many valuable data were offered by foreign and domestic researchers. The author wishes to acknowledge them:

The author wishes to express his thanks to his friends and colleagues for their kindness in reading and correcting the manuscript: Professor S. Sato, Hokkaido University; Professors I. Tamura and N. Nakanishi, Kyoto University; Professor Y. Shimomura, University of Osaka Prefecture, Professors F. E. Fujita, S. Nenno, H. Fujita, and K. Shimizu, Osaka University; Dr. S. Kajiwara, National Research Institute for Metals; and Mr. K. Sugino and Mr. H. Morikawa, Fundamental Research Laboratories, Nippon Steel Corporation. Further, the author expresses his gratitude to Professor J. Takamura, Kyoto University, for his valuable advice.

This book contains the experimental data obtained by the author and his colleagues at the Institute of Iron and Other Metals, Tohoku University, and at the Institute of Scientific and Industrial Research, Osaka University. The author expresses his appreciation for the research opportunities in these institutions.

1

Introduction to Martensite and Martensitic Transformation

Compared with that obtained by slow cooling, iron–carbon steel quenched from a high temperature has a very fine and sharp microstructure and is much harder. The mechanical properties and structure of quenched steels have long been studied because of their technological importance. The structure of quenched steel is called *martensite* in honor of Professor A. Martens, the famous pioneer German metallographer who greatly extended Sorby's initial work. Initially, the term was ambiguously adopted to denote the microstructure of hardened but untempered steels. As the essential properties of quenched steel have become better known, the meaning of the word has been gradually clarified as well as extended to nonferrous alloys in which similar characteristics occur. Although the term martensite has occasionally been used somewhat ambiguously, there exists a critical restriction on the use of the word. A substance's structure must have certain definite properties in order to be called martensitic structure; similarly, a phase transformation must have certain properties in order to be called a martensitic transformation. It is the object of this chapter to define martensite and martensitic transformations.

We shall take up first the basic properties of martensite in steels, particularly in carbon steels, and then discuss what martensite is in a wider sense.

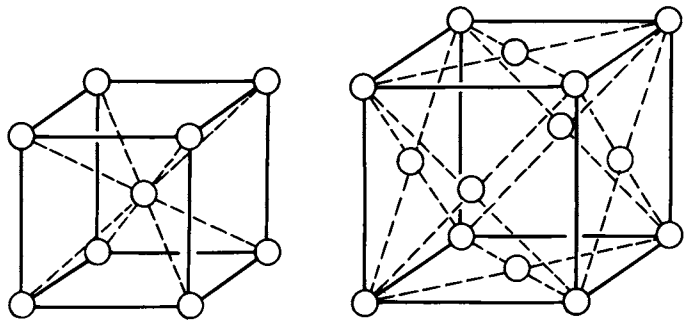

FIG. 1.1 (a) Body-centered cubic lattice (α iron). (b) Face-centered cubic lattice (γ iron).

1.1 Martensite in carbon steels

1.1.1 Allotropic transformations in iron

In order to discuss martensitic transformations in steel, we must consider first the allotropic transformation of elemental iron. Iron changes phase in the sequence $\alpha \rightarrow \beta \rightarrow \gamma \rightarrow \delta$ on heating. Alpha iron, which is the stable phase at room temperature, has the atomic arrangement shown in Fig. 1.1a, which depicts a unit cell of the body-centered cubic (b.c.c.) lattice, in which the atoms lie at the corners and body center of a cube. On heating to 790°C iron changes to the β phase, which has the same b.c.c. structure as α iron. The sole distinction is that α iron is ferromagnetic whereas β iron is paramagnetic. Since the magnetic change is not a change in crystal structure, we now use the term α iron to include β iron. The next transformation, which gives γ iron, takes place at 910°C (the A_3 point). Gamma iron has the face-centered cubic (f.c.c.) atomic arrangement, in which the unit cell contains atoms at the corners and face-centers of a cube, as shown in Fig. 1.1b. The last solid-state transformation on heating, $\gamma \rightarrow \delta$, takes place at 1400°C; δ iron has the same b.c.c. structure as α iron. The $\gamma \rightarrow \alpha$ transformation on cooling is closely related to the martensitic transformation which we will discuss later.

1.1.2 Phase diagram of carbon steels and the martensite start temperature, M_s

The outline of the phase diagram for a binary Fe–C alloy is given in Fig. 1.2. The ferrite α solid solution in this diagram has the b.c.c. arrangement of iron atoms, like pure α iron, the carbon atoms occupying randomly

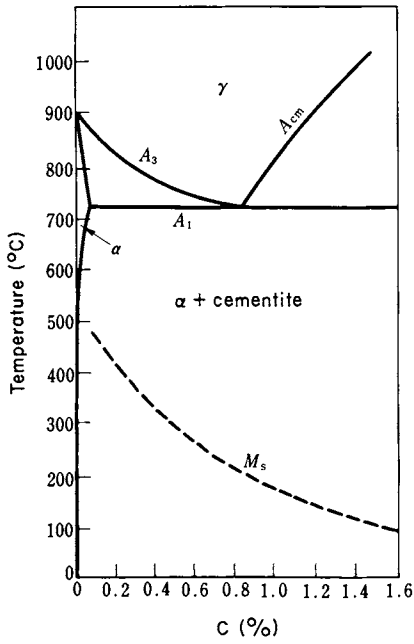

FIG. 1.2 Phase diagram of Fe–C system.

a small fraction of the sites marked ×, △, □ in Fig. 1.3a. Since these sites are interstitial sites lying between the iron atoms, the α phase is an interstitial solid solution of iron and carbon. The austenite, or γ phase is also an interstitial solid solution of iron and carbon, in which the iron atoms are arranged in an f.c.c. lattice like that of pure γ iron, the carbon atoms occupying randomly a fraction of the interstitial sites marked × in Fig. 1.3b. In addition to the difference in structure, the α phase and γ phase have different

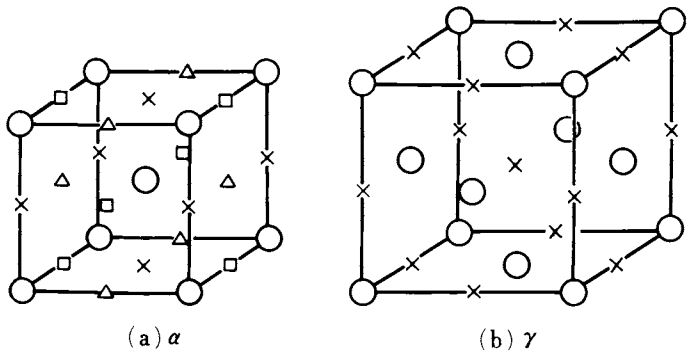

FIG. 1.3 Atomic arrangements in (a) ferrite (α) and (b) austenite (γ): ○, Fe atom; ×, △, □, positions available for C atom.

carbon solubilities. As is shown in the phase diagram, the solubility of carbon in the α phase is small and is at most 0.03% at the eutectoid temperature, 720°C, whereas the maximum solubility of carbon in the γ phase amounts to 1.7%,† corresponding to 8 at.%.

M_s temperature. Quenching of steel generally means that the steel is rapidly cooled to a low temperature from a temperature above the A_3 temperature or the eutectoid temperature (A_1). Any α phase or cementite that may be present in the heated condition is little changed on quenching. What is important is the γ phase. As the phase diagram shows, on slow cooling the γ phase is decomposed into α phase and cementite. This is not the case on quenching, for then the martensitic transformation, a main subject of this book, takes place. This can be detected by observed rapid changes of the physical properties, such as dilatation. The martensitic transformation starts at a temperature designated as the M_s temperature. Here M signifies martensite and the subscript s designates start. The M_s temperature depends upon the carbon content, as is indicated by the dotted line in Fig. 1.2. Note that this curve has a slope similar to that for the A_3 temperature but lies far below the A_3 temperature line. The M_s temperature of pure iron is only about 700°C, which is much lower than the A_3 point, 910°C. The reason for this difference will be presented later.

1.1.3 Crystal structure of martensite (α') in carbon steels

The crystal structure of martensite obtained by quenching the γ phase in carbon steels has a body-centered tetragonal (b.c.t.) lattice which may be regarded as an α lattice with one of the cubic axes elongated, as illustrated in Fig. 1.4b, where the vertical axis is elongated. This is the structure of martensite observed metallographically and the symbol α' is often used to denote it, since the martensite structure may be thought to be derived from the structure of the α phase. The prime is sometimes used as an indication of the tetragonality due to carbon atoms in ordered solid solution, but in this book α' will indicate the structure having characteristics of martensite, even including the b.c.c. phase without carbon atoms when this phase is produced by a martensitic transformation. The symbol (′) will be used generally to signify a martensite phase.

The lattice parameters of α' in steels vary with carbon content in a nearly linear fashion (see Figs. 2.1, 2.2). The tetragonality c/a and the volume of the unit cell increase with the carbon content. From this fact alone it can be deduced that α' is a solid solution of iron and carbon. The position for carbon atoms in the lattice as determined by various measurements is that marked × in Fig. 1.4b. Therefore, α' is also an interstitial solid solution, but

† Recently 2.0% was reported.

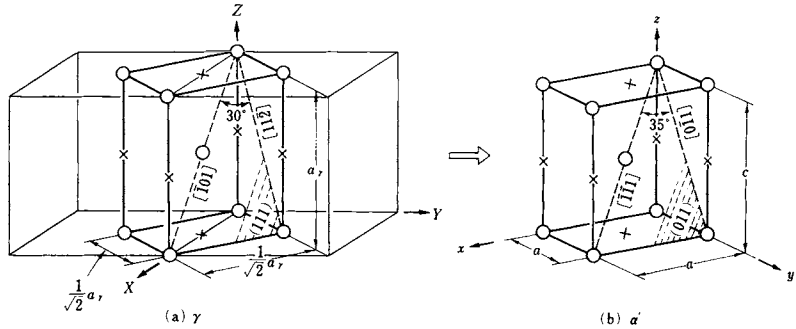

FIG. 1.4 Bain correspondence in the transformation of γ to α': ○, Fe atom; ×, positions available for C atom.

it differs from the ferrite shown in Fig. 1.3a: if the carbon atoms in α' occupy the sites marked ×, they cannot enter into the sites marked △ and □.

The solubility of carbon in α' is also small but not so small as in α, the maximum carbon content of α' being at most 8 at. %; hence only a small fraction of the sites marked × are occupied. In this case the portion of the lattice near the carbon atom is similar to that for the case of a carbon atom in the b.c.c. lattice, as shown in Fig. 3.13, but is such that the carbon atom pushes the nearest-neighbor iron atom marked 3 downward and the atom marked 4 upward, producing local lattice distortion. The latter is one of the main reasons why α' is hard.†

All the axes of lattice distortion due to the carbon atoms in the α' lattice are arranged in the same direction, for example, along the vertical c axis in Fig. 1.4b. These combine to make the lattice tetragonal along the c axis. This is not the situation in the α phase containing carbon; where the sites of the three sets marked ×, △, □ are occupied at random, as shown in Fig. 1.3a, the lattice is not tetragonal but cubic, with the three principal axes merely extended equally.

The α' lattice is similar to α, as already described, but it may be regarded as similar to γ from a different standpoint. Figure 1.4a shows two unit cells of the γ lattice. If in the heavy-lined portion of the figure we regard the axes rotated 45° around the vertical axis as the principal axes, the γ lattice can also be considered as a b.c.t. lattice with axial ratio $\sqrt{2}$, which is greater than that of α'. Therefore, if we regard α' as a distorted lattice of γ, α' may also be regarded as a transition phase between γ and α. A good correspondence is also obtained between the carbon sites in γ and α. The lattice correspondence between (a) and (b) in Fig. 1.4 is called the *Bain correspondence*

† Though such lattice distortion also exists in ferrite containing carbon atoms, it affects the hardness little because the carbon content is very small. Moreover, other sources of hardening in martensite (to be described later) are absent in ferrite and thus ferrite is not very hard.

and the concept that the α' lattice could be generated from the γ lattice by such a distortion as by decreasing the tetragonality from $\sqrt{2}$ was adopted in some earlier theories of the martensitic transformation mechanism in steels.

1.2 Characteristics of martensite in steel

The crystal structure of α' described in the preceding subsection is itself one of the characteristics of martensite. Other characteristics are as follows.

1.2.1 Diffusionless nature of the transformation

The γ phase retained after quenching has, of course, the same crystal structure as the γ phase stable at higher temperatures, the lattice parameters being unchanged except from contractions due to the decrease of temperature. It has the same carbon content as that of the γ phase at high temperature. The lattice of α' is expanded in relation to that of α, the amount depending on the carbon content. Moreover, there are no phases other than α' and retained γ in the specimen. The structure as observed under the microscope shows only these two phases. Therefore it may be considered that no chemical decomposition takes place during the martensitic transformation and a part or most parts of γ transform diffusionlessly to α', the compositions being unchanged. This is an extremely important factor in the martensitic transformation.

A necessary condition for the occurrence of the $\gamma \rightarrow \alpha'$ transformation is that the free energy of α' be lower than that of γ. Moreover, since additional energy, such as that due to surface energy and transformation strain energy, is necessary for the transformation to take place, the difference between the free energies of γ and α' must exceed the required additional energy. In other words, a driving force or excess free energy is necessary for the transformation to take place. Therefore, the γ to α' reaction cannot take place until the specimen is cooled to a particular temperature below T_0, the temperature at which the free energy difference between austenite and martensite of the same composition is zero (Fig. 1.5). The degree of supercooling is the greater the larger the difference between the two crystal structures, because it is more difficult for the change to occur when greatly differing structures are involved. In the case of steel the difference between the two structures is rather large and the difference between T_0 and M_s may be as large as 200°C. This great difference in structure is the reason why the M_s temperatures are markedly below the extended A_3 line in Fig. 1.2. (The A_3 temperature is higher than the T_0 temperature.[†])

[†] A_3 represents the temperature at which γ is in equilibrium with $\alpha + Fe_3C$, whereas T_0 represents the temperature at which γ and α' of the same carbon content are in metastable equilibrium.

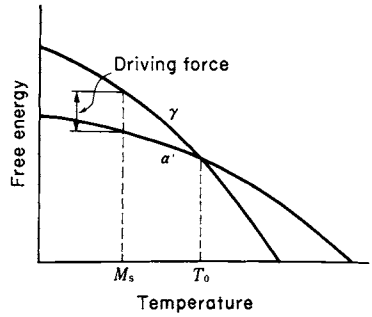

FIG. 1.5 Free energies of γ and α'.

1.2.2 Habit plane

When the temperature from which steels are quenched is high enough, the product structure becomes coarse and the individual crystals of α' can be distinguished in the optical microscope (Fig. 1.6). In the ultralow carbon steel the crystals appear lath-shaped in cross section; however, the actual shape is that of a plate or needle, where often the former is parallel to $\{111\}_\gamma$ and the latter to $\langle 110\rangle_\gamma$. In the medium and high carbon steels the crystals take the form of bamboo leaves or lenticular plates with a core, called the *midrib*, within them. This core is nearly parallel to $\{225\}_\gamma$ or $\{259\}_\gamma$, the latter being more frequent in high carbon steels. Thus martensite crystals have more or less definite habit planes† with respect to the crystal lattice of the parent phase γ.

1.2.3 Lattice orientation relationships

The crystallographic axes of α' crystals produced in a γ crystal also have a definite relation to those of the untransformed part of the γ crystal. In carbon steels the orientation relationships are

$$(111)_\gamma \| (011)_{\alpha'}, \qquad [\bar{1}01]_\gamma \| [\bar{1}\bar{1}1]_{\alpha'}.$$

These cannot be obtained directly from the parallel lines pictured in Fig. 1.4, but may be obtained by making parallel the two shaded triangular planes in (a) and (b), as well as one of the directions lying on each of those triangular planes. These relations are called the Kurdjumov–Sachs (K–S) relations, after their discoverers. In Fe–30% Ni alloys the orientation relationships are

$$(111)_\gamma \| (011)_{\alpha'}, \qquad [11\bar{2}]_\gamma \| [0\bar{1}1]_{\alpha'};$$

these are called the Nishiyama (N) relations. The parallel planes are the same as in the K–S relations, whereas the directional relationship is deviated

† In general, the indices of the habit plane are irrational.

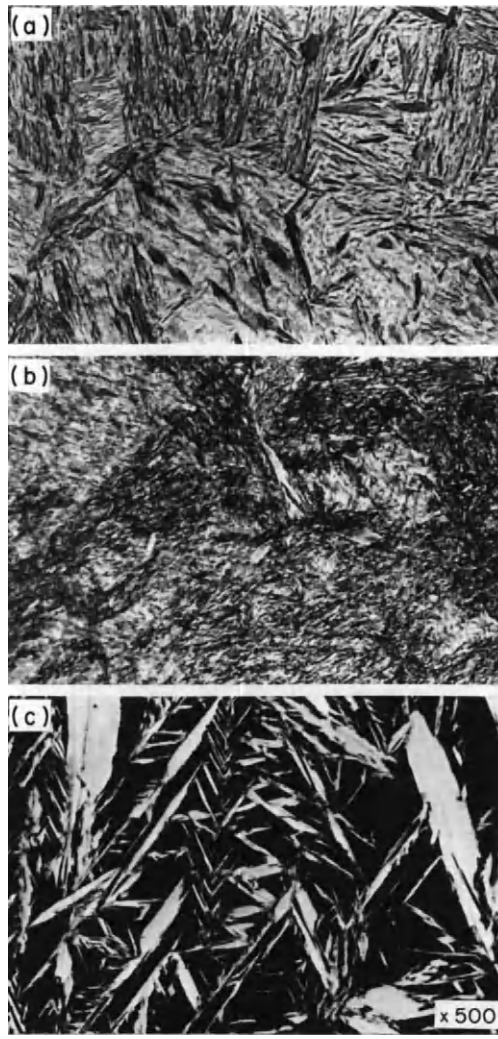

FIG. 1.6 Photomicrographs of quenched carbon steels (after Inoue and Matsuda[1]). (a) 0.2% C–1.5% Mn, water quenched from 1000°C (30 min); (b) 0.8% C–1.5% Mn, water quenched from 1000°C (30 min); (c) 1.4% C, water quenched from 1150°C (1 hr).

from the K–S relations by about 5°. In nickel steels (22% Ni–0.8% C) the orientation relationships are

$$(111)_\gamma \sim (011)_{\alpha'}, \qquad [\bar{1}01]_\gamma \sim [\bar{1}\bar{1}1]_{\alpha'},$$

within approximately 1° and 2.5°, respectively. These can be considered as intermediates between the two relations just described. These are called

the Greninger–Troiano relations. Thus one of the characteristics of the martensite transformation is that in steel of a given composition there are definite orientation relations.

1.2.4 Surface relief—shape change

An upheaval, or surface relief, is produced on a free surface when a martensite crystal forms. For example, in materials having M_s temperatures below room temperature, such as high Ni steels, surface upheaval may be studied on surfaces prepolished by electrochemical etching in the γ phase state at room temperature after having been cooled from a high temperature. As the martensite is formed subsequently by cooling below the M_s temperature, an upheaval is produced at the free polished surface, as illustrated in Fig. 1.7a. The surface relief is not irregular but the angle of incline of the upheaval has a definite value which depends on the crystal orientation. In the same way, a fiducial scratch line is bent at the γ–α' interface, as illustrated in Fig. 1.7b. The angle by which such a scratch has been bent is also definite in value, depending on the crystal orientation. The surface relief or bending of a scratch line is a surface manifestation of the definite shape change in the crystal that occurs during the γ–α' transformation.

1.2.5 Transformation by cooperative movement of atoms

As described earlier, the martensitic transformation is a diffusionless one and therefore a volume of γ changes to α' of a different structure without atomic interchange. How the α' crystal is formed in this case is important. It might be thought that the α' crystal could be formed from the γ crystal by individual atomic movements but this cannot be so. The fact that the α' crystal formed has a definite habit plane, definite orientation relations with γ, and definite surface relief leads us to the conclusion that these features

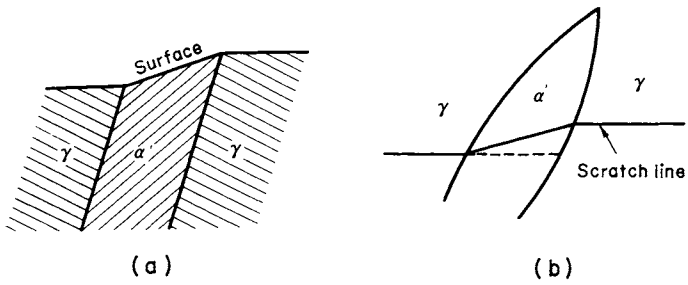

FIG. 1.7 (a) Surface relief and (b) bending of a fiducial (scratch) line.

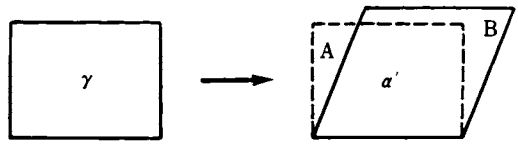

FIG. 1.8 Shape change during martensitic transformation.

are the results of coordinated and ordered rearrangement of the atomic configuration which takes place during transformation. It is considered that the atomic movements, though accompanied to some extent by thermal vibrations, are not free, as in a liquid or gas, but that as the transformation interface moves, the motions of neighboring atoms are coordinated to produce the new crystal.

1.2.6 Generation of lattice imperfections

As illustrated in Fig. 1.8, during transformation the framed volume of γ in (a) is imagined to change into that in (b). This produces a vacant volume in

inside the crystal in precisely this way because opposing stresses exerted by the surrounding matrix are applied to the transforming region to restrict the shape change. Elastic strains are not sufficient to relax these stresses, so the transforming region must undergo a considerable amount of plastic deformation. This complementary deformation may be produced by the movement of dislocations, as in the case of conventional plastic deformation. The motion of perfect dislocations gives *slip* and that of partial dislocations gives *stacking faults* or *internal twins* (Fig. 1.9).† Since a number of dislocations sufficient to make up for the lattice deformation is required, the dislocation density produced must be markedly larger for the $\gamma \rightarrow \alpha'$ transformation of steel than during ordinary plastic deformation. Lattice imperfections giving evidence of the so-called second distortion‡ are actually observed under the electron microscope within α' crystals. Figure 1.10 shows an example in which the specimens are the same as those used in Fig. 1.6. In low carbon steels (a), the α' crystals are lath-shaped and dislocations can be seen throughout the crystals. In medium carbon steels (b), a number of

† For simplicity, the plane of the transformation shear and that of the slip or twinning shear are considered to be parallel, but this is not generally so.

‡ The concept of a first deformation, consisting of a change in the shape of the unit cell, and a second deformation to relax the transformations is for convenience of thinking; the two deformations actually take place simultaneously.

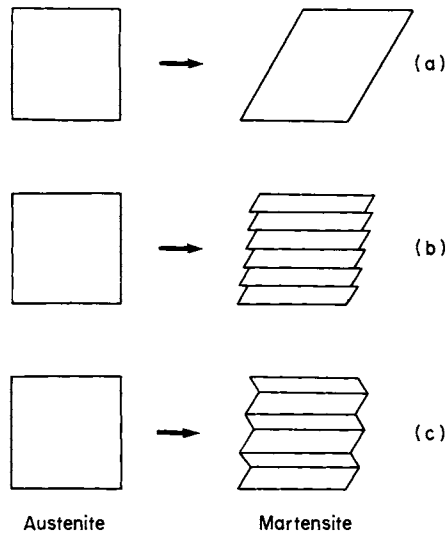

FIG. 1.9 Complementary shear—shear accompanying lattice deformation to relieve internal stresses. (a) No lattice-invariant shear. (b) Slip shear (leaving dislocations and stacking faults). (c) Twinning shear (leaving internal twins).

fine bands of internal twins can be seen, the spacing being about 100 Å. In high carbon steel (c), the portion that contains internal twins is increased.

One of the main characteristics of martensite is that it contains many lattice imperfections and this is an important feature that was overlooked in earlier studies.

1.3 General characteristics and definition of martensite

So far the characteristics of martensite have been described mainly for carbon steels. We will next consider which of these characteristics are essential to martensite in the broad sense.

First we consider the presence of carbon atoms in the lattice. Pure iron cooled at an extremely high velocity has all the characteristics of ordinary martensite except that no carbon is contained in the lattice. In this case, it is reasonable to call the quenched state of iron martensite: In such broad usage of the term martensite, the existence of carbon producing tetragonality is not a requirement.

All the other characteristics described in the preceding section are necessary for martensite. We can now give a general definition of martensite and the martensitic transformation: A martensitic transformation is a phase

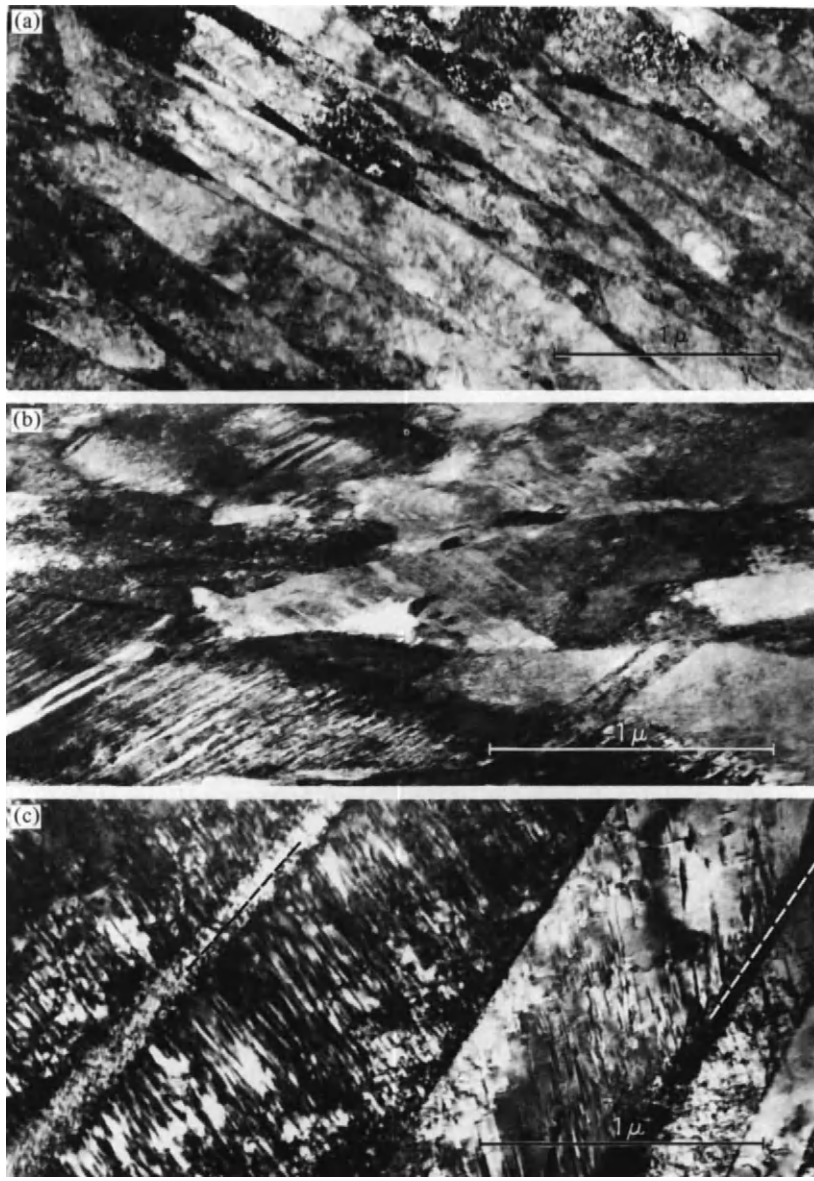

FIG. 1.10 Electron micrographs of quenched carbon steels (same steels as in Fig. 1.6). (After Inoue and Matsuda.[1]) (a) 0.2% C, lath-shaped martensite (α' crystals contain a large number of dislocations); (b) 0.8% C, lens-shaped martensite (α' crystals contain dislocations and internal twins); (c) 1.4% C, lens-shaped martensite (α' crystals contain many internal twins).

transformation that occurs by cooperative atomic movements. The product of a martensitic transformation is martensite. That a given structure is produced by a martensitic transformation can be confirmed by the existence of the various characteristics that have been discussed, especially the diffusionless character, the surface relief, and the presence of many lattice imperfections. Such characteristics are therefore criteria for the existence of martensite.

A given martensite may have many other characteristics which, though suggesting martensite, are not necessarily proofs in themselves that a martensitic transformation has occurred. For example, high hardness was a necessary property of martensite at the time when the word "martensite" was first adopted but it is no longer regarded as a good criterion. Equally, rapidity of transformation does not generally apply to martensite because, though in most steels the time of formation of an α' crystal is of the order of 10^{-7} sec, the growth in some alloys is so slow that the process may be followed under a microscope. Although the existence of a habit plane and an orientation relation is a necessary consequence of a martensitic transformation, it in turn is not a sufficient criterion, because some precipitates that are definitely not classified as martensite also have such characteristics. In the broad sense of the term, a great many examples of martensite have been confirmed in metals, as will be described in the following chapters. For example, there is another type of martensite in iron alloys, and a number of types of martensite have been observed in nonferrous alloys.

Reference

1. T. Inoue and S. Matsuda, Unpublished, Fundamental Research Labs., Nippon Steel Corp.

2

Crystallography of Martensite (General)

2.1 Introduction

As described in Chapter 1, the term martensite was originally adopted to denote a certain microstructure as seen in the optical microscope. Therefore, in early studies there existed confusion[1] as to whether martensite is a single phase or a duplex phase at the initial stage of precipitation. It was even theorized that martensite is composed of two bulk phases. But it is now known that martensite is a single phase, as described in the preceding chapter. Therefore, the martensitic transformation is a phase change from one single phase to another single phase.†

Moreover, since the chemical composition of the untransformed part was found to be unchanged, the composition of the transformed part must also be the same as that of the parent phase. This means that no atomic diffusion takes place during the transformation. In this sense the martensitic transformation is considered to be a kind of diffusionless transformation. ("Diffusion" in this case means long-range diffusion.) Since atomic migration of one atomic distance can readily occur, atoms may easily be spontaneously displaced to another lattice site if it is a stable position. For example, as a result of the Bain distortion, carbon atoms in the martensite lattice are considered to have a regular distribution so as to make the lattice tetragonal, but when the carbon content is very low ($<0.25\%$), the carbon atoms take

† When martensite is a multicomponent phase, then precipitation or other forms of phase separation may occur subsequent to the martensitic transformation. This was no doubt responsible for some of the early confusion.

a disordered arrangement so as to decrease the free energy. As a result, such martensite is cubic. Even when such local atomic diffusion occurs, the term martensitic transformation can be used.

One difference between precipitation in solids and the martensitic transformation is that there is no long-range diffusion in the latter. In addition, the martensitic transformation necessarily entails a definite orientation relationship, a definite habit plane, and regular surface relief. But the inverse is not always the case. The existence of a lattice orientation relationship is not a sufficient criterion for a martensitic transformation. For example, the precipitation reaction also gives a definite orientation relationship in many cases, and precipitates also often have a definite habit plane. Therefore, surface relief must be considered a most important determining property for the martensitic transformation, because it is not seen in the case of precipitation or phase separation by a diffusionlike mechanism. The surface relief that occurs during the martensitic transformation is a result of the mode of the crystal lattice transformation, in which atoms move not individually but cooperatively:† the motions of the neighboring atoms are coordinated. The Bain distortion is an example of a transformation occurring by cooperative movement of atoms. Some researchers[2,3] call the martensitic transformation a *military* transformation, in the sense that such a rearrangement of atoms takes place in an orderly, disciplined manner, like regimentation. But all the atoms do not move simultaneously and in reality atomic movement propagates successively in an ordered manner as a transformation front moves across the material. Therefore it is more appropriate to say that the martensitic transformation is like *Shōgidaoshi*‡ rather than like military motion.

The fine structures (fine grain size and lattice imperfections) will be considered next. Since martensitic transformation takes place by cooperative atomic movement, as just described, the growth of a martensite crystal across grain boundaries in the parent phase cannot occur. On the other hand, a great many martensite crystals can nucleate within a grain of the parent phase, and therefore martensite crystals must generally be of fine grain size.

As a result of the cooperative atomic rearrangement, the crystal shape tends to change. The change, however, is restricted by the surrounding matrix, so that plastic deformation necessarily takes place so as to lessen the effect of the shape change. Though plastic deformation may occur in the surrounding matrix, it occurs more easily in the martensite during transformation.

† Some researchers, particularly ceramists, have adopted the terms "displacive" for "cooperative" and "reconstructive" for transformations where the atoms move individually and are not coordinated with other atoms.[4,5]

‡ A Japanese word meaning "falling one after another in succession"—the domino effect.

In the case of the f.c.c.-to-b.c.c. transformation the amount of plastic deformation is very large: the shear angle is as great as 20°, so that an extremely large number of slips are necessary. Such slip is nothing more than the movement of a dislocation, and in the case of a partial dislocation a stacking fault remains in the wake of the dislocation within the crystal. It is very probable that many perfect dislocations also remain in the crystal, pinned there by impurities or other imperfections.

Instead of slip deformation, twinning may also occur in some alloys, especially if the transformation temperature is low. Such twins must generally be very thin, except for transformations with small shape changes, because thick twins produce large strains near their edges. In this sense the term "internal twin" is used to distinguish it from the usual twin, but the term "twin fault" may be more appropriate to emphasize the presence of the twin boundary. Formerly, Greninger[6] used the term "transformation twin" for a twin that was so large that it could be seen under the optical microscope and confirmed by x-ray diffraction. It is different from the internal twin described here. Greninger's transformation twin may be two transformation variants, one a crystallographic twin of the other, or they may be recrystallization twins. The term transformation twin in common usage today is synonymous with "internal twin."

In addition to the line defects and planar faults mentioned earlier, point defects may be produced. Interstitial atoms are one type of point defect, but more important are vacancies, which play an important role in rapidly cooled materials, although data on this possibility are lacking because vacancies have not yet been studied in relation to the martensitic transformation.

In short, since martensite is produced by cooperative atomic movements, lattice imperfections, such as dislocations, stacking faults, and twin faults, are inevitably introduced into it. Their amount is large when the transformation strains are large, and small when the strains are small. The presence of such lattice imperfections is an important feature of martensite and such imperfections cannot be neglected in a meaningful discussion of martensite.

2.2 f.c.c. (γ) to b.c.c. or b.c.t. (α') (iron alloys)

2.2.1 Tetragonal martensite containing carbon or nitrogen atoms

The crystal structure of martensite obtained by quenching carbon steels from the temperature range of the austenite (γ) phase region is body-centered tetragonal (b.c.t.). Although the symbol α_t is often used to denote tetragonal martensite, in this book we use the symbol α' to denote tetragonal martensite

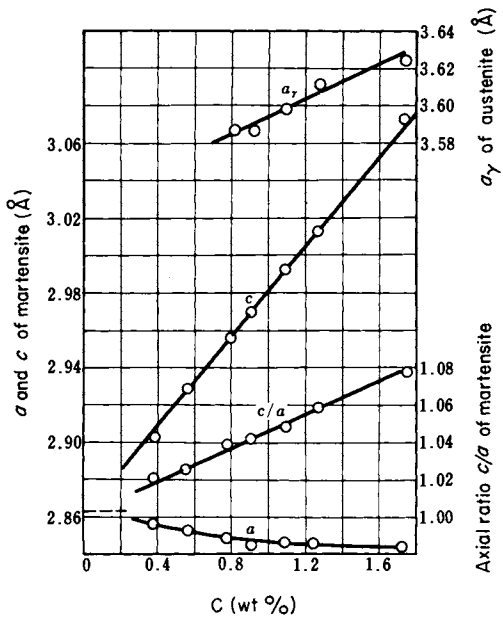

FIG. 2.1 Lattice constants of tetragonal martensite and austenite in quenched carbon steels. (After Honda and Nishiyama.[10])

as well as cubic martensite, which will be described more fully later.† Throughout this book the prime signifies a martensite phase.

Fink and Campbell[7] and Seljakov *et al.*[8] may have been the first to show the presence of tetragonal martensite in carbon steels (1926). This finding has been confirmed by many researchers, all of whom reported the same results‡ for the lattice parameters as those shown in Fig. 2.1.[9–11] That is, the a axis decreases a little and the c axis increases markedly with an increase in carbon content above 0.25%; therefore, the axial ratio c/a increases with the carbon content. This relation is given by the equation

$$c/a = 1.000 + 0.045 \quad \text{wt}\%\text{C}.^{12,13}$$

The volume of the unit cell also increases linearly with increasing carbon content. This suggests that carbon atoms are in interstitial sites in the iron lattice. The sites are $\frac{1}{2}\frac{1}{2}0$ and/or the equivalent sites, as shown in Fig. 1.4b. Further details will be presented in Chapter 3.

† In the early days there was an opinion that cubic martensite should be termed martensite-like, but this opinion is not warranted today.

‡ There is an opinion, not yet generally accepted, that something more complex is present; this opinion will be described in Section 3.8.

A large concentration of nitrogen (N) atoms,† like carbon atoms, can be dissolved interstitially in the f.c.c. lattice of iron at high temperatures; hence, martensite containing N atoms is produced by quenching, the lattice being cubic for nitrogen contents less than 0.7% and tetragonal for those greater than 0.7%. The lattice parameters are similar to those for martensite with C atoms. Plotting the lattice parameters as a function of the atomic percentage of N atoms, we find that the points are located on nearly the same lines obtained in the case of C atoms, as shown in Fig. 2.2.[9,14,16–19]

On adding special elements, such as Ni, Cr, or Mn, to steels containing C or N, we obtain tetragonal martensites, as in plain carbon or nitrogen steels, except for certain instances. Although the lattice parameters a and c change with the size of the added special element, the axial ratio c/a depends only on the carbon or nitrogen content.[20] This fact can be understood from the fact that the tetragonality is due to the ordered arrangement of the C or N atoms. An exception is the case of high Al steels, in which the axial ratio is larger by an amount due to the effect of the ordered arrangement of Al atoms (which will be described in the next section).[21]

2.2.2 Tetragonality due to the ordered arrangement of substitutional atoms

Even substitutional elements can bring about unusual phenomena, such as tetragonality, when they are added in large concentrations to steel and ordering occurs. For example, the addition of titanium to an Fe–30% Ni alloy can make the martensite tetragonal. As shown in Fig. 2.3,[22–24] the axial ratio increases with titanium content in a manner similar to that in carbon steels.

† A N atom dissolved in an interstitial site of the iron lattice differs from the C atom in the following way. The electronic structure of the C atom is $1s_2$, $2s_2$, $2p_2$, whereas that of the N atom is $1s_2$, $2s_2$, $2p_3$. According to self-consistent field computations, the atomic radii of both atoms are

	2s	2p	In the case of a single bond
C	0.67 Å	0.66 Å	0.77 Å
N	0.56 Å	0.53 Å	0.70 Å

This shows that a C atom is larger than a N atom. When they are dissolved interstitially,[14] however, both atoms behave as if they were the same size, as shown in Fig. 2.2. The reason for this is inferred from a diffusion experiment performed under an electric field.[15] In the γ phase at high temperatures C atoms migrated to the cathode whereas N atoms went to the anode. From this result it is considered that C atoms have a positive charge and N atoms a negative charge. Therefore, in the iron lattice C atoms behave as if their radius were smaller than that in the neutral condition and N atoms behave as if their radius were larger.

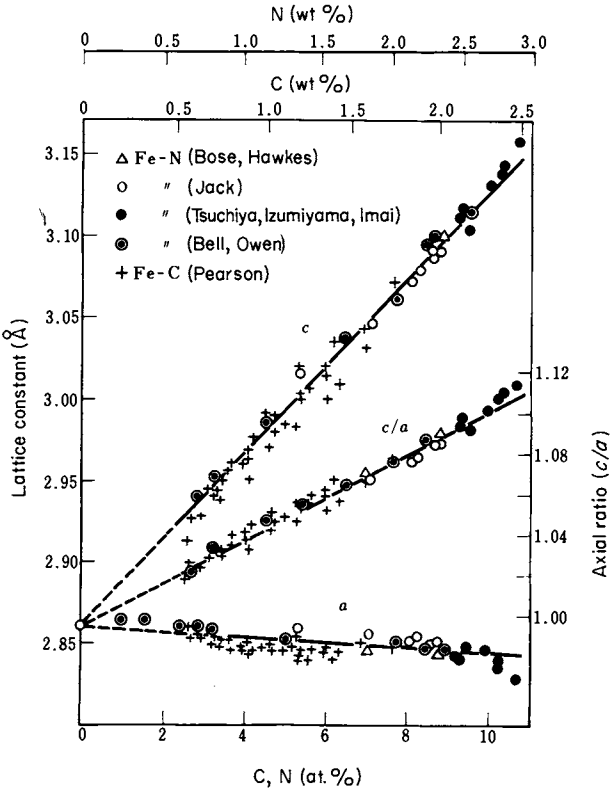

FIG. 2.2 Lattice constants of tetragonal martensite in quenched Fe–N and Fe–C alloys.[9,14–19]

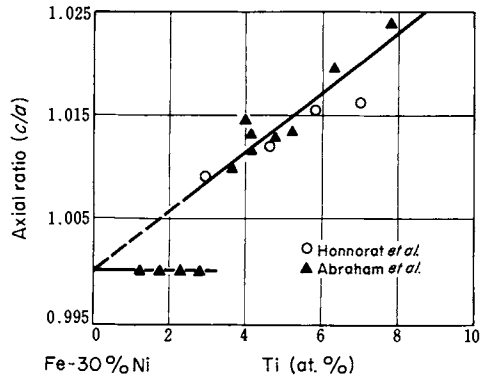

FIG. 2.3 Axial ratios of tetragonal martensite in substitutional solid solutions, Fe–30% Ni–Ti. (After Honnorat *et al.*[22,23] and Abraham *et al.*[24])

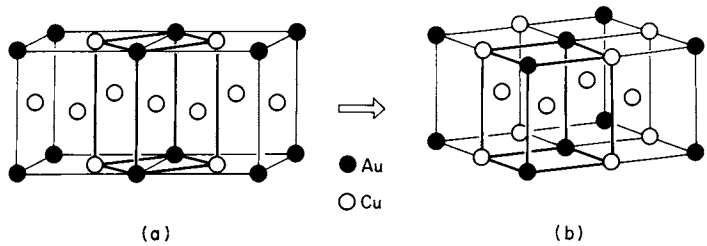

FIG. 2.4 Formation of a base-centered tetragonal lattice from Cu_3Au superlattice, (a) Cu_3Au superlattice. (b) Base-centered tetragonal (superlattice).

The cause of the tetragonality in this case is as follows: Ti atoms in the γ lattice are thought to form clusters of the ordered lattice Ni_3Ti, which has the Cu_3Au structure. As a consequence of the Bain distortion, the arrangement of Ti atoms along the compression axis in the transformation deformation is not equivalent to that along the perpendicular axes, as shown in Fig. 2.4. A consequence of such a condition is that the lattice is forced to be tetragonal because the Ti atom is larger than the Fe or Ni atom. This effect increases with the titanium content, and, as expected, the lattice parameters change as shown in Fig. 2.3. As the clusters of Ni_3Ti develop on aging at a temperature inside the γ phase region, the axial ratio of the product martensite increases,[25] supporting the above-mentioned assumption. Similar phenomena can be seen when martensites are obtained by quenching Fe–Al–C alloys where perovskite-type clusters form in the γ lattice.[26]

As is well known, boron of extremely small concentrations has a strong influence on the mechanical properties of iron alloys. This may be because, aside from the fact that boron makes iron boride, a small amount of boron dissolves in the iron lattice and plays an important role. Some properties support the opinion that the boron occupies interstitial sites,[27] but other facts favor a substitutional solution of boron.[28] This disagreement has long remained unresolved because of boron's very limited solubility. Nowadays, however, it is recognized that a large amount of boron can be dissolved in iron by splat quenching, providing some answers to this problem.

Ruhl and Cohen[29] investigated Fe–B, Fe–Ni, and Fe–Ni–B alloys by x-ray analysis after splat quenching and obtained experimental results that the martensites had a small degree of tetragonality and somewhat smaller lattice parameters. This means some but not all of the boron atoms are in the substitutional sites and form an ordered lattice. It is concluded from the lattice parameters that in Fe–9 at. % B alloy 0.6 at. % of the boron atoms are in the interstitial sites and 3.6 at. % of them are in substitutional sites, the

balance of the boron atoms being precipitated as $(Fe, Ni)_3B$.† It is reported[31] that oxygen also behaves like boron.

There is an example in the literature of the formation of tetragonal martensite in nonferrous alloys: ordered β brass, which has the CsCl structure β_1, is transformed by cold working to a tetragonal martensite (CuAu I structure), the axial ratio being 0.943 in a 61.3% Cu alloy.[32]

In both interstitial and substitutional solid solutions, the symmetries of the atomic positions are varied by the Bain distortion of the martensitic transformation, and therefore any ordered arrangement existing in the austenite state influences the symmetry of product martensite crystals as a whole.[33,34] The tetragonal martensites mentioned here constitute only one example, and in some cases martensites with more complex symmetries, such as orthorhombic, may be obtained.

2.2.3 Cubic martensite (α')

The martensite in substitutional alloys, such as Fe–Ni alloys,‡ that do not form an ordered lattice is likely to be cubic, as in pure iron. Even if these alloys contain interstitial atoms, the martensite is cubic as long as the interstitial content is small. This is why no data are shown in Fig. 2.1 for carbon contents less than 0.25%. There are two possibilities in this case: One is that the axial ratio is so close to unity that the tetragonality cannot be detected; the other, that the martensite can be cubic as long as the carbon content is small. Although this topic was discussed in Chapter 1, detailed aspects will be taken up again in Section 3.3.

The positions of the C atoms in the body-centered tetragonal lattice are the interstitial site $\frac{1}{2}\frac{1}{2}0$ and its equivalent sites, according to the tetragonal symmetry, as shown in Fig. 1.4b. But in the cubic lattice the three axes are equivalent, and therefore there are three times as many equivalent positions as in the tetragonal lattice, as shown in Fig. 1.3a. This distribution can be regarded as a union of the three kinds of tetragonal groups, each consisting of the positions marked □, △, or × in the tetragonal distribution, or from a different standpoint, each group in the tetragonal distribution can be seen as produced by the ordering of a group of positions in the cubic distribution.

2.2.4 Lattice orientation relationships

In all the crystals now called martensite, the crystal axes have a definite relation to those of the parent phase. For example, in steels there are the

† There is a report, however, that boron cannot be dissolved interstitially in high-purity alloys.[30]

‡ The lattice parameter in Fe–Ni alloys changes little with composition but there is a report[35] that it increases a little with Ni content up to 15% and then decreases with Ni content greater than 15%.

Kurdjumov–Sachs relations (K–S relations)

$$(111)_\gamma \| (011)_{\alpha'}, \qquad [\bar{1}01]_\gamma \| [\bar{1}\bar{1}1]_{\alpha'}. \tag{1}$$

These were first obtained for the relations between the orientations of α' and retained γ in a 1.4% C steel as determined by x-ray pole figure analysis.[36] They are also observed in ultralow carbon steels.[37] These relations are such

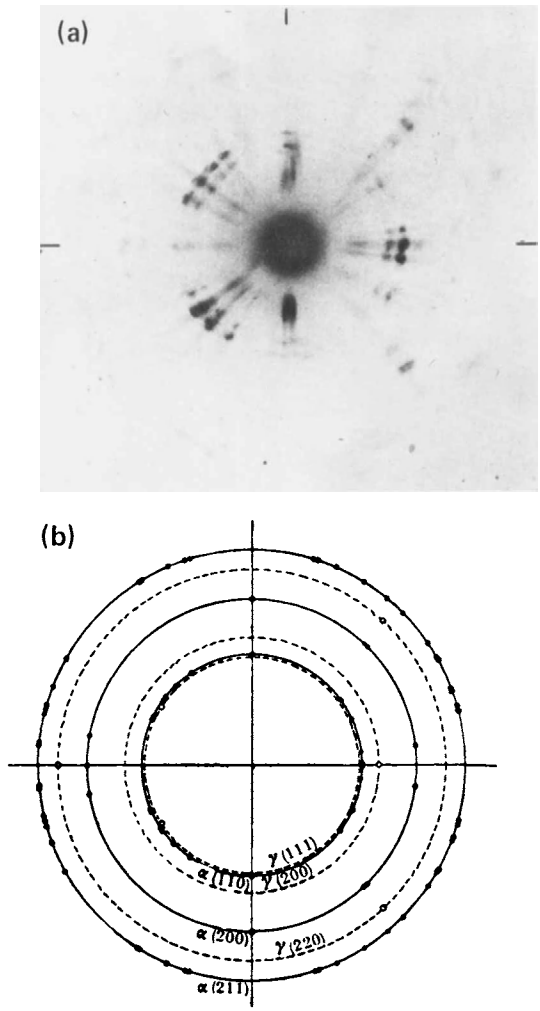

FIG. 2.5 X-ray oscillation photograph of Fe–30% Ni, showing Nishiyama orientation relations. (Specimen: a single γ crystal cooled in liquid nitrogen; x-rays: Mo–K; oscillation axis: $[001]_\gamma$; oscillation angle: 45° between $[100]_\gamma$ and $[110]_\gamma$.) (After Nishiyama.[38]) (a) Oscillation photograph; (b) pattern expected from N relation.

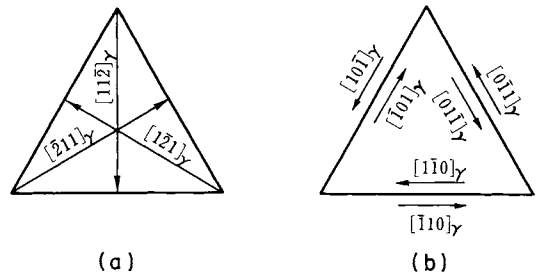

FIG. 2.6 Directions of shears in $(111)_\gamma$ plane. (a) N relationship. (b) K–S relationship.

that the close-packed plane of the γ lattice is parallel to that of the α' lattice, and the close-packed direction of the γ is parallel to that of the α'. Moreover, this direction is parallel to the Burgers vector, which is of physical importance. Strictly speaking, experimental results deviate a little from the foregoing relations.

In Fe–Ni alloys (Ni content more than 28%) the following relations are obtained.

$$(111)_\gamma \| (011)_{\alpha'}, \qquad [\bar{1}\bar{1}2]_\gamma \| [0\bar{1}1]_{\alpha'}. \tag{2}$$

Called the Nishiyama relations (N relations), they were first[38] obtained from the measurement of the positions of diffraction spots from several α' crystals that were produced from a γ single crystal of Fe–30% Ni alloy by cooling to the temperature of liquid nitrogen. Figure 2.5a shows an x-ray oscillation photograph in which the positions of the diffraction spots are in good agreement with those (Fig. 2.5b) predicted from the foregoing relations. These relationships were also confirmed by Wassermann[39] and others.[40–44†] Deviations of 1–2° from the Nishiyama relations were pointed out from very accurate measurements.

In the N relations, Eq. (2), the $(111)_\gamma$ plane of parallelism can be any one of four—(111), $(\bar{1}11)$, $(1\bar{1}1)$, or $(11\bar{1})$—planes. In each plane, any one of three different directions can be chosen, as illustrated in Fig. 2.6a. Therefore, this yields α crystals with $4 \times 3 = 12$ different orientations in a γ crystal. These crystals are called *variants*.

In the K–S relations four kinds of planes can also be considered, but six equivalent directions exist in each plane, as shown in Fig. 2.6b.‡ These consist

† There is a report[45] that different orientation relationships were obtained when martensites were formed by transformation in specimens thinned down to electron transparency for examination in the electron microscope. But it has been pointed out[46] that these results might have large errors due to a lack of proper analyses for thin specimens. Apart from this, the result that martensite induced under plastic deformation has different orientation relations was obtained in Fe–Ni alloys.[47]

‡ In the N relations, shears of opposite direction occur with difficulty and even if they take place, they do not generate different orientations.

of three pairs, with one direction the opposite of the other in each pair. Such pairs of crystals are twin related. Thus the K–S relations lead to $4 \times 6 = 24$ variants, or twice as many as those in the N relations. But the orientation of an α' crystal derived from the K–S relations differs by only 5°16′† from that derived from the N relations (Figs. 1.4, 6.5). Because of this there exist some alloys in which the K–S relations hold under some conditions and the N relations under others.‡

Orientation relationships also change with alloy composition. Greninger and Troiano[48] found that in a 22% Ni–0.8% C steel the orientation relations are a little different from both the K–S and N relations. For the experiment, a γ plate of grain size 1 cm was prepared. By cooling it to −70°C, α' crystals 2–3 mm long and 30 μm thick were produced. From this plate, specimens were cut out along one α' crystal boundary to expose a large area more than 1 mm in diameter. By measuring their orientations using the x-ray rotating crystal method, they obtained the following result:

$$(111)_\gamma \overset{1^\circ}{\sim} (011)_{\alpha'}, \qquad [\bar{1}01]_\gamma \overset{2.5^\circ}{\sim} [\bar{1}\bar{1}1]_{\alpha'}.$$

These are called the Greninger–Troiano relations (G–T relations). The accuracy in measurement of the angle was ±0.5°. These relations are midway between the K–S and N relations and the $(111)_\gamma$ and $(011)_{\alpha'}$ planes are not exactly parallel.

In 2.8% Cr–1.5% C steel[41] the orientation relations are near the G–T relations, but in 7.90% Cr–1.11% C steel[49] they are considerably different. Thus orientation relations may change with alloy composition and with transformation temperature. In all cases the parallel planes and directions usually deviate from planes and directions of low indices by 1° or several degrees and experimental scatter of about 1° always exists. Most of these deviations can be explained in terms of the phenomenological theory of martensitic transformation, which will be treated in Chapter 6.

2.2.5 Morphology and habit plane

The morphology of α' crystals has been well investigated and established for Fe–Ni alloys, so Fe–Ni alloys will be described first, to provide a basis for our discussion; then the morphology of martensites in carbon steels, nitrogen steels, and alloy steels will be described.

† In cases when the axial ratio of the α' crystal is 1.

‡ For example, there is a report[40] that in an Fe–31% Ni alloy the martensite formed at 240°C exhibited the K–S relations. This temperature is much higher than the M_s temperature, and if the specimen is held at the temperature for as long as six days, a considerable amount of the b.c.c. phase forms isothermally, as a result of gradual progressive transformation to a Widmanstätten structure. This might be placed in the category of massive transformation.

A. *In Fe–Ni alloys*

A close relation exists between the morphology of α' crystals and the transformation rate. Förster and Scheil[50] observed the change of electrical resistance during the martensitic transformation in Fe–Ni alloys by a cathode-ray oscilloscope and found two types of martensite; one formed extremely rapidly and the other rather slowly. The former was termed the "umklapp transformation" (*Umklappumwandlung*), since it resembled mechanical twinning; the latter was called the "schiebung transformation" (*Schiebungsumwandlung*), since it resembled slip deformation. Although these terms are rarely used now, we shall use them in this text.

Honma *et al.*[51,52] also reported two different morphologies resulting from the transformation; their findings were based on microstructure observations of α's with nickel contents of 2%–35%. One morphology, observed when the M_s temperature was higher than the ambient temperature, was massive† in shape for low nickel content but became platelike or lathlike as the nickel content was increased. This corresponds to the product of the "schiebung" transformation. In alloys containing more than 30% Ni and with the M_s below room temperature, the shape of the α' crystals was lenticular or bamboo-leaflike and the junction of two crystals had a jagged appearance, like lightning, suggesting that the martensite was produced by a chain reaction[53,54]. This corresponds to the product of the umklapp transformation.‡ Whether the schiebung or the umklapp transformation occurs depends to a great extent on the transformation temperature as well as on the chemical composition.[52,56]

Figure 2.7a[57] shows the morphology of α' of an Fe–30% Ni alloy that must have transformed by the umklapp process from immersion into liquid nitrogen. Though it shows a rough microstructure due to deep etching, it can be seen that the α' crystal is bamboo-leaflike. Figure 2.7b shows an electron micrograph (replica) of the framed area in part (a), where the triangular features seen at several places are etch pits. Since all of these etch pits are similar and of the same orientation, the whole region in this photograph is considered to be within one crystal. In earlier days an attempt was made to explain the hardness of martensite on the grounds that a crystal observed under the optical microscope might actually be composed of many fine crystals. This photograph shows that such an explanation was incorrect. Further, it should be noted that a straight "core" exists within the α' crystal in Fig. 2.7a. This is the *midrib*, which will be discussed in detail later. In this

† An α' crystal that is seen as massive under the optical microscope in many cases consists of a group of laths.

‡ There is an opinion[55] that the martensite produced from paramagnetic γ is lathlike whereas that produced from ferromagnetic γ is lenticular, but evidence for this opinion is lacking.

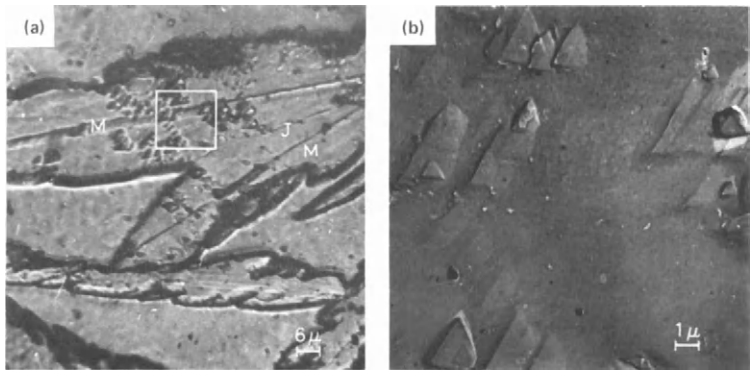

FIG. 2.7 Martensite in an Fe–30% Ni alloy (etched in a solution of 3% HCl and 2% zephiran chloride). (a) Optical micrograph: M, midrib; J, junction plane. (b) Electron micrograph of the white-framed area in (a): Triangular features are etch pits whose orientations on both sides of the midrib are similar. (After Nishiyama and Shimizu.[57])

figure a straight α'–α' interface, marked "J", can also be seen; this is called the *junction plane.*

Figure 2.8[58] shows an etched structure of the martensite in an Fe–32% Ni alloy, where α' crystals formed along two directions, and it appears that crystal II intersects crystal I. It is of interest that the midrib in crystal I is jogged in the vicinity of the intersection. Near the midrib are seen parallel striations oriented at an angle of about 50° to the midrib. These striations do not extend right up to the crystal boundary; rather, their ends form an interface that is roughly planar throughout the crystal. This is in contrast

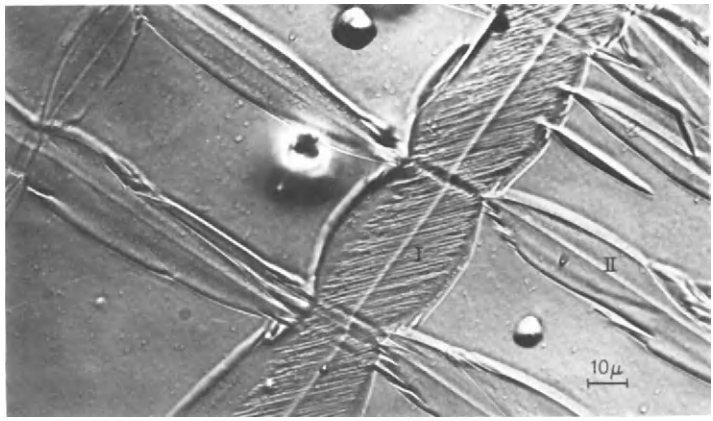

FIG. 2.8 Intersection of martensite plates in an Fe–32% Ni alloy (etching reagent 30% H_2O, 70% H_3PO_4). (After Patterson and Wayman.[58])

to the round α'–γ interface. It should also be noted that the growth tip of crystal II is not at the round interface with crystal I but at the end of the striations. This fact implies that the formation processes are different in regions with and without striations.

In the majority of cases there is some part of the α'–γ interface that has nearly a definite crystallographic orientation. As previously mentioned, this plane is called the habit plane and is of special significance in the crystallography of martensite. The habit plane is usually expressed as a plane in the parent phase. In the case of the umklapp transformation the shape of the martensite is lenticular and the α'–γ interface is not planar, so that a definite plane cannot be assigned. But even in this case the midrib has a definite plane, which is usually taken as the habit plane. Taking such a plane, in the case of the umklapp transformation in iron alloys the habit plane is approximately $(259)_\gamma$ or $(3\,10\,15)_\gamma$.[†] Though the habit plane is definite, a fairly large amount of scatter usually exists. This is due to the difference in the conditions under which martensite forms[‡] and is an important consideration in explaining the habit plane in terms of the phenomenological theory of martensite (Chapter 6).

The so-called surface martensites nucleate and grow on pricking by a needle. These have somewhat different morphologies. Okada and Arata[62] observed such martensite under the microscope, using the electropolished surface of an Fe–30% Ni alloy in the γ state. The shape of the α' crystals was nearly bamboo-leaflike but the crystals manifested somewhat unusual behavior in that in some cases the transformation took place on only one side of the midrib, whereas the γ on the other side remained untransformed and had many slip lines within it. Further, Klostermann and Burgers[63] examined an Fe–30.2% Ni–0.04% C alloy and found that the surface martensite contained platelike crystals with a $\{112\}_\gamma$ habit plane and propagated and stopped at a depth of 5–30 μm from the surface. Butterflylike martensite

[†] Details of the transformation occurring from explosive shock loading will be taken up in Section 3.7.2. Only the habit plane is presented here. In a study using Fe–30% Ni–0.026% C and Fe–28% Ni–0.1% C, Bowden and Kelly[59] found that α' began to change to f.c.c. martensite (γ') due to reverse transformation at 100-kbar peak pressure and virtually all the α' transformed to γ' when a 160-kbar peak pressure was reached. In this case the K–S relations held approximately while the habit plane was $(\bar{5}23)_{\alpha'}$ or $(\bar{1}21)_{\alpha'}$, which corresponds to $(225)_{\gamma'}$ or $(11\bar{2})_{\gamma'}$ referred to the γ' lattice. This was interpreted by assuming that the slip systems of $(101)\,[\bar{1}01]_{\alpha'}$ as well as of $(112)\,[11\bar{1}]_{\gamma'}$ are active during the transformation. These systems may not be peculiar to transformation by explosive shock loading because Zerwekh and Wayman[60] also observed slip of a similar system on heating a pure iron whisker crystal, in which the transformation is not purely martensitic.

[‡] Internal stress accompanying the transformation is one example of a factor that depends on transformation conditions. Habit plane scatter was observed to increase when the austenite had been strained plastically prior to transformation,[61] showing that prior deformation of the austenite is another variable factor.

was also often found. This was assumed to be an intermediate product between surface and "interior" martensite.

A martensite crystal formed by cold working is thinner than that formed by cooling.[64]

B. *In Fe–C and Fe–N alloys*

In carbon steels, the morphology of martensite changes with the carbon content; the α' crystal is platelike in medium carbon steels; it changes to lenticular with a midrib as the carbon content increases and M_s temperature decreases. The habit plane in most cases is $\{225\}_\gamma$ or $\{259\}_\gamma$ and in a given specimen the $\{259\}_\gamma$ habit predominates[65] for martensite produced at a low transformation temperature. The habit plane has a tendency to change with the carbon content, as shown in Fig. 6.35.[66] Martensite that has the $\{259\}_\gamma$ habit is considered to have formed by the process of umklapp transformation, as in Fe–Ni alloys. Sometimes the martensite region has a midrib parallel to the $\{259\}_\gamma$ plane but has a morphology suggesting it is divided into small parallel grains. The habit of these small grains is $\{225\}_\gamma$, which is called the secondary habit plane.[65,67] In other cases the γ–α' interfaces are so irregular that there are spikes on the interface. The habit plane of the spike segments is also $\{225\}_\gamma$[65] (see Fig. 2.9a).

In low carbon steels the martensite consists of bundles of laths, as was shown in Fig. 1.6. This is called lath martensite (the microstructure of which will be discussed later). Many investigators[37,68,69] have determined the crystallographic orientations and habit planes of each lath within a bundle; however, the results exhibit considerable scatter, because retained austenite was not generally found and the boundary of the laths was not always flat. In spite of this, it has been suggested that the habit is nearly $\{111\}_\gamma$ or $\{557\}_\gamma$.[70 †]

Careful two-surface analysis of martensite, utilizing annealing twins in the γ phase developed on heating prior to the transformation,[72] revealed that in Fe–10% Ni–(0.01–0.2)% C the habit plane departed approximately 12° from $\{111\}_\gamma$. The orientation relations were intermediate between the K–S and N relations but nearer the latter. The results above have also been discussed by others.[73]

Some studies[74,75] have suggested that in low carbon martensites, the $\{225\}_\gamma$ plates degenerate into needles with the $\langle 011\rangle_\gamma$ direction and that the needles lie in sheets on $\{111\}_\gamma$, which appears as the habit plane. Others[76] suggest that what is seen as a needlelike region is in reality like an airfoil section, the plane being $\{225\}_\gamma$ and the long direction $\langle 011\rangle_\gamma$. The habit

† In carbon steels with rather large carbon content the martensite formed by plastic deformation has a $\{111\}_\gamma$ habit.[71]

plane is also reported to be $\{123\}_{\alpha'}$ (long axis direction $\langle 111\rangle_{\alpha'}$) when referred to the α' lattice.[77] The martensite bundle in some cases consists of laths of different variants of the K–S relations (including twin relations) and in other cases it consists of laths all of the same variant with parallel growth directions giving the appearance of a bundle.

The habit planes of α' in nitrogen steels are the same as those in carbon steels.

C. *In other alloy steels*

The kinds of habit planes observed in carbon steels are also observed in alloy steels except in special cases. For example, in 18–8 stainless steel α' has a $\{225\}_{\gamma}$ habit.[78,79] In an Fe–30% Ni alloy containing about 5% titanium a $\{111\}_{\gamma}$ habit is reported.[24] The habit planes for many other iron alloys change with the chemical composition.[48,80] Such a change of the habit plane with composition for the same atomic arrangement may also be accounted for in terms of the phenomenological theory.

The habit plane of the hexagonal close-packed (h.c.p.) martensite produced in high manganese steels and 18–8 stainless steels will be described in the next section.

2.2.6 Shape change and surface relief

On the electropolished surface of austenite, an upheaval can be observed where a martensite plate forms and, as mentioned in Chapter 1, such an upheaval is called surface relief. Greninger and Troiano[48] examined the surface relief in an Fe–22% Ni–0.8% C alloy and observed that in each martensite plate macroscopically homogeneous shear takes place parallel to the plate.

Honma *et al.*[51,52] examined the surface relief of various Fe–Ni alloys by microinterferometry and found that the surface relief in the schiebung transformation resembled a slip band, whereas in the umklapp transformation a whole bamboo-leaflike crystal was elevated. The interference fringes changed their directions uniformly, indicating that the surface of a martensite crystal as a whole is tilted at a definite angle to the specimen surface. Thus, the surface relief is not irregular but each martensite crystal is subjected to a linear shape change.

Patterson and Wayman[58] also examined surface relief using an Fe–32% Ni alloy. Figure 2.9 shows the surface relief from two α' crystals produced in a specimen that was immersed in liquid nitrogen for a short time in order to produce a small amount of martensite. The crystals seen in the upper region have a somewhat complicated α' interface, but within the crystal a midrib can be seen (though not very clearly) in the central region.

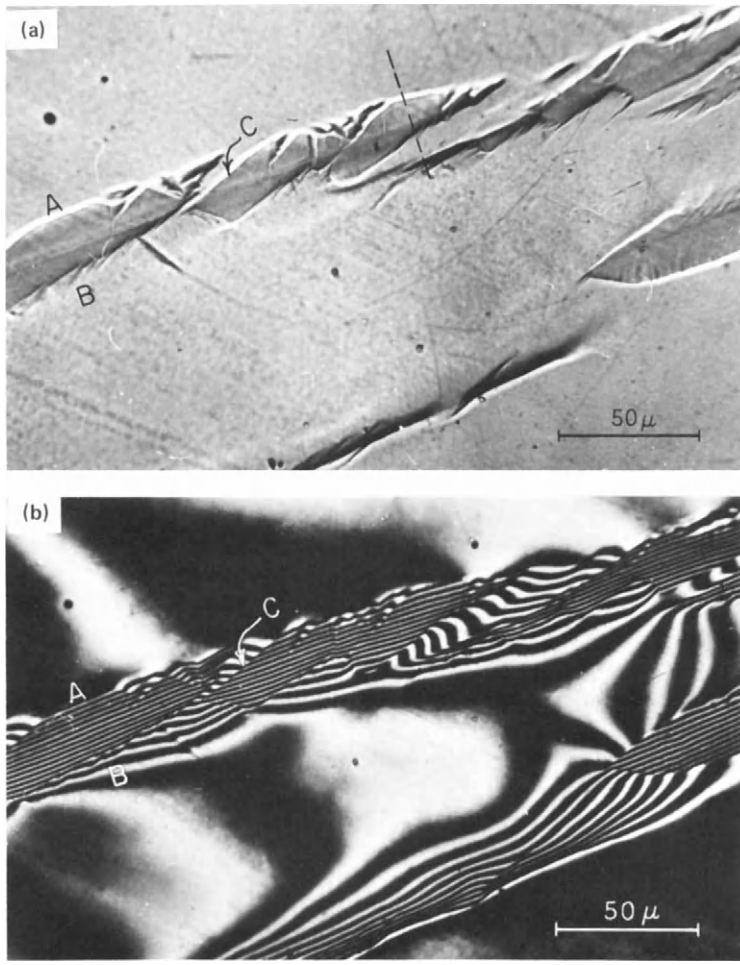

FIG. 2.9 Surface relief of martensite in an Fe–32% Ni alloy. (a) Ordinary optical micrograph. (b) Interference micrograph. (After Patterson and Wayman.[58])

Figure 2.9b is the corresponding interference micrograph. Since the phase plane of the light was adjusted approximately parallel to the surface of the γ matrix, the γ matrix shows slowly varying interferometer fringes,† whereas many fringes can be seen on the α' crystals, showing the presence of large upheavals. Moreover, the direction of the fringes is parallel to that of the

† One must not overlook the slight strain in the γ matrix near the α' crystal.

FIG. 2.10 Bending of scratch lines by martensitic transformation in an Fe–30% Ni alloy: plane of the paper, $(111)_\gamma$; habit plane, $\{259\}_\gamma$. (After Machlin and Cohen,[81] with permission of the American Institute of Mining, Metallurgical and Petroleum Engineers, Inc.)

midrib, indicating the absence of inclination along that direction. This fact is taken to be important in the theory of the transformation.

It has also been observed that a fiducial reference scratch bends where a martensite crystal has been produced (Fig. 2.10). Using this phenomenon, Machlin and Cohen[81] determined the shape change† and found that it can be represented as a transformation matrix. It was not a simple shear but a general one having a strain consisting of 0.20 in the shear direction and 0.05 perpendicular to it. This does not equal the amount of lattice distortion due to the crystallographic change. It is inferred from this fact that another deformation, as well as the distortion corresponding to the amount just stated, must occur in the crystal. This gives a basis for the phenomenological theory of the mechanism of the martensitic transformation (Chapter 6).

2.2.7 Substructure

As seen in the previous photographs, α' crystals are usually small. Detailed examination often reveals that what may look like a crystal under the optical microscope actually consists of many small subgrains with small misorientations. For example, it was observed[83,84] in Fe–28% Ni–0.04% C

† They used a single γ crystal of Fe–30% Ni alloy. A specimen was cut out along three orthogonal faces, $(111)_\gamma$, $(1\bar{1}0)_\gamma$, and $(\bar{1}\bar{1}2)_\gamma$, and scratch lines were drawn parallel to each edge. The specimen was then cooled to $-40°C$ to partially produce martensite. Examination of the surface revealed that the scratch lines were bent at the α'–γ interface. The shape change due to α' formation was estimated from the values of the angles of bending observed on the three orthogonal faces. Such measurements were done for 40 α' crystals. Various other methods have also been attempted.[82]

($M_s = -20°C$) that α' consists of small subgrains about 50 μm wide, misoriented by 10–20'.[†] Many investigations[85] of the fine structures in martensites are now being made in order to verify the existence of the lattice-invariant deformation inferred from the surface relief.

A. *Fe–Ni alloys*

Electron microscopic observations of the martensite of Fe–Ni alloys provide clear results because these alloys are easily electropolished and it is not difficult to obtain clean thin foil specimens.

In this alloy system, lath martensite[‡] forms when the nickel content is not very large or, even with fairly large nickel content, when the cooling rate is not very high. Figure 2.11 is an electron micrograph of the lath martensite produced in maraging steel[87§] quenched from 1000°C in water.

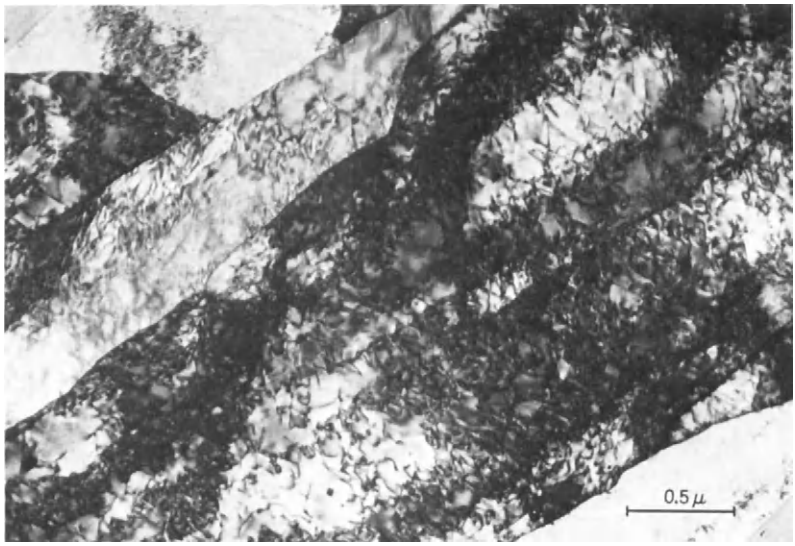

FIG. 2.11 Interior of a martensite crystal in a maraging steel (water quenched from 1000°C) having a lath structure containing numerous dislocations. (After Shimizu and Okamoto.[87])

[†] Using the microbeam x-ray technique (divergence $< 1°$).

[‡] The crystals within a bundle of laths have nearly the same orientations so that they are etched nearly identically, and under the optical microscope one bundle can appear to be one crystal because the lath boundaries are not clear. Because the morphology of the bundle appears massive, such α' is often called massive martensite.[86] This name, though convenient, is not ideal, since it is likely to be mistaken for the massive transformation (though there is no clear borderline between these two).

[§] Fe–19% Ni–10% Co–4.5% Mo–0.4% Ti–0.05% Al–0.03% C.

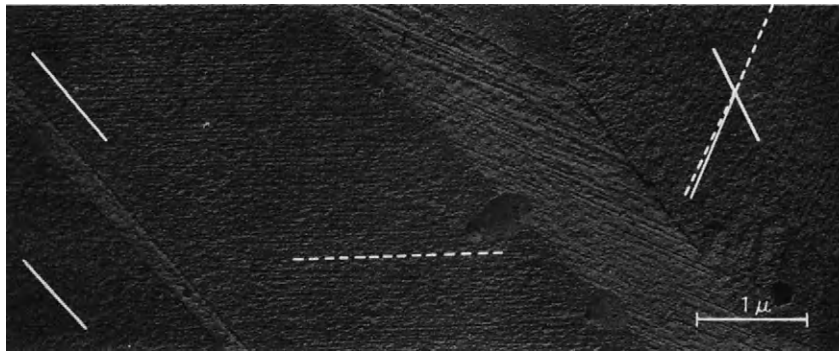

FIG. 2.12 Electron micrograph of a replica of surface relief of Fe–30.64% Ni alloy martensite showing substructure. (After Nishiyama, Shimuzu, and Sato.[96,97])

Many dislocations are seen in the lath.† They can be interpreted as the dislocations that remained after the lattice-invariant slip deformation necessary for the transformation (predicted from the surface relief).

In Fe–Ni alloys, with increasing Ni content, the M_s temperature decreases to below room temperature and the alloys undergo the umklapp transformation, where internal twins appear as another mode of lattice-invariant deformation. Figure 2.12, an electron micrograph that was taken by the present author *et al.*[96,97] in the pioneering age of electron microscopy,‡ shows a replica of the surface relief§ on an Fe–30.64% Ni martensite produced by subzero cooling after the specimen was furnace cooled from a high temperature and electropolished. In this figure each martensite plate is covered with striations, the spacing being about 100 Å. That these striations are due to internal twins can be confirmed by transmission electron micrography, as will be described next.

Figure 2.13[100,101] is an example of a transmission electron micrograph in which a number of parallel fine bands, all having the same direction,¶ are seen. Figure 2.14a is a selected-area electron diffraction pattern of area (a)

† In addition to dislocations, internal twins are occasionally observed in lath martensite. Das and Thomas[88] found internal twins in the α' of Fe–9% Ni–0.24% C and Fe–9% Ni–0.24% C–7% Co alloys. But some[89] consider such twins as deformation twins because they are short. There is a report[90] that such short deformation twins were observed in Fe, Fe–19.8% Ni, Fe–12.5% Cr–9.2% Ni, Fe–15% Cr–8.25% Ni, each containing about 0.03% C; there is also a report[91] that the α' in Fe–27% Ni–5.3% Ti had striations like internal twins. Thomas and Das[92,93] later studied α' in Fe–33% Ni and Fe–25% Ni–0.3% V and observed images that can be explained by double twinning. But there are other opinions[94,95] that dispute this explanation.

‡ Soon afterward Takeuchi and Honma[98] observed such structures in Fe–33% Ni. The spacing of the striations was 300–500 Å.

§ Fine striations are barely visible in the surface relief in the as-formed condition. Upon slight etching they can be seen clearly.[99]

¶ In the case of nickel content as high as 35%, the bands sometimes appear with three directions.[102]

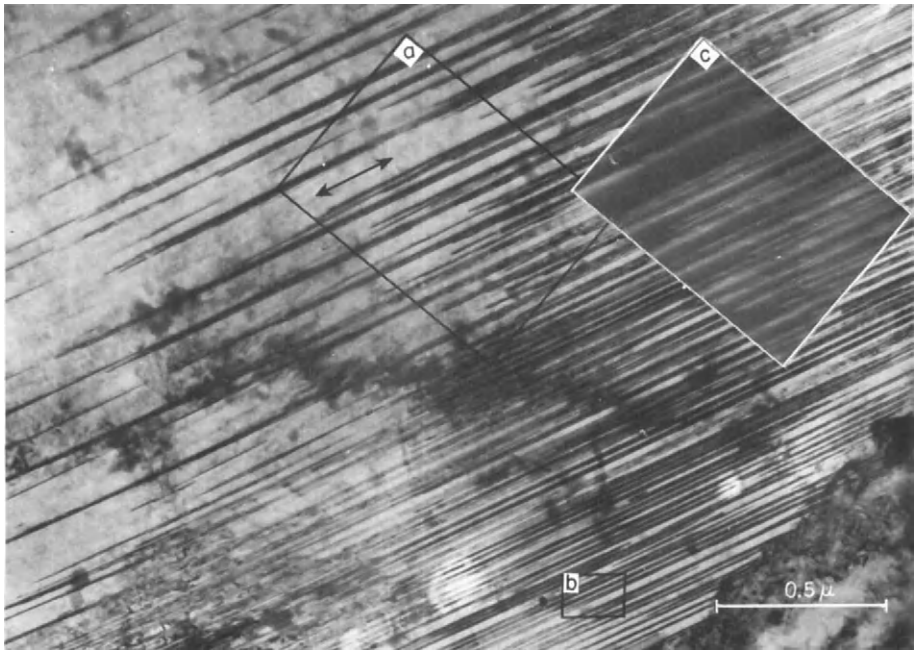

FIG. 2.13 Interior of a martensite crystal in an Fe–30% Ni alloy. Internal twins (dark thin bands) are evident. Inserted (c) is a dark-field image of area (a) obtained by using a twin spot. (After Shimizu.[101])

in Fig. 2.13. This diffraction pattern consists of two sets of reflections, as indicated by ● and ▲ in the key diagram (Fig. 2.14b). The two sets correspond to the $[\bar{1}10]$ and $[1\bar{1}0]^t$ zones, respectively, of the b.c.c. crystal structure. They are twin related to each other with respect to the (112) plane.

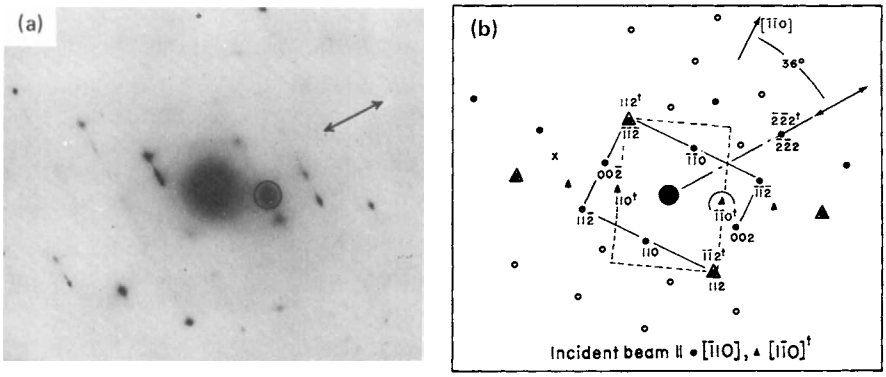

FIG. 2.14 (a) Electron diffraction pattern of martensite (area (a) in Fig. 2.13) in an Fe–30% Ni alloy. (b) Key diagram. (After Shimizu.[101])

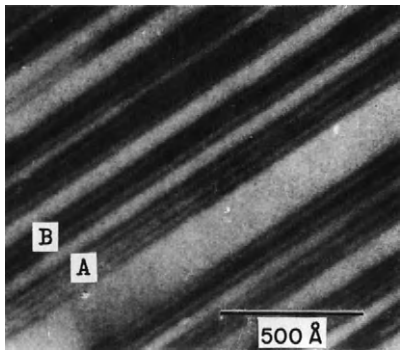

FIG. 2.15 Equi-thickness fringes due to internal twins enlarged from black-framed area (b) in Fig. 2.13. (After Shimizu.[101])

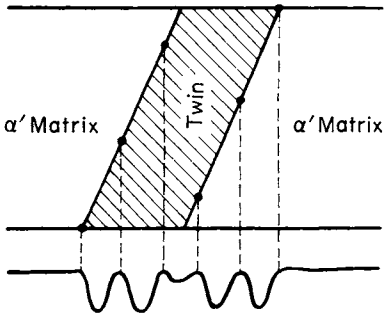

FIG. 2.16 Illustration of the formation of interference fringes due to an internal twin whose orientation is favorable for a Bragg reflection.

The surface trace of the twinning plane on the foil plane (indicated by a double-headed straight arrow in Fig. 2.14) is parallel to the fine bands. That these bands are twin plates is confirmed by the dark-field image in Fig. 2.13c produced by a spot $\bar{1}\bar{1}0^t$ encircled in Fig. 2.14b. Area (b) in Fig. 2.13 is enlarged in Fig. 2.15. It is seen that most of the bands consist of four lines and can be interpreted as the superposition of two sets of equal-thickness interference fringes on both sides of the twin plate, as illustrated in Fig. 2.16. The spacing of the fringes shows that the twin interface makes an angle of about 84° with the foil plane. From this analysis it is found that the thickness of the twin plate varies from 30 to 70 Å.

Figure 2.17 is an electron micrograph of another part of the same specimen. It appears quite different from Fig. 2.13, but by analyzing diffraction patterns it was found that the dark parallelograms have a twin relation to the matrix of the martensite plate with respect to the (112) plane.† The edges of the parallelograms parallel to the direction marked by the two-headed arrow are the traces of the twin plates on both surfaces of the foil; the other pair

† {112} has twelve variants. On which variant twinning occurs is important in the mechanism of the transformation. It will be described in detail later when the transformation mechanism is explained.

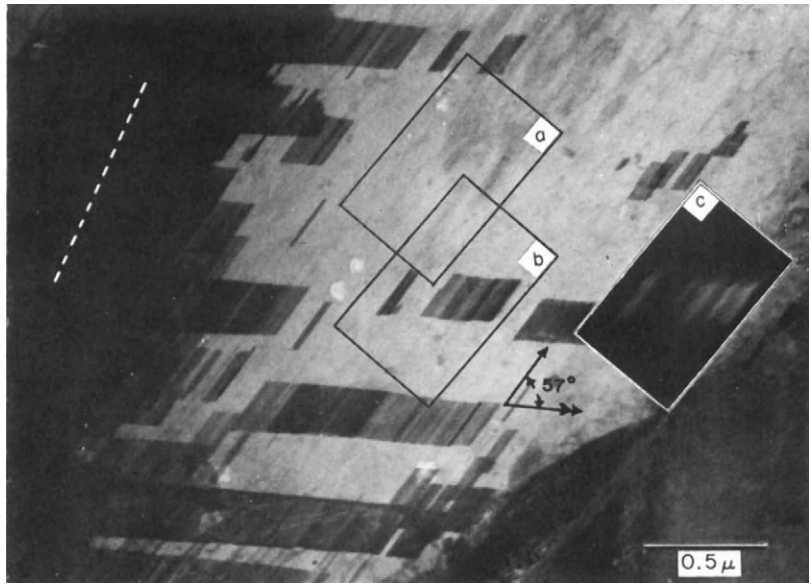

FIG. 2.17 Interior of a martensite crystal (in an Fe–30% Ni alloy) having internal twins whose sections are parallelograms. A dotted line shows the position of a midrib; pattern (c) is a dark-field image, obtained by using a twin spot of region (b). Region (a) did not reveal any strong twin spots. (After Shimizu.[101])

of edges, in the direction marked by the single-headed arrow, is parallel to the projection of the [111] direction onto the foil surfaces.† It is deduced from this fact that the twin plates are substantially thin ribbons elongated in the [111] direction and that sections of these ribbons cut by the foil surfaces are observed. The dotted line in this photograph (Fig. 2.17) shows the supposed position of a midrib near which twin bands are crowded together. The striations seen in the microphotograph in Fig. 2.8 are due to such twins,‡ and the ends of the twins are so uniform as to define a clear interface in the optical microphotograph; in the electron micrograph, however, the interface is observed to be quite irregular.

† Careful comparison of the electron micrograph and the corresponding electron diffraction pattern reveals that the twin boundary deviates from $(112)_{\alpha'}$ by 3°–21°. The deviation angle is constant in each α' crystal but different in different α' crystals. It is considered that the existence of such deviations is due to the occurrence of another slip in the crystal. Such deviations from $(112)_{\alpha'}$ have also been observed in later investigations.[103,104] But there is an opposing opinion[105] that such deviations are errors due to the buckling of the specimen foil. Therefore, further investigations are needed.

‡ There is a detailed review about internal twins.[106]

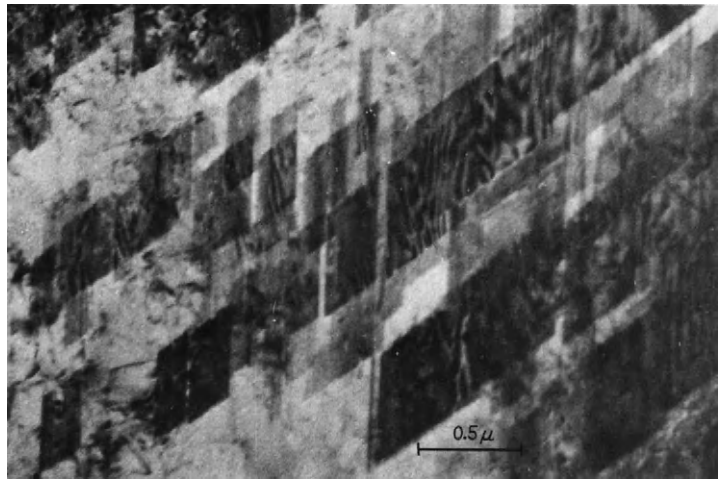

FIG. 2.18 Interior of a martensite crystal (in an Fe–30%Ni alloy) having internal twins that exhibit moiré fringes. (After Shimizu.[101])

Sometimes moiré fringes can be seen. They are caused by the interference of reflections from two overlapped twin plates[101] (Fig. 2.18).

In the untwinned region in a martensite crystal, a large number of perfect dislocations are seen.† Figure 2.19 is an example; in it, the direction of the incident electron beam was [110] and the contrast was caused by a strong $(1\bar{1}0)$ reflection. The long dislocations are arranged in two directions, $[1\bar{1}1]$ and $[1\bar{1}\bar{1}]$, to form diamondlike patterns. Since the slip direction in a b.c.c. crystal is usually $\langle 111 \rangle$, it is suggested that the observed dislocations in the two directions are both screw dislocations. The visibility condition of the dislocation is $\boldsymbol{g} \cdot \boldsymbol{b} \neq 0$[108,109] where $\boldsymbol{g}$ is the normal to the reflecting planes and $\boldsymbol{b}$ is the Burgers vector; this is actually satisfied in the present case.

In Fe–Ni alloys in which the microstructure of α' consists mainly of internal twins‡ and dislocations, the volume fraction of the twins is larger for alloys of lower M_s temperature§ and is small for specimens cold worked prior to transformation. On rare occasions stacking faults are also produced.

† Even in the case of martensite with internal twins, a few dislocations sometimes appear[107] if the specimen foil is tilted by an angle adequate to extinguish the reflection of the internal twins.

‡ There is a report[110] that twins about 1 μm thick were observed in Fe–33%Ni but they can be considered to be deformation twins.

§ There are three opinions about the increase in the amount of internal twins. The first[109] is that it is mainly due to the low M_s temperature; the second,[111] that it is due to the small stacking fault energy; and the third,[88] that it is mainly due to the small critical resolved shear stress for the formation of twins and slips.

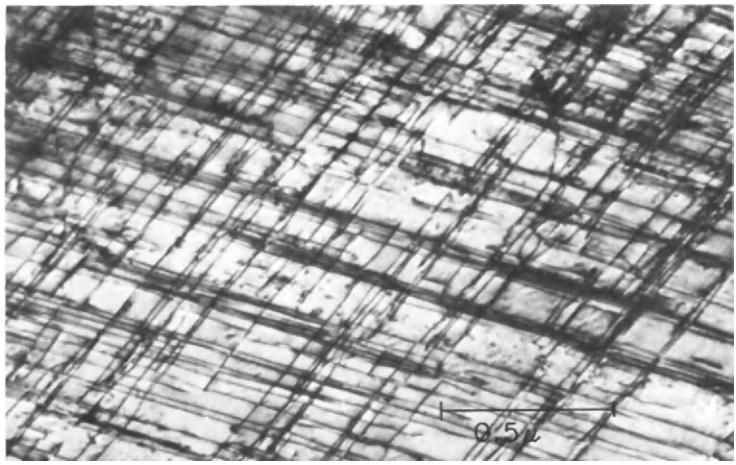

FIG. 2.19 Interior of a martensite crystal (in an Fe–29.8% Ni alloy) having long straight dislocations. (After Patterson and Wayman.[58])

Rowland *et al.*[112] observed {145} twins intersecting {112} internal twins in an Fe–32% Ni alloy. The former twins were rather coarse and considered to be the deformation twins. Striations parallel to {011} were also observed and considered to be slip dislocations retained in a bandlike form.

B. *Fe–C and Fe–N alloys*

Figure 1.10a is a transmission electron micrograph of the lath martensite in a 0.2% C steel formed by quenching. The boundaries of laths within a bundle are low-angle boundaries and those between bundles are high-angle boundaries. In each crystal there is a high density of dislocations.†

An electron micrograph of α' crystals in an 0.8% C steel is shown in Fig. 1.10b, where within a lenticular crystal, straight striations as well as many dislocations can be seen. Electron diffraction spots of (112) twins show that these striations are internal twins.[75,113] Such faults cannot be seen in lower carbon steels‡ but they gradually increase with increasing carbon content.

Figure 1.10c is an electron micrograph of the quenched structure in a 1.4% C steel showing part of two lenticular α' crystals in contact with each other. Within each crystal, dislocations as well as internal twins can be

† There is a report[88] that in the martensite crystals of Fe–9% Ni–0.24% C–(0–7)% Co alloys, internal twins as well as dislocations were observed.

‡ There is a report[114] that internal twins appeared even in a 0.5% C steel when the specimen was quenched rapidly.

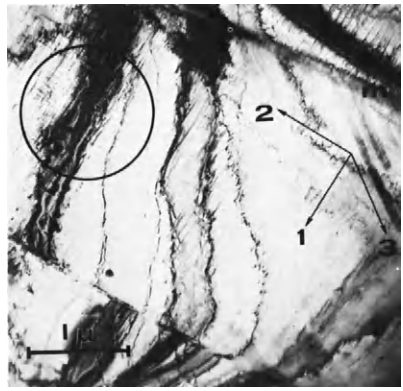

FIG. 2.20 Martensite plate (in an Fe–1.82%C alloy) having (011), (0$\bar{1}$1), and (101) internal twins, which are parallel to directions 1, 2, and 3, respectively. (After Oka and Wayman,[118] copyright American Society for Metals (1969).)

observed. The parts indicated by dotted lines are what are seen as midribs in the optical micrograph.

Application of the field ion microscope to the study of martensite has recently begun. An investigation[115,116] of α' crystals of Fe–0.88%C–0.45% Mn also revealed such internal twins of the $\{112\}$ type, the width being 15–40 Å and the spacing 15–50 Å. In internal twins produced layer by layer, alternate bright and dark bands were seen parallel to the (112) plane. The dark bands were interpreted as twin boundaries where preferential evaporation may have occurred.[117] In these experiments $\{145\}_{\alpha'}$ deformation twins were observed,[116] along with $\{112\}$ internal twins, as in the electron microscopic study described earlier.

Although the internal twins observed in 0.7%C and 1.4%C steels are of the $\{112\}$ type, plane faults of the $\{011\}$ type also appeared[118–120†] as the carbon content increased. Figure 2.20 is an example showing three types of plane faults, (011), (0$\bar{1}$1), and (101), which are parallel to arrows 1, 2, and 3, respectively, in the figure. Of the three, 1 and 2 are perpendicular to the foil plane and 3 is inclined to it. In other regions, (112) twins are also observed.

Let us next consider the origin of $\{011\}$ plane faults. These plane faults are obviously associated with thin twins but the concept that these are twin-related variants does not seem to apply because they must be derived from $\{111\}_\gamma$, considering the Bain correspondence. This is contradictory to the fact that $\{111\}_\gamma$ cannot become a mirror plane in transformation. Therefore, the $\{011\}$ twins must be nothing but twins caused by the plastic

† Before these researches striations of the $\{011\}_\alpha$ type observed in optical micrographs of etched martensite in high carbon steels had been interpreted[121] as the residues of the slip band produced on the $\{111\}_\gamma$ in the γ state.

deformation that relaxes the transformation strains. Such twins are expected to be easily formed, since in Fe–1.82%C steel the tetragonality is 1.08 and the magnitude of the shear for such twinning is 0.154, considerably smaller than the 0.71 required for the {112} deformation twin. That is, such twins have their origin in the tetragonality of the martensite.

Since nitrogen atoms, like carbon atoms, dissolve interstitially in the iron lattice, the morphology and fine structure of α' in Fe–N alloys resemble those of α' in carbon steels.[122–124]

C. *Alloy steels*

Addition of special elements to Fe–C or Fe–N alloys does not markedly change the fine structure as long as the amount of the added element is not very large. But due to the lowering of the transformation temperature caused by addition of the special element, the morphology of the martensite crystal and the proportion of dislocations and twin faults change somewhat.

For example, in Fe–3% Cr–1.5% C[119] and Fe–7.9% Cr–1.1% C[125] alloys, α' crystals sometimes exhibit $\{011\}_{\alpha'}$ plane† faults, but not as many as observed in the above-mentioned Fe–1.82%C alloy. Possibly because of this, the habit is intermediate between $\{225\}_\gamma$ and $\{259\}_\gamma$. But Fe–Ni alloy α' crystals without $\{011\}_{\alpha'}$ plane faults have the $\{259\}_\gamma$ habit and 18–8 stainless steels without even $\{112\}_\alpha$ twins have the $\{225\}_\gamma$ habit. Under what conditions the habit plane in carbon steels changes from $\{225\}_\gamma$ to $\{259\}_\gamma$ and whether or not the existence of the habit plane intermediate between the two is only due to the appearance of $\{011\}_{\alpha'}$ plane faults must be determined by future investigations.

In high carbon steels containing a large amount of aluminum, the habit plane is similar to that in carbon steels[21] but the internal twins and stacking faults are fine and extend throughout the crystal.[126,127] This steel is of theoretical importance and will be described in detail in Section 6.1.1.

Dissolving carbon in Fe–Ni alloys results in martensite with a somewhat different appearance. Figure 2.21 is an electron micrograph of an α' crystal, taken by Tamura *et al.*,[128] showing internal twins extending throughout the plate. In the twin plates mottled contrasts are seen. Figure 2.22 is an electron micrograph taken by Patterson and Wayman;[129] it shows internal twins that also extend completely to both interfaces and have mottled contrasts in the midrib region as well as in the twin regions. The reason mottled contrasts are observed is not yet well understood, but the contrasts may be related to the strain field due to clustering of carbon atoms in solution.

Thermal treatments that bring about the stabilization of austenite generally decrease the M_s temperature (Chapter 5), which results in a change of the

† Not all of $\{011\}_{\alpha'}$, but only one of the planes, as expressed in the orientation relationships.[125]

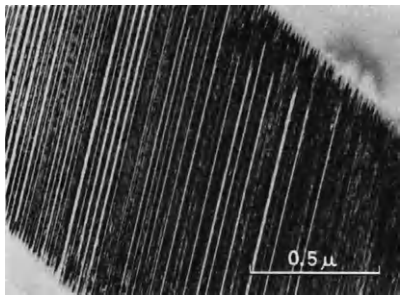

FIG. 2.21 Martensite plate filled with internal twins (in an Fe–29% Ni–0.4% C alloy). (After Tamura *et al.*[128])

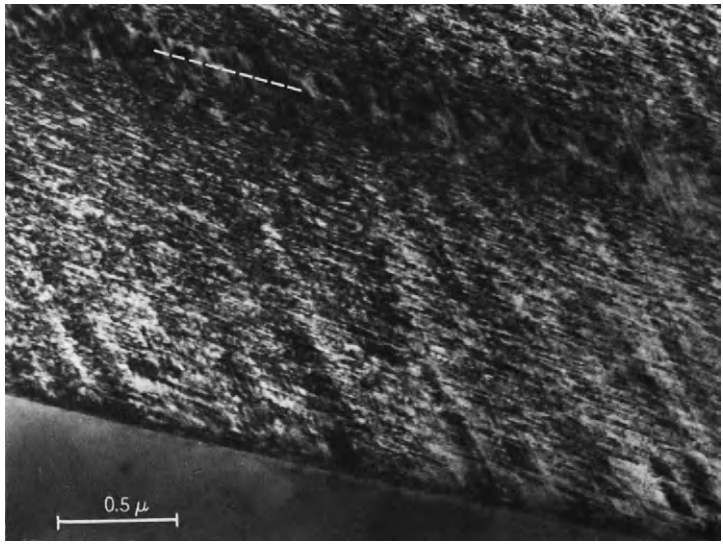

FIG. 2.22 Martensite plate in an Fe–21.7% Ni–1.0% C alloy. Note that internal twins are seen all over the martensite plate. A dotted line shows the position of the midrib. (After Patterson and Wayman.[129])

habit plane. This phenomenon in an Fe–31% Ni–0.28% C alloy has been studied by Tamura *et al.*[130,131†] Martensite with an M_s temperature of $-81°C$ consisted of lenticular α' crystals with midribs and partially twinned regions. As the M_s decreased, the twinned part increased and the twinning was completed at $-119°C$. With an M_s of $-171°C$, the α' crystals were not lenticular but thin, platelike, and completely twinned.

The thin platelike martensite formed at very low temperatures has a somewhat different morphology from that of lenticular martensite.[133] For

† Golikova and Izotov[132] used an Fe–24% Ni–3% Mn alloy.

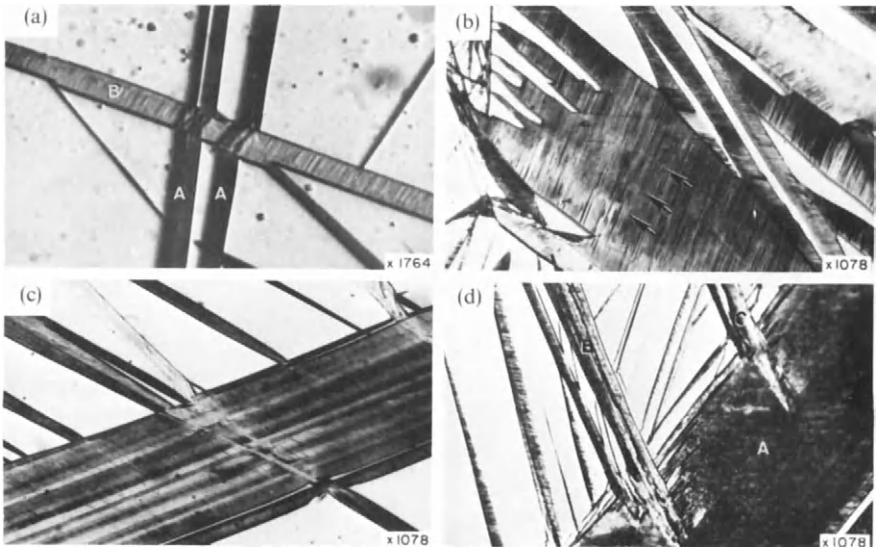

FIG. 2.22A Optical micrographs of martensite produced at very low temperatures. (a), (b) Fe–31% Ni–0.28% C cooled to −196°C. (c) Fe–33.5% Ni–0.22% C elongated 5% at −196°C. (d) Fe–33.5% Ni–0.22% C elongated 10% at −196°C. (After Maki *et al.*[133])

example, the intersection of martensite with different variants is frequently observed, as in Fig. 2.22Aa, where it appears that crystal A forms first and crystal B forms later, penetrating crystal A and deforming it at the crossing points. In thick martensite plates, faint striations parallel to the plate are always observed within it, as shown in Fig. 2.22Ab,c. This is considered to

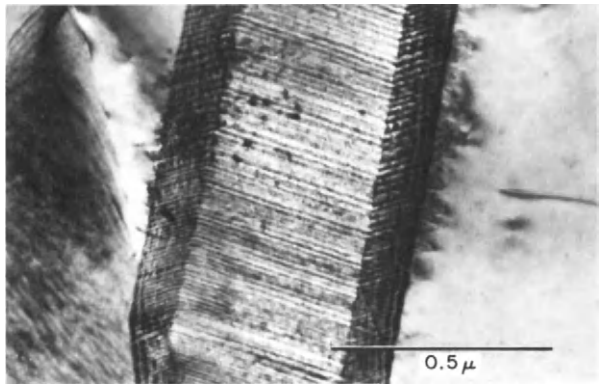

FIG. 2.22B Electron micrograph of a thin martensite crystal in Fe–31% Ni–0.23% C cooled to −196°C. (After Maki *et al.*[133])

be due to the nucleation of thin martensite plates that grow successively side by side and coalesce. In Fig. 2.22Ad, crystal A thickens after the impingement of other martensite crystals with different variants B and C (different directions), and it appears as if the B and C crystals penetrate the A crystal. Figure 2.22B is a high-magnification electron micrograph of a platelike crystal cut out obliquely; the two side bands are α'–γ interfaces and the central region is inside the martensite crystal, which shows internal twins in all regions.

2.2.8 Midribs

As described earlier, α' crystals with the $\{259\}_\gamma$ habit and occasionally with the $\{225\}_\gamma$ habit[125] have midribs which are planar. A midrib is not always located in the central region but it is probably the first part of the crystal to form. Although midribs have been studied extensively by electron microscopy and other methods, their basic character and origin are not yet completely understood. Since midribs seem very important for our understanding of the transformation mechanism, the facts observed so far are discussed further in this section in order to provide a basis for future progress.

Early in 1924, Lucas[134] and Sauveur[135] theorized that the midrib is the portion already transformed to *troostite*† and Desch[136] considered it to be a thin cementite plate about one molecular layer thick. Soon afterward Scheil[137] pointed out that such views are not correct, because he found that the midrib also appears in an Fe–29% Ni alloy without carbon atoms. There was another opinion—that the midrib is nothing but an interface between two variants of the martensite crystal—but this was also rejected by Scheil on the basis of his observation that the slip lines produced by plastic deformation after transformation pass through the midrib without kinking. No progress was made in understanding the midrib for several decades, but with the advent of the application of electron microscopy to metals, study of the midrib entered a second stage.

Figure 2.23[138] is an electron micrograph (replica) of the etched surface of one martensite crystal in quenched white cast iron. This crystal has a midrib (indicated by a solid white line) in the central region and parallel striations (broken line) on both sides of the midrib. These striations may be associated with the internal twins, as mentioned before.

Detailed inspection of the electron micrograph (replica) in Fig. 2.12 reveals that fine striations parallel to the internal twins (dotted lines) are bent at the point indicated by the thick solid line. The bending angle is small, at

† A microconstituent consisting of ferrite plus suboptical microscope carbide particles.

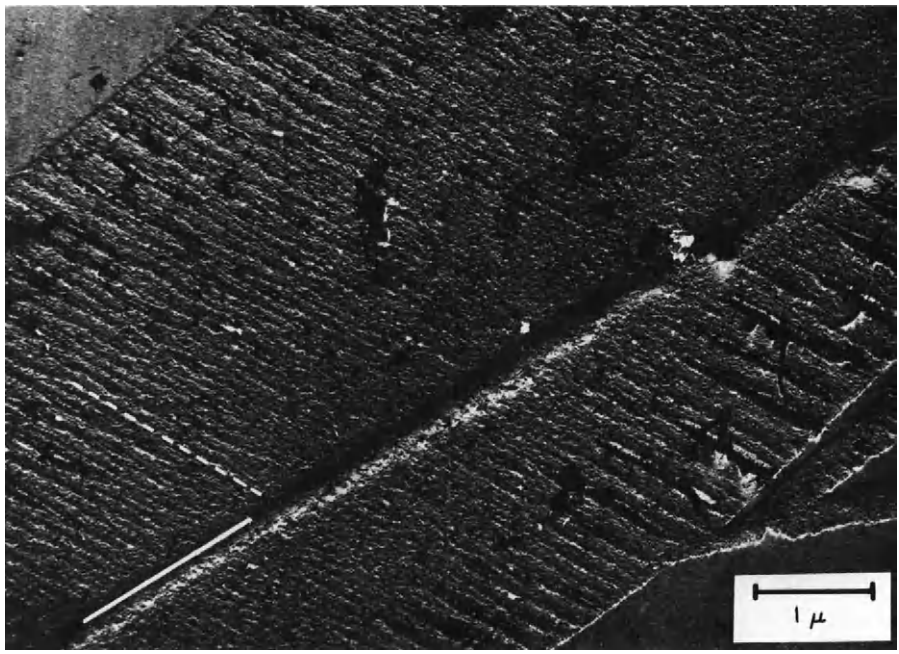

FIG. 2.23 Electron micrograph of a replica of a martensite crystal in quenched pig iron (Al deposited on the etched surface and Cr shadowed. Solid line: direction of the midrib; dotted line: direction of internal twin plane trace. (After Nishiyama and Shimizu.[138])

most about 7°. Since these linear zones appear quite different from the interface between variants, they may be considered midribs. It thus appears that midribs are very thin and can scarcely be observed in the electron micrograph. The midrib in Fig. 2.23 seems to be rather thick, but this must be interpreted as the result of preferential etching of the region near the midrib due to the existence of large internal strain. Therefore, as explained in interpreting the thin foil transmission electron micrograph (Fig. 2.17), the midrib is not a region in which there exist many internal twins; rather, internal twins are densely distributed near the midrib. This is also clear in Fig. 2.8, in which we see the midrib region as well as internal twin regions.

The midrib is usually, but not always, one line (actually one plane). Two midribs were first observed with an electron microscope[97,139] in a replica of the surface relief of martensite in an Fe–30% Ni alloy (Fig. 2.24). Two parallel midribs about 1 μm apart are visible in Fig. 2.24a. In some cases a transient region can be seen from one midrib to another, as in Fig. 2.24b. If the spacing is about 1 μm, as in these figures, the two lines will be unresolvable when the etched surface is examined by optical microscopy and thus it is observed as if it were only one midrib line.

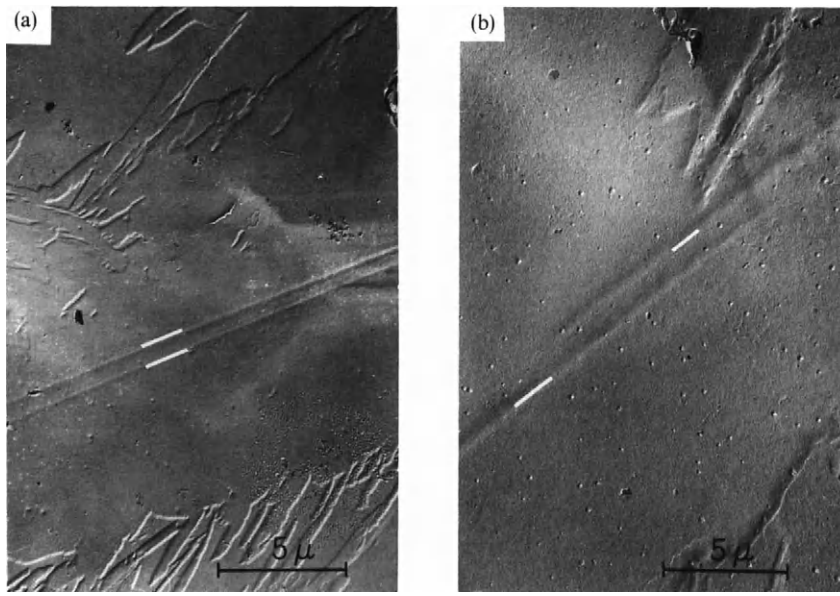

FIG. 2.24 Electron micrographs of replicas of lightly etched surfaces showing a martensite crystal (Fe–30% Ni) with two midribs. (a) Two parallel midribs. (b) Two midribs separated by shifting. (After Nishiyama *et al.*[97,139])

FIG. 2.25 Partitioning of martensite in a Kovar alloy. (After Nishiyama *et al.*[139])

Figure 2.25[139] shows an α' crystal in Kovar in which one crystal is subdivided into several regions by planes (parallel to the internal twins) where the midrib has steps. Recently, two midribs were also observed[140] by transmission electron microscopy in a Kovar alloy.† It was found that the region between the two midribs has a slightly different orientation from the outer regions.

† 27.69% Ni, 17.21% Co, 0.02% C, 0.18% Si, 0.56% Mn, balance Fe.

FIG. 2.26 Optical micrograph showing a martensite crystal (dark) with cone-shaped regions of retained austenite, like shadows, at phosphide particles (Fe–31.4% Ni–1.1% P alloy, etched in 1% alcoholic HNO_3). (After Neuhäuser and Pitsch.[141])

Recently Neuhäuser and Pitsch[141] observed the influence of incoherent precipitate particles in the austenite on subsequent transformation to martensite and obtained some results that might provide an understanding of the role of the midrib in the martensitic transformation. For their study, an Fe–31.4% Ni–1.1% P alloy was chosen. After being heat treated for 14 days at 910°C, it was quenched in water. As shown in Fig. 2.26 and its schematic drawing, Fig. 2.27a, small incoherent globular phosphide particles† are distributed uniformly in both the bright γ matrix and the darkly etched α'. Within the α' crystal, small austenite regions (bright) are retained around the phosphide particles. The morphology of such retained austenite is like a shadow behind the particle and the directions of these austenite shadows are all parallel but opposite on opposite sides of the midrib (the darkest central line). The lattice constants of γ and α' and the orientation relationships were obtained from Kossel patterns and the habit plane was measured. Using these data, the complementary shear predicted by the phenomenological theory of the martensitic transformation was obtained by numerical calculations. It was found that the direction of this shear and that of the shadow are not directly related;‡ rather, the projection of the direction of

† They are found to be isomorphous with Fe_3P and Ni_3P by x-ray diffraction of isolated residue.

‡ The length of the shadow measured on the surface of the specimen changes with the cutting plane. The longest was considered to be the real length of the shadow. The change of the shadow with increasing etching depth was also examined.

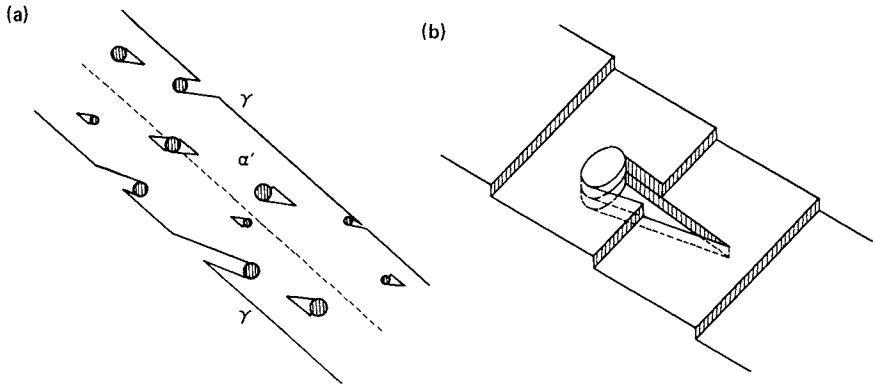

FIG. 2.27 (a) Schematic drawing of the typical features of austenite shadows in one martensite crystal. (b) Idealized picture of the formation of an austenite shadow at a particle when the transformation is proceeding. (After Neuhäuser and Pitsch.[141])

the shadow onto the habit plane is approximately antiparallel both to the direction of the maximum displacement of the shape deformation of the transformation and to the direction of the macroscopic shear involved in the shape deformation. The directions of the former and the latter deviate by 11° and 4°, respectively, from the projection of the shadow. From these results and the morphology of the shadows, the following process of the transformation was deduced.

The midrib plane is the plane of initiation of the transformation and the interface propagates on either side in opposite directions by means of ledges that are parallel to the midrib plane, as shown in Fig. 2.27b. The transformation front becomes pinned at the precipitated phosphide particles and these particles inhibit continuation of the transformation just behind them; thus, retained austenite regions are left, like shadows. This is the interpretation given by the investigators.

A similar midrib has also been observed in the case of deformation twins of α phases in Fe–Si[142] and Fe–V[143] alloys. This observation suggests that martensitic transformation by the umklapp process is similar to formation of the deformation twin, and the similarity is of significance in the theory of the mechanism of the martensitic transformation.

From the foregoing facts the nature of the midrib is suggested to be as follows: the α′ crystal forms initially at the midrib plane and grows laterally. This supposition is supported by the fact that the junction plane of two α′ crystals passes the point of intersection of two midribs. However, there still remain some questions about the nature of the midrib. Some investigators[54] believe that the midrib is a thin crystal plate but this is a matter for speculation. It may, therefore, be considered at present that the midrib may be the region in which some lattice imperfections are retained.

2.2.9 Relation of substructures to magnetic domains

The magnetic domains in ferromagnetic materials must be influenced by the fine structure of the crystals. In a study of a 3.24% Cr–1.4% C steel and a 10.1% Cr–1.02% C steel, Izotov and Utevskiy[144] observed that in spite of the fine structure the width of the magnetic domain is as large as 0.2–1.0 μm but the long direction of the magnetic domain coincides with the [001] of an α' crystal, as is predicted from magnetostriction. The magnetic domain has no relation to dislocations in martensite and is little influenced by the many internal twins near the midrib, but in some cases there are magnetic domains branching off at the midrib and combining again on the other side of the midrib. This behavior was observed in foils 1000–3000 Å thick and it is not known whether such is also the case in bulk material. The relation between the magnetic domain wall in the martensite crystal and the microstructure thus has not yet been clarified.

2.3 f.c.c. to h.c.p. (mainly in cobalt alloys and ferrous alloys)

2.3.1 h.c.p. martensite (ε) in cobalt alloys

Masumoto[145] found that cobalt has an allotropic transformation temperature at 403°C on cooling. As is well known, the high-temperature phase is f.c.c. and the low-temperature phase is h.c.p. (ε); (see Fig. 2.28). Since the addition of about 30% Ni to cobalt lowers the transformation temperature

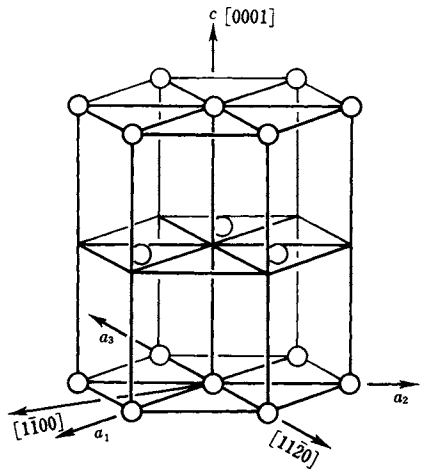

FIG. 2.28 Hexagonal close-packed (h.c.p.) lattice.

to about room temperature, h.c.p. martensite can be obtained even by slow cooling. The notation for h.c.p. martensite should perhaps be ε', where the prime is meant to signify martensite, as in the case of α'. In this book, however, h.c.p. martensite will be designated simply ε martensite, because the notation ε' is used for another crystal structure (see Section 3.8). The orientation relationship between ε and the retained f.c.c. phase is expressed as follows:[146,147]

$$(111)_{fcc}\|(0001)_{hcp},$$
$$[11\bar{2}]_{fcc}\|[1\bar{1}00]_{hcp}, \quad \text{or} \quad [1\bar{1}0]_{fcc}\|[11\bar{2}0]_{hcp}.$$

This is called the Shoji–Nishiyama relation (S–N relation).

Both the f.c.c. and h.c.p. crystals have a close-packed structure. The atomic arrangements of the $(111)_{fcc}$ plane and the $(0001)_{hcp}$ plane are quite the same; the only difference is the stacking of the atomic layers normal to these planes. Therefore, the lattice correspondence is geometrically simple. In addition, the volume change on transformation is only 0.3%, and therefore it is comparatively easy to establish the mechanism of the transformation (see Section 6.5.1).

Figure 2.29 shows the atomic arrangements of the two phases projected in the $[1\bar{1}0]_{fcc}$ and $[11\bar{2}0]_{hcp}$ directions, respectively. In this figure, the open and solid circles indicate the atoms lying on and above the plane of the paper, respectively. As can be seen from the figure, every two adjoining $(111)_{fcc}$ atomic planes are displaced toward the $[11\bar{2}]_{fcc}$ direction by $a/\sqrt{6}$ (a = lattice parameter) successively during the f.c.c.-to-h.c.p. transformation. By these successive displacements, an f.c.c. lattice is sheared by $\tan^{-1}(\sqrt{2}/4) \sim 19.5°$ as a whole. Shoji[131] was the first in Japan to note this matter. The axial ratio c/a in an h.c.p. lattice formed only by the foregoing shearing process from an f.c.c. lattice would be $\sqrt{8}/\sqrt{3} \fallingdotseq 1.633$. In a real crystal, however, the ratio is usually a bit different from this ideal value; e.g., cobalt has an axial ratio of 1.623 ($a = 2.507$ Å, $c = 4.069$ Å).[148]

In Co–Ni alloys, the ε martensite phase is produced even by slow cooling, exhibiting surface relief.[149–151] Figure 2.30a, a replica electron micrograph

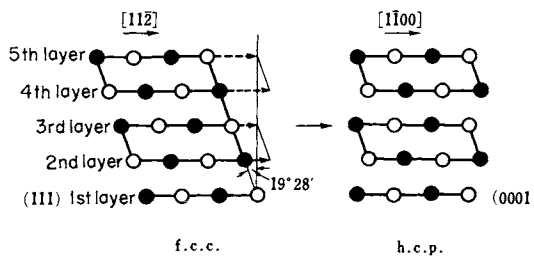

FIG. 2.29 Mechanism of the f.c.c.-to-h.c.p. transformation.

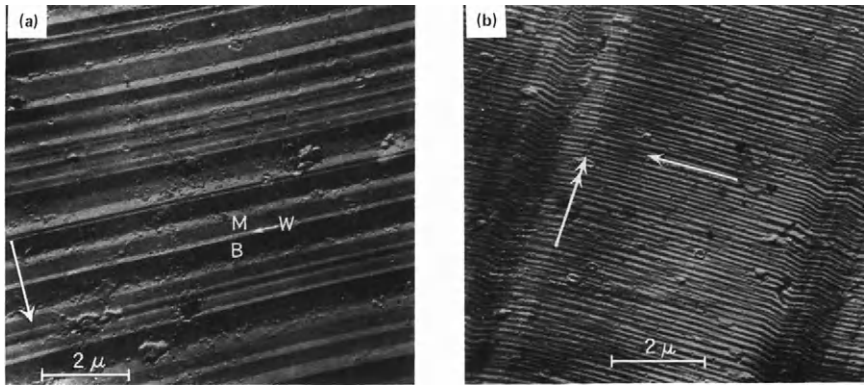

FIG. 2.30 Electron micrographs of replicas of the surface of martensite in a Co–24.61% Ni–0.052% C alloy. (a) Surface relief. (b) Thermally etched surface near $(112)_{fcc}$. (After Takeuchi and Honma.[149])

of the surface relief taken by Takeuchi and Honma, shows light and dark bands. The darkness of these bands is caused by shadowing (in the direction of the arrow) and indicates the degree of inclination of the surface. In this photograph, three kinds of bands showing different surface inclinations are arrayed repeatedly. The middle-tone regions might be untransformed areas. The less the nickel content in the cobalt alloy, the smaller is the width of each band.

The following experiment was done to measure quantitatively the surface inclination. Figure 2.30b is a replica electron micrograph showing the thermally etched structure on the surface plane near $(112)_{fcc}$ exhibiting the surface tilt of an ε martensite plate. In this figure, the striations parallel to the direction of the single-headed arrow are due to the $\{100\}_{fcc}$ planes revealed by thermal etching. The wide bands running in the direction of the double-headed arrow correspond to bands in Fig. 2.30a and the thermally etched striations due to the $\{100\}_{fcc}$ plane are bent at the boundaries of these bands. The bent angles were measured to be $-4°$, $-14°30'$, and $+18°$, and these values will be discussed shortly.

The f.c.c.-to-h.c.p. transformation, as shown previously in Fig. 2.29, occurs by shifting every other (111) plane in the f.c.c. lattice by $(a/6)[11\bar{2}]$. The shifts of $(a/6)[\bar{2}11]$ and $(a/6)[1\bar{2}1]$ on the $(111)_{fcc}$ planes also lead to h.c.p. crystals with the same orientation. The relations among these three shift vectors are shown in Fig. 2.31. The transformation deformation by only one kind of shift causes a total shear of 19.5°. If three variants with different shift vectors are stacked with the same thickness, the total transformation deformation becomes zero. That is, the transformation strains by shearing are canceled

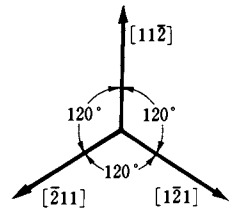

FIG. 2.31 The three kinds of shear direction in the f.c.c.-to-h.c.p. transformation.

in the bulk. Under these conditions the complementary shear for martensitic transformation can be small and, therefore, the formation of ε can occur easily.

The inclination angles of ε plates of three variants to the specimen surface near the $(112)_{fcc}$ plane were calculated to be $-3°12'$, $-14°18'$, and $+18°6'$,† and these values are in good agreement with the experimental values given before. This agreement affirms that the habit plane of the ε plates is $(111)_{fcc}$ and the shifts of atomic planes presumed in Fig. 2.29 actually occur. Furthermore, it is realized that stacking of crystal layers consisting of the three variants causes cancellation of their transformation strains. As for the ε martensite resulting from applied stress, such variants are formed to relieve the transformation stress and, therefore, possess a habit that appears like a slip band.[149,152]

The lattice defects in h.c.p. martensite of cobalt were first investigated by x-ray diffraction[153–155] and it was recognized that they caused the diffraction spots to be accompanied by streaks in the c^* direction. But only the spot with $h - k = 3n$ (n = integer) does not exhibit such a streak. It can be shown from diffraction theory that the origin of the streaks is not due to the thinness of the crystals in the [0001] direction, but that the streaks are due to many stacking faults parallel to the (0001) plane.[156]

The fine structure of ε martensite was made clear by Ogawa *et al.*[157–159] by means of electron microscopy. Figure 2.32a shows a transmission electron micrograph and Fig. 2.32b a diffraction pattern taken from a specimen of a Co–10% Ni alloy cooled slowly from 1000°C. From the pattern in part (b), it can be seen that a large portion of an f.c.c. crystal is transformed to ε and the foil plane is $(\bar{1}2\bar{1}0)_{hcp}$. Striations seen in part (a) are parallel to $(0001)_{hcp}$ and also to $(111)_{fcc}$ in the retained β phase. The intervals of these striations are much narrower than those in Fig. 2.30. This fact indicates that a variant crystal contains many planar defects. Since diffraction spots of $h - k \neq 3n$‡

† These values are corrected for the inclination of the specimen surface from $(112)_{fcc}$.

‡ The streak accompanying the central spot is considered to be due to multiple reflections, because it disappears when the specimen foil is tilted about the direction of the streak.

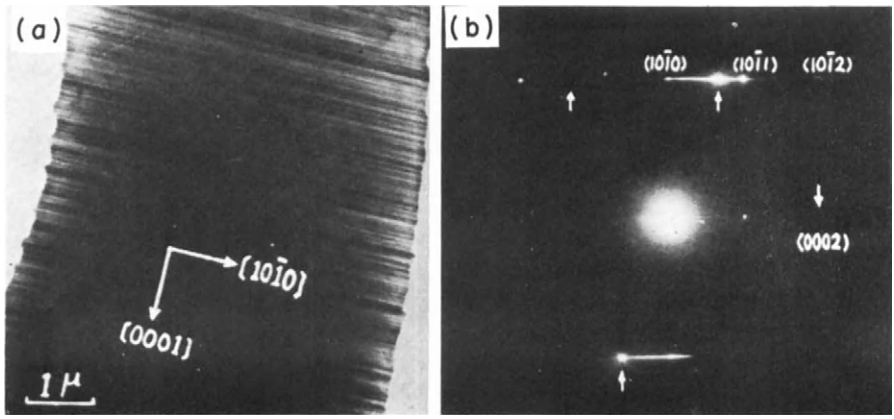

FIG. 2.32 Martensite in a Co–10% Ni alloy quenched from 1000°C. (a) Electron micrograph showing striations due to stacking faults. (b) Electron diffraction pattern showing ε phase and retained β phase. Note the streaks in the [0001] direction. (After Watanabe *et al.*[158])

are accompanied by streaks normal to $(0001)_{hcp}$, these streaks can be considered due to stacking faults on $(0001)_{hcp}$.†

The ε phase in cobalt and Co–Ni alloys is formed slowly. Utilizing this characteristic, researchers have studied the transformation process[158,160] during heating or cooling inside an electron microscope. According to their observations, stacking faults are formed by splitting perfect dislocations into partials, and two partial dislocations are combined into one perfect dislocation. The relation between the behavior of dislocations and the formation of the ε phase was determined. It should be remembered, however, that the observations in this experiment were made using thin films, which are different from bulk metals.‡

2.3.2 h.c.p. martensite (ε) in high manganese steels

As a typical ferrous alloy in which ε martensite occurs, high manganese steel will be described. In 1929[162–164] an h.c.p. phase was found in Fe–Mn alloys. At that time, it was designated the "h phase" and placed in the equilibrium phase diagram as the product of a peritectoid reaction. As a result of more recent research in the Soviet Union and elsewhere, it has been found that two types of martensitic transformations, $\gamma \rightarrow \alpha'$ and $\gamma \rightarrow \varepsilon$, occur, and that their transformation behavior is very complicated.§

† The existence of the stacking faults, if they are abundant, must be taken into account in any calculation of the inclination angle of the surface for the three martensite variants seen in Fig. 2.30.

‡ See reference 161 for cobalt whiskers.

§ There is an intermediate state before the formation of ε martensite, as will be explained in Section 3.8.

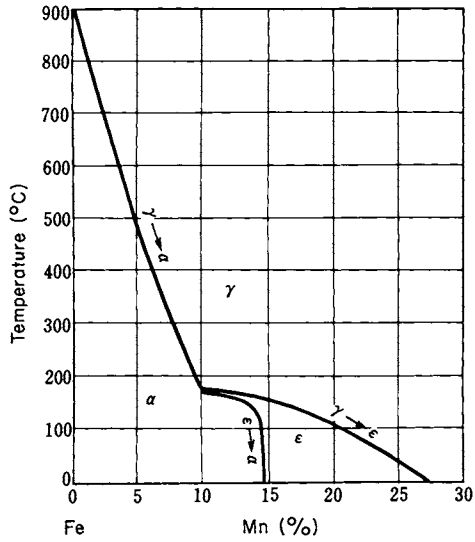

FIG. 2.33 Transformation temperatures of Fe–Mn alloys (extra-low carbon). (After Schumann.[165])

Schumann's work[165,166] on phase transformation of high manganese steels is particularly noteworthy. He examined steels with various manganese contents† by means of thermal dilatation, magnetic analysis, x-ray diffraction, optical microscopy, and other means. Thermal dilatation is of special interest. For example, in the case of a 13% Mn steel,

$$\delta l/l = 0.90\% \text{ (expansion)} \quad \text{for} \quad \gamma \rightarrow \alpha,$$
$$\delta l/l = -0.70\% \text{ (contraction)} \quad \text{for} \quad \gamma \rightarrow \varepsilon.$$

Therefore, in the $\varepsilon \rightarrow \alpha$ transformation a large expansion of

$$\delta l/l = 0.90 + 0.70 = 1.60\%$$

is expected. Hence, the three transformations can easily be distinguished from one another by a thermal dilatometer. Magnetic analysis is also convenient, because α is ferromagnetic and γ and ε are paramagnetic. Figure 2.33 shows the transformation temperatures determined with a cooling rate of 3°C/min, using these methods. In this alloy system, there is no appreciable difference in transformation temperatures even if the cooling rate is increased, except at high temperatures. Therefore, the transformation curves drawn in this figure are close to the true M_s temperatures for $\gamma \rightarrow \alpha'$, $\gamma \rightarrow \varepsilon$, and $\varepsilon \rightarrow \alpha'$, except for the part near pure Fe. This figure shows that α' forms below 10% Mn and ε forms above 10% Mn. It also indicates the possibility of the two-stage transformation $\gamma \rightarrow \varepsilon \rightarrow \alpha'$ in the range between

† (2.35–31.1)% Mn, (0.035–0.09)% C.

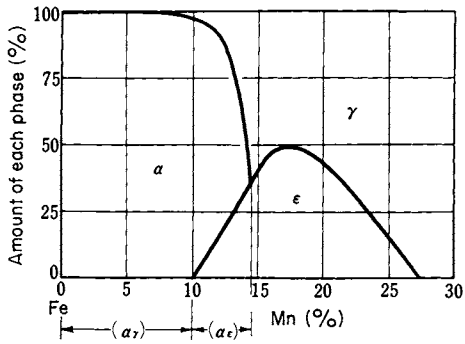

FIG. 2.34 Amounts of transformed products in extra-low carbon manganese steels air cooled from 1000°C. (After Schumann.[165])

10 and 14.5% Mn. Schumann deduced the occurrence of the second stage from his metallographic examinations, as will be described later. Figure 2.34 shows the relative amounts of the α', ε, and γ phases in specimens air-cooled from 1000°C.

A. $\gamma \rightarrow \varepsilon$

Figure 2.35 shows the typical structure of the ε phase formed by water quenching. In this figure, ε plates appear along the $\{111\}_\gamma$ planes, giving a Widmannstätten structure. When so many ε plates are formed, it is difficult,

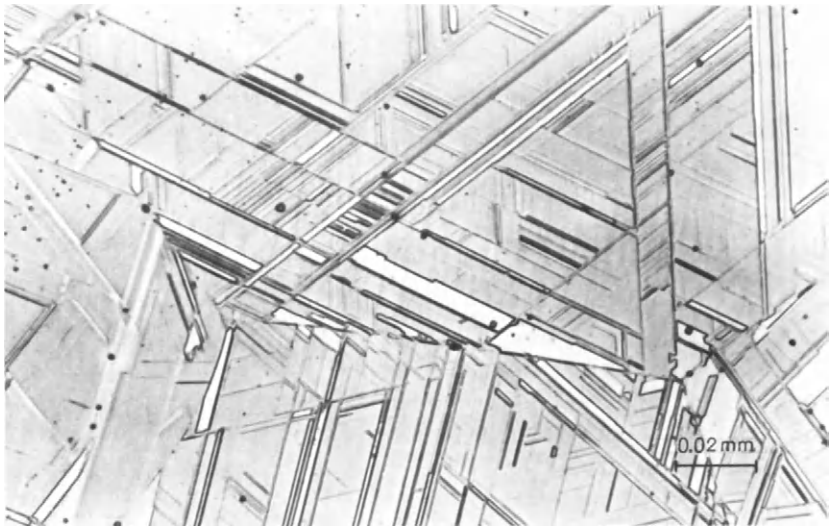

FIG. 2.35 Widmanstätten ε martensite in a steel of 16.4% Mn–0.09% C water quenched from 1150°C (etched in nital). (After Schumann.[165])

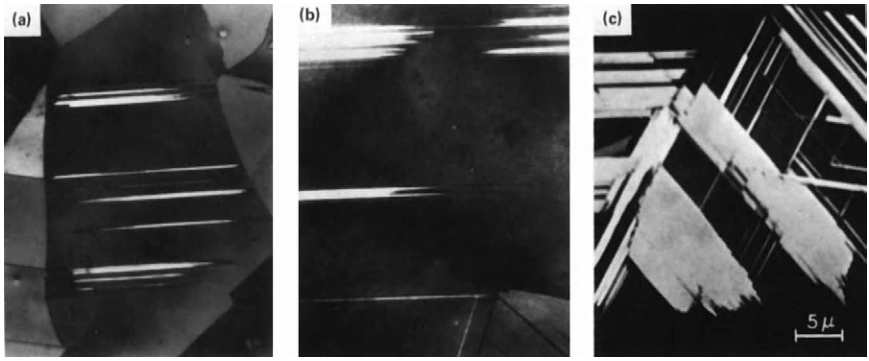

FIG. 2.36 Growth of ε martensite in a 26.12% Mn steel air cooled from 1000°C. (a) Initial stage of ε martensite formation along $(111)_\gamma$. (b) Side-by-side formation of two ε plates. (c) Successive formation of adjacent ε plates along three kinds of $(111)_\gamma$ planes. (After Schumann.[165])

in some regions, to distinguish the retained austenite from the ε phase. Therefore, in order to make the distinction easier, the manganese content was increased to 26%, the specimen was air-cooled, and an etching solution† different from that in Fig. 2.35 was used. The results are shown in Fig. 2.36a, where the ε plates appear acicular shaped (the true form is platelike), and are clearly distinguishable because of the strong etching of the γ matrix, and Fig. 2.36b, where the ε plates appear adjacent to each other. In Fig. 2.36c, the ε plates are parallel to three of the four $\{111\}_\gamma$ planes, and are thicker, exhibiting notches at the ends. This sequence suggests that thickening occurs by the successive formation of thin ε plates in contact with their neighbors; ε plates do not thicken by growth in the lateral direction.

B. $\varepsilon \rightarrow \alpha'$

Figure 2.37 is an optical micrograph of a 13.83% Mn steel air-cooled from 1000°C. In a steel of this composition it is possible to display the $\gamma \rightarrow \varepsilon \rightarrow \alpha'$ transformation process. The etchant used in Fig. 2.37 is the same as in Fig. 2.36. The bright regions are ε plates (thin ε plates look black, probably due to etching of their boundaries), the grey regions are austenite retained between the ε plates, and the darkest, granular regions are α′ martensite. The α′ crystals intrude into the ε plates but not into the retained austenite.[167] It is inferred from this fact that the α′ crystal seen here is not transformed directly from the austenite but is formed from the ε phase.

Recently, Oka *et al.*[168] studied Fe–Mn–C alloys by electron microscopy and observed two types of α′: one was formed through ε and the other directly from the austenite. The habit planes of the former were $(\bar{2}\bar{2}5)_\gamma$, $(\bar{5}22)_\gamma$, and

† 100 cm³ of a saturated solution of sodium thiosulfate and 10 g of potassium metabisulfite.

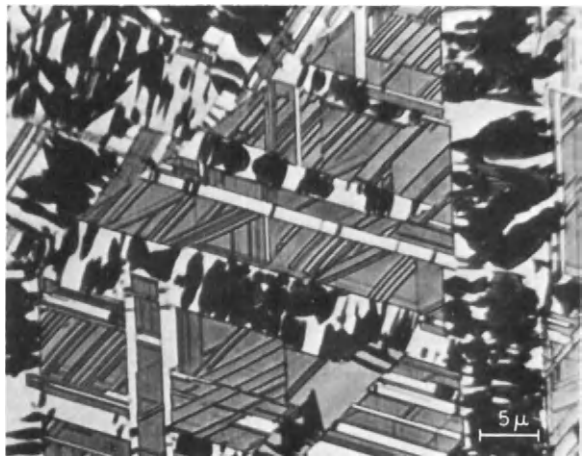

FIG. 2.37 Optical micrograph of a 13.83% Mn steel air cooled from 1000°C. Bright regions: ε; gray regions: retained γ interposed between two ε plates; dark regions: α' produced from ε. (After Schumann.[165])

$(2\bar{5}2)_\gamma$, which make an angle of about 85° with $(111)_\gamma$; and that of the latter was $\{225\}_\gamma$, which makes an angle of about 25° with $(111)_\gamma$. It was frequently observed that the former had dislocations parallel to $\{011\}_\alpha$ whereas the latter had $\{112\}_\alpha$ internal twins. As for the orientation relationship, in the former[169] it was close to that derived from the combination of the Shoji–Nishiyama relation in the $\gamma \rightarrow \varepsilon$ transition and the Burgers relation in the $\varepsilon \rightarrow \alpha'$ (Section 2.4.1), whereas in the latter it was close to the K–S relation.

Since the α' crystals formed by transformation of the ε phase are naturally smaller than the parent ε crystals, they are extremely small compared to

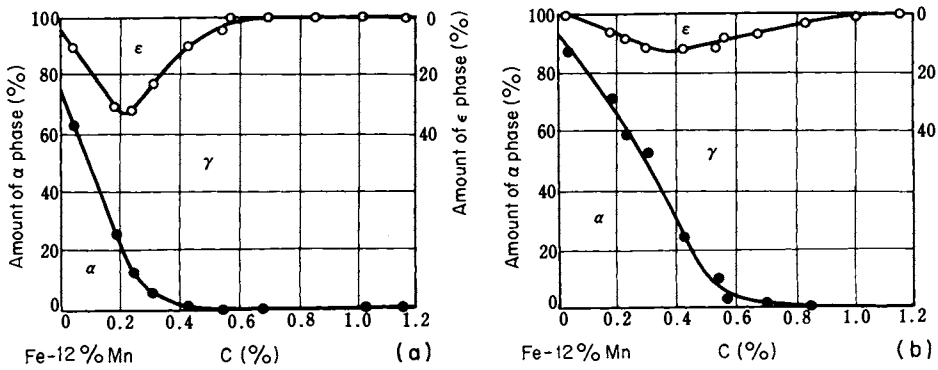

FIG. 2.38 Amounts of γ, α, and ε phases produced in an Fe–12% Mn–C alloy. (a) As quenched from 1100°C. (b) Hammered after quenching. (After Imai and Saito.[177])

the α' martensite formed directly from the austenite. Lysak and Nikolin[170] had also observed α' martensite formed through the ε phase and reported that the orientation of the α' satisfies the K–S relation, although the transformation occurs via the intermediate state, the ε phase.

The $\gamma \rightarrow \varepsilon \rightarrow \alpha'$ transformation can be induced by plastic deformation, like the $\gamma \rightarrow \alpha'$.[171] On heating, the α' formed by the $\varepsilon \rightarrow \alpha'$ transition does not revert to the ε phase but transforms to austenite.[165]

C. *ε martensite formed by cold working*

It is now well known† that in high manganese steels ε martensite is formed easily by cold working. This has been extensively studied.[174–181] During the $\gamma \rightarrow \varepsilon$ transformation, the $\gamma \rightarrow \alpha'$ transformation also occurs simultaneously.‡ Whether the $\gamma \rightarrow \varepsilon$ or $\gamma \rightarrow \alpha'$ transformation occurs faster or more abundantly is markedly affected by the carbon content[182,183] as well as the manganese content. Figure 2.38, from Imai and Saito,[178] shows the volume percentages of γ, α', and ε in 12% Mn steels with various carbon contents quenched from 1100°C. These amounts were estimated from dilatometer curves. (See Section 5.3 for the relation between the degree of working and the volume of transformation products.) Figure 2.38a shows the results for as-quenched specimens, Fig. 2.38b the results for specimens hammered from 70 to 72 mm in length. From these figures, it can be seen that cold working affects the amounts of α and ε.§

† In about 1942, Nishiyama and Arima[172] made an experiment on a Hadfield steel (12% Mn–1.2% C), which is austenitic in the as-quenched state. In those days it was believed that when such a steel is tempered at 550°C, martensite appears along with the precipitated carbides and the troostite. Since it seemed curious that martensite is formed by slow cooling after tempering, they examined this question. At that time, electropolishing was beginning to be applied to polish specimens for optical microscopy, so they used this method. On mechanically polished surfaces, x-ray patterns showed diffraction lines due to the existence of an h.c.p. structure but not on the electropolished surface. That is, it was found that martensite does not appear in the tempered steel and it was confirmed that the $\gamma \rightarrow \varepsilon$ transformation occurs due to the stress during mechanical polishing in the austenite matrix when the dissolved carbon is decreased by tempering. Thus mechanical polishing may not be suitable for specimens that are easily transformed by deformation. Later Imai and Saito[173] examined a 13.7% Mn–1.2% C steel tempered at 500°C for 10–100 hr to precipitate the carbides fully, and observed that the ε phase formed during cooling of a tempered, unpolished specimen.

‡ According to a report[179] of an investigation with the Bitter pattern (the pattern formed by sprinkling ferromagnetic fine powder over a specimen), the ferromagnetic powder adhered to the regions where slip bands crossed each other, and therefore α' might have formed at the crossings.

§ Discussing again the experiment on tempered Hadfield steel by the author and his coworkers described earlier, we note that if carbides are precipitated by tempering, and the carbon content of the austenite matrix is consequently lowered from 1.2% C to between 0.6% and 1.0% C, then the austenite matrix is subject to structural changes from mechanical polishing, which may be inferred from Fig. 2.38b, but not from electropolishing, which may be inferred from Fig. 2.38a.

D. *Lattice defects and surface relief of ε martensite*

Lysak and Nikolin[184] investigated the phase transformations in various steels containing 4–18% Mn and 0.2–1.4% C by means of x-ray diffraction. First, a γ single crystal that was transformed by quenching and dipping into liquid nitrogen was x-rayed by the rotating crystal method. The diffrac-

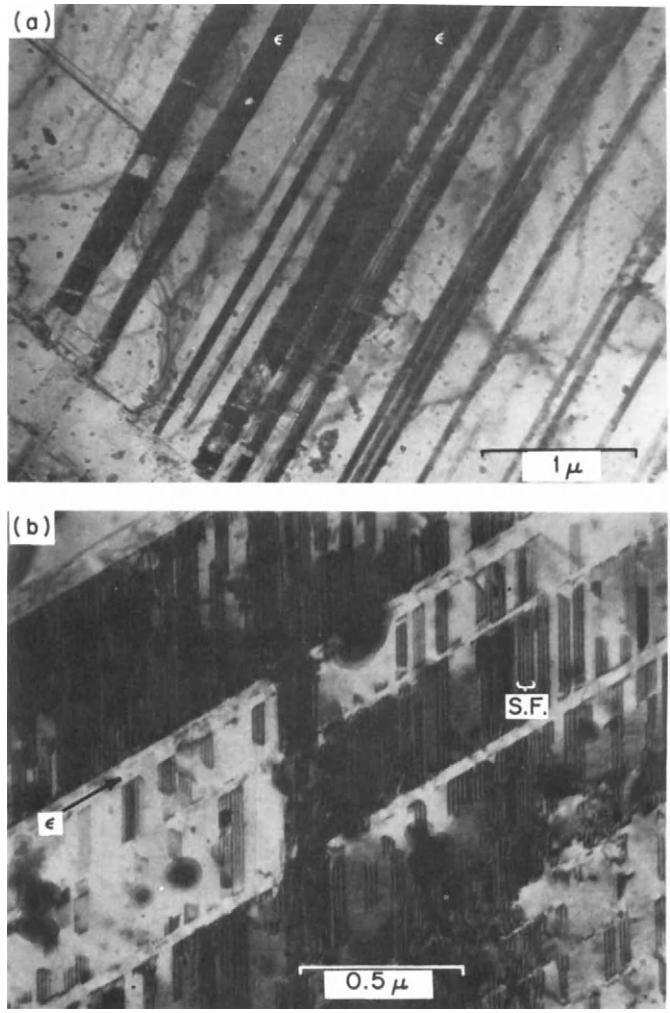

FIG. 2.39 Electron micrographs of a high manganese steel (9.75% Mn–0.97% C) quenched and hammered. (a) A region containing numerous ε plates (dark bands). (b) A region containing numerous stacking faults (parallel interference fringes are labeled "S.F."). (After Nishiyama and Shimizu.[186])

tion patterns showed that each of the h.c.p. spots satisfying the condition $h - k \neq 3n$ was accompanied by a streak parallel to the [0001] direction. This fact indicates the existence of stacking faults on the (0001) planes. The microhardness of the 14% Mn–0.4% C steel treated as above was as high as 420 kg/mm^2. The formation of the surface relief was also confirmed on the surface of the h.c.p. crystal by means of interference microscopy. This result indicates that the h.c.p. phase observed is the ε phase formed by the martensitic transformation.

Before these studies, Nishiyama *et al.* observed ε martensite in a manganese steel with an electron microscope, first by the replica method[185] and later by direct transmission.[186] The specimen used was a 9.75% Mn–0.97%C steel that was f.c.c. in the as-quenched state. The electron micrographs in Fig. 2.39 were obtained from a specimen quenched and deformed by hammering. In Fig. 2.39b, bands consisting of three or four interference fringes (labeled "S.F.") are due to stacking faults that were formed on the {111} planes of the austenite (two of four possible $\{111\}_\gamma$ planes in this figure). The large bands labeled "ε" are ε plates parallel to one of the $\{111\}_\gamma$ planes. Within the ε plates many striations can be seen. These are believed to be caused by stacking faults because streaks are observed accompanying the electron diffraction spots. In this respect manganese steels appear similar to cobalt alloys. In some regions bands appeared due to deformation twins of austenite.[187]

Suemune and Ōoka,[188] who studied several manganese steels by transmission electron microscopy, observed that the α′ appearing in 13.5% manganese steels contains many dislocations and the habit of the α′ is quite different from that of ε martensite, as shown in Fig. 2.40 (the α′ crystals

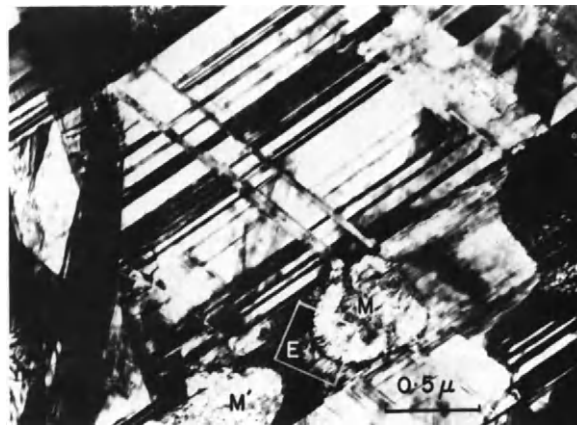

FIG. 2.40 Electron micrograph of a high manganese steel (13.5% Mn–0.02% C) quenched from 1100°C (30 min), showing α′ and ε martensities. (After Suemune and Ōoka.[188])

are labeled M and M'). These results are consistent with those shown in Fig. 2.37. Furthermore, it was observed that the formation of ε was induced by that of α' in some cases and a small amount of α' was occasionally formed by hammering even in steel containing manganese as high as 18.3%.

According to Bogachev *et al.*,[189] who also made similar observations in a manganese steel, the ε plates formed previously are obstacles to the formation of new ones. In rare cases the ε plates formed crossing the old ε plates. Furthermore, when a quenched 20% Mn steel was heated up to 70°C, the stacking faults in the retained austenite were increased. This temperature is nearly equal to the temperature at which the formation rate of ε is maximum. Considering these facts, Bogachev *et al.* stressed that the formation of stacking faults in the austenite is related closely to the formation of the ε phase. They also examined the effects of third elements, such as Cr, Ni[190], Mo, and W,[191] on these phase transformations.

2.3.3 h.c.p. (ε) and b.c.c. (α') martensites in Cr–Ni stainless steels

Although 18–8 stainless steel is usually austenitic, by some treatments martensites are formed. These affect the mechanical properties of the steel; therefore, numerous studies[192–197] of these martensites have been previously reported. In this alloy system, an h.c.p. martensite as well as a b.c.c. martensite is observed. The former martensite is usually denoted ε, as with high Mn steels.†

Schumann and von Fircks[198] prepared a number of alloys with various Cr and Ni contents and measured the M_s temperatures and the amounts of ε and α' martensite by dilatometry, magnetic analysis, and other methods, as in the study of Mn steels. Figure 2.41 shows the transformation starting temperatures of Cr:Ni = 5:3 alloys for a cooling rate of 5°C/min. It is seen from this figure that below Cr + Ni = 24% (15% Cr–9% Ni) only α' (designated by α_γ) is formed directly from the austenite, whereas above Cr + Ni = 24% α' (designated by α_ε) is always formed through ε.‡ The α_ε has a structure[165] similar to that in the Mn steels shown in Fig. 2.37. The volume ratio of α' (α_γ or α_ε) and ε that formed by cooling to -196°C is shown in Fig. 2.42.

Prior to the study of Schumann *et al.*, Imai *et al.*[200] found that in steels with approximately 17% Cr and 8% Ni, both $\gamma \rightarrow \varepsilon$ and $\gamma \rightarrow \alpha'$ transformations occur isothermally (Section 4.5) with separate C curves of the rate of trans-

† Some researchers[192] use the notation θ for h.c.p. martensite.

‡ There is a paper[199] reporting that an Fe–25% Cr–20% Ni alloy quenched from 1150°C is f.c.c. ($a = 3.59$ Å) and becomes f.c.t. ($a = 3.28$ Å, $c/a = 1.33$) by deformation at 77°K. But electron micrographs suggest that the latter may be ε. The discrepancy requires further research for its solution.

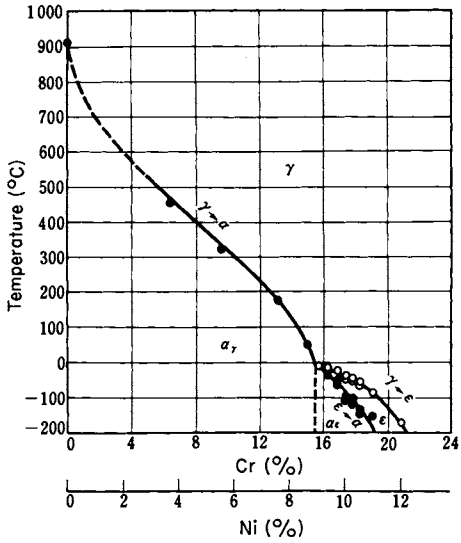

FIG. 2.41 Transformation temperatures of Fe–Cr–Ni alloys (Cr: Ni = 5:3). (After Schumann and von Fircks.[198])

formation versus temperature, the temperatures of the maximum rates being −100°C and −135°C, respectively. In this case, α' forms directly from γ. The $\gamma \rightarrow \varepsilon$ transformation in this steel occurs even by only cooling to low temperatures in the same way as in high Mn steels, and it is markedly promoted by deformation at low temperatures. The occurrence of this phenomenon is due to the low stacking fault energy.

Schumann[201] investigated the behavior of the ε phase in the quaternary Fe–Mn–Cr–Ni alloy system and found phenomena similar to those in Mn steels and Cr–Ni steels. In samples with component ranges of 0.58–16.84% Mn, 3.05–19.50% Cr, and 2.80–11.85% Ni, the $\gamma \rightarrow \alpha$ transformation always occurred through ε and not directly from γ.

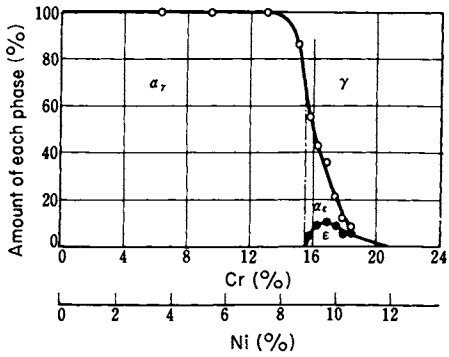

FIG. 2.42 Amounts of transformed products in Fe–Cr–Ni alloys (Cr:Ni = 5:3) water quenched from 1050°C and cooled to −196°C. (After Schumann and von Fircks.[198])

TABLE 2.1 Appearance of α' and ε martensites due to cold working in 304-type stainless steel[a]

Specimen	Cooling process[b]	Deformation conditions: Temperature	Deformation conditions: Elongation (%)	Martensite
A	Furnace cooling	Room	3	None
B	Furnace cooling	Room	7	ε
C	Furnace cooling	−195°C	0	None
D	Furnace cooling	−195°C	3.6	ε
E	Furnace cooling	−195°C	7	$\varepsilon + \alpha'$
F	Quenching	−195°C	0	$\varepsilon + \alpha'$

[a] After Nishiyama *et al.*[202]
[b] After heating for 30 min at 1000°C.

Nishiyama *et al.*[202] also studied a 304-type stainless steel.† In the experiment, six kinds of samples were made with varying heat treatment and tensile deformation, as shown in Table 2.1, and were investigated by electron microscopy. First, the structures of specimens furnace-cooled after heating for 30 min at 1000°C were examined. In specimen A, deformed by 3% at room temperature, dislocations and stacking faults (exhibiting interference fringes) were seen, as shown in Fig. 2.43a,‡ and in specimen B, deformed by 7% at room temperature, the stacking faults increased in number, appearing as dark bands that may have finally become ε plates (Fig. 2.43b). With increase of the elongation up to 30%, those defects increased but α' was not yet observed. In specimens C, D, and E, deformed at −195°C, ε plates were abundantly evident after elongation of 3.6% (Fig. 2.44a) and α' grains were formed between the ε plates by elongation of 7% (Fig. 2.44b).

Specimen F, quenched to room temperature, will be discussed next. When this specimen was cooled to −195°C, ε and α' martensites appeared even without deformation. This is remarkably different from the furnace-cooled specimen C. The optical micrograph shown in Fig. 2.45a exhibits martensites here and there. It seems that they were formed not by cooling but by the internal stress induced by quenching. In Fig. 2.45b, an electron micrograph, the region between ε bands A and B is crowded with α' crystals of the lath form in which many dislocations can be seen. In Fig. 2.45c the α' plates

† 18.1% Cr, 9.7% Ni, 0.06% C, 0.5% Si, 1.03% Mn, 0.04% P, 0.23% Mo.

‡ There is some suspicion that all of the transformation products might have been produced during electropolishing of the specimen film. It is, therefore, necessary to confirm these facts with the ultrahigh-voltage electron microscope using thicker specimens.

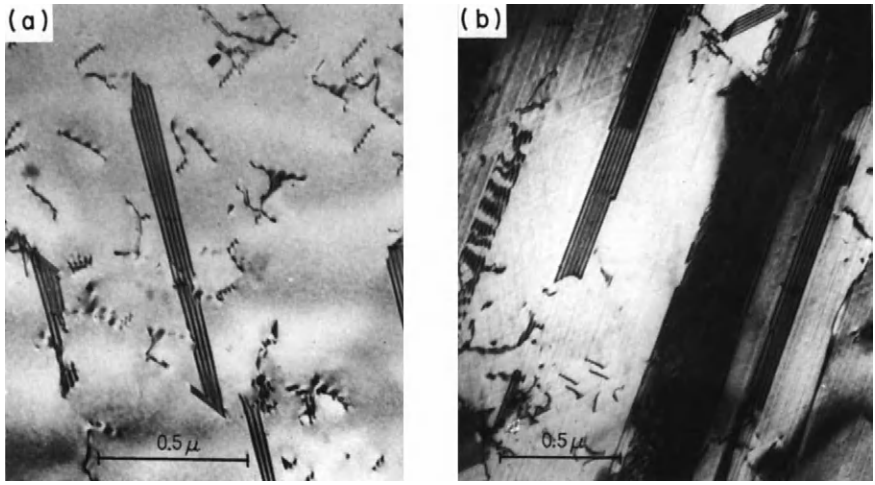

FIG. 2.43 Electron micrographs of a 304-type stainless steel furnace cooled and cold worked at room temperature. (a) Extended 3% (stacking faults and dislocations are formed). (b) Extended 7% (ε plates are formed). (After Nishiyama *et al.*[202])

appear granular, probably due to the approximately parallel orientation to the specimen film. Figure 2.45d is the same portion of the film tilted about the arrow in part (c) to make dislocation images in the α′ crystals clear. Since the α′ crystals in these photographs are seen between two ε

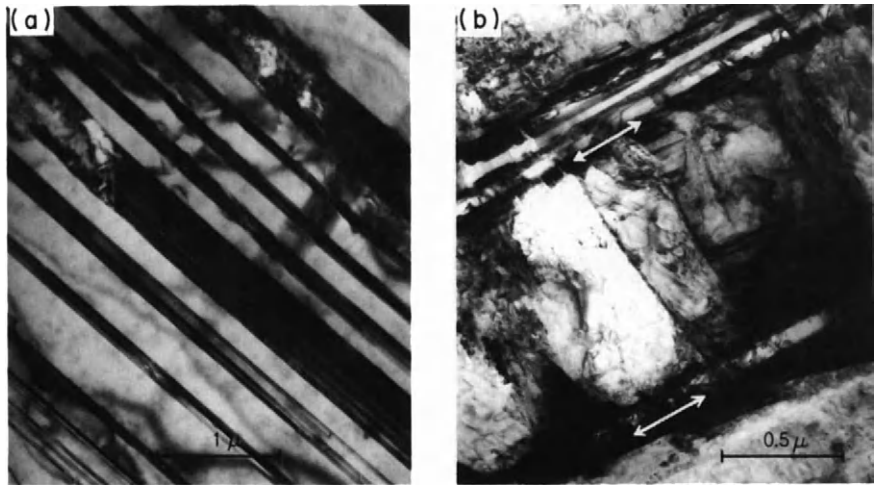

FIG. 2.44 Electron micrographs of a 304–type stainless steel furnace cooled and cold worked at −195°C. (a) Extended 3.6% (ε plates are formed). (b) Extended 7% (α′ phases are formed between the ε plates). (After Nishiyama *et al.*[202])

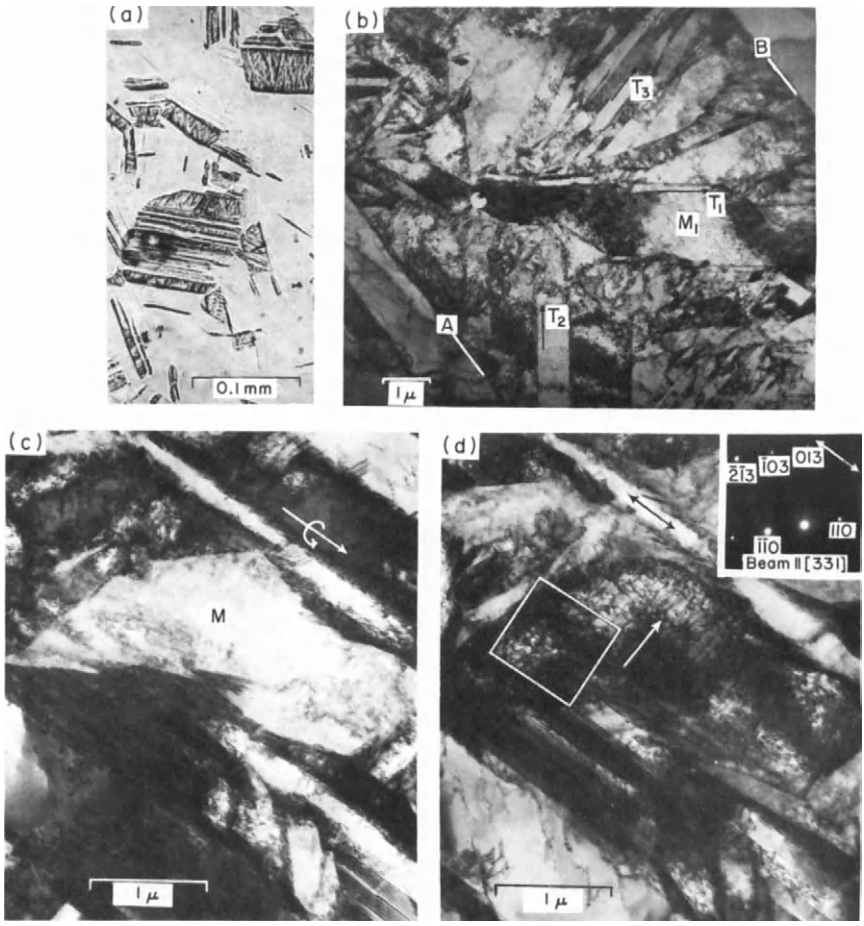

FIG. 2.45 Optical (a) and electron (b–d) micrographs of a 304-type stainless steel water quenched and cooled to $-195°C$. (a) Formation of martensite. (b) α' crystals of the plate form. (c) α' crystals of the massive form. (d) Dislocations in martensite crystals are revealed by tilting the specimen from (c). (After Nishiyama *et al.*[202])

plates, it appears that the ε plates were formed first and that the α' crystals were then formed between them. On whether the ε plates form first or not there are three opinions, as follows.

A. *Transformations occur in the sequence γ to ε to α'*

Cina[203] estimated the amounts of the transformation products in an 18–8 stainless steel from data obtained by x-ray diffraction and magnetic measurement; he found that ε was first formed by deformation at room

temperature, and then with increasing deformation the amount of ε decreased while α′ formed. From this result, he thought that some of the α′ crystals were formed from ε, though others were formed directly from γ. Lagneborg[204] and Mangonon and Thomas[205] supported this opinion.

B. *ε plates are formed first and α′ crystals nucleate at the interface between ε plate and γ matrix and grow into the latter*

Venables[206] examined, by means of electron microscopy, the phase changes during deformation of an 18–8 stainless steel. He observed the formation of α′ at the intersection of two ε plates parallel to $\{111\}_\gamma$ planes crossing each other (see Fig. 3.19a). At an early stage of formation, α′ is a needle crystal parallel to the $\langle 110\rangle_\gamma$ direction, which is the direction of the intersection of the ε bands, and later it grows to a plate with the $\{225\}_\gamma$ habit plane in the γ matrix. Breedis and Robertson[207] agreed initially with the first A opinion, but later [208†] they preferred the second B opinion, because the morphology of α′ was affected by lattice defects and other features in the γ matrix. Kelly [169] reached a similar opinion from electron microscope observations of the habit planes of martensites in a 17% Cr–9% Ni steel and a 12% Mn–10% Cr–4% Ni steel.

C. *α′ is formed first and ε is formed subsequently by internal stress due to the α′ formation*

Dash and Otte,[209,210] using mainly 18% Cr–12% Ni stainless steels cooled to −196°C, observed the martensites shown in Fig. 2.46. They considered that the regions between two α′ crystals transform to ε plates as a result of the stress arising from the formation of the two α′ crystals. Supporting evidence for this consideration is as follows. Since the ε plates between the two α′ crystals contain many planar defects, the α′ should also show traces of planar defects if α′ crystals were formed at the both sides of ε plates subsequently to the ε formation. This is not the case in the photograph.[‡] Goldman *et al.*[211] also agreed with this opinion.

Further research is needed to determine which of these three opinions is correct, but at present it may be concluded that the formation mechanisms of martensite in this alloy system vary with the conditions: composition, treatments, and so forth.

† The morphology of α′ is lathlike in a steel whose composition ratio is approximately Ni:Cr = 18:8 and it changes to platelike with increase of this ratio.

‡ This fact may not be strong evidence of the initial formation of α′ martensite, because it may be that during the transformation lattice defects existing in the ε plates were removed and new lattice defects were introduced into the α′ crystals.

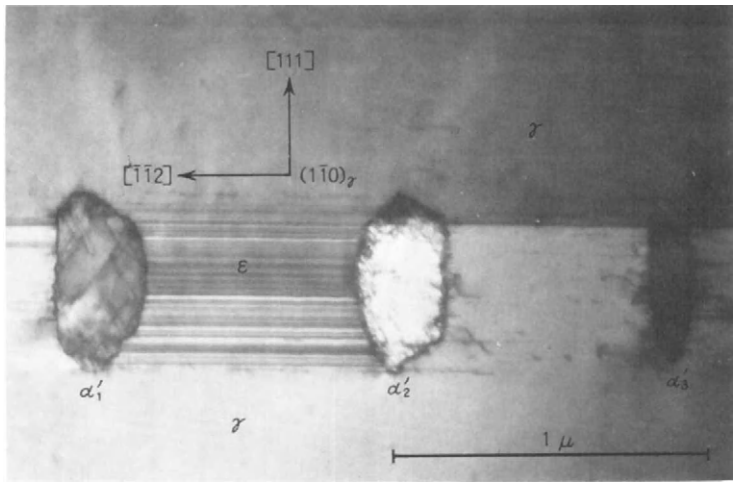

FIG. 2.46 Epsilon martensite produced between two α′ crystals by transformation stress in an Fe–18% Cr–12% Ni alloy cooled to −196°C. (After Dash and Otte.[209,210])

2.3.4 h.c.p. martensite (ε) in other alloy systems

Besides the alloys previously described, there are other alloys with both h.c.p. and b.c.c. phases produced by transformations similar to those in Fe–Mn alloys. For example, Fe–Ir alloys have such product phases;[212] the transformation temperatures are shown in Fig. 2.47.[213,214] Since both product phases in this alloy exhibit surface relief, they must be martensitic. As for their crystallographic properties, such as lattice defects, according to Miyagi and Wayman,[213] α′ in alloys with less than 30% Ir is similar to α′ in Fe–Ni alloys, α′ and ε occurring in alloys of from 30% to 43% Ir are similar to α′ and ε in Cr–Ni stainless steels, and in alloys of from 43% to 53% Ir only ε appears, as in Co alloys. Since Fe–Ru alloys[215] also have transformation-temperature curves resulting in h.c.p. and b.c.c. product phases similar to those for Fe–Ir alloys, both phases may be martensitic and their lattice defects may be similar to those in Fe–Ir alloys.

The h.c.p. phase may also be produced in a quite different fashion. For instance, the supersaturated α solid solution (f.c.c.) in Cu–Si alloys can be transformed partly to an h.c.p. phase with many stacking faults by plastic deformation.[216,217] Such faults are characteristic of martensite. Nevertheless, it might be thought (incorrectly) that this product is merely a precipitate, since in the Cu–Si equilibrium phase diagram the h.c.p. (κ) phase exists at equilibrium in higher silicon alloys, though at high temperatures. But precipitation cannot occur only by plastic deformation at room temperature, and therefore the foregoing product is considered to have formed as a

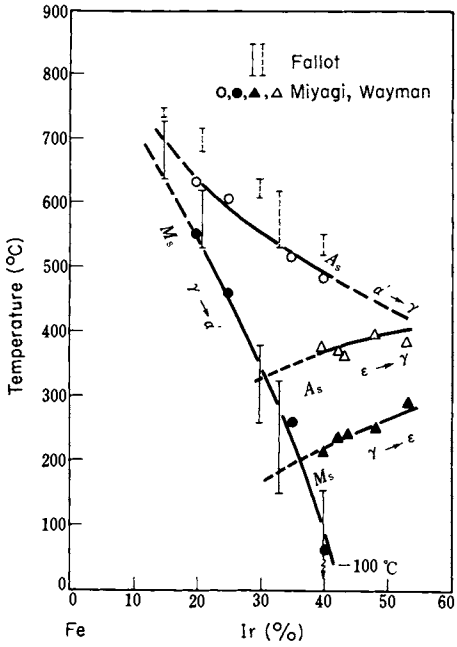

FIG. 2.47 Transformation temperatures of Fe–Ir alloys. (After Fallot[214] and Miyagi and Wayman.[213])

metastable phase without diffusion, that is, by a martensitic transformation. Phenomena resembling the above sometimes appear when supersaturated solid solutions are tempered.[217,218] The product in this case should be considered a precipitate, because the diffusivity is sufficiently high.

2.4 b.c.c. to h.c.p. (mainly titanium alloys and zirconium alloys)

Examples of metals undergoing b.c.c.-to-h.c.p. transformations are Li, Ti, Zr, and Hf. When these metals are quenched from temperatures at which the (b.c.c.) β phase is stable, they transform to an h.c.p. α phase. Although the α has the same crystal structure as that formed by slow cooling, it also has the characteristics of martensite. If these metals are alloyed, their ability to be quenched is enhanced, and martensitic products are more easily formed.

2.4.1 Orientation relationships and transformation mechanism

The lattice orientation relationship for the b.c.c.-to-h.c.p. transformation was first studied in Zr by x-ray diffraction[219] and the following result was obtained:

$$(110)_{bcc} \| (0001)_{hcp}, \qquad [\bar{1}11]_{bcc} \| [11\bar{2}0]_{hcp},$$

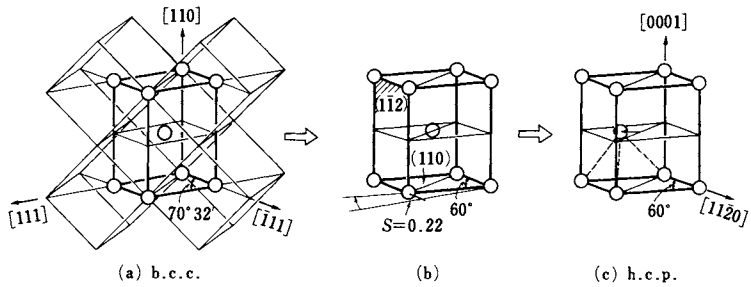

FIG. 2.48 Burgers' mechanism for the b.c.c.-to-h.c.p. transformation.

which is called the Burgers relationship, after its discoverer. This relation may be considered to have arisen by the following two processes, as shown in Fig. 2.48. The first, (a) to (b), proceeds by shearing in the $[\bar{1}11]_{bcc}$ direction along the $(1\bar{1}2)_{bcc}$ plane, and the second, (b) to (c), proceeds by shuffling of every other atomic plane of $(110)_{bcc}$. Therefore, it is significant that the foregoing relation is rewritten as follows:

$$(1\bar{1}2)_{bcc}\|(1\bar{1}00)_{hcp}, \qquad [\bar{1}11]_{bcc}\|[11\bar{2}0]_{hcp}.$$

In zirconium, the lattice parameters are $a_{bcc} = 3.61$ Å, $a_{hcp} = 3.245$ Å, and $c_{hcp} = 5.165$ Å. Hence, the transformation expands the lattice by 1.2% in the c direction and contracts the lattice by 1.2% in the plane perpendicular to the c direction.

2.4.2 Substructure of martensite in titanium of commercial purity

Figure 2.49[220] is an optical micrograph of h.c.p. martensite (α) in commercially pure titanium formed by water quenching from the β phase at high temperatures, revealing wedge-shaped crystals. Their habit plane is $(133)_\beta$. Within the wedge-shaped crystals many dislocations can be observed by electron microscopy. Sometimes several bands can be seen in the martensite plates, as shown in Fig. 2.50. These bands are $\{10\bar{1}1\}$ twins. Usually twins with this index are formed abundantly by deformation above 400°C, whereas only a few are formed at room temperature.[221] Therefore the $\{10\bar{1}1\}$ twins observed here are considered to have been formed during transformation† or by transformation stress after transformation at high temperatures. The thickness of these twins is much larger than that of internal twins in steels and the dislocations are seen not only in the matrix but also inside twin bands.

† A theory[222] interpreting the formation of $\{10\bar{1}1\}$ twins by transformation has been published and theoretical calculations[223] of the energy of various stacking faults in close-packed hexagonal structures have been made.

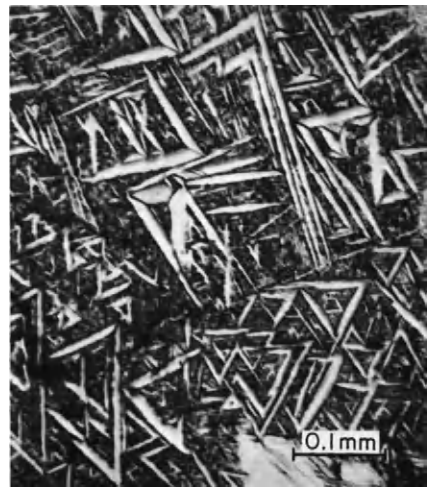

FIG. 2.49 Optical micrograph of commercially pure titanium, water quenched, showing wedge-shaped martensite crystals. (After Nishiyama *et al.*[220])

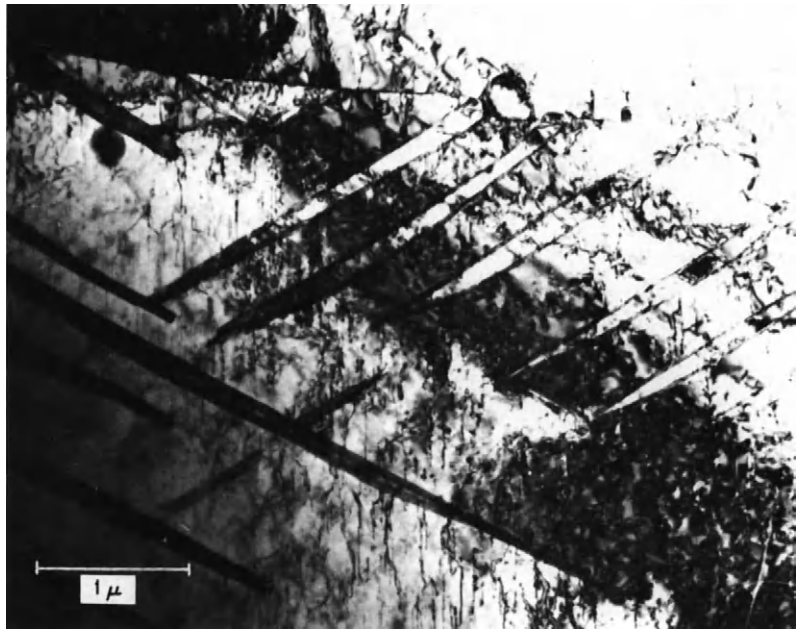

FIG. 2.50 Electron micrograph of a martensite crystal in titanium. (Bands running obliquely are internal twins parallel to $(10\bar{1}1)$; irregularly curved short lines are dislocations.) (After Nishiyama *et al.*[220])

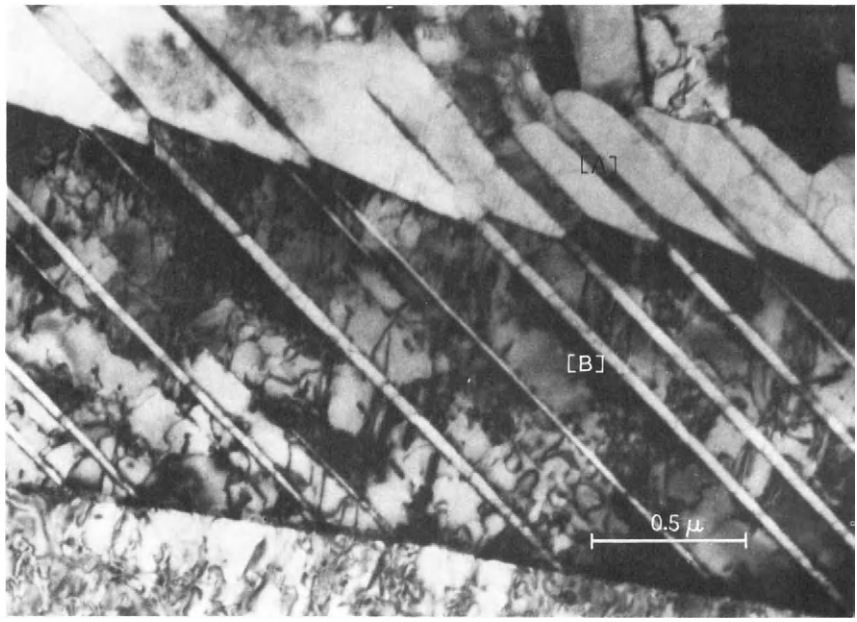

FIG. 2.51 Electron micrograph of a Ti martensite crystal consisting of twin layers. (After Nishiyama *et al.*[220])

The repeated twins as shown in Fig. 2.51[220] are rarely found. In this photograph, a number of threefold nodes of twin boundaries (coherent and incoherent) are recognized between crystal groups [A] and [B]. At these nodes, however, the angles among the adjoining boundaries are not those given by thermal equilibrium, as in the recrystallized states. The same crystal habit was also observed in a Ti–5% Mn alloy.[224] Stacking faults are frequently observed in Ti martensite. Figure 2.52 is an example in which stacking faults with six interference fringes at intervals of about 0.2 μm are observed.

It has been reported that on deformation three kinds of slip planes, $\{10\bar{1}0\}$, $\{10\bar{1}1\}$, and (0001), are observed; however, slip on the (0001) plane is not considered to occur easily due to the large value of the critical resolved shear stress. Nevertheless, most of the dislocations and stacking faults in the photographs shown previously lie on the (0001) plane. Therefore, all these defects are thought to have occurred during the transformation.

In short, in commercially pure titanium the wedge-shaped crystals formed by quenching have the same h.c.p. structure as that obtained by slow cooling. But they involve many dislocations and stacking faults. Therefore, they can be said to be martensite crystals. In material of high purity the so-called

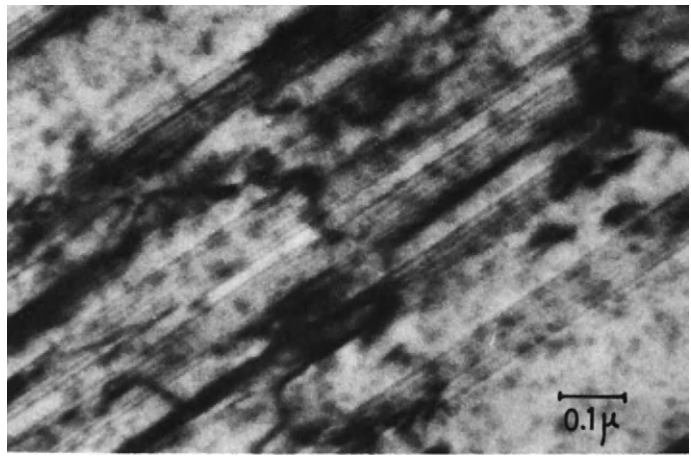

FIG. 2.52 Electron micrograph of the interior of a Ti martensite crystal, showing parallel interference fringes (running obliquely) due to stacking faults along (0001) planes. (After Nishiyama *et al.*[220])

lath martensite is obtained; it consists of a bundle of platelike crystals, all having a common direction and no internal twins.[225]

2.4.3 Substructure of martensite in titanium alloys

When titanium dissolves other elements, its M_s temperature is lowered, as will be described in Section 4.3, and the α' martensites can easily be obtained and observed without a self-tempering effect. Ti–Cu alloys are examples. Fujishiro and Gegel[226] examined the α' phase in Ti–0.5% Cu and Ti–1% Cu alloys and Williams *et al.*[227] examined the α phase in Ti–(4–8)% Cu alloys by means of electron microscopy. Here we describe mainly the results of the latter investigation, which have been reported in detail. There are two kinds of morphologies of α' in this alloy system: one is lath-type,† which occurs in alloys below 4% Cu, and the other is platelike, occurring between 6% and 8% Cu. The former consists of bundles of parallel laths (layers of platelike crystals) similar to the lath martensites in low carbon steels and Fe–Ni alloys. The lath plane is approximately parallel to the $\{10\bar{1}1\}_\alpha$ plane, the orientation difference being only 1–1.5° between lath layer crystals, and the lath boundary consists of an array of dislocations with $\boldsymbol{b} = \frac{1}{3}\langle 2\bar{1}\bar{1}3\rangle_\alpha$. Inside the lath, there are dislocations with $\boldsymbol{b} = \frac{1}{3}\langle 11\bar{2}0\rangle_\alpha$, internal twins of $\{1012\}_\alpha$ type,‡ and stacking faults with fault vector $\frac{1}{3}\langle 10\bar{1}0\rangle_\alpha$. The fine

† The workers used the terminology "massive martensite."

‡ A very small amount of internal twins of this type was found in the martensite of Ti–Cr alloys.[225]

structures in the platelike crystals are almost the same as those in commercially pure Ti and their internal twins are of the $\{10\bar{1}1\}_\alpha$ type.

Zangvil *et al.*[228] subsequently performed a similar experiment using Ti–(1–5)% Cu alloys. The orientation relationship between β and α' was found to be that of Burgers with the habit plane of α' within 4° from $(10\,\bar{7}\,9)_\beta$ or $(10\,\bar{9}\,7)_\beta$. These characteristics of α' are in agreement with the phenomenological theory of Bowles and Mackenzie. The internal twin plane was confirmed to originate from the original $\{110\}_\beta$ plane.

There has been considerably more research on other titanium-base alloys, but most of the results are similar to those just described. Therefore, only a short note will be added here about Ti–Fe alloys, which are slightly different in character from the others. The iron lowers the M_s temperature of the alloy most effectively and increases the hardness of the martensite. Figure 2.53[229] is an optical micrograph of a Ti–3% Fe alloy quenched from 1050°C into water at room temperature. In this figure a large β grain is seen, divided into a large number of α' crystals by the $\beta \rightarrow \alpha$ transformation, and a fine structure can be seen in each α' crystal. The x-ray diffraction pattern of the martensite phase displays only one diffuse Debye–Scherrer ring because of the fineness of the grains and the presence of many lattice defects. Electron microscopy reveals that the martensite has fine grains about 1 μm long and 0.2 μm wide, as shown in Fig. 2.54. By electron diffraction, they were identified to be h.c.p. α' crystals. A little β phase is found to remain. Face-centered cubic martensite, which is described in the next subsection, was also found in some regions.

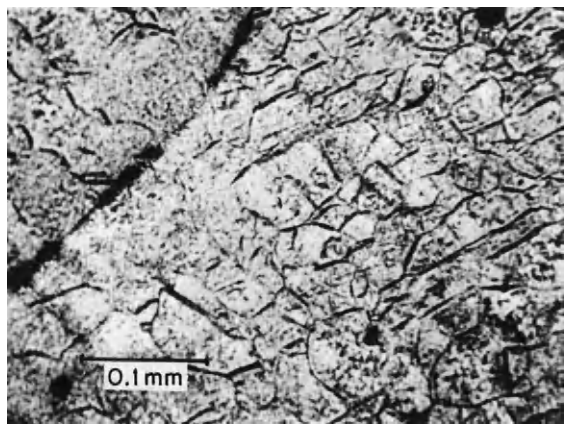

FIG. 2.53 Optical micrograph of martensite in a Ti–3% Fe alloy showing fine α' grains. (The broad line running obliquely at the upper left is a β grain boundary produced at a high temperature.) (After Nishiyama *et al.*[229])

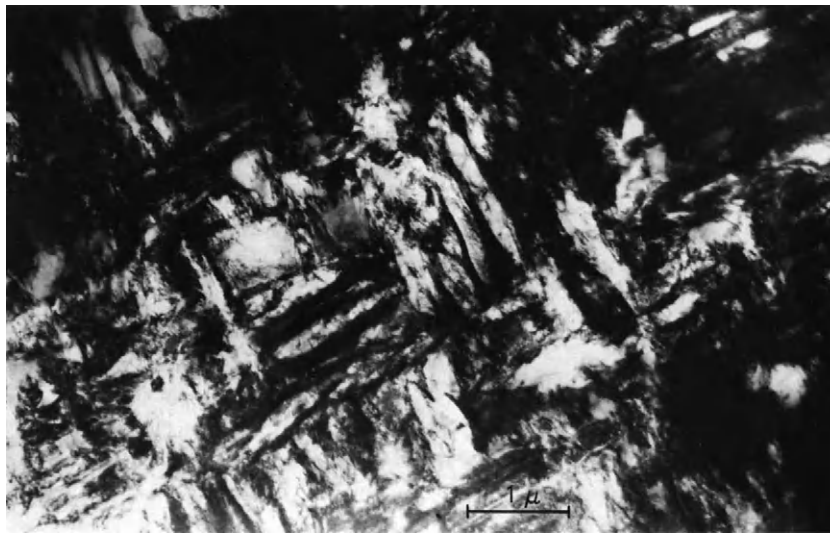

FIG. 2.54 Electron micrograph of a quenched Ti–3% Fe alloy, showing martensite crystals 1 μm long and 0.2 μm wide. (After Nishiyama *et al.*[229])

2.4.4 f.c.c. martensite in titanium alloys

Although martensite with an f.c.c. structure might be unexpected, it has actually been found in Ti–V,[230,231] Ti–Al,[232] Ti–Cr,[233] and Ti–8% Al–1% Mo–2% V[234] alloys, in addition to Ti–Fe alloy. Such martensite has {111} twins within which there are planar faults along the {110} plane.

It has been reported that the f.c.c. martensite in Ti–10% Mo, Ti–15% Mo, and Ti–5% Mn alloys is formed only in thin films.[224] The lattice parameter of the f.c.c. martensite in a Ti–5% Mn alloy is $a = 4.5$ Å, which is considerably larger than 4.13 Å expected from the size of the atomic diameter of titanium. Thus it may be imagined[224] that hydrogen atoms have intruded, assuming interstitial positions in the f.c.c. lattice, but this has not been confirmed.†

The orientation relationship[233] between f.c.c. martensite and the β matrix was determined, using thin films of Ti–Cr alloys, to be as follows: $(110)_\beta \| (111)_{fcc}$; $[111]_\beta$ deviates from $[110]_{fcc}$ by 0–6° toward the $[011]_{fcc}$ direction.

This is almost the same as in ferrous alloys except for the large scatter. Discussion of the martensite in the TiNi compound will be deferred to the next section.

† Hydrides of Ti, Zr, and Hf undergo martensitic transformation with a resulting fine structure.[235]

2.4.5 Martensite in zirconium alloys

Since Zr is similar in nature to Ti, Zr alloys are similar in crystallographic behavior to Ti alloys. For example, in Zr–Nb alloys, the habit plane of the martensite is close to the {334} plane,[236] as in Ti alloys. Below 0.8% Nb the martensite is massive and the only lattice defects are dislocations, but above 0.8% Nb the martensite is platelike and has $\{1\bar{0}11\}$ internal twins.[236–238] The thickness ratio of the matrix and adjoining twin is approximately 3:1.[236] The number of twins increases with increasing Nb content. Therefore, the more the transformation temperature is lowered, the more easily internal twins are formed, as observed in Fe–Ni alloys. The situation in Zr–Nb is actually more complicated. In some cases large martensite crystals, which from their morphology seemed to have formed first, contain internal twins, whereas small ones in the same specimen formed subsequently at lower temperatures do not contain internal twins. From this fact it is thought that a fast cooling rate promotes the formation of internal twins.[236]

2.5 Close-packed layer structures of martensites produced from β phase in noble-metal-base alloys

Most β phases of noble-metal alloys with a 3:2 electron-to-atom ratio are b.c.c. This fact was first pointed out by Hume-Rothery, and the so-called electron compounds are often called Hume-Rothery phases.† Copper-, silver-,‡ or gold-based alloys belong to this category. The β phase has a fairly wide range of solid solution at high temperatures, but the stability of the β phase decreases with decreasing temperature, narrowing the range of solid solution. The β phase then usually decomposes below several hundred degrees Celsius. If cooled rapidly to suppress the diffusion of atoms, however, the β phase transforms to a martensite without decomposition.

The crystal structures of the transformation products are close-packed layer structures, such as f.c.c. and h.c.p. It may be assumed from the Burgers relations mentioned in Section 2.4.1 that the close-packed layer is transformed from a $\{110\}_{bcc}$ plane, that is, the transformation shear plane. For the shear direction there are two possibilities, $\pm[1\bar{1}0]$, on each plane. If

† According to the electron theory of metal, the b.c.c. structure is considered to be stable in these alloys because, near a 3:2 electron-to-atom ratio, the Fermi surface is almost in contact with the first Brillouin zone of the b.c.c. structure; hence the energy of the conduction electrons is lowered.[239]

‡ Silver-based alloys have not been so extensively studied as Cu-based alloys, but one study[240] reported that when Ag–Ge alloys with 5–22 at.% Ge were splat-cooled from the melt, an h.c.p. phase containing stacking faults appeared. It is not clear, however, whether this transformation is martensitic or massive.

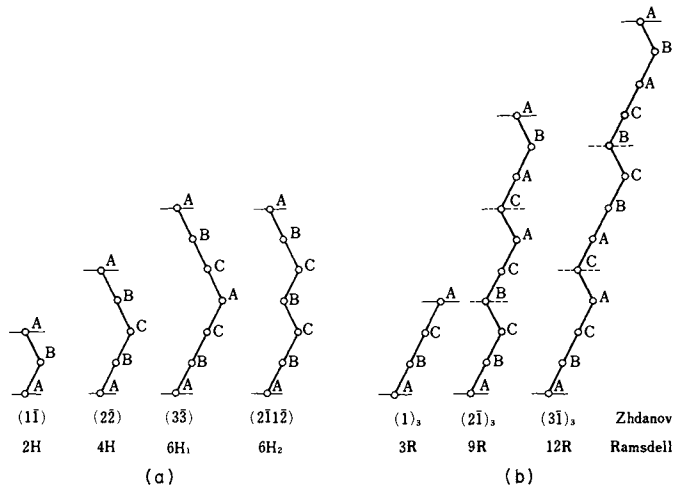

FIG. 2.55 Various kinds of close-packed layer structures.

shear takes place in the same direction on every plane parallel to (110), the resulting structure is f.c.c. If alternate shear on every other plane takes place, the resulting structure is h.c.p. If plus and minus shears occur randomly, it can be said that stacking faults are introduced in either the f.c.c. or h.c.p. structure. If plus and minus shears occur periodically, this is referred to as "shuffling." When the resulting structures are energetically favorable, their existence is possible. Various examples are shown in Fig. 2.55 and Table 2.2. The first column in Table 2.2 shows the Ramsdell notation,[241] in which

TABLE 2.2 Notations for various close-packed layer structures

Notation			Examples of martensites produced from		
Ramsdell	Zhdanov	Stacking mode[a]	DO_3	B2	b.c.c.
2H	(1$\bar{1}$)	AB$^-$	Cu–Al γ_1' Cu–Sn γ_1'	Au–Cd γ_1'	Ag–Cd
4H	(2$\bar{2}$)	AB$^-$A$^-$C	Cu–Sn β_1'	TiNi (low temp.)	—
6H$_1$	(3$\bar{3}$)	ABCA$^-$C$^-$B$^-$	—	—	—
6H$_2$	(2$\bar{1}$1$\bar{2}$)	ABC$^-$BC$^-$B$^-$	—	—	—
3R	(1)$_3$	ABC	—	Au–Cd α_1'	Ag–Zn
9R	(2$\bar{1}$)$_3$	ABC$^-$BCA$^-$CAB$^-$	Cu–Al β_1'	Cu–Zn β_1' Au–Cd β_1'	—
12R	(3$\bar{1}$)$_3$	ABCA$^-$CABC$^-$BCAB$^-$		TiNi (room temp.)	—

[a] The superscript minus sign denotes negative shifting (shuffling) between atomic layers.

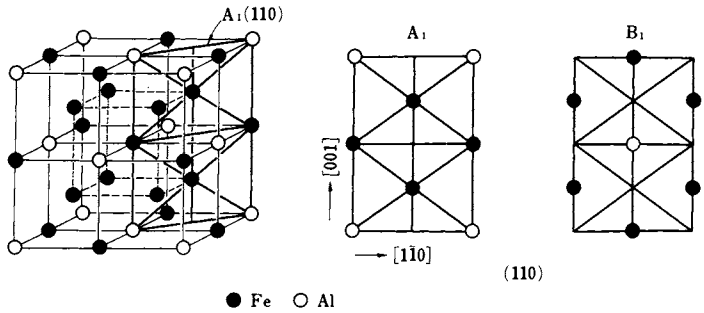

FIG. 2.56 Crystal structure of Fe_3Al-type superlattice (β_1), regarded as an alternate stacking of atomic planes A_1 and B_1.

the Arabic numeral indicates the number of layers in one period and the letter (H or R) following it stands for hexagonal or rhombohedral symmetry. The subscript numerals indicate different kinds of stacking order with the same symmetry and the same period. According to this notation, in the case of rhombohedral symmetry the number preceding R represents the total period of the stacking and within that period there are subperiods† whose intervals are $\frac{1}{3}$ of the total period. The notation in the second column is that of Zhdanov;[243–244] it represents stacking order rather than symmetry. For example, 12R is expressed as $(3\bar{1})_3$ in the Zhdanov notation, in which the first number in the parentheses shows the number of layers undergoing uniform positive shear and the second number (with the overbar) shows the number of layers undergoing negative shear following the positive shear. The subscript outside the parentheses indicates the number of repeat cycles that give one total period.

In many cases these close-packed structures have superlattices. The superlattices are considered to be formed because the product phases in the martensitic transformation inherit the atomic ordering of the parent phases. Most β phases in noble-metal-based alloys have the Fe_3Al-type (DO_3) superlattice or CsCl-type (B2) superlattice. All of these superlattices are denoted by β_1 in this book.‡ The subscript 1 means that the β phase has a superlattice. In the Fe_3Al-type structure two kinds of atomic planes, A_1 and B_1, parallel to $(110)_{bcc}$ are alternately stacked, as shown in Fig. 2.56. It is then considered that the martensite structures resulting from shears on these $(110)_{bcc}$ planes consist of six kinds of close-packed layers that are

† H. Sato[242] used the notation 1R, 3R, and 4R instead of 3R, 9R, and 12R, by taking into account these subperiods.

‡ In some papers the Fe_3Al-type superlattice is denoted by β_1 and the CsCl-type superlattice is denoted by β_2.[245]

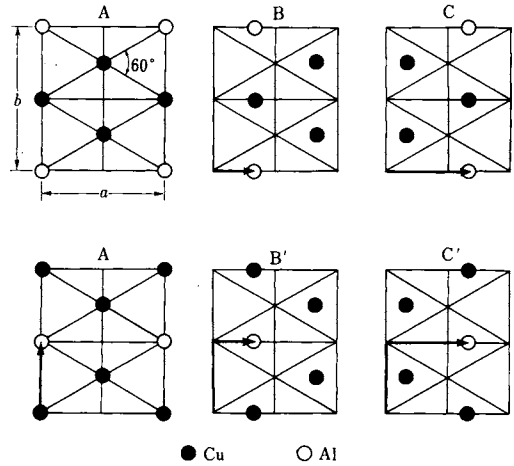

FIG. 2.57 Six kinds of atomic layers in close-packed structures of martensite transformed from the Fe_3Al-type superlattice (β_1). (The arrows indicate the displacement vector of each layer referred to layer A.)

shifted relative to each other in the directions parallel to the close-packed plane. For example, the 2H structure has the AB′ stacking order, where the prime represents a change in the superlattice structure and the A′, B′, and C′ planes are produced by shifting the A, B, and C planes, respectively, by $b/2$ along the b axis in Fig. 2.57. In the case of the 9R structure, such as in samarium, three layers constitute one subperiod, but if atomic ordering is involved, six layers constitute one subperiod. If these subperiods are taken as the unit cell, the symmetry of the resulting structures is monoclinic. If the nine layers $ABC^-BCA^-CAB^-$ are taken as the unit cell,† the symmetry is then orthorhombic. The a and b axes in the orthorhombic coordinate system are shown in Fig. 2.57 and the c axis is perpendicular to the close-packed plane. (See Fig. 2.55.)

In the case of CsCl-type structures two kinds of atomic planes, A_2 and B_2, are stacked alternately, as shown in Fig. 2.58. The kinds of layers in close-packed structures resulting from transformation of the CsCl-type structure are expected to be those shown in Fig. 2.59. Examples of close-packed structures with such layers are also shown in Table 2.2.

One reason for the existence of the layer structures listed in Table 2.2 was explained by H. Sato *et al.*,[242,246] in terms of the electron theory of metals. They thought that the explanation for the existence of long-period

† The superscript minus is used in this book to denote negative shuffling between atomic layers only for helping intuitive understanding.

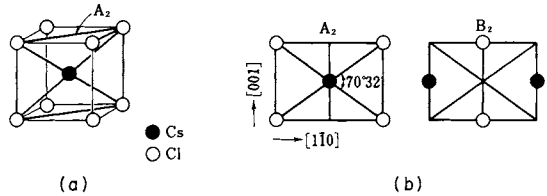

FIG. 2.58 Crystal structure of the CsCl-type superlattice (β_1). (This structure can be regarded as an alternate stacking of atomic layers A_2 and B_2.) (a) Unit cell. (b) Two kinds of (110) atomic layers.

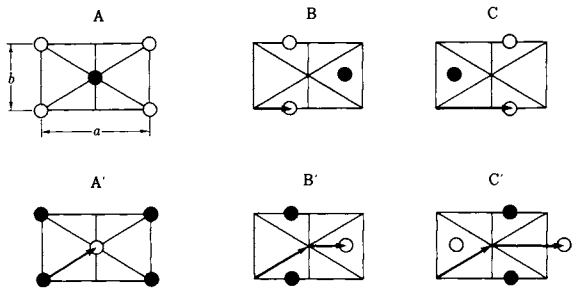

FIG. 2.59 Six kinds of atomic layers in close-packed structures of martensite produced from the CsCl-type superlattice (β_1). (The arrows indicate the displacement vector of each layer referred to layer A.)

superlattice structures applied to the present case as follows. If stacking faults are introduced periodically into a crystal, the crystal has a long-period stacking order, resulting in a new Brillouin zone boundary produced near the origin of the reciprocal lattice. If the electron-to-atom ratio happens to be such that the Fermi surface is almost in contact with the newly created zone boundary, then the energy of the conduction electron is lowered. If such a reduction in the energy of the conduction electrons is greater than the increase in strain energy accompanying the introduction of stacking faults at regular intervals, long-period stacking structures with shuffling will be stable.

Since the energy differences among the various kinds of long-period stacking structures are small, there are a number of factors other than the alloying content for deciding which long-period stacking structure can exist. The conditions for the formation of martensite are among these factors. For example, in Cu–Al alloys (whose phase diagram is shown in Fig. 2.60), martensite in bulk specimens has the 9R structure, but in thin foils the 2H structure appears in addition.[247] In some alloys a mixture of two kinds of long-period stacking structures is formed. For example, in the Au–Cd system the 2H and 9R structures are found in lamellar form.[246]

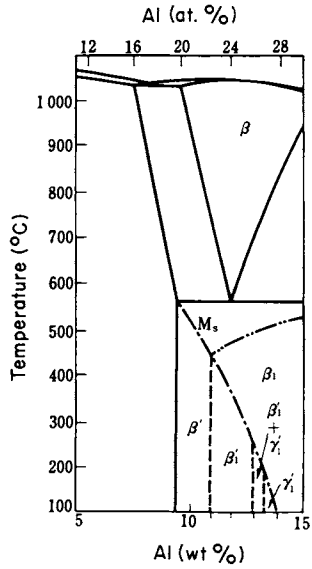

FIG. 2.60 Phase diagram of the Cu–Al system.

The structure factor for a long-period stacking structure can conveniently be expressed as

$$F = V_O \cdot V_L$$

where V_O is the structure factor for one layer (a–b plane in orthorhombic coordinates) and V_L is the structure factor associated with stacking order along the c axis. Therefore, electron diffraction patterns with a zone axis parallel to the c axis have hexagonal symmetry as far as the fundamental spots are concerned. The positions of diffraction spots of these patterns are determined only by V_O, although their intensities are also affected by the stacking order along the c axis, that is, by V_L. Superlattice spots are formed in accordance with the atomic ordering in the a–b plane. In diffraction patterns containing the $\boldsymbol{c}^*$ axis, a diffraction spot in the $\boldsymbol{c}^*$ direction for the f.c.c. structure is split with equal intervals by V_L into a number of spots that are equal to the number of layers in one subperiod. For example, the spot is split into two spots for the 2H structure and into three spots for the 9R structures. The intensity distributions of such patterns for H-type structures are symmetrical with respect to the $\boldsymbol{a}^*$–$\boldsymbol{b}^*$ plane, but for R-type structures the intensity distributions are asymmetrical.

The crystal structures of the various martensites formed by rapid quenching of the β phases of noble metal alloys were not clarified until the selected-area diffraction technique of electron microscopy was applied to the structure analyses; in the past, therefore, these martensites were often

said to have complicated orthorhombic structures. Recently, however, it was found that these structures are the close-packed layer structures mentioned in this section.

2.5.1 β', β_1', and γ_1' martensites in Cu–Al alloys and γ_1' martensite in Cu–Al–Ni alloys

The high-temperature β phase (b.c.c.) in Cu–Al alloys undergoes eutectoid transformation at 570°C (Fig. 2.60), but upon quenching it transforms martensitically.[248–251] The martensite phases formed upon quenching are denoted β' for less than 11% Al (22.5 at.%), β_1' for 11–13% Al, and γ_1' for more than 13% Al.† With more than 11% Al the β phase becomes ordered before the martensitic transformation takes place.

A. *β_1' martensite*

β_1' has an ordered 9R structure.‡ The determination of the crystal structure of β_1' was first made possible by electron microscopy.[252] The unit cell of this structure in orthorhombic coordinates consists of 18 layers, as shown in Fig. 2.61. The stacking of the layers in one period is

$$AB'C^-B'CA'^-CA'B^-A'BC'^-BC'A^-C'AB'.$$

Therefore, taking account of the atomic ordering, this ordered 9R structure should be labeled 18R in the Ramsdell notation.

In the case of ideal atomic ordering with 25 at.% Al, the crystal structure factor of β_1' is

$$\begin{aligned} F = &\left[f_{Al} + f_{Cu}\left\{\exp\left(2\pi i\frac{k}{2}\right) + \exp\left[2\pi i\left(\frac{h}{2}+\frac{k}{4}\right)\right] + \exp\left[2\pi i\left(\frac{h}{2}-\frac{k}{4}\right)\right]\right\}\right] \\ &\times\left\{1 + \exp\left[2\pi i\left(\frac{h}{3}+\frac{k}{2}+\frac{l}{18}\right)\right] + \exp\left[2\pi i\left(\frac{2h}{3}+\frac{2l}{18}\right)\right]\right\} \\ &\times\left\{1 + \exp\left[2\pi i\left(\frac{h}{3}+\frac{k}{2}+\frac{3l}{18}\right)\right] + \exp\left[2\pi i\left(\frac{2h}{3}+\frac{6l}{18}\right)\right]\right\} \\ &\times\left\{1 + \exp\left[2\pi i\left(\frac{k}{2}+\frac{9l}{18}\right)\right]\right\} \end{aligned}$$

† The subscript 1 in β_1', γ_1' means that the parent phases are ordered. Swann and Warlimont[245] denote a parent phase with the CsCl-type superlattice by β_2 and the martensite transformed from β_2 by β_2'. Throughout this book, however, the subscript 1 is used regardless of the type of superlattice.

‡ The lattice constants of β_1' are $a_0 = 4.49$ Å, $b_0 = 5.19$ Å, and $c_0 = 38.2$ Å ($a_0:b_0:c_0 = \sqrt{3}:2:18\sqrt{2/3}$). In monoclinic coordinates the unit cell has six layers and the lattice constants are $a_m = a_0$, $b_m = b_0$, $c_m = (c_0/3)\,\mathrm{cosec}\,\beta = 13.1$ Å, $\beta = 103°16'$.

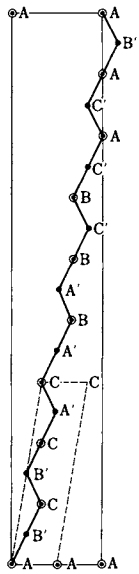

FIG. 2.61 Ordered 9R structure transformed from β_1 superlattice. (Solid-line rectangle is the orthorhombic unit cell; broken-line parallelogram is the monoclinic unit cell.)

where f_{Al} and f_{Cu} are the atomic scattering factors of Al and Cu, respectively, and h, k, l are the Miller indices in orthorhombic coordinates. The reciprocal lattice determined with this equation is shown in Fig. 2.62. The filled circles in the figure show the fundamental spots and open circles show the superlattice spots. All the spots in the reciprocal lattice are aligned in the directions of the $\boldsymbol{a}_m^*$ and $\boldsymbol{c}_m^*$ axes, which are the monoclinic coordinate axes with the six-layer unit cell. This means that the atomic arrangement can also be expressed by monoclinic coordinates. One of the characteristic features of this reciprocal lattice is that for $h \neq 3n$ three spots aligned in the $\boldsymbol{c}^*$ direction constitute one period of intensity distribution along the $\boldsymbol{c}^*$ direction. This is due to the fact that three layers constitute one subperiod of stacking order in the crystal. If there are no stacking faults in the crystal, these three spots are spaced with equal intervals and their intensity ratios are $S:M:W = 231:65:28$.

Figure 2.63 shows an electron diffraction pattern of martensite in Cu–23.7 at.% Al obtained by water quenching from 950°C. This diffraction pattern corresponds to the pattern for $k = 4n$ shown in Fig. 2.62. The diffraction spots seen along the $[001]_o$ direction† in Fig. 2.63 indicate that there is a three-layer period in the stacking order.‡ The streaks running

† Subscript "o" indicates that the Miller indices are expressed by orthorhombic coordinates.

‡ Spots for $h = 3n$ seen in Fig. 2.63 include those which are due to multiple reflections. They apparently have intensity distributions similar to those for $h = 3n \pm 1$.

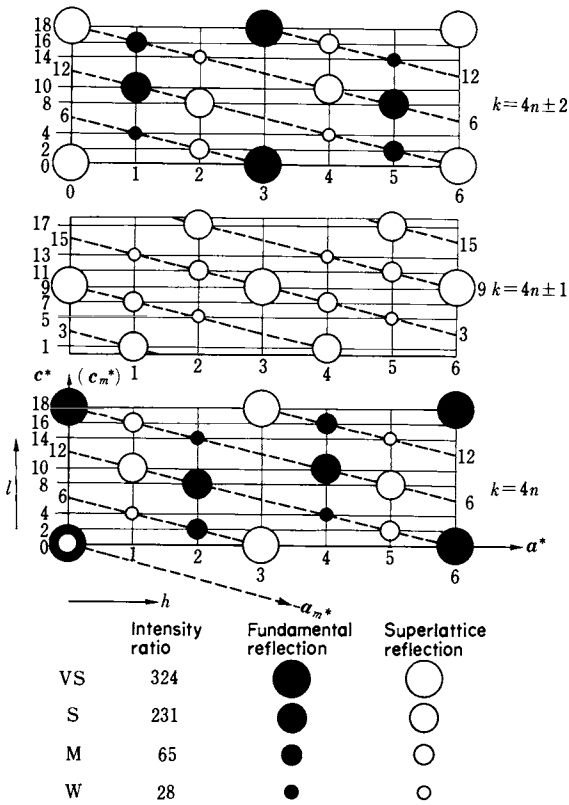

FIG. 2.62 Reciprocal lattice of ordered 9R structure of β_1' martensite of Cu–25 at. % Al. (After Nishiyama and Kajiwara.[252])

through these spots are due to stacking faults on the $(001)_0$ plane. Details on the probabilities for the occurrence of these stacking faults will be given later.

The electron diffraction patterns clearly show the existence of a superlattice in this martensite. This fact is also shown by dark-field image electron micrographs, which reveal antiphase domains (Fig. 2.64). The boundaries of the domains extend across the martensite plates, as seen in Fig. 2.64, indicating that the superlattice in the martensite is inherited from the parent phase.

It is considered that the β_1' structure is produced from the β_1 structure by shear accompanied by shuffling of the atomic planes. The streaks in the [001] direction in electron diffraction patterns, however, indicate that there are a number of errors in the shuffling. Figure 2.65 shows a typical transmission electron micrograph of β_1' martensite: Several martensite plates

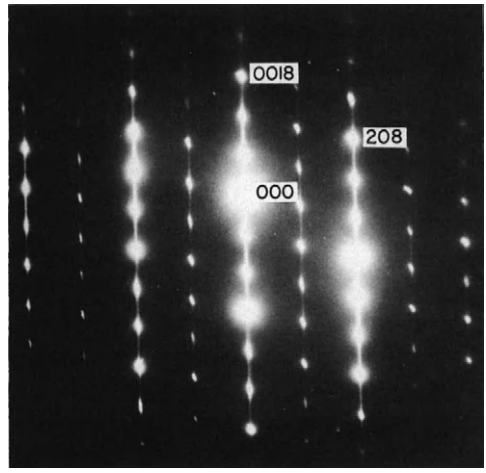

FIG. 2.63 Electron diffraction pattern (9R $[010]_0$) of β_1' martensite in Cu–23.7 at.% Al alloy. Three spots aligned in the [001] (vertical) direction constitute one period. (After Nishiyama and Kajiwara.[252])

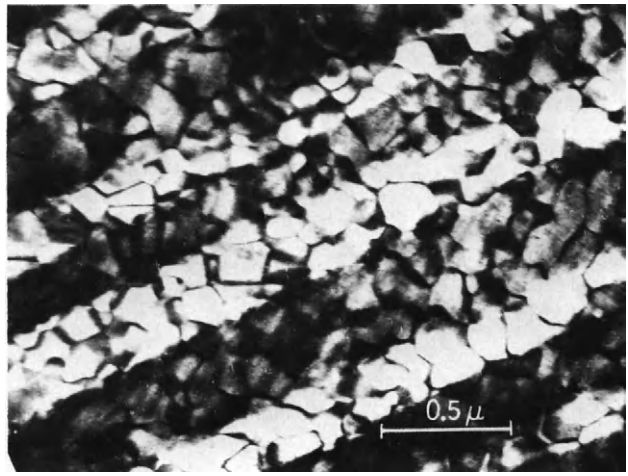

FIG. 2.64 Dark-field image formed by a superlattice reflection of β_1' martensite in Cu–24.6 at.% Al. The boundaries of granular antiphase domains extend across the interfaces of the martensite plates. (After Swann and Warlimont.[245])

are seen in the layer structure and striations tending in the same direction are observed in every other plate. Figure 2.66 shows the details of the striations. The directions of these striations in the photographs coincide with surface traces of the (001) plane and the direction of the streaks seen in the

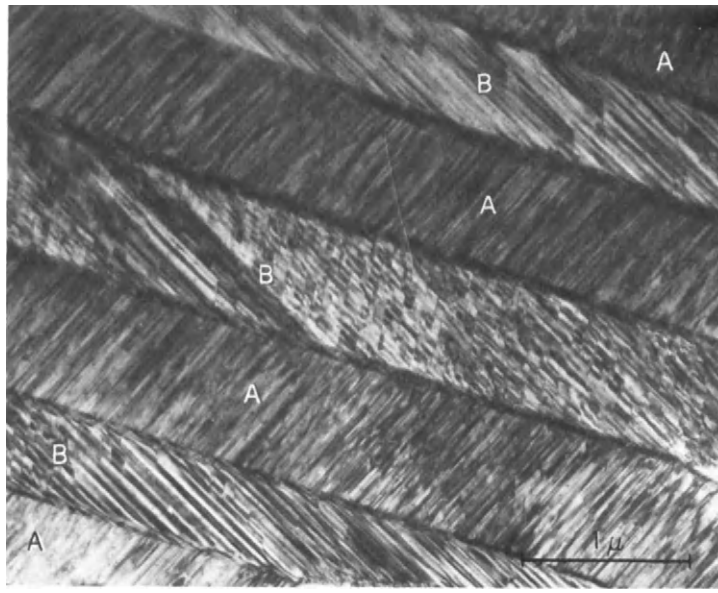

FIG. 2.65 Electron micrograph of β_1' martensite in Cu–23.7 at. % Al water quenched from 950°C; alternate bands are two kinds of variants; striations in each band are stacking faults. (After Nishiyama and Kajiwara.[252])

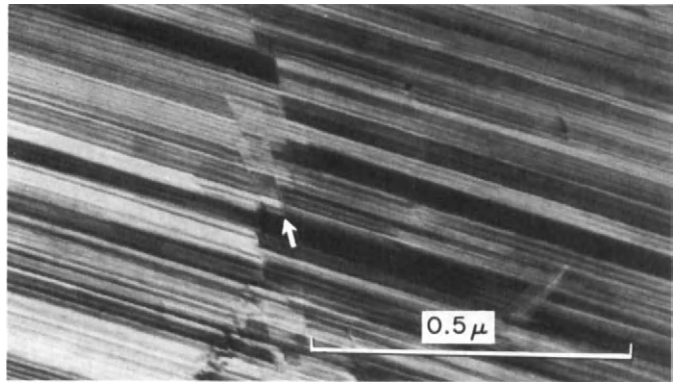

FIG. 2.66 Stacking faults and partial dislocations in β_1' martensite in Cu–23.7 at. % Al. (Interference fringes due to a stacking fault exhibit four or five striations; the arrow indicates partial dislocations.) (After Nishiyama and Kajiwara.[252])

electron diffraction pattern is perpendicular to the (001) plane. Therefore, the striations are due to stacking faults on the (001) plane.

The crystal structure of β_1' martensite was determined to be the 9R structure, for every third layer is shuffled. However, since this martensite

FIG. 2.67 Electron micrograph revealing the lattice image of three atomic layer periods in 9R β_1' in Cu–23.5 at. % Al. Disturbance of the fringe spacing shows random stacking faults. (After Toth and Sato.[255])

contains many stacking faults, its crystal structure might be thought to have a periodicity different from that mentioned above.† This possibility was ruled out by Toth and Sato.[255] Figure 2.67 is a high-resolution electron micrograph showing lattice images with 6.5 Å spacing. This observed lattice periodicity corresponds to the spacing between neighboring shufflings, namely, the three-layer interval of the (001) plane (6.37 Å). Some irregularities are seen from place to place in these lattice images; these are due to stacking faults. This photograph shows clearly that the β_1' martensite of Cu–Al alloys has the 9R structure. It is not clear whether the observed stacking faults have resulted from errors in the shuffling or from lattice-invariant shear in the transformation. However, a study of Cu–Sn martensite described in the next section suggests that the latter is the case.

When high pressure is applied during the transformation, a slightly different structure appears for β_1'. When Cu–Al alloys with 24.3–27.0 at. % Al were cooled under a pressure of 30 kbar, a mixture of 9R and 2H structures appeared in layer form with 100 Å thickness.[256‡] The phase with these mixed structures was named β_1''.

The orientation relationships between β_1' and β_1 in the case of cooling have not yet been determined, but those in the case of heating have been made clear.[260] A specimen of β_1' martensite formed by quenching from a high temperature was thinned by electrolytic polishing for transmission electron

† For example, a 22-layer unit cell with a different stacking order was assumed for β_1' in some reports.[245,253] However, this analysis was later found to be incorrect.[254]

‡ Structures similar to this were reported to form in Cu–Zn–Ca,[257] Cu–Zn–Al,[258] and Cu–Zn–Si[259] alloys on cooling as well as by deformation.

FIG. 2.68 Electron micrograph revealing reverted β_1 crystals produced in β_1' martensite of Cu–24.1 at.% Al by heating at 450°C in an electron microscope. (After Kajiwara and Nishiyama.[260])

microscopy observation. These thin foils were heated in an electron microscope by using a heating stage to cause them to revert to β_1. Figure 2.68 shows a transmission electron micrograph of coexisting β_1' martensite and β_1 phase produced by heating to 450°C. The striated region in this photograph is β_1' martensite and the bright parallel plates are the β_1 phase. These plates grew lengthwise and then sidewise during observation.†

An electron diffraction pattern of this region showed a pattern of the Fe_3Al-type structure as well as that of β_1'. The Fe_3Al-type pattern is due to the β_1 phase. The orientation relations between β_1 and β_1' were found to be

$$(110)_{\beta_1} \| (12\bar{8})_{\beta_1'}, \qquad [1\bar{1}1]_{\beta_1} \| [2\bar{1}0]_{\beta_1'}.$$

The β_1' phase is considered to be metastable because it can be easily transformed into other phases by deformation[261] (Chapter 3, Section 3.2.4C). In some cases, β_1' is mixed with γ_1' in a lamellar form.[262]

B. *γ_1' martensite*

The phase γ_1' has an h.c.p. structure.[263–265] If the atomic ordering is taken into account, its structure should be regarded as orthorhombic.‡

† Before the β_1 phase appeared, the whole area of Fig. 2.68 was β_1' martensite. This region corresponds to a martensite plate like those shown in Fig. 2.65. The width of the martensite plate was very large.

‡ The lattice constants of the γ_1' phase are $a_0 = 4.51$ Å, $b_0 = 5.20$ Å, and $c_0 = 4.22$ Å.[244,266]

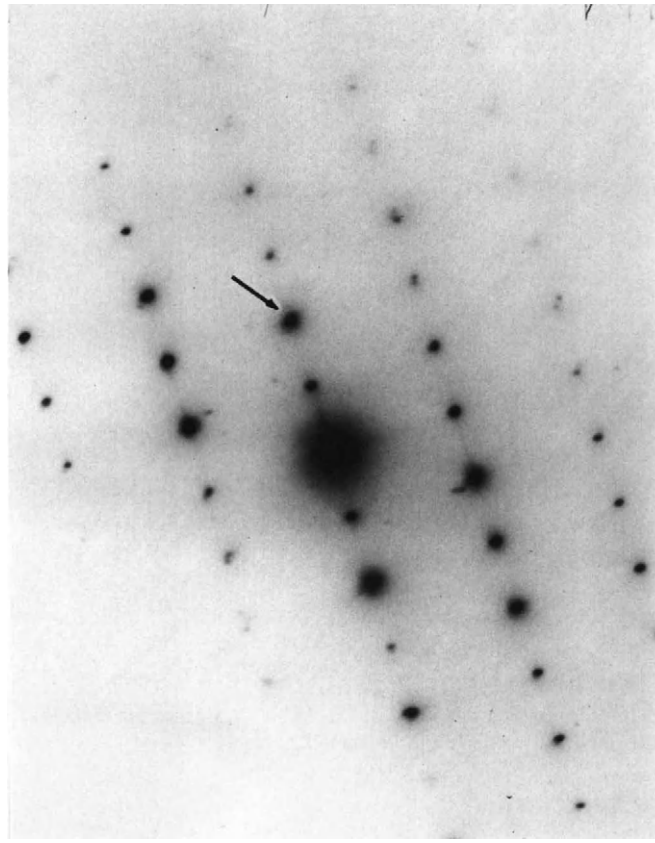

FIG. 2.69 Electron diffraction pattern of γ_1' martensite (in Cu–27 at.% Al) showing 2H structure. The zone axis is $[210]_o$. The spot shown by an arrow corresponds to the spacing of stacking layers. (After Sato *et al.*[265])

Figure 2.69 shows that this structure is the AB′ stacking layer structure (2H). The appearance of γ_1' martensite in the optical microscope is hardly distinguishable from that of β_1', but their electron microscopic substructures are quite different; transformation twins are seen in γ_1' (Fig. 2.70). The twinning plane of the transformation twins is $\{201\}$ or $\{121\}$ in orthorhombic coordinates and $\{1\bar{1}01\}$ in hexagonal coordinates.[244] Fine striations are seen in these twins. These are due to a high-order twinning. The γ_1' also has a superlattice, which was confirmed not only by electron diffraction, but also by the microscopic observation of antiphase boundaries. The atomic ordering in γ_1' is inherited from the parent β_1, as in the case of β_1'.

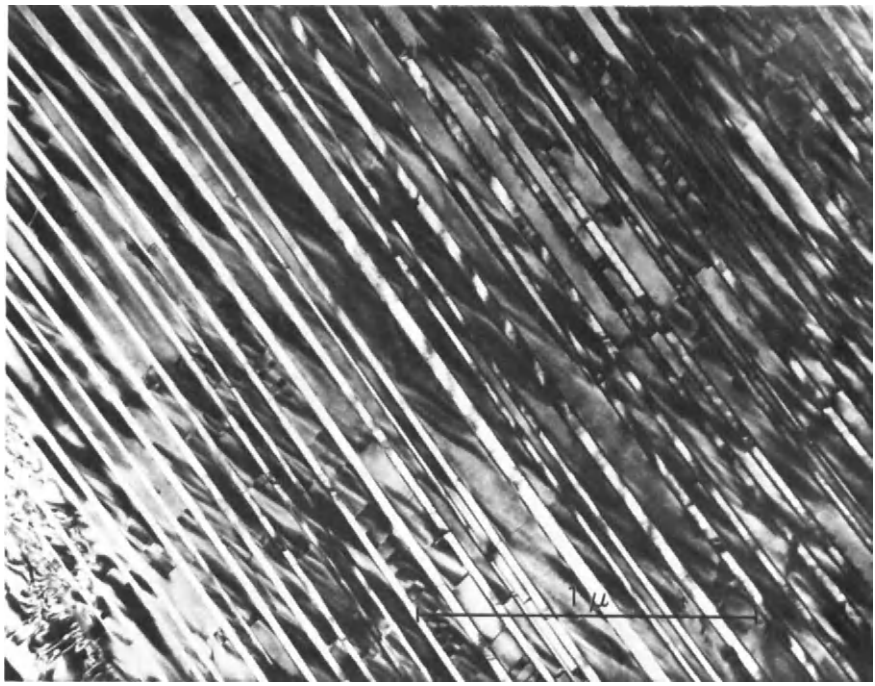

FIG. 2.70 Electron micrograph of γ_1' in Cu–27.9 at.% Al (showing the fine cross striations within $(10\bar{1}1)$ twins). (After Swann and Warlimont.[245])

C. *β′ martensite*

In a Cu–Al alloy with less than 11% Al, β' martensite is formed, which also has a 9R structure containing stacking faults parallel to (001), but no superlattice spots have been observed. The phase diagram in Fig. 2.60 shows that an extrapolated order–disorder transition curve is situated below the M_s temperature curve. This suggests a possibility that a martensite crystal formed below the extrapolated order–disorder transition curve may be ordered, although a martensite crystal formed above that curve will be disordered. Figure 2.71, an electron micrograph taken from a Cu–10% Al specimen that was quenched from 1100°C in water kept at 100°C, may support this possibility. Striations owing to stacking faults are also seen in this figure. There is a more transparent region in the center of a large martensite plate. The region is thinner than the other part and must have been preferentially polished during thinning of the specimen. The thinner part may be associated with a more disordered region of the martensite plate, that is, the central portion of the plate may be disordered but the surrounding region may be in a short-range ordered state. If this assumption is correct,

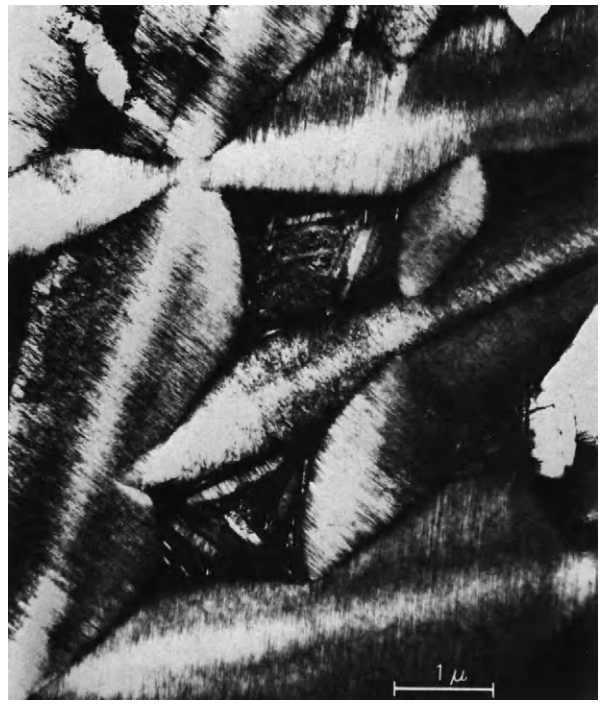

FIG. 2.71 Electron micrograph of β' martensite in Cu–20.7 at.% Al quenched from 1000°C to 100°C. The central region of each β' crystal is transparent due to the preferential etching of the specimen foil. (After Swann and Warlimont.[245])

it is considered that a thin martensite plate formed first and it widened after the adjacent β_1 region had become short-range ordered because of the slow quenching rate there. This may support a parallel assumption that in steel a midrib of martensite is produced first in the formation of a martensite plate.

D. *γ_1' in Cu–Al–Ni alloys*

Thermoelastic martensite has been observed in some Cu–Al–Ni alloys.[267] In this kind of martensite, the transformation proceeds in balance between a driving force of chemical free energy and a force owing to an elastic energy and is reversible in a thermal cycle. Details of the kinetics of this transformation will be described later (Section 5.2.6). The morphology and substructures of this type of martensite are quite interesting.†

† Martensitic transformation in Au–20.7% Cu–30.9% Zn is also thermoelastic. The parent phase in this case is of the Heusler type.[267]

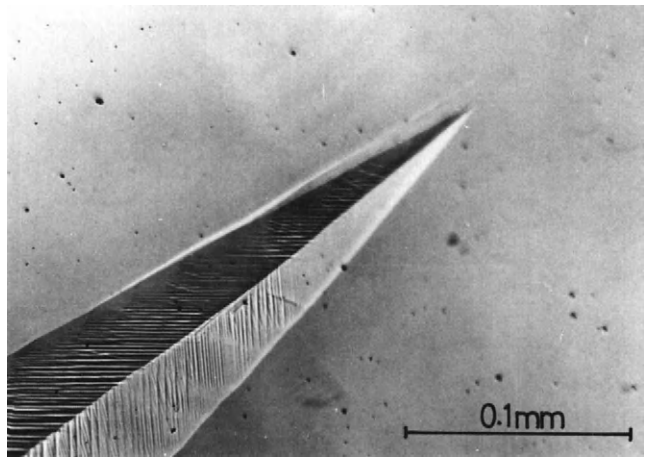

FIG. 2.72 Optical micrograph showing a spearlike γ_1' crystal in a Cu–14.2% Al–4.3% Ni alloy. Both sides of the ridge are {121} twinned with each other; the striations are twins of other kinds of {121} (rarely {101}). (After Otsuka and Shimizu.[268])

Otsuka and Shimizu[268,269] reported that a large γ_1' martensite plate formed when a Cu–14.2% Al–4.3% Ni alloy was quenched from 1000°C in water kept at 100°C.† This martensite looks like the tip of a sharp spear, as in Fig. 2.72. There are striations symmetrical with respect to the central plane of the plate, which looks like a ridge.‡ The central plane is parallel to $(121)_{\gamma 1'}$, that is, $(10\bar{1}1)_{\text{hex}}$ and each side separated by this plane is in a twin relationship with the other. The orientation relationships between martensite and parent phase are the same for these two martensite crystals. They are in accordance with the Burgers relationships

$$(110)_{\beta_1} \| (121)_{\gamma_1'}, \qquad [11\bar{1}]_{\beta_1} \| [2\bar{1}0]_{\gamma_1'}.$$

The two martensite crystals separated by the central plane are variants having a twin relationship with each other. Therefore, the central boundary is not a midrib. The boundaries between martensite and parent phase in Fig. 2.72 are {331}§ and they are considered to be habit planes because they are very straight.

† If this alloy is deformed after quenching to room temperature, thin plates of β_1' martensite are produced.[270]

‡ Martensitic transformation does not occur for Cu–14% Al or Cu–14.5% Al merely by quenching from 1000°C in water. However, an isothermal martensitic transformation takes place at room temperature. The morphology of the isothermal martensite is similar to that shown in Fig. 2.72 and looks like a sharp spear. The martensite plates sometimes cross each other during growth.[271] In some cases a growing martensite plate pierces a martensite plate already formed.[272] A spearlike morphology is also seen in Cu–12.8% Al–7.7% Ni.[273]

§ In an earlier work,[274] the habit plane was reported to be oriented by 2 from $\{221\}_{\beta_1}$ for Cu–14.5% Al–(0.5–3.0)% Ni.

Narrow bands seen in both crystals separated by the central boundary are internal twins for which the twinning plane is $\{121\}$.† This twinning plane belongs to the same $\{121\}$ plane family as that of the twinning plane forming the central boundary. It can be explained that these substructures in the martensite were produced as a result of relaxation of transformation strains; that is, the variants in twin relationship with respect to the central boundary plane greatly reduce the transformation strain, and the internal twins correspond to the lattice-invariant strain in the phenomenological theory. A further study by electron microscopy showed that there are fine striations in the internal twins. Since streaks perpendicular to $(001)_{\gamma_1'}$ were observed in the electron diffraction patterns, these are due to stacking faults on the $(001)_{\gamma_1'}$. It is considered that these stacking faults were produced to relax remaining transformation stresses, which had not been relaxed completely by the internal twinning on account of an unfavorable orientation. This is an example of double lattice-invariant shears. The shape memory effect in Cu–Al–Ni alloys will be described in Section 5.2.6.

2.5.2 β_1' and γ_1' martensites in Cu–Sn alloys

Although the martensites in Cu–Sn alloys‡ have been studied since the early days,[277] their crystallography was not clear until electron microscopic observations were made.

A. *Parent phase* β_1

The high-temperature β phase of this alloy is also b.c.c. and undergoes a eutectoid phase transformation at 580°C. The order–disorder transition of the β phase has not been determined, but recently a high-temperature electron diffraction study[278] showed that the β phase becomes an ordered Fe_3Al-type lattice below 750°C.§

B. β_1' *martensite*

When a Cu alloy containing approximately 15 at.% Sn is quenched from a high temperature, straight lines that resemble slip lines appear in the matrix phase (Fig. 2.73a). An electron microscopic observation[276,280] reveals that these lines are bands containing striations (Fig. 2.74a). From the electron diffraction pattern in Fig. 2.74b and some other diffraction patterns it was determined that this martensite has the 4H structure with

† According to a recent paper,[275] a small amount of $\{101\}_{\gamma_1'}$, i.e., $\{10\bar{1}2\}$, twins is contained.

‡ In a report by Nishiyama *et al.*[276] the notations β' and β'' were employed for β_1' and γ_1', respectively.

§ A recent report[279] confirmed that the temperature at which β changes to β_1 is around 725–750°C. The lattice constants of β_1 were reported to be $a = 2.98$ Å, $c = 3.07$ Å, and $c/a = 1.03$.

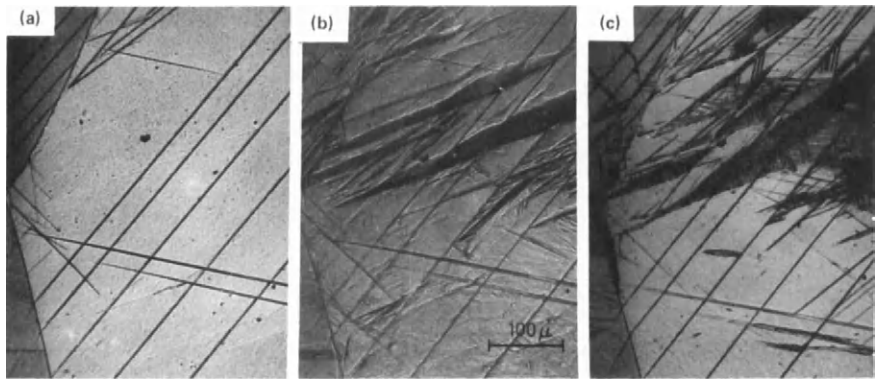

FIG. 2.73 Optical micrograph of martensite in a Cu–14.80 at.% Sn alloy heated for 1 hr at 700°C followed by water quenching. (a) As quenched and etched, showing narrow bands of β_1' martensite. (b) Same area as (a), after dipping in liquid nitrogen, showing the surface relief of newly formed lens-shaped γ_1' martensites. (c) Re-etched surface of the same area as in (b), clearly revealing the lens-shaped γ_1' martensites. (After Nishiyama *et al.*[276])

AB′AC′ stacking order.† The lattice orientation relationships‡ were determined from Fig. 2.75 to be

$$(001)_{\beta_1'} \| (110)_{\beta_1}, \qquad [\bar{2}\bar{1}0]_{\beta_1'} \| [\bar{1}11]_{\beta_1}.$$

If β_1' is expressed in hexagonal coordinates, $(001)_{\beta_1'}$ corresponds to $(0001)_{\text{hex}}$, and $[\bar{2}\bar{1}0]_{\beta_1'}$ corresponds to $[11\bar{2}0]_{\text{hex}}$. Therefore, the foregoing orientation relationships are equivalent to the Burgers relations in the b.c.c.-to-h.c.p. transformation.

The habit plane was determined from electron micrographs such as Fig. 2.75 to be $(223)_{\beta_1}$. This plane is very close to $\{112\}_{\beta_1}$, which contains an invariant line direction. The phenomenological theory may predict this habit plane (Chapter 6).

The foregoing relation suggests that β first becomes β_1 by ordering and then is transformed into β_1'. A possible transformation mechanism is that there will be $\pm[1\bar{1}0]_{\beta_1}$ shears on $(110)_{\beta_1}$, as in the case of Cu–Al alloys, but for the present case the shear direction is reversed every two layers to form the AB′AC′ stacking layer structure. If there are errors in that

† The lattice constants of this martensite were found by x-ray diffraction[281] to be $a_0 = 4.558$ Å, $b_0 = 5.042$ Å, $c_0 = 4.358 \times 2$ Å.

‡ The β_1 phase in this case begins to change into an aggregate, β_x, containing precipitates due to heat evolution by the electron beam during the electron microscopic observation.[276,278] However, since the orientation of β_1 coincides with that of β_x, the orientation relationships between β_x and β_1' are considered to be equivalent to those between β_1 and β_1'. In Fig. 2.75, β_2 means the matrix of β_x.

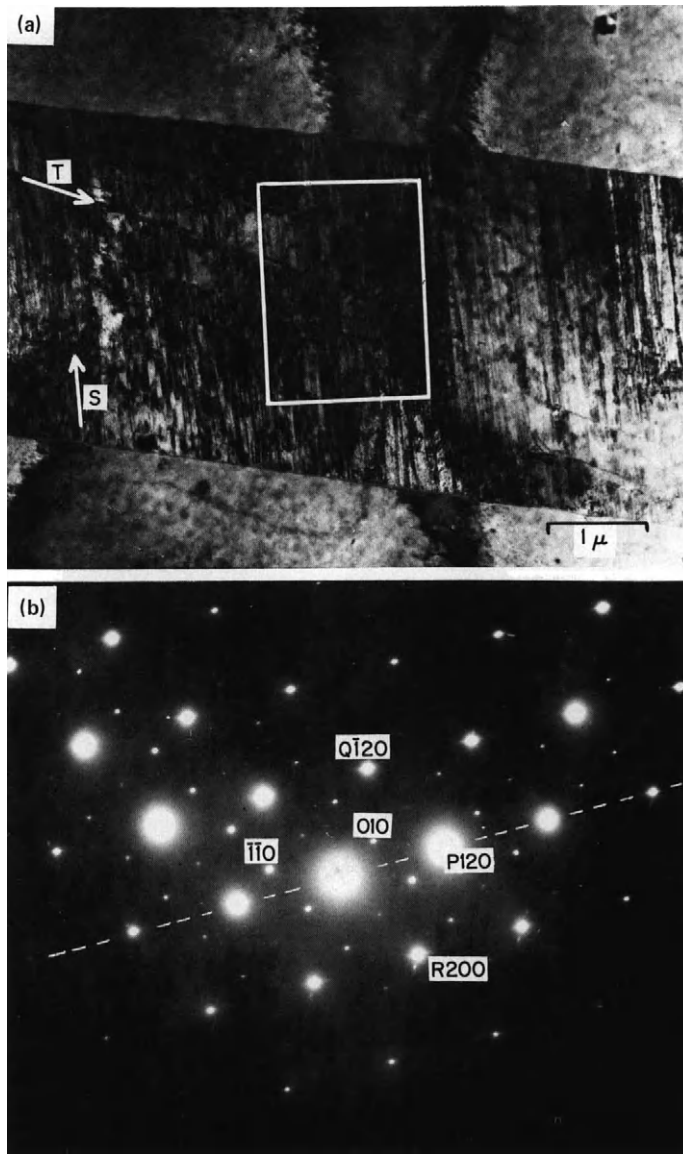

FIG. 2.74 β_1' martensite of Cu–14.80 at. % Sn. (a) Electron micrograph showing a β_1' crystal having stacking faults. (b) Electron diffraction pattern of the white-framed area in (a), showing the [001] zone. (After Nishiyama *et al.*[276])

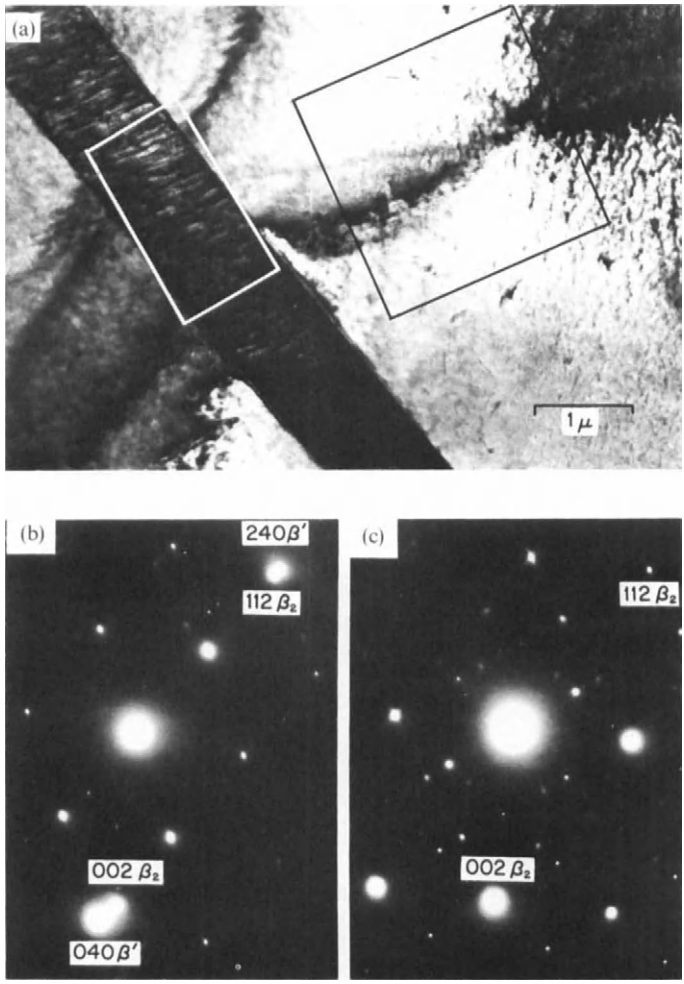

FIG. 2.75 Lattice orientation relationship between β_1' and β_1 in Cu–14.80 at. % Sn. (a) Electron micrograph showing a β_1' crystal in a β_1 matrix. (b) Electron diffraction pattern of the white-framed area in (a), showing the [001] zone of β_1' martensite. (c) Electron diffraction pattern of the black-framed area in (a), showing the [110] zone of β_1 matrix. (After Nishiyama *et al.*[276])

regular shear, stacking faults on the $(001)_{\beta_1'}$ will be produced. However, no such stacking faults have been observed so far, although a more detailed observation might prove the existence of such stacking faults. The striations in Fig. 2.74a are due to stacking faults on the $(122)_{\beta_1'}$, that is, on $(10\bar{1}1)_{hex}$. These stacking faults should be considered to be lattice-invariant strain rather than errors in the regular shear in the transformation mechanism.

The reason why the slip has occurred on the $(122)_{\beta_1'}$ instead of the $(001)_{\beta_1'}$ may be as follows. If the transformation of this alloy takes place by the mechanism mentioned above, there would be an 11.6% expansion and an 8.8% contraction along the a axis and b axis, respectively, but along the c axis only a 3.0% expansion will be required. Moreover, the inclination of the c axis to the basal plane does not change during the transformation. Therefore, a resolved shear stress on the $(122)_{\beta_1'}$ caused by the transformation strain will be much greater than that on the $(001)_{\beta_1'}$ basal plane, and consequently slip occurs more frequently on the $(122)_{\beta_1'}$ than on the $(001)_{\beta_1'}$ and many stacking faults are produced on the $(122)_{\beta_1'}$. Slip on the $(124)_{\beta_1'}$, that is, $(10\bar{1}2)_{\text{hex}}$, was not observed. This is probably due to the rough and uneven atomic arrangement of the $(124)_{\beta_1'}$ plane in the AB′ AC′ structure as compared with that on the $(122)_{\beta_1'}$.

C. γ_1' *martensite*

When the alloy is further cooled to a subzero temperature after being quenched from the β phase region, a new wedge-shaped surface relief feature appears on the specimen surface. Figure 2.73b shows such surface relief. The photographed area is identical to that in Fig. 2.73a. Figure 2.73c shows a chemically etched pattern of the area revealing the substructure more clearly. These wedge-shaped regions are also considered to be martensite because they showed a surface relief effect, and are designated γ_1'. The habit plane of this martensite is $\{133\}_{\beta_1'}$.[282] The crystal structure of this γ_1' is the same one as that of the γ_1' in Cu–Al alloys, namely, a hexagonal structure with AB′ stacking order.

The orientation relationships between γ_1' and β_1 are the same as those between β_1' and β_1. That is, they are the Burgers relations. Therefore, there will be $\pm[1\bar{1}0]_{\beta}$ shear on $(110)_{\beta_1}$, as in the case of $\beta_1 \rightarrow \beta_1'$, but in this case the shear direction alternates at every layer to produce the AB′ structure. Weak streaks in $[001]_{\gamma_1'}$ observed in electron diffraction patterns of γ_1' suggest the existence of stacking faults owing to errors in the transformation shear.

The twinning plane of the internal twins of γ_1' is $(121)_{\gamma_1'}$ in most cases. This plane corresponds to $(10\bar{1}1)_{\text{hex}}$, as in the case of the β_1' martensite in which the twinning plane is $(122)_{\beta_1'}$; $(122)_{\gamma_1'}$, that is, $(10\bar{1}2)_{\text{hex}}$, could also be a twinning plane. In Fig. 2.76 striations within each twin are not parallel to the twinning plane. These striations coincide with $(1\bar{2}1)_{\gamma_1'}$ surface traces, and hence, they are due to stacking faults produced by the lattice-invariant shear. There are very few stacking faults on the basal plane. This may be explained in the same way as the case of β_1' martensite.

As described earlier, even in an alloy with the same composition, two different martensite structures, β_1' and γ_1', appear, depending on the transformation temperature. The martensite structures are also dependent on

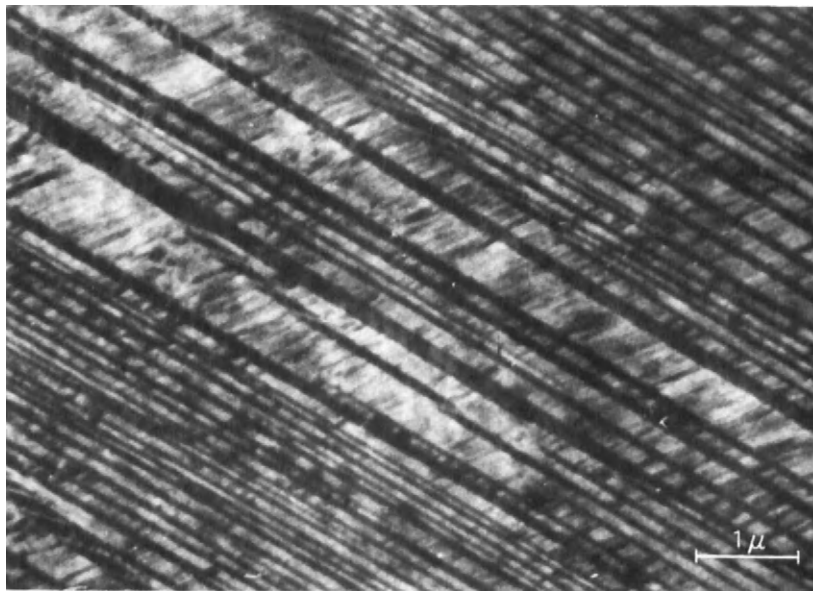

FIG. 2.76 Interior of a γ_1' crystal (in Cu–14.80 at.% Sn), consisting of internal twin lamellae within which are seen striations (due to stacking faults) having alternate inclination for alternate twins. (After Morikawa *et al.*[280])

the alloy composition, as in the case of Cu–Al alloys. In the composition range of 13.1–15.0 at.% Sn, β' or β_1' martensite forms. Above 14.5 at.% Sn, however, γ_1' martensite frequently appears. For 13.8–15.0 at.% Sn, β_1' and γ_1' coexist in lamellar form.[283–285]

2.5.3 β_1' martensite in Cu–Zn alloys

Despite extensive early studies, the crystal structure of β_1' martensite in Cu–Zn alloys was not clear until an electron microscope study was completed. The high-temperature β phase of this alloy becomes ordered on cooling and assumes a CsCl-type superlattice (β_1).[284–287] On quenching to room temperature, straight lines like slip lines were observed by optical microscope, as in Cu–Sn alloys.† S. Sato *et al.*[287,289] found by electron microscopy that the crystal structure of such straight-line regions is 9R. Within these regions stacking faults were also observed on the (001) plane. The orientation relationships between the martensite (β_1') and its parent

† It was reported[288] that a martensitic transformation to a twinned f.c.c. structure took place during the thinning procedure for electron microscopy although the as-quenched specimen was austenitic at room temperature.

phase (β_1) are

$$(001)_{\beta_1}\|(104)_{\beta_1}', \qquad [010]_{\beta_1}\|[010]_{\beta_1}',$$

which deviate a little from those for the $\beta_1' \rightarrow \beta_1$ transformation of Cu–Al alloy. By an earlier x-ray study,[290] the crystal structure of martensite formed at a subzero temperature was reported to be h.c.p. However, an electron microscope study by Sato *et al.*[289,291] showed that it is also 9R.†

As is known from before,[277] the martensitic transformation of this alloy is induced by plastic deformation. It was recently found by Kajiwara[292] that the strain-induced martensite of Cu–40.6 at. % Zn consists of a crystal of the f.c.t. structure with a CuAu I-type superlattice and a very thin platelike crystal of 9R structure. The axial ratio of the f.c.t. structure differs from martensite plate to martensite plate, ranging from 0.93 to 0.97. There are many stacking faults in martensite crystals of both the f.c.t. and 9R structures.

Murakami *et al.*[293] studied an $Au_xCu_{55-x}Zn_{45}$ alloy that was obtained by partial replacement of the Cu atom with an Au atom in the Cu–Zn alloy system. They found that a three-step transformation occurred as follows:

$$\beta \xrightarrow{T_c} \text{CsCl type} \xrightarrow{T_c'} \text{Heusler type} \xrightarrow{M_s} \text{Orthorhombic (2H + 18R)}$$

As the Au composition x increases, the transition temperature T_c of the first transformation step increases, starting from 455°C at $x = 0$. The transition temperature T_c' in the second transformation step has a maximum value of 390°C at $AuCuZn_2$. The third transformation is martensitic and its M_s temperature reaches a maximum 45°C at 26% Au. The crystal structure of this martensite is 2H or 9R (18R if the superlattice is considered). The substructures in these martensites are stacking faults on $(001)_0$ of 18R and internal twins on $(121)_0$ of 2H.[294]

2.5.4 α', β_1', and γ_1' martensites in Au–Cd alloys‡

The β phase in Au–Cd alloys exists near 50 at. % Cd and its crystal structure is b.c.c. If the Cd composition is not too low, the β phase becomes β_1, which is ordered with a CsCl-type superlattice.[299] Upon quenching from a high

† In one reference[284] martensite formed at low temperature was denoted β''.

‡ Nakanishi and Wayman[295] reported that when an Au–47.5 at. % Cd alloy was slowly cooled from a high temperature, a $\beta \rightarrow \beta'$ (orthorhombic) transformation took place at 60°C, but when the alloy was quenched to a temperature just above 60°C, a $\beta \rightarrow \beta''$ (triclinic) transformation occurred on further slow cooling.[296] Ferraglio *et al.*[297] reported that when an Au–50 at. % Cd alloy was splat quenched from the liquid phase kept at 300°C (quenching rate: 10^7/sec), the β_1 phase with the CsCl-type superlattice was retained and after having been kept at room temperature for several months, the β_1 phase was transformed into martensite. Changes in elastic constants during the transformation were also measured.[298]

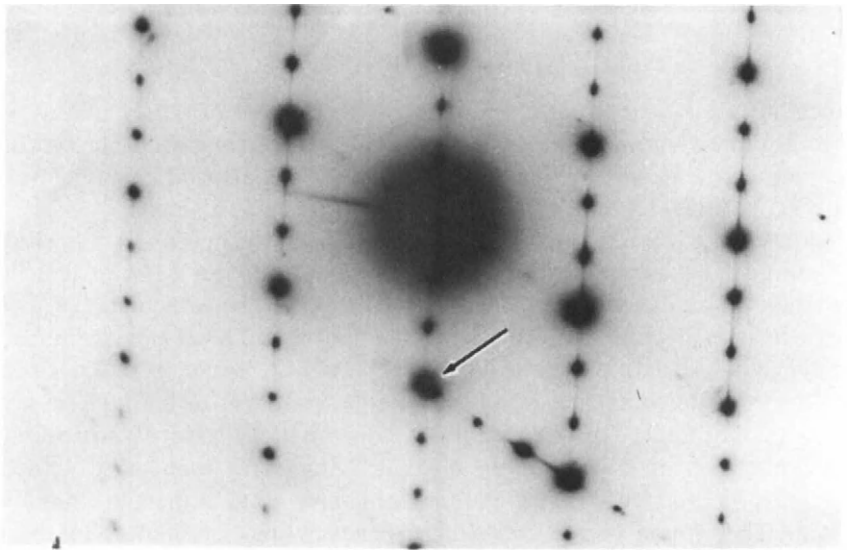

FIG. 2.77 Electron diffraction pattern of β_1' martensite in Au–47.5 at.% Cd (9R $[1\bar{1}0]_o$). (After Toth and Sato.[301])

temperature, three kinds of martensite, α', β_1',[300] and γ_1', appear. The quenching rate does not need to be very high. Toth and Sato[301] studied these martensite structures with the electron microscope and obtained the following results. The α' martensite has a disordered f.c.c. structure and contains a high density of stacking faults and twin faults which cause streaks in the electron diffraction pattern in the direction perpendicular to the (111) plane. This α' martensite appears in a relatively low Cd composition range, that is, near 45% Cd. Since the α' martensite is disordered, its parent phase must have been disordered around this composition range.

The crystal structure of β_1' martensite is 9R. As in the case of the β_1' martensite of Cu–Al alloys, one period of intensity distribution in the reciprocal lattice along the c^* direction contains three spots (Fig. 2.77),[301†] although the reciprocal lattice of β_1' in Au–Cd is different from that of β_1' in Cu–Al owing to a different atomic ordering in the close-packed layer. The β_1' of this alloy consists of alternate bands, as in the β_1' of Cu–Al. There are two kinds of crystallographic relations between the neighboring bands. In one, the c axes of the neighboring martensite crystals are parallel to each other; in the other, they make an angle of 60°. In each band there are stacking faults on the $(001)_{\beta_1'}$ as in the β_1' of Cu–Al. Most often, β_1'

† This electron diffraction pattern is symmetrical with respect to the central vertical line because the incident electron beam is parallel to the $[1\bar{1}0]$ direction.

appears at 46.5 at.% Cd, though it sometimes appears at 47.5 at.% Cd. The transformation to β_1' occurs on slow cooling and more abundantly on quenching. The growth behavior of this martensite will be described in Section 3.5.2.

The β_1' further transforms into γ_1' on tempering. The γ_1' has a 2H stacking layer structure with a superlattice (Fig. 2.78). The superlattice is considered to be inherited from the superlattice of β_1. Since the M_s temperature in the transformation of β_1 to γ_1' is about 60°C, the martensitic transformation to γ_1' occurs on slow cooling as well as on quenching. As mentioned earlier, the γ_1' is also transformed easily from β_1' on tempering, which suggests that the γ_1' is relatively stable. There are substructures in γ_1' martensite similar to those in Cu–Zn alloys. Figure 2.79a shows internal twins on the

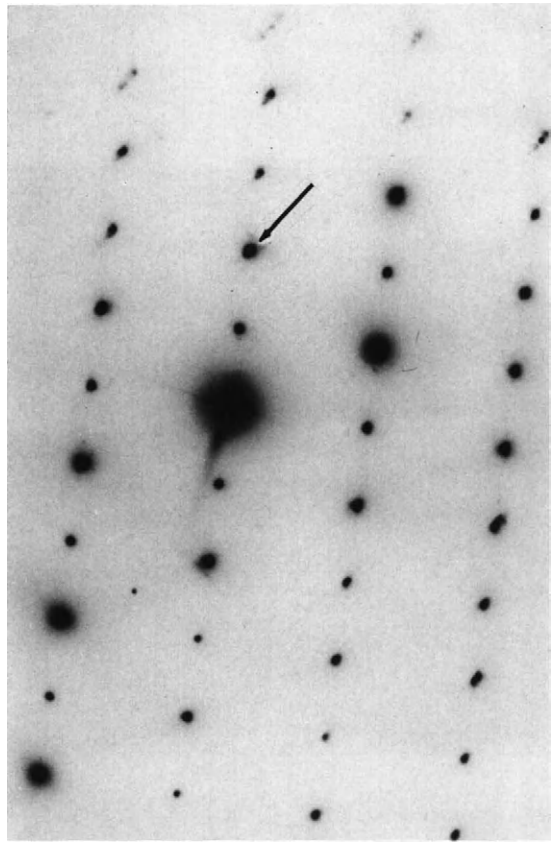

FIG. 2.78 Electron diffraction pattern of γ_1' martensite in Au–46.5 at.% Cd (2H $[1\bar{1}0]_o$). (After Toth and Sato.[301])

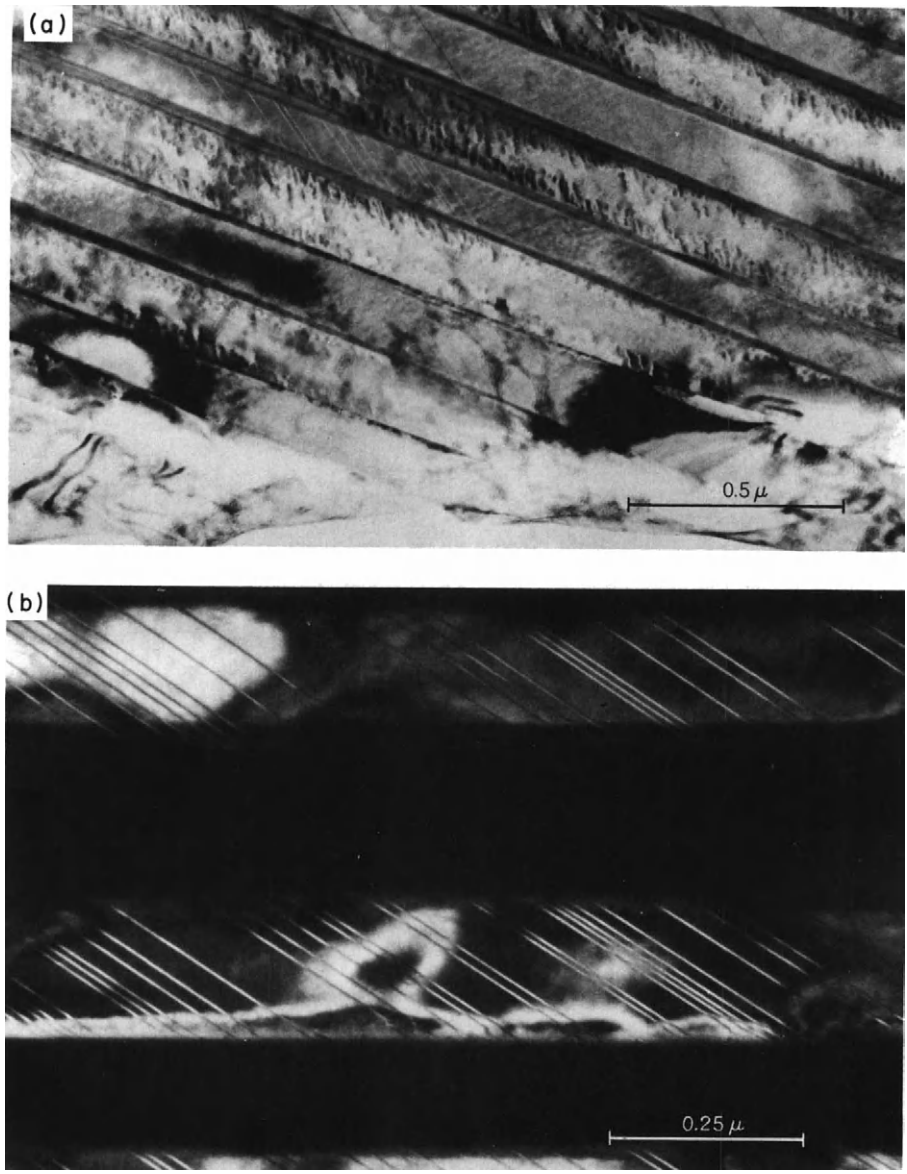

FIG. 2.79 Interior of γ_1' martensite (in Au–47.5 at. % Cd), consisting of internal twin lamellae within which are seen striations due to stacking faults. (a) Bright-field image. (b) Dark-field image. (After Toth and Sato.[301])

$\{10\bar{1}1\}$ plane and stacking faults on the (0001) plane in each twinned crystal. These stacking faults can be seen clearly in the dark-field photograph (Fig. 2.79b). The γ_1' usually appears in a higher Cd composition range than does the β_1'. There is also a composition range in which β_1' and γ_1' coexist in lamellar form.

Suppose that a specimen of β_1 in Au–49 at.% Cd is transformed into γ_1' by cooling and that this specimen is then deformed in the γ_1' temperature range. If the deformed specimen is reversely transformed into the β_1 phase by heating, the original specimen form is recovered. This is called the *shape memory effect* (Section 5.2.6). A specimen of γ_1' shows such great elasticity that it can be deformed like rubber by an external force. The same behavior was observed in Ag–Cd alloys.[302,303]

2.5.5 Martensite in TiNi alloys

Approximately equiatomic Ti–Ni alloys are known by the name of Nitinol, and the alloys recently came into the limelight because they have many special properties, such as *shape memory*, and have been utilized for industrial purposes. Thus the alloys have been the subject of many studies. The results, however, especially on the crystallographic nature of the martensitic transformation, are not in agreement with one another. Such disagreement may be attributed to the complexities of the parent structure and the simultaneous occurrence of martensitic transformation and precipitation.† We will discuss the parent phase first.

A. *Parent phase*

The high-temperature parent phase of the approximately equiatomic Ti–Ni alloys is generally accepted to be of the B2 type (the order–disorder transition temperature is 625°C[306]). Strictly speaking, however, the structure is not so simple. According to an experiment by Chandra and Purdy,[307] the parent phase rapidly cooled to temperatures above 100°C is simply the B2 type, but it undergoes a change to a premartensitic state while the specimen temperature is lowered to about 30°C. The change occurs continuously as the temperature decreases, and diffraction patterns taken from the premartensitic state reveal extra reflections whose radial positions are $\frac{1}{3}$ of those of fundamental spots. Wang *et al.*[308] explained the extra reflections as due to a superlattice (the lattice constant is $a_0 = 9$ Å and it is three times

† There is a report that the parent phase undergoes a eutectoid reaction at 640°C and decomposes into Ti_2Ni (f.c.c.) and $TiNi_3$ (h.c.p.), and that an intermediate precipitate is produced at an early stage of the eutectoid reaction.[304] This report, however, is criticized in another paper.[305]

that of the B2). Nagasawa[309] also studied the crystal structure of an alloy quenched from 800°C, using electron diffraction. He proposed a modulated structure of the B2's to account for the diffraction patterns. The modulation was such that the B2 lattice is periodically sheared, with shufflings, on every third $(\bar{1}10)$ and $(\bar{1}01)$ plane along the $[111]$ and $[1\bar{1}1]$ directions, respectively. They proposed this modulated structure to be a kind of martensite because it was also produced by deformation.†

Otsuka *et al.*[311,312] studied the same problem by taking electron diffraction patterns from a thin specimen cooled in an electron microscope. Figure 2.80a shows an electron micrograph and the corresponding diffraction pattern taken from an as-quenched thin specimen at 18°C. The diffraction pattern corresponds to the B2 type. If the specimen is cooled to −196°C in an electron microscope, some parts undergo a martensitic transformation, as will be described later. Other parts, especially thin parts of the specimen edge, do not show any structural change, as seen from the micrograph in part (b), which was taken from the same area as that in part (a) (the artifact indicated by the arrow identifies the area). In spite of such stability of structure, the corresponding diffraction pattern reveals extra reflections (at the right in part (b)). The extra reflections are located at $\frac{1}{3}$ positions in the same manner as those obtained by the previous workers. If the specimen is again heated to 18°C, then the extra reflections disappear, as can be seen in the diffraction pattern of part (c). Therefore, the phase change responsible for the extra reflections must be a reversible one. Otsuka *et al.*[311] thus speculated that the phase change may be attributed to some electronic ordering or lattice modulation due to some periodic atomic displacements. In any case, the phase change may not be an ordinary martensitic one, but a premartensitic one. In fact, no trace of the lattice-invariant shear of the martensitic transformation is observed in the micrograph in Fig. 2.80b.

Premartensitic phase changes just above the M_s temperature are occasionally observed. Sandrock *et al.*[313] examined this phenomenon in detail in a Ti–Ni alloy. According to their experiment, electrical resistivity versus temperature curves during cooling,‡ exhibit a gradual increase and finally a peak below a temperature about 30°C above the M_s temperature; electron diffraction patterns reveal streaks along the 111 reciprocal lattice vector in addition to $\frac{1}{3}$ extra reflections at about 30°C above the M_s temperature. These phenomena were attributed to anomalous lattice vibrations that are induced by a decrease in the elastic modulus as the temperature decreases. Such an explanation was also presented by Delaey *et al.*[316]

† There is another report[310] with results substantially in agreement with this as well as those obtained by Nagasawa,[309] as mentioned later.

‡ A few studies of this phenomenon by electrical resistivity measurement have been reported.[314,315] in addition to that described in the text.

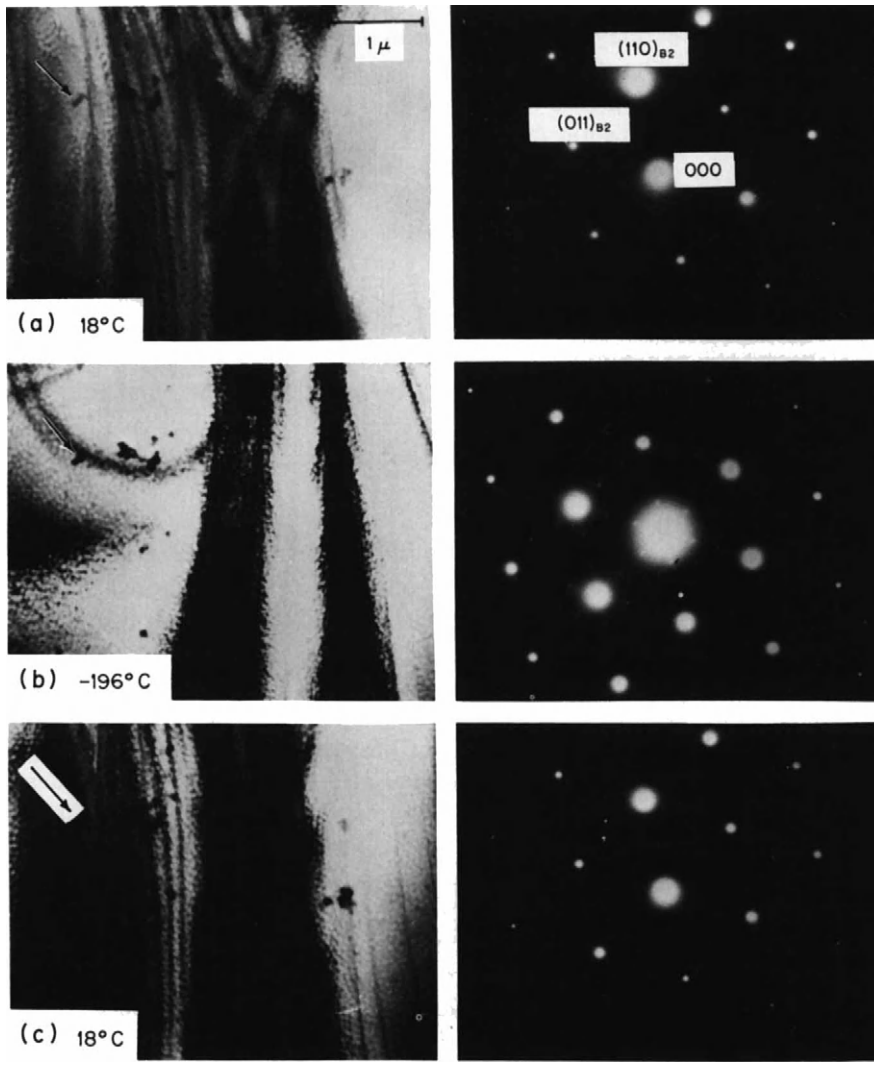

FIG. 2.80 Change of structure as seen by the electron microscope and its diffraction pattern due to a premartensitic transition and its reverse transition in a Ti–49.75 at.% Ni alloy. (a) As quenched to 18°C. (b) Cooled to −196°C. (c) Returned to 18°C. (After Otsuka *et al.*[311])

Wayman *et al.*[317] examined the behavior of the peak in the electrical resistivity versus temperature curves during thermal cycling, and found that on cooling the peak appears at the M_s temperature and has no direct relation to the martensitic transformation. They have attributed the peak to a scattering effect of conduction electrons due to a magnetic or electronic

ordering before the martensitic transformation starts. On the other hand, a specimen cooled to about $-100°C$ that has completely undergone a martensitic transformation does not exhibit any peak during heating. They explained this phenomenon as due to the disappearance, during the martensitic transformation, of the foregoing magnetic or electronic ordering. The peak does not appear during cooling provided that the specimen has not been heated to a temperature above the A_s temperature.

Honma *et al.*[318] measured the specific heat of a TiNi alloy, and suggested the existence of an intermediate phase.

Wang *et al.*[319] studied the crystal structure of the parent phase by means of x-ray and neutron diffraction, and reported that the matrix phase consists of the B2 and $P\bar{3}ml$ lattices at temperatures just above M_s, and that the martensite consists of three lattices, $P\bar{1}$, P1, and P6/m. There has thus not been a consensus on the crystal structure of parent phase.

B. *Martensite phase*

Otsuka *et al.*[311] studied the martensitic transformation in a TiNi alloy by examining the surface relief effect. Figure 2.81 is a series of optical micrographs taken from a specimen continuously cooled to subzero temperatures below the M_s temperature ($-40°C$ to $-50°C$).† This series shows that surface relief appears and grows gradually as the temperature decreases (photos (a) to (d)), and that it shrinks and disappears as the temperature increases (photos (e) to (h)). This fact clearly indicates the occurrence of a martensitic transformation.‡ It was also verified by a subsequent experiment [321,322] which reported that martensite plates did not grow continuously but grew discontinuously, although the units of growth could not be resolved by an optical microscope. This martensitic transformation is a thermoelastic one, and at temperatures near M_s, the martensitic specimen exhibits anomalies in elasticity,[323] internal friction,[306,324] electrical resistivity,[306,325,326] magnetic properties,[325] transformation behavior,[327–329] and so on. Moreover, the martensitic specimen exhibits a shape memory effect, which will be discussed in detail in Chapter 5.2.6.

Some workers have defined this to be a first-order transformation[306,330] but others consider it a second-order one.[331–333] Recently Otsuka *et al.* have clearly verified that it is first order by examining the variation of x-ray diffraction lines with temperature.

Various crystal structures of the TiNi martensite have been reported.[334–337] According to a recent electron diffraction study by Nagasawa *et al.*[309,338] the martensite phases have various close-packed structures,

† It is also reported that $M_s = 160°C$ and $M_f = -120°C$.[320]

‡ Wang *et al.*[308] concluded that this phase change is not martensitic since the surface relief effect was not detected in their experiment.

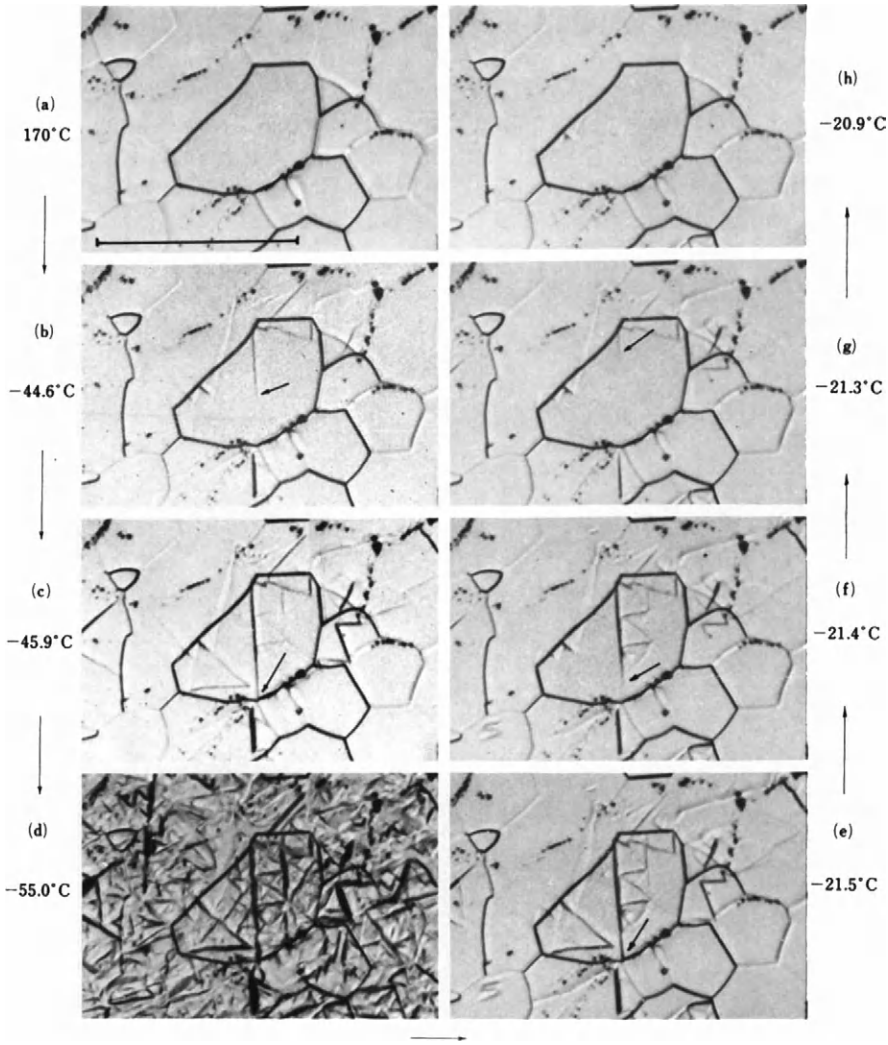

FIG. 2.81 Continuous observation of the surface relief from the thermoelastic growth and shrinking of the martensite in Ti–49.75 at. % Ni. (a)–(d) Cooling. (e)–(h) Heating. (After Otsuka *et al.*[312])

which are obtained from the B2-type parent lattice. In particular, it is of the 12R and 4H structures at room and subzero temperatures, respectively, but the 2H and 18R structures are also observed occasionally. The 12R and 4H structures are closely connected with each other in such a way that one structure transforms to the other, depending on the parameters of the stacking faults on the basal (001) planes.[309] Otsuka *et al.*[310] studied the

crystal structure as well as the internal defects of martensite. They examined acicular martensites produced at thicker parts of thin foils by cooling in an electron microscope. Figure 2.82a is an electron micrograph of a martensite displaying many planar defects. From the corresponding diffraction pattern in photo (b) and the trace analysis, the planar defects were determined to be internal twins on the $(11\bar{1})$ planes. The crystal structure was identified to be nearly the B19 type, more exactly a distorted B19

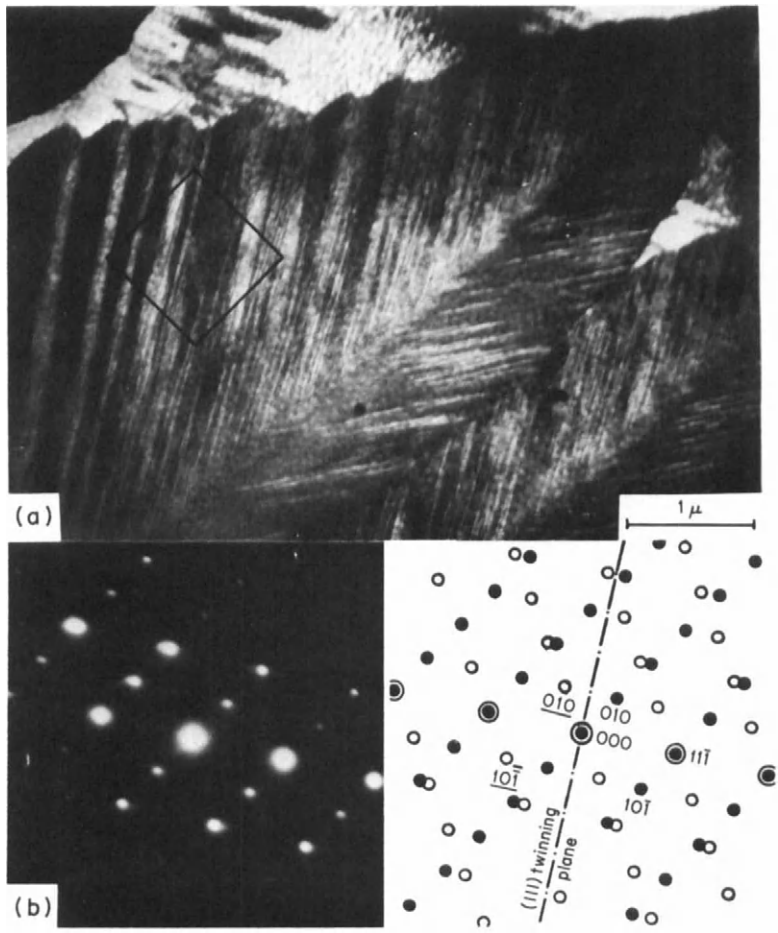

FIG. 2.82 TiNi martensite. (a) Electron micrograph of a martensite crystal having internal twins on the $(11\bar{1})$ plane. (b) Electron diffraction pattern of the black-framed area in (a) and its key diagram, showing that it consists of two [101] zones having the twin relationship with respect to the $(11\bar{1})$ twinning plane. Indices of twin reflections are underlined. (After Otsuka *et al.*[311])

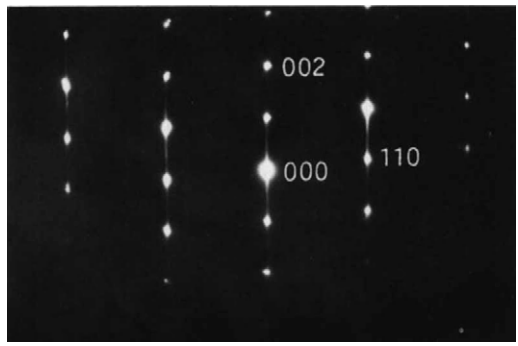

FIG. 2.83 Electron diffraction pattern of TiNi martensite showing [1$\bar{1}$0] zone. (After Otsuka *et al.*[311])

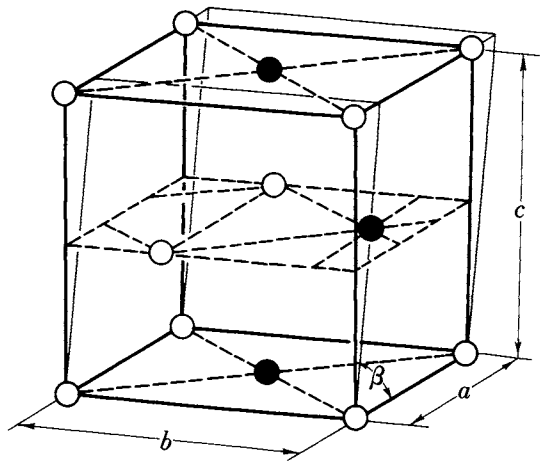

FIG. 2.84 Unit cell of TiNi martensite. $a = 2.889$ Å, $b = 4.120$ Å, $c = 4.622$ Å, $\beta = 96.8°$. (After Otsuka *et al.*[311])

structure. The analysis of Fig. 2.83 and other diffraction patterns gave the structure shown in Fig. 2.84.† The unit cell is monoclinic with the c axis slightly inclined ($=96.8°$). Such a monoclinic structure was recently confirmed by a neutron diffraction study.[339] The atomic arrangement in the unit cell, however, might not be exactly that of Fig. 2.84, since the (001) line was observed in the x-ray diffraction patterns.

In addition to the (11$\bar{1}$) twin faults, (001) stacking faults were also found in the martensite. Streaks parallel to the c^* axis in Fig. 2.83 are evidence of

† This structure is supported by other workers.[312,315]

the stacking faults. The orientation relationship between the martensite and parent lattices was determined to be

$$(001)\ \overset{6.5^\circ}{\underset{M}{\sim}}\ (101)_{B2}, \qquad [\bar{1}10]_M \| [\bar{1}\bar{1}1]_{B2}.$$

This is nearly the Burgers relation, though a difference of 6.5° exists between their planar relations.

2.6 Martensitic transformation behavior of the second-order transition

All the martensitic transformations previously described are first-order transitions.† The martensitic transformation, however, is not necessarily limited to first-order transitions. Cooperative movement of atoms without long-range diffusion is a primary requirement, which may be satisfied in second-order transitions, such as order–disorder, magnetic, or dielectric transitions. Therefore, if these second-order transitions are accompanied by a lattice deformation and take place upon rapid change of temperature, the new phases will be formed by cooperative movement of atoms, so that lattice imperfections will be produced, as in the case of ordinary martensite.

2.6.1 f.c.c. to f.c.t. martensitic transformations

In In–Tl alloys, where the equilibrium diagram is as shown in Fig. 2.85,[340–342] the boundary line between the α and β phases is inclined to the temperature axis. Hence, when the temperature is lowered below the line, the $\beta \rightarrow \alpha$ transformation occurs. The β phase is f.c.c. and the α phase is f.c.t., which is distorted only a little from f.c.c. The lattice constants of the α phase, a_t and c_t, are as shown in part (b) of the figure, both gradually approaching the lattice constant a_c of the β phase as the composition approaches the boundary line. Such variations in the lattice constants are suggestive of a second-order transition.

Under this small lattice change, the transformation strain is very small and can easily be relaxed in many ways. Guttman *et al.*,[340,343] Luo *et al.*,[341] and Pollock and King,[342] studied this transformation. Figure 2.86a is an optical micrograph of the surface relief of the α phase in an In–20.75 at.% Tl alloy that occurred at 57°C on cooling the β phase from a temperature of 90°C. In this micrograph, each parent grain consists of parallel bands;

† In first-order transformations, at constant pressure, there is a discontinuity in the enthalpy versus temperature curve, corresponding only to a change in the slope of the free energy versus temperature curve; i.e., the discontinuity is in $(\partial F/\partial T)_p$. In second-order transformations there is no discontinuity in $(\partial F/\partial T)_p$ but a discontinuity occurs in $(\partial^2 F/\partial T^2)_p$.

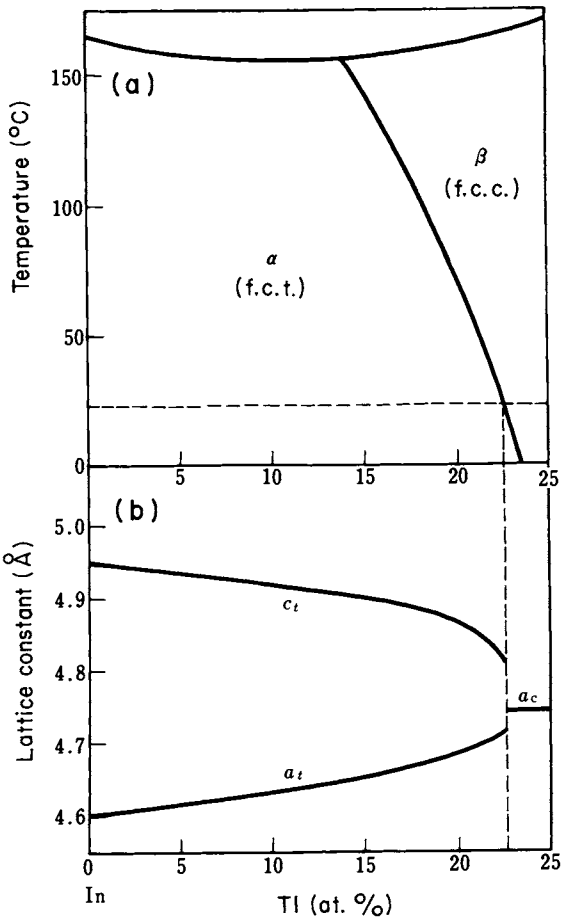

FIG. 2.85 Phase diagram and lattice constants of In–Tl alloys. (a) Pertinent portion of phase diagram. (b) Lattice constants at 24°C. (After Guttman.[340])

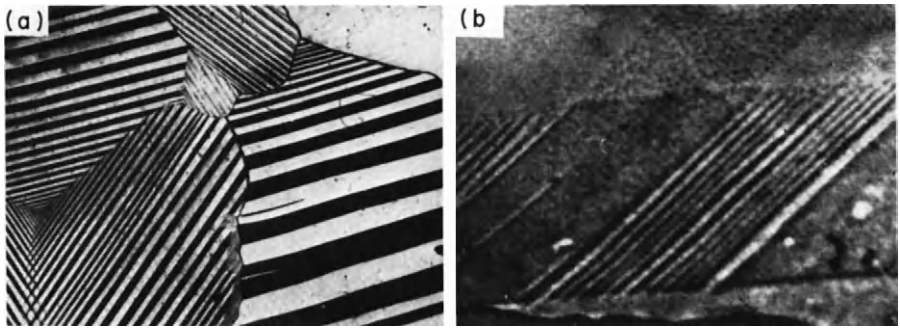

FIG. 2.86 Optical micrographs of martensite in an In–20.75 at.% Tl alloy. (a) Surface relief showing alternate lamellae of two variants of martensite in each parent grain. (After Bowles *et al.*[343]) (b) Etched surface showing internal twins within each variant. (After Guttman.[340])

adjacent bands are parallel to a (101) twin plane of the tetragonal lattice, whereas alternate bands have the same surface inclination. These neighboring bands are considered to be two variants that together relax the transformation strains.

High-magnification examinations of etched specimens reveal that each of the bands contains finer subbands. The subbands are always parallel to the $\{011\}$ planes lying at 60° to the main bands, and the subbands in the alternate main bands have the same orientation, forming two different sets. The interface between these subbands is parallel to (011) for one set and to $(01\bar{1})$ for the other set; thus the crystals of the different sets are at about 90° to each other; that is, all these interfaces are twin faults. It can therefore be concluded that the transformation has occurred by double shear processes, $(101)\,[\bar{1}01]$ and $(011)\,[0\bar{1}1]$, in the case of the (011) set. This doubly twinned structure was formerly taken as evidence of the double distortion theory of the martensite transformation mechanism that was advanced a number of years ago.

Heating to reverse the transformation causes the surface relief bands to disappear, which proves that the transformation occurs by a reversible mechanism.[340,344] Such a phenomenon cannot be found in ordinary steels. In the transformation of In–Tl alloys, the lattice deformation is very small, and after one variant is formed, another variant by the opposite shear is formed adjacent to it, so as to decrease the total strain of the transformation. Therefore, the substructure may be coarse and hence can be observed optically, whereas in steels it is so fine that the observation must be made by electron microscopy. In In–Tl alloys, the heat of transformation has been reported to be small, 2.66×10^{-3} cal/g.[345†] Other transformation behaviors of this alloy will be described in Section 3.5.1.

When a specimen of transformed f.c.t. α phase is stressed by bending,[344,345] some of the fine twins are detwinned with a clicking sound to relax the stress, but they become twinned again on removal of the stress and thus the specimen becomes unstrained. This rubberlike behavior is like that of the γ_1' phase of Au–Cd alloys, the details of which will be described in Section 3.6. The transformation of this alloy proceeds only with falling temperature and does not take place isothermally. Alloys of In–(4–5)% Cd[346] and V–(6–8) at.% N[347] have a cubic-to-tetragonal transformation and microscopic structures like those in In–Tl alloys have been found.

Manganese–copper alloys having more than 60% Mn also show a similar equilibrium diagram and similar concentration dependence of lattice constants; therefore, similar f.c.c.-to-f.c.t. transformation is observed. The

† Second-order transitions do not have a heat of transformation; the heat effect is spread over a temperature range.

occurrence of the f.c.t. lattice in these alloys, however, originates from the antiferromagnetic spin ordering of the Mn ion.[348] This phase has a banded structure with fine subbands and surface relief characteristic of martensite.[349,350] Since this transformation is reversible, there is large internal friction at temperatures just below the M_s temperature (Section 5.2.7). Similar phenomena are seen in alloys containing 13–29 at % Ni in place of Cu.[351–353] An alloy of the composition $MnZn_3$, which is of the Cu_3Au type, becomes antiferromagnetic and tetragonal ($c/a = 0.95$) by cooling to temperatures below 130°K.[352] Therefore, a transformation similar to that in Mn–Cu alloys is expected to occur.

2.6.2 b.c.c. to b.c.t. martensitic transformations

Manganese–gold alloys near the atomic composition 1:1 are b.c.c. at high temperatures, forming a superlattice of the CsCl type referred to as the c phase.[354] When the temperature is lowered to 500°K, the alloys become antiferromagnetic by a second-order transformation and the lattice changes to b.c.t. with an axial ratio less than one (called the t_1 phase). The composition dependence of the Néel temperature is shown in Fig. 2.87.[354] In the composition range of less than 50 at. % Au, the t_1 phase transforms further to a t_2 phase at lower temperatures. At these transformation temperatures the lattice constants change discontinuously, as shown in Fig. 2.88[354] for a Mn–47 at. % Au alloy. By neutron diffraction it is found that during this transition, the direction of the magnetic moment of the Mn atom changes, as shown in Fig. 2.89.[355]

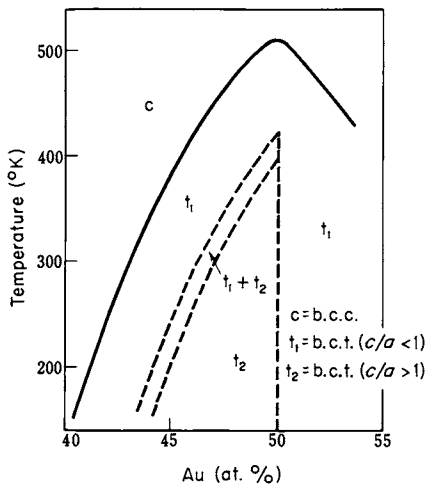

FIG. 2.87 Change of transformation temperature of Mn–Au alloys with Au content. (After Smith and Gaunt.[354])

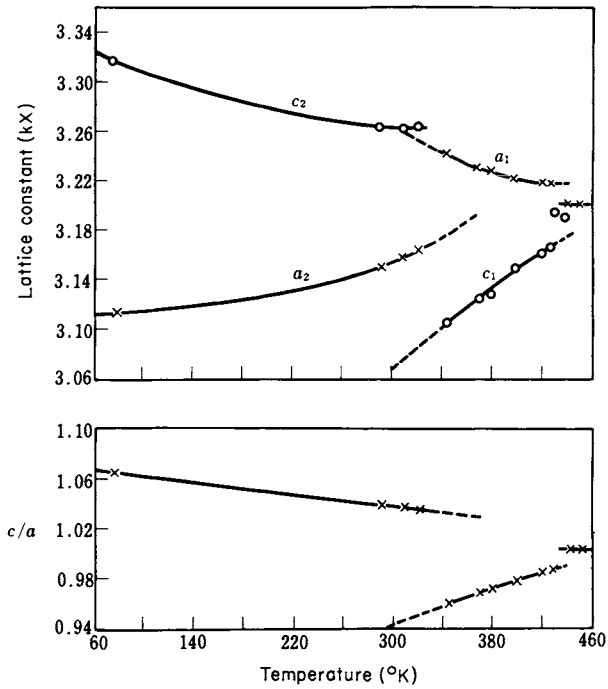

FIG. 2.88 Change of lattice constants of Mn–47at.% Au alloy with temperature. (After Smith and Gaunt.[354])

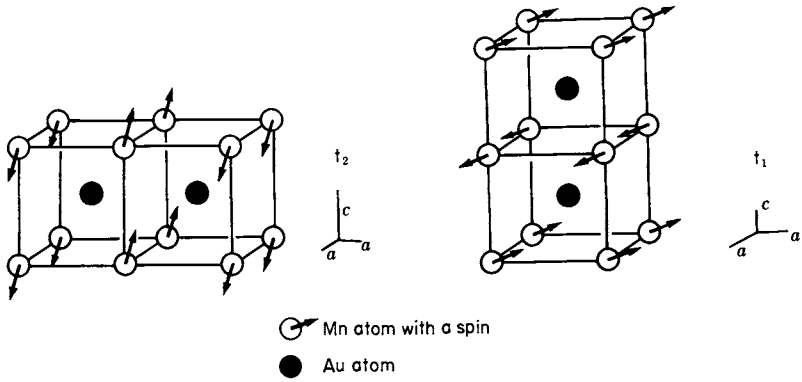

FIG. 2.89 Direction of the magnetic moment of the Mn atom in the t_1 and t_2 phases of MnAu. (After Bacon.[355])

TABLE 2.3 Surface relief on $(011)_c$ plane of t_1 and t_2 phases in Mn–47.5 at. % Au[a]

Phase	Temperature	Thickness ratio of twins	Surface relief Angle of inclination (radian)
t_1	341°K	1.8 ± 0.3	0.029
t_2	296°K	1.9 ± 0.3	0.026

[a] After Finbow and Gaunt.[356]

Both transitions, $c \rightarrow t_1$ and $t_1 \rightarrow t_2$, are considered to be martensitic because they are accompanied by surface relief. In the surface relief, gross twin layers and subtwin layers of the {011} type are seen. Since the lattice deformations in these transitions are very small, as in the case of In–Tl alloys, the gross twins are so thick that they can be seen with the naked eye and the subtwins can be seen by light microscopy. Table 2.3 shows the ratio of twin thicknesses and the inclination of the surface relief.[356] The surface relief occurred in each of these transitions disappears on the reverse transformation. Under atmospheric pressure a single crystal of the c phase transforms to a number of many-banded b.c.t. crystals (t_1 or t_2 phase). But if adequate pressure is applied during the transition, a single crystal of the b.c.t. structure can be obtained.

Manganese–nickel alloys of near-equiatomic composition have antiferromagnetism and cubic-tetragonal transitions similar to those in the MnAu alloy.[357] Therefore, a martensitic transformation may also take place in these alloys.

In FeRh, which is of the CsCl type, a transition from antiferromagnetic to ferromagnetic is accompanied by a change in the lattice constants and the diffused diffraction lines.[358] Therefore, phenomena similar to those observed in the MnAu are expected.

In Ta–Ru alloys near the equiatomic composition, according to Schmerling *et al.*,[359] the high-temperature μ phase is subject, on cooling, to transformation from μ (CsCl type) to μ' (b.c.t.), and the transformation is reversible without hysteresis. Surface relief and planar defects are found and, consequently, this transformation can be considered to be martensitic. The M_s temperature is about 1370°C for 55 at. % Ru and 700°C for 45 at. % Ru. The alloy whose composition is near 1:1 has a second-order $\mu' \rightarrow \mu''$ transformation (body-centered orthorhombic), with an M_s temperature of 820°C for 50 at. % Ru and 680°C for 47.5 at. % Ru. This transformation is also reversible and the product μ'' has surface relief and twin faults; hence, it too can be considered martensitic. The reversibility of these two transformations is due to the fact that the lattice change at high temperatures is

small. Both of them are probably first-order transformations. Nevertheless, they are described here for the sake of convenience.

In Nb–Ru alloys, a similar transformation is found, exhibiting large bands that are probably internal twins.[360]

2.7 Tables of crystallographic properties of various martensites

Tables 2.4–2.9 are summaries of the crystallographic properties of various martensites reported in the literature.

TABLE 2.4 f.c.c. to b.c.c. (b.c.t.)

Alloy system	Composition (wt %)	Crystal structure of martensite	M_s (°C)	Orientation relationship[a]	Habit plane	Lattice defects[b]	Reference no.
Fe	—	α′ b.c.c.	< 720	—	—	—	
Fe–Ni	0–34 Ni	α′ b.c.c.	720 to −100	K–S (hi), N (lw)	{259} (lw)	tw $(112)_{\alpha'}$, ds	38–47, 58, 90, 100, 103, 105, 110, 129
Fe–Ni–Ti	30 at. % Ni, 3–8 at. % Ti	—	—	—	—	—	22–44
Fe–C	0–0.2 C	α′ b.c.c.	~460	—	{111}	ds	7–13, 36, 37, 65–70, 77, 81, 84, 113
	0.2–1.4 C	α′ b.c.t.	~100	K–S	{225} {259}	tw (112), ds	
	1.5–1.8 C	α′ b.c.t.	~0	K–S	{259}	tw (112) (011)	
Fe–N	0.7–3 N	α′ b.c.t.	—	—	—	—	16–19, 122–124
Fe–Ni–C	11.5–29 Ni, 0.4–1.2 C	α′ b.c.t.	—	—	—	tw (112) (011)	71, 75, 88, 109, 128
	22 Ni, 0.8 C	α′ b.c.t.	—	G–T	{259}	tw (112) (011)	48
Fe–Al–C	7–10 Al, 1.5–2.0 C	α′ b.c.t.	—	G–T	{3 10 15}	tw (112)	21, 125
Fe–Cr–C	2.8–8 Cr, 1.1–1.5 C	α′ b.c.t.	−36	—	{225}	tw (112) (011), ds (011)	41, 49, 111, 119, 125, 144, 361
Fe–Pt	25 at. % Pt	α′ b.c.c.	−50	~G–T	{3 10 15} {295}	tw $(112)_{\alpha'}$	362–365
Fe–Ir	0–53 Ir	α′ b.c.c.; ε h.c.p.	—	—	—	—	212, 366

[a] Key: K–S $\begin{cases}(111)_{fcc}\|(011)_{bcc}\\ [10\bar{1}]_{fcc}\|[\bar{1}1\bar{1}]_{bcc}\end{cases}$ N $\begin{cases}(111)_{fcc}\|(011)_{bcc}\\ [\bar{2}11]_{fcc}\|[01\bar{1}]_{bcc}\end{cases}$ G–T $\begin{cases}\{111\}_{fcc} \overset{1^\circ}{\sim} \{110\}_{bcc}\\ \langle 110\rangle_{fcc} \overset{2.5}{\sim} \langle 111\rangle_{bcc}\end{cases}$; lw, low temperature; hi, high temperature.

[b] Key: ds, dislocations; tw, internal twins.

TABLE 2.5 f.c.c. to b.c.c. (b.c.t.) and h.p.

Alloy system	Composition (wt %)	Crystal structure of martensite	M_s (°C)	Orientation relationship[a]	Habit plane	Lattice defects[b]	Reference no.
Fe–Mn	1–15 Mn	α′ b.c.c.	860–180	—	—	—	162–165
	13–25 Mn	ε h.c.p.	200–120	S–N	{111}	—	
Fe–Mn–C	—	α′, ε	—	—	—	—	168–189
Fe–Cr–Ni	17–18 Cr, 8–9 Ni	α′ b.c.c.	—	K–S	{225}	ds	75, 76, 78, 79, 169,
		ε h.c.p.	—	S–N	⟨111⟩ {111}	st(0001)	192–211, 367
Fe–Mn–Cr–Ni	—	α′ b.c.c.	—	K–S	{112}	—	201, 367
	—	ε h.c.p.	—	S–N	{111}	—	367

[a] S–N: $(111)_{fcc}\|(0001)_{hcp}$; $[11\bar{2}]_{fcc}\|[1\bar{1}00]_{hcp}$ or $[1\bar{1}0]_{fcc}\|[11\bar{2}0]_{hcp}$. [b] Key: ds, dislocations; st, stacking faults.

TABLE 2.6 f.c.c. to h.c.p. stacking structure

Alloy system	Composition (wt %)	Crystal structure of martensite	M_s (°C)	Orientation relationship[a]	Habit plane	Lattice defects[b]	Reference no.
Co	—	ε h.c.p.	—	S–N	{111}	—	146, 147, 153–161
Co–Ni	0–30 Ni	ε h.c.p.	380–20	S–N	{111}	st(0001)	149–151, 158, 368
Co–Be	10 at. % Be	ε h.c.p.	—	—	—	st(0001)	369
La	—	4H	—	—	—	—	370
Ce	—	4H	$\begin{pmatrix} M_s = -10, M_d = 225, \\ A_s = 110, A_f = 150 \end{pmatrix}$			—	371, 372

[a] S–N: $(111)_{fcc}\|(0001)_{hcp}$, $[11\bar{2}]_{fcc}\|[1\bar{1}00]_{hcp}$ or $[1\bar{1}0]_{fcc}\|[11\bar{2}0]_{hcp}$. [b] Key: st, stacking faults.

TABLE 2.7 b.c.c. to h.c.p. (or f.c.c.)[a]

Alloy system	Composition (wt %)	Crystal structure of martensite	M_s (°C)	Orientation relationship[a]	Habit plane	Lattice defects[b]	Reference no.
Ti	—	h.c.p.	800	B	{8 9 12} {133}	tw (10$\bar{1}$1), ds (0001)	220, 222, 225, 373–376
Ti–V	0–7.5, 13 V	h.c.p.	600–270	—	—	tw (10$\bar{1}$1)	230, 231, 377
Ti–Nb	0–25 at. % Nb	h.c.p.[c]	871–212	—	—	—	402, 403
	35 Nb	Ortho (α'')	~175	Ba	—	—	404
Ti–Ta	0–22 Ta	h.c.p. (α')	—	—	—	tw $(10\bar{1}1)_{\alpha'}$	378, 379
	23–53 Ta	Ortho (α'')	—	—	—	tw $(\bar{1}11)_{\alpha''}$	
Ti–Cr	6.9–20 Cr	h.c.p.	320–67	—	{334}	tw (10$\bar{1}$1), (1$\bar{1}$02)	225
	5.5–18.7 at. % Cr	h.c.p. + f.c.c.	—	K–S (f.c.c.)	—	—	235, 380, 381
Ti–Mo	6 Mo	h.c.p.	600	—	—	tw (10$\bar{1}$1), ds (0001)	382
	11 Mo	h.c.p.	340	B	(8 9 12)4°	—	381, 383
					($\bar{3}$44) 4°	—	
	11, 12.5 Mo	h.c.p.	340	—	—	—	384
Ti–Mn	4.3–5.2 Mn	h.c.p.	~300	B	{334} {344}	tw (10$\bar{1}$1)	224, 385
Ti–Fe	3 Fe	h.c.p. + [f.c.c.]	370	—	{334}	tw (10$\bar{1}$1)	229, 381, 386
Ti–Ni	2–5.45 Ni	h.c.p. ω	680–540	—	—	—	387, 388
Ti–Cu	0.56–8 Cu	h.c.p.	740–570	—	$\{10\bar{1}1\}_{\alpha'}$	tw (10$\bar{1}$1), (1$\bar{1}$02)	226–228
Ti–Al	8 Al	h.c.p. [f.c.c.]	—	—	—	—	232
Ti–Al–Mo–V	8 Al–1 Mo–2 V	h.c.p.	—	—	—	tw (10$\bar{1}$1)	233
Zr	—	h.c.p.	—	B (0–2°)	{569} {145}	—	219, 389–391

TABLE 2.7—*Continued*

Alloy system	Composition (wt %)	Crystal structure of martensite	M_s (°C)	Orientation relationship[a]	Habit plane	Lattice defects[b]	Reference no.
Zr–Nb	2.5–5.5 Nb	h.c.p.	650	B	{334}	tw $(10\bar{1}1)$, ds	236
Zr–Mo	11–12.5 Mo	h.c.p.	—	—	{334} {344}		384
Li	—	h.c.p.	−252	B (3°)	{441}	—	392–395, 400
Li[d]	—	f.c.c.	—	—	—	—	396
Li–Mg	0–40 Mg	h.c.p.	—	—	—	—	397, 398, 400
Na	—	h.c.p.	—	—	—	—	401

[a] Burgers (B) relations: $(110)_{bcc} \| (0001)_{hcp}$; $[\bar{1}11]_{bcc} \| [11\bar{2}0]_{hcp}$. (Angle in parentheses shows deviation.); Ba: $[100]_{\alpha''}^{2^\circ} \sim [111]_\beta$, $[010]_{\alpha''}^{2^\circ} \sim [110]_\beta$, $[001]_{\alpha''} \sim [110]_\beta$.

[b] Key: ds, dislocations; tw, internal twins.

[c] Slightly deformed to be orthorhombic.

[d] Cold-worked in liquid nitrogen.

TABLE 2.8 β **phase (b.c.c.) to close-packed layer structure in noble metals and alloys**

Alloy system	Composition (wt %)	Crystal structure: Parent phase	Crystal structure: Martensite	M_s (°C)	Orientation relationship[a]	Habit plane	Lattice defects[b]	Reference no.
Cu–Al	~11 Al	β	β' 9R	~450	—	—	st (0001)	245
	11–13 Al	β_1 DO_3	β_1' 9R	450–240	B (p 4°)[d] B″ (rev.)[e]	(133) (2°) ($12\bar{8}$)	st (0001)	245, 252, 255, 260, 405–409, 410, 411
	13–15 Al	β_1 DO_3	γ_1' 2H	~240	~B	(122) (3°)	tw ($10\bar{1}1$)	245, 264–266
Cu–Ga	20–25 at.% Ga	β_1 DO_3	β_1'	430–460	—	—	—	412–414
Cu–Al–Ni	12.8 Al, 7.7 Ni	β_1 DO_3	β_1 Γ_0, $\gamma_1'\Gamma_0$,	—	—	β_1', (155); γ_1', (277)	—	273
	14 Al, 4 Ni	β_1 DO_3	γ_1' Γ_0	−10 to −15	B′	(221)–(331)	tw ($10\bar{1}1$) st (0001)	268–275, 415, 416
Cu–Al–Mn	12.5–13.6 Al, 4–5.7 Mn	β_1 DO_3	γ_1' Γ_0	—	—	—	—	417, 418
Cu–Sn	23.35–24.5 Sn	β_1 DO_3	β_1' 4H	—	B	(223)	st ($10\bar{1}1$)	276, 281, 299
	24.5–24.5 Sn	β_1 DO_3	γ_1' 2H	—	B	(133)	tw ($10\bar{1}1$) st ($01\bar{1}1$)	276, 282, 419, 420
Cu–Zn	29–40 Zn	β_1 B2	β_1' 9R	—	B‴	(155) (166) (169)	st (0001)	284, 287–289, 291, 399, 421–423, 424–426
Cu–Zn[c]	45–48 Zn	β_1 B2	—	—	—	(2 11 12)–(110)	—	427
Cu–Zn–Si	33.5 Zn, 1.8 Si	β_1 B2	β_1' 9R + f.c.c.	30	—	—	—	259
	27 Zn, 5.0 Si	β_1 B2	β_1' 9R + f.c.c.	200	—	—	—	259
Cu–Zn–Al	0–36 at. % Zn 3–20 at. % Al	—	—	—	—	—	—	258

TABLE 2.8—*Continued*

Alloy system	Composition (wt %)	Crystal structure: Parent phase	Crystal structure: Martensite	M_s (°C)	Orientation relationship[a]	Habit plane	Lattice defects[b]	Reference no.
Cu–Zn–Ga	—	—	—	—	—	—	—	257, 428, 429
Au–Cu–Zn	20.7 Cu, 30.9 Zn	β	$\beta'T_0$	—	B′	(133)–(011)	—	267, 293, 294, 430
Au–Cu–Zn	$Au_xCu_{55-x}Zn_{45}$	—	β_1' 18R γ_1' 2H	—	—	—	—	263
Ag–Cd	50–53 at. % Cd	β	Γ_0	—	—	—	—	431, 432
	44–47 at. % Cd	β_1 B2	2H	−44–137		(133)		302, 303
Ag–Zn	49 at. % Zn	β_1 B2	h.c.p., f.c.c.	—	—	—	—	433–436
Ag–Ge	15 at. % Ge	β	h.c.p., f.c.c.	—	—	—	—	437
Au–Zn	48–56 at. % Zn	β' B2	$Pmc2_1$	−252 to −168	B′	‖⟨110⟩	—	438–440
Au–Cd	45–46.5 at. % Cd	β	α' f.c.c.	—	—	—	tw (111), st (111)	301
	46.5–47.5 at. % Cd	β_1 B2	β_1' 9R	—	—	—	st (0001)	301
	47.5 at. % Cd	β_1 B2	γ_1' 2H	60–30[f]	B	(133)	tw ($10\bar{1}1$) st (0001)	300, 301, 441–444

Au–Cd–Cu	47.5, 49.0 at.% Cd 0–5 at.% Cu	β_1 B2	Trig.	60 to −180	—	—	—	445, 446
Au–Cd–M[g]	50 at.% Cd, M	β_1 B2	—	—	—	—	—	447
Ni–Ti	50.0 at.% Ti	B2	12R, 4H	—	—	—	st (001)	309, 338
	50.3% at. Ti	B2[h]	~B19	−40 to −50	B (p 65°)[i]	—	tw ($11\bar{1}$) st (001)	311, 312
Ni–Al	34–38 at.% Al	B2	Ll_0 (AuCu)	—	—	—	tw (111)	448–450
Ni–Al	39–41 at.% Al	—	—	873–243	—	—	tw (111)	449, 450
Ni–Sn	25 at.% Sn	DO_3	γ' 2H	—	—	—	—	451

[a] B′, $(101)_{\beta_1}\|(001)_{\gamma_1'}$, $[010]_{\beta_1}\|[010]_{\gamma_1'}$; B″, $(110)_{\beta_1}\|(12\bar{8})_{\beta_1'}$, $[1\bar{1}1]_{\beta_1}\|[2\bar{1}0]_{\beta_1'}$; B‴, $(001)_{\beta_1}\|(104)_{\beta_1'}$, $[010]_{\beta_1}\|[010]_{\beta_1'}$.
[b] Referred to the hexagonal indices even in the orthorhombic crystal. Key: st, stacking faults; tw, internal twins; Γ_O, simple orthorhombic.
[c] Cold worked.
[d] Deviation 4° in the plane relation.
[e] In the reverse transformation.
[f] The critical temperature of order–disorder change is just below the melting point.
[g] M: In, Hg, Mg, Zn.
[h] The size of the unit cell is three times the B2 lattice.
[i] Deviation 65° in the plane relation.

TABLE 2.9 Other alloys

Alloy system	Composition (wt %)	Crystal structure: Parent phase	Crystal structure: Martensite	M_s (°C)	Orientation relationship[a]	Habit plane	Lattice defects[b]	Reference no.
In–Tl	20.75 at. % Tl	β f.c.c.	α f.c.t.	53	S	—	tw (101)	340–343
In–Cd	4–5 Cd	β f.c.c.	α f.c.t.	60	S	—	—	346
Mn–Cu	5–40 Cu	β f.c.c.	α f.c.t.	—	—	—	tw (101)	348, 350, 452
Mn–Ni	13–15 at. % Ni	β f.c.c.	α ($c/a<1$)	—	—	—		351, 353
	14–22 at. % Ni	β f.c.c.	α ($c/a>1$)	—	—	—	—	
	50 at. % Ni	B2	θ CuAlI	—	—	—	—	357
Mn–Au	45–55 at. % Au	c B2	t_1 b.c.t.	—	—	—	tw (101)	354
	45–50 at. % Au	t_1 b.c.t.($c/a<1$)	t_2 b.c.t.($c/a>1$)	—	—	—		354
Ru–Ta	45–55 at. % Ta	μ' B2	μ' b.c.t.	1370–700	—	—	plane	359
	50–52.5 at. % Ta	μ'' b.c.t.	μ' b.c.o.	820–680	—	—	tw	359
U–Mo	5 at. % Mo	γ b.c.c.	$\alpha\Gamma_0'$	—	—	—	tw {130} {021} {112} {111}	453, 454
U–Cr	1, 1.4 at. % Cr	β tet	$\alpha\Gamma_0'$	270	(a)–(c)	(321) (441)		455–457

U–Ti	0–6% Ti	γ f.c.c.	$\alpha\,\Gamma_0$	—	—	—	tw	458, 459
Nb_3Sn	23–25 at.% Sn	β–W	Γ_t	~40 K	—	—	—	460–465
V_3Si	—	β–W	Γ_t	~22 K	—	—	—	462, 466, 467
V_3Ga	—	β–W	Γ_t	~50 K	—	—	—	468
Pu	—	β 12/m	$\alpha\,P2_1/m$[c]	120°	N–B	—	—	469
Ce	—	—	4H	—	—	—	—	470
Hg[d]	—	α f.c. Rh[f] (98°22′)	γ f.c. Rh[f] (~82°)	—	—	$\{\bar{1}13\}\langle 110\rangle$	—	471
$Ar–N_2$	0–50 mol% N_2	h.c.p.	f.c.c.	$M_d = 76$ −22°K[c]	—	—	—	472, 273
$Ar–O_2$	0–20 mol% O_2	h.c.p.	f.c.c.	$M_d = 76$ −20°K[e]	—	—	—	473

[a] (a) $\{101\}_\beta \| (001)_\alpha$; (b) $\{212\}_\beta \| (001)_\alpha$; (c) $\{410\}_\beta \| (001)_\alpha$; S: $(111)_\beta \| (111)_{\alpha'}$, $[01\bar{1}]_\beta \| [01\bar{1}]_{\alpha'}$; N–B: $(010)_\alpha \| (\bar{1}11)_\beta$, $[10\bar{2}]_\alpha \| [32\bar{1}]_\beta$.

[b] Key: tw, internal twins.

[c] The atomic arrangement is complicated. The transformation is accompanied by some individual movement of atoms besides shuffling of the atomic layers.

[d] Cold worked in liquid helium.

[e] The transformation does not occur without deformation.

[f] Rh: rhombohedral.

References

1. A. Sauveur, *Trans. AIME* **73**, 859 (1926).
2. F. C. Frank, *NPL Conf. Relation Between Structure Strength Met. Alloys* p. 248. HM Stationary Office, London, 1963.
3. J. W. Christian, Iron Steel Inst. Spec. Rep. 93, p. 1 (1965).
4. W. D. Kingery, "Introduction to Ceramics." Wiley, New York, 1960.
5. A. G. Guy, *Metall. Trans.* **3**, 2535 (1972).
6. A. B. Greninger, *Trans. AIME* **120**, 393 (1936).
7. W. Fink and E. Campbell, *Trans. Am. Soc. Steel Treat.* **9**, 717 (1926).
8. N. Seljakov, J. Kurdumoff, and N. Goodtzow, *Nature (London)* **119**, 494 (1927).
9. W. B. Pearson, "Handbook of Lattice Spacings and Structure of Metals and Alloys," p. 921. Pergamon, Oxford, 1958.
10. K. Honda and Z. Nishiyama, *Sci. Rep. Tohoku Univ.* **21**, 299 (1932).
11. C. S. Roberts, *Trans. AIME* **197**, 203 (1953).
12. C. S. Roberts, B. L. Averbach, and M. Cohen, *Trans. ASM* **45**, 576 (1953).
13. P. G. Winchell and M. Cohen, *Trans. ASM* **55**, 347 (1962).
14. K. H. Jack, *Proc. Roy. Soc.* **A208**, 200 (1951).
15. W. Seith, "Diffusion in Metallen," p. 125. Springer-Verlag, Berlin, 1939.
16. M. Tsuchiya, M. Izumiyama, and Y. Imai, *Sci. Rep. RITU* **A17**, 173 (1965); Sci. Rep. 50th Anniv. p. 207 (1966).
17. B. N. Bose and M. F. Hawkes, *J. Met.* **188**, 307 (1950).
18. W. Pitsch, *Phil. Mag.* **4**, 577 (1958).
19. T. Bell and W. S. Owen, *J. Iron Steel Inst.* **205**, 428 (1967).
20. Z. Nishiyama, *Sci. Rep. Tohoku Univ.* **24**, 128, 517 (1935).
21. M. Watanabe and C. M. Wayman, *Scr. Metall.* **5**, 109 (1971).
22. Y. Honnorat, G. Henry, and J. Manenc, *Mém. Sci. Mét.* **62**, 429 (1965).
23. Y. Honnorat, G. Henry, G. Murry, and J. Manenc, *C. R. Acad. Sci. Paris* **260**, 221 (1965).
24. J. K. Abraham and J. S. Pascover, *Trans. AIME* **245**, 759 (1969).
25. R. E. Miner, *Metall. Trans.* **2**, 1250 (1971).
26. R. Oshima and C. M. Wayman, *Metall. Trans.* **3**, 2163 (1972).
27. A. K. Shevelev, *Sov. Phys.-Dokl.* **3**, 1254 (1958).
28. P. M. Strocchi, B. A. Melandri, and A. Tamba, *Nuovo Cimento* **B51**, 1 (1967).
29. R. C. Ruhl and M. Cohen, *Trans. AIME* **245**, 253 (1969).
30. A. Lucci, G. Della Gatta, and G. Venturello, *Met. Sci. J.* **3**, 14 (1969).
31. J. L. Swisher and E. T. Turkdogang, *Trans. AIME* **239**, 426 (1967).
32. E. Hornbogen, A. Segmüller, and G. Wassermann, *Z. Metall.* **48**, 379 (1957).
33. P. G. Winchell and G. R. Speich, *Acta Metall.* **18**, 53 (1970).
34. J. W. Cahn and W. Rosenberg, *Scr. Metall.* **5**, 101 (1971).
35. L. Zwell, D. E. Carnahan, and G. R. Speich, *Metall. Trans.* **1**, 1007 (1970).
36. G. Kurdjumov and G. Sachs, *Z. Phys.* **64**, 325 (1930).
37. P. Dörnen and W. Hofman, *Arch. Eisenhütt.* **30**, 627 (1959).
38. Z. Nishiyama, *Sci. Rep. Tohoku Univ.* **23**, 637 (1934).
39. G. Wassermann, *Mitt. K-W-I Eisenforsch.* **17**, 149 (1935)
40. R. F. Mehl and G. Derge, *Trans. AIME* **125**, 482 (1937).
41. H. M. Otte, *Acta Metall.* **8**, 892 (1960).
42. A. Kochendörfer and G. Otto, *Arch. Eisenhütt.* **30**, 227 (1959).
43. J. F. Breedis and C. M. Wayman, *Trans. AIME* **224**, 1128 (1962).
44. I. P. Sorokin, *Fiz. Met. Metall.* **30**, 653 (1970).

45. W. Pitsch, *Arch. Eisenhütt.* **30**, 503 (1959); *J. Inst. Met.* **87**, 444 (1959); *Phil. Mag.* **4**, 577 (1959).
46. Z. Nishiyama, K. Shimizu, and K. Sugino, *Acta Metall.* **9**, 620 (1961); *Mem. ISIR Osaka Univ.* **18**, 71 (1961).
47. A. J. Bogers, *Acta Metall.* **10**, 260 (1962).
48. A. B. Greninger and A. R. Troiano, *Trans. AIME* **145**, 289 (1941); **185**, 590 (1949).
49. C. M. Wayman, J. E. Hanafee, and T. A. Read, *Acta Metall.* **9**, 391, 912 (1961).
50. F. Förster and E. Scheil, *Z. Metall.* **32**, 165 (1940).
51. S. Takeuchi, T. Honma, and H. Suzuki, *J. Jpn. Inst. Met.* **21**, 51 (1957).
52. T. Honma, *J. Jpn. Inst. Met.* **21**, 122, 126, 263 (1957).
53. J. C. Bokros and E. R. Parker, *Acta Metall.* **11**, 1291 (1963).
54. R. Brook and A. R. Entwisle, *J. Iron Steel Inst.* **203**, 905 (1965).
55. R. G. Davies and C. L. Magee, *Metall. Trans.* **1**, 2927 (1970).
56. H. Suzuki and T. Honma, *J. Met.* **4**, 519 (1952).
57. Z. Nishiyama and K. Shimizu, *Acta Metall.* **6**, 125 (1958); *Mem. ISIR, Osaka Univ.* **15**, 105 (1958).
58. R. L. Patterson and C. M. Wayman, *Acta Metall.* **14**, 347 (1966).
59. H. G. Bowden and P. M. Kelly, *Acta Metall.* **15**, 1489 (1967).
60. R. P. Zerwekh and C. M. Wayman, *Acta Metall.* **13**, 99 (1965).
61. R. P. Reed, U.S. Dept. of Commerce, Nat. Bur. Std. Rep. 9256 (1966).
62. M. Okada and Y. Arata, *Tech. Rep. Osaka Univ.* **5**, 169 (1955).
63. J. A. Klostermann and W. G. Burgers, *Acta Metall.* **12**, 355 (1964).
64. M. M. Shteynberg, Yu. N. Goykhenberg, D. A. Mirzayev, and O. P. Morozov, *Fiz. Met. Metall.* **30**, 1200 (1970).
65. R. F. Mehl and D. M. Van Winkle, *Rev. Métall.* **50**, 465 (1953).
66. A. B. Greninger and A. R. Troiano, *Trans. AIME* **140**, 307 (1940).
67. E. E. Lähteenkorva, Ann. Acad. Sci. Fennicæ, A. VI, Physica No. 86 (1961).
68. C. J. Altstetter and C. M. Wayman, *Acta Metall.* **10**, 992 (1962).
69. A. R. Entwisle, "The Mechanism of Phase Transformations in Metals," p. 315. Inst. of Metals, London, 1956.
70. A. R. Marder and G. Krauss, *Trans. ASM* **62**, 957 (1969).
71. V. V. Nemirovskiy, *Fiz. Met. Metall.* **25** 900 (1968).
72. F. J. Schoen, J. L. Nilles, and W. S. Owen, *Metall. Trans.* **2**, 2489 (1971).
73. P. M. Kelly and P. McDougall, *Metall. Trans.* **3**, 2294 (1972).
74. J. S. Bowles, *Acta Crystall.* **4**, 162 (1951).
75. P. M. Kelly and J. Nutting, *J. Iron Steel Inst.* **197**, 199 (1961).
76. R. P. Reed, *Acta Metall.* **10**, 865 (1962).
77. J. M. Chilton, C. J. Barton, and G. R. Speich, *J. Iron Steel Inst.* **208**, 184 (1970).
78. J. A. Venable, *Phil. Mag.* **7**, 35 (1962).
79. A. G. Crocker and B. A. Bilby, *Acta Metall.* **9**, 678 (1961).
80. V. M. Schastlivtsev, *Fiz. Met. Metall.* **33**, 326 (1972).
81. E. S. Machlin and M. Cohen, *Trans. AIME* **191**, 1019 (1951).
82. D. P. Dunne and C. M. Wayman, *Acta Metall.* **18**, 981 (1970).
83. S. M. Abdykulova, V. G. Gorbach, and Ye. A. Izmaylov, *Fiz. Met. Metall.* **26**, 144 (1968).
84. A. R. Marder and G. Krauss, *Trans. ASM* **60**, 651 (1967).
85. Z. Nishiyama and K. Shimizu, *Tetsu to Hagane* **50**, 2215 (1964).
86. For example, W. S. Owen, E. A. Wilson, and T. Bell; "Zackey: High Strength Materials," Chapter 5, p. 167. Wiley, New York, 1964.
87. K. Shimizu and H. Okamoto, *J. Jpn. Inst. Met.* **35**, 204 (1971).
88. S. K. Das and G. Thomas, *Metall. Trans.* **1**, 325 (1970).

89. C. M. Wayman, *Metall. Trans.* **1**, 2009 (1970).
90. I. N. Bogachev, N. V. Zvigintsev, and V. M. Faber, *Fiz. Met. Metall.* **27**, 720 (1969).
91. J. K. Abraham and J. S. Pascover, *Trans. AIME* **245**, 759 (1969).
92. G. Thomas and S. K. Das, *J. Iron Steel Inst.* **209**, 801 (1971).
93. G. Thomas, *Metall. Trans.* **2**, 2373 (1971).
94. W. Wirth and J. Bickerstaffe, *Metall. Trans.* **3**, 3260 (1972).
95. D. S. Sarma and J. A. Whiteman, *Metall. Trans.* **3**, 3264 (1972).
96. Z. Nishiyama, *I. U. Cr. Congr., 3rd, Paris Symp.* p. 5 (1954).
97. Z. Nishiyama, K. Shimizu, and S. Sato, *J. Jpn. Inst. Met.* **20**, 325, 386 (1956); *Mem. ISIR Osaka Univ.* **13**, 1 (1956).
98. S. Takeuchi and T. Honma, *Phys. Soc. Jpn. Spring Meeting* Branch 6, p. 88 (1955).
99. Z. Nishiyama, K. Shimizu, and R. Kawanaka, *J. Jpn. Inst. Met.* **23**, 311 (1959); *Mem. ISIR Osaka Univ.* **16**, 87 (1959).
100. Z. Nishiyama and K. Shimizu, *Acta Metall.* **7**, 432 (1959).
101. K. Shimizu, *J. Phys. Soc. Jpn.* **17**, 508 (1962).
102. R. P. Reed, *Acta Metall.* **15**, 1287 (1967).
103. P. C. Rowlands, E. O. Fearon, and M. Bevis, The Mechanism of Phase Transformation in Crystal Solids. Inst. Met. Spec. Rep. No. 33, p. 194 (1969).
104. M. G. H. Wells, *Acta Metall.* **12**, 389 (1964).
105. T. J. Patrician, H. M. Ledbetter, and R. P. Reed, *Acta Metall.* **3**, 947 (1972).
106. K. Otsuka and K. Shimizu, *Bull. Jpn. Inst. Met.* **11**, 12 (1972).
107. Z. Nishiyama, K. Shimizu, and S. Katagiri, *Mem. ISIR Osaka Univ.* **21**, 51 (1964).
108. P. B. Hirsch, A. Howie, and M. J. Whelan, *Phil. Trans. Roy. Soc.* **A252**, 499 (1960).
109. O. Johari and G. Thomas, *Acta Metall.* **13**, 1211 (1965).
110. G. Krauss and W. Pitsch, *Acta Met.* **12**, 278 (1964); *Arch. Eisenhütt.* **35**, 667 (1964); *Trans. AIME* **233**, 919 (1965).
111. K. Shimizu and C. M. Wayman, *Acta Metall.* **14**, 1390 (1966).
112. P. C. Rowland, E. O. Fearon, and M. Bevis, *J. Mater. Sci.* **5**, 769 (1970).
113. P. M. Kelly and J. Nutting, *Proc. Roy. Soc.* **A259**, 45 (1960).
114. G. S. Ansell, V. I. Lizunov, and R. W. Messler, Jr., *Trans. JIM* **9** (*Suppl.*), 933 (1968).
115. P. C. Sekhar, M. E. Schreiner, and M. H. Richman, *Field Emission Symp. 17th, Connecticut* p. 45 (1970).
116. P. C. Sekhar and M. H. Richman, *Metallography* **4**, 133 (1971).
117. B. N. Ranganathan and H. E. Grenga, *Phil. Mag.* **26**, 265 (1972).
118. M. Oka and C. M. Wayman, *Trans. AIME* **242**, 337 (1968); *Trans. ASM* **62**, 370 (1969).
119. M. Oka and C. M. Wayman, *Trans. JIM* **10**, 411 (1969).
120. V. I. Izotov and L. M. Utevskiy, *Fiz. Met. Metall.* **25**, 98 (1968).
121. P. G. McDougall and J. S. Bowles, *Acta Metall.* **12**, 779 (1964).
122. Y. Imai, M. Izumiyama, and M. Tsuchiya, *Sci. Rep. RITU*, 50th Ann., p. 207 (1966).
123. M. G. A. Biswas and I. Cood, *J. Iron Steel Inst.* **206**, 496 (1968).
124. K. J. Albutt and S. Garber, *J. Iron Steel Inst.* **206**, 1037 (1968).
125. K. Shimizu, M. Oka, and C. M. Wayman, *Acta Metall.* **19**, 1 (1971).
126. Z. Nishiyama, K. Shimizu, and M. Harada, *Trans. JIM* **11**, 152 (1970).
127. M. Watanabe and C. M. Wayman, *Metall. Trans.* **2**, 2221 (1971).
128. I. Tamura, H. Yoshimura, M. Ibaragi, and M. Tagaya, *J. Jpn. Inst. Met.* **27**, 206 (1963).
129. R. L. Patterson and C. M. Wayman, *Acta Metall.* **12**, 1306 (1964).
130. T. Maki, S. Shimooka, and I. Tamura, *Metall. Trans.* **2**, 2944 (1971).
131. T. Maki, S. Shimooka, M. Umemoto, and I. Tamura, *Trans. JIM* **13**, 400 (1972).
132. V. V. Golikova and V. I. Izotov, *Fiz. Met. Metall.* **34**, 1323 (1972).
133. T. Maki, S. Shimooka, T. Arimoto, and I. Tamura, *Trans. JIM* **14**, 62 (1973).
134. F. F. Lucas, *Trans. Am. Soc. Steel Treat.* **6**, 669 (1924).

135. A. Sauveur, "The Metallography and Heat Treatment of Iron and Steel." McGraw-Hill, London, 1938.
136. C. H. Desch, "The Chemistry of Solid." Cornell Univ. Press, Ithaca, New York, 1934.
137. E. Scheil, *Arch. Eisenhütt* **9**, 61 (1935).
138. Z. Nishiyama and K. Shimizu, *J. Electronmicrosc.* **4**, 51 (1956).
139. Z. Nishiyama, S. Sato, K. Shimizu, and M. Doi, *J. Electronmicrosc.* **5**, 4 (1956).
140. T. Tadaki, T. Sahara, and K. Shimizu, *J. Jpn. Inst. Met.* **35**, 609 (1971); *Mem. ISIR Osaka Univ.* **29**, 85 (1972).
141. H. J. Neuhäuser and W. Pitsch, *Acta Metall.* **19**, 337 (1971).
142. Z. Nishiyama, K. Shimizu, and A. Kamada, *Acta Metall.* **12**, 446 (1964); *Trans. JIM* **6**, 40 (1965).
143. H. Suzuki, M. Tanino, and K. Aoki, *Jpn. J. Appl. Phys.* **5**, 879 (1966).
144. V. I. Izotov and L. M. Utevskiy, *Fiz. Met. Metall.* **25**, 751 (1968).
145. H. Masumoto, *Sci. Rep. Tohoku Imp. Univ.* **15**, 461 (1928).
146. H. Shoji, *Z. Kristallogr.* **77**, 381 (1931).
147. Z. Nishiyama, *Sci. Rep. Tohoku Imp. Univ.* **25**, 79 (1936).
148. W. C. Ellis and E. S. Greiner, *Trans. ASM* **29**, 215 (1941).
149. S. Takeuchi and T. Honma, *J. Jpn. Inst. Met.* **19**, 652 (1955); *Sci. Rep. RITU* **A9**, 508 (1957).
150. H. Bibring, *Acta Metall.* **7**, 684 (1959).
151. H. Bibring, G. Lenoir, and F. Sebilleau, *Rev. Métall.* **56**, 279 (1959).
152. P. Gaunt and J. W. Christian, *Acta Metall.* **7**, 529 (1959).
153. O. S. Edwards and H. Lipson, *Proc. Roy. Soc.* **A180**, 268 (1942).
154. O. S. Edwards and H. Lipson, *J. Inst. Met.* **69**, 177 (1943).
155. C. R. Houska, B. L. Averbach, and M. Cohen, *Acta Metall.* **8**, 81 (1960).
156. A. J. C. Wilson, *Proc. Roy. Soc.* **A180**, 277 (1942).
157. S. Ogawa, D. Watanabe, Y. Onuma, and K. Shiraishi, *J. Electronmicrosc.* **8**, 159 (1959).
158. D. Watanabe, S. Fujime, and S. Ogawa, *J. Phys. Soc. Jpn. Suppl. B-II* **17**, 205 (1962); *J. Phys. Soc. Jpn.* **19**, 711 (1964).
159. L. Habraken, *J. Inst. Met.* **90**, 85 (1961/62).
160. E. Votava, *J. Inst. Met.* **90**, 129 (1961/62); *Acta Metall.* **8**, 901 (1960).
161. R. T. Johnson and R. D. Dragsdorf, *J. Appl. Phys.* **38**, 618 (1967).
162. T. Ishiwara, *Kinzoku no Kenkyu* **7**, 115 (1930).
163. W. Schmidt, *Arch. Eisenhütt.* **3**, 293 (1929/30).
164. V. N. Krovobok, *Trans. Am. Soc. Steel Treat.* **15**, 893 (1929).
165. H. Schumann, *Arch. Eisenhütt.* **38**, 647 (1967); **40**, 1027 (1969).
166. H. Schumann and J. Dührkop, *Neue Hütte* **17**, 18 (1972).
167. H. Schumann, *Neue Hütte* **17**, 203 (1972).
168. M. Oka, Y. Tanaka, and K. Shimizu, *Jpn. Inst. Met.*, Fall Meeting, p. 116 (1970).
169. P. M. Kelly, *Acta Metall.* **13**, 635 (1965).
170. L. I. Lysak and B. I. Nikolin, *Fiz. Met. Metall.* **17**, 708 (1964).
171. B. Cina, *Acta Metall.* **6**, 748 (1958).
172. Z. Nishiyama and H. Arima, *J. Jpn. Inst. Met.* **6**, 569 (1942).
173. Y. Imai and T. Saito, *J. Jpn. Inst. Met.* **25**, 57 (1961).
174. G. Collette, C. Crussart, A. Kohn, J. Plateau, G. Pomey, and M. Weisz, *Rev. Métall.* **54**, 433 (1957).
175. C. H. White and R. W. K. Honeycombe, *J. Iron Steel Inst.* **200**, 457 (1962).
176. G. P. Sanderson and R. W. Honeycombe, *J. Iron Steel Inst.* **200**, 934 (1962).
177. Y. Imai and T. Saito, *J. Jpn. Inst. Met.* **26**, 73, 77 (1962).
178. Y. Imai and T. Saito, *J. Jpn. Inst. Met.* **26**, 283 (1962).
179. K. Hans v. Klitzing and W. Wesselhöft, *Arch. Eisenhütt.* **26**, 755 (1955).

180. L. S. Yershova, I. N. Bogachev, and R. S. Shklyar, *Fiz. Met. Metall.* **12**, 670 (1961).
181. L. S. Yershova and I. N. Bogachev, *Fiz. Met. Metall.* **13**, 107 (1962).
182. K. Ono, *J. Jpn. Inst. Met.* **13**, 22 (1949).
183. T. Saito, *Trans. JIM* **6**, 240 (1965).
184. L. I. Lysak and B. I. Nikolin, *Fiz. Met. Metall.* **17**, 40, 703 (1964).
185. Z. Nishiyama, K. Shimizu, and M. Oka, *J. Jpn. Inst. Met.* **22**, 532 (1958); *Mem. ISIR, Osaka Univ.* **16**, 73 (1959).
186. Z. Nishiyama and K. Shimizu, *J. Phys. Soc. Jpn.* **15**, 1963 (1960).
187. Z. Nishiyama, M. Oka, and H. Nakagawa, *Trans. JIM* **28**, 403 (1964).
188. K. Suemune and K. Ooka, *J. Jpn. Inst. Met.* **30**, 428 (1966).
189. I. N. Bogachev, L. V. Zhuravel, and V. F. Yegolayev, *Fiz. Met. Metall.* **25**, 708 (1968).
190. I. N. Bogachev and L. S. Malinov, *Fiz. Met. Metall.* **14**, 828 (1962).
191. I. N. Bogachev and V. F. Yegolayev, *Fiz. Met. Metall.* **16**, 710 (1963).
192. B. Cina, *J. Iron Steel Inst.* **177**, 406 (1954).
193. H. C. Fiedler, B. L. Averbach, and M. Cohen, *Trans. ASM* **47**, 267 (1955).
194. P. Bastien and J. M. B. Dedieu, *J. Iron Steel Inst.* **183**, 254 (1956).
195. H. M. Otte, *Acta Metall.* **5**, 614 (1957).
196. J. Ménard and L. Weil, *C. R. Acad. Sci. Paris* **250**, 4160 (1960).
197. R. P. Reed, *Acta Metall.* **10**, 865 (1962).
198. H. Schumann and H. J. von Fircks, *Arch. Eisenhütt.* **40**, 561 (1969).
199. R. Voyer, F. Bertaut, and J. Geneste, *C. R. Acad. Sci. Paris* **258**, 4975 (1964).
200. Y. Imai, M. Izumiyama, and K. Sasaki, *Sci. Rep. Tohoku Univ.* **A18**, 39 (1966).
201. H. Schumann, *Arch. Eisenhütt.* **4**, 1169 (1970).
202. Z. Nishiyama, K. Shimizu, and S. Morikawa, *J. Jpn. Inst. Met.* **27**, 497 (1963); *Mem. ISIR Osaka Univ.* **21**, 41 (1964).
203. B. Cina, *Acta Metall.* **6**, 748 (1958).
204. R. Lagneborg, *Acta Metall.* **12**, 823 (1964).
205. L. Mangonon, Jr. and G. Thomas, *Metall. Trans.* **1**, 1577 (1970).
206. J. A. Venables, *Phil. Mag.* **7**, 35 (1962).
207. J. F. Breedis and W. D. Robertson, *Acta Metall.* **10**, 1077 (1962); **11**, 547 (1963).
208. J. F. Breedis, *Trans. AIME* **230**, 1583 (1964); *Acta Metall.* **13**, 239 (1965).
209. J. Dash and H. M. Otte, *Int. Congr. Electron Microsc., 5th* HH-4 (1962); *Acta Metall.* **11**, 1169 (1963).
210. H. M. Otte and J. Dash, *Eur. Conf. Electron Microsc., 3rd, Prague* (1964).
211. A. J. Goldman, W. D. Robertson, and D. A. Koss, *Trans. AIME* **230**, 240 (1964).
212. E. A. Plekhanova, S. Kh. Kurumchina, and V. F. Yegolayev, *Fiz. Met. Metall.* **27**, 473 (1969).
213. M. Miyagi and C. M. Wayman, *Trans. AIME* **236**, 806 (1966).
214. M. Fallot, *Ann. Phys.* **10**, 291 (1938).
215. L. D. Blackburn, L. Kaufman, and M. Cohen, *Acta Metall.* **13**, 533 (1965).
216. H. Schumann, *Z. Metall.* **58**, 207 (1967).
217. C. S. Barrett, *Trans. AIME* **188**, 123 (1950); "Imperfection in Nearly Perfect Crystals," p. 97, 1952; *Trans. AIME* **188**, 123 (1950).
218. S. D. Dahlgren, W. F. Flanagan, and D. H. Polonis, *Trans. AIME* **236**, 1071 (1966).
219. W. G. Burgers, *Physica* **1**, 561 (1934).
220. Z. Nishiyama, M. Oka, and H. Nakagawa, *Trans. JIM* **7**, 168, 174 (1966).
221. N. E. Paton, and W. A. Backofen, *Trans. AIME* **245**, 1369 (1969).
222. J. K. Mackenzie and J. S. Bowles, *Acta Metall.* **5**, 137 (1957).
223. K. Schwartzkoff, *Acta Metall.* **17**, 345 (1969).
224. C. Hammond and P. M. Kelly, *Acta Metall.* **17**, 869 (1969).
225. R. H. Erikson, R. Taggart, and D. H. Polonis, *Acta Metall.* **17**, 553 (1969).

226. S. Fujishiro and H. L. Gegel, *Int. Congr. Electron Microsc., 6th*, 441 (1966).
227. J. C. Williams, R. Taggart, and D. H. Polonis, *Metall. Trans.* **1**, 2265 (1970).
228. A. Zangvil, S. Yamamoto, and Y. Murakami, *Metall. Trans.* **4**, 467 (1973).
229. Z. Nishiyama, M. Oka, and H. Nakagawa, *J. Jpn. Inst. Met.* **30**, 16 (1966).
230. J. C. McMillan, R. Taggart, and D. H. Polonis, *Trans. AIME* **239**, 739 (1967).
231. M. Oka, C. S. Lee, and K. Shimizu, *Metall. Trans.* **3**, 37 (1972).
232. W. K. Armitage, Iron and Steel Inst., Spec. Rep. No. 93, p. 76 (1965).
233. R. H. Erikson, R. Taggart, and D. H. Polonis, *Trans. AIME* **245**, 359 (1969).
234. M. J. Blackburn, *Trans. ASM* **59**, 876 (1966).
235. D. Whitwham, *Mém. Sci. Rev. Métall.* **57**, 1 (1960).
236. S. Banerjee and R. Krishnan, *Acta Metall.* **19**, 1317 (1971).
237. G. T. Higgins and E. Banks, *Iron Steel Inst.* Spec. Rep., **93**, 102 (1965).
238. C. D. Williams and R. W. Gilbert, *Trans. JIM* **9**, *Suppl.* 625 (1968).
239. T. B. Massalski and H. W. King, *Progr. Mater. Sci.* **10**, 1 (1961).
240. P. Furrer, T. R. Anantharaman, and M. Warlimont, *Phil. Mag.* **21**, 873 (1970).
241. L. C. Ramsdell, *Am. Mineralog.* **32**, 64 (1947).
242. H. Sato, *Metall. Soc. Conf.* **29**, 295 (1963); *J. Cryst. Soc. Jpn.* **10**, 50 (1968).
243. G. S. Zhdanov and Z. V. Minervina, *C. R. Akad. Sci. USSR* **48**, 182 (1945).
244. A. L. Patterson and J. S. Kasper, "International Tables for X-ray Crystallography," Vol. II, p. 344. *Intern. Union Cryst.* 1959.
245. P. R. Swann and H. Warlimont, *Acta Metall.* **11**, 511, 1099 (1963).
246. H. Sato, R. S. Toth, and G. Honjo, Pub. Preprint, Sci. Lab., Ford Motor Co. (Nov. 3, 1965); *J. Phys. Chem. Solid* **28**, 137 (1967).
247. S. Kajiwara, *J. Phys. Soc. Jpn.* **22**, 795 (1967).
248. V. Gawranek, E. Kaminsky, and G. Kurdjumov, *Metallwirtschaft* **17**, 370 (1935).
249. H. Mitani and N. Nakanishi, *J. Jpn. Inst. Met.* **22**, 208 (1958); **23**, 48 (1959); **24**, 748 (1960); **25**, 639 (1961).
250. N. Nakanishi, *Trans. JIM* **2**, 37 (1961); *Bull. Univ. Osaka Pref.* **A9**, 95, 109 (1961).
251. J. Jellison and E. P. Klier, *Trans. AIME* **233**, 1694 (1965).
252. Z. Nishiyama and S. Kajiwara, *Jpn. J. Appl. Phys.* **2**, 478 (1963); *Trans. JIM* **3**, 127 (1962); *Mem. ISIR Osaka Univ.* **19**, 59 (1962).
253. H. Warlimont and M. Wilkens, *Z. Metall.* **56**, 850 (1965).
254. J. Kakinoki, *J. Cryst. Soc. Jpn.* **7**, 66 (1965); **8**, 15 (1966).
255. R. S. Toth and H. Sato, *Acta Metall.* **15**, 1397 (1967).
256. J. Brettschneider and H. Warlimont, *Z. Metall.* **59**, 740 (1968).
257. L. Delaey and H. Warlimont, *Z. Metall.* **56**, 437 (1965); **57**, 793 (1966).
258. L. Delaey, *Z. Metall.* **58**, 388 (1967).
259. H. Pops and L. Delaey, *Trans. AIME* **242**, 1849 (1968).
260. S. Kajiwara and Z. Nishiyama, *Jpn. J. Appl. Phys.* **3**, 749 (1964).
261. S. Kajiwara, *J. Phys. Soc. Jpn.* **23**, 656 (1967).
262. L. Delaey and I. Lefever, *Trans. JIM* **10**, 372 (1969).
263. G. V. Kurdjumov and T. Stelletskaya, *Metallwirtschaft* **13**, 304 (1934).
264. I. Isaitschev, E. Kaminsky, and G. V. Kurdjumov, *Trans. AIME* **128**, 361 (1938).
265. H. Sato, R. S. Toth, and G. Honjo, *Acta Metall.* **15**, 1381 (1967).
266. G. V. Kurdjumov, V. Miretskii, and T. Stelletzkaya, *J. Tech. Phys. USSR* **8**, 1959 (1938); *J. Phys.* **3**, 297 (1940).
267. M. J. Duggin, *Acta Metall.* **12**, 529, 1015 (1964); **14**, 123 (1966).
268. K. Otsuka and K. Shimizu, *Jpn. J. Appl. Phys.* **8**, 1196 (1969).
269. K. Otsuka and K. Shimizu, *Trans. JIM* **15**, 103, 109 (1974).
270. K. Otsuka and K. Shimizu, *Phil. Mag.* **24**, 481 (1971).
271. R. Kumar and V. Balasubramanian, *Trans. AIME* **218**, 185 (1960).

272. V. A. Lobodyuk and L. G. Khandros, *Dokl. Akad. Nauk SSSR* **153**, 807 (1963).
273. D. Hull and R. D. Garwood, *J. Inst. Met.* **86**, 485 (1957/58).
274. C. W. Chen, *Trans. AIME* **209**, 1202 (1957).
275. K. Otsuka and K. Shimizu, *J. Phys. Soc. Jpn.* **28**, 804 (1970).
276. Z. Nishiyama, K. Shimizu, and H. Morikawa, *Trans. JIM* **8**, 145 (1967); **9**, 307 (1968).
277. For example, A. B. Greninger and V. G. Mooradian, *Trans. AIME* **128**, 337 (1938).
278. Z. Nishiyama, K. Shimizu, and H. Morikawa, *Jpn. J. Appl. Phys.* **6**, 815 (1967).
279. V. A. Lobodyuk, V. K. Tkachuk, and L. G. Khandros, *Fiz. Met. Metall.* **31**, 643 (1971).
280. H. Morikawa, K. Shimizu, and Z. Nishiyama, *Trans. JIM* **9**, *Suppl.* 317, 930 (1968).
281. T. Soejima, H. Hagiwara, and N. Nakanishi, *Trans. JIM* **5**, 273 (1964).
282. N. F. Kennon and J. S. Bowles, *Acta Metall.* **17**, 373 (1969).
283. H. Warlimont, Iron Steel Inst. Spec. Rep. No. 86, *Scarborough Conf.* p. 107 (1964).
284. G. Kunze, *Z. Metall.* **53**, 329, 396, 565 (1962).
285. N. F. Kennon and T. M. Miller, *Trans. JIM* **13**, 322 (1972).
286. H. Pops, *Trans. AIME* **236**, 1532 (1966).
287. S. Sato, A. Murayama, and Z. Nishiyama, *Mem. ISIR Osaka Univ.* **23**, 59 (1966).
288. D. Hull, *Phil. Mag.* **7**, 537 (1962).
289. S. Sato and K. Takezaea, *Trans. JIM* **9**, *Suppl.* 925 (1968).
290. T. B. Massalski and C. S. Barrett, *Trans. AIME* **209**, 455 (1957).
291. S. Sato, T. Otani, and N. Sugeno, *Jpn. Inst. Met.*, Spring Meeting, p. 52 (1971).
292. S. Kajiwara, *J. Phys. Soc. Jpn.* **30**, 1757 (1971); *Trans. JIM* **12**, 297 (1971).
293. Y. Murakami, H. Asano, N. Nakanishi, and Y. Kachi, *Jpn. J. Appl. Phys.* **6**, 1265 (1967).
294. Y. Murakami, N. Nakanishi, and Y. Kachi, *Jpn. J. Appl. Phys.* **11**, 1591 (1972).
295. N. Nakanishi and C. M. Wayman, *Trans. JIM* **4**, 179 (1963); *Trans. AIME* **227**, 500 (1963).
296. H. M. Ledbetter and C. M. Wayman, *Metall. Trans.* **3**, 2349 (1972).
297. P. Ferraglio, K. Mukherjee, and L. S. Castleman, *Acta Metall.* **18**, 1067 (1970).
298. Y. Gefen and M. Rosen, *Phil. Mag.* **26**, 727 (1972).
299. H. Warlimont and D. Härter, *Int. Conf. Electron Microsc., 6th, Kyoto* p. 453 (1966).
300. L.-C. Chang, *Acta Cryst.* **4**, 320 (1951).
301. R. S. Toth and H. Sato, *Acta Metall.* **16**, 413 (1968).
302. R. V. Krishnan and L. C. Brown, *Metall. Trans.* **4**, 1017 (1973).
303. A. Nagasawa, *J. Phys. Soc. Jpn.* **32**, 864 (1972).
304. D. Koskimaki, M. J. Marcinkowski, and A. S. Sastri, *Trans. AIME* **245**, 1883 (1969).
305. R. J. Wasilewski, S. R. Butler, and J. E. Hanlon, *Metall. Trans.* **1**, 1459 (1970).
306. V. S. Postnikov, V. S. Lebedinskiy, V. A. Yevsyakov, I. M. Sharshakov, and M. S. Pesin, *Fiz. Met. Metall.* **29**, 364 (1970).
307. K. Chandra and G. R. Purdy, *J. Appl. Phys.* **39**, 2176 (1968).
308. F. E. Wang, W. J. Buchler, and S. J. Pickert, *J. Appl. Phys.* **36**, 3232 (1965).
309. A. Nagasawa, *J. Phys. Soc. Jpn.* **29**, 1386 (1970); **31**, 1683 (1971).
310. S. P. Gupta, A. A. Johnson, and K. Mukherjee, *J. Phys. Soc. Jpn.* **31**, 605 (1971).
311. K. Otsuka, T. Sawamura, and K. Shimizu, *Phys. Status Solidi (a)* **5**, 457 (1971).
312. K. Otsuka, T. Sawamura, K. Shimizu, and C. M. Wayman, *Metall. Trans.* **2**, 258 (1971).
313. G. D. Sandrock, A. J. Perkins, and R. F. Hehemann, *Metall. Trans.* **2**, 2769 (1971).
314. F. E. Wang, B. F. De Savage, W. J. Buehler, and W. R. Hosler, *J. Appl. Phys.* **39**, 2166 (1968).
315. Y. Takashima and T. Horiuchi, *Jpn. Inst. Met.*, Spring Meeting, p. 50 (1971).
316. L. Delaey, J. Van Paemel, and T. Struyve, *Scr. Metall.* **6**, 507 (1972).
317. C. M. Wayman, I. Cornelis, and K. Shimizu, *Scr. Met.* **6**, 115 (1972).

318. T. Honma, M. Matsumoto, and Y. Shugo, *Jpn. Inst. Met.*, Spring Meeting, p. 26 (1972).
319. F. E. Wang, S. J. Pickert, and H. A. Alperin, *J. Appl. Phys.* **43**, 97 (1972).
320. F. E. Wang and D. W. Ernst, *J. Appl. Phys.* **39**, 2192 (1968).
321. R. F. Hehemann and G. D. Sandrock, *Scr. Met.* **5**, 801 (1971).
322. G. D. Sandrock and R. F. Hehemann, *Metallography* **4**, 451 (1971).
323. R. J. Wasilewski, *Trans. AIME* **233**, 1691 (1965).
324. R. Hashiguchi and K. Iwasaki, *J. Appl. Phys.* **39**, 2182 (1968).
325. J. E. Hanlon, S. R. Butler, and R. J. Wasilewski, *Trans. AIME* **239**, 1325 (1967).
326. F. E. Wang, B. F. DeSavage, W. J. Buehler, and W. R. Hosler, *J. Appl. Phys.* **39**, 2166 (1968).
327. A. S. Sastri and M. Marcinkowski, *Trans. AIME* **242**, 2393 (1968).
328. R. Hashiguchi and K. Iwasaki, *Trans. JIM* **9**, *Suppl.* 288 (1968).
329. T. Suzuki, *J. Jpn. Inst. Met.* **34**, 337 (1970).
330. R. J. Wasilewski, S. R. Butler, and J. E. Hanlon, *Met. Sci. J.* **1**, 104 (1967).
331. D. P. Dautovich, Z. Melkui, G. R. Purdy, and C. V. Stager, *J. Appl. Phys.* **37**, 2513 (1966).
332. H. A. Berman, E. D. West, and A. G. Rozner, *J. Appl. Phys.* **38**, 4473 (1967).
333. F. E. Wang, B. F. De Savage, W. J. Buehler, and W. R. Hosler, *J. Appl. Phys.* **39**, 2166 (1968).
334. R. J. Wasilewski, S. R. Butler, J. E. Hanlon, and D. Worden, *Metall. Trans.* **2**, 229 (1971).
335. G. R. Purdy and J. Gordon Parr, *Trans. AIME* **211**, 636 (1961).
336. D. P. Dautovich and G. R. Purdy, *Can. Metall. Q.* **4**, 130 (1965).
337. M. J. Marcinkowski, A. S. Sastri, and D. Koskimaki, *Phil. Mag.* **18**, 945 (1968).
338. A. Nagasawa, T. Maki, and J. Kakinoki, *J. Phys. Soc. Jpn.* **26**, 1560 (1969).
339. M. Matsumoto, Y. Shugo, and T. Honma, *Bull. Res. Inst. Min. Dress. Met.* **28**, 65 (1972).
340. L. Guttman, *Trans. AIME* **188**, 1472 (1950).
341. H. L. Luo, J. Hagen, and M. F. Merriam, *Acta Metall.* **13**, 1012 (1965).
342. J. T. A. Pollock and H. W. King, *J. Mater. Sci.* **3**, 372 (1968).
343. J. S. Bowles, C. S. Barrett, and L. Guttman, *Trans. AIME* **188**, 1478 (1950).
344. Z. S. Basinski and J. W. Christian, *Acta Metall.* **2**, 101, 148 (1954).
345. M. W. Burkart and T. A. Read, *J. Met.* **5**, 1516 (1953).
346. T. Heumann and B. Predel, *Z. Metall.* **53**, 240 (1962).
347. D. I. Potter and C. J. Altstetter, *Acta Metall.* **20**, 313 (1972).
348. J. A. Hedley, *Mater. Sci. J.* **2**, 129 (1968).
349. Z. S. Basinski and J. W. Christian, *J. Inst. Met.* **80**, 659 (1951/52).
350. E. P. Butler and P. M. Kelly, *Int. Congr. Electron Microsc., 6th* **1**, 451 (1966).
351. W. R. Patterson, *Trans. AIME* **233**, 438 (1965).
352. H. Uchishiba, T. Hori, and Y. Nakagawa, *J. Phys. Soc. Jpn.* **27**, 600 (1969).
353. H. Uchishiba, T. Hori, and Y. Nakagawa, *J. Phys. Soc. Jpn.* **28**, 792 (1970).
354. J. H. Smith and P. Gaunt, *Acta Metall.* **9**, 819 (1961).
355. G. E. Bacon, *Proc. Phys. Soc.* **79**, 939 (1962).
356. D. Finbow and P. Gaunt, *Acta Metall.* **17**, 41 (1969).
357. E. Krên, E. Nagy, I. Nagy, L. Pál, and P. Szabo, *J. Phys. Chem. Solids* **29**, 101 (1968).
358. A. I. Zakharov, *Fiz. Met. Metall.* **24**, 84 (1967).
359. M. A. Schmerling, B. K. Das, and D. S. Lieberman, *Metall. Trans.* **1**, 3273 (1970).
360. B. K. Das, M. A. Schmerling, and D. S. Lieberman, *Mater. Sci. Eng.* **6**, 248 (1970).
361. K. Shimizu, M. Oka, and C. M. Wayman, *Acta Metall.* **18**, 1005 (1970).
362. E. J. Efsic and C. M. Wayman, *Trans. AIME* **239**, 873 (1967).
363. T. Tadaki and K. Shimizu, *Trans. JIM* **11**, 44 (1970).

364. C. M. Wayman, *Scr. Metall.* **5**, 489 (1971).
365. D. P. Dunne and C. M. Wayman, *Metall. Trans.* **4**, 137, 147 (1973).
366. M. Miyagi and C. M. Wayman, *Trans. AIME* **236**, 806 (1966).
367. P. M. Kelly, *Acta Metall.* **13**, 635 (1965).
368. S. Takeuchi and T. Honma, *Sci. Rep. Tohoku Univ.* **A9**, 492 (1957).
369. S. Kajiwara, *Jpn. J. Appl. Phys.* **9**, 385 (1970).
370. M. J. Marcinkowski and E. N. Hopkins, *Trans. AIME* **242**, 579 (1968).
371. C. C. Koch and C. J. McHargue, *Acta Metall.* **16**, 1105 (1968).
372. M. S. Rashid and C. J. Altstetter, *Trans. AIME* **236**, 1649 (1966).
373. C. J. McHargue, *Acta Cryst.* **6**, 529 (1953).
374. J. B. Newkirk and A. H. Geisler, *Acta Metall.* **1**, 370 (1953).
375. A. J. Williams, R. W. Cahn, and C. S. Barrett, *Acta Metall.* **2**, 117 (1954).
376. M. Sorel, *C. R. Acad Sci. Paris* **248**, 2106 (1959).
377. J. C. McMillan, R. Taggart, and D. H. Polonis, *Trans. AIME* **237**, 739 (1967).
378. T. Yamane and J. Ueda, *Acta Metall.* **14**, 438 (1966).
379. K. A. Bywater and J. W. Christian, *Phil. Mag.* **25**, 1249 (1972).
380. R. H. Erikson, R. Taggart, and D. H. Polonis, *Trans. AIME* **239**, 124 (1967).
381. Y. C. Liu, *Trans. AIME* **206**, 1036 (1956).
382. M. Oka, *Trans. JIM* **8**, 215 (1967).
383. S. Weinig and E. S. Machlin, *Trans. AIME* **200**, 1280 (1954).
384. P. Gaunt and J. W. Christian, *Acta Metall.* **7**, 534 (1959).
385. Y. C. Liu, and H. Margolin, *Trans. AIME* **197**, 667 (1953).
386. Z. Nishiyama, S. Sato, M. Oka, and H. Nakagawa, *Trans. JIM* **8**, 127 (1967).
387. J. W. Barton, G. R. Purdy, R. Taggart, and J. Gordon Parr, *Trans. AIME* **218**, 844 (1960).
388. E. D. Lee, E. E. Underwood, and O. Johari, *Int. Congr. Electron Microsc., 6th* **1**, 433 (1966).
389. A. P. Komar and V. N. Shrednik, *Fiz. Met. Metall.* **5**, 452 (1957).
390. J. P. Langeron and P. Lehr, *C. R. Acad. Sci. Paris* **212**, 1734 (1958).
391. J. P. Langeron and P. Lehr, *Mém. Sci. Rev. Mét.* **56**, 307 (1959).
392. J. S. Bowles, *Trans. AIME* **189**, 44 (1951).
393. V. Hovi, E. Mäntysalo, and K. Tinsanen, *Acta Metall.* **14**, 67 (1966).
394. D. L. Martin, *Phys. Rev. Lett.* **1**, 447 (1958).
395. Z. S. Basinski and L. Verdini, *Phil. Mag.* **4**, 1311 (1959).
396. C. S. Barrett, *Phys. Rev.* **72**, 245 (1947).
397. D. B. Masson, *Acta Metall.* **10**, 986 (1962).
398. C. S. Barrett and D. F. Clifton, *Phys. Rev.* **78**, 639 (1950).
399. R. D. Garwood and D. Hull, *Acta Metall.* **6**, 98 (1958).
400. C. S. Barrett and O. R. Trautz, *Trans. AIME* **175**, 579 (1948).
401. D. L. Martin, *Phys. Rev. Lett.* **1**, 4 (1958).
402. A. R. G. Brown, D. Clark, J. Eastabrook, and K. S. Jepson, *Nature (London)* **201**, 914 (1964).
403. C. Hammond, *Scr. Met.* **6**, 569 (1972).
404. C. Baker, *Met. Sci. J.* **5**, 92 (1971).
405. D. F. Toner, *Trans. AIME* **215**, 223 (1954).
406. G. Wassermann, *Metallwirtschaft* **8**, 133 (1934).
407. A. B. Greninger, *Trans. AIME* **133**, 204 (1939).
408. I. Tarora, *J. Jpn. Inst. Met.* **8**, No. 6, 298 (1944); **13**, No. 3, 6 (1949).
409. A. J. Bradley and P. Jones, *J. Inst. Met.* **51**, 131 (1933).
410. N. Nakanishi, *Trans. JIM* **2**, 79 (1961).
411. M. Wilkens and H. Warlimont, *Acta Metall.* **11**, 1099 (1963); *Z. Metall.* **55**, 382 (1964).

412. T. Saburi and C. M. Wayman, *Trans. AIME* **233**, 1373 (1965).
413. J. E. Kittl and T. B. Massalski, *Acta Metall.* **15**, 161 (1967).
414. J. E. Kittl and C. Rodriguez, *Acta Metall.* **17**, 925 (1969).
415. M. J. Duggin and W. A. Rachinger, *Acta Metall.* **12**, 529 (1964).
416. C. W. Chen, *Trans. AIME* **9**, 1202 (1957).
417. S. Sugino, N. Nakanishi, and H. Mitani, *J. Jpn. Inst. Met.* **29**, 751 (1965).
418. L. G. Khandros, *Akad. Nauk Ukr. SSR* No. 4, 30 (1953).
419. I. Isaichew, *Zh. Tyek. Fiz.* **17**, 829 (1947).
420. V. A. Lobodyuk, V. K. Tkachuk, and L. G. Khandros, *Fiz. Met. Metall.* **30**, 1082 (1970).
421. W. Jolley and D. Hull, *J. Inst. Met.* **92**, 129 (1963/64).
422. D. B. Masson and R. K. Govila, *Z. Metall.* **54**, 293 (1963).
423. H. Pops and T. B. Massalski, *Trans. AIME* **230**, 1662 (1964).
424. G. Bassi and B. Ström, *Z. Metall.* **47**, 16 (1956).
425. M. Ahlers and H. Pops, *Trans. AIME* **242**, 1267 (1968).
426. J. D. Ayers and C. P. Herring, *J. Mater. Sci.* **6**, 1325 (1971).
427. H. Pops and M. Ahlers, Inst. Met. Monogr. Rep. No. 33, p. 197 (1969).
428. R. K. Govila, *Acta Metall.* **12**, 273 (1964).
429. D. B. Masson and R. K. Govila, *Z. Metall.* **54**, 293 (1963).
430. M. J. Duggin and W. A. Rachinger, *Acta Metall.* **12**, 1015 (1964).
431. D. B. Masson and C. S. Barrett, *Trans. AIME* **212**, 260 (1958).
432. D. B. Masson, *Trans. AIME* **218**, 94 (1960).
433. L. C. Brown and M. J. Stewart, *Trans. AIME* **242**, 1353 (1968).
434. H. W. King and T. B. Massalski, *Trans. AIME* **221**, 1063 (1961).
435. W. D. Hoff and W. J. Kitchingman, *Brit. J. Appl. Phys.* **16**, 353 (1965).
436. W. J. Kitchingman and J. I. Buckley, *Acta Metall.* **8**, 373 (1960).
437. P. Furrer, H. Warlimont and T. R. Anantharaman, *Proc. Indian Acad. Sci.* **75**, 103 (1972).
438. A. Ball and R. E. Smallman, *Acta Metall.* **13**, 1011 (1965).
439. H. Pops and T. B. Massalski, *Trans. AIME* **233**, 728 (1965).
440. H. Iwasaki, *J. Phys. Soc. Jpn.* **20**, 2129 (1965).
441. L.-C. Chang and T. A. Read, *Trans. AIME* **189**, 47 (1951).
442. W. Wallace, W. D. Hoff, and W. J. Kitchingman, *Acta Cryst.* **A24**, 680 (1968).
443. H. K. Birnbaum, *J. Appl. Phys.* **29**, 1773 (1958).
444. H. K. Birnbaum, *Trans. AIME* **215**, 508 (1959).
445. M. E. Brookes and R. W. Smith, Inst. Met. Monogr. No. 33, p. 266 (1969).
446. H. M. Ledbetter and C. M. Wayman, *Acta Metall.* **20**, 19 (1972).
447. M. E. Brookes and R. W. Smith, *Met. Sci. J.* **2**, 181 (1968).
448. S. Rosen and J. A. Goebel, *Trans. AIME* **242**, 722 (1968).
449. K. Enami, S. Nenno, and K. Shimizu, *Trans. JIM* **14**, 161 (1973).
450. V. S. Litvinov, L. P. Zelenin, and R. Sh. Shklyar, *Fiz. Met. Metall.* **31**, 138 (1971).
451. R. Boku, T. Saburi, and S. Nenno, *J. Jpn. Inst. Met.* **37**, 1128 (1973).
452. F. T. Worrell, *J. Appl. Phys.* **19**, 929 (1948).
453. G. H. May, Int. Res. Develop. Co., Res. Rep. (IRD 66-71).
454. J. Lehmann, *C. R. Acad. Sci. Paris* **248**, 2098 (1959).
455. B. R. Butcher and A. H. Rowe, Inst. Met. Monogr. No. 18, p. 229 (1955).
456. W. M. Lomer, Inst. Met. Monogr. No. 18, p. 243 (1955).
457. Mlle J. Beaudier, G. Cabane, and P. Mouturat, *Mém. Sci. Rev. Mét.* **58**, 176 (1961).
458. M. Anagnostidis, R. Baschwitz, and M. Colombie, *Rev. Métall.* **63** e (2), 163 (1966).
459. D. L. Douglass, *Trans. ASM* **53**, 163 (1966).
460. H. W. King, Inst. Met. Monogr. No. 33, p. 196 (1969).
461. R. Mailfert, B. W. Batterman, J. J. Hanak, *Phys. Lett.* **24A**, 315 (1967).

462. H. W. King, F. H. Cocks, and J. T. A. Pollock, *Phys. Lett.* **26A**, 77 (1967).
463. S. A. Medvedev, K. V. Kiseleva, and V. V. Milshailov, *Sov. Phys.-Solid State* **10**, 584 (1968).
464. L. J. Vieland, *J. Phys. Chem. Solids* **33**, 581 (1972).
465. K. R. Keller and J. J. Hanak, *Phys. Rev.* **154**, 628 (1967).
466. B. W. Batterman and C. S. Barrett, *Phys. Rev. Lett.* **13**, 390 (1964); *Phys. Rev.* **145**, 296 (1965).
467. M. J. Goringe, U. Valdré, "The World through the Electron Microscope," Metallurgy, Vol. III, p. 96. JEO Lab. Co., 1965; *Phys. Rev. Lett.* **14**, 823 (1965); *Proc. Roy. Soc.* **A295**, 192 (1966).
468. E. Nembach, K. Tachikawa, and S. Takano, *Phil. Mag.* **21**, 869 (1970).
469. R. D. Nelson and F. E. Bowman, *Trans. AIME* **245**, 967 (1969).
470. C. J. McHargue and H. L. Yakel, *Acta Metall.* **8**, 637 (1960).
471. J. S. Abell and A. G. Crocker, Inst. Met. Monogr. No. 33, p. 192 (1969).
472. C. S. Barrett and L. Meyer, *J. Chem. Phys.* **42**, 107 (1965).
473. C. S. Barrett, Inst. Met. Monogr. No. 33, p. 313 (1969).

3

Crystallography of Martensites—Special Phenomena

3.1 Kinds of imperfections in martensite lattices

Many kinds of lattice defects are observed in martensites. They may be classified as[†]

1. Point defects
   (a) Lattice vacancies
   (b) Interstitial atoms (ordered or disordered)
   (c) Substitutional atoms (ordered or disordered)
2. Line defects—dislocations
3. Plane defects
   (a) Stacking faults[‡]
      (i) Stacking faults (deformation faults)[§]
      (ii) Twin faults (growth faults)
   (b) Cell boundaries (subboundaries) and other boundaries between crystal segments
   (c) Antiphase domain boundaries
   (d) Boundaries between variant crystals
      (i) Produced to minimize transformation strains
      (ii) Produced by chance

[†] There are other defects not included in this classification, such as clusters of point defects, precipitates, dynamic crowdions, and phonons.

[‡] In the broad sense.

[§] In the narrow sense.

(e) Grain boundaries of parent phase
4. Elastic strains (long range)—quenching strains

The morphology and distribution of these defects have already been discussed in Chapter 2. Quantitative descriptions of defects in item 1 will be given in Section 3.3 and of the defects in items 2–4 in Section 3.2.

3.2 Amount of lattice imperfections in martensite measured by diffraction

Because of the overlapping effects of different defects on diffraction patterns, it is usually difficult to obtain information concerning the amount of each kind of defect in martensite. The correspondence of the diffraction effects to the lattice defects can be considered as shown in the accompanying tabulation.

Diffraction effect	Lattice defects
Change in intensity	Short-range strains, point defects
Line broadening	Internal strain effect—Line defect, stacking faults, elastic strain Size effect—Stacking faults, cell structure, substructure
Peak shift	Stacking faults, anisotropic strains[a]

[a] This refers to strains varying with the crystallographic direction. Anisotropic strains can be produced in martensite by special shears for transformation.

3.2.1 X-ray analysis using polycrystals

A. *Simple analysis*

It is well known that the diffraction lines from martensite in steel are very much broadened. Roughly speaking the origin of the broadening lies in the internal strains and small crystal domains previously listed.

The broadening due to small domain size can be related to the incomplete interference caused by the insufficient number of scattering elements, that is, to the number of atomic planes t. In this case the width of the diffraction line β_s may be expressed as

$$\beta_s = \frac{k\lambda}{t\cos\theta} \quad \text{or} \quad \beta_s \cos\theta = \frac{k\lambda}{t}.$$

This relation is called the *Scherrer formula*;[1] in it, θ is the Bragg angle, λ the wavelength, and k a constant close to 1. The formula shows that the

values of $\beta_s \cos\theta$ are constant for all the diffraction lines in a diffraction pattern.

The broadening due to internal strains, corresponding to the fluctuation in d values, can be roughly estimated by differentiating the Bragg equation. The integral width β_ε is expressed by

$$\beta_\varepsilon = 2\langle\varepsilon^2\rangle^{1/2} \tan\theta \quad \text{or} \quad \beta_\varepsilon \cos\theta = 2\langle\varepsilon^2\rangle^{1/2} \sin\theta,$$

where $\langle\varepsilon^2\rangle^{1/2}$ represents the root mean square strain (rmss) in the crystal. This equation means that a simple relation pertains, $\beta_\varepsilon \cos\theta \propto \sin\theta$.

If the above two kinds of broadening occur simultaneously, the resultant width β may be expressed as

$$\beta \cos\theta = (\beta_s + \beta_\varepsilon) \cos\theta = (k\lambda/t) + 2\langle\varepsilon^2\rangle^{1/2} \sin\theta.$$

Therefore, a plot of $\beta \cos\theta$ versus $\sin\theta$ may give a rough estimate of the strain ε and domain size t, since the slope of the plot gives $\langle\varepsilon^2\rangle^{1/2}$ and the intercept of the plot with the ordinate gives the value $k\lambda/t$. Many investigations[2–7] of the origin of the broadening of martensite lines have been made by this method. Unfortunately, the results are subject to some complex effects due to the presence of interstitial atoms, as described in the following section.

Sato,[8] using an Fe–27% Ni alloy containing a comparatively small amount of carbon (0.06% C), investigated the lattice defects produced in martensite. Annealed filings 20–50 μm in particle size were cooled to liquid nitrogen temperature to produce martensite with the b.c.c. structure. The diffraction profiles of the martensite lines were obtained by the fixed-count method using a diffractometer. Figure 3.1 represents an example of the intensity profiles of the 200 reflections. One sees a very large broadening of the martensite lines compared with those of filed iron. Figure 3.2 shows the plots of $\beta \cos\theta$ versus $\sin\theta$ for both the lines from the subzero martensite and those from the filed iron obtained in the experiment. As described above, the slope of the plot corresponds to the internal strain of the crystal. The broken lines in the figure show that the average amount of strain in the subzero martensite was about twice as much as that in the filed iron. Abnormally large β values of the 200 lines may be understood mainly by the elastic anisotropy of the crystal. These results were investigated in detail by analyzing the intensity profiles of the diffraction lines as shown in Fig. 3.1.

B. *Fourier analysis*

According to diffraction theory,[9] the intensity per unit length of the diffracting line at position 2θ in the profile of a powder line $00l$† from a

† Any atomic plane (hkl) in a cubic crystal can be expressed as a $(00l)$ plane of the corresponding orthorhombic crystal.

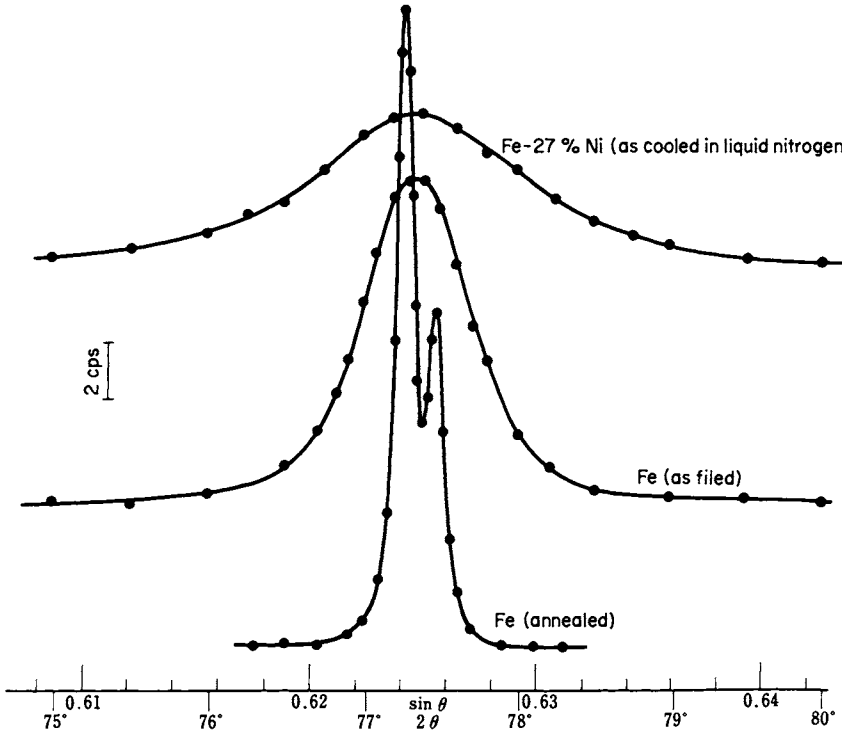

FIG. 3.1 X-ray diffraction profiles of 200 reflections. (After Sato.[8])

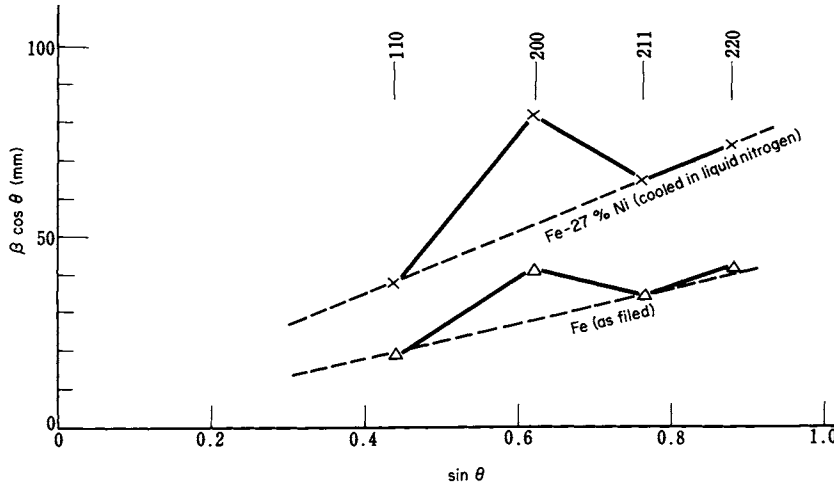

FIG. 3.2 Relation between $\beta \cos\theta$ and $\sin\theta$ (β is the integral breadth). (After Sato.[8])

microcrystal containing distortion will be expressed as

$$P_{2\theta}' = C \sum_n \{A_n \cos 2\pi nl + B_n \sin 2\pi nl\} \tag{1}$$

where C is a gradually varying function of θ that depends on the nature of specimen and the experimental conditions and l is a variable in reciprocal space in the direction perpendicular to the (001) atomic planes. The Fourier coefficients A_n and B_n consist of two components, with the superscripts S denoting domain size and D denoting distortion:

$$A_n = A_n^{\mathrm{S}} A_n^{\mathrm{D}}, \qquad B_n = B_n^{\mathrm{S}} B_n^{\mathrm{D}}, \tag{2}$$

$$A_n^{\mathrm{S}} = B_n^{\mathrm{S}}, \qquad A_n^{\mathrm{D}} = \langle \cos 2\pi l Z_n \rangle, \qquad B_n^{\mathrm{D}} = -\langle \sin 2\pi l Z_n \rangle, \tag{3}$$

where Z_n means the relative displacement (in units of atomic distance) between the 0th and nth atomic planes measured perpendicular to the (001) planes; $\langle\ \rangle$ denotes the average for different pairs with the same n.† Z_n may be either positive or negative, and if the distribution of strains is assumed to be symmetrical with respect to their signs, the term B_n will vanish and the diffraction profile will be symmetrical.

In the actual treatment, the Fourier analyses are first performed for $00l$ profiles with several orders l, using Eq. (1). For symmetrical profiles the sine coefficients B_n become zero. In Eq. (3), A_n^{D} can be expressed approximately as

$$\begin{aligned} \ln A_n^{\mathrm{D}} &= \ln\langle \cos 2\pi l Z_n \rangle \fallingdotseq \ln(1 - 2\pi^2 l^2 \langle Z_n^2 \rangle) \\ &\fallingdotseq -2\pi^2 l^2 \langle Z_n^2 \rangle. \end{aligned} \tag{4}$$

This approximate treatment is accurate if the distribution of strains happens to be Gaussian, or if both l and Z_n are small. In this case,

$$\ln A_n = \ln A_n^{\mathrm{S}} - 2\pi^2 l^2 \langle Z_n^2 \rangle \tag{5}$$

and, consequently, a plot of $\ln A_n(l)$ against l^2 will give straight lines whose intercepts with the ordinate represent $\ln A_n^{\mathrm{S}}$. The A_n^{S} values are then plotted against n. Treating this plot as a continuous function of A_n^{S} versus n, we can relate the slope of this function at $n = 0$, by diffraction theory,[9] to the spacing d of the $(00l)$ plane and the grain dimension (coherent domain size) D as

$$-\left(\frac{dA_n^{\mathrm{S}}}{dn}\right)_{n=0} = \frac{d}{D}; \tag{6}$$

Eq. (6) is often used to estimate D from diffraction experiments. Moreover, the slope of the line in the $\ln A_n - l$ plot will give the Z_n^2 value, as seen in

† For the statistical treatment of strain, Z_n values with different n's are considered. n is a measure of distance in real crystals. It has been derived from diffraction theory that this n corresponds to the harmonic number in the Fourier analysis of the diffraction line.

Eq. (5). Putting $Z_n d = \Delta L$ and $nd = L$, the root mean square strain is given by

$$\langle \varepsilon_L^2 \rangle^{1/2} = \langle (\Delta L/L)^2 \rangle^{1/2} = \left\langle \left(\frac{Z_n}{n} \right)^2 \right\rangle^{1/2} = \frac{d}{L} \langle Z_n^2 \rangle^{1/2}. \tag{7}$$

For *hkl* reflections of a cubic crystal, the same treatment can be used by replacing l^2 in Eq. (5) by $l_0^2 = h^2 + k^2 + l^2$.

The broadening due to the strains and the small domain size can thus be separated, at least in principle, by Fourier analysis of the intensity profile. The Fourier method is more rigorous than the method described in Section 3.2.1A, which utilizes only the θ-dependent nature of the width β separately for the two effects, disregarding their combined effects on the diffraction.

The Fourier method has often been used to analyze the diffraction lines from martensite.[10–13] Sato[8] analyzed his data for subzero-cooled martensite in Fe–27% Ni alloy in this way. The rmss obtained in martensite are compared with those for filed iron in Fig. 3.3. The figure shows that the strains in the ⟨100⟩ direction are larger than those in other directions and that the strains in martensite are about twice as large as those in filed iron. The values obtained by Sato are consistent with other data in the literature.

In Table 3.1 are listed the values of domain size (D_{obs}) obtained in Sato's analysis. In comparing these values with the data of other investigations,[11–13]

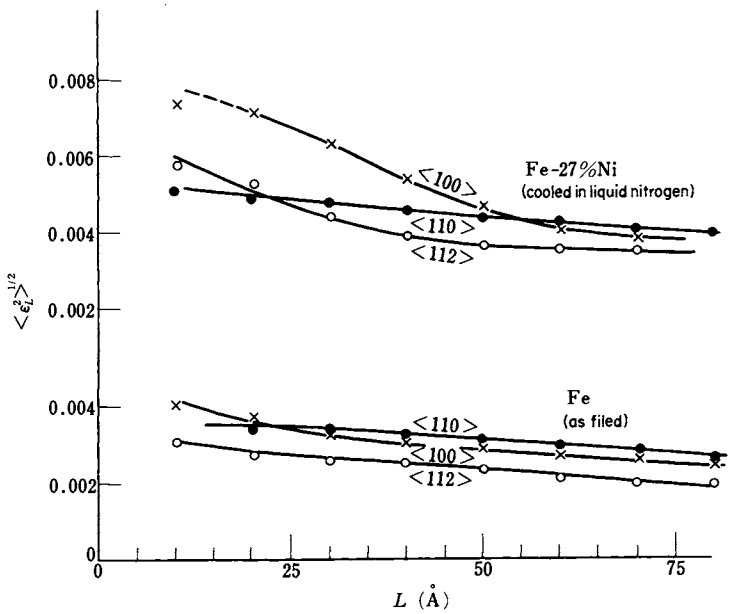

FIG. 3.3 Root mean square strain in filed iron and in martensite in an Fe–27% Ni alloy. (After Sato.[8])

TABLE 3.1 Apparent domain size D_{obs} in martensite and in filed iron[a]

hkl	110		200		211
Ratios of theoretical values of D_{sf}	2.83	:	1	:	1.63
Fe–27% Ni (α′)					
D_{obs}	200 Å		65 Å		100 Å
ratio	3.0	:	1	:	1.5
Pure iron (filed)					
D_{obs}	335 Å		155 Å		195 Å
ratio	2.2	:	1	:	1.3

[a] After Sato.[8]

we find that the values of the ratios of D_{obs} for different directions are almost equal, although the absolute values are quite different.†

It is worth noting that the value of D_{obs} obtained represents not the real but the apparent domain size, corresponding to the diffraction broadening due to various lattice defects in martensite. The broadening is caused mostly by the stacking faults on {112} martensite planes, produced in large quantities during transformation. According to the calculation by Guentert and Warren,[13] the apparent domain size D_{obs} is related to the real domain size D as follows:

$$1/D_{obs} = 1/D + 1/D_{sf},$$
$$1/D_{sf} = \{(1.5\alpha + \beta)/(u + b)l_0 a\} \sum_b |-h - k + 2l|$$

where we assume that deformation faults with probability α and twin faults with probability β occur independently and at random on (112) planes. The values of α and β are also assumed to be sufficiently small. The terms b and u represent, respectively, the number of component reflections of the same family that are broadened and unbroadened by faulting. The value of $1/D_{sf}$, due to the stacking faults, depends on the Miller index of reflection, and the ratio $D_{sf}(110)$: $D_{sf}(200)$: $D_{sf}(211)$ calculates to 2.83:1:1.63, independent of the amount of faulting. Since the observed ratios of domain size D_{obs} for different directions for martensite are very close to these calculated values, as shown in Table 3.1, it may be assumed that the stacking faults contribute a great deal to the broadening of martensite lines. Using the observed values of D_{sf} for the 110, 200, and 211 directions, the value of $1.5\alpha + \beta = 0.033$ was

† The discrepancies in absolute values of D_{obs} may arise from different experimental conditions, especially from different estimates of background intensity.

obtained for subzero-cooled martensite. If only the effect of stacking faults were predominant in filed iron, $1.5\alpha + \beta = 0.01$ would be obtained.† However, this assumption seems improbable because the number of stacking faults observed in deformed iron by electron microscopy is not very large. Therefore, the effects of the dislocations and anisotropic strains due to transformation shear must greatly influence the *hkl* dependence of broadening. These effects will also occur in Fe–27% Ni martensite.[14] The foregoing argument is further supported by the research work on single crystals of martensite that will be described in the next section.

The distribution of elastic stresses produced by transformation is usually very complicated. Some attempt has been made to analyze the problem by the theory of elasticity.[15]

3.2.2 X-ray analysis using single crystals

Diffraction theory predicts the peak shifts of diffraction spots for b.c.c. single crystals containing deformation faults on their (112) planes. The amount and direction of the shift depend on the index of reflection and are different among those of the same family such as (310) and (130). Since each component of the family has a shift in a different direction, the net effect is not a shift but a broadened powder line. Accordingly, it is impossible to obtain definite information on the deformation faults in b.c.c. crystals directly from the peak shift of powder lines,‡ contrary to the case of f.c.c. crystals. This is also true for the effects of anisotropic strains. Therefore, it is desirable to study these problems by single crystal diffractometry.

Sato and Nishiyama[18] attempted to irradiate an individual martensite leaf by microbeam x rays to measure the shift of the diffraction spots. First, they prepared large γ grains (~ 5 mm) of an Fe–30.6% Ni alloy by annealing for 12 hr at 1300°C. After cutting a coarse-grained block into slices 0.1 mm thick and removing the surface layer by etching, they annealed the slices again. The specimens were then cooled to -25°C to obtain a few large martensite α' leaves in a large γ grain. The small amounts of peak shift for individual diffraction spots were measured by a back reflection x-ray camera having a pinhole collimator of a few tenths of a micrometer in diameter. The diameter of the x-ray beam on the specimen was about 50 μm and was small enough to hit only one martensite single crystal. Successive oscillation photographs were taken to obtain reflections from the planes belonging to the $\{hkl\}$ group.

† For other b.c.c. metals, such as V, Ta, Nb, β CuZn, and β AlNi, almost the same values have been obtained so far.

‡ The expansion of spacing, if any, at a fault plane ε_f, produces a particular shift the amount of which depends on the *hkl* of the powder line.[16] Shifts of this kind have already been observed,[17,18] and yet it is not known if all the shifts are produced only by ε_f.

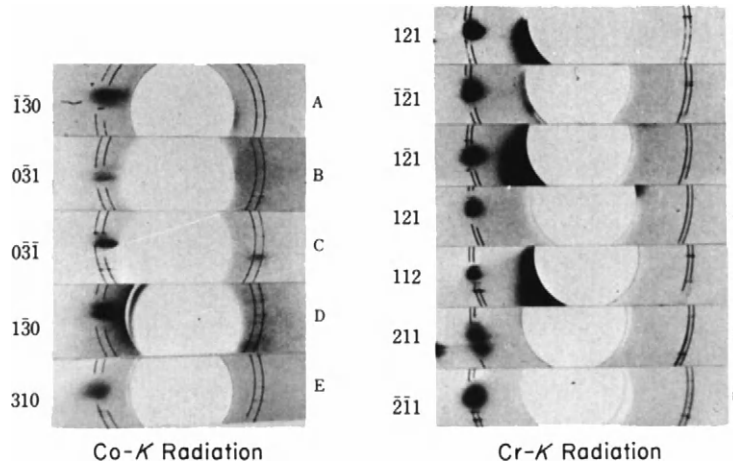

FIG. 3.4 Oscillation x-ray photographs for a single α' crystal of Fe–30.6% Ni alloy. (The α' crystal was produced by subzero cooling to $-25°C$. X-ray microbeams (50 μm) were used.) (After Sato and Nishiyama.[18])

Figure 3.4 shows two series of photographs taken from one α' crystal. The index written in each pattern was determined by taking the N orientation relationship between the γ and α' crystals to be

$$(111)_\gamma \| (011)_{\alpha'}, \qquad [\bar{1}\bar{1}2]_\gamma \| [0\bar{1}1]_\alpha.$$

The sharp doublet lines seen in the photograph are powder lines from annealed pure iron, doubly exposed as a standard. It is clearly seen that the diffraction spots from the single crystal of martensite are broader than the standard lines. Nevertheless, we must bear in mind that the broadening of diffraction spots from a single crystal is much less than that of the α' powder line at the same 2θ position. The powder lines of martensite at the back reflecting position always broaden too much for us to recognize them.

Measuring the position of the α' spots with respect to the standard lines, we obtain clear shifts that depend on the *hkl* indices of the reflection planes. By analyzing the amount and direction of the shifts, it was suggested that they were caused by residual elastic strains,† expansion or contraction,

† Elastic strains of this kind should be distinguished from macroscopic strains, such as quenching strains. The residual macroscopic strain in quenched steel was measured[19] through the change in length of a cylindrical specimen with an outer diameter of 103 mm and inner diameter of 25 mm, upon etching of the inner wall layer by layer. For the water-quenched specimen, compression stress, in both the longitudinal and circumferential directions, as high as 38 kg/mm^2 was observed. In the oil-quenched specimen, on the other hand, tension stress as high as 42 kg/mm^2 was detected. Another x-ray work[20] reported residual macroscopic strains corresponding to a stress of ± 3000–4000 lb/in.^{2}

opposing the Bain distortion of the transformation, and stacking faults on $\{112\}$ in the α' crystal with a particular crystallographic relation to the matrix γ crystal.[13]

From the profile of the diffraction spots seen in Fig. 3.4, broadening was detected in addition to the characteristic shift of peak position, as stated earlier. The broadening may be produced in part by the small domain size and by other lattice defects in the α' crystals. Lysak and Vork[21] observed the broadening of spots† from α' single crystals of six manganese steels containing 0.52%–0.88% C and 8.2%–7.3% Mn. The broadening was more prominent for the spots at the higher 2θ values. If the broadening in this case is caused by the inhomogeneous distribution of carbon atoms in the martensite lattice, the width of the diffraction profile should be proportional to $\tan\theta$. But this was not the case. The authors utilized the Fourier method to analyze the broadening. The numerical values obtained, for example, in a 0.76% C–7.8% Mn steel, were

$$D_{[110]} = 23 \times 10^{-7}\,\text{cm}, \qquad \langle \varepsilon^2 \rangle^{1/2} = 5 \times 10^{-3},$$
$$D_{[110]}:D_{[200]}:D_{[211]} = 3.8:1.00:1.75.$$

This ratio is in fair agreement with the theoretical value listed in Table 3.1, meaning that stacking faults exist in the martensite lattice. The absolute values of $D_{[hkl]}$ depended on the carbon content: the more carbon introduced into the martensite, the smaller the $D_{(hkl)}$ values.

3.2.3 X-ray analysis of internal elastic strain in martensite, using extracted powders

It is expected that the elastic internal strains in α' crystals in a bulk specimen would be released on extraction of the individual α' crystals from the matrix. Russian workers have attempted to determine if this is true. Arbuzov *et al.* reported that the broadening of the powder lines from α' crystals extracted electrolytically‡ from plain carbon steels (0.80%–1.51% C)[22] and chromium steels (0.84% C–1.00% Cr)[23] was much less than that of bulk martensite, even though the lattice constants were virtually unchanged from the bulk specimen. This experiment supports the concept that the tetragonal nature of martensite is an inherent property and is not due to the effect of the surrounding matrix. Moreover, the experiment showed that the internal strains produced by the surroundings may be removed through extraction from the matrix. This elastic strain may be the same kind of strain as the residual microstrain in single crystals of Fe–Ni martensite on which Sato *et al.* reported.

† The range of oscillation was chosen to be $\pm(5°–7°)$.

‡ The electrolyte used was an aqueous solution of KCl and citric acid or chloric acid.

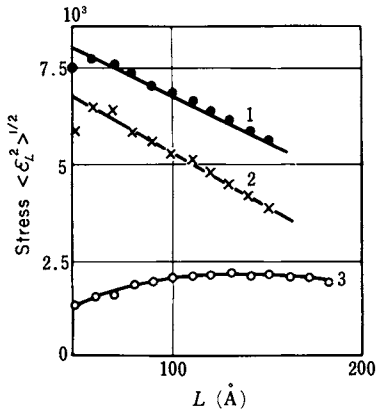

FIG. 3.5 Root mean square strain for ⟨110⟩ in martensite of a carbon steel containing 1.2% C. Curve 1, rod with 12 mm diameter; curve 2, filings; curve 3, electrolytically extracted powder. (After Kurdjumov and Nesterenko.[24])

Kurdjumov and Nesterenko[24] have made a similar experiment. They quenched a specimen of carbon steel containing 1.2%C from 1020°C and took x-ray diffraction profiles of the (110) and (220) reflections. The coherent domain size $D = 2.3 \times 10^{-6}$ cm was obtained by Fourier analysis of these profiles. Figure 3.5 shows part of their results; in it, the rmss values for three different forms of specimens are plotted. Curve 1 was obtained from a rod specimen with 1.2 mm diameter, curve 2 from filings, and curve 3 from α' martensite grains electrolytically extracted from bulk cylindrical specimens (10–12 mmϕ). We can readily see that the rmss in extracted α' grains is very much less than that in the other specimens. The result was not contrary to the initial expectation.

3.2.4 Stacking disorder in martensites with close-packed layer structures

The amounts of stacking faults in martensites of ferrous alloys are very difficult to measure accurately. On the other hand, for close-packed structure martensites, such as those in noble-metal-based alloys, a diffraction theory dealing with stacking faults was established by Kakinoki and Komura,[25,26†] and using fundamental equations developed in this theory, it is reasonably easy to estimate the density of stacking faults in these martensite crystals.

As an example, an analysis of stacking faults in β_1' martensite in a Cu–Al alloy is presented here. As noted in Section 2.5.1, electron diffraction spots of β_1' martensite are elongated and have streaks in the c^* direction, which

† Theories[27] other than that by Kakinoki and Komura are not applicable to these martensite structures.

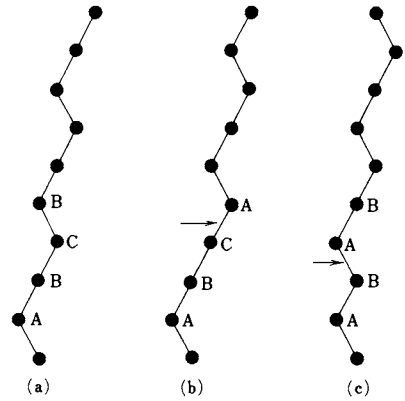

FIG. 3.6 Kinds of stacking faults in the 9R structure. (a) No fault; (b) cubic-type fault; (c) hexagonal-type fault.

suggests the existence of stacking faults. A detailed inspection of these diffraction patterns reveals that three kinds of spots, S, M, and W, aligned in the c^* direction are not equally spaced and their intensities differ from those of a perfect crystal (Fig. 3.8). Spots S, M, and W should be equally spaced if there were no stacking faults in the crystal. The forgoing experimental facts are explained as due to stacking faults by the Kakinoki–Komura theory. The outline of the treatment by that theory is as follows.

Stacking faults are classified as "cubic type" and "hexagonal type," rather than as "deformation faults" and "twin faults," which have been used in most diffraction theories treating stacking faults. Figure 3.6 illustrates the two types of stacking faults. The basic stacking order in the 9R structure[†] is $ABC^-BCA^-CAB^-$, in which ABC is followed by B (Fig. 3.6a), but if an error in the stacking order occurs at the place indicated by the arrow in Fig. 3.6b, the stacking becomes ABCA, which is the same stacking order as that in an f.c.c. crystal. This type of stacking fault is called the *cubic-type stacking fault*. The probability of such a stacking fault occurring is expressed by α. The probability $\alpha = 1$ means that the whole crystal is a perfect f.c.c. crystal. On the other hand, if an error in the stacking order occurs in the location indicated by the arrow in Fig. 3.6c, the stacking becomes ABAB, which is the same stacking order as that in an h.c.p. crystal. This is called the *hexagonal-type stacking fault*. The probability of such a stacking fault occurring is expressed by β. The probability $\beta = 1$ means that the whole crystal is a perfect h.c.p. crystal.

Figure 3.7a, b, c shows the positions (abscissas) and intensities (ordinates) of spots aligned in the c^* direction of f.c.c., 9R, and h.c.p. structures, respec-

[†] β_1' has the 18R structure but may be expressed as 9R if the superlattice is ignored. For simplicity the structure is treated as 9R in this chapter.

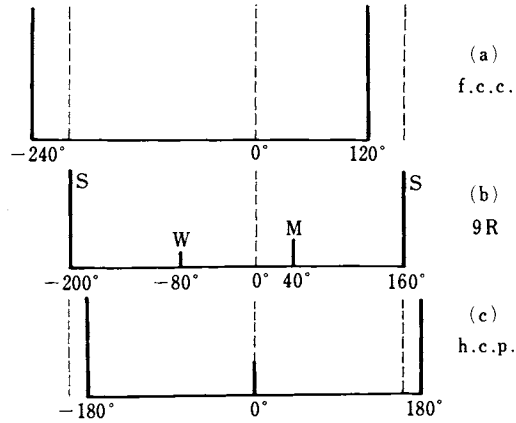

FIG. 3.7 Arrangements of diffraction spots ($h = 3n - 1$) in the c^* direction in three kinds of close-packed layer structures. (The abscissas indicate 360° (l/18) where l is the index referred to the c^* axis, and the ordinates indicate the intensity of diffraction.)

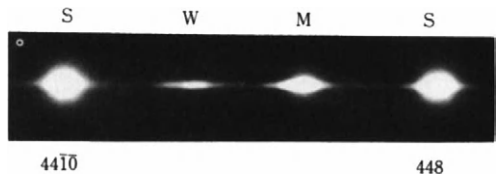

FIG. 3.8 A series of spots in the c^* direction in an electron diffraction pattern of β_1' martensite of a Cu–24.7 at.% Al alloy, the incident beam being in the $[1\bar{1}0]_{\beta_1'}$ direction. (After Nishiyama *et al.*[28])

tively. It is then expected that if cubic-type faults occur in a 9R crystal (Fig. 3.7b), the spots will shift toward those in Fig. 3.7a, whereas if hexagonal-type faults occur, the spots will shift toward those in Fig. 3.7c. This was confirmed by more rigorous numerical calculations.[28] Calculated intensity curves were obtained for various values of α and β ranging from 0 to 1.† According to those calculations, diffraction spots are shifted as well as diffused by the existence of stacking faults, and separations between spots S–W–M–S vary as the stacking fault densities change. These separations were plotted as functions of α and β. Stacking fault parameters α and β, corresponding to the observed separations between the spots, can be obtained by using such relations. Figure 3.8 shows an example of a spectrum of

† In the case of the 9R structure, "Reichweite," s must be equal to 3 or greater than 3, according to the Kakinoki–Komura theory. This means that four fault parameters, α, β, α', and β', must be used in principle to describe stacking disorder in the crystal. However, since only two parameters α and β satisfactorily explained the observed experimental facts, the other parameters α' and β' may be assigned equal to 0.

TABLE 3.2 Reflection spot distances and stacking fault parameters in the 9R structure[a]

Index of spot	$(44\bar{1}0)$	$(44\bar{4})$	(442)	(448)	Parameters	
Sign of spot	S	W	M	S	α	β
Spot distance						
$2\pi\Delta l/18$ (No fault)	120°	120°	120°		0	0
Cu–Al β_1' (Fig. 3.8)	124.8°	104.8°	130.3°		0.260	0.396

[a] After Nishiyama *et al.*[28]

electron diffraction spots of β_1' martensite in Cu–24.7 at.% Al.† The separations between the spots in this figure were measured (see Table 3.2). The measured separations are wider than 120° for S–W and M–S, but narrower than 120° for W–M. In the case of a perfect unfaulted crystal, those values should all be equal to 120° ($2\pi\Delta l/18$ radian). From the measured values of the separations between the spots, the corresponding stacking fault parameters α and β were obtained, using the above-mentioned relations. They are listed in the last two columns of Table 3.2. By this procedure α and β were obtained from many martensite crystals. The results for cubic-type faults are $\alpha = 0.004$–0.27; for hexagonal-type faults, $\beta = 0.12$–0.40. Thus, stacking fault parameters vary from crystal to crystal in a specimen, resulting in a wide range of observed values of α and β. It is then expected that the fault parameters may be significantly affected by such other factors as alloying content, specimen surface, and external stresses. The following are results of studies by Kajiwara and others on these effects.

A. *Dependence on alloy composition*[29]

Five different Cu–Al alloys‡ containing between 22.5 and 26 at.% Al were studied by x-ray diffraction photography and diffractometry. The positions of the diffraction lines of the β_1' martensite were all consistent with those expected from the 9R structure except for a certain amount of line shifting. The stacking fault parameters shown in Fig. 3.9 were obtained from the line shifts; the hexagonal-type stacking faults increases with increasing Al content.§ This result shows that β_1' martensite tends to approach γ_1' martensite by an increase in the parameter β as the Al content increases. This seems to be quite reasonable, for the existence of the γ_1' structure

† The specimens were thinned by electrolytic polishing from 0.35-mm-thick plates that had been quenched from 950°C.

‡ Specimens for x-ray diffraction consisted of filings less than 250 mesh in size quenched in brine from 950°C or 1000°C.

§ In this case, to a first approximation, only parameter β is sufficient to describe the stacking disorder.[28,30]

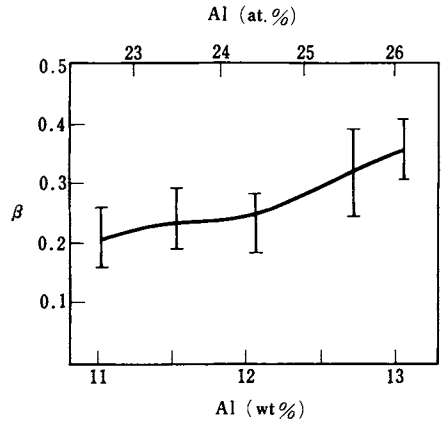

FIG. 3.9 Composition dependence of stacking fault parameter β in β_1' martensite of Cu–Al alloys. (After Kajiwara.[29])

at a higher Al content indicates that the h.c.p. structure is the more stable one in the high Al range. Recently, Delaey and Cornelis[31] studied the variation of stacking fault probability in β_1' and γ_1' with alloy composition in Cu–Zn, Cu–Zn–Ga, and Cu–Zn–Si alloys. They found that cubic-type stacking faults are predominant at low Zn concentrations whereas hexagonal stacking faults are predominant at high Zn concentrations. In the case of Fe–Ni alloys, the values of α and β are also dependent on composition.[32]

B. *Surface effect (thin foil specimens)*

In an experiment examining surface effects, thin foils of Cu–24.0 at.% Al[30,33] with various thicknesses were transformed martensitically by quenching from 700°C and examined with a 500 kV electron microscope. Figure 3.10 shows electron diffraction patterns taken from such martensite crystals of different thicknesses. As shown at the right of each photograph in this figure, various values of β were obtained. Among these even $\beta = 1$ is found. It appears† that β approaches 1 as the foil thickness decreases, indicating clearly the existence of a surface effect. On the other hand, in low Al content alloys, such as Cu–19.7 at.% Al, the concentration of cubic-type stacking faults tends to increase with decreasing foil thickness.[34]

C. *Effect of deformation*

It has been well known from early research on martensite that plastic deformation brings about some change in the crystal structure of martensites. In the case of the Cu–Al alloys, β_1' martensite had been believed to transform

† The spectra of diffraction spots in Fig. 3.10 are arranged in order of β value but not necessarily in order of foil thickness.

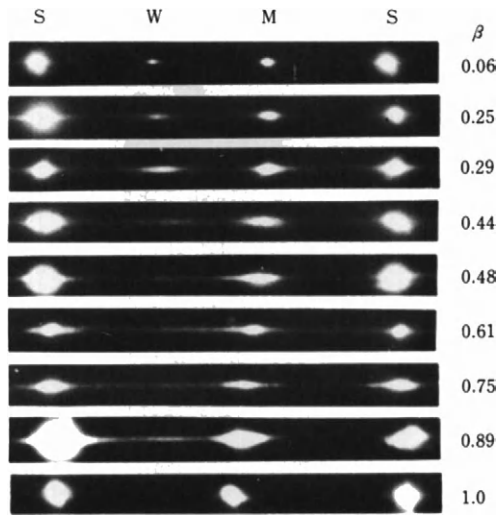

FIG. 3.10 Variation of the distribution of diffraction spots with stacking fault probability β. (Thin foils of Cu–24.0 at.% Al alloy.) (After Kajiwara.[33])

simply into an h.c.p. structure.[35,36] According to recent x-ray diffraction studies,[37,38] however, the strain-induced transformations are not so simple in Cu–(21–26) at.% Al alloys. In these alloys, powder specimens (250 mesh size) brine quenched from a high temperature had martensites of the 9R structure over the whole composition range. When these powder specimens were deformed by grinding in a mortar or when a quenched bulk specimen (β_1' martensite) was filed, the crystal structure changed to f.c.c. for low Al contents, h.c.p. for high Al contents, and a mixture of these two structures for intermediate Al contents. Thus, it can be said that for any Al composition, the 9R structure is not stable.

The effect of deformation was also studied by electron diffraction using a Cu–22.5 at.% Al alloy.[39] This alloy composition is in the range where the strain-induced structures are a mixture of f.c.c. and h.c.p. The results of the study showed that cubic-type stacking faults are predominant in some cases and hexagonal faults in other cases. In the former, α ranged from 0 to 0.6, but 0.6 was the maximum value of α that could be obtained even by applying severe deformation; instead, new structures with long-period stacking orders appeared, such as $(7\bar{1})$, $(8\bar{1})_3$, $(10\ \bar{1})$, and $(11\ \bar{1})_3$ structures in the Zhdanov notation.†

The β_1' martensite formed in a Cu–Zn alloy by quenching also has the 9R structure and contains a high density of stacking faults. An electron

† These structures correspond to those formed by introducing stacking faults into an f.c.c. crystal at every 8, 9, 11, and 12 layers, respectively.

diffraction study of a Cu–38.6 at. % Zn alloy† showed that the predominant type of stacking fault involved is cubic with $\alpha = 0.13–0.43$.[40] As mentioned before, the martensite structures induced by deformation are a mixture of the 3R (f.c.t.) and 9R structures, both containing stacking faults. The stacking faults are such that the stacking order in 3R changes to approach that in 9R (9R-type stacking faults).[41]

Analysis of the fault parameter by electron diffraction was also performed on h.c.p. martensites in Co, Co–12.2 at. % Be, and Co–19.5 at. % Ni that had been formed by quenching from a high temperature.[42] This case is relatively simple; only cubic-type faults associated with the parent phase were involved, and the existence of stacking faults shifted two diffraction spots arrayed in the c^* direction toward an f.c.c. phase spot. From the measurement of such shifts it was found that $\alpha = 0.03–0.3$. In some martensite plates, diffraction spots were not shifted but were only accompanied by streaks. This may be the case for $\alpha = \alpha'$, which means that faults of the cubic type in the normal and reverse directions occurred with the same probability.

3.3 Lattice imperfections due to interstitial atoms

3.3.1 Location of interstitial atoms

As described in Chapter 2, steel martensites contain carbon and/or nitrogen atoms interstitially, and hence the lattices are considerably distorted. The subject is important because of the strong effects of these lattice distortions on the mechanical properties of steel. We begin our discussion of this subject with the possible occupied interstitial positions in the b.c.c. lattice.

Figure 3.11 shows two possible sites for interstitial atoms where relatively large open spaces are surrounded by iron atoms. In this figure, (a) $(\frac{1}{2}\frac{1}{4}0)$ and (b) $(\frac{1}{2}\frac{1}{2}0)$ correspond to the so-called tetrahedral site and octahedral site, respectively. The former is 1.60 Å from the centers of four iron atoms that form a tetrahedron. The octahedral site, which is bounded by six iron atoms, is 1.43 Å from the centers of the atoms at the body-centered positions and 2.02 Å from those at the corner positions in part (b). If only the distances to the nearest-neighbor atoms were important, the interstitial atoms would prefer the tetrahedral sites. However, if relaxation of the surrounding iron atoms occurs easily, then the occupancy will not depend on spacing alone.

According to theoretical calculations by Shatalov and Khachaturyan,[43] in b.c.c. lattices the interstitial atoms may enter either tetrahedral or octahedral sites, depending on the kind of matrix atoms. For example, the occupied

† Specimens 0.13 mm thick were quenched in a 10% NaOH solution to form some martensite plates.

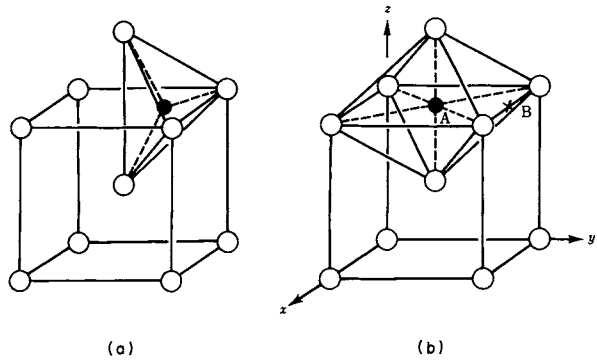

FIG. 3.11 Possible positions of the carbon atom (●) in b.c.c. iron (○, Fe atom) (a) Tetrahedral site ($\frac{1}{2}\frac{1}{4}0$); (b) octahedral site ($\frac{1}{2}\frac{1}{2}0$).

site is octahedral for iron and tetrahedral for vanadium. In tantalum and niobium, both kinds of sites may be occupied.

The interstitial atoms in austenite are at the octahedral sites in the f.c.c. lattice.† This site in austenite keeps its surroundings during the Bain transformation; in other words, the octahedral site in the f.c.c. lattice directly corresponds to the octahedral site in the b.c.c. lattice. Hence, interstitial atoms may be expected to stay in these sites during transformation. However, it can be imagined from Fig. 3.11 that interstitial atoms may move from octahedral to tetrahedral sites without difficulty. Therefore, the interstitial site in martensite will not be determined by a simple consideration of the Bain correspondence.

3.3.2 Detection of dipole strains by x-ray diffraction

Neither interstitial site in the b.c.c. lattice has enough space for an interstitial atom like carbon or nitrogen. When interstitial atoms are introduced, the original lattice must expand, generating short-range strains. At the tetrahedral sites, the effects with respect to the three principal axes are equivalent and, hence, the strain produced will be isotropic. For the octahedral sites in the b.c.c. lattice, however, the strain in the vertical direction of Fig. 3.11b is larger than that in the horizontal directions. This type of strain has been called a *dipole strain*, the defect being called a *dipole defect*.

† For the f.c.c. lattice, the largest interstitial site is the octahedral site $\frac{1}{2}\frac{1}{2}\frac{1}{2}$ and no other space in the lattice is as large. Though there was little doubt that the interstitial atoms occupy these sites, Petch[44] confirmed this by x-ray diffraction. He quenched a manganese steel (13% Mn–1.43% C) to form austenite crystals and measured the integrated intensity of various reflections. The best fit between the calculated intensities and the observed intensities was obtained for carbon atoms occupying octahedral sites.

In an early study of the line broadening of α' martensite in steel, it was thought that the strain due to interstitial atoms was one of the important origins of the broadening. However, since the strain is only short range, the effects should be detectable only through the integrated intensity rather than through the width of the diffraction line. From this point of view, the author and a co-worker made the following experiment about 30 years ago.[45] Gamma crystals of Fe–10 wt % Al alloy can contain more than 2% of carbon in solution[46] and, hence, tetragonal martensites having a large axial ratio can be obtained by quenching these aluminum steels. Figure 3.12 shows a typical x-ray Debye-Scherrer pattern of a quenched aluminum steel obtained in that experiment. We clearly see the tetragonal doublets of the

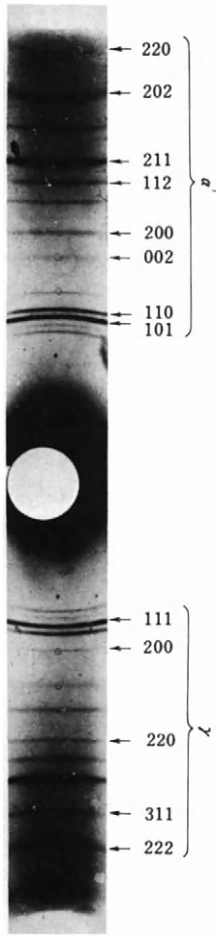

FIG. 3.12 Debye–Scherrer photograph of martensite in an Al steel (Fe–10% Al–2.4%C, quenched from 1170°C in ice water). (After Nishiyama and Doi.[45])

TABLE 3.3 Intensity ratios of component lines of tetragonal doublets of martensite (Al steel)[a]

hkl	*I/KH*	Ratio
101	0.254	0.55
110	0.465	
002	0.145	0.66
200	0.220	
112	0.174	0.62
211	0.280	
202	0.142	0.65
220	0.218	

[a] After Nishiyama and Doi.[45]

α' reflection which made possible an estimate of the intensity of each component of the reflection. In Table 3.3 the measured values of integrated intensity and their ratios are listed. The integrated intensities in this table have been divided by the frequency factor H, so the values for both components should be nearly equal if no other effects on the intensity are present. As can be seen in the last column of Table 3.3, the observed ratios are less than unity; that is, the intensity of the component with the higher l index was much less than that having the lower l index. The results suggest that some of the iron atoms are locally displaced parallel to the c axis. The larger the short-range strain component perpendicular to the reflecting plane, the weaker the reflected intensity is. These experimental results provide evidence supporting the occupation of octahedral sites by carbon atoms, as shown in Fig. 3.13, since tetrahedral occupation will give equal strains in the principal directions.

Lipson and Parker[47] obtained results similar to the foregoing for carbon steels containing 1.57% C. Il'ina *et al.*[48] detected weakening of particular reflections for low carbon steels, containing 0.35% or 0.41% C,[48] from which they predicted special short-range strains similar to the foregoing. They repeated the same experiment for a high carbon steel containing 1.3% C[49] and obtained results like the author's, from which they calculated the mean square strain to be 0.15 Å in the [001] direction. Arbuzov *et al.*[50] and Kurdjumov[51] also reported, for 0.98% C steels, that the mean square strain in the c direction was about twice that in the a direction.

All of these experiments have proved that the solute carbon atoms in the iron lattice produce dipole strains. Moreover, the evidence tells us that

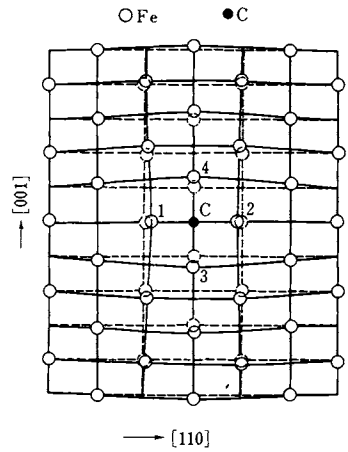

FIG. 3.13 Dipole strain around a carbon atom in martensite (○ Fe, ● C).

the dipole strains are distributed almost entirely in one direction, because if this were not the case (i.e., if the dipole strains were distributed equally in all three principal directions), the intensity ratio presented in Table 3.3 would be unity for all the doublet reflections. The experiments suggest the possibility of carbon atom ordering in a particular direction. This problem will be examined in detail later, in Section 3.3.5.

3.3.3 Mössbauer effect due to interstitial atoms

The preceding section showed that dipole strains are a kind of short-range strain that may be produced by interstitial atoms. It is expected that the local distortion between neighboring atoms affects the Mössbauer effect.† Several researches[52–58] on this problem using the Mössbauer method have been reported.

Fujita *et al.*[54–57] made Mössbauer measurements on thin carburized steels 30 μm thick containing 0.7%–1.1% C, quenched in ice water from 850°C. A ^{57}Co was used as the source. Gamma rays having an energy of 14.4 keV and originating from ^{57}Fe* were produced by the β decay of the

† The Mössbauer effect is a resonance absorption effect of γ rays due to the change in the energy levels of atomic nuclei. By this effect we obtain information on the following phenomena: (1) the internal magnetic field at the nucleus, which is affected by the surrounding atoms; (2) the energy difference due to the electric quadrupole, which reflects the difference in potential gradient due to the distortion of the crystal lattice and of electron orbits; (3) the isomer shift, which shows the change in interaction between the nucleus and s electrons. The isomer shift is also affected by the screening effect due to the d electrons and accordingly is sensitive to the exchange of electrons between neighboring atoms. These three phenomena provide information on the short-range interactions of atoms for which the diffraction method is less effective.

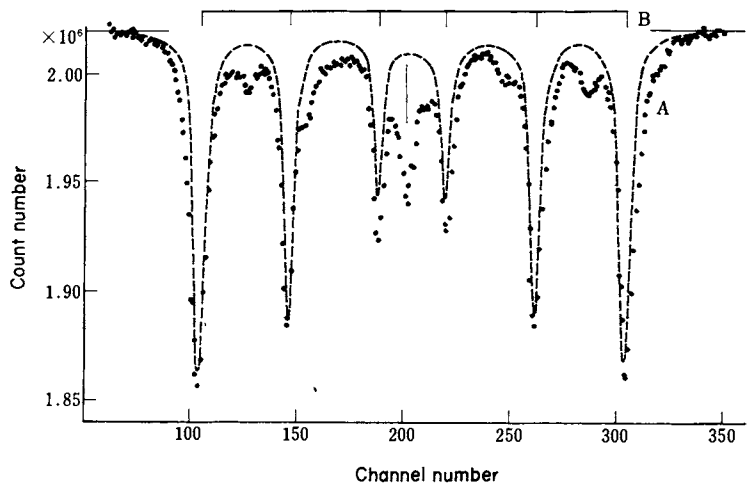

FIG. 3.14 Mössbauer spectrum of martensite in Fe–4.2 at.% C. (After Moriya *et al.*[57])

source. The energy of the γ rays was modified by the Doppler effect. The absorption spectrum due to ^{57}Fe naturally contained in the specimens was measured at room temperature.

Figure 3.14 is an example of the spectra, in which the ordinate represents the measured counts of transmitted γ rays† and the abscissa shows the channel number of a multichannel-type pulse height analyzer, which corresponds to the energy change due to the Doppler effect.‡ The broken line represents the spectrum from pure iron, used as a reference. Six absorption peaks, produced by the nuclear Zeeman effect, are obvious. For a quenched specimen, a sharp absorption peak with no splitting can be observed at the center in the figure. This absorption is produced by the paramagnetic retained austenite. The other absorption peaks are very much like those of α iron. This is because α' martensite is ferromagnetic and the relations between neighboring atoms are similar to those in b.c.c. α iron, even though interstitial carbon atoms are present. Elsewhere in the pattern, however, very small absorption peaks in addition to the main peaks are clearly observed. Small peak shifts can also be seen in the figure. These additional small peaks become clearer as the carbon content increases; hence, it is to be expected that they are produced by the modification in nuclear energy of iron atoms due to the neighboring carbon atoms. The effect of carbon can be seen in the difference between the spectra from the carburized iron and from pure iron. Suppose we have a carbon atom at the octahedral site, $\frac{1}{2}\frac{1}{2}0$, in Fig. 3.15. The number of iron atoms that are influenced by the

† The measured counting rate was 4000–12,000 counts/sec.

‡ The maximum channel number was 400, the Doppler velocity being 10 mm/sec.

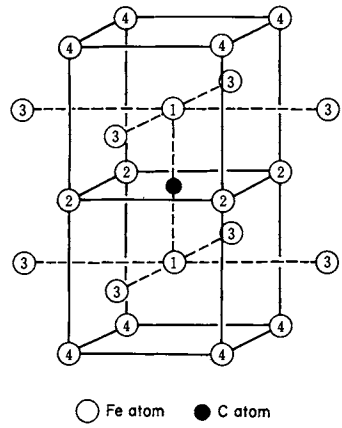

FIG. 3.15 Fe atoms around a C atom at an octahedral site in a b.c.c. lattice. ① 2, ② 4, ③ 8, ④ 8 atoms.

carbon atom will be 2, 4, 8, and 8 for the first, second, third, and fourth nearest neighbors, respectively. More distant iron atoms are assumed not to be influenced by the carbon atom. The difference between the two spectra was analyzed to consist of three components having the parameters shown in Table 3.4. The degree of absorption for each component also suggests that these absorptions are indeed produced by atoms at the first, second, and third plus fourth nearest neighbors.

As seen in Table 3.4, the parameters for the first nearest-neighbor atoms are quite different from those for others. The value of the internal field H_i for these atoms is 20% smaller than that of the others. Moreover, the spectrum has a negative isomer shift δ and a large quadrupole effect ε. These anomalous parameters of the spectrum were suggested to be related to the formation of covalent coupling between the 2s and 2p levels of the carbon atoms and the 3d level of the first nearest-neighbor iron atoms. On the other hand,

TABLE 3.4 Mössbauer parameters of α' martensite in Fe–4.2 at. % C[a]

	Number of Fe atoms (%)	Internal field H_i (kOe)	Isomer shift δ (mm/sec)	Quadrupole effect ε (mm/sec)
Nearest Fe atoms				
First	8.2	265 ± 2	-0.03 ± 0.05	0.13 ± 0.05
Second	14.5	342 ± 2	0.02 ± 0.05	-0.02 ± 0.05
Third and fourth	38	334 ± 2	0.01 ± 0.05	0.01 ± 0.05
Pure iron	—	330	0	0

[a] After Moriya *et al.*[54–57]

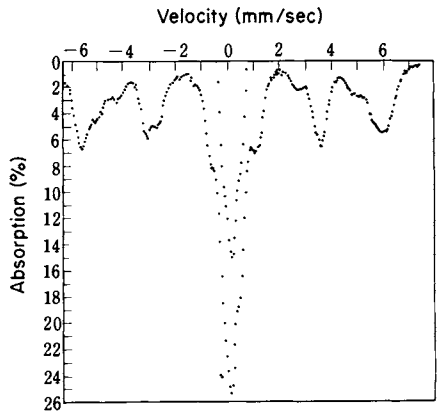

FIG. 3.16 Mössbauer spectrum of martensite in Fe–1.96% C. (After Genin and Flinn.[58])

iron atoms farther away than the second nearest neighbors are much less affected by the carbon atoms, and their effect on the Mössbauer pattern may be thought of as due simply to lattice distortion,[59] that is, the second and the third atoms move closer together, the fourth moves farther away.

The parameters for first nearest-neighbor atoms tell us that the iron atoms at these positions are strongly influenced by interstitial carbon atoms, though this may not necessarily be a direct evidence of large displacements of atoms in the c direction. However, including the results of the effect of atoms at the second, third, and fourth nearest neighbors, this experiment strongly suggests the existence of dipole strains due to interstitial atoms. The knowledge obtained here may also apply to the problem of carbon atoms dissolved in ferrite. The tetragonality of martensite is not due to short-range strains, but is related to the ordered occupation of octahedral sites by carbon atoms, which will be discussed later.

Soon after the study of Fujita *et al.*,[54–57] Genin and Flinn[58] made a similar study of the same problem with slightly different procedures and analyzed the data in another way. They carburized a thin iron foil to make carbon steel containing 1.96% C.† Since the quenched specimen consisted of γ crystals, due to the high carbon content, it was cooled in liquid nitrogen to obtain a large amount of α' crystals. The measurements were made at 77°K to avoid the smearing of absorption peaks due to thermal vibration. Figure 3.16 is the spectrum that was obtained.‡ The ordinate shows the degree of absorption and the abscissa the velocity of the source for the

† The x-ray diffraction pattern for the carburized specimen gave $a_\gamma = 3.638$ Å. By substituting this value in the general equation relating a_γ to the carbon content w (wt %), $a_\gamma = 3.572 + 0.033w$, $w = 1.96\%$ was obtained.

‡ The figure is reproduced upside down from the original to facilitate comparison with Fig. 3.14.

TABLE 3.5 Mossbauer parameters of α′ martensite in Fe–1.96% C[a]

Group	No. of neighboring C atoms	Internal field H_i (kOe)	Isomer shift (mm/sec)	Quadrupole effect ε (mm/sec)
0	0	350	+0.188	−0.06
1	1	340.74	+0.544	+0.063
2	>2	277.50	+0.210	+0.159

[a] After Genin and Flinn.[58]

Doppler effect, that is, the energy of γ rays absorbed. At the center of the figure, as before, there is a large absorption peak due to the retained austenite, γ, which is paramagnetic. In addition to this peak, we recognize six main peaks at almost the same positions as those of pure iron, with small subsidiary peaks, which can be classified into three groups having the Mössbauer parameters given in Table 3.5. Group 0 has parameter values close to those of pure iron; hence, this spectrum is produced by the iron atoms that are little affected by carbon atoms. This group corresponds to the spectrum that was used by Fujita *et al.* as the reference for their raw spectra. The parameters for group 2, on the other hand, differ a great deal from those of pure iron, so this spectrum may be attributed to the first nearest-neighbor atoms in the data by Fujita *et al.* However, Genin *et al.* gave another explanation. They interpreted the spectrum of this group as being produced by iron atoms influenced by two or more carbon atoms.[60]

Later, Fujita *et al.*[61,62] repeated their experiment at low temperatures. They cooled a steel containing 1% carbon to −196°C and measured the Mössbauer spectrum at this temperature. They obtained peaks similar to Genin's but interpreted them in another way; that is, they theorized that just after the subzero cooling the carbon atoms were situated at both the octahedral and tetrahedral sites, and that the atoms at the latter sites moved to the former positions as the temperature was raised to room temperature. After this experiment, Lesoille and Gielen[63] obtained results that could be interpreted similarly.

3.3.4 Internal friction from interstitial atoms

As described in Section 3.3.1, the interstitial atom in Fig. 3.11b will push apart the iron atoms at the first nearest-neighbor sites, which are located above and below the carbon atom. So, when the lattice is extended vertically, the short-range stress will be more or less relaxed. On the other hand, extension in a horizontal direction, for example, in the x direction, will

produce the opposite effect. Therefore, the movement of the interstitial atom from A to B may occur to reduce the applied stress. That is, the interstitial atom will change its position so as to have the axis of dipole strain in the tensile direction. In the case of compression, the opposite will occur. In other words, the external force will produce a newly ordered distribution of the carbon atoms in the specimen. When we apply an alternating force, the interstitial atoms may move back and forth between stable sites. Then elastic energy will be dissipated in the crystal, giving rise to internal friction. This is the origin of the phenomenon occurring at the so-called Snoek peak,[64] which for α ferrite crystals appears at about 40°C when the internal friction is plotted against the temperature at a frequency of about 1 Hz.

Since the internal friction curve shows only one peak, and since the atoms at the tetrahedral sites would not be sensitive to an external force, because of their symmetrical location with respect to the principal axes, it is natural to conclude that the interstitial atoms occupy octahedral sites. The magnetic aftereffect[65] and the elastic aftereffect[66] are also related to the behavior of interstitial atoms at octahedral sites.

These phenomena are caused by the effect of dipole strains, so the strength of the dipole strain can be roughly estimated from the relaxation strength of the Snoek peak. The results obtained by anelasticity measurements in various stress modes for single crystals of ferrite are listed, along with the x-ray results for martensite, in Table 3.6, where λ_1 and λ_2 are respectively, the strain values (per atom fraction) in the directions of the dipole and transverse axes, and $\lambda_1 - \lambda_2$ corresponds to the dipole strength. The values obtained for ferrite in Fe–C and Fe–N systems by anelasticity measurements are in agreement with those calculated for tetragonal martensite by using c/a from x-ray diffraction. This would mean that most of the carbon atoms occupy octahedral sites in ferrite as well as in martensite. The difference is that in ferrite the carbon atoms are randomly distributed, whereas in martensite their distribution is ordered.

TABLE 3.6 Average value of dipole strains produced by interstitial atoms

Alloy		Researchers	Method of measurement	$\lambda_1 - \lambda_2$
Fe–C	Ferrite	Dijkstra,[69]	Bending oscillation	1.07
		Swartz *et al.*[70]	Torsional oscillation	0.87
		Ino *et al.*[71]	Bending and torsional oscillation	0.78
	Martensite	Roberts[72]	X-ray diffraction	0.94
Fe–N	Ferrite	Dijkstra,[69]	Bending oscillation	0.97
		Swartz *et al.*[70]	Torsional oscillation	0.80
	Martensite	Bell *et al.*[73]	X-ray diffraction	0.90

The internal friction experiments just discussed are concerned with the Snoek peak for ferrite. On the other hand, in tetragonal martensite the carbon atoms are all in ordered sites and cannot contribute to produce the Snoek peak; the experiments confirm this absence. An internal friction peak for martensite appears at 220°C[67] for Fe–C alloys and at 180°C for Fe–N alloys.[68] These may correspond to the Köster peaks in deformed steel.

3.3.5 Tetragonality due to configurational ordering of the interstitial atoms

Ordering of the interstitial atoms in b.c.c. crystals can occur without external stress, provided that the interstitial content exceeds a certain value. The origin of this ordering can be considered as follows: If the dipoles are spaced closely together, so that their strain fields interact with each other, the dipole axes will all orient in one direction, mutually relaxing the strains and resulting in a diminution of the strain energy in the whole system. Such ordering of the distribution of the interstitial atoms distorts the lattice so as to produce tetragonality. This is the origin of tetragonal martensite. Though the ordered state possesses a lower strain energy, its configurational entropy term is smaller because of the smaller number of states, which tends to increase the free energy. The state of ordering will be controlled by a balance of these two effects. The situation is quite similar to that in conventional superlattice alloys. This ordering is often called *Zener ordering*, since Zener[74] first studied this problem thermodynamically.

Sato[75] carried out a statistical mechanics calculation of the ordering of interstitial atoms, utilizing the Bragg–Williams theory[76] of the order–disorder transition. The interactions of neighboring atoms were generalized, instead of limiting them to the elastic interaction. He concluded that the critical temperature T_c (°K) for the ordering of carbon atoms was proportional to the carbon content c (defined as the ratio of the number of carbon atoms to iron atoms), that is,

$$T_c \fallingdotseq \frac{\Gamma}{2.743k}\, c \qquad (\Gamma = 2\Gamma_1 + 4\Gamma_2), \tag{1}$$

where k is the Boltzmann constant and Γ_1 and Γ_2 are the interaction energies between two carbon atoms separated by $(a/2)\langle 100\rangle$ and $(a/2)\langle 110\rangle$, respectively. It is difficult to make an accurate theoretical evaluation of Γ; however, assuming that the tetragonal lattice is formed by balancing the interaction energy with the strain energy, we obtain

$$\Gamma = \tfrac{2}{3}N\lambda^2 E_{100} \tag{2}$$

where N is the number of iron atoms in a unit volume, λ is the tetragonal strain produced by a carbon atom (in a unit volume) moving to an ordered site, and

E_{100} is the Young modulus of iron in the [100] direction. Substituting Eq. (2) into Eq. (1) gives

$$T_c \fallingdotseq 0.243 \frac{N\lambda^2 E_{100}}{k} c. \tag{3}$$

Using X_c, the weight percent of carbon, instead of c, and letting $N_c = 3.92 \times 10^{21} X_c$, $E_{100} = 1.3 \times 10^{12}$ dyn/cm^2, $\lambda = 1.2 \times 10^{-23}$ (obtained from the lattice constant of the tetragonal martensite), we finally get

$$T_c \fallingdotseq 1330 X_c \quad (°\text{K}). \tag{4}$$

This equation agrees well with the result obtained by Zener, who used a simple statistical method.

Figure 3.17 shows the variation of T_c with X_c, Eq. (4). The region below the line corresponds to the tetragonal range in which the ordering of carbon atoms occurs. For instance, at room temperature, α' crystals containing less than 0.22 wt % of carbon have a cubic lattice, whereas those containing more than 0.22 wt % of carbon are tetragonal. This critical value is very close to 0.25 wt % C,[77] which has been obtained experimentally as the minimum value of carbon in tetragonal martensite. In the case of high nickel steels, the critical values are smaller.[78]

The carbon atoms in cubic martensite are thought to be distributed at random. This means that cubic martensite has the same crystal structure as supersaturated ferrite, except that lattice defects introduced during the martensitic transformation are present.

It should be noted that in carbon steels with very low carbon contents the theory above is applicable only to the ideal quench, that is, to situations in which no other reaction takes place during and after the quench. This is

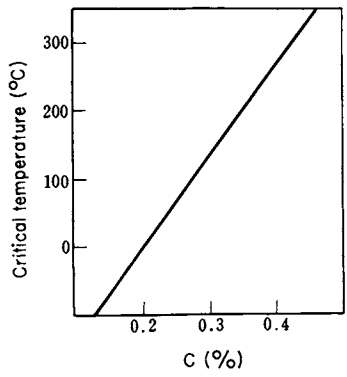

FIG. 3.17 Critical temperature for the ordering of C atoms in a b.c.c. lattice. (After Zener[74] and Sato.[75])

not expected to occur in reality because the M_s temperature for low carbon steel is usually very high, for example, 542°C for 0.026% C and 478°C for 0.18% C steel.[79] During quenching, the martensite must pass through a high-temperature region, though for only a short period, during which the carbon atoms may possibly move to nearby, more stable sites.

Speich[80] studied this problem for various carbon steels.† Specimens 0.25 mm thick were rapidly quenched in ice water containing NaCl (10%) and NaOH (2%). The quenching speed in that experiment was 10^4°C/sec. The specimen was put in liquid nitrogen just after quenching in order to suppress the diffusion of carbon atoms after quenching. Nevertheless, an evidence that carbon atoms had moved during quenching was observed. The electrical resistivity in the quenched state increased almost linearly with the carbon content, but below 0.2% C, the slope, that is, the contribution of carbon to the resistivity was smaller than that above this concentration. This fact indicates the occurrence of some phenomenon in the martensites containing less than 0.2% carbon. The intensity of the Snoek peak of those martensites was as small as one fifth of that of the ferrite when a comparison was made at the 0.026% C content.

These two observations support the concept that in steels containing less than 0.2% C, some of the carbon atoms in martensite cluster on defects, for example, on dislocations or lath boundaries. In this case, 90% of the carbon atoms is thought to have clustered during quenching. Even if this value is an overestimate, the foregoing phenomenon and Zener's condition for the disordering of carbon atoms explain why martensite in very low carbon steel maintains the cubic structure.

It should be added that disordering by deformation has been observed in specimens in which all the carbon atoms had been in ordered sites. Al'shevskiy and Kurdjumov[81] quenched an Fe–14% Ni–1% C alloy ($M_s = -24$°C), cooled it to −197°C, and took an x-ray diffraction photograph. Next, they deformed the specimen by 29% without changing the temperature and took an x-ray photograph again at the same temperature. A comparison between the two photographs revealed that the 110 line, a component of the tetragonal doublet, was broadened and shifted to a low-angle position by deformation, which corresponds to a decrease in the tetragonal ratio c/a. Decomposition of the martensite, had it occurred, would have produced a shift of the 011 line to the high-angle side. Therefore, the change in c/a may be considered the result of a disordering of the carbon atoms by cold working. After being cold worked, the specimen was kept at room temperature and an increase in c/a was observed. This suggests that ordering of the carbon atoms again occurred at room temperature.

† Impurities are Si, 40; Mn, 20; S, 30; P, 10; N, 10 ppm.

3.3.6 Amount of local strain around a dipole

So far, we have seen that interstitial atoms in the b.c.c. lattice produce dipole strains. Let us now consider the local distribution of strains around such a dipole, not the averaged strain field described in Section 3.3.2. The strain distribution due to a point defect has already been calculated by the theory of elasticity. If the point defect stresses an elastically homogeneous isotropic medium of infinite size, the displacement will have spherical symmetry, as expressed by[82]

$$\boldsymbol{\mu}_s = \boldsymbol{i}_r C_s / r^2. \tag{1}$$

If it stresses the elastic medium in only one direction, the displacement will have an axis of symmetry and be expressed as[83]

$$\boldsymbol{\mu}_d = \boldsymbol{i}_r \frac{C_d}{r^2}\left[-\left(\frac{\lambda+\mu}{2\mu}\right)+\left(\frac{5\mu+3\lambda}{2\mu}\right)\cos^2\phi\right] - \boldsymbol{i}_\phi \frac{C_d}{r^2}\sin\phi\cos\phi \tag{2}$$

where r and ϕ are the polar coordinates (r is the distance from the point defect and ϕ the angle from the axis of symmetry), $\boldsymbol{i}_r$ and $\boldsymbol{i}_\phi$ are the unit vectors in directions r and ϕ, respectively, λ and μ are the Lamé constants, and C_s and C_d are measures of the strength of the point defect and are proportionality constants determined by experiment. Consider now the case in which carbon atoms are introduced interstitially in the b.c.c. lattice of iron. If we assume that the tetragonality is formed by homogeneous distribution of carbon dipoles having a common axis, [001], the proportionality constants can be obtained from the values of lattice constants of martensite. Goland and Keating[84,85] determined the proportionality constants by this assumption, and obtained the strain distribution as

$$\boldsymbol{\mu} = \boldsymbol{i}_r\left(\frac{D + E\cos^2\phi}{r^2}\right) + \boldsymbol{i}_\phi\left(\frac{F\sin\phi\cos\phi}{r^2}\right) \tag{3}$$

where

$$D = -0.44191\,\text{Å}^3, \qquad E = 2.42760\,\text{Å}^3, \qquad F = -0.56551\,\text{Å}^3$$

and the r values are in angstroms.

Figure 3.18 shows the strain map obtained from Eq. (3), indicating an equi-displacement locus around a dipole. Table 3.7[84,86–88] shows the calculated values of the displacement produced by a carbon atom at $\frac{1}{2}\frac{1}{2}0$. The $\mu_1{}^c$ is the displacement of an iron atom at $\frac{1}{2}\frac{1}{2}\frac{1}{2}$ in the c direction, and $\mu_2{}^a$ is the displacement at 000 in the a direction. These values support the previous assumption that the distortion in the c direction must be the largest, although the absolute values are quite different among researchers.

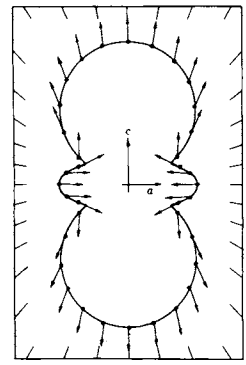

FIG. 3.18 Elastic displacement field around a dipole. The solid curve is the locus of displacements of constant magnitude. The tetragonal axis is denoted by c and the direction of the displacements is indicated at points on the locus at 10° intervals. (After Keating and Goland.[84])

Next we examine whether the theoretically calculated strain is consistent with the average strain obtained from x-ray diffraction data as described in Section 3.3.2. The intensity of an x-ray diffraction line will be decreased by the short-range displacement of atoms as follows:

$$I = KH \exp(-L) \tag{4}$$

where H is the frequency factor, K includes the Lorentz polarization factor and the atomic scattering factor, and L is a quantity related to the displacement of the atoms. K will be approximately the same for the tetragonal doublet. Because of the large displacement of iron atoms near the carbon, we may not simply say that L is proportional to $\langle \mu^2 \rangle^{1/2}$, as in the case of thermal vibrations. Krivoglaz[89] obtained an equation,

$$L = -\sum_n \ln\{1 + 2p(1-p)[\cos(\boldsymbol{\mu}_n \cdot \boldsymbol{k}) - 1]\}, \tag{5}$$

in which $\boldsymbol{\mu}_n$ is the displacement of the nth atom, $\boldsymbol{k}$ is the vector perpendicular to the reflecting plane and has a magnitude of $4\pi \sin\theta/\lambda$ (θ is the Bragg angle), λ is the wavelength of the x rays, and p is the ratio of the number of carbon atoms to that of iron atoms.

TABLE 3.7 Displacement of Fe atoms due to the presence of a C atom at $\frac{1}{2}\frac{1}{2}0$ in a b.c.c. lattice

	Keating and Goland[84]	Johnson *et al.*[86]	Krivoglaz and Tikhonova[87]	Fisher[88]
$\mu_1{}^c$	+0.968 Å	+0.320 Å	+0.486 Å	+0.272 Å
$\mu_2{}^a$	−0.078 Å	−0.060 Å	−0.003 Å	−0.069 Å

TABLE 3.8 Intensity ratios of tetragonal doublets of martensite (experimental: 1.33% C steel)[a]

	$I'(002)/I'(200)$	$I'(112)/I'(211)$
As quenched	0.481	0.578
Aged 3 weeks at room temperature	0.353	0.474

[a] After Moss.[90]

TABLE 3.9 Intensity ratios of tetragonal doublets of martensite (theoretical)[a]

$\mu_1{}^c$ (Å)	$I'(002)/I'(200)$	$I'(112)/I'(211)$
0.45	0.604	0.689
0.60	0.522	0.642
0.755	0.490	0.643

[a] After Moss.[90]

Using Eqs. (3), (4), and (5), and comparing with the observed intensity ratios of the component reflections in the tetragonal doublet, we may check whether or not the theoretical displacements are quantitatively reasonable. Moss[90] checked this point for subzero-cooled martensites in a 1.33% C steel. He used Fe–K_{α_1} radiation monochromatized by a curved LiF crystal and measured the diffracted intensity accurately by using a pulse height analyzer to remove the $\frac{1}{2}\lambda$ contribution. The observed intensity ratios are listed in Table 3.8, where the intensities I' were corrected for the frequency factor and other factors. The calculated ratios for values of $\mu_1{}^c$ are listed in Table 3.9 for comparison. We might say that the two sets agree fairly well. The data are also very similar to those in Table 3.3. The experimental data in Table 3.8 indicate that aging increases the dipole strain effect, which suggests that further ordering occurs at room temperature.

3.4 Initial stage of the formation of martensite crystal

It is very difficult to determine the process of nucleation or embryo formation of martensite experimentally; therefore, the only attempts to solve this problem that have been made so far have been theoretical. Martensite nucleation remains one of the main unsolved problems in transformation

theory. Isotropic models based on classical thermodynamic theory similar to the case of precipitation from a liquid solution were proposed at one time. But they can never be adapted to a solid-state transformation, and a more detailed crystallographic model based on the atomistic rearrangements is required. Thus, it is necessary to investigate the problem with tools, such as the field ion microscope that have enough resolution to distinguish individual atoms. Unfortunately, however, no such results have been obtained in this area, so in this chapter a few results on the early stage of martensite transformations determined by transmission electron microscopy are presented.

3.4.1 Initial stage of the f.c.c.-to-h.c.p. transformation

High Mn steel is a representative alloy in which h.c.p. martensite (hereafter denoted by ε) forms. In the initial stage of the formation of ε, as discussed in Chapter 2 and shown in Fig. 2.36, many very thin parallel plates of the ε phase are formed first, and these combine so that a bulkier ε phase results. No continuous increase in the thickness of the individual ε plates occurs in this process. The mechanism of nucleation of the initial thin ε plate remains unclear.

On the other hand, ε plates induced by plastic deformation are formed in a slightly different way. To examine the process, many studies have been done of 18–8 stainless steels and several facts have been reported by Venables[91] and by Fujita and Ueda,[92] in addition to those already mentioned in Section 2.3. Fujita and Ueda, by means of transmission electron microscopy, continuously observed the formation of stacking fault groups and their accumulation, utilizing the heating effect of electron irradiation. They examined the distinction between overlapping stacking faults and an ε plate, making use of their effects on the appearance of extinction contours. The specimens were 18–8 stainless steel plates annealed for 5 hr at 900°C and subjected to tension to give a 5% elongation at -196°C. Some of the results are shown in Figs. 3.19 and 3.20. Figure 3.19c is an electron diffraction pattern taken from area (a), showing the h.c.p. structure. The dark-field image from the $(1\bar{1}01)$ reflection is shown in Fig. 3.19b. From these micrographs, it was concluded that the banded structures seen in Fig. 3.19a, b are ε phase crystals.

Figure 3.20 is a micrograph of another field, in which stacking faults inclined to the surface exhibit parallel interference fringes. Each stacking fault is terminated by a pair of partial dislocations. The parallel fringes are often abruptly shifted, indicating that the number of overlapping stacking faults changes. The number of stacking faults increases with increasing deformation. In this micrograph, many stacking faults are already overlapping in some regions. These overlapping stacking faults are quite similar to the

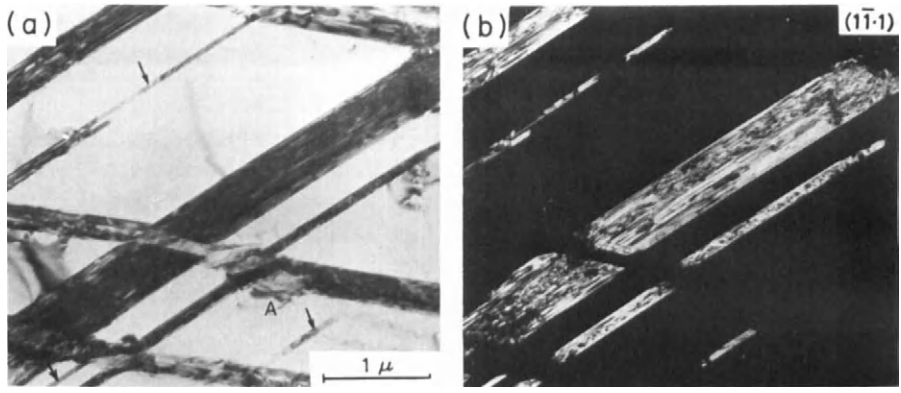

FIG. 3.19 ε martensite produced by tensile deformation (5%) at −196°C in 18–8 stainless steel.
(a) Bright-field image of electron micrograph.
(b) Dark-field image by (1$\bar{1}$01) reflection.
(c) Electron diffraction pattern of [25·3] zone.
(After Fujita and Ueda.[92])

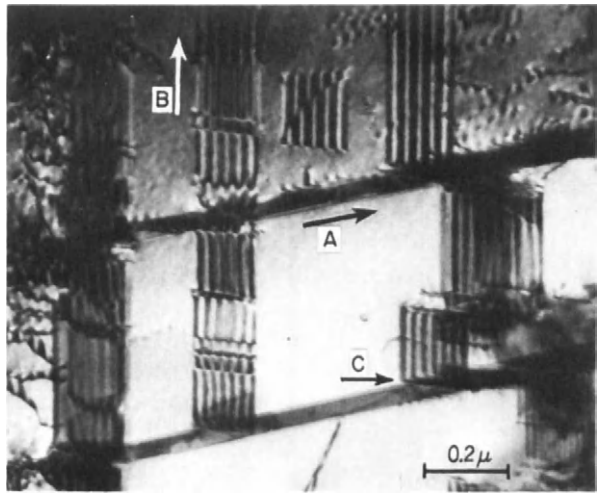

FIG. 3.20 Electron micrograph showing the initial stage of the formation of ε martensite and stacking faults produced by tensile deformation (5%) at −196°C in 18–8 stainless steel. (Bands in direction A are the ε martensite at the initial stage, and stripes in direction B are stacking fault fringes.) (After Fujita and Ueda.[92])

structure of an ε plate, because the f.c.c. structure with stacking faults in every other (111) plane is nothing but the ε phase.

The bands along direction A in Fig. 3.20 and the thin plates indicated by the arrows in Fig. 3.19 are considered to be the initial stage of ε formation. From the surface of the ε band, indicated by arrow C in Fig. 3.20, stacking faults of the secondary slip system are successively generated by the stair-rod mechanism. It is possible that the front partial dislocations on the primary slip system move to the secondary slip planes by cross slip in every other atomic layer. This has been considered to be the process by which ε forms. When the cross slip of partial dislocations occurs on secondary slip planes separated by more than two atomic layers, the result is stacking faults in the ε phase. In fact, one can recognize this phenomenon from the contrast of ε bands in Fig. 3.19. Furthermore, it is evident that the ε band contains many (0001) stacking faults, since the individual spots in the electron difffraction pattern always have long streaks when the incident beam is parallel to the (0001) plane.

From these facts, Fujita *et al.* concluded that the nucleus of the ε phase induced by plastic deformation does not form three dimensionally, but is formed by overlapping of stacking faults.

3.4.2 Initial stage of the f.c.c.-to-b.c.c. (or b.c.t.) transformation

As described in Chapter 6, Jaswan speculated that a half dislocation further divided into halves in the f.c.c. austenite is possibly able to develop into a nucleus of b.c.c. martensite because the atomic arrangements at the quarter dislocation and in the b.c.c. structure are very similar to each other. On the other hand, Otte[93] examined stacking faults in an austenitic steel by means of x-ray diffraction and optical microscopy, and he concluded that Jaswan's speculation is questionable, since no direct relation has been found between the occurrence of stacking faults and the formation of b.c.c. martensite. However, Venables[91] found small α′ crystals at the intersection of two ε plates of different systems. The α′ crystal had the shape of a rod along a ⟨110⟩ direction since it was formed along the intersection of two {111} planes. The small crystal indicated by A in Fig. 3.19a may be an α′ crystal occurring where two ε plates cross.

Dash and Brown[94] studied the nucleation problem of martensite by means of electron microscopy of an Fe–32.3% Ni alloy, but could find no evidence of a nucleus of an α′ crystal.† In the initial stages of α′ formation, however,

† Previously another research group[95] observed an Fe–Ni alloy by transmission electron microscopy and found small parallelogram crystals. At that time they considered these crystals to be martensite nuclei. However, it was clarified in subsequent works[96–99] that these crystals were nothing more than sections of ribbonlike transformation twins in martensites.

they always observed {111} shears in austenite grains. Those shears were occasionally found to have originated from the end of a lenticular martensite plate and to be parallel to the habit plane. Dash and Brown theorized from these results that {111} shears might play a certain promotive role in α' formation.

Shimizu *et al.*[100] also studied the initial stages of martensitic transformation in an Fe–7.90% Cr–1.11% C alloy, which is a typical specimen for $\{225\}_\gamma$-type martensites. When a specimen of the alloy was cooled to $-40°C$ to $-50°C$, about 20%–30% martensite was produced in the specimen, since the M_s temperature was about $-36°C$. Figure 3.21 is an example of transmission electron micrographs taken from a thin specimen. In the figure, the parts marked S.F. are considered to be stacking faults parallel to the {111} planes in austenite because of their appearance, the relation with neighborhood dislocations, and the corresponding diffraction pattern. Other features, marked M_1 and M_2, were parallel to a (252) plane (precisely speaking, to a plane between the (252) and (121) planes); moreover, moiré fringes can be seen in M_1. These morphologies suggest that the M_1 and M_2 regions may be thin martensite platelets. The S.F. regions are connected with the M_1 and M_2 regions. If the martensite (M regions) was produced first, the stacking faults (S.F. regions) might have occurred to accommodate the transformation strains; on the other hand, if the stacking faults were produced first, martens-

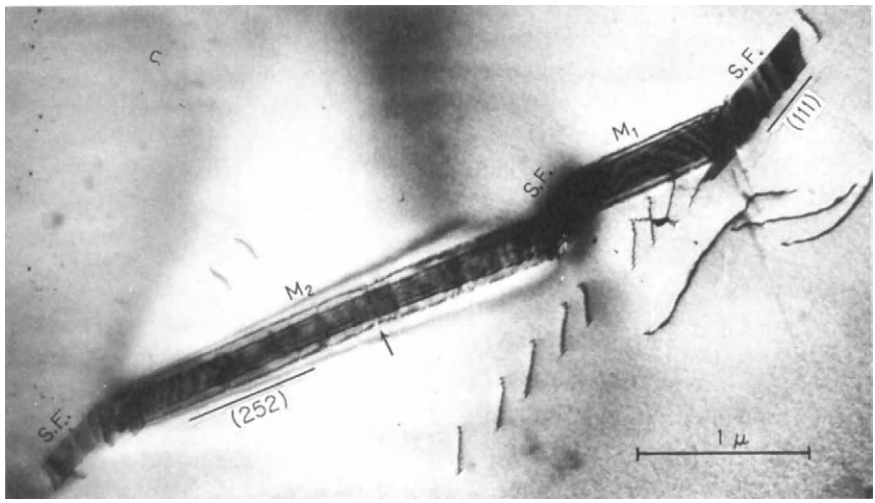

FIG. 3.21 Electron micrograph taken from an Fe–7.90% Cr–1.11% C alloy cooled to $-40°C$, showing that martensite platelets (M_1 and M_2) are formed connecting with stacking faults (S.F.) in an austenite, and that small $\{112\}_{\alpha'}$ transformation twins (arrow) are recognized in the platelets. (After Shimizu *et al.*[100])

ite might then have nucleated at the stacking faults. Striations are visible at M_2, as indicated by the arrow. These striations were parallel to the projection of a $[\bar{1}01]_\gamma$ or $[\bar{1}\bar{1}1]_\alpha$ direction onto the specimen surface and they can be considered to be very small twins produced by lattice-invariant shears during the martensitic transformation. Such twins were clearly observed in larger martensite crystals, and the twin plane was verified to be the $(112)_\alpha$ plane, which is inclined to the tetragonal c axis by a larger angle than in other twin variants. The habit planes of martensites connected with a special $(111)_\gamma$ stacking fault plane are only $(252)_\gamma$, $(225)_\gamma$, and $(522)_\gamma$, all of which are inclined to the $(111)_\gamma$ plane by 25°. This fact must be taken into account in martensite nucleation theories.

On the other hand, some experiments indicate that martensite does not always nucleate at a stacking fault but can also nucleate at other defects, such as austenite grain boundaries and other interphase boundaries. An example of nucleation at an interphase boundary was reported by Warlimont[101]. The specimen he used was an Fe–1.15% C–5.1% Mn alloy that was quenched from 1100°C and aged for 30 min at 450°C, after which it was quenched in iced brine. In this case, cementite crystals were produced in the austenite grains, and α' martensite was nucleated at the interphase boundaries between the austenite and cementite crystals. The orientation relationships between the martensite and cementite (θ) crystals were determined to be

$$(010)_\theta \| (111)_{\alpha'}, \qquad [001]_\theta \| [1\bar{2}1]_{\alpha'} \quad \text{within } 4°,$$

or

$$(103)_\theta \| (011)_{\alpha'}, \qquad [010]_\theta \| [\bar{1}1\bar{1}]_{\alpha'}.$$

Such a crystallographic relation seems to suggest the possibility that cementite plays some role in the formation of α' martensites.

3.5 Single-interface growth of martensite

Martensite in some alloys grows very quickly, whereas in others it grows slowly. Such a difference in growth rate may be attributed to the amount of lattice deformation during the martensitic transformation. When the amount is large, the transformation occurs only with difficulty and can begin only after extreme supercooling of the specimen. The heat of transformation in such a case can easily be absorbed, so martensites can grow quickly once the nuclei are produced. On the other hand, if the amount of lattice deformation is small, the transformation can begin more easily and does not require so much supercooling. The transformation propagation, however, ceases soon because of the temperature rise due to the heat of

transformation. Thus, the transformation does not progress unless the temperature becomes low enough to enable the material to absorb transformation heat without raising its temperature to the critical transformation temperature. It is, therefore, possible to reduce the transformation rate by reducing the cooling rate. In addition, when the lattice deformation is small, transformation strains may be relieved easily. Therefore, it is also possible to give rise to single-interface transformation by cooling the specimen under a suitable temperature gradient. In fact, such a mode of transformation has been observed in detail for some alloys in which the transformation rate may be fairly slow. Two examples of such transformations are described next.

3.5.1 In–Tl alloys

As mentioned in Section 2.6.1, this alloy system exhibits an f.c.c.-to-f.c.t. martensitic transformation. In the case of 20.75 at. % Tl, the transformation strain can be expressed in a matrix form.

$$\begin{bmatrix} a_t/a_c & 0 & 0 \\ 0 & a_t/a_c & 0 \\ 0 & 0 & c_t/a_c \end{bmatrix} = \begin{bmatrix} 0.988 & 0 & 0 \\ 0 & 0.988 & 0 \\ 0 & 0 & 1.021 \end{bmatrix},$$

using the lattice constants of the parent and martensite, $a_c = 4.75$ Å, $a_t = 4.69$ Å, and $c_t = 4.85$ Å. The value of this matrix is nearly 1 and the shear angle is as small as 3°. Thus, a single-interface transformation, as mentioned above, can be expected to occur in In–Tl alloys. Moreover, the transformation temperature on cooling differs from that on heating by only 2°.

In an experiment by Basinski and Christian,[102] a fully annealed single crystal of the alloy exhibited a single-interface martensitic transformation when the crystal was cooled under a suitable temperature gradient. The transformation proceeded by motion of a single interface traveling from the cooled (53°C) end of the crystal to the other end. The traveling interface was parallel to a {110} plane. The martensite obtained was internally twinned, as mentioned previously, but the twins just behind the interface were so narrow that the surface relief effect in that region was not detectable by optical microscopy. Such a region, the accommodation region, is about 10 times as wide as that of the twins. The accommodation region was narrower on heating, but wider on cooling; its width increased as the velocity of the traveling interface increased, becoming as large as 1 mm. As mentioned previously, the velocity of the interface was proportional to the cooling rate of the specimen. For example, the velocity was 0.05 cm/sec when the cooling rate was 20°C/min. This value, however, is an average of nonuniform velocities. If the temperature at the interface is raised by heating, the

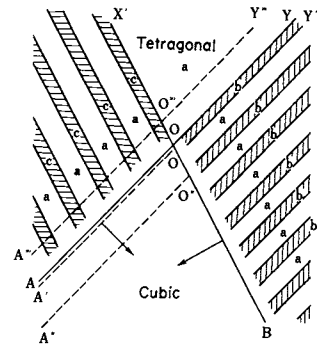

FIG. 3.22 A schematic illustration of the crossing of two transformation fronts in an In–Tl alloy. (After Basinski and Christian.[102])

interface moves in the opposite direction, the martensite phase reverts to the parent phase, and the lamellar structure completely disappears. Thus, the specimen returns to a single crystal, and therefore the transformation may be said to be perfectly reversible.

A more interesting phenomenon is observed[103] when the interfaces of two martensite crystals within the parent crystal cross each other. This is shown schematically in Fig. 3.22, where one interface, AO, crosses another interface, BO. If the first shear in one martensite has the same elements as the second shear in the other martensite, interface AO advances, producing two variant crystals, a and c, and interface BO produces a and b variants; thus the region swept by the two interfaces becomes a single crystal, the twinned structure disappearing. Such a disappearance of the twin is reasonable considering the relation of the two shears.

If the interface motion is stopped for a time, a stabilizing effect occurs in the neighborhood of the arrested interface. This effect can be attributed to a relaxation of transformation strains during the arrest period, even though the strains are very small.

This alloy exhibits a shape memory effect, in that a plastically deformed specimen reverts to the undeformed original shape when the deformed specimen is heated to a temperature above its A_s point. The shape memory effect, together with similar effects in other alloys, will be described in Section 5.2.6. The rubberlike elasticity of martensite specimens is discussed in Section 3.6.

3.5.2 Au–Cd alloys

As described in Section 2.5.4, the Au–Cd alloy with a composition of 47.5 at.% Cd exhibits a martensitic transformation from the CsCl-type ordered β_1 phase ($a_0 = 3.3165$ kX) to an orthorhombic (2H-type) γ_1' phase

($a = 3.1476$ kX, $b = 4.7549$ kX, $c = 4.8546$ kX). The lattice deformation in this transformation expressed in a matrix form is

$$\begin{bmatrix} b/\sqrt{2}a_0 & 0 & 0 \\ 0 & c/\sqrt{2}a_0 & 0 \\ 0 & 0 & a/a_0 \end{bmatrix} = \begin{bmatrix} 1.0138 & 0 & 0 \\ 0 & 1.0350 & 0 \\ 0 & 0 & 0.9491 \end{bmatrix}.$$

The value of the determinant of this matrix is also nearly 1 and the shear angle is about 3°. The M_s and A_s temperatures of this alloy are 60°C and 80°C, respectively, the difference between them being only 20°C. It is therefore expected that this alloy will exhibit a single-interface transformation, like the In–Tl alloy.

The transformation behavior of this alloy was observed in detail by Chang.[104] Figure 3.23a shows the behavior of a traveling interface on heating; the abscissa and the ordinate represent the frame number and the interface position, respectively, in cinemicroscopy. The curve has irregular steps but forms a straight line on the average; that is, it represents a constant interface velocity. Figure 3.23b shows the behavior on cooling; the curve is also a straight line on the average, although it has little irregularities and small steps. Thus, the interface velocity V is proportional to the heating or cooling velocity (dT/dt), so it can be represented as

$$V = k(dT/dt)$$

where the constant k depends on the transformation temperature. Since the constant k can also be considered to depend on the activation energy

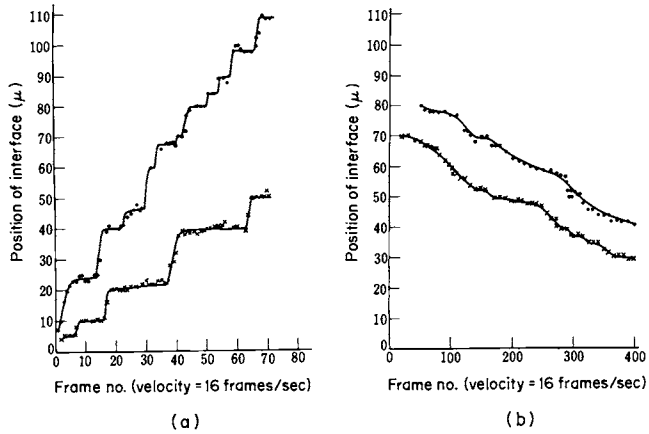

FIG. 3.23 Traveling behavior of transformation front on (a) heating and (b) cooling (Au–47.5 at.% Cd). (After Chang.[104])

Q', it may be represented in the form

$$k = k_0 \exp(-Q'/RT).$$

The activation energy in this expression was found from the experimental data to be 22–27 kcal/mole.

Consider the case in which a single interface moves across a specimen after it has been stopped at a place for a time by interrupting the cooling. If such a specimen is again heated and undergoes a reverse transformation, the returning interface may be stopped for a time at the place where the advancing interface had been stopped on cooling, notwithstanding that the specimen is still being heated. After a further increase in temperature, the interface starts to return and regains its previous velocity. The stopping period t' of the interface may be represented by the expression

$$t' = ft \exp(-Q/RT)$$

where t is the time period during which the cooling was interrupted. Putting experimental data into this expression gives $Q = 24$ kcal/mole. This value is nearly equal to that of Q' determined from the variation in k with T.

The value of the activation energy obtained in the foregoing two experiments is not very accurate, and its true meaning is ambiguous at present. Nevertheless, considered together with the results of x-ray diffraction studies, the interface-stopping phenomenon seems to suggest that the stabilization effect was due to stress relaxation. Another possibility should also be considered: atomic diffusion in the vicinity of the stopped interface may play a role in the stabilization effect.

3.6 Rubberlike elasticity of martensite

Ölander[105] and Benedicks[106] were the first to point out that a bar composed of β_1' or γ_1' martensite of a Au–Cd alloy has rubberlike characteristics such that a bar drastically deformed by applied stress returns to its original form with removal of the stress. Chang and Read[107] observed the following facts about this rubberlike elasticity,† in a bar specimen made by converting a β_1 single crystal of Au–47.5 at. % Cd into a β_1' martensite by multi-interface transformation. The elastic modulus was measured in three-point bending, with the results shown in Fig. 3.24, where the ordinate represents the load, and the abscissa the deflection of the center point of the specimen. The specimen is apparently elastic when subjected to large strains because it straightens completely with removal of the load. The load-deflection curve, however, is not linear; the apparent modulus decreases with an increase in

† This characteristic is also called *ferroelasticity*.[108]

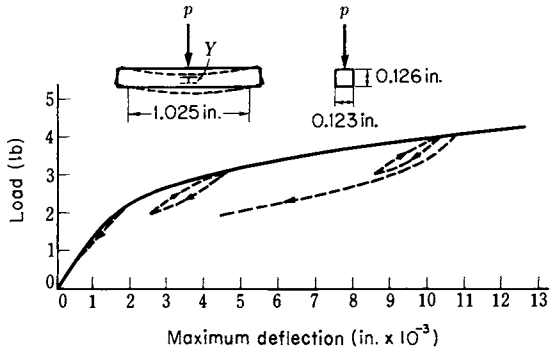

FIG. 3.24 Rubberlike elasticity of a Au–47.5 at.% Cd alloy. (After Chang and Read.[107])

the load. Considering E as the apparent modulus for one point on the curve and treating the specimen as a conventional elastic body, we get

$$Y = -Pl^2/48EI$$

where I is the moment of inertia of the cross section of the bar, l the distance between the fulcrums, P the load, and Y the amount of deflection of the center point. The apparent modulus calculated at each point on the curve using this formula decreases by a factor of 2 with the load over the range investigated, as can be seen in Table 3.10. Even the largest modulus, at a load near 0, is one seventh of that for aluminum and one twentieth of that for iron, and in this respect the alloy behaves as if it were a rubber.

Such rubberlike elasticity is also found in the tetragonal martensite of In–Tl alloys. The smaller the axial ratio, the more easily (101) twins nucleate and the more pronounced the rubberlike characteristics are. Burkart and Read[109] observed the following. First, when the martensite specimen is

TABLE 3.10 Apparent Young's modulus of γ' martensite in an Au–47.5 at. % Cd alloy[a]

Load (lb)	E (lb/in.^{2})
0	1.5×10^6
2	1.1×10^6
3	0.55×10^6
4	0.61×10^6
6	0.66×10^6

[a] After Chang and Read.[107]

strained, sounds due to twinning can be heard. Under a microscope during the straining it is observed that the twin boundaries migrate; one of the twin pair becomes wider while the other becomes narrower with increasing strain, and finally the boundaries disappear, so that the specimen is seen to be uniformly bright. Once this stage is reached, it is difficult to increase the strain further.[110] In conclusion, the strain in this phenomenon is not a true elastic strain, but is deformation by detwinning; that is, the deformation is really plastic. When the load is removed, however, the initial internal twins appear and the specimen returns to its initial shape.†

Basinski and Christian[113] proposed that although one of the twin pair seems to have entirely disappeared as a result of the application of a load, small stressed portions remain, and when the load is removed, those portions act as nuclei of the original internal twins, and the specimen returns to its initial shape.‡ However, unless the stressing temperature is sufficiently low, the specimen does not return completely to the initial shape when the stress is removed. This fact seems to be related to the relaxation of strains at sufficiently high temperatures and to stabilization owing to the migration of impurity atoms. On the other hand, rubberlike elasticity does not appear in specimens that have just been transformed, but appears in specimens that have been aged for some time (about one day for the Au–Cd alloy).

Basinski and Christian,[113] using the idea of twinning dislocations, explained the reversion of internal twins (detwinning) by stress. The rubberlike elasticity appears when the distortion by detwinning is small, as in alloys with a small tetragonality ratio, c/a. Therefore, this behavior is also expected in Cu–Mn,[117] Cr–Mn,[118] In–Cd,[119] and $BaTiO_3$.[120]

There are some alloys in which original shape does not recur upon removal of the load at room temperature, but does reappear at slightly higher temperatures. Enami and Nenno[121] found such a phenomenon in the CuAu-I-type martensite produced from the β_1 phase (B2 type) of a Ni–Al alloy. They used a specimen of Ni–35.3 at. % Al–1 at. % Co alloy and quenched it in ice water from 1250°C to form 100% martensite. The specimen was then bent§ at room temperature, and it remained bent even after the load was removed. Shape recovery was induced by heating to about 280°C. Therefore, if the temperature during bending had been above that temperature, the specimen

† In the γ_1' martensite of a Cu–14.2% Al–4.3% Ni alloy, similar phenomena have been observed.[111,112]

‡ Without such a hypothesis it is possible to explain this phenomenon by the pole dislocation mechanism.[114,115] According to another theory,[116] twinning does not take place directly, but portions with favorable orientations revert to the parent phase and then the reverted phase is transformed to martensite with favorable orientations, so that the internal stress is relaxed, and thus the result is the same as in the case of twinning.

§ According to another experiment[122] applying compression, the shape recovery is almost complete provided that the load is not too much greater than the yield point.

would have returned to its original shape upon removal of the load, exhibiting rubberlike elasticity. The shape recovery in the foregoing example may be regarded as a kind of shape memory effect. But this kind of memory effect is different in nature from that occurring in the reverse transformation of some alloys, such as Au–Cd (Section 5.2.6), because in this alloy the temperature of the reverse transformation is above 500°C. The memory effect in the present case is considered to be due to the detwinning, for the martensite in this alloy contains internal twins (Section 5.2.6).

3.7 f.c.c. martensite produced by reverse transformation

Face-centered cubic structure has frequently been observed in the course of heat treatment, being produced from b.c.c. martensite (α') by reverse transformation. The appearance of the reverted γ (γ_r) is an important phenomenon because the nature of this γ_r differs from that of the retained austenite γ, though their crystal structures are the same. Since there have been no definitive studies of the reverse transformation in commerical alloys, we will discuss the results obtained for iron, Fe–Ni and Fe–Ni–C alloys, about which basic information has been obtained. The discussion is divided into two parts: reverse transformation induced by heating and that induced by high pressure.

3.7.1 Reverse transformation (α' to γ_r) by heating

Even in the case of pure iron, α' martensite can be produced by ultrahigh-speed quenching. The γ_r reverted from such martensite by heating is not different from ordinary f.c.c. iron. However, Fe–Ni alloys of higher nickel content where the reverse transformation temperature (A_s temperature) is lower than the recrystallization temperature give interesting results.

We reconsider an old experiment done by Nishiyama using an Fe–30% Ni alloy.[123] As cooled from high temperatures, this alloy has an f.c.c. structure, since its M_s point is below room temperature. Figure 3.25a shows a Laue photograph of a single crystal of this alloy taken by white x rays incident to the [111] direction.

Figure 3.25b was taken of the same orientation of the specimen after transformation to martensite by cooling in liquid air. It shows Laue spots from polycrystals with some texture. It was clarified, from photographs taken with characteristic x rays, that this texture was composed of twelve variants of the transformed b.c.c. phase, and was different from that produced by deformation. Then, after heating for 15 min at 500°C followed by slow

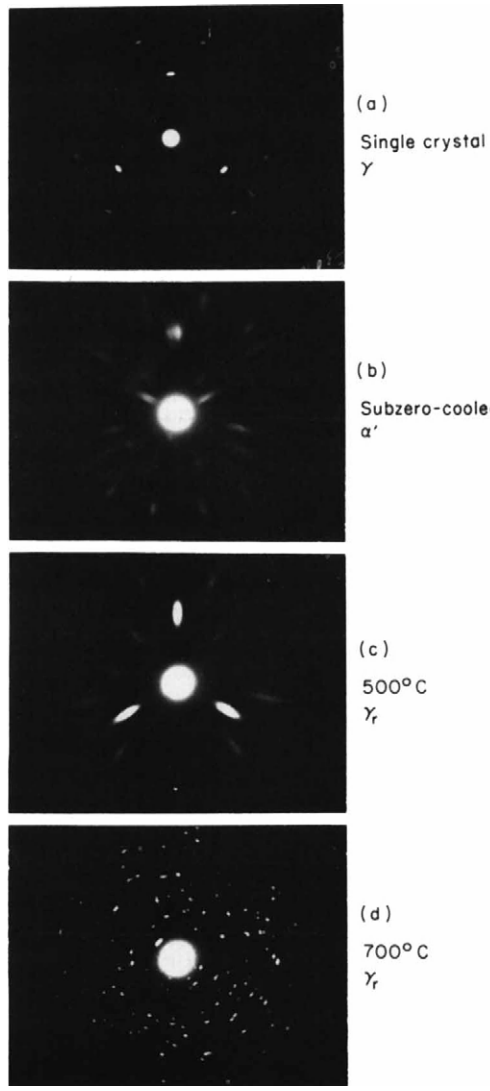

FIG. 3.25 Transformation of γ to α' to γ_r in an Fe–30% Ni alloy. (After Nishiyama.[123])

cooling, the photograph in Fig. 3.25c was taken of the same specimen with the same incident direction. This shows the somewhat diffuse Laue spots of a single f.c.c. crystal of the same orientation as in part (a). That is, all the α' variants composed of the different orientations return to the f.c.c. structure (γ_r) with almost the same orientation as that of the initial specimen.

In the transformation of α' to γ_r, twelve γ_r variants can be produced from one α' crystal in general, and hence about $12 \times 12 - 11 = 133$[†] variants of γ_r might be produced through the transformation of γ to α' to γ_r. In the present case, however, the transformation by just the reverse process is dominant for each variant. This memory effect is due to the residual transformation stress accompanying each α' martensite. The stress generated by the $\gamma \rightarrow \alpha'$ transformation naturally favors the reverse shape change when the $\alpha' \rightarrow \gamma_r$ transformation takes place. Therefore, α' returns to γ_r with the same orientation as before transformation, again yielding a single crystal. However, the Laue spots of the γ_r exhibit asterism, as shown in Fig. 3.25c. This means that lattice defects exist in the γ_r and that the γ_r is made up of subcrystals with slightly different orientations.[‡]

The lattice defects are not decreased by heating for 15 min at 550°C, but they are slightly decreased by further heating for 30 min at 600°C. Further annealing for 30 min at 700°C gives Fig. 3.25d, which shows a polycrystalline γ phase with random orientations due to recrystallization.

The mechanical properties of γ_r with such a high density of lattice defects must differ from those of retained austenite. In an Fe–33% Ni alloy,[127] the yield stress and maximum elongation values of the γ_r produced by heating α'[§] for 2 min at 400°C are, respectively, twice and one half of those for retained austenite. Thus the lattice defects in γ_r do indeed markedly influence the mechanical properties of γ_r.

The mechanisms for the reverse α' to γ_r transformation will now be described. There are two opinions regarding the character of this transformation: it is diffusional[127,128] and diffusionless.[129–131] In practical cases, however, the reverse transformation will manifest both characteristics to a certain degree, depending on the conditions of the heat treatment.

A. *Rapid heating*

The facts just presented suggest that the process of reverse transformation of α' to γ_r is not the exact inverse of the transformation of γ to α'. In our discussion of the mechanism of reverse transformation, the case of rapid heating, in which the effect of annealing is avoided, will be considered first. Lacoude and Goux[132] investigated this problem using an Fe–9.8% Cr alloy. The specimens were heated to 750°C, which is below the temperature of the γ loop in the equilibrium diagram of the alloy, and then rapidly heated to a temperature within the γ loop. After being held at that temperature, the

[†] When transformation of b.c.c. to f.c.c. to b.c.c. occurs with the K–S relationships, 528 variants of the b.c.c. phase with different orientations can be produced.[124]

[‡] This problem was subsequently fully investigated by microbeam x-ray diffraction[125] and by x-ray diffraction microscopy.[126]

[§] Sixty percent of the specimen was changed to α' by cooling to -195°C after quenching in water from 1000°C.

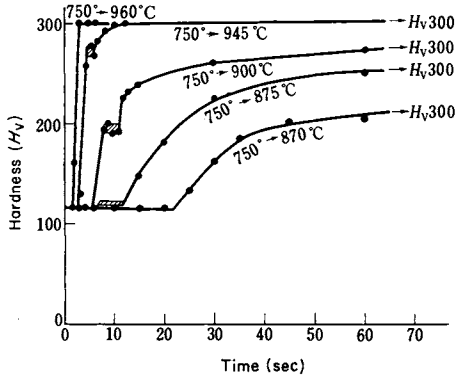

FIG. 3.26 Variation of hardness as a function of isothermal heating at a γ state temperature followed by rapid quenching (Fe–9.8% Cr alloy). (After Lacoude and Goux.[133])

specimens were quenched in water and the hardness was measured. As shown in Fig. 3.26, the hardness versus holding time curves have two stages. The first stage of hardness increase is assumed to correspond to the diffusionless transformation† of α to γ occurring in part of the specimen, and the second stage to the formation of fine-grained γ by diffusional transformation in the residual part. This assumption is consistent with the results of optical microscopy, in which two kinds of structures were observed in the γ phase. By dilatometry, rapid expansion was observed first, immediately followed by contraction. This rapid expansion can be assumed to be due to the diffusionless $\alpha \rightarrow \gamma'$ transformation, and the subsequent contraction to the diffusional $\alpha \rightarrow \gamma$ transformation. Although these observations are noteworthy, more detailed investigations should be performed to prove the foregoing assumptions.‡

These assumptions are also supported by the results of Kidin *et al.*[134] They heated an Fe–5% Cr–0.02% C alloy at a speed of 5000°C/sec from just below the A_1 point, quenched it, and then observed by microinterferometry the surface of the α phase obtained by the transformation of α to γ to α. Traces of shear having occurred at the time of the α to γ transformation were found. Therefore, Kidin *et al.* concluded that this transformation was martensitic.

† This may be a massive transformation; see the "Applications" volume of "Martensitic Transformation" (Maruzen, Tokyo, 1974, in Japanese).

‡ Lacoude and Goux[133] quenched an Fe–Cr alloy rapidly from a temperature above the γ loop and examined its microscopic structure; they always found martensite. So they concluded that the δ phase does not change directly to the α phase even by rapid quenching, but always through the γ phase. Either or both the $\delta \rightarrow \gamma$ and $\gamma \rightarrow \alpha$ transformations was/were considered to be martensitic. However, if more rapid quenching is performed, the direct transformation of δ to α may take place instead of the martensitic transformation.

Sekino and Mori[135] also studied this problem, using four kinds of high-strength steels containing AlN, and concluded that reverse transformation occurred martensitically with the aid of fine precipitates of AlN.

Further, Kessler and Pitsch[136] observed crystallographic phenomena, including surface relief of the γ_r, in an Fe–32.5% Ni–0.026% C alloy. The M_s point of this alloy is $-90°C$. The A_s point is between 300° and 320°C in the regions near retained austenite and 320° and 420°C at the interior of the α'. In the experiment the alloy was first quenched to room temperature and then cooled to $-90°$ to $-140°C$, where 50%–60% of the specimen had changed to α'. Figure 3.27a shows the surface structure. The α' and retained γ can be distinguished as dark and bright constituents, respectively, due to ZnSe vapor deposited on the surface.[137] Following the described treatment, a specimen was transformed by heating to 345°C in 3 min. The results are shown in Fig. 3.27b; the γ_r phase is found along the boundary between the α'

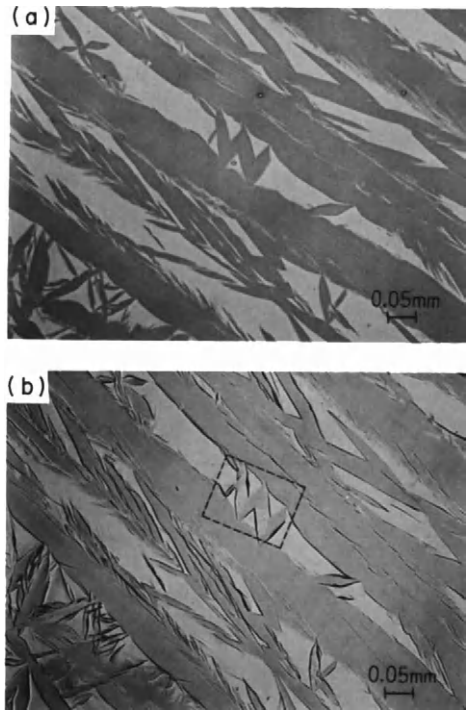

FIG. 3.27 Subzero-cooled state and the initial stage of reverse transformation in an Fe–32.5% Ni alloy. (a) Cooled at $-97°C$ after quenching, ZnSe vapor deposited (grayish crystals are α' martensite and the bright matrix is austenite). (b) Treated as (a) and heated up to 345°C. The narrow regions along the boundary between α' and γ appear dark due to the surface relief of the newly formed γ_r. (After Kessler and Pitsch.[136])

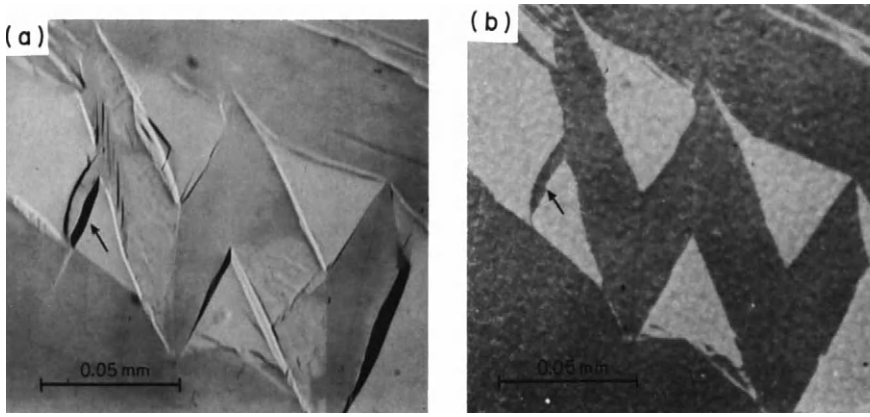

FIG. 3.28 Initial stage of reverse transformation in Fe–32.5% Ni. (a) Enlargement of the framed region in Fig. 3.27b. (b) Electropolished surface of specimen in (a), on which ZnSe vapor has been deposited. (The reverted γ_r region appears equally bright as the retained γ.) (After Kessler and Pitsch.[136])

and γ, and appears dark due to the change in the angle of the reflected light from the surface relief produced by transformation to γ_r. This effect is more clearly observed in Fig. 3.28a, which was obtained by further magnification of the region framed by the broken lines in Fig. 3.27b. That the bright regions of contrast have the f.c.c. structure can be deduced from the fact that the regions are indistinguishable from retained γ after evaporation of ZnSe on a slightly repolished surface of the specimen, as shown in Fig. 3.28b. On further heating at higher temperatures, the γ_r phase is also formed within the α' phase which exhibits the surface relief.

The orientation relationships between γ_r and α' were examined by x rays and by electron microscopy, with the result (with a scatter of 8°):

$$[100]\gamma_r \| [\overline{0.052} \quad 0.707 \quad \overline{0.695}]_{\alpha'}$$
$$[010]\gamma_r \| [\overline{0.139} \quad 0.695 \quad 0.695]_{\alpha'}$$
$$[001]\gamma_r \| [0.390 \quad 0.139 \quad 0.070]_{\alpha'}$$

These relations are close to the Nishiyama relations for the transformation of γ to α'. From this we may be able to understand why the pattern in Fig. 3.25c is single-crystal-like.

The habit plane of γ_r measured by electron microscopy was found to be $(0.21, 0.55, 0.81)_{\alpha'}$, which was close to the $(0.23, 0.62, 0.75)_{\alpha'}$[138,139] obtained from the Kossel pattern.† These orientation relations and the habit plane are

† This relationship is slightly different from the $(0.174, 0.307, 0.935)_{\alpha'} \pm 3°$ and $(0.375, 0.545, 0.749)_{\alpha'} \pm 3°$ values that were obtained by Shapiro and Krauss[140] using an Fe–32.9% Ni–0.006% C alloy.

in good agreement with those expected from the crystallographic phenomenological theory of the martensitic transformation[141] (Chapter 6). Further, γ_r has surface relief and many lattice defects. These facts show that the γ_r produced by the reverse transformation is a kind of martensite, although the transformation may be slightly massive in character due to the temperature effect because the heating rate was not sufficiently rapid in this experiment.

As described above, the γ_r produced by rapid heating is almost fully martensitic in nature. Consequently, the α' produced from such γ_r by subzero cooling has a finer substructure with many more lattice defects and a higher hardness[142] than α' produced from ordinary γ. Habrovec *et al.*[143] investigated the microscopic structure of such α' by electron microscopy using an Fe–24.5% Ni–0.42% C alloy.

It is expected that the reverse transformation temperature on rapid heating is higher than T_0, in contrast to the M_s point on rapid cooling. Especially in pure iron the A_s temperature is high and hard to measure. In spite of this difficulty, Miwa and Iguchi[144] tried to measure it. They heated a specimen at 10^7°C/sec with a power source for spot welding, and measured the temperature by a radiation pyrometer. They found that the A_s is 1100°C. This value is higher than A_3 by 190°C, which is almost equal to $T_0 - M_s$. This fact suggests that the reverse transformation in this experiment was martensitic.

B. *Slow heating*

When α' was heated at rates slower than those just described, almost the same results were obtained;[145†] the γ_r had not only surface relief but also lattice defects, which were observed as fine striations by electron microscopy.[140] Since the γ_r has the character of martensite even when the heating rate is relatively slow, thermal analysis may be used to examine the martensitic transformation process. Kessler and Pitsch[146] employed this method to study an Fe–32% Ni alloy, the same alloy previously described.[136] A specimen of this alloy was transformed to 80%–90% α' by immersion in liquid nitrogen after quenching. It was then subjected to microcalorimetry. Figure 3.29a is a heating curve at the rate of 0.3°C/min. In this curve, regions I and III show heat absorption and region II heat evolution.

In order to examine the cause of the heat absorption and evolution, the heating was interrupted on the way, followed by rapid cooling to room temperature, and the microstructure was examined. Then the specimen was reheated from room temperature to a temperature higher than before, followed by rapid cooling, and the structure was reexamined. Figure 3.29b shows the successive heating curves obtained in this way.

† Discrimination of the f.c.c. phase from the b.c.c. phase was made by vapor depositing TiO_2 on the specimen surface. In this method, f.c.c. and b.c.c. crystals are also contrasted as bright and dark, respectively.

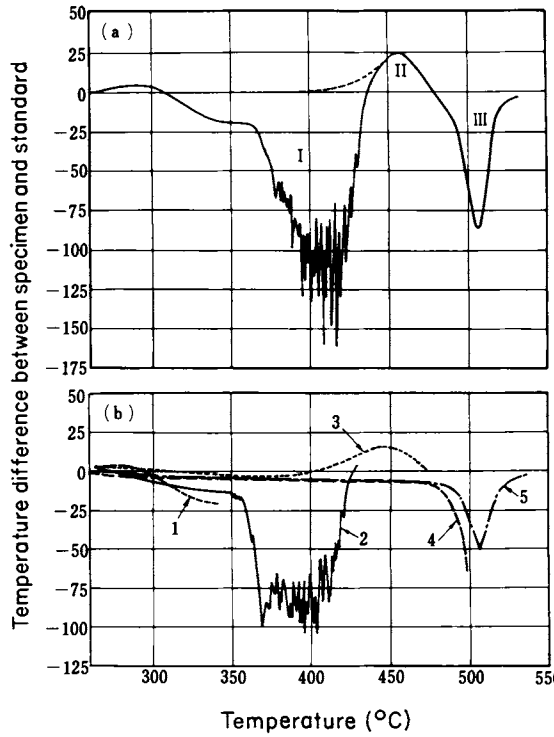

FIG. 3.29 Thermal analysis by continuous heating of an Fe–32.5% Ni alloy containing 80%–90% of α' martensite. (Abscissa: temperature of a standard sample; ordinate: temperature difference, the scale 25 corresponding to a temperature difference of 0.125°C; the heating rate is 0.3°C/min.) (a) A heating curve up to the highest temperature. (b) The consecutive heating curves: Curve 1, first heating, to 342°C; curve 2, second heating, to 430°C; curve 3, third heating, to 473°C; curve 4, fourth heating, to 498°C; curve 5, fifth heating, to 535°C. (After Kessler and Pitsch.[146])

When the specimen was heated to the end of curve 1 in this figure (342°C), γ_r in narrow and long relief was observed along the boundary between α' and retained γ, as shown in Fig. 3.27b. It is therefore suggested that the small amount of heat absorption in the curve is caused by the formation of γ_r.

Curve 2 shows the second heating, to 420°C, at which temperature the heat absorption I is almost completed. At this stage additional γ_r crystals had been formed, displaying new relief features even inside the α' crystal, and the volume of α' decreased to 35%. Therefore it is certain that heat absorption I is the endothermic heat of transformation due to the change in phase from α' to γ_r. If the heating is stopped before the completion of heat absorption I and started again after an interval, the heat absorption does not begin until the temperature is raised higher than before. That is, stabilization of the matrix α' has occurred.

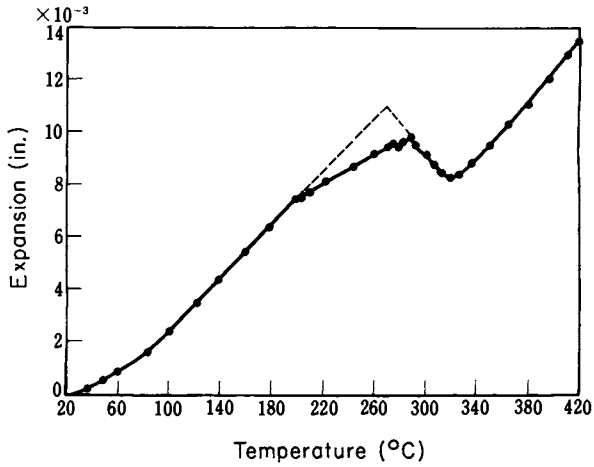

FIG. 3.30 Dilatation curve of Fe–33.95% Ni alloy containing 40% α' martensite, showing gradual contraction followed by a more abrupt contraction. Heating rate, 1°C/min. (After Jana and Wayman.[147])

Curve 3 shows the third additional heating to the end of heat evolution II (473°C), and at this stage neither increase nor decrease of γ_r could be seen. If heat evolution II was caused by the diffusion of atoms, though slight, between the residual α' and γ_r, the α' may have been stabilized because the composition around the interface between both phases would have approached the equilibrium state stopping the transformation of α' to γ_r.

Curve 4 shows the fourth additional heating, to 498°C, which is a little prior to the peak of the second heat absorption. At this stage, the reverse transformation had advanced still further and rose-flowerlike crystals had appeared. But microanalysis revealed that there was no difference in composition between a flowerlike region and its neighbor, which indicates that there was no diffusion of atoms. Therefore, these flowerlike structures are considered to have been produced by massive transformation.

Jana and Wayman[147] also studied this problem by dilatometry and microstructure analysis. Figure 3.30 shows a dilatation curve on heating at the rate of 1°C/min using an Fe–33.95%Ni alloy, which had been transformed to 40% α' by cooling in liquid nitrogen after annealing at 1200°C for 24 hr. It is worth noting that there is a gradual deviation of the curve from normal thermal expansion in the temperature range of 200°–280°C. Examining the structure near this temperature, some of the internal twins in the martensite were found to have disappeared. However, the investigators explain† that the deviation of the curve is not related to the decrease of the internal twins

† Some investigators[139] suggest that this explanation is not yet conclusive.

but is caused by formation of γ by diffusional transformation in part of the specimen. When the temperature reaches 280°C, abrupt contraction begins. At this point, f.c.c. crystals with surface relief were found; they are considered to have been produced by a shear mechanism. When the heating rate was increased to 4°C/sec, no gradual deviation was observed, indicating that the whole specimen was transformed by the shear mechanism. Watanabe *et al.*[148] studied the reverse transformation in a 9% Ni steel and noticed that lattice defects also influence this transformation. The reverse transformation in carbon steel also exhibits surface relief.[149,150] In this case, however, the transformation is accompanied by the diffusion of carbon atoms; therefore it cannot be regarded as a purely martensitic transformation but is rather a bainitic transformation.

Apple and Krauss[151] examined the influence of the heating rate, in the range 3°–28,000°C/sec, on the A_f temperature and the microstructure. The components of the steel specimens were varied in the ranges 0.04%–0.6% C and 32%–22% Ni so as to keep the M_s point constant. The A_f temperature of the 0.004% C steel was constant no matter what the heating rate may be (the A_s point cannot be measured accurately), but for steels containing more carbon it was always lower for the slower heating rate. This was caused by the precipitation of carbide during the heating. In this case, the shape of the γ particles produced as nearly spherical, probably being strongly affected by heating. But when the heating rate was increased, the A_f temperature became higher, the surface relief was distinct, and the shape of the γ crystals was platelike or acicular. These facts clearly prove that the transformation in this case is martensitic.

In the case of heating steels with a high A_f temperature, the situation is complicated: not only is internal stress produced in the γ formed by reverse transformation, but the diffusion of solute atoms also takes place.[152]

3.7.2 Reverse transformation by high-pressure loading

Iron, with respect to pressure and temperature, has the phase diagram shown in Fig. 5.1. The A_3 temperature of iron decreases with increasing pressure, and it reaches about 500°C at 90 kbar. When the pressure is higher than this value, iron is γ phase at high temperatures and below the γ phase region the h.c.p. phase appears. In the case of iron alloys with high nickel content, the $\gamma \rightarrow \alpha'$ transformation occurs at about room temperature even at 1 atm, and thus it may readily be assumed that the $\alpha' \rightarrow \gamma_r$ transformation occurs promptly under high pressure.

In what follows, two cases of this reverse transformation will be described, transformation from ferrite (α), and from martensite (α').

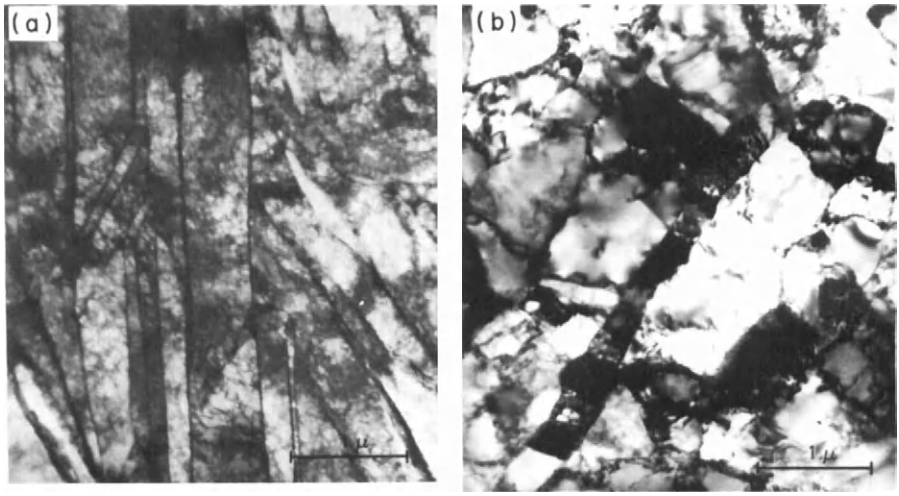

FIG. 3.31 Electron micrographs of martensite produced from ferrite in pure iron by explosive loading. (a) α to γ' to α' by 155 kbar. (b) α to γ' to α' by 310 kbar (cell structures are seen). (After Leslie *et al.*[153])

A. *Transformation of ferrite by explosive loading*

Leslie *et al.*[153] observed the change in microscopic structure due to explosive loading of annealed pure iron (Ferrovac E†). According to their results, only dislocations, with a density of 10^9–10^{10} per square centimeter, and deformation twins are observed in a specimen subjected to pressures up to 110 kbar. At 155 kbar, however, a new plate-shaped phase appears, and its structure is similar to that obtained by quenching very rapidly from above the A_3 temperature, as shown in Fig. 3.31. It seems that on application of an explosive wave, the iron is first transformed to the γ_r phase or ε martensite due to high pressure, and then, after the passage of the explosive wave, it reverts to the α' phase which has the b.c.c. structure. Therefore, the α' phase contains many lattice defects.

When an explosive load of 220 kbar is applied, the phase transformation occurs all over the specimen, and the thickness of the crystals produced diminishes. The hardness also increases, the maximum being at about 300 kbar. Above 300 kbar, a cell structure is formed, as shown in Fig. 3.31b, probably because of the occurrence of recovery from the rise of temperature due to the explosive load. When the pressure is increased to 550 kbar, a small amount of recrystallized particles is found, and at 750 kbar, they spread out

† Containing 0.005% C, 0.013% O, and 0.005% Mn.

over the whole specimen. It has been reported that quite similar phenomena are observed in ferrite of alloy steel.[154]

The following study, which was published before those just discussed, is also concerned with the present problem. Agarwala and Wilman[155] observed that when a plate of α iron was polished at room temperature, the f.c.c. phase appeared along with small $\{111\}_\gamma$ twins in the surface layer.† They suggested that the f.c.c. phase might have been induced by the localized heating from polishing. It is possible, however, that the local high pressure that occurs on polishing is the cause of the γ formation. Moreover, according to the results of this experiment, the lattice orientation relationship in the formation of the f.c.c. phase agrees with neither the K–S relation nor the N relation, but is rather $\{001\}_\gamma \| \{110\}_\alpha$ and $\langle 110\rangle_\gamma \| \langle 111\rangle_\alpha$. Therefore, they proposed a transformation mechanism involving shear along the $[\bar{1}11]_\alpha$ direction on $(211)_\alpha$. This means that the reverse $\alpha \rightarrow \gamma$ and normal $\gamma \rightarrow \alpha$ transformations are not completely the reverse of each other.

B. *Transformation of martensite in Fe–Ni alloys by explosive loading*

Since the A_s temperature of an Fe–Ni alloy containing a large amount of nickel is low, the $\alpha' \rightarrow \gamma'$ transformation takes place even at room temperature under explosive loading. Leslie *et al.*[154] conducted the following experiment. First, Fe–32% Ni and Fe–23% Ni–0.67% C alloy specimens were annealed at 1000°C. They were then quenched to room temperature and further cooled to −195°C, which transformed them to α′. Next, an explosive load of 170 or 270 kbar was applied. Some specimens were again cooled to −195°C. Table 3.11 gives some of the results and shows the following facts:

(a) The α′ phase prepared by subzero cooling can be transformed to f.c.c. by explosive deformation. Since this transformation occurs instantaneously, the transformed phase must not be the same in nature as the original austenite but may be categorized as a martensite and designated the γ′ phase. Comparing the optical microscopic structures before and after applying the explosive load reveals that they are quite similar to each other (Fig. 3.32). But the transmission electron microscope image of the specimens subjected to the explosive load exhibits a finer substructures than those of α′, as shown in Fig. 3.33. In this micrograph, there are regions containing internal twins. Of course, the twin surface is the (111) plane. From the elongation of the spots in the electron diffraction pattern, the thickness of the twins was estimated

† The specimen used was a single crystal plate of very low carbon iron, and the crystal was abraded with emery paper while immersed in benzene, etched in 1% picral for 4–6 min, and then electropolished for 5–10 sec.

TABLE 3.11 Change of structures by explosive loading and subzero cooling in an Fe 32% Ni alloy[a]

Heat treatment after quenching from 1000°C			Microscopic structure[b]	Ratios of phases (%)			Hardness (DPH)		Internal stress ($\times 10^{-3}$)
Subzero cooling	→ Loading →	Subzero cooling		γ	α'	γ'	1 kg	25 g	
	No		A	100	—	—	112	119	—
−196°C	—	—	M	12	88	—	241	243 (α')	2.8
	270 kb	—	Deformed A	100	—	—	213	233	1.75
	270 kb	→ −195°C	Ausformed M	20	80	—	259	271 (α')	5.5
−196°C →	270 kb	—	M (f.c.c.)	—	10	90	292	—	2.4
−195°C →	270 kb	→ −195°C	M (f.c.c. + b.c.c.)	—	33	67	309	—	—
−195°C →	270 kb	→ −269°C	M (f.c.c. + b.c.c.)	—	39	61	301	—	—

[a] After Leslie *et al.*[154]

[b] A, austenitic; M, martensitic.

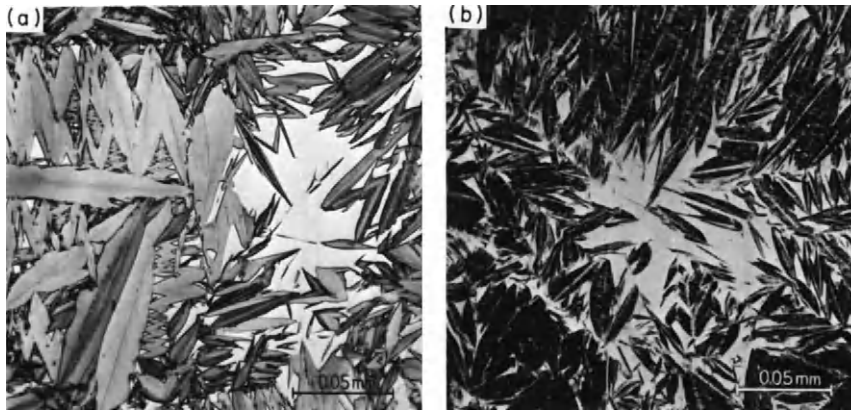

FIG. 3.32 Optical micrographs of α' and γ' martensite in Fe–38% Ni alloy. (a) $\gamma \xrightarrow{-196°C}$ $12\%\gamma + 88\%\alpha'$. (b) $\gamma \xrightarrow{-196°C} 12\%\gamma + 88\%\alpha' \xrightarrow{270\ kbar} 10\%\alpha' + 90\%\gamma'$. (After Leslie *et al.*[154])

to be a few angstroms. The hardness is also large, but conversely, the internal strain is rather small compared with those in the parent α' phase.

(b) When the γ' phase produced by explosive deformation was again cooled to $-195°C$ or $-269°C$, only a small portion of the γ' phase changed to b.c.c., but the rest remained unchanged. This fact means that the γ' phase had been stabilized. The origin of this stabilization is thought to be due to the presence of abundant lattice defects, and not due to such a chemical origin as

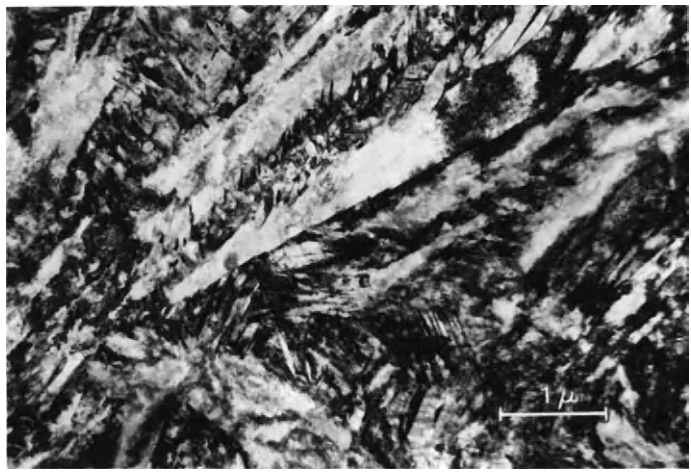

FIG. 3.33 Electron micrograph of γ' martensite in Fe–32% Ni alloy ($\gamma \xrightarrow{-196°C} \alpha' \xrightarrow{170\ kbar} \gamma'$). (After Leslie *et al.*[154])

atomic diffusion because the specimens were kept at such low temperatures during the treatments. Of course, both the α' and γ' phases in these specimens had internal twins.

According to the study of Bowden and Kelly,[156] when an explosive load was applied to Fe–30% Ni–0.026% C and Fe–28% Ni–0.1% C alloys, the $\alpha' \rightarrow \gamma'$ transformation began to occur at 100 kbar, and was completed at 160 kbar. In this case, the K–S orientation relationship was approximately satisfied. Since two kinds of habit plane were found, they concluded that two kinds of slip system had operated to give complementary shear, as follows:

$$\begin{aligned} \text{slip system I:} \quad & (110)_{\gamma'}[1\bar{1}0]_{\gamma'} = (112)_{\alpha'}[11\bar{1}]_{\alpha'} \\ & \text{for habit plane:} \quad (\bar{5}23)_{\alpha'} = (225)_{\gamma'} \\ \text{slip system II:} \quad & (111)_{\gamma'}[\bar{1}2\bar{1}]_{\gamma'} = (101)_{\alpha'}[\bar{1}01]_{\alpha'} \\ & \text{for habit plane:} \quad (\bar{1}21)_{\alpha'} = (11\bar{2})_{\gamma'} \end{aligned}$$

Since slip system I is the exact reverse of that of the $\gamma \rightarrow \alpha'$ transformation, the γ' phase produced by this system can have the same orientation as the original γ phase. But this is not so for the γ' phase due to slip system II.† Quantitatively, the former is much more prevalent than the latter. The internal twins in the parent α' phase are inherited in the γ' phase due to slip system II. The greater proportion of the γ' phase produced at 160 kbar has $(111)_{\gamma'}$ microtwins. The twin interfaces were found to be only the planes, which were perpendicular to the habit plane, of four kinds of $\{111\}_{\gamma'}$. This may be understood by assuming that these twins are not deformation twins but are accommodation internal twins induced by the $\alpha' \rightarrow \gamma'$ phase transformation. This fact suggests that these twins are formed by slip system II.

Christou[158] studied this problem using an Fe–7.37% Mn alloy and obtained almost the same results except that much more of the γ' phase was due to slip system II. The experiment was extended to the α phase of an Fe–14% Mn alloy. In this case, however, α' phase without internal twins, instead of γ', was produced by a shock wave of 90 kbar as well as by a 150-kbar wave. Therefore it was inferred that this transformation occurred through the sequence α to ε to α'.

Rohde[159] proposed that formation of the γ' phase due to a shock load should be treated as an adiabatic transformation. In an experiment,[160] an Fe–29.5% Ni–0.50% Mn–0.10% C alloy was first slowly cooled to room temperature and then subzero cooled to −196°C, giving 75.8% α'. When a hydrostatic pressure of 21 kbar was applied to the specimen, no phase transformation occurred. On the other hand, when a shock wave was applied, transformation occurred at 18 kbar. From this result it was concluded that a shear component rather than pressure is essential to the present trans-

† A shear displacement similar to slip system II was observed when a whisker was heated.[157]

formation. It was also observed that the transformed γ' regions were local and exhibited banded structures along the forward direction of the shock wave.

Another experiment[161] on a nickel steel where a shock shear stress was applied also gave evidence of the formation of the γ' phase. It is certain that the transformation in this case was also martensitic, although it may have been accompanied by a rise of temperature due to heat evolution by the shock wave.

3.8 The $\gamma \rightarrow \varepsilon' \rightarrow \varepsilon \rightarrow \kappa' \rightarrow \alpha_m$ mechanism of the course of martensitic transformation in steels

Lysak proposed that the martensitic transformation in steels takes place by four consecutive steps.[162] Since this proposal differs drastically from those discussed earlier in this book, it was not included in Chapter 2 to avoid confusion. This view will be discussed next.

Its description will begin with the initial stage of the transformation, namely, the proposed formation of an ε' phase that is preliminary to the formation of ε martensite, and will continue to the last stage, namely, the formation of α_m. This phase corresponds to the α' martensite mentioned before but is described by Lysak as an orthorhombic phase slightly deformed from tetragonal. Finally, the proposition that the κ' phase appears as an intermediate between the ε and α_m phases will be discussed.

3.8.1 The ε' phase as a preliminary stage to the formation of ε martensite

As described in Section 2.3, in some cases for Mn steels, the ε phase appears as an intermediate phase in the $\gamma \rightarrow \alpha'$ transformation. Furthermore, Lysak and Nikolin[163,164] reported that another new phase, designated ε', preceded the transformation to ε martensite.

They investigated this phase by means of the rotating crystal method of x-ray diffraction, using (10–12)% Mn–(0.4–0.7)% C steels. Figure 3.34a shows an x-ray diffraction pattern of a single γ crystal of the alloy obtained by slow cooling to room temperature from a high temperature. Figure 3.34b shows the pattern of the same crystal after it had been cooled in liquid nitrogen. It exhibits some new diffraction spots besides those seen in part (a). These new diffraction spots, which were interpreted as due to the new ε' phase, are connected by streaks arranged in parabolas intersecting Debye–Scherrer rings, six spots being arrayed in one period.† This pattern corresponds to the

† Such diffraction spots of the new phase were not found in a carbon-free Fe–20% Mn alloy.[165]

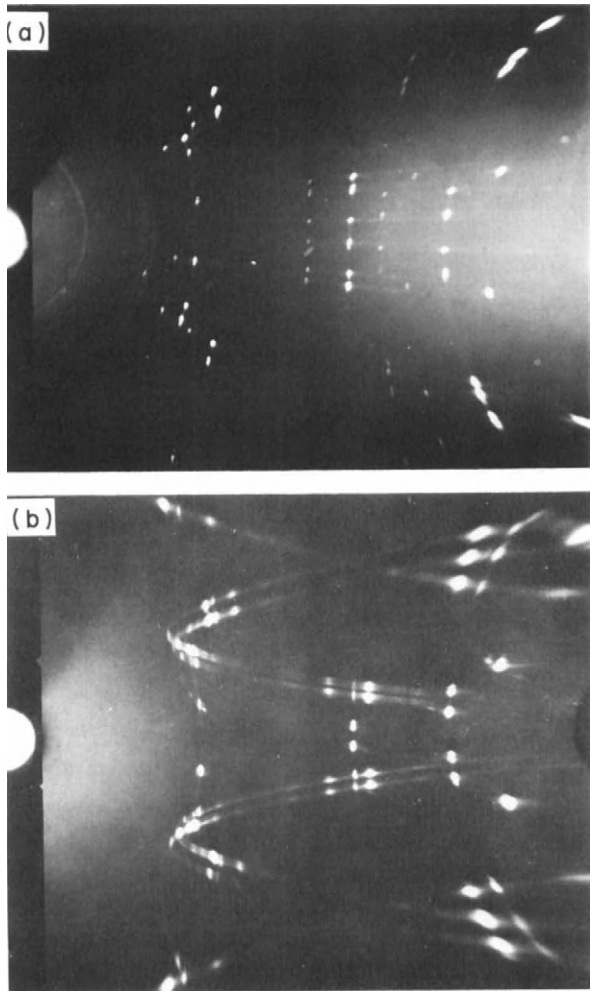

FIG. 3.34 X-ray rotation photographs at the initial stage of the transformation of an Fe–12% Mn–0.5% C alloy. (a) Specimen slowly cooled from 1100°C (single γ crystal), Fe–$K_{\alpha,\beta}$ radiation. (b) Same crystal cooled to -196°C ($\gamma + \varepsilon'$) Fe–K_α (monochromatized). (After Lysak and Nikolin.[163])

reciprocal lattice shown in Fig. 3.35, in which the open circles represent γ spots and the closed circles are due to the ε' phase. Indices assigned to the ε' spots are referred to a hexagonal lattice.

The relation between lattice orientations of the ε' and γ phases satisfies the Shoji–Nishiyama relationship in the same way as that between ε and γ.

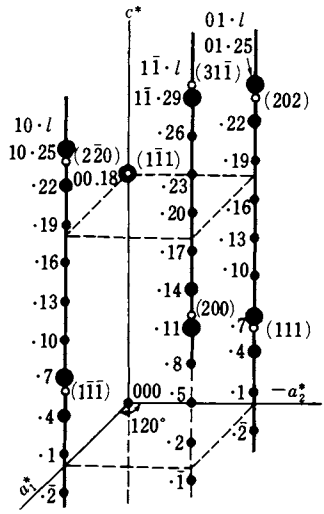

FIG. 3.35 Schematic illustration of reciprocal lattice drawn from the diffraction pattern in Fig. 3.34b. (After Lysak and Nikolin.[163])

From this relation it is suggested that the lattice of ε' is a stacking sequence structure consisting of atomic planes parallel to the $(111)_\gamma$ plane. Since six diffraction spots on the c axis (which corresponds to the direction of the streaks) constitute one period, the period of the stacking sequence must be six layers. For the six-layer period there are three kinds of stacking sequences. Among them, the $(5\bar{1})_3$

$$\mathrm{ABCABC^-BCABCA^-CABCAB^-}$$

type sequence explains the intensities of the diffraction spots best. This structure is formed by shuffling every six $\{111\}_\gamma$ layers from the f.c.c. lattice. Thus it is very close to the γ phase. The unit cell of the ε' phase consists of 18 atomic layers and its lattice parameters are $a_h = 2.533$ Å and $c_h = 37.280$ Å referred to the hexagonal axes and $a_r = 12.50$ Å and $\alpha = 11°41'$ referred to the rhombohedral axes.

Even when the time of holding the specimen in liquid nitrogen is prolonged to 500 hr, the amount of ε' is not changed. By heating the ε' to 60°C, the reverse transformation of ε' to γ occurs and then by recooling in liquid nitrogen, the ε' crystal forms with the same orientation as before. That is, this transformation is reversible.

The ε' phase is paramagnetic and its hardness is not very high. The degree of surface relief due to the $\gamma \rightarrow \varepsilon'$ transformation is so small that it cannot be detected by a microscope at 600×. The weak surface relief is considered to be due to the small lattice distortion during the $\gamma \rightarrow \varepsilon'$ transformation. But

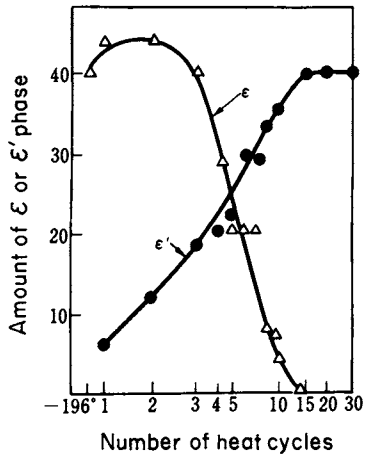

FIG. 3.36 Change in the amounts of ε and ε′ induced by thermal cycles of 400°C ⇄ −196°C (Fe–16% Mn–0.35% C). (After Lysak and Nikolin.[164])

taking into consideration other properties, the ε′ phase may come within the category of martensite.

Although it has been observed that ε′ transforms to ε by plastic deformation, there is no evidence for the occurrence of the ε′ → ε transformation in other experiments. Nevertheless, Lysak *et al.* consider that the ε phase always forms through the ε′ phase. That is, according to Lysak's view on the γ → ε transformation, the ε′ lattice forms first, and then the number of stacking faults increases in the lattice until every other layer becomes a stacking fault, which constitutes formation of the h.c.p. ε phase.

As was explained earlier, the ε′ is an intermediate phase, but it does not always appear. Whether the ε′ appears during the γ → ε transformation or not may be determined by preexisting lattice defects. This problem has been studied by experiments on the effects of thermal and mechanical treatment.[166] In what follows we shall explain studies on the effect of thermal cycles. In the experiment, a 16% Mn–0.35% C steel was air cooled to obtain the γ phase and was immersed in liquid nitrogen to form a mixture of γ and ε.† Subsequently, it was repeatedly heated to 400°C and then cooled to −196°C. The amount of ε decreased gradually and that of ε′ increased as shown in Fig. 3.36.‡ This phenomenon occurred more rapidly when plastic deformation was added and when the carbon content was increased. The latter fact seems to indicate that carbon atoms in solution compose Cottrell atmospheres at

† At this stage, the ε′ phase does not appear in this alloy, whose composition is different from that of the alloy used before.[163]

‡ This was also confirmed by thermal analysis.[164]

dislocations and the Suzuki effect at stacking faults, by which the $\gamma \rightarrow \varepsilon$ transformation is suppressed. The work on the effect of thermal cycling was continued and interesting results were obtained.[167]

As for the cause of the formation of the ε' phase, Lysak and Goncharenko[168] thought that when γ crystals are rapidly cooled or crystallized from the melt, stacking faults form in them. The ε' phase is formed when these faults increase in number and order on subsequent thermal treatment. Such a phenomenon also occurs in rhenium steels.[169] In cases of Fe–0.7% C–20.0% Re and Fe–0.5% C–25.0% Re alloys, the stacking fault probability in the initial γ matrix was as small as $\alpha_\gamma = 0.0175 \pm 0.005$ and the distribution of the lattice defects was random. However, by rapid cooling to liquid nitrogen temperature, the probability was increased to $\alpha_{\varepsilon'} = 0.170 \fallingdotseq \frac{1}{6}$ and partial formation of the ε' phase occurred by an ordering of the stacking faults corresponding to shufflings every six layers. An increase in the stacking fault probability to $\alpha_{\varepsilon'} = 0.522 \fallingdotseq \frac{1}{2}$ and an ordering equivalent to lattice plane shuffling every other layer bring the formation of the ε phase to completion. Thus, stacking faults existing at the outset in the γ matrix become nuclei of the ε' and ε phases. On the assumption that the formation of the ε' and ε phases is related to stacking faults and twin faults, further investigations were made.[170]

Oka *et al.*[171] studied this problem in detail by means of electron microscopy, using a steel with almost the same composition (16.5% Mn–0.26% C) as Lysak's. As the number of thermal cycles between -196°C and 400°C was increased, a more complex phenomenon was noted.

First, after quenching to room temperature followed by cooling to -196°C, a mixture of γ and ε phases was found both containing planar faults. With a specimen subjected to 20–25 thermal cycles, however, the electron diffraction pattern showed streaks that increased in length with cycling. In electron micrographs bright γ regions and dark $\gamma + \varepsilon$ regions were seen. The ε phase especially contained many defects. Increasing the number of cycles to 50 caused the diffraction spots due to the ε phase to weaken and become hardly recognizable; only the γ phase with planar faults existed. This fact indicates that the ε phase was destroyed. In a specimen subjected to about 100 cycles, four new diffraction spots appeared between the 000 and 111 spots, and they became clearer after 150 cycles, as shown in Fig. 3.36A. From their intensity distribution, the crystal structure was determined to be 15R of the $(3\bar{2})_3$ type (see Section 2.5).

After the number of thermal cycles was increased to 200, five diffraction spots appeared in one period along the reciprocal lattice axis parallel to the [0 0 18] direction; they are due to the $(5\bar{1})_3$ structure found by Lysak *et al.* Upon increasing the number of thermal cycles, the diffraction spots corresponding to the γ structure appeared. These γ crystals were formed in some

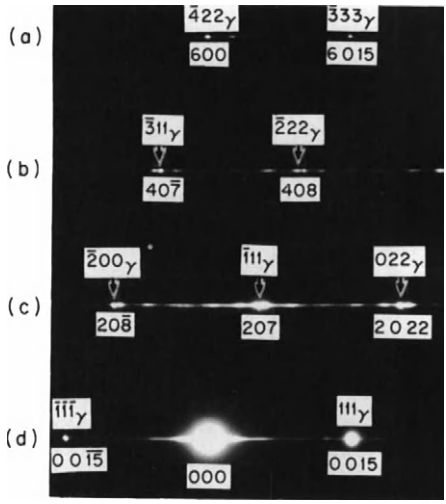

FIG.3.36A Electron diffraction patterns of a 16.5% Mn–0.26% C steel after 150 thermal cycles of 400°C ⇄ −196°C, showing diffraction spots due to 15R $(3\bar{2})_3$ and γ structures. (After Oka *et al.*[171])

regions of the specimens by transition from the 18R structure; this is the so-called reverted γ phase. Finally, these crystals covered in the entire specimen. That is, when the number of thermal cycles is increased, the following transition processes take place:

$$\gamma \rightarrow \underset{(3R)}{\gamma} + \underset{(2H)}{\varepsilon} \rightarrow \text{faulted } \gamma \rightarrow 15R(3\bar{2})_3 \rightarrow 18R(5\bar{1})_3 \rightarrow \text{reverted } \gamma.$$

In order to examine the nature of the last transition, a specimen that was subjected to 200 cycles and exhibited the 18R structure was held for 5 min at 400°C and then quenched in water at room temperature. It still exhibited the 18R structure. Therefore, it was concluded that the reverse transition, ε' to γ, did not occur yet as a result of heating to 400°C for a few minutes.

Considering the foregoing results together with the facts that in the electron micrographs, fine dots appeared in the γ phase formed in the last transition and the boundaries between the γ phase and the 18R structure were irregular, it may be inferred that the carbon atoms precipitated as carbides by autotempering and that the regularly arrayed stacking faults, which had been stabilized by the clustering (Suzuki effect) of the carbon atoms, shrank away. Therefore, it is thought that the 18R structure was destroyed, giving the reverted γ. From the fact that such long-period stacking order structures as the 15R and 18R structures did not appear in carbon-free Fe–Mn binary alloys, carbon atoms can be considered to play an important role in the formation of long-period stacking order structures.

Further, the problem of stabilization of the γ for $\gamma \rightarrow \varepsilon$ transformation will be described in Section 5.7.9B.

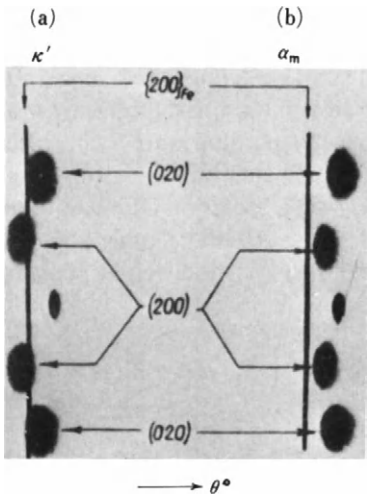

FIG. 3.37 (200) and (020) diffraction spots of (a) κ' and (b) α_m martensite in an Fe–4% Mn–1.42% C alloy. (After Lysak *et al.*[174])

3.8.2 Structure of α_m martensite

Lysak *et al.* earlier recognized α' to be body-centered tetragonal, as described in Chapter 2, and denoted it α_t,[172,173] but the notation was changed to α_m based on the following results.

Lysak *et al.*[174] examined the x-ray diffraction patterns of martensite that had transformed from a single γ crystal of 1.55%–1.83% C steel. They found that the (200) diffraction spot appears at a different angle from the (020) spot, as seen at the right in Fig. 3.37, and thus the two a axes, which have so far been considered to be the same length, are a little different in length from each other. Therefore, they regarded this crystal lattice as body-centered orthorhombic and changed the phase symbol to α_m. Table 3.12 shows the parameters of the lattice.

TABLE 3.12 Lattice constants of α_m martensite[a]

Composition (%)							
C	Ni	Cu	a (Å)	b (Å)	c (Å)	c/a	c/b
1.55	—	—	2.856	2.844	3.032	1.061	1.066
1.70	—	—	2.855	2.836	3.059	1.071	1.079
1.74	7	—	2.855	2.829	3.063	1.073	1.083
1.83	—	14	2.847	2.826	3.079	1.078	1.086

[a] After Lysak *et al.*[174]

3.8.3 Structure of κ martensite

Lysak *et al.*[172,173] found a b.c.c. phase mixed with the usual b.c.t. martensite when they examined C steel, Ni steel, and Mn steel quenched in a salt solution kept at room temperature, and named it the κ phase, thinking it a new phase. Subsequently, however, they correctly pointed out[175] that the κ phase is nothing but a low carbon martensite affected by auto-tempering during quenching. The κ phase contains 0.25%–0.35% carbon and its lattice parameter a_κ is 2.880 Å. In high carbon steels, the κ phase becomes slightly tetragonal with an axial ratio $c/a = 0.9956 + 0.012p$ (p is the weight percent of carbon)[176] because it contains a coherent low-temperature carbide (not ε carbide).

3.8.4 Structure of κ' martensite

In Mn steels,† Lysak *et al.*[177,178] found a b.c.t. martensite whose axial ratio is smaller than that of α_m when the steel was quenched to a temperature as low as -160°C. The M_s temperature of this steel is below room temperature. This newly found martensite was named the κ' phase; its x-ray diffraction pattern is shown at the left in Fig. 3.37.‡ As will be described later, when the temperature was raised to -35°C, the κ' phase decomposed into $\kappa + \alpha_m$. Therefore, if such a steel is quenched to room temperature as usual, the $\kappa + \alpha_m$ mixture may be mistakenly regarded as the directly formed product. From this it can be understood that the κ described in Section 3.8.3 is an α phase resulting from the decomposition of κ'.

Al'Shevskiy and Kurdjumov[180] also recognized the presence of κ' in 4% Mn–1.25% C and 6.3% Mn–0.95% C steels. In these alloys the κ' also transformed gradually, as shown in Fig. 3.38, which indicates the change in the axial ratio with time of aging above the M_s temperature. The axial ratio

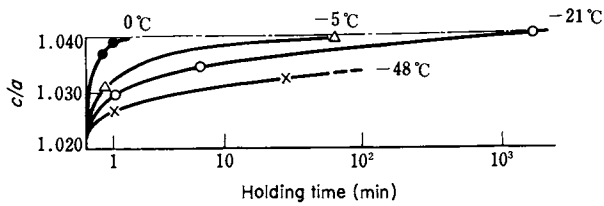

FIG. 3.38 The c/a ratio of martensite as a function of holding time at different temperatures above the M_s point (-57°C) in an Fe–6.3% Mn–0.97% C alloy quenched from 1100°C to liquid nitrogen temperature. (After Al'Shevskiy.[181])

† Their compositions were (8.5–7.5)% Mn–(0.6–0.76)% C[177] and (4–2)% Mn–(1.3–1.8)% C.[178]

‡ The orientation of κ' is of course the same as that of α_m.[179]

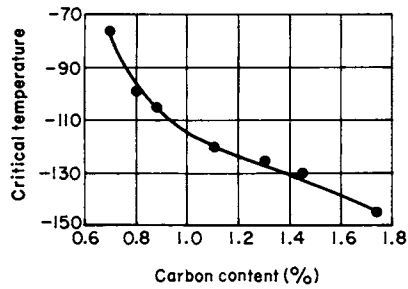

FIG. 3.38A Critical temperature of the $\kappa' \rightarrow \alpha_m$ transition as a function of the carbon concentration in manganese steels. (After Lysak and Kondrat'yev.[182])

approaches the standard ratio corresponding to α_m.[181] But in the case of 5.0% Cr–8.5% Ni–0.5% C and 16% Cr–0.4% C steels, the pattern of the κ' was obscure. It is not obvious whether it could not be detected because of the small carbon content or whether it simply was not present in these alloys.

There is a lowest critical temperature for the transformation of κ' to α_m. The critical temperature depends on the composition. By studying eight kinds of Mn steel with (2.0–8.0)% Mn–(1.75–0.7)% C, where the Mn content decreased with increasing C content, it was determined that the critical temperature decreases as the C content increases, as shown in Fig. 3.38A.[182] That is, the κ' phase becomes unstable as the carbon content increases.

Lysak and Nikolin[183] later found that the orthorhombic κ' phase is also formed in alloys with rhenium, which has characteristics similar to manganese. A 10% Re–1.4% C steel is an example; in it, the lattice parameters in the state cooled in liquid nitrogen are $a = 2.874$ Å, $c = 2.997$ Å. At room temperature they change to $a = 2.866$ Å, $c = 3.230$ Å. The former are those of κ'. Figure 3.39 shows the effect of carbon content on the lattice parameters of the alloys at $-180°C$. In these alloys the M_s points are maintained below room temperature by reducing the Re content from 20% to 6% as the carbon content is increased from 0.8% to 1.7%.

The κ' phase was also examined in detail by x-ray diffraction, using the martensite produced from a single γ crystal of Mn steel by quenching to $-180°C$; it was found that the structure of κ' is body-centered orthorhombic, like that of α_m. Table 3.13 compares the lattice parameters of κ' at $-180°C$ with those of α_m at room temperature.

In Re steel, both the orthorhombic κ' and α_m are obtained.[183] They can be clearly recognized in alloys with a high carbon content. When the carbon content is less than about 1.4%, it is difficult to confirm the presence of the orthorhombic phase by measuring the lattice constants due to the diffuseness of the diffraction spots.

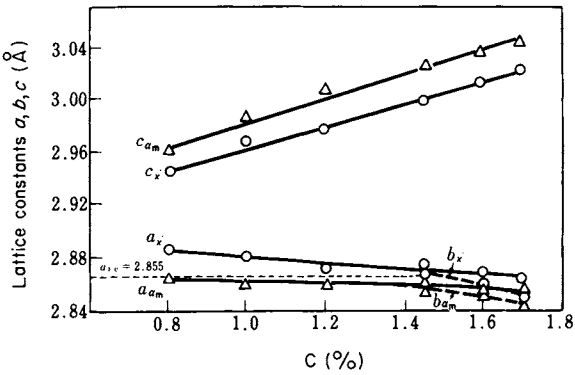

FIG. 3.39 Lattice parameters of κ' and α martensite as functions of the carbon concentration in rhenium steels. (After Lysak and Andrushchik.[183])

C (%)	0.8	1.0	1.2	1.45	1.6	1.7
Re (%)	20	17	15	10	8	6

TABLE 3.13 Lattice constants of κ' martensite and of α_m martensite produced from the κ' by keeping at room temperature[a]

Composition (%)		κ'			α_m		
C	Mn	a (Å)	b (Å)	c (Å)	a (Å)	b (Å)	c (Å)
1.42	4	2.869	2.861	3.000	2.862	2.851	3.018
1.52	2	2.866	2.856	3.003	2.859	2.848	3.022

[a] After Lysak *et al.*[174]

Lysak and Vovk[177] claim that the ε phase is sometimes transformed to κ' by plastic deformation.

3.8.5 Reason for formation of κ' and the $\kappa' \rightarrow \alpha_m$ process

Why does κ' of a lower axial ratio appear instead of α_m of a higher axial ratio on quenching to very low temperatures? Lysak *et al.* explained this question on the assumption that the κ' is formed through the sequence of γ to ε' to ε to κ' and that this course of the transformation influences the carbon atom sites.

Although the sites of carbon atoms in the ε' lattice have not been determined experimentally, they can be presumed from the transformation process to be as follows.[184,185] Consider two $\{111\}_\gamma$ atomic planes between which the shuffling has occurred (Section 2.3) during the $\gamma \rightarrow \varepsilon'$ transformation. In this case a C atom that was at the octahedral site (O site) in the γ lattice

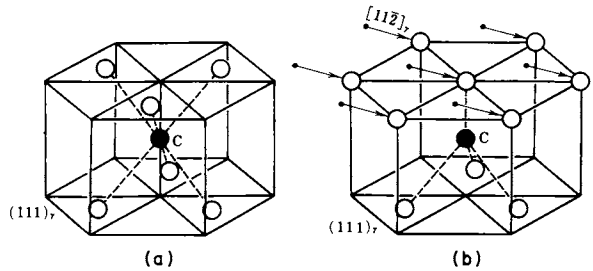

FIG. 3.40 Transition of a carbon atom from an O site to a T site by slipping along $(111)_\gamma$. (a) Octahedral site. (b) Tetrahedral site.

moves together with the atomic plane either above or below in order to occupy the largest space. The resulting position is a tetrahedral site (T site) in the ε' lattice, as illustrated in Fig. 3.40b. On the other hand, a C atom lying between two atomic planes without shuffling, of course, remains at the O site. Since in the f.c.c. to h.c.p. transformation shuffling occurs in every other atomic plane, half of the C atoms remain at O sites and the others occupy T sites.

In the course of the $\varepsilon \rightarrow \kappa'$ transformation,† a carbon atom at the T site in the ε lattice occupies a T site on the *b* axis in the κ' lattice, and hence the lengths of the *a* axis and *b* axis become different. When the κ' phase is warmed to room temperature, some of the C atoms at the T sites on the *b* axis move to the more stable O sites on the *c* axis, so that the axial ratio becomes larger, although some of the C atoms still remain at the T sites. Thus, the κ' changes to a slightly orthorhombic structure, α_m. The investigators considered that these phenomena must be able to occur not only in the Mn steel but also in other alloys. For the appearance of κ', however, confirmation by x-ray diffraction has been made only in Mn steels, Re steels, and carbon steels.[186] Notwithstanding, they supposed that κ' would also be produced in other alloys, on the basis of the following evidence.

Koval' *et al.*[187] studied this problem by electrical resistivity as well as x-ray diffraction. Manganese steels and carbon steels were quenched in liquid nitrogen to produce martensite, and as the temperature was gradually raised from that of the liquid nitrogen, the electrical resistivity increased at first but began decrease at about $-100°C$, as shown in Fig. 3.41. X-ray diffraction confirmed that the increase in electrical resistivity in the first stage is due to the transformation of the retained austenite to martensite, and the decrease in the subsequent stage is due to the transformation of κ' to α_m.‡

† There is no direct experimental evidence of an $\varepsilon \rightarrow \kappa'$ transformation.

‡ It was confirmed by magnetic measurement that there was no change in the amount of martensite.[188]

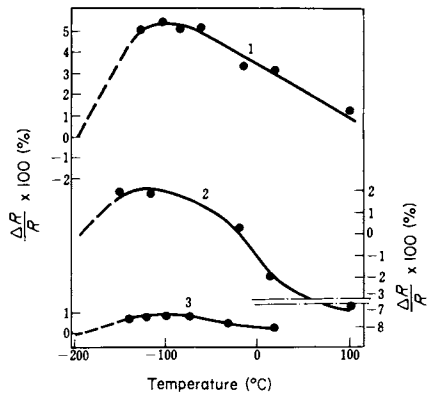

FIG. 3.41 Change in electrical resistivity of martensite on heating after quenching in liquid nitrogen at −197°C. Curve 1, Fe–7.5% Mn–0.75% C; curve 2, Fe–4.5% Mn–0.60% C; curve 3, Fe–1.6% C. (After Koval' *et al.*[187])

Lysak *et al.*,[189] using Mn steels and Re steels, observed similar tendencies in the variation of electrical resistivity, as shown in Fig. 3.42, although the temperature of the resistance decrease differs, depending on the composition. Such a phenomenon was also observed in Ni steels (Fig. 3.43).[190] This result indicates that a decrease in resistivity corresponding to the $\kappa' \rightarrow \alpha_m$ transformation starts from about −220°C, indicating that this transformation can complete at the liquid air temperature. In one investigator's opinion, this was one reason why the κ' phase could not be detected after a quench into liquid air.

Later,[191] the κ' phase in 8% Ni–1.75% C steel was detected by x-ray diffraction at 6°K using liquid helium. Compared with the case of Mn steel or Re steel, however, the diffraction spots were broad and the difference of the lattice parameters from those of α_m was small. The reason for this was believed to be that the $\kappa' \rightarrow \alpha_m$ transformation took place during quenching, because the presence of Ni atoms was considered to enhance the mobility of the C atoms. In 28% Ni–1.1% C steel, the κ' phase could not be found.

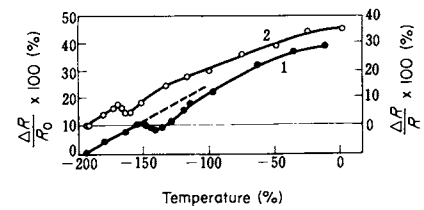

FIG. 3.42 Change in electrical resistivity of martensite on heating after quenching in liquid nitrogen. Curve 1, Fe–4.0% Mn–1.4% C; curve 2, Fe–10% Re–1.4% C. (After Lysak *et al.*[189])

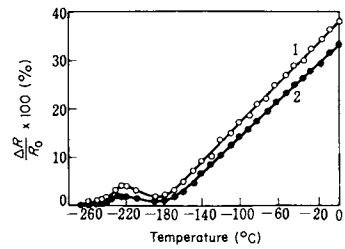

FIG. 3.43 Change in electrical resistivity of martensite on heating after quenching in liquid helium. Curve 1, Fe–7% Ni–1.7% C; curve 2, Fe–16% Ni–1.4% C. (After Lysak and Artemyuk.[190])

It was, therefore, inferred that in this case the α_m might be produced directly from the γ phase, probably due to a different mechanism of transformation.

To clarify the $\kappa' \rightarrow \alpha_m$ transformation process in detail, Lysak and Kondrat'yev[192] prepared single γ crystals of 2% Mn–1.75% C steel, and used a low-temperature x-ray diffraction camera First these crystals were cooled in liquid nitrogen to produce κ' martensite, then the temperature was gradually raised. With this treatment, the $\kappa' \rightarrow \alpha_m$ transformation was noted at about -110°C, where the width of the (002) diffraction spot reached the maximum value. Above this temperature, the width decreased with increasing temperature. This observation suggests that the $\kappa' \rightarrow \alpha_m$ transformation does not occur continuously in a single phase but discontinuously with coexistence of two phases, $\kappa + \alpha_m$.

Furthermore, it was found that Re steels ((20–6)% Re–(0.8–1.7)% C) quenched to a very low temperature showed an anomalous expansion at $-160°$ to -135°C during the raising of the temperature. This fact is also regarded as evidence of the $\kappa' \rightarrow \alpha_m$ transformation.[193–195]

As described in Section 3.3, Fujita *et al.*[196,197] examined the Mössbauer spectra of 1.0% C steel quenched to -200°C, and recognized that there are C atoms at the T sites. This finding supports the inference of Lysak *et al.* that not only Mn steel and Re steel but other steels become κ' when quenched to a very low temperature.

About the reason for the formation of the κ', Roitburd and Khachaturyan[198] presented a different interpretation. They believed the $\gamma \rightarrow \alpha'$ transformation to consist of two processes, $(111)_\gamma[\bar{2}11]_\gamma$ shear and $(1\bar{2}1)_\gamma[10\bar{1}]_\gamma$ shear. In the former process, there is another shear along the opposite direction, $[2\bar{1}\bar{1}]_\gamma$, which forms $(011)_{\alpha'}$ twins. The amount of displacement of each atomic plane in the $[\bar{2}11]_\gamma$ shear is one sixth of the period of atomic arrangement in the shearing direction, while it is five sixths in the opposite ($[\bar{1}\bar{1}2]_\gamma$) shear. The site of C atoms in the latter twin is regarded as a disordered position with respect to the matrix crystal. Since such twins are

mixed, the whole crystal—that is, the κ' crystal—has a small axial ratio. Usikov[199] observed $\{101\}_{\alpha'}$ twins and a small axial ratio in Fe–3.5%Mn–1.42%C by x-ray diffraction and supported the interpretation of Roitburd *et al.* This interpretation, however, has two weak points. One of them is the great difficulty that atoms must encounter in moving over a large potential for the shuffling of the $\frac{5}{6}$ atomic period. The other is that the amount of $(011)_{\alpha'}$ twins, as observed by electron microscopy, is actually small (Section 2.2.7), and therefore the number of C atoms in the disordered sites must be small. Consequently, the $(011)_{\alpha'}$ twins considered here must be different from the observed ones and are only hypothetical.

Lysak *et al.*[200] observed, in Al steels ((3–4)%Al–(2.0–2.4)%C), that in some cases the axial ratio of the tetragonal martensite decreased inversely during the room-temperature aging. This fact shows that C atoms move from O sites to T sites, contrary to the case mentioned earlier. According to Beshers' calculation,[201] the C atom in a T site has a lower energy than in an O site, when the ratio of the elastic moduli for [210] and [001] directions is less than unity. Lysak *et al.* therefore assumed that this condition is satisfied due to the ordering of Al atoms in the Al steel, which is contrary to the cases of other iron alloys.

References

1. P. Scherrer, *Göttingen Nachr.* **98**, (1918).
2. S. Sekito, *Kinzoku no Kenkyu* **3**, 482 (1926); **4**, 297, 478 (1927).
3. J. A. Wheeler and M. A. Jaswon, *J. Iron Steel Inst.* **157**, 161 (1947).
4. J. Mazur, *Nature (London)* **164**, 358 (1949).
5. J. Mazur, *Cryogenics* **4**, 36 (1964).
6. M. A. Jaswon, *Nature (London)* **164**, 712 (1949).
7. J. Mazur, *Nature (London)* **164**, 712 (1949).
8. S. Sato, *Jpn. J. Appl. Phys.* **1**, 210 (1962).
9. B. E. Warren and B. L. Averbach, *J. Appl. Phys.* **21**, 595 (1950); **23**, 497, 1059 (1952).
10. R. A. Smith, *J. Iron Steel Inst.* **173**, 147 (1953).
11. C. N. J. Wagner, *Arch. Eisenhüttenwes.* **29**, 489 (1958).
12. A. J. Goldman and C. N. J. Wagner, *Acta Metall.* **11**, 405 (1963).
13. O. J. Guentert and B. E. Warren, *J. Appl. Phys.* **29**, 40 (1958).
14. S. V. Volkov, A. A. Vaynshteyn, and M. L. Komissarova, *Fiz. Met. Metalloved* **22**, 823 (1966).
15. S. Sato, Private Communication, Hokkaido Univ. (1971).
16. C. N. J. Wagner, A. S. Tetelman, and H. M. Otte, *J. Appl. Phys.* **33**, 3030 (1962).
17. A. J. Goldman and C. N. J. Wagner, *Acta Metall.* **11**, 405 (1963).
18. S. Sato and Z. Nishiyama, *Jpn. J. Appl. Phys.* **4**, 84 (1965).
19. D. M. Naklimov, *Chem. Abstr.* **43**, 1966f (1949).
20. A. L. Christian and E. S. Rowland, *Trans. ASM* **45**, 638 (1953).
21. L. I. Lysak and Ya. N. Vovk, *Fiz. Met. Metalloved.* **21**, 430 (1966).
22. M. P. Arbuzov, *Ber. Akad. Wiss. UdSSR (N.S.)* **74**, 1085 (1950).

23. M. P. Arbuzov and I. G. Barantseva, *Fiz. Met. Metalloved.* **19**, 158 (1965).
24. G. V. Kurdjumov and Ye. G. Nesterenko, *Fiz. Met. Metalloved.* **12**, 883 (1961).
25. J. Kakinoki and Y. Komura, *Acta Crystallogr.* **19**, 137 (1965).
26. J. Kakinoki, *Acta Crystallogr.* **23**, 875 (1967).
27. B. E. Warren, *Progr. Met. Phys.* **8**, 147 (1959).
28. Z. Nishiyama, J. Kakinoki, and S. Kajiwara, *J. Phys. Soc. Jpn.* **20**, 1192 (1965).
29. S. Kajiwara, *Jpn. J. Appl. Phys.* **7**, 342 (1968).
30. S. Kajiwara, *J. Phys. Soc. Jpn.* **22**, 795 (1967).
31. L. Delaey and I. Cornelis, *Acta Metall.* **18**, 1061 (1970).
32. D. K. Chaudhuri, P. A. Ravindran, and J. J. Wert, *J. Appl. Phys.* **43**, 778 (1972).
33. S. Kajiwara and H. Fujita, *J. Phys. Soc. Jpn.* **21**, 400 (1966).
34. S. Kajiwara, *J. Phys. Soc. Jpn.* **27**, 268 (1969).
35. I. Isaitshev, E. Kaminsky, and G. V. Kurdjumov, *Trans. AIME* **128**, 361 (1938).
36. A. B. Greninger, *Trans. AIME* **133**, 204 (1939).
37. S. Kajiwara, *J. Phys. Soc. Jpn.* **23**, 656 (1967).
38. S. Kajiwara, *Trans. Nat. Res. Inst. Met.* **10**, 295 (1968); *Trans. JIM* **9**, *Suppl.* 543 (1968).
39. S. Kajiwara, *J. Phys. Soc. Jpn.* **25**, 1741 (1968); **27**, 712 (1969).
40. S. Kajiwara, *J. Phys. Soc. Jpn.* **30**, 768 (1971).
41. S. Kajiwara, *J. Appl. Crystallogr.* **4**, 329 (1971).
42. S. Kajiwara, *Jpn. J. Appl. Phys.* **9**, 385, 1555 (1970).
43. G. A. Shatalov and A. G. Khachaturyan, *Fiz. Met. Metalloved.* **25**, 637 (1968).
44. N. J. Petch, *J. Iron Steel Inst.* **145**, 111 (1942).
45. Z. Nishiyama and M. Doi, *J. Jpn. Inst. Met.* **8**, 305 (1944).
46. K. Löhberg and W. Schmidt, *Arch. Eisenhüttenwes.* **11**, 607 (1938).
47. H. Lipson and A. M. B. Parker, *J. Iron Steel Inst.* **149**, 123 (1944).
48. V. A. Il'ina, V. K. Kritskaya, and G. V. Kurdjumov, *Dokl. Akad. Nauk SSSR* **85**, 773 (1952).
49. V. A. Il'ina, V. K. Kritskaya, and G. V. Kurdjumov, *Dokl. Akad. Nauk SSSR* **85**, 997 (1952).
50. M. P. Arbuzov, L. I. Lysak, and Ye. G. Nesterenko, *Dokl. Akad. Nauk SSSR* **90**, 375 (1953).
51. G. V. Kurdjumov, *J. Iron Steel Inst.* **195**, 26 (1960).
52. P. M. Gielen and R. Kaplow, *Acta Metall.* **15**, 49 (1967).
53. M. Ron, A. Kidron, H. Schechter, and S. Niedzwiedz, *J. Appl. Phys.* **38**, 590 (1967).
54. H. Ino, T. Moriya, F. E. Fujita, and Y. Maeda, *J. Phys. Soc. Jpn.* **22**, 346 (1967).
55. F. E. Fujita, H. Ino, and T. Moriya, *Tetsu to Hagane* **53**, No. 5, S. 131 (1967).
56. H. Ino, T. Moriya, and F. E. Fujita, *Tetsu to Hagane* **54**, 34 (1968).
57. T. Moriya, H. Ino, F. E. Fujita, and Y. Maeda, *J. Phys. Soc. Jpn.* **24**, 60 (1968).
58. J.-M. R. Genin and P. A. Flinn, *Trans. AIME* **242**, 1419 (1968).
59. D. N. Pipkorn, C. K. Edge, P. Debrunner, G. DePasquali, H. G. Drickamer, and H. Frauenfelder, *Phys. Rev.* **135**, A1604 (1964).
60. R. A. Johnson, *Acta Metall.* **13**, 1259 (1965).
61. F. E. Fujita, H. Ino, T. Moriya, and H. Hirose, Japan Inst. Metals, Spring Meeting, p. 78 (1969).
62. F. E. Fujita, T. Moriya, and H. Ino, *Int. Conf. Sci. Tech. Iron Steel, Tokyo* 6-14-1, p. 658 (1970).
63. M. Lesoille and P. M. Gielen, *Metall. Trans.* **3**, 2681 (1972).
64. J. L. Snoek, *Physica* **8**, 711 (1941).
65. J. L. Snoek, *Physica* **9**, 862 (1942); **6**, 161 (1939).
66. J. L. Snoek, *Physica* **6**, 591 (1939).

67. R. Ward and J. M. Capus, *J. Iron Steel Inst.* **201**, 1038 (1963).
68. M. Sakamoto, Japan Inst. Metals, Fall Meeting, p. 219 (1972).
69. D. J. Dijkstra, *Phillips Res. Rep.* **2**, 375 (1947).
70. J. C. Swartz, J. W. Shilling, and A. J. Schwoeble, *Acta Metall.* **16**, 1359 (1968).
71. H. Ino and Y. Inokuti, *Acta Metall.* **20**, 157 (1972).
72. C. S. Roberts, *Trans. AIME* **197**, 203 (1953).
73. T. Bell and W. S. Owen, *J. Iron Steel Inst.* **205**, 428 (1967).
74. C. Zener, *Trans. AIME* **167**, 550 (1946); *Phys. Rev.* **74**, 639 (1948).
75. H. Sato, *J. Jpn. Inst. Met.* **17**, 601 (1953).
76. W. L. Bragg and H. J. Williams, *Proc. Roy. Soc.* **A145**, 699 (1934).
77. A. G. Khachaturyan, *Fiz. Met. Metalloved.* **19**, 343 (1965).
78. P. G. Winchell and M. Cohen, *Trans. ASM* **55**, 347 (1962).
79. R. A. Grange and H. M. Stewart, *Trans. AIME* **167**, 467 (1946).
80. G. R. Speich, *Trans. AIME* **245**, 2553 (1969).
81. Yu. L. Al'shevskiy and G. V. Kurdjumov, *Fiz. Met. Metalloved.* **30**, 413 (1970).
82. J. D. Eshelby, *J. Appl. Phys.* **25**, 255 (1954).
83. J. R. Townsend, *Acta Metall.* **15**, 325 (1965).
84. D. T. Keating and A. N. Goland, *Acta Metall.* **15**, 1805 (1967).
85. A. N. Goland and D. T. Keating, *J. Phys. Chem. Solids* **29**, 785 (1968).
86. R. A. Johnson, G. J. Dienes, and A. C. Damask, *Acta Metall.* **12**, 1215 (1964).
87. M. A. Krivoglaz and E. A. Tikhonova, *Ukr. Fiz. Zh.* **5**, 174 (1960).
88. J. C. Fisher, *Acta Metall.* **6**, 13 (1958).
89. M. A. Krivoglaz, *Fiz. Met. Metalloved.* **7**, 650 (1959).
90. S. C. Moss, *Acta Metall.* **15**, 1815 (1967).
91. J. A. Venables, *Phil. Mag.* **7**, 35 (1962).
92. H. Fujita and S. Ueda, *Acta Metall.* **20**, 759 (1972).
93. H. M. Otte, *Acta Metall.* **5**, 614 (1957).
94. S. Dash and N. Brown, *Acta Metall.* **14**, 595 (1966).
95. M. H. Richman, M. Cohen, and H. G. F. Wilsdorf, *Acta Metall.* **7**, 819 (1959).
96. Z. Nishiyama and K. Shimizu, *Acta Metall.* **7**, 432 (1959); **9**, 980 (1961).
97. Z. Nishiyama, K. Shimizu, and K. Sugino, *Acta Metall.* **9**, 620 (1961); *Mem. ISIR, Osaka Univ.* **18**, 71 (1961).
98. J. Gaggero and D. Hull, *Acta Metall.* **10**, 995 (1962).
99. K. Shimizu and C. M. Wayman, *Congr. Electron Microsc., 6th* **1**, 459 (1966).
100. K. Shimizu, M. Oka, and C. M. Wayman, *Acta Metall.* **18**, 1005 (1970).
101. H. Warlimont, *Trans. AIME* **224**, 495 (1962).
102. Z. S. Basinski and J. W. Christian, *Acta Metall.* **2**, 148 (1954).
103. Z. S. Basinski and J. W. Christian, *Acta Metall.* **4**, 371 (1956).
104. L.-C. Chang, *J. Appl. Phys.* **23**, 725 (1952).
105. A. Ölander, *Z. Kristallogr.* **83A**, 145 (1932).
106. C. Benedicks, *Ark. Mat. Astron. Fys.* **27A**, No. 18 (1940/41).
107. L.-C. Chang, and T. A. Read, *Trans. AIME* **189**, 47 (1951).
108. D. S. Lieberman, "Phase Transformation," Chapter 1, p. 1, Amer. Soc. of Metals, 1968.
109. M. W. Burkart and T. A. Read, *Trans. AIME* **197**, 1516 (1953).
110. H. K. Birnbaum and T. A. Read, *Trans. AIME* **218**, 662 (1960).
111. K. Otsuka, *Jpn. J. Appl. Phys.* **10**, 571 (1971).
112. A. L. Kuporev and L. G. Khandros, *Fiz. Met. Metalloved.* **32**, 1322 (1971).
113. Z. S. Basinski and J. W. Christian, *Acta Metall.* **2**, 101 (1954).
114. S. G. Khayutin and Ye. S. Shpichinetskij, *Fiz. Met. Metalloved.* **22**, 432 (1966).
115. S. G. Khayutin, *Fiz. Met. Metalloved.* **25**, 730 (1968); **26**, 742 (1968).

116. R. J. Wasilewski, *Scr. Metall.* **5**, 127 (1971).
117. F. T. Worrell, *J. Appl. Phys.* **19**, 929 (1948).
118. S. J. Carlile, J. W. Christian, and W. Hume-Rothery, *J. Inst. Met.* **77**, 169 (1949).
119. W. Betteridge, *Proc. Phys. Soc.* **50**, 519 (1938).
120. B. Mathias and A. von Hippel, *Phys. Rev.* **72**, 1378 (1945).
121. K. Enami and S. Nenno, *Metall. Trans.* **2**, 1487 (1971).
122. K. Enami, S. Nenno, and Y. Inagaki, Japan Inst. Metals, Fall Meeting, p. 233 (1972).
123. Z. Nishiyama, *Sci. Rep. Tohoku Univ.* **23**, 637 (1934).
124. H. Hu, *Trans. AIME* **233**, 1071 (1965).
125. A. G. Yakhontov, *Fiz. Met. Metalloved.* **21**, 43 (1966).
126. Ye. A. Izmaylov and V. G. Gorbach, *Fiz. Met. Metalloved.* **20**, 114 (1965).
127. G. Krauss, Jr., *Acta Metall.* **11**, 499 (1963).
128. G. Wassermann, *Mitt. K. W. I. Eisenf.* **17**, 149 (1935), *Stahl Eisen* **55**, 1117 (1935).
129. J. Grewen and G. Wassermann, *Arch. Eisenhüttenwes.* **12**, 863 (1961).
130. V. G. Gorbach and E. D. Butakova, *Fiz. Met. Metalloved.* **16**, 292 (1963).
131. G. Krauss and M. Cohen, *Trans. AIME* **224**, 1212 (1962); **227**, 278 (1963).
132. M. Lacoude and C. Goux, *C. R. Groupe 7* **259**, 1856 (1964).
133. M. Lacoude and C. Goux, *C. R. Groupe 7* **259**, 1117 (1964).
134. I. N. Kidin, M. A. Shtremel', and V. I. Lizunov, *Fiz. Met. Metalloved.* **21**, 585 (1966).
135. S. Sekino and N. Mori, *Trans. ISIJ Proc. ICSTIS* Pt. II, p. 1181 (1971).
136. H. Kessler and W. Pitsch, *Arch. Eisenhüttenwes.* **38**, 321 (1967).
137. H. E. Bühler, W. Pepperhoff, and H. J. Schüller, *Arch. Eisenhüttenwes.* **36**, 457 (1965).
138. H. Hälbig, H. Kessler, and W. Pitsch, *Acta Metall.* **15**, 1894 (1967).
139. W. Pitsch, *Trans. AIME* **242**, 2019 (1968).
140. S. Shapiro, G. Krauss, *Trans. AIME* **239**, 1408 (1967); **242**, 2021 (1968).
141. H. Kessler and W. Pitsch, *Arch. Eisenhüttenwes.* **38**, 469 (1967); *Acta Metall.* **15**, 401 (1967).
142. For example, H. Yamanaka, *Rep. Ind. Res. Inst., Osaka Prefecture* **23**, 14, 22 (1960).
143. F. Habrovec, J. Skarek, P. Ryš, and J. Kounicý, *J. Iron Steel Inst.* **205**, 861 (1967).
144. Y. Miwa and N. Iguchi, *J. Jpn. Inst. Met.* **37**, 945 (1973).
145. H. Kessler and W. Pitsch, *Acta Metall.* **13**, 871 (1965).
146. H. Kessler and W. Pitsch, *Arch. Eisenhüttenwes.* **39**, 223 (1968).
147. S. Jana and C. M. Wayman, *Trans. AIME* **239**, 1187 (1967).
148. M. Watanabe, G. Watanabe, and Y. Yoshino, Japan Inst. Metals, Fall Meeting, p. 207, 208 (1970).
149. B. K. Sokolov and V. D. Sadovskij, *Fiz. Met. Metalloved.* **3**, 6 (1958).
150. V. N. L'nianoi, I. V. Salli, *Fiz. Met. Metalloved.* **9**, 460 (1966).
151. C. A. Apple and G. Krauss, *Acta Metall.* **20**, 849 (1972).
152. I. N. Roshchina and V. J. Kozlovskaya, *Fiz. Met. Metalloved.* **31**, 589 (1971).
153. W. C. Leslie, E. Hornbogen, and G. E. Dieter, *J. Iron Steel Inst.* **200**, 622 (1962).
154. W. C. Leslie, D. W. Stevens, and M. Cohen, "High Strength Materials" (V. F. Zackey, ed.) *Proc. 2nd Berkeley Int. Mater. Conf.* (1964), 382. Wiley, New York.
155. R. P. Agarwala and H. Wilman, *Proc. Phys. Soc.* **66B**, 717 (1953); *Proc. Roy. Soc.* **A223**, 167 (1954).
156. H. G. Bowden and P. M. Kelley, *Acta Metall.* **15**, 1489 (1967).
157. R. P. Zerwekh and C. M. Wayman, *Acta Metall.* **13**, 99 (1965).
158. A. Christou, *Scr. Metall.* **4**, 437 (1970).
159. R. W. Rohde, *Acta Metall.* **18**, 903 (1970).
160. R. W. Rohde, J. R. Holland, and R. A. Graham, *Trans. AIME* **242**, 2017 (1968).
161. R. J. Russel and P. G. Winchell, *Metall. Trans.* **3**, 2403 (1972).

162. L. I. Lysak, *Metallofizika* **27**, 40 (1970).
163. L. I. Lysak and B. I. Nikolin, *Dokl. Akad. Nauk SSSR* **152**, 812 (1963).
164. L. I. Lysak and B. I. Nikolin, *Fiz. Met. Metalloved.* **20**, 547 (1965); **23**, 93 (1967).
165. V. L. Kononenko, L. N. Larikov, L. I. Lysak, B. I. Nikolin, and Yu. F. Yurchenko, *Fiz. Met. Metalloved.* **28**, 889 (1969).
166. Yu. N. Makogon and B. I. Nikolin, *Fiz. Met. Metalloved.* **32**, 1248 (1971).
167. L. I. Lysak, Yu. N. Makogon, and B. I. Nikolin, *Fiz. Met. Metalloved.* **25**, 562 (1968).
168. L. I. Lysak and I. B. Goncharenko, *Fiz. Met. Metalloved.* **31**, 1004 (1971); Institut Metallofiziki, 71.1 (1971).
169. L. I. Lysak and I. B. Goncharenko, *Fiz. Met. Metalloved.* **30**, 967 (1970).
170. D. A. Mirzayev and S. V. Rushchits, *Fiz. Met. Metalloved.* **37**, 912 (1974).
171. M. Oka, Y. Tanaka, and K. Shimizu, *Jpn. J. Appl. Phys.* **11**, 1073 (1972); *Trans. JIM* **14**, 148 (1973).
172. L. I. Lysak and Ya. N. Vovk, *Fiz. Met. Metalloved.* **19**, 599 (1965).
173. L. I. Lysak, Ya. N. Vovk, and E. L. Khandros, *Fiz. Met. Metalloved.* **19**, 933 (1965).
174. L. I. Lysak, Ya. N. Vovk, A. G. Drachinskaya, and Yu. M. Polishchuk, *Fiz. Met. Metalloved.* **24**, 299 (1967).
175. L. I. Lysak and A. G. Drachinskaya, *Fiz. Met. Metalloved.* **25**, 241 (1968).
176. L. I. Lysak and Yu. M. Polishchuk, *Fiz. Met. Metalloved.* **27**, 148 (1969).
177. L. I. Lysak and Ya. N. Vovk, *Fiz. Met. Metalloved.* **20**, 540 (1965).
178. L. I. Lysak, Ya. N. Vovk, and Yu. M. Polishchuk, *Fiz. Met. Metalloved.* **23**, 898 (1967).
179. L. I. Lysak, Yu. M. Polishchuk, and Ya. N. Vovk, *Fiz. Met. Metalloved.* **22**, 275 (1966).
180. Yu. L. Al'Shevskiy and G. V. Kurdjumov, *Fiz. Met. Metalloved.* **25**, 172 (1968).
181. Yu. L. Al'Shevskiy, *Fiz. Met. Metalloved.* **27**, 716 (1969).
182. L. I. Lysak and S. P. Kondrat'yev, *Fiz. Met. Metalloved.* **32**, 637 (1971).
183. L. I. Lysak and L. O. Andrushchik, *Fiz. Met. Metalloved.* **26**, 380 (1968); **28**, 348 (1969).
184. L. I. Lysak and B. J. Nikolin, *Fiz. Met. Metalloved.* **22**, 730 (1966).
185. L. I. Lysak, *Ukr. Zh.* **14**, 1604 (1969).
186. L. I. Lysak and Ya. N. Vovk, *Fiz. Met. Metalloved.* **31**, 646 (1971).
187. Yu. M. Koval', P. V. Titov, and L. G. Khandros, *Fiz. Met. Metalloved.* **23**, 52 (1967).
188. L. I. Lysak, L. O. Andrushchik, N. A. Storchak, and V. G. Prokopenko, *Fiz. Met. Metalloved.* **30**, 661 (1970).
189. L. I. Lysak, L. O. Andrushchik, and Yu. M. Polishchuk, *Fiz. Met. Metalloved.* **27**, 827 (1969).
190. L. I. Lysak and S. A. Artemyuk, *Fiz. Met. Metalloved.* **27**, 1122 (1969).
191. L. I. Lysak and V. Ye. Danil'yenko, *Fiz. Met. Metalloved.* **32**, 639 (1971).
192. L. I. Lysak and S. P. Kondrat'yev, *Fiz. Met. Metalloved.* **30**, 973 (1970).
193. L. I. Lysak, L. O. Andrushchik, and N. A. Storchak, Ordena Lenija *Akad. Nauk USSR Inst. Metall.* (1970).
194. L. I. Lysak and L. O. Andrushchik, *Fiz. Met. Metalloved.* **28**, 478 (1969).
195. L. I. Lysak, L. O. Andrushchik, S. A. Artemyuk, and N. A. Storchak, *Fiz. Met. Metalloved.* **31**, 221 (1971).
196. F. E. Fujita, T. Moriya, and H. Ino, *Int. Conf. Sci. Tech. Iron Steel, Tokyo* p. 658 (1970).
197. F. E. Fujita, H. Ino, T. Moriya, M. Funabashi, and T. Irie, Phys. Soc. Japan, Spring Branch Meeting, I, p. 127 (1971).
198. A. L. Roitbourd and A. G. Khachaturyan, *Fiz. Met. Metalloved.* **30**, 1189 (1970).
199. M. P. Usikov, *Fiz. Met. Metalloved.* **33**, 1047 (1972).
200. L. I. Lysak, A. G. Drachinskaja, and N. A. Storchak, Institut Metallofiziki, 71.5 (1971).
201. D. N. Beshers, *J. Appl. Phys.* **36**, 290 (1965).

4

Transformation Temperature and Rate of Martensite Formation

The crystallography of martensites, which has been described in previous chapters, serves to examine statically the states of existence without regard to such parameters as temperature. Hence, it is only part of the picture. In this chapter, a description of the kinetics[1] of the martensitic transformation (e.g., the conditions of temperature or other variables under which it occurs) is presented.

The formation of martensite is most commonly observed when the temperature changes, but sometimes it occurs while a sample is held at a constant temperature. In the latter case, the temperature at which the sample is held is an important factor for the kinetics. The propagation of a martensitic transformation front can be either rapid or slow. Since all these phenomena must proceed toward decreasing the free energy, it is necessary to bear this fact in mind when making a thermodynamic analysis of the martensitic transformation. In this chapter we will discuss mainly the case of steels. Details of various conditions that influence the formation of martensites will be described in the next chapter.

4.1 Chemical free energy changes in transformations

4.1.1 Transformation in pure iron

Let us consider the chemical free energy change accompanying the $\alpha \rightarrow \gamma$ transformation in pure iron, which is the basis for the martensitic transformation in steels. Since the α and γ phases differ in crystal structure, the

temperature dependence of the chemical free energy is different between the two phases, as was shown in Fig. 1.5. Therefore, the quantity $\Delta F^{\alpha\to\gamma}$ as defined here must be zero at, negative above, and positive below the A_3 temperature.

$$F^{\gamma} - F^{\alpha} = \Delta F^{\alpha\to\gamma} \tag{1}$$

where F^{γ} and F^{α} are the chemical free energies of the γ and α phases, respectively. Attempts have been made to calculate $\Delta F^{\alpha\to\gamma}$ using measured values of various thermodynamic quantities and a number of numerical equations for $\Delta F^{\alpha\to\gamma}$ as a function of the absolute temperature T have been given.[2–11] For example, Kaufman and Cohen[6] proposed

$$\Delta F_{\mathrm{Fe}}^{\alpha\to\gamma} = 1202 - 2.63 \times 10^{-3}T^2 + 1.54 \times 10^{-6}T^3 \quad \text{cal/mol} \tag{2a}$$

for $T = 200°$–$900°$K. Owen and Gilbert[7] gave

$$\Delta F_{\mathrm{Fe}}^{\alpha\to\gamma} = 1474 - 3.4 \times 10^{-3}T^2 + 2 \times 10^{-6}T^3 \quad \text{cal/mol} \tag{2b}$$

for $T = 800°$–$1000°$K. If the ferromagnetism of α iron is taken into account, this type of equation becomes slightly modified.[12,13] Figure 4.1 shows $\Delta F_{\mathrm{Fe}}^{\alpha\to\gamma}$ plotted against temperature; note that the data given by various investigators are in fairly good agreement at high temperatures.

The enthalpy change $\Delta H^{\alpha\to\gamma} = \Delta F^{\alpha\to\gamma} - T\,\partial\Delta F^{\alpha\to\gamma}/\partial T$, which corresponds to heat evolution due to the $\gamma \to \alpha$ transformation, can be calculated by replacing $\Delta F^{\alpha\to\gamma}$ in this equation by Eq. (2). The result of this calculation is shown in Fig. 4.2, from which the heat of the $\gamma \to \alpha$ transformation in pure iron is seen to be large.

In the case of the martensitic transformation, as will be discussed later, additional energy changes besides the chemical free energy change are required.

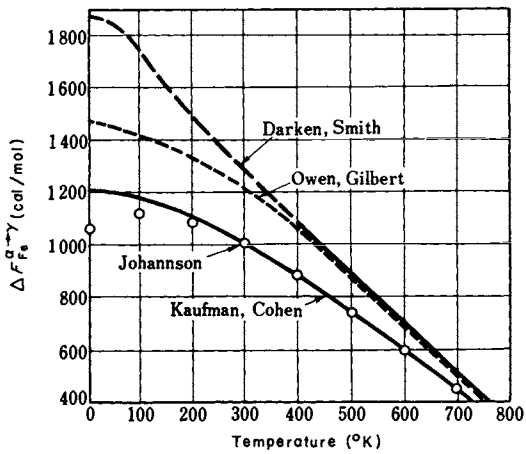

FIG. 4.1 Free energy difference in the $\gamma \to \alpha$ transformation of iron.[2,4,6,7]

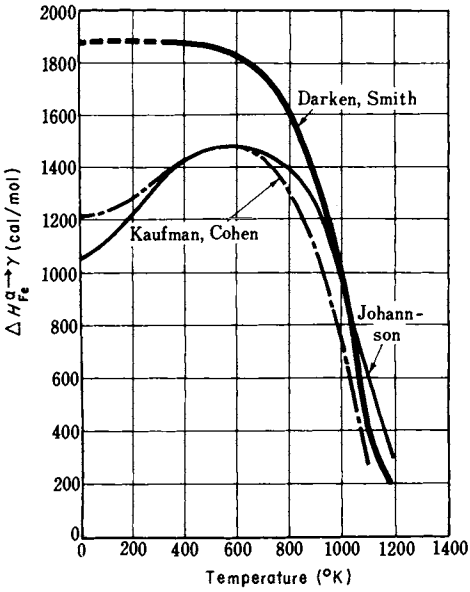

FIG. 4.2 Enthalpy change due to the $\gamma \to \alpha$ transformation in iron.[2,4,6]

Hence the transformation does not occur at temperature T_0, at which $\Delta F^{\gamma\to\alpha} = 0$, but starts at a lower temperature called the M_s temperature.

4.1.2 Martensitic transformation in iron alloys

When a γ solid solution of an Fe–A alloy transforms into an α solid solution of the same composition, the chemical free energy change ΔF_{Fe-A} accompanying it is formally expressed by a sum of three terms, as follows:

$$\Delta F_{Fe-A}^{\gamma\to\alpha} = (1 - x)\Delta F_{Fe}^{\gamma\to\alpha} + x\Delta F_{A}^{\gamma\to\alpha} + \Delta F_{M}^{\gamma\to\alpha} \tag{3}$$

where x is the concentration of component A in atom fraction. In Eq. (3), the first, second, and third terms represent respectively solvent Fe atoms, solute A atoms, and the mixture (solid solution) of the two species. The first term can be estimated by using Eq. (2), but the second and third terms are difficult to estimate. A few examples of the efforts that have been made to estimate these quantities will be discussed next.

Zener[14] has derived the thermodynamic properties of medium alloy steels by assuming the phases to be ideal solutions and therefore the mixing term $\Delta F_{M}^{\gamma\to\alpha}$ to be negligible. He further assumed $\Delta S_{A}^{\gamma\to\alpha} = 0$[15] in the second (solute) term $\Delta F_{A}^{\gamma\to\alpha} = \Delta H_{A}^{\gamma\to\alpha} - T\,\Delta S_{A}^{\gamma\to\alpha}$ and so

$$\Delta F_{A}^{\gamma\to\alpha} \fallingdotseq \Delta H_{A}^{\gamma\to\alpha}. \tag{4}$$

TABLE 4.1 Difference in heat of solution between γ and α′ Fe phases[a]

Alloying element	$\Delta H_A^{\gamma\to\alpha'}$ (cal/mol)	Alloying element	$\Delta H_A^{\gamma\to\alpha'}$ (cal/mol)	Alloying element	$\Delta H_A^{\gamma\to\alpha'}$ (cal/mol)
C	8100	Cu	1280	Mo	−1360
N	5360	Zn	590	V	−2830
Mn	2440	Si	−475	P	−4180
	2700[17]	Be	−810	Sn	−5500
Ni	1600	Al	−1300	Ti	−9000
	2500[17]	W	−1360	Cr	1200[18]

[a] Data from Zener[14] unless otherwise specified.

He finally obtained

$$\Delta F^{\gamma\to\alpha} = (1 - x)\Delta F_{Fe}^{\gamma\to\alpha} + x\Delta H_A^{\gamma\to\alpha}. \tag{5}$$

Here $\Delta H_A^{\gamma\to\alpha}$ is the difference between the heats of solution of component A in the α and γ solid solutions and is nearly equal to $\Delta H_A^{\gamma\to\alpha'}$ (α′ denotes martensite); numerical values† are listed in Table 4.1.[14,17,18] Elements for which $\Delta H_A^{\gamma\to\alpha'}$ is positive lower T_0 and those with negative $\Delta H_A^{\gamma\to\alpha'}$ elevate T_0.‡ The T_0 value is the main factor in determining the M_s temperature.

Kaufman and Cohen[6] made a more rigorous treatment, to be applicable to high alloy steels. In their treatment, the mixing term was considered, assuming a regular solid solution, and the parameters used were determined from the observed concentrations[22] of the γ and α phases in equilibrium. They obtained the following equation for Fe–Ni alloys applicable up to 1000°K:

$$\Delta F_{Fe-Ni}^{\gamma\to\alpha} = (1 - x)\Delta F_{Fe}^{\gamma\to\alpha} - x(-3700 + 7.09 \times 10^{-4}T^2 + 3.91 \times 10^{-7}T^3) - x(1 - x)[3600 + 0.58T(1 - \ln T)] \quad \text{cal/mol}. \tag{6}$$

The temperature T_0 at which $\Delta F_{Fe-Ni}^{\gamma\to\alpha}$ vanishes will be shown later in Fig. 4.7. This result is subject to a slight modification when the ferromagnetism is taken into account.[23]

The mixing term is also taken into account in calculating the free energy of formation of interstitial solid solutions, as in Fe–C and Fe–N alloys.[24,25] In the case in which tetragonal martensite forms, the free energy change due to the ordering of interstitial atoms should be taken into account.[26] Along this line, Imai *et al.*[27] made a statistical mechanics calculation. First they calculated the free energy change $\Delta F^{\gamma\to\alpha'}$ for disordered lattice (cubic crystal)

† Scheil and Normann[16] have determined this quantity for Fe–Ni alloys.

‡ Chromium is an exception.[19–21] The reason is that the heats of solution used in the calculation were obtained by extrapolating the values obtained at low chromium concentrations to high concentrations.

formation by using equilibrium concentrations of the α and γ phases. They obtained the following expressions.

Fe–C case:

$$-\Delta F^{\gamma\to\alpha'}$$

$$= (1-x)\,\Delta F_{\mathrm{Fe}}^{\gamma\to\alpha} - x(5552 + 1.65RT) - RT\left[x\ln\frac{x}{1-2x} - x\ln\frac{x}{3(1-2x)}\right]$$
$$- RT\frac{3x^2}{1-x}\left\{\left[1-\exp\left(\frac{-1032}{RT}\right)\right]^2\left[2-\exp\left(\frac{-1032}{RT}\right)\right]\right.$$
$$\left.+\frac{2064}{RT}\exp\left(\frac{-1032}{RT}\right)\right\} + 1.8\times 10^4\left(\frac{x}{1-x}\right)^2 \quad \text{cal/mol;} \tag{7}$$

Fe–N case:

$$-\Delta F^{\gamma\to\alpha'}$$

$$= (1-x)\,\Delta F_{\mathrm{Fe}}^{\gamma\to\alpha} - x(5360 + 1.92RT) - RT\left[x\ln\frac{x}{1-2x} - x\ln\frac{x}{3(1-2x)}\right]$$
$$- RT\frac{3x^2}{1-x}\left\{\left[1-\exp\left(\frac{-1180}{RT}\right)\right]^2\left[2-\exp\left(\frac{-1180}{RT}\right)\right]\right.$$
$$\left.+\frac{2360}{RT}\exp\left(\frac{-1180}{RT}\right)\right\} + 1.8\times 10^4\left(\frac{x}{1-x}\right)^2 \quad \text{cal/mol.} \tag{8}$$

Second, for the case of a tetragonal crystal in which interstitial atoms take an ordered arrangement, they obtained the following relations by adapting Sato's calculation:[26]

$$-\Delta F^{\gamma\to\alpha'} = -\Delta F^{\gamma\to\alpha} - F \tag{9}$$

$$F = \frac{1}{3}N\phi\left(\frac{x}{1-x}\right)^2(1-S^2)$$
$$+ NRT\left\{\frac{1}{3}\frac{x}{1-x}(2S+1)\ln\left[\frac{1}{3}\frac{x}{1-x}(2S+1)\right]\right.$$
$$+\left[1-\frac{1}{3}\frac{x}{1-x}(2S+1)\right]\ln\left[1-\frac{1}{3}\frac{x}{1-x}(2S+1)\right]$$
$$+\frac{2}{3}\frac{x}{1-x}(1-S)\ln\left[\frac{1}{3}\frac{x}{1-x}(1-S)\right]$$
$$\left.+2\left[1-\frac{1}{3}\frac{x}{1-x}(1-S)\right]\ln\left[1-\frac{1}{3}\frac{x}{1-x}(1-S)\right]\right\} \tag{10}$$

where N is the number of Fe atoms and S, the long-range order parameter for the arrangement of interstitial atoms, is zero for the cubic crystal. The interaction energy between interstitial atoms in the lattice, ϕ, is estimated to be 3.74×10^{-2} ergs for both the Fe–C and Fe–N cases, assuming that the energy decrease due to ordering of interstitial atoms in the tetragonal crystal balances the increase of elastic energy due to the tetragonal distortion. Putting this value into Eq. (10) and utilizing Eq. (2b) for $\Delta F_{Fe}^{\gamma\to\alpha}$ enables us to express $-\Delta F^{\gamma\to\alpha'}$ as a function of x and T. The temperatures T_0 at which $\Delta F^{\gamma\to\alpha'}$ becomes zero are also included in Fig. 4.6.

Wada[20] discussed the free energy change, taking into consideration the contribution from ferromagnetism.

4.2 Nonchemical free energy for martensitic transformation

Martensitic transformations do not start at T_0, where $\Delta F^{\gamma\to\alpha'} = 0$, but begin to occur† only when the M_s temperature is reached after further cooling. For steels the difference between T_0 and M_s amounts to something like 200°C, whereas in some other cases it is small. The free energy change, which corresponds to the temperature difference between T_0 and M_s, amounts to about 300 cal/mol in the steels and this constitutes the driving force for the transformation. This energy is necessary because the following nonchemical energy terms must be considered in order to start the reaction.

4.2.1 Interfacial energy between martensite and matrix

The interfacial energy between the martensite and its matrix depends on the coherency of the two phases, that is, on the orientations and indices of the interface of the two crystals. Assuming the interfacial energy constant, the total energy of the interface is equal to the surface energy σ (per unit area) multiplied by the surface area. If a martensite crystal is lenticular in shape and not too thick, the surface area is near $2\pi r^2$ and hence the energy of the interface is expressed by $2\pi r^2\sigma$ where r is the radius of the martensite crystal. If the interface is like Frank's interface[29] (to be described in Section 6.5.4), σ is estimated[24,30] to be about $(1.2\text{–}2.4) \times 10^{-5}$ cal/cm^2.

† This "begins to occur" is not meant in the strict sense. It means that the transformation is first discerned rather clearly by a standard measuring method. It is a fact[28] that with increasing accuracy of measurement the beginning temperature rises accordingly and approaches the temperature T_0. This extreme case corresponds to "true nucleation," in which the phenomenon at a particular spot of the sample where the nonchemical energy is extremely small is detected by the measurement.

4.2.2 Energy for plastic deformation due to the transformation

As discussed in Chapter 2, a large amount of slip or twinning occurs within martensite crystals in order to relax the stress due to the shape change associated with the lattice transformation. Slip (or twinning) also occurs to some extent within the matrix that surrounds the martensite crystals. The energy necessary to cause such deformations is supposed to be very large, but there seems to be no formula available that can be used to estimate it quantitatively. However, the amount of this nonchemical free energy is very important in discussing martensitic transformation, and microscopic factors must be considered when estimating this energy. Unfortunately, however, the present state of research is such that the phenomenon can be treated only macroscopically by averaging the microscopic factors.

4.2.3 Energy for elastic deformation accompanying transformation

In addition to the strain energy due to plastic deformation mentioned in the previous subsection, an elastic distortion occurs over a wide range inside and outside of a martensite crystal and the corresponding energy is stored. If the martensite crystal is lenticular in shape, this energy is given by

$$\pi r t^2 A = \pi r^2 t (At/r)$$

where t is the thickness, r the radius, and $\pi r^2 t$ the volume of the martensite crystal. The constant A is estimated to be 480–1440 cal/cm^3 by Fisher,[25] and to be 500 cal/cm^3 at 25°C by Knapp and Dehlinger,[31] under certain assumptions.

Lyubov and Roitburd[32] regarded a martensite plate as a flat elliptic cylinder (major axis a, minor axis b) of infinite length and calculated the change of b/a accompanying the growth of the martensite plate. In this calculation, they obtained the ratio b/a by minimizing the sum of the interfacial energy and the elastic energy stored around the martensite crystal. When growth has progressed, the ratio eventually becomes

$$(b/a)_{\text{lim}} = [\alpha^2/(k^2 + \alpha^2)]^{1/2}$$

where α is the expansion due to the transformation and k is a shear strain which is assumed to occur parallel to the surface of the martensite plate. For an iron alloy in which $\alpha = 0.01$ and $k = 0.18$, $(b/a)_{\text{lim}}$ becomes 1/19. Next, in order for the martensite plate to grow, it is necessary that the chemical free energy change accompanying the transformation be greater than the elastic energy due to an expansion associated with the transformation. The critical value is estimated to be 400 cal/mol for iron alloys.

In the foregoing calculation the energy of lattice defects accumulated within the martensite plate was not taken into account and the crystal was assumed isotropic.

4.2.4 Energy of elastic vibration produced during transformation

This is the energy of sound occurring during the transformation and it is thought to be small.

4.2.5 Experiments concerning nonchemical energy

Since each of the nonchemical energies mentioned earlier is complex in content, it is not easy to estimate each term separately. In the following, three examples of nonchemical free energies are given without resolving them into individual terms.

According to research[33] in which the enthalpy change accompanying the f.c.c.-to-h.c.p. transformation in cobalt was measured, it is 113 cal/mol during heating and 84 cal/mol during cooling, and this difference is interpreted to be due to the difference between the nonchemical energies required for both transformations.

According to research[34] using Fe–Ni base alloys with C, Cr, or Co additions, the heat evolution, which mainly reflects the driving force of the transformation, is nearly proportional to the rigidity modulus μ. This is a manifestation of the fact that the nonchemical energy is mainly dependent on the elastic constants, since for every alloy concerned here, the transformation is f.c.c. to b.c.c. and hence the transformation distortion is nearly equal. The fact is that a Co addition raises the M_s temperature and lowers the heat evolution and this in turn corresponds to a lowering of the rigidity modulus. Theories concerning this problem will be given in Section 6.7.

Singh and Parr[35] have measured nonchemical energy using the electrode potential method. The specimen was a cube of iron (0.005% C–0.02% Si–0.06% N) with an edge length of 3/64 in. It was quenched by a jet of He gas at a cooling rate of 5×10^3°C/sec. The quenched specimen was confirmed to be martensite from its surface relief. The electrode potential was measured by making this specimen one electrode and a slow-cooled piece of ferritic iron with isotropic crystal grains the other. The electrode potential measured was 6.4 mV, the equivalent of 300 cal/mol of heat. This heat, which corresponds to the difference between the free energies of martensite and ferrite, is very close to the value, 290 cal/mol (as estimated from chemical free energies), of the driving force for the martensitic transformation. These authors suggest that this agreement indicates the validity of the thermodynamic treatment. However, there is reservation about this research.[36,37]

4.3 Transformation temperature

4.3.1 Effect of cooling rate

In general, the martensitic transformation temperature is dependent on the cooling rate when the cooling rate is not high; above a critical cooling rate, however, the starting temperature of the transformation is constant. (Usually this temperature at which the formation of martensite starts is called the M_s temperature.) Although the constant starting temperature had been established many years ago, the issue whether the M_s is constant and independent of the cooling rate was often raised.[38] In iron-base alloys, as will be discussed later, it is often observed that the transformation temperature versus cooling rate curve shows two plateaus when cooling rates exceed a critical cooling rate (see Fig. 4.4). In such a case, the plateau at the lower temperature is thought to be the M_s temperature and the one at the higher temperature to be the A_3 temperature (for iron-base alloys), corresponding to the largest supercooling.

In titanium, however, there is no plateau on the transformation temperature versus cooling rate curve. Duwez[39] changed the cooling rate up to 1.5×10^4°C/sec, and Bibby and Parr[40] made similar experiments up to 5×10^4°C/sec. According to the latter authors, the transformation temperature is 882°C on slow cooling; it decreases linearly with increasing cooling rate, and goes down to 800°C at a cooling rate of 5×10^4°C/sec. Therefore, the critical cooling rate at which the curve becomes horizontal might be much higher. On the other hand, at a cooling rate of 200°C/sec surface relief as evidence of martensite formation is observed. Therefore, within the scope of the experiments, the transformation should be interpreted to occur by both the individual and cooperative movement of atoms.

Similarly, the transformation temperature of Zr is 865°C on slow cooling and decreases to 850°C on rapid cooling (1.5×10^4°C/sec).[39] If this lower value is taken as the M_s temperature, the degree of supercooling in Zr is an order of magnitude smaller than that of iron-base alloys. Therefore, the driving force for the transformation in Zr is small, 50 cal/mol.[41]

On the other hand, for cooling rates ranging from a low rate to 1.5×10^4°C/sec the temperature at which the transformation starts for Tl is constant at 230° ± 4°C. This is not independent of the fact that the heat of transformation of Tl has so small a value as 74 cal/mol, which is an order of magnitude smaller[39] than the heat of transformation of Zr, 710 cal/mol. Considering these examples, when the transformation temperature versus cooling rate curve has a single plateau, it is questionable whether the transformation product formed there is completely martensitic. Conversely, it

may be possible that the transformation product formed below the critical cooling rate is partly martensitic in nature.

According to Lieberman,[42] the M_s temperature of a nearly equiatomic Au–Cd alloy is constant (32°C), independent of the cooling rate. Furthermore, below M_s the relation between the amount of transformation product and temperature is expressed by a single curve that is independent of the cooling rate, provided the cooling rate is lower than a critical value. He proposed to call this curve an *eigentherm.*

In some alloys in which the cooling rate has an influence on the stabilization of the matrix, the transformation temperature is lower at slower cooling rates. This subject will be treated in Section 5.7.8.

4.3.2 M_s temperatures of pure iron, carbon steels, and nitrogen steels

Upon heating, iron undergoes the transformations α (b.c.c.) to γ (f.c.c.) to δ (b.c.c.). This sequence is thought to be due to the following reasons: In general, the b.c.c. lattice is not close packed and atoms within this lattice are easier to move. The entropy of lattice vibration due to this instability is large,† and thus at high temperatures the free energy $F = H - TS$ (H is the enthalpy) is small. Therefore, the b.c.c. structure is very stable at high temperatures. For this reason the b.c.c. structure exists as a high-temperature phase in many metals and alloys. Iron also takes the b.c.c. structure as the δ phase at high temperatures.

However, iron with the b.c.c. structure is again stable at lower temperatures (below the lowest temperature for the stable γ phase). This is due to another reason, [43] namely, that the d electrons in Fe cause the electronic structure of an Fe atom to be anisotropic, thereby contributing to a directional binding of Fe atoms. With a rise in temperature, however, this directional binding tends to become isotropic, and eventually the close-packed structure of γ iron becomes more stable. With further increase in temperature the b.c.c. structure again becomes stable, for the reason already mentioned.

We now consider the martensitic transformation in pure iron. It has been a long time since it was pointed out that pure iron undergoes martensitic transformation. In 1929, Sauveur and Chou[44] quenched a piece of electrolytic iron in mercury from 1000°C and found surface relief indicating a martensitic transformation. However, the purity of the specimen was not known at the time, and the M_s temperature was not measured.

Later, a number of researchers[7,45–51] confronted this problem. In 1930, Wever and Engel[45] determined the transformation temperature by quenching a small sample of reduced pure iron. The sample was a ribbon in shape,

† Among metals with the b.c.c. structure, Fe has a particularly large elastic anisotropy and strong vibrations in the direction of elastic weakness.

TABLE 4.2 M_s **temperatures of iron**[a]

Carbon (%)	Cooling rate (°C/sec)	M_s (°C)
0.037	$3.36–5.76 \times 10^3$	440–438
0.025	9.47×10^3	435
0.014	6.60×10^3	440
<0.01	7.15×10^3	Not detected

[a] After Wever and Engel.[45]

0.03 mm thick, and was heated by passing current through it in a vacuum. The quenching was carried out by spraying water or blowing argon gas and the temperature change was measured by a thin thermocouple spot-welded on the specimen. The microstructure was also observed. The transformation temperatures obtained in this experiment are given in Table 4.2. Thus, above 0.014% carbon the martensite was positively identified and the M_s temperature determined, but it was not possible to detect the M_s temperature of the iron having the highest purity, probably because the cooling rate was not rapid enough.

In 1951 Duwez[39] determined the transformation temperature of 0.001% C iron as 750°C by gas-jet-type quenching at a cooling rate of 1.5×10^4°C/sec. In 1964 Bibby and Parr[49] obtained a cooling rate of more than 3.5×10^4°C/sec by gas-jet-type quenching and succeeded in producing martensite in iron containing less than 0.0017% C. The M_s temperature was found to be 750°C.

In 1966, using Ferrovac E (0.0029% C) iron, Speich *et al.*[50] heated specimens by a ruby laser ray and super-rapid-cooled them at a rate of 10^5°C/sec by blasting them with a gas mixture of argon and water vapor. They obtained a martensitic microstructure whose hardness is reported to be 150 DPH, but unfortunately the M_s temperature is not recorded in this report.

Izumiyama *et al.*[51] studied this problem using iron of the highest-purity grades. The carbon and nitrogen contents in the iron specimens are listed in Table 4.3, from which other impurities, such as Si, Mn, P, and S, are omitted, but their amounts are small. Specimen A in Table 4.3 is purest and was prepared by synthesizing and purifying a stable organometallic compound.[52] The cooling method was gas-jet-type quenching similar to that used by Bibby and Parr[49] but using a tapered nozzle. In this experiment argon or hydrogen gas was used. The specimen size was $0.2 \times 0.25 \times 0.25$ mm. An 0.08-mm alumel–chromel thermocouple was spot-welded onto the specimen. The other ends of the thermocouple were connected to a synchroscope on which the cooling curves were obtained. Using the method

TABLE 4.3 Carbon and nitrogen contents in high-purity iron specimens

Specimen	C (%)	N (%)	Method of preparation
A	0.001	0.001	From pure organic compound
B	0.002	0.001	Johnson and Matthey
C	0.003	0.002	Electrolytic iron
D	0.006	0.002	Electrolytic iron and pig iron
E	0.018	0.001	
F	0.039	0.002	

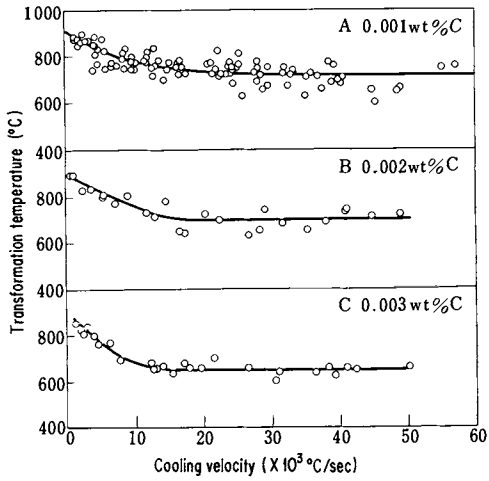

FIG. 4.3 Relation between the transformation temperature of iron and the cooling rate (0.001–0.003% C). (After Izumiyama *et al.*[51])

just described and adjusting the gas pressure at the outlet of the gas container, cooling rates ranging from 10^2 to 6×10^4°C/sec could be obtained. Quenching was performed after heating for 2 hr at 1000°C.

The experimentally determined transformation temperatures are plotted against the cooling rate in Figs. 4.3 and 4.4. These curves show that the critical cooling rate is around 2×10^4°C/sec and each curve consists of two stages† for carbon contents greater than 0.006% and of a single stage for iron of higher purity than this. The horizontal temperature at the second stage is clearly M_s. However, even for the purest iron, containing 0.001% C, which had only a single stage, surface relief was observed on the specimen

† According to Wilson,[53] between the two stages there occur two additional stages due to bainitic reactions in a steel containing 0.011% C.

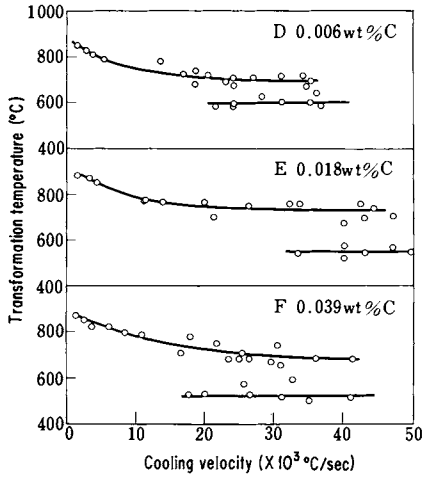

FIG. 4.4 Relation between the transformation temperature of iron and the cooling rate (0.006–0.039%C). (After Izumiyama *et al.*[51])

when it was cooled faster than the critical cooling rate. This indicates that the single-stage transformation possesses the characteristics of the martensitic transformation.† Therefore, the transformation that occurs when iron with less than 0.006% C is cooled faster than the critical cooling rate is regarded by the researchers as a supercooled A_3 transformation, namely it occurs partly by diffusion-controlled and partly by shear mechanisms. In other words, the former is due to individual movement of atoms and the latter has a martensitic element due to the cooperative movement of atoms. In Fig. 4.4 transformation temperatures appear in two stages, as represented by the two horizontals. In this case, usually one of the two stages appears on the cooling curve, although in rare cases two stages appear. This is because the specimen is small. Taking this smallness into consideration, it seems that although the transformation temperature curves for high-purity specimens A, B, and C (Fig. 4.3) consist of a single stage, they would in reality consist of two stages that would lie too close to each other to be resolved.‡ At such high temperatures, individual movement of atoms takes part in the martensitic transformation to some extent. Therefore it might be impossible to measure the true M_s temperature by present-day techniques.

As mentioned previously, the fact that surface relief appeared in titanium when the cooling rate was still below the critical rate seems to be a phenomenon similar to the one for iron with less than 0.006% C.

† Electron microscope observation of quenched iron of good purity revealed a substructure[54] characteristic of martensite.

‡ Since the specimen is small, local fluctuation of concentration of impurity might have great influence on the results of measurements for the case of iron with very low carbon concentration. Morozov *et al.*[55] reported four stages in the transformation temperature of iron containing 0.01% C. The plateau temperatures were 820°, 720°, 540°, and 420°C.

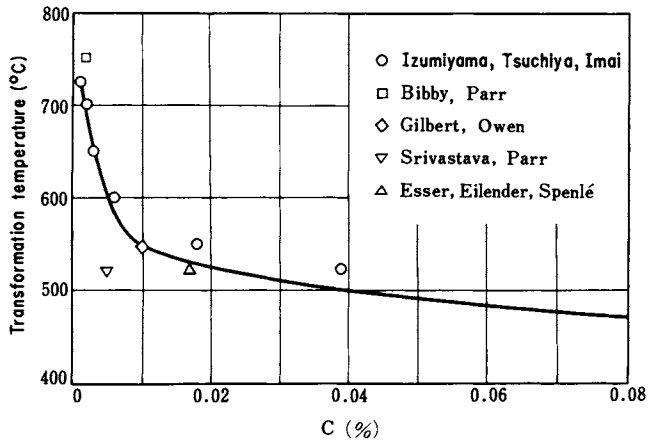

FIG. 4.5 Transformation temperatures of Fe–C alloys (low carbon). (After Izumiyama *et al.*[51])

In summary, transformation temperature data that were determined by the method just described are plotted against carbon concentration in Fig. 4.5; data of some other researchers are also included. Most researchers[56] report that below 0.006% C the transformation temperature drastically increases with decreasing carbon content. The solid curve in Fig. 4.5 indicates that the transformation temperature of pure iron is 720°C and this value coincides with the one obtained by extrapolating the M_s temperatures of high-purity binary Fe-base alloys to pure iron. Hence, this value can be taken as the transformation temperature of pure iron within the limit of the cooling rates achieved. In a rigorous sense, however, this temperature should not be interpreted as the M_s temperature of pure iron,† because as mentioned previously, the transformation is not considered to be effected solely by the cooperative movement of atoms, but to some extent by individual movement of atoms as well. This is also the case for alloys containing elements that apparently raise the M_s temperature. Considering these facts, the M_s temperature of pure iron can be obtained by extrapolating M_s temperatures of carbon steels to zero carbon concentration; it turns out to be below 720°C. However, one more thing remains to be considered for pure iron. As described before, the martensitic transformation requires nonchemical energy, especially for the transformation shear distortion. But a relatively low value of nonchemical energy is required for the transformation of an extremely pure iron, because the elastic limit near the transformation

† Gilbert and Owen[8] reported on Fe–(0–15) at. % Ni, Fe–(0–10) at. % Cr, Fe–(0–2.7) at. % Si alloys, stating that with a high cooling rate, such as 5500°C/sec, martensites were not obtained; instead, massive α was always observed.

TABLE 4.4 Effect of carbon impurity on elastic limits of iron[a]

Carbon content (wt %)	Elastic limit (kg/mm^2)	
	20°C	890°C
$<10^{-6}$	3	0.21
10^{-3}	12	1.1

[a] After Kamenetskaya *et al.*[57]

temperature markedly decreases (Table 4.4) when the purity of the iron is increased. This situation thus raises the M_s temperature. Kamenetskaya *et al.*[57] report that the M_s temperature of pure iron increases up to 800°–900°C when the carbon content is decreased below 10^{-6}–10^{-7} wt %.

There are a number of measured values[58–61] of M_s temperatures of carbon steels that are not as low in carbon content as those described so far. A few examples are shown in Fig. 4.6, which reveals that the M_s temperature decreases with increasing carbon content. A similar relation holds for

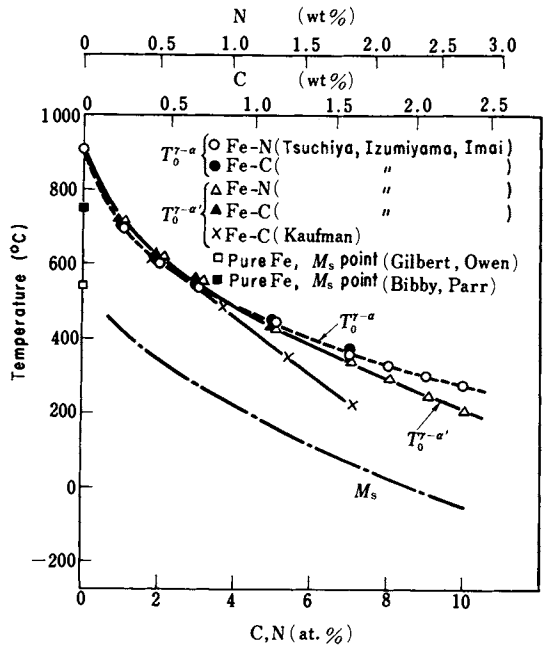

FIG. 4.6 The M_s and T_0 temperatures of carbon steels and nitrogen steels (Imai *et al.*[27]; others[5,6,49]).

nitrogen steels. The experimentally determined M_s versus solute concentration curve for carbon and nitrogen steels runs nearly parallel to and lies lower (by about 200°C) than the curves for T_0 that were obtained from the relation $\Delta F^{\gamma \to \alpha'} = 0$. When the value of $\Delta F^{\gamma \to \alpha'}$ at the M_s temperature is calculated using Eqs. (9) and (10) in Section 4.1, it is found to be about 300 cal/mol, not depending[†] appreciably on carbon concentration. This value corresponds to the total amount[‡] of nonchemical free energies, as described before, and constitutes the driving force for the transformation.

When the martensite of a carbon steel is heated, it decomposes before the reverse transformation takes place. Therefore it is difficult to measure the A_s temperature, but it can be done by rapid heating. According to Gridnev and Trefilov,[62] the A_s temperature was found to be higher than the M_s by 300°–400°C[§] at a heating rate of 600°C/sec. Figure 4.6 also shows that the M_s temperature versus nitrogen content curve experimentally determined almost coincides with that for the Fe–C system, when the concentration is expressed in atomic percent of solute. Other investigators[64] agree with this observation.

4.3.3 M_s and A_s temperatures of iron-base binary substitutional solid solutions

Since the $\gamma \to \alpha$ transformation temperature in Fe–Ni alloys markedly decreases with Ni content, martensite can be more easily obtained with an increase in Ni content. Moreover, at higher Ni contents atomic diffusion is not involved in the reverse transformation on heating; hence, the diffusionless $\alpha \to \gamma$ transformation can be studied. This problem was undertaken by Chevenard[65] in 1914 and it was disclosed that the M_s and A_s temperatures were far apart, that is, the so-called hysteresis phenomenon was marked.

Figure 4.7 shows the observed values[¶] of the M_s and A_s temperatures of Fe–Ni alloys (M_d and A_d temperatures will be explained in Section 5.2.1). In this figure, T_0, which was determined from $\Delta F^{\gamma \to \alpha'} = 0$, is also included.

[†] Regarding the dependence of $\Delta F^{\gamma \to \alpha'}$ on carbon content, it is argued that either it increases with carbon content or it does not change to any remarkable extent, depending on approximations used in the calculation.[20]

[‡] Since an activation energy is necessary for the transformation, strictly speaking, the 300 cal/mol value should be in excess of the total nonchemical free energies.

[§] According to a report,[63] superheating in the reverse transformation does not exceed 50°C even at a heating rate of 2×10^4°C/sec when the carbon content decreases to a low value, as in Armco iron.

[¶] On this topic there are a number of references available. The determinations of these quantities are usually made by thermal analysis, thermal expansion, and electrical resistance measurements. But in some cases[66] the temperature at which surface relief appears on the prepolished surface of a specimen was measured during continuous observation under the optical microscope. There was no difference in the results between conventional methods and this one.

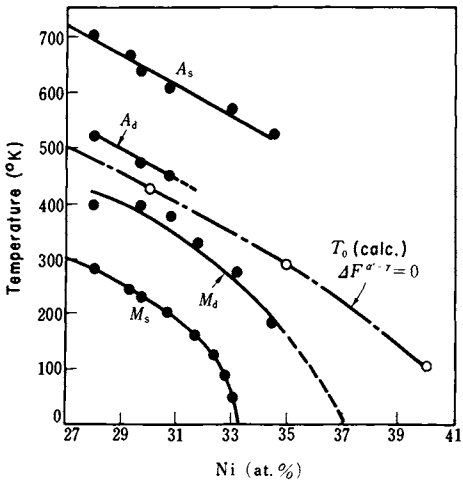

FIG. 4.7 Transformation temperatures of Fe–Ni alloys (with Ni contents higher than 27%). (After Kaufman and Cohen[6].)

From the figure it is seen that $T_0 \fallingdotseq \frac{1}{2}(M_s + A_s)$.† This means that the driving forces of both martensitic transformations, γ to α' and α to γ', are nearly equal. This driving force can be calculated from $\Delta F^{\gamma\to\alpha'}$ at the M_s temperature. A calculation[6] shows that the driving force is 350 cal/mol at 27% Ni; it is greater with more Ni and smaller than this value with less Ni. For low Ni concentrations, ΔF, which was calculated from the experimentally determined transformation temperature by the usual method, cannot be considered the driving force for the martensitic transformation. One reason for this is that for low Ni contents the transformation temperature is high and hence at a cooling rate obtainable by ordinary quenching individual movement of atoms takes part in the transformation; that is, the so-called massive transformation occurs. Another reason is that, as described before, ordinary iron-base binary substitutional alloys usually contain impurities,‡ such as C and N, which greatly influence the transformation characteristics of steels, and therefore they cannot be considered genuine binary alloys.

Considering this point, Izumiyama *et al.*[51] measured the transformation temperature of high-purity (less than 0.002% for each of C and N) Fe–Ni alloys using the same rapid cooling method as that employed for Fe–C alloys.

† The two boundary lines $\alpha/\alpha+\gamma$ and $\gamma/\alpha+\gamma$ in the equilibrium phase diagram lie below and above the T_0 curve and show a concentration dependence tendency similar to the two curves for M_s and A_s. However, the two boundary curves are essentially different in nature from the M_s and A_s curves.

‡ This factor has particularly great influence on the transformation characteristics of Fe-base substitutional alloys containing carbide- or nitride-forming elements. Even without such elements, for example, in Fe–(0.1–0.5)% Co alloys containing only 0.009% C, an anomalous phenomenon has been observed[67] that seems attributable to the presence of C atoms.

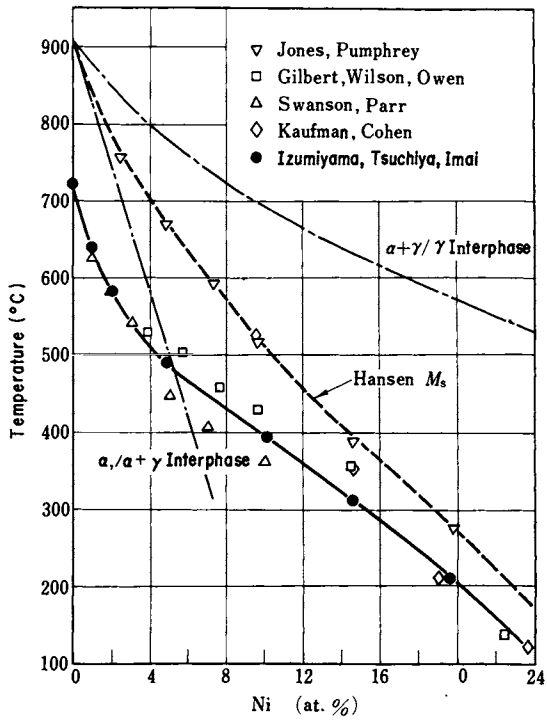

FIG. 4.8 Transformation temperatures of Fe–Ni alloys (with Ni contents lower than 24%). (After Izumiyama *et al.*[51])

The data are included in Fig. 4.8 and are seen to agree with the lower values among the transformation temperatures in the literature,[68–70] which are also included in the figure. As in the Fe–C alloys, the M_s temperature curve (solid line) rises steeply with decreasing Ni content below 1% toward the transformation temperature 720°C of pure iron. This behavior may be largely due to the effect of individual movement of atoms, as previously described for Fe–C alloys.

Izumiyama *et al.*,[71] using a similar method, made measurements on other Fe-base binary alloys. Figure 4.9 shows the results. The transformation start temperature, which was attained by extrapolating the curves of Fig. 4.9 to pure iron, is found to be 720°C, in agreement with the cases of Fe–C and Fe–Ni alloys. Some of the curves do not seem to agree with the previously reported data[72–77] on binary alloys. This disagreement is probably due to impurities contained in those alloys. From the curves in Fig. 4.9 it is seen that the alloying element that lowers T_0 generally decreases the M_s temperature. In such cases the A_s also decreases. It is thought that in alloys with high M_s temperatures the individual movement of atoms must have affected

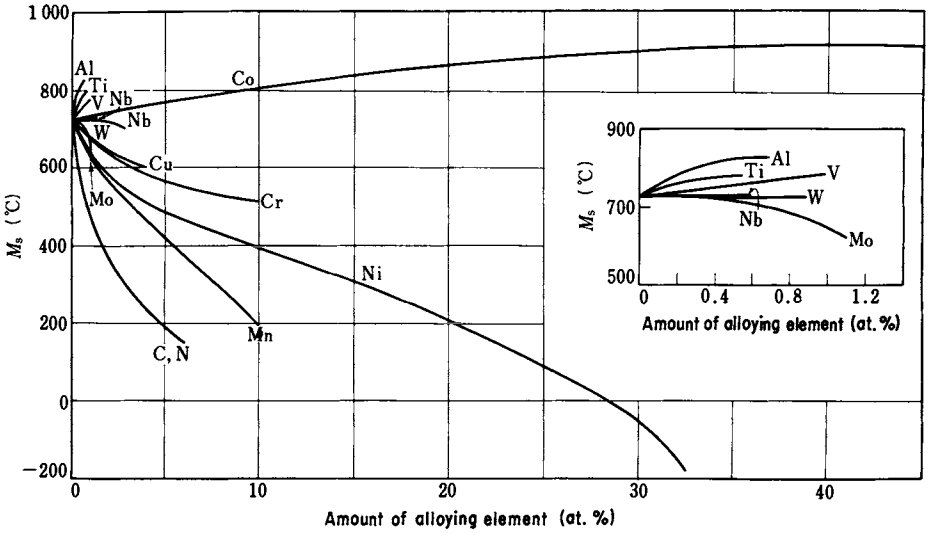

FIG. 4.9 M_s temperatures of Fe-base binary alloys. (After Izumiyama *et al.*[71])

the transformation. Such an argument is supported by the experimental fact that in alloys with high M_s temperatures the surface relief effects due to martensitic transformation are so weak that the effects are difficult to discern.

The effect of hydrogen on the M_s temperature in steels is not uniformly established.[78,79] In some cases it raises M_s by 50°C and in other cases it has no effect.

4.3.4 M_s temperatures of ternary iron-base alloys

In estimating the effect of alloying elements on the M_s temperature in alloys of more than three elements,[78–85] the effects of C and N are additive relative to each other, but the effects of C or N are not additive with those of other substitutional elements. The effects of substitutional elements can be mutually additive except for a few cases.[86] For example, with additions of third elements to Fe–Ni alloys the M_s and A_s temperatures vary as shown in Table 4.5.

The data concerning Fe–Cr–Ni alloys are also given in Fig. 2.41. There is a report[87] that for 18–8 stainless steel the Ni equivalents of the fourth elements are Si, 0.45; Mn, 0.55; Cr, 0.08; C, 27; and N, 27. In the $\gamma \rightarrow \varepsilon$ transformation in these alloys the fourth elements that raise the stacking fault energy (e.g., C) decrease the transformation temperature, whereas those that lower the stacking fault energy (e.g., Si) raise the transformation temperature.[88] Addition of Co to an Fe–13% Cr alloy prolongs the incubation period and decreases the fraction transformed.[89]

TABLE 4.5 Effect of third elements on the transformation temperatures of Fe–Ni alloys[a]

Mother alloy Fe–Ni(%)	Ti M_s A_s	V M_s A_s	Nb M_s A_s	Cr M_s A_s	Mo M_s A_s	W M_s A_s	Mn M_s A_s	Co M_s A_s	Ni M_s A_s	Cu M_s A_s	Al M_s A_s	Si M_s A_s	Reference
22.5%	↷	↷	↷	↓ ↓				↑ ↑	↓ ↓		—	↷	82
27–30%			↷	↓	↓	↓	↓				—	↓	83
18, 30%		↑ ↓		↓ ↓	↑ ↓		↓ ↓	↑ ↑		↓ ↓	↓ ↓	↓ ↑	84

[a] Key: ↓ fall; ↑ rise; ↷ rise and then fall; — no change.

In Fe–Mn–C alloys with more than 10% Mn, ε martensite forms and its M_s temperature decreases with increasing Mn as well as with an increase in C.[90]

4.3.5 M_s temperatures of other alloys

As previously described, the transformation start temperature of pure Ti depends on the cooling rate (below 10^4°C/sec). However, its alloys, like Fe alloys, have fixed M_s temperatures. The M_s temperatures of various Ti alloys are shown in Fig. 4.10,[39,91,92] from which it is seen that the M_s temperature usually decreases with increased alloying element concentration, except for high concentrations of added Al, Sn, Ag, or Pt. The trend is related to that in the T_0 versus composition relation. The larger the difference in radii between solvent and solute atoms, the more markedly the M_s temperature is lowered.[80] This is also observed on T_0. The driving force, which is denoted by $T_0 - M_s$, is necessary for the transformation to overcome the nonchemical energies. Hence, $T_0 - M_s$ should not depend strongly on the amount of an alloying element and this is actually the case. For Co–(0–30)% Ni alloys the difference between M_s and A_s temperatures is only about 20°C.[93]

It is generally true that the M_s temperature decreases upon ordering of the arrangement of solute atoms. For example,[94] when quenched from a disordered state at 1000°C to room temperature, the alloy Fe_3Pt partly undergoes a martensitic transformation, but it does not transform at all upon quenching to room temperature after annealing at 650°C for about 30 min to induce ordering, for in this case the M_s temperature is −50°C.

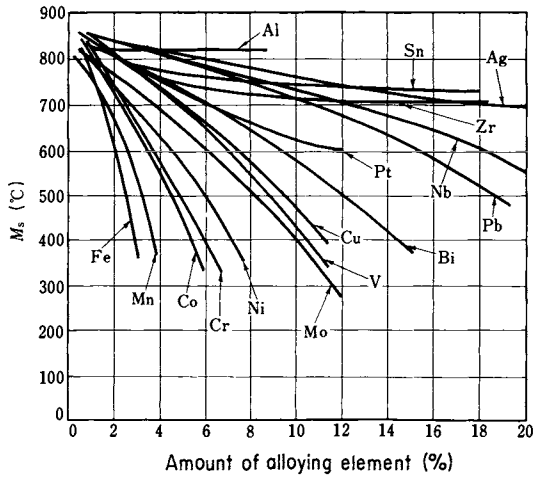

FIG. 4.10 M_s temperatures of Ti-base binary alloys.[39,91,92]

In Li–Mg alloys, the M_s temperature has a maximum at about 15 at.% Mg.[95] The M_s temperature of β brass decreases by 7.4°C with every 1% increase in Zn content.[96,97] Addition of Al also lowers the M_s temperature. But if the Zn content is adjusted so as to keep the electron:atom ratio constant, the M_s temperature rises[98] with increasing Al content. Gallium addition raises the M_s temperature, but indium addition lowers it.

The β phase in Ag–Zn alloys containing less than 39.5 at.% Zn undergoes a martensitic transformation and the decrease in M_s with increasing Zn concentration is 80°C/at.% Zn.[99]

The effect of a third element on the M_s temperature has also been studied in Au–50.0 at.% Cd,[100] Au–47.5 at.% Cd,[101] and TiNi.[102]

4.4 Transformation velocity

The rate of a martensitic transformation consists of the probability of formation of a martensite nucleus and the rate of growth. The rate of growth can be classified roughly into three modes. The fastest mode is of the order of the velocity of formation of mechanical twins, as in the umklapp transformation (Section 2.2.5) in iron-base alloys. The second fastest one is of the order of the velocity of slip deformation, as in the schiebung transformation. The slowest mode is represented by In–Tl alloys, in which the transformation occurs only where heat is removed, since the degree of supercooling is small. In the following we present the observed facts pertaining to these three typical modes.

4.4.1 Umklapp transformation velocity

In 1932, Wiester[103] tried to measure the rate of growth of α' martensite crystals of a 1.65% C steel using an optical microscope. Since the M_s temperature of this steel is below 100°C, the specimen was first quenched from a temperature in the γ phase region in a metal bath kept at 100°C. The specimen was polished and etched at this temperature and it was confirmed that all the γ phase was retained. The specimen was further cooled to room temperature or liquid air temperature. During cooling, motion pictures with 20 frames/sec were taken of the microstructure of surface relief occurring due to the transformation. It was found from this experiment that the growth process of a single α' plate did not extend over several frames, but reached its completion within the time of single frame and that the number of α' plates increased successively with time. It was concluded then that the time for formation of a single α' plate is less than 1/20 sec.

In 1957, Honma[104] took motion pictures with 64 frames/sec, using an Fe–31% Ni alloy having γ crystals about 10 mm in diameter; these were

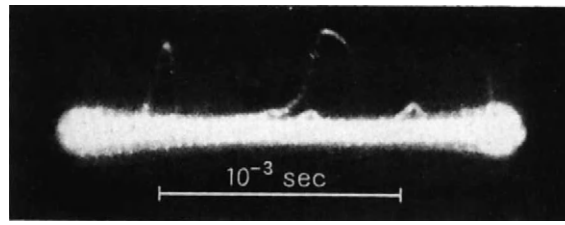

FIG. 4.11 Magnetic pulses during martensitic transformation. (Fe–20% Ni–2% Cr–0.6% C, –127.5°C). (After Okamura *et al.*[107])

100 times larger than those used in Wiester's experiment. However, his result was that groups of α' plates formed as a burst within the time of a single frame. From his observation, the time for formation of a burst was estimated to be less than 1/250 sec.

As another phenomenon, audible clicks are often heard in martensitic transformations on subzero quenching of the retained γ phase in quenched steels. In 1936, Förster and Scheil[105] recorded these audible clicks on an electromagnetic oscillograph using an Fe–29% Ni alloy. The vibrations lasted less than 2×10^{-3} sec. At the same time, the researchers observed a local temperature rise in the specimen.

The same investigators in 1940[106] recorded the change in electrical resistance on a cardiograph† during the transformation in the same alloy and obtained a pulse signal lasting about 8×10^{-5} sec.‡ This value is for the umklapp transformation occurring below room temperature. Above room temperature a reaction of slower velocity was observed. This corresponds to the schiebung transformation.

In 1942 Okamura *et al.*[107] studied a change in the intensity of magnetization during transformation of the paramagnetic γ phase to the ferromagnetic α' phase. Their method was to record the magnetization intensity on a Brown tube oscillograph using the technique of measuring the Barkhausen effect§ during cooling of a Ni steel specimen¶ in a magnetic field of 550 Oe. Figure 4.11 shows an example of oscillograph signals obtained in this experiment. It can be seen in this figure that the α' plates are formed intermittently, as expected. The duration of a single pulse was about $(1-36) \times 10^{-4}$ sec. The volume of α' crystallites corresponding to the magnetic change is estimated to be 3.4×10^{-6} cm^3, which is equivalent to a total volume of about 100 α' plates of the size observed. The foregoing observations suggest

† The frequency response of the equipment was 30 kHz.

‡ Such a pulse time value has also been observed in deformation twinning in Bi.

§ When a ferromagnetic substance is magnetized by progressively increasing the magnetic field, the intensity of magnetization increases discontinuously in the early stages, when the magnetic field is weak. This effect is called the Barkhausen effect.

¶ $M_s = -130$°C.

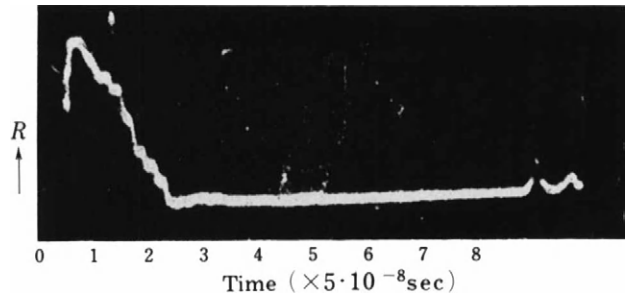

FIG. 4.12 Electrical resistance pulse during martensitic transformation (Fe–29.5% Ni). (After Bunshah and Mehl,[108] with permission of the American Institute of Mining, Metallurgical and Petroleum Engineers, Inc.)

the existence of an autocatalytic phenomenon. Thus it was theorized then that the time for formation of a single α' plate might be less than 10^{-6} sec.

Later, in 1953, Bunshah and Mehl[108] reinvestigated this process by the use of electrical resistance measurements, like Förster and Scheil.[105] They used an improved equipment in which the values of frequency response of the amplifiers were 40 kHz to 80 MHz and 100 kHz to 200 MHz, and that of the oscilloscope was 200 Hz to 75 MHz. An Fe–29.5% Ni alloy† was chosen as the specimen, because the electrical resistance decreases by about 50% upon martensitic transformation in this alloy and thus the $\gamma \rightarrow \alpha'$ transformation can be detected very clearly.

It is seen, from the observation of the pulse as shown in Fig. 4.12, that the electrical resistance of the sample first increases slightly to a maximum and then decreases greatly to a value lower than the initial value. Aside from the small initial increase in resistance, the subsequent large decrease seems to correspond to the growth of martensite crystals. The duration of a pulse was found to depend on the size of the martensite crystal formed and to vary from 0.5×10^{-7} to 5.0×10^{-7} sec.‡

To investigate the nature of a single pulse, the martensitic transformation in a large-grained γ phase sample was allowed to occur so as to form only a very small amount of α' martensite crystals. Since the number of pulses was found to correspond roughly to the number of α' crystals formed in the sample, it was thus supposed that each pulse corresponds to formation of a single martensite crystal. The duration of a pulse observed in the initial stage of the transformation was found to be approximately proportional to the width of the α' plate. Therefore, assuming that the martensite plate

† Impurity content 0.027% C, 0.135% Mn, and 0.094% Si.

‡ These signals correspond to a frequency of 10 MHz, which is well within the frequency response of the apparatus (75 MHz), thus these values are reliable and the errors involved are ±5%.

grows in the width direction, the velocity of propagation of the transformation front was estimated to be 1100 m/sec, which is about one third the velocity of sound propagating in metals. This result suggests that the propagation of the transformation is very similar to the propagation of shock waves in metals.

This velocity of propagation of martensite was found to be constant within $\pm 20\%$, whether the transformation temperature was $-20°C$ or $-195°C$. This result is very important for the following reasons. If atoms were activated individually, the rate of transformation should be proportional to $\exp(-Q/RT)$ according to the Arrhenius law, as will be described later. However, the observed results have shown that the transformation rate does not depend appreciably† on the transformation temperature. Thus, the mechanism of transformation should be such that the structure of martensite is not formed by activation of individual atoms, but by the cooperative movement of atoms.

Even in so-called isothermal martensite formed during holding at a fixed temperature, the time for formation of a martensite crystal was approximately 0.1 μsec, which is similar to the case of athermal transformation. The prolonged pulse signals appear when the burst-type transformation, consisting of simultaneous and autocatalytic formation of a large number of α' crystals, occurs.

Following the research of Bunshah and Mehl,[108] Lähteenkorva[110] carried out similar research on an Fe–20% Ni–0.5% C alloy, Ti, and Zr. The observed duration of a pulse in the Fe–Ni–C alloy is 0.4–8 μsec, which corresponds to one burst, and the 0.1 to 2-μsec pulses observed in Ti or Zr correspond to the formation of large martensite plates.

Beisswenger and Scheil[111] continued their earlier research by improving their apparatus and obtained results agreeing with those of Bunshah and Mehl. They also investigated the causes of the initial increase in electrical resistance appearing in the pulse, which had not been interpreted by Bunshah and Mehl, and showed that this anomaly appeared when the specimen had been deformed plastically before testing; it disappeared, or sometimes the electrical resistance decreased from the initial value, when the specimen was carefully treated to avoid deformation. It was also shown that the electrical resistance increased when α' plates formed perpendicular to the specimen axis, and decreased for α' plates parallel to the axis.

After Scheil's death, Kimmich and Wachtel,[112] following Scheil's suggestion, continued their investigation by adding a new experimental technique, the external application of a magnetic field, and reported their results as

† In 18–8 stainless steel, 1% C steel, and Fe–20% Ni alloys Kulin and Cohen[109] observed that martensitic transformations had occurred even at very low temperatures (near 0°K). If the atoms had been activated one by one, such a reaction would never have occurred.

follows: The reason for the existence of maxima and minima in the pulse was the voltage change induced by magnetization of the specimen by formation of martensite plates; thus only the decreasing portion of the pulse corresponds to a true decrease in resistance due to the formation of martensite.

Recently, Suzuki and Saito[113] magnetically measured the transformation velocity in an Fe–31% Ni alloy by using an apparatus that has a far quicker response than those used in earlier research. They reported that a single martensite crystal forms in 0.5×10^{-7} sec and the propagation velocity is 8×10^4 cm/sec. Further, they made measurements for the case of isothermal martensite and found that the formation velocity of a single martensite crystal is as fast as the values they obtained for the athermal case. This finding indicates that in the case of isothermal martensites in an iron-base alloy the nucleation itself is isothermal, but the growth does not seem isothermal.[114]

4.4.2 Schiebung transformation velocity

Fe–Ni Alloys

In Fe–Ni alloys, if the M_s temperature is above room temperature, the martensite is not lenticular in shape, but has a morphology like a bundle of slip bands. Thus, the transformation is called the schiebung transformation, as already noted in Chapter 2. The rate of transformation in this case is not so fast that the change in microstructure with time during the transformation can be followed under a microscope. Takeuchi *et al.*[115] studied this by taking motion pictures (16–24 frames/sec) during the transformation in Fe–(20–29)% Ni alloys and obtained the following results:

(i) First, a faulted region like a slip band occurs at a certain place and grows straight until its growth is stopped at such obstacles as grain boundaries. This faulted region grows parallel to the $(111)_\gamma$ plane in alloys with Ni contents less than 27%. In alloys with Ni contents near or above 29%, however, martensite plates are produced deviating from the $(111)_\gamma$ plane initially and then growing along the $(111)_\gamma$ plane only in the later stage.

(ii) The relation between the length of a single faulted line and the time of growth is parabolic and the velocity of progress of the transformation front v at time t is expressed as

$$v = at$$

where a is a constant depending on the cooling rate.

(iii) By decreasing the cooling rate to suppress the generation of martensite nuclei to some extent, the transformation can be made to occur at different temperatures even in an alloy with the same Ni concentration. In this case the relationship between the velocity v and the transformation

temperature T is approximately

$$v = b(T_1 - T)$$

where b is a constant and T_1 is a constant temperature. This equation means that v is proportional to the degree of supercooling. The previous result (item ii) can be interpreted in such a way that the increase in degree of supercooling is proportional to the time elapsed, since the specimen is cooled at a constant rate.

(iv) When transformation occurs at a temperature very close to T_1, the rate of growth is very small. Since at that temperature the probability of nucleation of martensite is extremely small, the transformation does not take place at all, even after the specimen is held for a few hours. For example, it took 27 sec for a martensite crystal to grow 0.5 mm in length.

About 14 years after the research of Takeuchi *et al.*,[115] Yeo[116] carried out similar research after confirming that in Fe–Ni alloys isothermal martensite forms more easily with decreasing carbon content. By taking motion pictures, he observed the isothermal transformation to martensite in an Fe–28.8% Ni–0.008% C alloy held at 27°C. According to his results, the radial growth rate of individual martensite plates is 0.11 mm/sec, which is slower by a factor of about 10^{-7} than that measured by Bunshah and Mehl.[108] This slow rate of growth is about the same as for the schiebung transformation.

The foregoing results were obtained from observation of martensite crystals formed on the surface of the specimen; thus it must be borne in mind that the features should be somewhat different inside the specimen. There are other investigations[117–120] on the rate of martensite transformation at the surface. According to them, martensites grow gradually, when held at a constant temperature, in response to so small a strain as that induced by a needle scratch. According to investigations using an Fe–30.2% Ni–0.04% C alloy,[119,120] the rate of lengthwise growth of an α' crystal at room temperature lies in the 0.001–100 mm/sec range; in the sidewise direction, on the other hand, growth proceeds sluggishly, although it continues for a few weeks.

These observations, however, merely indicate that the transformation front grows continuously within the resolution limits of optical microscopy. It is questionable whether the transformation front moves continuously on the electron microscopic scale.

Co–Ni alloys

In the f.c.c. to h.c.p. transformation in cobalt and Co–Ni alloys the amount of transformation shear is relatively large, that is, 0.34. However, since this shear is relieved by the formation of variant crystals and stacking faults

(Section 2.5.1), the difference between M_s and A_s is only about 20°C. Moreover, the temperature dependences of the free energies of both phases are almost similar to each other. Therefore, the free energy difference accompanying the transformation is only 3 cal/mol. This is about one one-hundredth that accompanying the $\gamma \rightarrow \alpha'$ transformation in Fe–base alloys.

As mentioned earlier, the transformation velocity is low when the degree of supercooling is small. According to the microstructure studies by Takeuchi and Honma,[121] using Co–(0.35–30.24)% Ni alloys, the transformation is similar to the schiebung transformation in Fe–Ni alloys and the velocity in the edgewise direction of a martensite crystal is 1–100 mm/sec, which is less than one ten-thousandth that for the umklapp transformation in steels. According to the hot stage microscope study by Bibring *et al.*,[93] the rate of growth of a martensite crystal varies over a wide range. At slower rates of growth it takes several tens of seconds to complete the growth in some cases and less than 0.0001 sec in other cases, whereas at the fastest rates audible clicks occur, as in the umklapp transformation. They[122] also used a technique to record on an oscilloscope the amplified piezoelectricity caused by the martensitic transformation.

4.4.3 Transformation velocity with small degree of supercooling

In martensitic transformations in which the transformation deformation is small, the nonchemical energy required is small. Thus, the transformation can start almost without supercooling. Therefore, the transformation takes place as long as the specimen is cooled and it stops when cooling is stopped. For this reason, the transformation rate appears to be proportional to the cooling rate. Although this tendency has been seen for the schiebung transformation in the Fe–Ni alloys mentioned earlier, the most typical example has been found in In–Tl alloys. In these alloys, the velocity of transformation is slow, as was mentioned in Section 2.6.1. The velocity of propagation of the transformation front is proportional to cooling rate and amounts to 0.5 mm/sec[123] when the cooling rate is 20°C/sec.

4.5 The martensite nucleus and isothermal martensite

4.5.1 The martensite nucleus[124]

It is well known that crystallization from a supercooled liquid is controlled by nucleation and that the presence of a favorable nucleation site greatly enhances the reaction. In martensitic transformations, which are solid-state reactions as well as diffusionless reactions, the generation of embryos will be more difficult. Therefore, martensitic nucleation does not generally occur

randomly. For example, it has long been known that in β brass[125] some of the martensite crystals always form at identical positions in repeated heating and cooling transformation cycles, and this is a kind of memory effect. Furthermore, the number of martensite crystals decreases with increasing homogenization treatment. There is even a case in which only one martensite crystal forms from one parent phase crystal when transformed after homogenizing at a high temperature. In such a case the lattice deformation for transformation is very small, as in the Au–47.5 at.% Cd alloy.[126] From these facts it is supposed that there are preferred sites for nucleation and that the lattice defects may provide those sites.[127]

Metastable atomic arrangements suitable for martensitic transformation may exist in some lattice defects. These metastable arrangements may be transformed into stable martensite by thermal vibrations, elastic waves, or other fluctuations, and the transformation may proceed by the propagation of strain waves. The lattice must pass through an activated state in the process to convert the atoms at metastable sites into stable sites of the new phase, and the activation is achieved by thermal vibrations or by applied stresses. This is the so-called activation energy for nucleation. If such strain embryos[128–135] are assumed, there is no need to assume the critical size for the martensite nuclei, as in the classical theory.

The probability of nucleation in martensitic transformation has long been studied, since it influences the transformation susceptibility, which is one of the basic factors for the hardenability of steels. However, it is very difficult to grasp the details of nucleation itself and thus the theories on nucleation probability do not seem based on well-established observations. Therefore, a detailed description will not be given here.

4.5.2 Isothermal martensite and its growth

In many of the martensitic transformations discussed so far, the reactions start at the M_s temperature and proceed while the temperature is falling. When the cooling is stopped, the reactions stop, and when the cooling is resumed, they start again. The reactions proceed only while the temperature is changing. Therefore, martensite produced by this type of reaction is referred to as *athermal martensite.* Most of the martensites in steels belong to this category.

In some cases, however, martensites form isothermally above or below the M_s temperature. This type of martensite is referred to as *isothermal martensite.* Although occurrence of this type of martensite has long been known,[136,137] at one time it was treated as just a "tailing-off effect" that generally appears at the beginning and final stages of athermal transformations. Kurdjumov *et al.* treated it as a separate phenomenon. They first observed isothermal

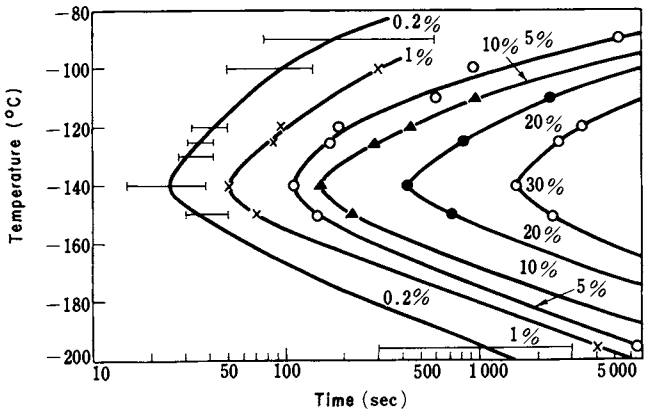

FIG. 4.13 C curves for isothermal transformation to martensite in an Fe–23.2% Ni–3.62% Mn–0.016% C alloy. (After Shih *et al.*[154])

martensite transformation in Fe–6.0% Mn–2% Cu–0.6% C[138] and Fe–23% Ni–3.4% Mn[139,140] alloys and subsequently in an Fe–2.3% Mn–0.8% C[140] alloy. Thereafter, this phenomenon attracted much attention and many investigations have been made.[129,141–154]

In a *TTT* (transformation–temperature–time) diagram (Fig. 4.13), which represents the amount of isothermal martensite in relation to holding time and temperature, the C curves characteristic of isothermal transformation represent stages from the beginning to the end of the transformation. Therefore, this isothermal transformation cannot be attributed to a tailing-off effect of the athermal martensitic transformation. It seems more logical to treat the isothermal transformation as a normal one and the athermal one as special, because it is the athermal transformation that has singularities affected by other factors. For example, in stress-sensitive alloys once a few martensite crystals have happened to form initially, the transformation instantly proceeds to the fullest extent possible at that particular temperature (in some cases in an autocatalytic manner) with help of transformation-induced stress. Thus the time-dependent change is hardly detected.†

We shall now proceed to a quantitative description of martensite nucleation. The driving force for nucleation is considered to be the difference in chemical free energy between the parent phase and the martensite. Therefore, the amount of transformation product f in the early periods of the

† According to the work by Philibert and Crussard[155] on an Fe–2.5% Cr–1.4% C alloy, martensites formed athermally during cooling to a certain temperature by a conventional cooling method and further transformation occurred isothermally during holding at this temperature. But with appropriate treatment, only the isothermal transformation occurred. This seems to imply that the normal transformation is the isothermal rather than the athermal one.

transformation is considered to be proportional to the degree of supercooling. That is,

$$f = \alpha(M_s - T_q) \tag{1}$$

where T_q is the temperature of the medium in which the specimen is quenched and α is a proportionality constant. This equation was found to hold experimentally to some extent.[156] For carbon steels α is 0.011 when f is expressed as the volume fraction and the temperature in degrees Celsius.[157,158] The value of α changes, depending largely on the difference in entropy of the two phases, as well as on the composition of the alloy, the crystallography of the martensite habit, and the cooling rate.[159]

The constant α represents the factors (except the degree of supercooling) that influence the nucleation probability. In examining these, we see that the rate of nucleation may be expressed as

$$\dot{N} = A \exp(-\Delta W/RT) \tag{2}$$

where $\dot{N}$ is the number of nuclei formed per unit volume per unit time, ΔW the activation energy for nucleation, and A the frequency factor for nucleation. Both ΔW and A are considered to be temperature dependent and will be discussed in the following paragraphs.

In general, the observation of nucleation phenomena is complicated, since we do not actually observe nucleation independent of accompanying growth. Particularly in athermal martensitic transformations one can observe only the combined effect of nucleation and growth. Therefore, an example of isothermal transformation will be given, since it is easier to treat nucleation phenomena in this case.

Shih *et al.*[154] measured the amount of transformation product by electrical resistivity change for three kinds of Mn steels, of which the Fe–23.2% Ni–3.62% Mn–0.016% C alloy is most convenient for our present purpose, since it has an M_s temperature below -196°C and athermal martensites do not form above this temperature. The specimen was water quenched from 1100°C, held for 1 hr at 650°C in order to anneal out the quenching strain, and then cooled to liquid nitrogen temperature. At this stage, martensite had not yet appeared. Subsequently the specimen was heated to a temperature between -196° and -90°C to allow isothermal transformation. As a result Shih *et al.* obtained the C curves illustrated in Fig. 4.13. The left-most curve represents the 0.2% transformation. Since the accuracy is 0.2%, this curve is meant to express the times for detectable transformation products to appear. If τ_i (in seconds) is the period prior to this curve (i.e., the induction period) and v the volume of an α' crystal (see the second footnote on p. 288, then the following equation will hold.

$$0.002 = \dot{N} v \tau_i. \tag{3}$$

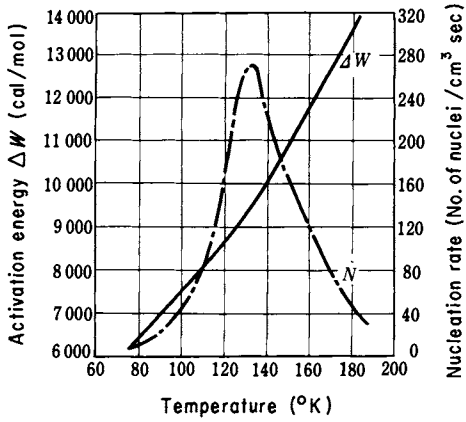

FIG. 4.14 Initial rate of isothermal nucleation and the activation energy of nucleation in an Fe–23.2% Ni–3.62% Mn alloy. (After Cech and Hollomon.[145])

The metallographic observation gave 1.6×10^{-2} and 8×10^{-4} cm, respectively, for the radius r and the thickness δ of an α' martensite plate. The volume $v = \pi r^2 \delta$ is computed to be 0.6×10^{-6} cm^3.† Substituting this value into Eq. (3) and using the τ_i obtained from the 0.2% curve in Fig. 4.13, we obtain values for $\dot{N}$. The result is shown in Fig. 4.14, where a peak appears at -130°C.‡

The frequency factor A in Eq. (2) is expressed by $A = n_i \nu$, where ν is the lattice vibration frequency, which is estimated to be of the order of 10^{13} sec^{-1}, and n_i is the total number of nucleation sites. If we assume that one nucleus forms in each grain, and the number of grains in a unit volume is 10^5/cm^3, then $A = 10^{18}$. Substituting the values for A and $\dot{N}$ in Eq. (2), we obtain ΔW as a function of the temperature T. ΔW increases with increasing temperature and is about 9.5 kcal/mol§ at -130°C where $\dot{N}$ is maximum. This value is very small compared to the activation energy for self-diffusion of Fe atoms, 60 kcal/mol. The curves in Figs. 4.13 and 4.14 are similar to those for diffusional transformations when compared only in shape. This similarity seems to come from the present situation, namely, that only nucleation is involved, and different curves are expected for phenomena involving the growth process.

† The size of an α' crystal is influenced by the size of the γ grains and accordingly by the austenitizing temperature. Thus $\dot{N}$ is also influenced. This effect will be discussed in Section 5.3.5.

‡ Isothermal martensite form also in high-speed steels by subzero cooling after quenching. Preaging treatment at room temperature lowers the temperature for the maximum transformation rate. The longer the aging period, the lower this temperature is and the smaller the amount of transformation product.

§ Kurdjumov and Maksimova[139] have obtained, for an Fe–23% Ni–3.4% Mn alloy, an activation energy of nucleation of 0.6 kcal/mol and work for nucleation at -50°C of 1.4 kcal/mol.

In the calculation of the activation energy ΔW, the classical nucleation theory[160] assumes that embryos are transformation products already grown to a certain size. In this theory, the shape of the embryos is assumed to be such that the sum of the difference in the chemical free energies between the parent phase and the nucleus, the energy of the interface with the parent phase, and the strain energy of the nucleus is minimal. An embryo can become a nucleus when it grows to a critical size, and thus the activation energy ΔW for the process has been estimated. Since martensitic transformations, however, do not seem to take place in such an equilibrium fashion, the classical approach† does not seem appropriate without any correction.

Knapp and Dehlinger[31] and Cohen[132] developed a theory by regarding the martensite embryo as a small crystallite with dislocation loops in the interface on the basis of Frank's model (described in Chapter 6) and taking into consideration the free energy balance of the embryo. Later, Raghavan and Cohen[133–135] further developed this type of calculation. Although these calculations are more refined than the classical theory, they are still based on the classical equilibrium concept and still seem unsatisfactory. This type of theory will not be commented on further.

Even in the case of isothermal transformation, one cannot entirely reject the possibility that autocatalytic nucleation takes part in the transformation. Pati and Cohen,[162] using an Fe–24% Ni–3% Mn alloy, determined the amounts of isothermal martensite from the electrical resistivity measurements, and determined the mean volume per martensite plate as a function of percentage transformation at various temperatures by quantitative metallography. These results were analyzed in terms of autocatalytic nucleation. Utilizing the results of the mean volume per martensite plate, they found that the number of embryos generated per unit volume of martensite formed is approximately constant at 10^{10} per cubic centimeter over the entire temperature range from $-80°$ to $-196°C$. They also found that the activation energies of the overall isothermal reaction are of the order of 10 kcal/mol and decrease with decreasing temperature.

4.5.3 Condition for formation of f.c.c.-to-b.c.c. isothermal martensite and its morphology

Whether a martensitic transformation is isothermal or athermal depends primarily on the chemical composition of the material. It is usual, however, for both isothermal and athermal transformations to take place even in the same alloy; only the temperatures for these two types of transformations to occur and the amounts of transformation product differ, depending on the chemical composition. Imai and Izumiyama[148] investigated the effect of

† There is an experimental work[161] to attempt to prove this theory.

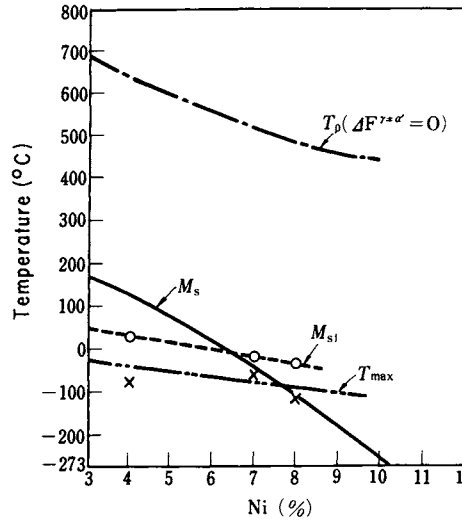

FIG. 4.15 T_0, M_s, M_{si}, and T_{max} of Fe (17–18)% Cr–Ni alloy with varying Ni content. (After Imai and Izumiyama.[148])

chemical composition. Figure 4.15 shows the effect of Ni content on the highest temperature for the isothermal martensitic transformation to occur M_{si}, and on the nose temperature T_{max} of the C curves, for Fe–Cr–Ni alloys with the Cr content kept approximately constant at 17%–18%.† Compared to the M_s temperatures, which are also included in the figure, the decrease in M_{si} and T_{max} with increasing Ni content are gradual; these two curves cross the M_s curve at about 7% Ni. Thus it can be said that in the lower Ni range athermal martensite tends to form first and in the higher Ni range isothermal martensite tends to form earlier. The same parallelism holds for the driving force versus Ni content plot (Fig. 4.16). The situation is about the same for Fe–Cr–Mn steels.[148]

Whether isothermal or athermal martensite forms in the same alloy depends on preheat treatment. For example,[163] it was observed that an Fe–27% Ni (C < 0.01%) alloy annealed at a high temperature (1100°) for a long time (24 hr) forms athermal martensite whose M_s is −30°C, whereas the same alloy, when brought back to the γ state by heating for 2 hr at 500°C after it had been plastically deformed in the α state, undergoes isothermal transformation to martensite and has an M_s of −5°C. This difference is considered to be due to the change in the austenite grain size.

It is reported[164] that when the impurities (carbon and nitrogen) that stabilize austenite are removed, isothermal transformation to martensite

† In Fe–Cr–Ni alloys, with increasing Cr and decreasing Ni, the amount of isothermal martensite increases.[149] In Fe–Mn–C steels, the greater the Mn and C contents, the more isothermal martensite tends to form.[152]

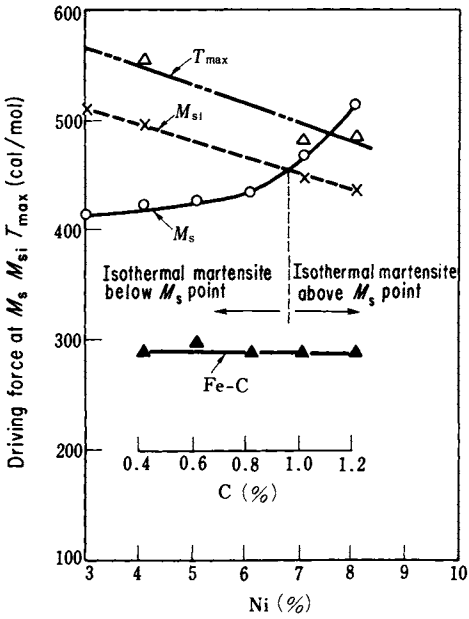

FIG. 4.16 Driving force for the transformation of Fe–(17–18)% Cr–Ni alloy with varying Ni content. (After Imai and Izumiyama.[148])

occurs more easily. In general, the formation of isothermal martensite is markedly affected by the conditions of formation.[165]

The isothermal and athermal martensites that appear in the same alloy differ in morphology. According to the investigation of an Fe–21.3% Ni–5.2% Mo alloy by Georgiyeva *et al.*,[166] the M_s temperature for athermal martensite is $-185°C$, the temperature range for isothermal transformation is from $-50°$ to $-150°C$, and the temperature for maximum transformation rate is closer to T_0 than M_s. The occurrence of isothermal martensite depends largely on surface conditions and does not appear in a mechanically polished specimen. Plates of either martensite have midribs and contain many internal $\{112\}\langle 111\rangle$ twins but the plate thickness is larger in the isothermal martensite. The habit plane in an athermal martensite plate is parallel to its midrib but not that in an isothermal one. Later, by replacing the Mo in this alloy with Mn, Georgiyeva *et al.*[167] obtained a similar result for Fe–24% Ni–3% Mn. An interesting feature of the microstructure is that many parallel platelike crystals of isothermal martensite are aligned in a characteristic row making an angle with the plates. The direction of the row is analyzed and found to lie on the $(259)_\gamma$ plane, which coincides with the plane of the midrib of an athermal martensite. The habit plane of each martensitic plate is found to be $(0.745, 0.490, 0.449)_\gamma$, which makes an angle with the $(259)_\gamma$ plane. The internal twin thickness ranges from 100 to 1000 Å for isothermal martensite, being thicker than 60 Å for the athermal twins. The

ratio of twin thickness to intertwin spacing is above unity for isothermal martensite and about 0.6 or larger for athermal martensite. The dislocation density is smaller than that for the athermal case and diminishes toward the periphery of the martensite plate. This is probably because dislocations generated by the accommodation shear of the transformation move easily and only a few are retained, since the formation of isothermal martensites occurs gradually.

Recently,[168] Georgiyeva and Maksimova studied isothermal martensite in 35 nickel steels of varying compositions in the range (12–35)% Ni–(0.02–1.00)% C. According to them, the relation between M_s temperature and composition is as shown in Fig. 4.16A. In this figure the alloys studied can be divided into groups I, II, and III, each with its own peculiar kinetics. Alloys of group I have the capacity for isothermal formation of martensite, particularly at temperatures near M_s. The martensite crystals have irregular, broken boundaries, giving quite a complex outline, and have dislocations of high density within them. In alloys of group II, martensites form at slightly lower temperatures. They form initially by burst and later grow as isothermal martensites. The external shape of the martensite crystals is relatively well defined and lenticular. Each martensite crystal has within it a midrib near which there are internal twins. In alloys of group III, martensite crystals form entirely by burst in the lowest temperature range. The martensite crystals are perfectly regular plates with straight, clearly defined boundaries and have internal twins all over each plate. The surface relief is uneven and blurred in alloys of group I, but in group III alloys the transformation results in the formation of exceptionally pronounced relief, all the elements of which have straight sides and flat faces. These features indicate that the transformation has occurred entirely by a shear mechanism. The surface relief effects for group II are about midway between those in group I and group III.

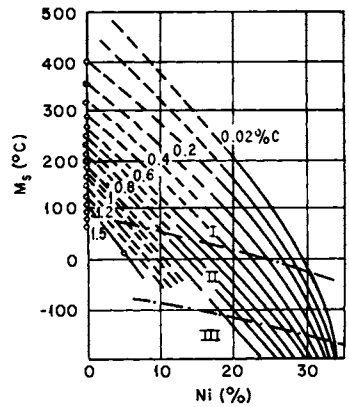

FIG. 4.16A Composition dependence of M_s in Fe–Ni–C. (After Georgiyeva and Maksimova.[168])

According to the research of Jones and Entwisle,[169] replacing Mn in an Fe–Ni–Mn alloy by Cr at a ratio of 1.5% Cr to 1% Mn does not produce any difference in the features of martensite formation. In the case of Fe–25.7% Ni–2.95% Cr, however, isothermal martensite forms in the temperature range $-78.5°$ to $-140°C$ and its habit plane is $\{225\}_\gamma$, whereas below this temperature range, the burst transformation takes place and the habit plane is $\{259\}_\gamma$.

4.5.4 Isothermal martensite of h.c.p. and other structures

Isothermal martensitic transformations are also found in f.c.c.-to-h.c.p. transformations, for example, in high manganese steels and 18–8 stainless steels. In the case of high manganese steels[170,171] the temperature for the maximum amount of transformation product is lowered with increasing manganese or carbon contents. Thus, the transformation no longer takes place when the carbon content exceeds a critical value. In the case of stainless steels, according to the investigation of an Fe–17% Cr–8% Ni alloy by Imai *et al.*,[150] the *TTT* diagram (Fig. 4.17) is composed of double C curves. The upper C curves, with a nose at about $-100°C$, are associated with the γ (f.c.c.) $\rightarrow \varepsilon$ (h.c.p.) transformation, and the lower curves, with a nose at about $-135°C$, are associated with the $\gamma \rightarrow \alpha'$ transformation.

In a martensitic transformation with a small activation energy (those with a small transformation deformation) for nucleation, as in In–Tl alloys, the

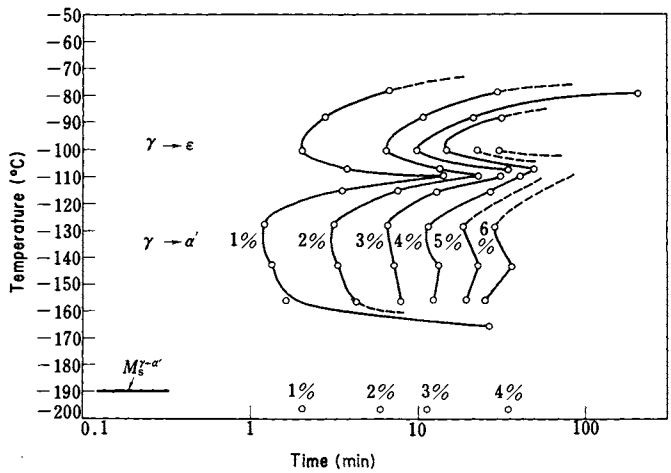

FIG. 4.17 Transformation–temperature–time curves for isothermal transformation to martensite in an Fe–17% Cr–8% Ni alloy. (Specimens were held for 1 hr at 1100°C and water quenched.) (After Imai *et al.*[150].)

M_s temperature is only a little below T_0 and the heat evolution accompanying the transformation is small. Therefore, the transformation appears to be isothermal, but strictly speaking it may not be. If such is the case, it may not be appropriate to classify the martensites into the two types, athermal and isothermal.

We still have to ask why martensites nucleate after different periods of holding at the same temperature in the isothermal transformation. A detailed discussion is left for Chapter 5, where the temperature range for transformation is treated; however, a possible reason is hinted at in the example cited next. In U–Cr alloys[172,173] gradual transformation at room temperature can be detected by observing the surface relief. This phenomenon is explained as follows: once transformation occurs at a certain place, transformation strain is produced around the region to suppress further transformation. However, when the strain is relieved gradually in a time-dependent manner as in creep, the transformation can proceed further. Yershov and Aslon[174] observed such a phenomenon in Cr steels and Ni steels. They made a metallographic measurement of the amount of isothermal martensite produced during holding at a constant temperature after introducing some athermal martensite by initial quenching to that temperature. They also measured the decrease in transformation-induced strain in the retained γ phase from the $(200)_\gamma$ line width of x-ray diffraction, and found a parallelism between the amount of isothermal martensite and the decrease in strain.

Uranium–molybdenum alloys are very suited for kinetic studies of the isothermal martensite transformation, because the transformation of these alloys is very sluggish.[175] Hence, an extensive study[176] has been made on this system. In the case of U–0.45% Mo alloy, at 80°C the incubation period is 1 hr and only 50% of the specimen is transformed after 5 hr. Since the transformation is so slow, it is difficult to define the transformation temperature, which corresponds to the conventional M_s temperature, but a TTT diagram for the transformation of certain amounts can be obtained. When such measurements are made, the $\beta \rightarrow \alpha'$ (martensite) transformation can be represented by a C curve that lies well below the C curve for the $\beta \rightarrow \alpha$ transformation. Therefore, if these two curves are drawn on the same graph, there appears to be a bay at approximately 300°C.

4.6 Adiabatic nature of the formation of athermal martensite

4.6.1 Athermal martensite and its growth[177]

In athermal martensitic transformation, because of its high transformation velocity, it is extremely difficult to observe the growth process of each martensite crystal formed. This is especially true for the umklapp transfor-

mation. Even in such a case, however, it can be surmised, from the facts described in Section 4.4.1, that each crystal grows at a constant velocity during a certain period of time. In regard to the growth morphology of a martensite plate having a midrib, this midrib is thought to be a starting site of growth, as was described in Chapter 2. It may not always be true that only after the midrib of a martensite plate has grown edgewise to its full extent does the plate grow sidewise. Rather, as soon as a part of the midrib forms, it might begin to grow sidewise, even during edgewise growth. The formation of the midrib must precede the growth of martensite.

4.6.2 Temperature distribution near the transformation front during adiabatic transformation

The transformation rate depends on the probability of formation of martensite nuclei and their subsequent growth. The nucleation can be treated isothermally. But it is questionable to treat the growth rate isothermally based on classical thermodynamics when a growth rate as fast as that with the umklapp transformation and the considerable evolution of transformation heat are taken into account. For example, in the case of Fe–30% Ni alloy the heat evolution is 10 cal/g; hence, a drastic temperature rise of a few tens of degrees Celsius is expected if this heat is not removed. In fact, upon measuring the temperature of a specimen on which a very thin thermocouple was spot-welded, a local temperature rise of about 10°C was observed.[104,178]

In order to judge how to treat the growth process of a martensite crystal thermodynamically, it is necessary to see the temperature distribution near the transformation front. However, since measuring it is difficult, Nishiyama *et al.*[179] have estimated it by calculation.

To simplify the problem, let us assume the following: (i) Martensite (α') and austenite (γ) have the same density ρ, specific heat c, and thermal conductivity κ. (ii) In a γ crystal extending infinitely, a thin martensite plate nucleates at $x = 0$ and grows symmetrically into both the plus and minus directions of x. In such a model one-dimensional treatment is permissible. Such a model does not alter the essential nature of the transformation and may be used for estimating the general aspect of the temperature distribution. Let v denote the velocity of propagation with which the α' phase grows in the γ phase, and Q_0 the heat of the transformation. For the present model the following heat conduction equation can be obtained.

$$\frac{\partial \theta}{\partial t} = a^2 \frac{\partial^2 \theta}{\partial x^2} + b\,\delta(x - vt) \qquad (x \geqq 0) \tag{1}$$

where θ is the temperature, $a^2 = \kappa/c\rho$, $b = Q_0 v/c$, and $\delta(x)$ is Dirac's δ function.

Equation (1) can be solved under the following initial and boundary conditions.

$$\text{Initial condition:} \quad \theta(x, t) = 0 \quad \text{for} \quad t \leqq 0; \tag{2}$$

$$\text{Boundary condition:} \quad (\partial\theta(x, t)/\partial x)_{x=0} = 0, \quad \theta(\infty, t) \text{ finite} \tag{3}$$

The result of calculation is given by

$$\theta = \frac{b}{v}\left\{\exp\left[\frac{v^2}{a^2}\left(t - \frac{x}{v}\right)\right] E\left(\frac{2vt - x}{\sqrt{2t}\, a}\right) - \exp\left[\frac{v^2}{a^2}\left(t + \frac{x}{v}\right)\right]\left[1 - E\left(\frac{2vt + x}{\sqrt{2t}\, a}\right)\right]\right\} \tag{4}$$

where

$$E(x) \equiv \int_{-\infty}^{x} (2\pi)^{-1/2} \exp(-\omega^2/2)\, d\omega.$$

By inserting the numerical values of the physical constants for pure iron, namely, $\kappa = 0.11$ cal/cm sec deg, $c = 0.11$ cal/g deg, $\rho = 7.9$, $Q_0 = 10$ cal/g, and $v = 1.1 \times 10^6$ cm/sec into Eq. (4), we can calculate the temperature distribution at the time when the half thickness of an α' plate has grown to 10, 100, and 1000Å. The results appear in Fig. 4.18. As shown in the figure, the temperature falls steeply in the vicinity of the transformation front. Such a sharp temperature gradient is very important from thermodynamical considerations. If the propagation of the transformation is steady even in a microscopic sense, these curves will show the true temperature distribution. If it is intermittent, however, these curves do not show the true temperature distribution, but must be regarded as showing merely the smoothed-out values, because the propagation speed value adopted here is only an average one.

Next, it can easily be predicted that the thermal change at the transformation front is neither purely adiabatic nor isothermal. In order to see where the real situation lies between the two extreme cases, consider a

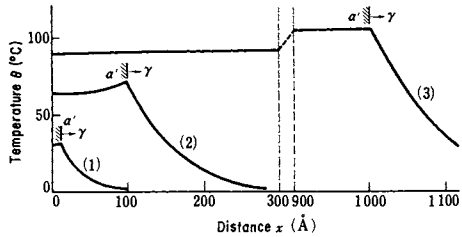

FIG. 4.18 Temperature distribution in a martensite plate and in the matrix near the transformation front (half thickness of martensite plate: (1) 10 Å; (2) 100 Å; (3) 1000 Å).

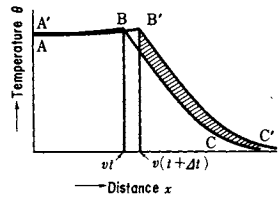

FIG. 4.19 Growth of a martensite plate and the change of temperature distribution in a time interval Δt.

parameter p, which denotes the fraction of heat removal at the transformation front. If $p = 0$, it is adiabatic; if $p = 1$, it is isothermal. In Fig. 4.19, ABC is the temperature distribution at time t, and A′B′C′ applies at $t + \Delta t$. The forward (toward γ) heat conduction during the transformation of the region between $x = vt$ and $x = v(t + \Delta t)$ can be measured by the area S of the shaded region. Thus, the p in question is expressed by

$$p = S/(b\,\Delta t) \tag{5}$$

where

$$S = \int_{v(t+\Delta t)}^{\infty} \{\theta(x, t + \Delta t) - \theta(x, t)\}\, dx, \tag{6}$$

and $b\,\Delta t$ is the heat evolution during Δt divided by $c\rho$. The proportion of the backward (toward the already transformed region) heat conduction is calculated to be very small.[179] Therefore, the parameter p may be taken as a quantity to measure approximately the proportion of the transformation heat removed by the surrounding regions. Using Eqs. (4), (5), and (6), we can calculate p and express it as

$$p = p^{(0)} + p^{(1)}\,\Delta t + p^{(2)}(\Delta t)^2 + \cdots. \tag{7}$$

The relation between $p^{(0)}$ and t is plotted in Fig. 4.20. This curve shows that if the propagation of the transformation is steady ($\Delta t = 0$), the process may be nearly isothermal. The deviation of p from unity is at most about 10%; p would differ significantly from this value for the intermittent transformation. Let us assume that a sudden transformation occurred in the small region $v\,\Delta t$, which is called here the *transformation unit* and is regarded as a physical unit of the intermittent transformation. The justification for using such a transformation unit will be examined later.

The value of p after infinite time has passed is calculated to be

$$p_{t\to\infty} = \frac{1 - \exp[(-v^2/a^2)\,\Delta t)]}{(v^2/a^2)\,\Delta t}. \tag{8}$$

The relations between $p_{t\to\infty}$ and the transformation unit $v\,\Delta t$ for $a^2/v = 900$, 90, and 9 Å are shown in Fig. 4.21. From these curves it is noted that the

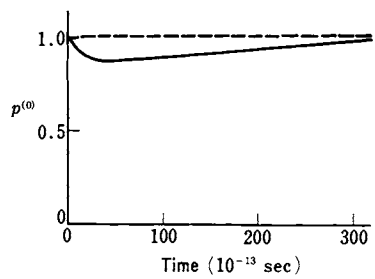

FIG. 4.20 Curve of $p^{(0)}$ versus t.

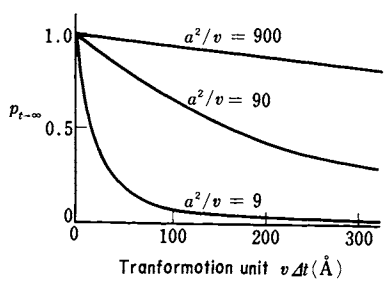

FIG. 4.21 Curves of $p_{t\to\infty}$ versus $v\,\Delta t$.

transformation occurs more adiabatically as the transformation unit becomes large. In a state where the martensite has not yet grown large, $t \ll \infty$, the transformation process must be more adiabatic, because those curves lie considerably below the corresponding ones in Fig. 4.21. It can be seen in this figure that if the value of a^2/v is 90 Å, the transformation process is nearly isothermal for $v\Delta t$ less than 10 Å and that the adiabatic element increases with increasing $v\Delta t$. If the value of a^2/v is 9 Å, it is isothermal for a few angstroms or less, but it is nearly adiabatic for 40 Å or more. For an Fe–30% Ni alloy the value of κ is 0.028 cal/cm sec deg, which is about one fifth that of pure iron, and a^2 is accordingly small. Therefore the transformation process in the alloy is more adiabatic than in pure iron.

If the transformation goes on intermittently, the transformation unit $v\Delta t$ just described plays an important role in the thermodynamics of the martensitic transformation. Equation (1), however, assumes the steady transformation. Therefore, in the exact treatment of the intermittent transformation, the term representing the heat evolution in Eq. (1) must be rewritten in a more appropriate form. To carry out this calculation, we must know in detail the experimental facts concerning the discontinuous transformation mechanism. However, there are no such established data available at the present time. On the other hand, as long as the transformation unit $v\Delta t$ is small, the calculation presented in the preceding paragraph is a good approximation. Therefore, the results drawn from the calculation are considered to be valid, at least qualitatively.

Summing up these results, we note that at the nucleation stage the martensitic transformation is an isothermal process, but the matter is not so simple for the growth process. If the transformation proceeds continuously (i.e., the transformation unit is smaller than a certain value), it is considered an isothermal process, just like nucleation. If the transformation proceeds intermittently (i.e., the transformation unit is large), it is an adiabatic process. In this case the magnitude of the transformation unit is very important. At present, however, assigning a concrete physical meaning to the transformation unit is very difficult because the model adopted here is not exact. For a thermodynamic consideration of the martensitic transformation, the stress due to the transformation strain must also be considered.

So far the transformation has been treated on the assumption that the transformation front is planar. This is, of course, a first approximation. For rigorous treatment it is better to assume that the transformation front is as close as possible to the actual shape. As described in Section 4.2.3, Lyubov and Roitburd[180] assumed the martensite crystal to be an elliptic cylinder and treated its growth in such a way that the sum of the elastic energy stored in the matrix and the surface energy is minimal. According to their result, the growth in the major axis direction of the ellipse (in the direction

of the width of the martensite plate) becomes faster. In this case, the result of calculation of the temperature distribution shows that in the early stage of the transformation the temperature rise is small in every direction, that is, nearly isothermal, and that contrary to the foregoing, if the growth reaches a steady state beyond the early stage, the temperature rise in the matrix adjacent to the tip of the ellipse in the major axis direction becomes large and the process is found to be adiabatic, whereas the temperature rise in the minor axis direction (normal to the martensite plate) is not so large.

4.6.3 Thermodynamic treatment of adiabatic transformation

If the growth of α' phase occurs by the umklapp transformation, which is a nearly adiabatic process, thermodynamic treatment of the growth should be made accordingly.[181] To simplify the problem, let us consider the limiting case in which the transformation takes place by a perfect adiabatic process.

In the case of adiabatic treatment, it is convenient to consider the problem on the basis of the entropy S and internal energy U. Figure 4.22a shows S–U relations for the γ and α' phases (for simplicity, α' will be replaced by α). For both phases the curves are such that U increases with increasing S and are concave upward, meeting at point K. The U versus T curves for both phases are shown in Fig. 4.22b, where U increases with T. The free energy F curves decrease with increasing temperature, as shown in Fig. 4.22c. In this figure the point of intersection O of the two curves represents the

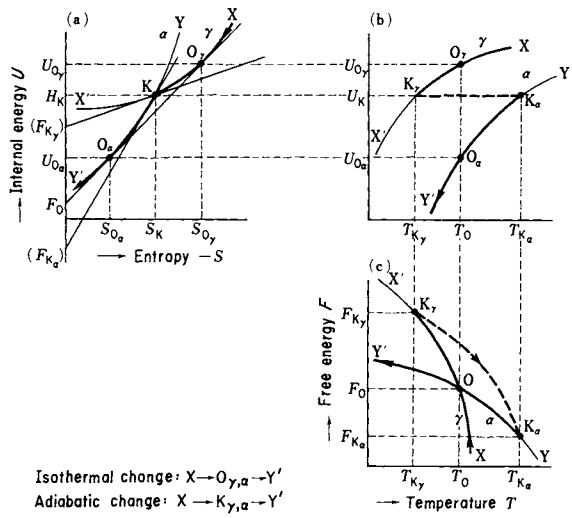

FIG. 4.22 U–S, U–T, and F–T relations near the transformation temperature (in case non-chemical energy is not required).

equilibrium coexistence of the two phases in the case of isothermal transformation.

For simplicity, let us first consider a transformation which is not accompanied by nonchemical energy, the cause of the irreversibility of the transformation. In this case, on cooling from the γ state at X in the figures, the process follows a course X–O–Y′ in Fig. 4.22c if the transformation is isothermal. On cooling from X in Fig. 4.22a, once a state O_γ, which is one contact point of the common tangent to the two U–S curves, is reached, the path does not continue to go in the direction $O_\gamma \rightarrow K$, but rather switches from O_γ to O_α at the same temperature on the α curve, and then proceeds along the curve toward the $O_\alpha Y'$ direction. In Fig. 4.22b, the transformation follows the path $X \rightarrow O_\gamma \rightarrow O_\alpha \rightarrow Y'$. During this phase change, if both the temperature T and free energy F ($= F_O$) are invariant, at or near the transformation front the entropy S must drop abruptly from S_{O_γ} at state O_γ to S_{O_α} at state O_α.

However, since the transformation in the present case is assumed to be adiabatic, S cannot drop abruptly. If the transformation does not have irreversible factors, S does not rise abruptly either. Therefore S must change continuously during the transformation. In order for this to occur, starting from X in Fig. 4.22a the process is bound to proceed along the γ curve as far as K via O_γ and at point K to switch to the α curve. In Fig. 4.22a the tangent at K of the U–S curve for the γ phase meets the U axis at F_{K_γ} (this is the free energy of the γ phase, represented by point K) and its gradient is equal to the temperature T_{K_γ} of the γ phase represented by point K. F_{K_α} and T_{K_α} are the corresponding physical quantities for the α phase. It is obvious from the foregoing that T_{K_α} is larger than T_{K_γ}. When the transformation occurs, the temperature rises discontinuously from T_{K_γ} to T_{K_α}, as shown in Fig. 4.22b, and the free energy decreases precipitously from F_{K_γ} to F_{K_α}, as shown in Fig. 4.22a. For this case the relation between F and T is shown in Fig. 4.22c. On cooling from state X in this figure, the process proceeds along the γ curve, passing O ($T = T_O$) without switching to the α curve until state $K_\gamma(T_{K_\gamma}, F_{K_\gamma})$ of high F value at lower temperature is reached. Then it jumps to $K_\alpha(T_{K_\alpha}, F_{K_\alpha})$ on the α curve and continues along $K_\alpha Y'$. In other words, in an adiabatic transformation S is invariant, F decreases discontinuously, and the temperature rises steeply.†

When nonchemical energy is required, as is the case in real transformations, this energy must be supplied by chemical energy. On cooling from state X in the γ phase, as shown in Fig. 4.23, the process continues to proceed along the γ curve via point K until point U (at which the transformation commences) is reached. Since the transformation is assumed adiabatic, the

† As shown in Fig. 4.22c, the fact that the transformation does not occur at T_O but does at the lower temperature T_{K_γ} means that an adiabatic transformation alone requires supercooling even when nonchemical energy is not required.

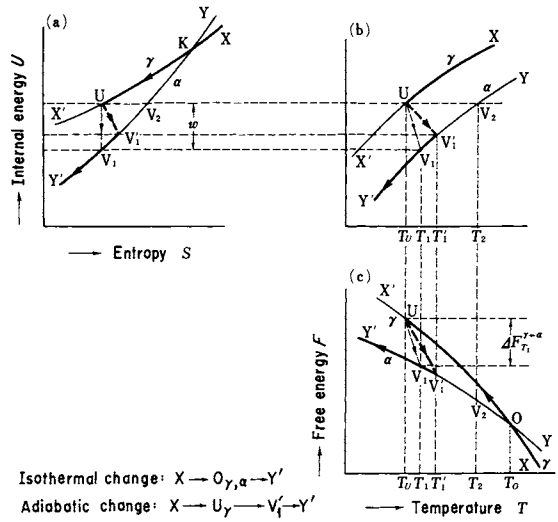

FIG. 4.23 *U–S*, *U–T*, and *F–T* relations during the transformation (in case nonchemical energy is required).

internal energy of the γ phase at the state U must be higher† than that of α by an amount w, which is the nonchemical energy necessary for the transformation. The temperature T_U corresponding to the point U is far below T_{K_γ}. Since a transformation in real cases involves irreversible factors, S must increase, and hence the temperature at which the transformation starts is further depressed below T_U. The amount of this depression varies, depending on the conditions and details of α formation, and its minimum is zero. In the following we consider the case in which the depression is zero.

The α phase at V_1 just after transformation contains the transformation strain (lattice defects and elastic strain). When a part of this strain energy is relieved after the transformation, it contributes to a temperature rise. If all of the transformation strain is relieved, the final internal energy should become the value at V_2 in Fig. 4.23a. But in reality there is dissipation of energy in such forms as residual lattice defects and scattered elastic waves. Therefore, the temperature rises to T_1' (corresponding to state V_1'), which is between T_1 (state V_1) and T_2 (state V_2). After this has happened, the temperature decreases along the path $V_1'Y'$.

To sum up, by its very nature, the adiabatic transformation starts at a temperature far below the temperature T_O at which the free energies of the γ and α phases are equal. Furthermore, in case nonchemical energy w is

† It may also be regarded that the point of intersection K of the two curves is displaced to point U by shifting the U–S curve of the α phase as a whole upward by an amount w.

required, the transformation starts only when the temperature is lowered to such a value that $\Delta U^{\gamma\to\alpha}$ instead of $\Delta F^{\gamma\to\alpha}$ as the driving force balances with w. This is why the transformation occurs upon severe supercooling.

Krisement *et al.*[182†] presented a similar argument in their paper, utilizing a graph like Fig. 4.23b. According to them, among the various factors contributing to w the predominant one is the strain energy due to the lattice expansion upon transformation. Considering this strain energy to depend on the amount of martensite transformed, they estimated the value of w for a 0.7% C steel from the degree of reduction in the lattice parameter of the retained γ as compared with the normal value, and obtained 48 cal/mol as a minimum and 400 cal/mol as a maximum.[‡] If the temperatures T_U corresponding to the minimum and maximum values of w are the M_s and M_f temperatures, respectively, the existence of the transformation temperature range can be explained, as Krisement *et al.* state. In their arguments they assume w to be equal to $\Delta F^{\gamma\to\alpha}$ at T_1. However, such an assumption may not be warranted in the case of an adiabatic change.

Hillert[184] is also critical of such an assumption. In order to estimate T_1 and T_U, he considered the process $U \to V_1$ in Fig. 4.23a as an adiabatic change requiring the work w; that is,

$$dU + w = 0, \tag{9}$$

$$dS = 0, \tag{10}$$

and discussed the problem starting with these equations. In Eq. (9) dU can be expressed by

$$dU = U_{T_1}{}^{\alpha} - U_{T_U}{}^{\gamma} \equiv (U_{T_1}{}^{\gamma} - U_{T_U}{}^{\gamma}) + (U_{T_1}{}^{\alpha} - U_{T_1}{}^{\gamma}).$$

Since $U_{T_1}{}^{\alpha} - U_{T_1}{}^{\gamma}$ is constant, being independent of the temperature T_1, within a narrow temperature range, it is denoted by ΔU. $U_{T_1}{}^{\gamma} - U_{T_U}{}^{\gamma}$ is expressed by $c(T_1 - T_U)$ where c is the specific heat of the parent phase. Therefore Eq. (9) becomes

$$c(T_1 - T_U) + \Delta U + w = 0. \tag{11}$$

Similarly, Eq. (10) can be written as

$$S_{T_1}{}^{\alpha} - S_{T_U}{}^{\gamma} \equiv (S_{T_1}{}^{\gamma} - S_{T_U}{}^{\gamma}) + (S_{T_1}{}^{\alpha} - S_{T_1}{}^{\gamma}) = 0,$$

and since $S_{T_1}{}^{\alpha} - S_{T_1}{}^{\gamma}$ is considered independent of T_1 within a narrow temperature range, it is denoted by ΔS. Since $S_{T_1}{}^{\gamma} - S_{T_U}{}^{\gamma}$ is equal to

† Crussard[183] also emphasized the adiabatic nature of the martensitic transformation and proposed a mechanism in which the propagation of the transformation is similar to that of an explosion wave.

‡ There are papers[24,182] that report w to be 65 cal/mol.

$c \ln(T_1/T_U)$, Eq. (10) becomes

$$c \ln(T_1/T_U) + \Delta S = 0. \tag{12}$$

From Eqs. (11) and (12), the following equations are obtained.

$$T_1 = \frac{\Delta U + w}{c[\exp(\Delta S/c) - 1]} \qquad T_U = \frac{\Delta U + w}{c[1 - \exp(-\Delta S/c)]}. \tag{13}$$

Now, let us consider

$$T_i = \frac{\Delta U + w}{\Delta S}. \tag{14}$$

Since T_i satisfies $\Delta U - T_i \Delta S + w = 0$, it corresponds to the equilibrium temperature under isothermal conditions. Combining Eq. (13) and (14) gives the relations

$$T_1 = T_i \frac{\Delta S}{c[\exp(\Delta S/c) - 1]}, \qquad T_U = T_i \frac{\Delta S}{c[1 - \exp(-\Delta S/c)]}, \tag{15}$$

$$T_1 - T_U = -\frac{\Delta U + w}{c} = T_i \frac{-\Delta S}{c}. \tag{16}$$

Therefore, if w can be estimated, T_1 and T_U can be obtained from Eqs. (15) and (16) by using ΔU, ΔS, and c.

Plastic deformation changes the martensitic transformation temperature. When the degree of deformation is increased, the transformation temperatures, namely, the M_d temperature (on cooling) and A_d temperature (on heating), approach one another and sometimes coincide. In the latter case, w is considered to be zero. There are some cases in which the M_d and A_d temperatures never coincide. An example close to this is an Fe–Ni alloy having its M_s temperature below room temperature. According to measurement made on an Fe–30% Ni alloy, $A_d - M_d$ is found to be 100°C (Fig. 4.7).[6] For this alloy, $T_i = T_O = 450$°K, $-\Delta S = 1.5$ cal/mol °K, and $c = 70$ cal/mol °K. Putting these values into Eq. (16), we obtain

$$T_1 - T_U = 95°,$$

which agrees very well with the observed $A_d - M_d$ value. It is consistent in this case to assume that M_d is equivalent to T_U for $w = 0$, that is, to T_{K_γ}, and A_d is equivalent to T_1 for $w = 0$, that is, to T_{K_α}. From this, the reason the M_d and A_d of the Fe–30% Ni alloy do not coincide, however heavily the alloy is deformed plastically, can be attributed to the adiabatic nature of the umklapp transformation in this alloy.

Usually, in the case where a martensitic transformation is treated as an isothermal process, Eq. (14) is used to obtain the value of w, regarding M_s

as the T_i temperature. So the value of w for Fe–C alloys is found to be 350 cal/mol. If M_s is regarded as T_U and Eq. (15) is utilized to obtain w, $w = 200$ cal/mol is obtained. This value is closer to the w value (65 cal/mol) estimated directly, although there is still considerable discrepancy. This difference may be due to either an incorrect estimate of w or the fact that the estimated w corresponds to the work between V_1' and V_2 in Fig. 4.23.

References

1. L. Kaufman and M. Cohen, Thermodynamics and kinetics of martensitic transformations, *Progr. Met. Phys.* **7**, No. 3, 165 (1958).
2. C. H. Johannson, *Arch. Eisenhüttenwes.* **11** 241 (1937).
3. J. C. Fisher, *Trans. AIME* **185** 688 (1949).
4. L. S. Darken and R. P. Smith, *Ind. Eng. Chem.* **43**, 1815 (1951).
5. R. J. Weiss and K. J. Tauer, *Phys. Rev.* **102**, 1490 (1956).
6. L. Kaufman and M. Cohen, *Trans. AIME* **206**, 1393 (1956).
7. W. S. Owen and A. Gilbert, *J. Iron Steel Inst.* **196**, 142 (1960).
8. A. Gilbert and W. S. Owen, *Acta Metall* **10**, 45 (1962).
9. R. Kohlhaas and M. Braun, *Arch. Eisenhüttenwes.* **34**, 391 (1963).
10. L. Kaufman, E. V. Clougherty, and R. J. Weiss, *Acta Metall.* **11**, 323 (1963).
11. R. L. Orr and J. Chipman, *Trans. AIME* **239**, 630 (1967).
12. C. Zener, *Trans. AIME* **203**, 615 (1955).
13. U. Roesler, H. Sato, and C. Zener, "Theory of Alloy Phases," p. 255. Am. Soc. Metals, (1955).
14. C. Zener, *Trans. AIME* **167**, 513 (1946).
15. L. S. Darken, *Trans. AIME* **167**, 468 (1946).
16. E. Scheil and W. Norman, *Arch. Eisenhüttenwes.* **30**, 751 (1959).
17. F. W. Jones and W. I. Pumphrey, *J. Iron Steel Inst.* **163**, 121 (1949).
18. J. C. Fisher, J. H. Hollomon, and D. Turnbull, *Trans. AIME* **185**, 691 (1949).
19. L. Kaufman, *Trans. AIME* **215**, 218 (1959).
20. T. Wada, *Trans. Iron Steel Inst. Jpn.* **8**, 1 (1968).
21. D. A. Mirzayev, Yu. N. Goykhenberg, and M. M. Shteyberg, *Fiz. Met. Metalloved.* **26**, 857 (1968).
22. E. A. Owen and Y. H. Liu, *J. Iron Steel Inst.* **163**, 132 (1949).
23. M. Hillert, T. Wada, and H. Wada, *J. Iron Steel Inst.* **205**, 539 (1967).
24. M. Cohen, E. S. Machlin, and V. G. Paranjpe, "Thermodynamics in Physical Metallurgy," p. 242. Am. Soc. Metals, (1949).
25. J. C. Fisher, "Thermodynamics in Physical Metallurgy," p. 201. Am. Soc. Metals, (1940).
26. H. Sato, *J. Jpn. Inst. Met.* **17**, 601 (1953).
27. Y. Imai, M. Izumiyama, and M. Tsuchiya, *Sci. Rep. RITU* **17**, 173 (1965).
28. V. L. Snezhnoy, F. D. Miroshnichenko, and V. G. Kanibolotskij, *Fiz. Met. Metalloved.* **31**, 158 (1971).
29. F. C. Frank, *Acta Metall.* **1**, 15 (1952).
30. E. S. Machlin, *Trans. AIME* **200**, 684 (1954).
31. H. Knapp and U. Dehlinger, *Acta Metall.* **4**, 289 (1956).
32. B. Ya. Lyubov, A. L. Roitburd, *Dokl. Akad. Nauk SSSR* **131**, 303 (1960) [*English transl.*: *Sov. Phys.-Dokl.* **5**, 376 (1960)].
33. R. Adams and C. Altstetter, *Trans. AIME* **242**, 139 (1968).

34. A. J. Goldman and W. D. Robertson, *Acta Metall.* **13**, 391 (1965).
35. K. P. Singh and J. Gordon Parr, *Acta Metall.* **9**, 1073 (1961).
36. H. H. Uhlig, *Acta Metall.* **10**, 1107, 1109 (1962).
37. S. V. Radcliffe, L. Kaufman, and M. Cohen, *Acta Metall.* **10**, 1110 (1962).
38. For example, C. L. M. Cottrell, *J. Iron Steel Inst.* **176**, 269 (1954).
39. P. Duwez, *Trans. AIME* **3**, 765 (1951); *J. Inst. Met.* **80**, 525 (1951/52); *Trans. ASM* **45**, 934 (1952).
40. M. J. Bibby and J. Gordon Parr, *J. Inst. Met.* **92**, 341 (1964).
41. L. Kaufman, *Acta Metall.* **7**, 575 (1959).
42. D. S. Lieberman, *Int. Conf. Sci. Tech. Iron Steel, Tokyo* 6-8-3, 590 (1970).
43. S. Mizushima and I. Ichijima, "Essays in Structural Chemistry," Chapter 9. MacMillan, New York, (1971).
44. A. Sauveur and C. H. Chou, *Trans. AIME* **84**, 350 (1929).
45. F. Wever and N. Engel, *Mitt. K. W. I. Eisenforsch.* **12**, 93 (1930).
46. H. Esser, W. Eilender, and E. Spenlé, *Arch. Eisenhüttenwes.* **6**, 389 (1933).
47. W. S. Owen and A. Gilbert, *J. Iron Steel Inst.* **196**, 142 (1960).
48. L. P. Srivastava and J. Gordon Parr, *Trans. AIME* **224**, 1295 (1962).
49. M. J. Bibby and J. Gordon Parr, *J. Iron Steel Inst.* **202**, 100 (1964).
50. G. R. Speich, A. Szirmae, and R. M. Fisher, *Adv. Electron Microgr. Am. Soc. Test. Mater.* **6**, 97 (1966).
51. M. Izumiyama, M. Tsuchiya, and Y. Imai, *J. Jpn. Inst. Met.* **34**, 286 (1970).
52. K. Arakawa, *Nippon Butsuri Gakkai Shi* **21**, 523 (1966).
53. E. A. Wilson, *Scr. Metall.* **4**, 309 (1970).
54. For example, C. M. Wayman and C. J. Altstetter, *Acta Metall.* **10**, 992 (1962).
55. O. P. Morozov, D. A. Mirzayev, and M. M. Shteynberg, *Fiz. Met. Metalloved.* **32**, 1290 (1971).
56. For example, L. I. Kogan and R. I. Entin, *Fiz. Met. Metalloved.* **23**, 956 (1967).
57. D. S. Kamenetskaya, T. B. Piletskaya, and V. I. Shiryaev, *Fiz. Met. Metalloved.* **27**, 842 (1969).
58. H. Hanemann and H. J. Wiester, *Arch. Eisenhüttenwes.* **5**, 377 (1952).
59. T. G. Digges, *J. Res. Nat. Bur. Std.* **23**, 151 (1939); *Trans. ASM* **28**, 575 (1940).
60. A. B. Greninger and A. R. Troiano, *Trans. ASM*, **28**, 357 (1940).
61. R. A. Grange and H. M. Stewart, *Trans. AIME* **167**, 467 (1946).
62. V. N. Gridnev and V. I. Trefilov, *Dokl. Akad. Nauk SSSR* **95**, 741 (1954), Brutcher transl. No. 3385.
63. W. L. Haworth and J. Gordon Parr, *Trans. ASM* **58**, 476 (1965).
64. T. Bell, *J. Iron Steel Inst.* **206**, 1017 (1968).
65. P. Chevenard, *Rev. de Métall.* **11** (1914).
66. B. R. Banerjee and J. J. Hauser, *Metallography* **1**, 157 (1968).
67. J. Gordon Parr, *J. Iron Steel Inst.* **205**, 426 (1967).
68. C. A. Clark, *J. Iron Steel Inst.* **193**, 11 (1959).
69. E. Scheil and E. Saftig, *Arch. Eisenhüttenwes.* **31**, 623 (1960).
70. W. D. Swanson and J. Gordon Parr, *J. Iron Steel Inst.* **202**, 104 (1964).
71. M. Izumiyama, M. Tsuchiya, and Y. Imai, *J. Jpn. Inst. Met.* **34**, 291 (1970).
72. H. H. Chiswik and A. B. Greninger, *Trans. ASM* **32**, 483 (1944).
73. P. Payson and C. H. Savage, *Trans. ASM* **33**, 261 (1943).
74. J. B. Bassett and E. S. Rowland, *Trans. AIME* **180**, 439 (1949).
75. L. I. Kogan and R. I. Entin, *Zh. Tekh. Fiz.* **20**, 683 (1950); *Chem. Abstr.* **44**, 8751 h.
76. D. W. Gomersall and J. Gordon Parr, *J. Iron Steel Inst.* **203**, 275 (1965).
77. J. M. Wallbridge and J. Gordon Parr, *J. Iron Steel Inst.* **204**, 119 (1966).
78. R. Kumar and A. G. Quarrell, *J. Iron Steel Inst.* **187**, 195 (1957).

79. K. J. L. Iyer, *Scr. Metall.* **6**, 721 (1972).
80. G. H. Eichelman, Jr. and F. C. Hull, *Trans. ASM* Reprint No. 9, 19 (1952).
81. W. Steven and A. G. Hayes, *J. Iron Steel Inst.* **183**, 349 (1956).
82. R. B. G. Yeo, *Trans. AIME* **227**, 884 (1963).
83. M. M. Shteynberg, V. V. Golikova, L. G. Zhuravlev, and V. N. Gonchar, *Fiz. Met. Metalloved.* **26**, 331 (1968).
84. K. Ishida and T. Nishizawa, *J. Jpn. Inst. Met.* **36**, 270 (1972).
85. D. A. Mirzayev, M. M. Shteynberg, and Yu. N. Goykhenberg, *Fiz. Net. Metalloved.* **28**, 362 (1969).
86. L. A. Carapella, *Met. Progr.* **46**, 108 (1944).
87. G. H. Eichelman and F. C. Hull, *Trans. ASM* **45**, 77 (1953).
88. I. N. Bogachev, V. F. Yegolayev, and G. Ye. Zvigintseva, *Fiz. Met. Metalloved.* **28**, 885 (1969).
89. P. Nicolaides, D. Coutsouradis, and L. Habraken, *Trans. AIME* **215**, 702 (1959).
90. H. Schumann, *Neue Hütte* **17**, 605 (1972).
91. H. Kaneko and Y.-C. Huang, *J. Jpn. Inst. Met.* **27**, 387, 393, 398, 407 (1968).
92. T. Sato, S. Fukai, Y.-C. Huang, and S. Suzuki, *Sumitomo Light Met.* **1**, 173 (1960).
93. H. Bibring, G. Lenoir, and F. Sebilieau, *Rev. Métall* **56**, 279 (1959).
94. T. Tadaki and K. Shimizu, *J. Jpn. Inst. Met.* **34**, 77 (1970).
95. C. S. Barrett, *Trans. ASM* **49**, 53 (1957).
96. A. L. Titchener and M. B. Bover, *Trans. AIME* **200**, 303 (1954).
97. H. Pops and T. B. Massalski, *Trans. AIME* **230**, 1962 (1964).
98. H. Pops and N. Ridley, *Metall. Trans.* **1**, 2653 (1970).
99. J. D. Ayers and C. P. Herring, *J. Mater. Sci.* **6**, 1325 (1971).
100. M. E. Brookes and R. W. Smith, *Met. Sci. J.* **2**, 181 (1968).
101. M. Jovanović, M. E. Brookes, and R. W. Smith, *Met. Sci. J.* **5**, 230 (1971).
102. T. Honma, Y. Shugo, and M. Matsumoto, Res. Inst. Min. Dress. Metall. Rep. No. 672 (1972).
103. H. J. Wiester, *Z. Metallk.* **24**, 276 (1932).
104. T. Honma, *J. Jpn. Inst. Met.* **21**, 263 (1957).
105. F. Förster and E. Scheil, *Z. Metallkd.* **28**, 245 (1936).
106. F. Förster and E. Scheil, *Z. Metallkd.* **32**, 165 (1940); *Naturwissenschaften* **25**, 439 (1937).
107. T. Okamura, S. Miyahara, and T. Hirone, *Rikagaku Kenkyusho Iho* **21**, 985 (1942).
108. R. F. Bunshah and R. F. Mehl, *J. Met.* **5**, 1250 (1953).
109. S. A. Kulin and M. Cohen, *Trans. AIME* **188**, 1139 (1950).
110. E. E. Lähteenkorva, *Ann. Acad. Sci. Fennicae, A. VI. Physica* No. 87 (1961).
111. H. Beisswenger and E. Scheil, *Arch. Eisenhüttenwes* **27**, 413 (1956).
112. H. Kimmich and E. Wachtel, *Arch. Eisenhüttenwes.* **35**, 1193 (1964).
113. Y. Suzuki and H. Saito, Jpn. Inst. Metals, Fall Meeting, p. 233 (1972).
114. V. I. Izotov, P. A. Khandarov, and A. B. Chormonov, *Fiz. Met. Metalloved.* **33**, 214 (1972).
115. S. Takeuchi, H. Suzuki, and T. Honma, Jpn. Inst. Metals, Spring Meeting, p. 21 (65) (1950).
116. R. B. G. Yeo, *Trans. ASM* **57**, 48 (1964).
117. M. Okada and Y. Arata, *Tech. Rep. Osaka Univ.* **5**, 169 (1955).
118. P. Bastien and G. Stora, *C. R. Acad. Sci. Paris* **244**, 2613 (1957).
119. J. A. Klostermann and W. G. Burgers, *Acta Metall.* **12**, 355 (1964).
120. J. A. Klostermann, "The Mechanism of Phase Transformations in Crystalline Solids." Inst. of Metals, Spec. Rep. No. 33, p. 143 (1969).
121. S. Takeuchi and T. Honma, *Sci. Rep. RITU* **A9**, 492 (1957).

122. H. Bibring and F. Sebilleau, *Rev. Métall.* **56**, 609 (1959).
123. Z. S. Basinski and J. W. Christian, *Acta Metall.* **2**, 143 (1954).
124. C. L. Magee, "Phase Transformation," ASM Seminar, p. 115 (1968).
125. A. B. Greninger and V. G. Mooradian, *Trans. AIME* **128**, 337 (1938).
126. L.-C. Chang and T. A. Read, *Trans. AIME* **189**, 47 (1951).
127. K. C. Jones and A. R. Entwisle, *J. Iron Steel Inst.* **209**, 739 (1971).
128. M. Cohen, E. S. Machlin, and V. G. Paranjpe, "Thermodynamics in Physical Metallurgy," p. 242. Amer. Soc. Metals (1949).
129. E. S. Machlin, and M. Cohen, *Trans. AIME* **4**, 489 (1952).
130. L. Kaufman, and M. Cohen, Inst. Metals, Monograph and Rep. Series No. 18, p. 187 (1955).
131. R. E. Cech and D. Turnbull, *Trans. AIME* **206**, 124 (1956).
132. M. Cohen, *Trans. AIME* **212**, 171 (1958).
133. V. Raghavan and M. Cohen, *Acta Metall.* **20**, 333 (1972).
134. M. Cohen, *Metall. Trans.* **3**, 1095 (1972).
135. V. Raghavan and M. Cohen, *Acta Metall.* **20**, 779 (1972).
136. A. B. Greninger and A. R. Troiano, *Trans. ASM* **28**, 537 (1940); *Stahl Eisen* **60**, 761 (1940).
137. B. L. Averbach, M. Cohen, and S. C. Fletcher, *Trans. ASM* **40**, 728 (1948).
138. G. V. Kurdjumov and O. P. Maksimova, *Dokl. Akad. Nauk SSSR* **61**, 83 (1948).
139. G. V. Kurdjumov and O. P. Maksimova, *Dokl. Akad. Nauk SSSR* **73**, 95 (1950).
140. G. V. Kurdjumov and O. P. Maksimova, *Met. Progr.* January, 122 (1952); *Dokl. Akad. Nauk SSSR* **81**, 565 (1951).
141. F. C. Thompson and M. D. Jepson, *J. Iron Steel Inst.* **164**, 27 (1950).
142. B. L. Averbach, M. Cohen, and S. G. Fletcher, *Trans. ASM* **40**, 728 (1948).
143. S. C. Das Gupta and B. S. Lement, *Trans. AIME* **191**, 727 (1951).
144. S. A. Kulin and G. R. Speich, *Trans. AIME* **194**, 258 (1952).
145. R. E. Cech and J. H. Hollomon, *Trans. AIME* **197**, 685 (1953).
146. M. Okamoto and R. Tanaka, *J. Jpn. Inst. Met.* **20**, 285 (1956).
147. R. B. G. Yeo, *Trans. AIME* **224**, 1272 (1962); *Trans ASM* **57**, 48 (1964).
148. Y. Imai and M. Izumiyama, *J. Jpn. Inst. Met.* **27**, 170 (1963); *Sci. Rep. RITU* **A17**, 135 (1965).
149. E. D. Butakova and K. A. Malyshev, *Fiz. Met. Metalloved.* **32**, 353 (1972).
150. Y. Imai, M. Izumiyama, and K. Sasaki, *Sci. Rep. RITU* **A18**, 39 (1966).
151. V. Raghavan and A. K. Entwistle, Iron and Steel Inst., Spec. Rep. No. 93, p. 30 (1965).
152. E. Schmidtmann, K. Vogt, and H. Schenck, *Arch. Eisenhüttenwes.* **38**, 639 (1967).
153. A. R. Entwisle, *Met. Sci. J.* **2**, 153 (1965).
154. C. H. Shih, B. L. Averbach, and M. Cohen, *Trans. AIME* **202**, 183, 1265 (1955).
155. J. Philibert and C. Crussard, *J. Iron Steel Inst.* **180**, 39 (1955).
156. W. J. Harris, Jr. and M. Cohen, *Trans. AIME* **180**, 447 (1949).
157. K. R. Satyanarayan, W. Eliasz, and A. P. Miodownik, *Acta Metall.* **16**, 877 (1968).
158. D. P. Koistinen and R. E. Martburger, *Acta Metall.* **7**, 59 (1959).
159. R. Brook, A. R. Entwisle, and E. F. Ibrahim, *J. Iron Steel Inst.* **195**, 292 (1960).
160. J. H. Hollomon and D. Turnbull, *Progr. Met. Phys.* **4**, 333 (1965).
161. For example, A. V. Anandaswaroop and V. Raghavan, *Scr. Metall.* **3**, 221 (1969).
162. S. R. Pati and M. Cohen, *Acta Metall.* **19**, 1327 (1971).
163. Ye. Ye. Yurchikov and A. Z. Men'shikov, *Fiz. Met. Metalloved.* **32**, 168 (1971).
164. R. B. G. Yeo, *Trans. AIME* **224**, 1222 (1962).
165. I. Ya. Georgiyeva and I. I. Nikitina, *Fiz. Met. Metalloved.* **33**, 144 (1972).
166. L. Ya. Georgiyeva, V. I. Izotov, I. I. Nikitina, and P. A. Khandarov, *Fiz. Met. Metalloved.* **27**, 1129 (1969).

167. I. Ya. Georgiyeva, V. I. Izotov, M. N. Pankova, L. M. Utevskiy, and P. A. Khandarov, *Fiz. Met. metalloved.* **32**, 626 (1971).
168. I. Ya. Georgiyeva and O. P. Maksimova, *Fiz. Met. Metalloved.* **32**, 364 (1971).
169. W. K. C. Jones and A. R. Entwisle, *Met. Sci. J.* **5**, 190 (1971).
170. L. S. Yershova, *Fiz. Met. Metalloved.* **15**, 571 (1963).
171. I. N. Bogachev, V. F. Yegolayev, and L. S. Malinov, *Fiz. Met. Metalloved.* **17**, 49 (1964).
172. A. N. Holden, *Acta Metall.* **1**, 617 (1952).
173. B. W. Mott and H. R. Haines, *Rev. Métall.* **51**, 614 (1954).
174. V. M. Yershov and N. L. Oslon, *Fiz. Met. Metalloved.* **27**, 166 (1969).
175. A. Mihajlovic and A. Mance, *J. Nucl. Mater.* **32**, 357 (1969).
176. A. Mihajlovic, *J. Mater. Sci.* **5**, 955 (1970).
177. A. R. Entwisle and J. A. Feeney, Inst. of Metals, Spec. Rep. No. 33, p. 156 (1969).
178. F. Förster and E. Scheil, *Z. Metallkd.* **32**, 165 (1940).
179. Z. Nishiyama, A. Tsubaki, H. Suzuki, and Y. Yamada, *J. Phys. Soc. Japan* **13**, 1084 (1958).
180. B. Ya. Lyubov and A. L. Roitburd, *Dokl. Akad. Nauk SSSR* **131**, 809 (1960).
181. Z. Nishiyama and Y. Shimomura, *J. Jpn. Inst. Met.* **12**, No. 2/3, 9; No. 5, 1 (1948).
182. O. Krisement, E. Houdremont, and F. Wever, *Rev. Metall.* **51**, 401 (1954).
183. C. Crussard, *C. R. Acad. Sci. Paris* **240**, 2313 (1955).
184. M. Hillert, *Acta Metall.* **6**, 122 (1958).

5

Conditions for Martensite Formation and Stabilization of Austenite

In general, a phase transformation is caused by the free energy difference between two phases. The free energy is influenced by pressure as well as temperature. The martensitic transformation is also markedly influenced by other factors (e.g., external stress) because it occurs mainly by the cooperative movement of atoms. It is, therefore, important to know the conditions under which martensite forms. This chapter will consider various conditions for martensite formation, and finally, the stabilization of austenite, which is of engineering importance.

5.1 **Effect of pressure** (hydrostatic pressure)[1]

Pressure, as well as temperature, is a factor that determines the state of materials. Hydrostatic pressure, if great, would shrink the atomic distance and influence the electron distribution, hence causing an appreciable change in the transformation temperature. For example, in the case of Cs metal subjected to increasing pressure, discontinuous contractions are observed at 22 kbar and 45 kbar. The first contraction is due to a b.c.c.-to-f.c.c. phase transformation. The second contraction is as large as 11%, but the arrangement of atoms does not change. The latter contraction is interpreted to be caused by the change in cohesive strength of the lattice due to the electronic transition from the 6s to the 5d state. Transformation temperature is a function of pressure. Similar phenomena are observed in Ce and Rb. In Tl,

which (like Ti) transforms from b.c.c. to h.c.p., the transformation temperature is lowered from 505°K to 300°K by applying 36.7 kbar.[2] This is coincident with the value predicted from theoretical calculations.[3] If transformation temperatures are very low in comparison with the Debye temperature, a martensitic transformation may occur.

In this chapter, the effect of pressure on the phase diagram for pure iron will be briefly explained and then the effect of pressure on martensitic transformation will be described, mainly with reference to iron alloys.

5.1.1 Pressure–temperature diagram for iron

As was discussed in Chapter 1, in pure iron the α (β, δ) and γ phases exist over ranges of temperature under 1 atm. The temperature ranges for phase stability are changed by increased pressure. First, let us discuss the effect of pressure on the decrease in T_0 for the A_3 transformation. If the pressure (p) is not too high, the change in the A_3 point can be estimated thermodynamically from the Clausius–Clapeyron equation, $\Delta H = T(dp/dT_0)\Delta V$, where ΔH is the enthalpy change, estimated to be 215 cal/mol, taken from the heat of transformation at the A_3 point at 1 atm. The volume change ΔV is estimated to be $-3 \times 3.5 \times 10^{-3}$ per unit volume from the measurement of the lattice constant.[4] Consequently, the result

$$dT_0/dp = -9.8°\text{C/kbar}$$

is obtained. That is, T_0 decreases with increasing pressure due to the negativity of ΔV. The value estimated here coincides with the result obtained from electrical resistance measurements at a moderate pressure.[5,6] In the high-pressure range, the rate of decrease of T_0 with pressure decreases, as shown in Fig. 5.1. With a further increase in pressure, a new phase, ε (h.c.p.), appears with a triple point (115 kbar, 500°C). The α–ε boundary in Fig. 5.1

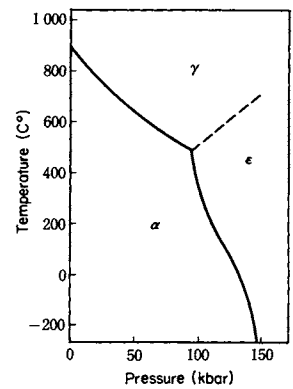

FIG. 5.1 p–T diagram for pure iron.

was determined by structure observations,[7] changes in x-ray diffraction patterns,[8] and changes in time-pressure curves during impact compression,[9] and the γ–ε boundary was determined by x-ray diffraction.[8†]

The ε phase is considered to be the same phase as the ε martensite that forms in high manganese and 18–8 stainless steels. It is expected that, even in pure iron, ε martensite can be obtained by carrying out the $\gamma \rightarrow \varepsilon$ transformation by rapid cooling under high pressure (more than 115 kbar), or the $\alpha \rightarrow \varepsilon$ transformation may be brought about by an increase in pressure at a low temperature. This has been confirmed by many investigations since Bancroft *et al.*[11] initially made studies using shock waves. Giles *et al.*[12] have observed, by means of x-ray diffraction, the change in crystal structure in pure iron compressed under hydrostatic pressure (piston method). They observed that both α and ε coexisted under a pressure between 45 and 163 kbar, and that the transformation occurred abarically with considerable hysteresis. Therefore, the pressure P_0 at which the free energies of both phases are equal at constant temperature has the same significance as T_0, the temperature at which the free energies of the two phases are equal at constant pressure. At 300°K, the critical pressure values are

$$P_{M_s}^{\alpha \rightarrow \varepsilon} = 133 \quad \text{kbar (for the } \alpha \rightarrow \varepsilon \text{ start)},$$
$$P_{M_f}^{\alpha \rightarrow \varepsilon} = 163 \quad \text{kbar (for the } \alpha \rightarrow \varepsilon \text{ finish)},$$
$$P_{M_s}^{\varepsilon \rightarrow \alpha} = 81 \quad \text{kbar (for the } \varepsilon \rightarrow \alpha \text{ start)},$$
$$P_{M_f}^{\varepsilon \rightarrow \alpha} = 45 \quad \text{kbar (for the } \varepsilon \rightarrow \alpha \text{ finish)}.$$

Then, at 300°K

$$P_0 = \tfrac{1}{2}(P_{M_s}^{\alpha \rightarrow \varepsilon} + P_{M_s}^{\varepsilon \rightarrow \alpha}) = 107 \quad \text{kbar}.$$

These values are approximately coincident with the results obtained by electrical resistance measurement.[13]

5.1.2 Effect of pressure on the equilibrium concentration of interstitial atoms and vacancies[14]

The pressure dependency of the equilibrium concentration (c_p) of vacancies or interstitial atoms, such as carbon and nitrogen, is expressed as

$$c_p = c_0 \exp(-pV/RT)$$

† The ε phase has been also obtained by splat cooling in an Fe–(3.8–4.8) wt % C[10] alloy. In this case, the maximum solubility of carbon in the ε phase is nearly the same as the composition corresponding to Fe_4C, and the interstitial carbon atoms occupy octahedral sites in the h.c.p. lattice. This structure is almost the same as ε carbide. The difference between the ε phase and ε carbide appears to be that the carbon concentration in the ε phase is not as high as in ε carbide and the distribution of carbon in the ε phase is disordered. Furthermore, with the addition of Si,[10] the ε phase is likely to appear even when the carbon content is less than 3.8%.

where c_0 is a constant, V the molar volume change due to the formation of point defects, R the gas constant, and T the absolute temperature. For example, taking $T = 500°K$, $V = 5\,cc/mol$, we have

$$\begin{aligned} c_p/c_0 &= 0.87 \qquad (\text{for } p = 1\,\text{atm}) \\ &= 4 \times 10^{-6} \qquad (\text{for } p = 100\,\text{kbar}). \end{aligned}$$

With this large difference, the solubility line in the phase diagram of an alloy containing interstitial atoms is shifted to the low-concentration side with increasing pressure.

The decrease in vacancy content with increasing pressure would reduce nucleation sites for transformation; furthermore, it would delay the diffusion of substitutional atoms through vacancies. These effects are associated with the stabilization of austenite, which will be mentioned in later sections.

5.1.3 Effect of pressure on T_0 and M_s temperatures for the $\gamma \rightarrow \alpha$ transformation and the equilibrium diagrams of iron alloys

The effect of pressure on the transformation temperature of an iron alloy can be calculated from the Clausius–Clapeyron equation, as for pure iron. However, a rough estimate can also be obtained in the following way. Since the ΔH and ΔV of an iron alloy are not much different from those of pure iron, it can be considered that the T_0–composition curve for an iron alloy is lowered by the same amount as for pure iron when the pressure is increased. Consequently, the M_s temperature is also lowered. This problem was first investigated by Kulin *et al.*[15] They showed that the M_s temperature of an Fe–30% Ni alloy was lowered at the rate of 8°C/kbar under hydrostatic pressure. Similar phenomena were experimentally confirmed in Fe–Cr,[16–18] Fe–Si,[19] Fe–V,[20] Fe–Ru,[21] and Fe–Ni.[22–27] In Fe–Cr alloys, with an increase in pressure, the A_3 point is lowered, and the γ loop region is widened up to 20% Cr.[16] Therefore, the $\gamma \rightarrow \alpha'$ martensitic transformation can take place even in high chromium alloys under high hydrostatic pressure. In Fe–Mn alloys, as shown in Fig. 5.2, the $\gamma \rightarrow \varepsilon$ boundary is shifted to the high-temperature side and the α–ε boundary is shifted to lower manganese contents with an increase in pressure.[28–30] On the other hand, an Fe–22% Cr–8% Ni alloy does not transform, even under 124 kbar.[31]

In Fe–C alloys, since the equilibrium concentration of interstitial atoms is markedly decreased with pressure, as mentioned earlier, the solubility of carbon atoms in both the α and γ phases is markedly reduced with pressure. Because the specific gravity is larger, in the order α, γ, and cementite, both the A_3 and A_1 points are lowered and the eutectoid composition is shifted to the lower carbon content with increasing pressure.[14,32,33] Figure 5.3 shows the Fe–C diagram obtained under 34 katm. Accordingly, the M_s point

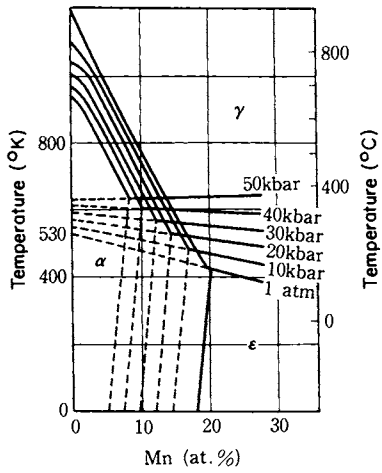

FIG. 5.2 Effect of pressure on Fe–Mn phase diagram. (After Yershova and Ponyatovskij.[28])

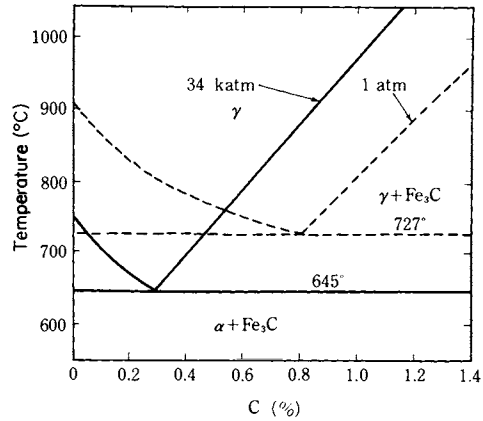

FIG. 5.3 Effect of pressure on Fe–C phase diagram. (After Hilliard and Cahn.[14])

is lowered with an increase in pressure, as shown in Fig. 5.4.[34,35] Therefore, the martensite formed under high pressure is microstructurally fine-scaled and hard in comparison with that formed under 1 atm. The required driving force for the martensitic transformation under high pressure is 60–70 cal/mol larger than that under 1 atm in 0.22–0.56% C steels.[35] Furthermore, the hardenability is improved by an increase in pressure.[36–38] For example, in a 0.09% C steel at 29 kbar,[39] the martensitic structure is easily obtained, even with a cooling rate as low as 200°C/sec. The A_s temperature is also lowered with an increase in pressure.[40] For example, the A_s point of an Fe–28.4% Ni–0.5% C alloy is 380°C under 1 atm, and is decreased 4°C/kbar with an increase in pressure.[41]

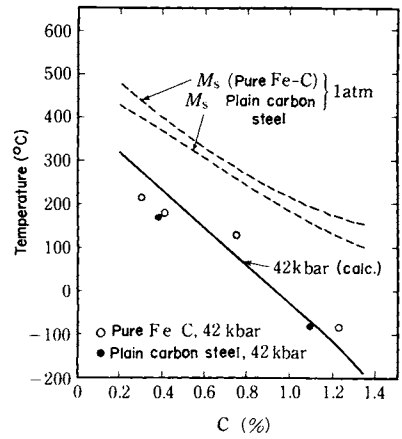

FIG. 5.4 Effect of pressure on M_s temperature of Fe–C alloys. (After Radcliffe and Schatz.[34])

The substructure of martensite is also affected by pressure. In carbon steel martensites under 1 atm, internal twins are observed only in steels containing more than 0.4% C, whereas under 40 kbar twins are observed at carbon concentrations down to 0.2%.

As mentioned earlier, in almost all iron alloys the γ phase is stabilized with pressure. Even in the usual case of quenching under 1 atm, however, the martensite exerts a compressive stress on the surrounding austenite because of volume expansion due to transformation. Therefore, it is considered that the retained austenite is somewhat stabilized by such a stress.

Similarly, in the case of reverse transformation, the A_s point is lowered by hydrostatic pressure. Pope and Edwards[42] investigated this phenomenon using Fe–Ni base alloys. They found that the A_s decreased at first at 30°C/kbar with increasing pressure in an Fe–30.3% Ni alloy. At around 2.3 kbar pressure, however, the A_s temperature suddenly increased and then, when the pressure exceeded 6 kbar, gradually fell. They suggested that the rise in A_s between 2.3 and 6 kbar was due to strain hardening of the martensite.

5.1.4 Nonferrous alloys

Phenonema similar to those just described for iron alloys are observed in nonferrous alloys. For example, the M_s temperature of the β phase in Cu–Al alloys is depressed below room temperature under a pressure of 30 kbar.[43] This change is also related to the volume expansion upon transformation.

5.1.5 Transformation induced by ultrahigh pressure

High pressures above 100 kbar are usually obtained by utilizing explosives. Since explosion waves consist of cycles of expansion and contraction in one direction, an attendant plastic deformation occurs, which will be men-

tioned later. However, the effect of high hydrostatic pressure due to a shock wave is considered to be predominant because one cycle of the wave is very short. Furthermore, the temperature of the specimen would be increased locally by the explosive wave. Transformations induced by explosions have been described in Section 3.7.2.

5.2 Stress-induced transformation

5.2.1 Reasons for the formation of stress-induced martensite

It has long been known that in some alloys the martensitic transformation occurs by deformation.[44,45] A typical example is stainless invar (Co–36% Fe–8.7% Cr).[46] Figure 5.5 displays x-ray photographs showing the phase transformation induced by tensile deformation. Even though this alloy is f.c.c., after slow cooling from a high temperature to room temperature, as shown in Fig. 5.5a, it transforms almost completely to martensite (b.c.c.) by a tensile deformation of 46%, as shown in Fig. 5.5b.

First consider the effect of tensile stress. As mentioned in the preceding section the transformation temperature is lowered by pressure in alloys that expand on transformation (such as the $\gamma \rightarrow \alpha'$ transformation in iron alloys). By the same reasoning, the transformation temperature must be raised if the specimens are subjected to negative pressure. Although we cannot practically obtain a negative hydrostatic pressure, in effect a negative pressure is operative when a tensile stress is applied, and doing so raises the transformation temperature. Thus, transformation is induced by the application of a tensile stress at a temperature just above the M_s.

Shear stresses also induce transformations. The martensitic transformation in effect takes place by a lattice deformation of the parent crystal, as described

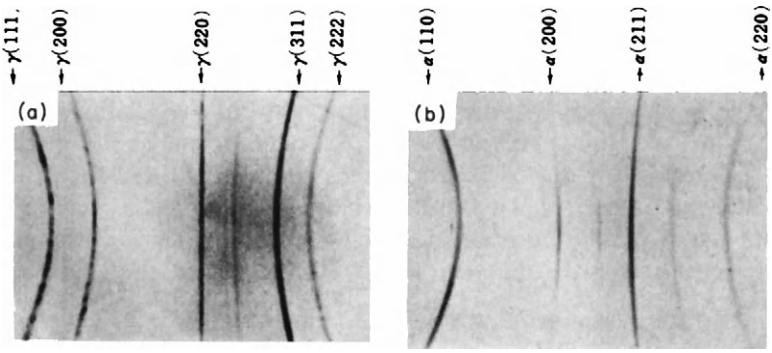

FIG. 5.5 Debye–Scherrer photographs showing transformation induced by tensile deformation (stainless invar, Co–36% Fe–8.7% Cr, Co–K radiation). (a) Before deformation (f.c.c.). (b) After 46% deformation by tension (b.c.c.). (After Nishiyama.[46])

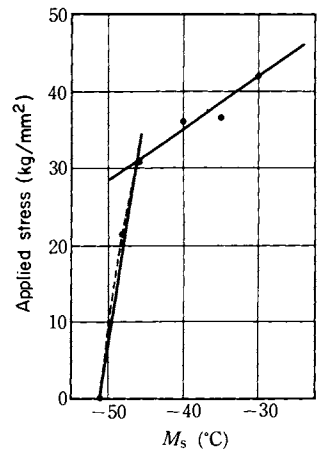

FIG. 5.6 Correlation of M_s temperature with applied stress (Fe–31.7% Ni). (After Hosoi and Kawakami.[53])

in Chapter 1. Such lattice deformation is brought about by shear deformation. Therefore, the transformation must be favored by applying a shear stress of suitable sense.[47–49] The driving force necessary for transformation is reduced by a portion of the mechanical work performed by the shear stress.[50] The M_s is thus raised when stress is applied to the specimen.† If the M_s resulting from external stress is above room temperature, martensite will form by the application of stress at room temperature. This lends support to the embryo theory for the nucleation of martensite.

We now introduce the study by Hosoi and Kawakami[52] as an example showing that the M_s temperature is raised by stress.‡ These workers used austenitic specimens of an Fe–31.7% Ni alloy ($M_s = -51°C$) that was heated for 60 min at 1100°C and then air cooled. These specimens were deformed in tension at various temperatures, and the stress–strain curves were recorded. In general, serrations were observed in the stress–strain curves when martensite was induced during deformation. The stresses at which serrations began to appear at various temperatures were measured to determine the M_s temperature under stress. Their results are shown in Fig. 5.6, which indicates that the M_s is raised by an increase in stress, but the relationship is not linear. In discussion, the workers theoretically estimated the increase in the M_s temperature due to external stress by applying the theory proposed by Patel and Cohen[54] that assumes the mechanical work (U) from the action of applied stress during transformation reduces the driving force for the martensitic transformation. The work (U) varies with the angle between

† In the case of fine particles, the M_s temperature is also raised by external stress, as in the case of large particles.[51]

‡ There is another investigation in which the rise in M_s temperature caused by stress was measured in several Fe–Ni–C alloys.[53]

the specimen axis and the normal to the martensite habit plane. It was assumed that the M_s temperature is associated with martensite plates having the maximum work (U_{max}). It is known, regarding the transformation strain, that the shear strain is 0.20 and the normal component is 0.05; consequently, U_{max} becomes 2.0 cal/mol under 1 kg/mm^2 tension. On the other hand, applying the equation proposed by Kaufman and Cohen[55] for the difference in chemical free energy ($\Delta F^{\gamma\to\alpha'}$), we obtain $d\Delta F^{\gamma\to\alpha'}/dT = 1.2$ cal/mol °C. Then the rate of increase of the M_s due to an applied stress is

$$\frac{dM_s}{d\sigma} = U_{max}\Big/\frac{d\Delta F}{dT} = 1.6 \quad (°C/kg/mm^2).$$

Although this result is slightly larger in comparison with that derived from Fig. 5.6, it may be concluded that the experimental result is generally in agreement with the theoretical one, if one allows for approximations used in the theory. As shown in Fig. 5.6, the rate of rise of the M_s temperature is larger in the higher stress region. This may be due to the effect of plastic deformation in addition to the applied stress.

The transformation start temperature, which can be raised by an externally applied stress or by plastic deformation, is called the M_d temperature. The M_d temperature has an upper limit, which must be T_0, since the external stress or plastic deformation can only supplement the driving force for the martensitic transformation.

A similar phenomenon is observed for the A_s temperature; that is, the reverse transformation takes place at a temperature lower than A_s in the presence of an externally applied stress or plastic deformation. The start temperature of the reverse transformation under stress is called the A_d temperature. The A_d and M_d temperatures approach T_0 with an increase in stress or plastic strain, and would theoretically coincide with T_0 if the adiabatic transformation effect (cf. Section 4.6.3) were absent.

5.2.2 Examples of stress-induced transformations

Besides the examples described in the preceding section, many investigations have been made of the $\gamma \to \alpha'$ transformation induced by applied stress.[56–61] The most popular example is that in stainless steels. The variation of martensite content with elongation in an Fe–14.8% Cr–12.6% Ni alloy ($M_s = -78$°C) is shown in Fig. 5.7.[62] Here the martensite content is barely increased from small strains, but is rapidly increased above about 6% strain. However, the formation of martensite slows down above about 15% strain, which indicates that the stabilization of austenite occurs. Of course, such a tendency would vary with a change in chemical composition.[63] Similar behavior has also been observed in Fe–Ni–C alloys.[64]

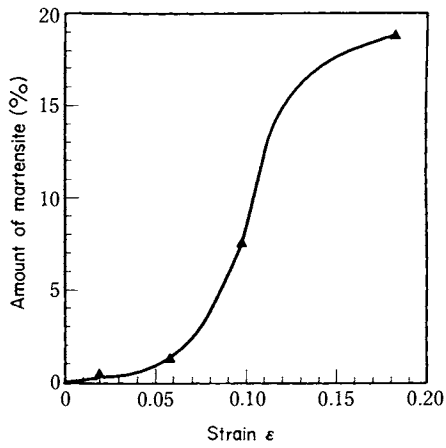

FIG. 5.7 Change in amount of martensite during deformation at −40°C (Fe–14.8% Cr–12.6% Ni). (After Breedis.[62])

Strain-induced transformation has also been observed in an Fe–30% Ni alloy, although the amount of transformation is small.[56] In this alloy, even when the surface of a specimen is barely picked with a needle, α' martensite is induced (Chapter 2). In this case, the transformation is considered to be of the schiebung type.[57] For this alloy, stress-induced transformation is more pronounced at lower deformation temperatures, and the lattice orientation relationship deviates slightly from the N relationship.[58] The behavior of this transformation depends markedly on the nature of the stress (negative or positive) and orientation of the crystals.[65–69]

Stress-induced martensite is frequently seen on a fractured surface due to the high stress there. For example, in 3.5% Ni[70] and 1.5% Cr steels,[71] retained austenite transforms completely at the fractured surface. It is also reported that a small amount of transformation occurred upon neutron irradiation in a 347 stainless steel.[72]

The transformation from the γ (f.c.c.) to the ε (h.c.p.) phase is also easily induced by stress. The reason is that the lattice strain in this transformation is a typical shear mode and the chemical free energy difference between phases is small over a relatively wide temperature range. As already described in Section 2.3, the $\gamma \rightarrow \varepsilon$ transformation occurs in high manganese steels. In this case, ε martensite forms at an early stage of deformation and α' martensite is induced later.[73†] As already mentioned, in 18–8 stainless steel ε martensite as well as α' are induced, although in small amounts, by deformation at liquid air temperature.[75‡] For these steels, the transformation proceeds even at low (near 0°K) temperatures. This observation is regarded

† The $\varepsilon \rightarrow \alpha'$ transformation also occurs at a later stage of deformation.[74]

‡ Guntner and Reed[76] showed the amount of α' and ε martensite produced by deformation.

as experimental evidence that the martensitic transformation takes place by a shear mechanism.[77]

The ordered β_1 phase in the Cu–Pd system is transformed to a disordered f.c.c. structure by deformation.[78] In Cu–14.2% Al–4.3% Ni the β_1' phase forms by deformation,† whereas γ_1' forms upon cooling.[79,80] In the case of deformation of β brass, the f.c.t. structure is induced at low strains and the f.c.c. structure at high strains, as mentioned in Section 2.5.2. Such a phenomenon has also been observed in Ag–Cd[81] and Ag–Zn[82] alloys. Furthermore, stress-induced transformations have been observed in Ti alloys,[83–87] Pu,[88,89] and alloys that exhibit a second-order-like transformation, such as In–Tl,[90,91] Au–Cd,[90,91] and Ti–Ni.[92] In some alloys, for example, a Ti–6% Al–4% V alloy, transformation induced by external stress takes place at elevated temperatures.[93]

5.2.3 Transformation-induced plasticity and TRIP steel[94]

Martensite formed by deformation is called *strain-induced martensite.* When such a transformation occurs, the ductility of the alloy increases substantially.‡ The phenomenon was recognized by Sauveur[96] in 1924 in torsion tests of iron bars, and is termed transformation-induced plasticity.[97,98] Recently, this phenomenon has attracted special interest because of its practical applications. Steels having such properties are called TRIP (for *tr*ansformation-*i*nduced *p*lasticity) steels.[99]

Tamura *et al.*[100,101] investigated the TRIP phenomenon using metastable austenite iron alloys. They studied the transformation behavior and tensile properties during deformation. Figure 5.8a§ shows the effect of deformation temperature on martensite content after tensile tests on an Fe–29% Ni–0.26% C alloy ($M_s = -35°C$, f.c.c. in the annealed state). It indicates that with lowering test temperature, the transformation begins to occur at the M_d temperature, which is 40°C above M_s, and that at the M_s temperature as much as 80% martensite is formed. Typical TRIP behavior is represented in Fig. 5.8b; with decreasing test temperature the elongation rapidly increases from just below M_d, reaches a maximum value around $-10°C$, and then decreases abruptly. It is evident that the enhanced elongation is caused by the martensitic transformation upon deformation.

Three possible causes have been considered for the temperature dependence of elongation. First, just below the M_d temperature, variants whose

† Above the A_f temperature.

‡ The anomalous improved ductility due to transformation under stress has also been observed for diffusional phase transformations.[95]

§ The strain rate was 5.5×10^{-4}/sec, and the amount of martensite was measured from the ratio of integrated intensities of $(110)_\alpha$ and $(111)_\gamma$ reflections in x-ray diffraction patterns.

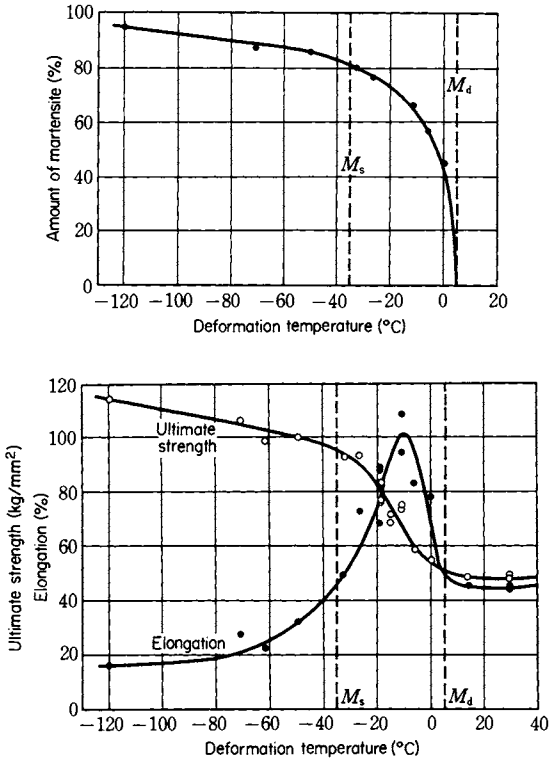

FIG. 5.8 Transformation-induced plasticity in tensile tests at various temperatures (Fe–29% Ni–0.26% C). (a) Amount of martensite after tensile tests. (b) Elongation and tensile strength. (After Tamura, *et al.*[101])

formation contributes to the elongation of the specimen are formed preferentially. As the large chemical driving force becomes available at temperatures near M_s, variants of all orientations can form. This randomized behavior lowers the elongation. Almost all martensites formed below the M_s are not stress induced. Therefore, the elongation must be caused only by the plastic deformation and thus is generally small. The second cause is the suppression of necking. When martensite is formed during tensile deformation, the strain hardening becomes large. Under such conditions, it is expected that necking be suppressed and uniform elongation enhanced. Third cause is the suppression of the initiation and propagation of microcracks by relaxation of stress concentrations due to the formation of strain-induced martensites. The variation of tensile strength with test temperature corresponds well with the percentage of martensite, as shown in Fig. 5.8.

In an Fe–Ni–C alloy, the morphology of strain-induced martensite formed at a certain temperature range is butterflylike or needlelike, and the interface between the martensite and its matrix is irregular, which is quite different from that of thermally transformed martensite (which takes the form of lenticular plates). Generally speaking, since the M_s temperature is raised by deformation, the martensite exhibits morphologies similar to those characteristic of martensite having higher M_s temperatures.[102] Such a morphology change in strain-induced martensite is expected to affect the mechanical properties.

A large elongation is also produced when a specimen under constant load is subjected to thermal cycles through the transformation temperature. For example, an elongation of 160% was obtained in an Fe–15.4% Ni alloy after 150 cycles in the temperature range 204°–646°C under a tensile stress of 7900 lb/in.^{2}.[103]

5.2.4 Autocatalytic effect[104–106]

It has already been mentioned that a martensite plate produces a stress field in the surrounding austenite and that additional transformation is induced by stress. Especially in the case of the umklapp transformation, the stress field accompanied by kinetic energy is very large, and therefore the umklapp transformation occurs as a chain reaction. This behavior is called the *autocatalytic effect*. In some cases of the $\gamma \rightarrow \alpha'$ transformation in iron alloys, the transformation occurs explosively. Such transformation behavior is called the *burst effect*. It has been considered that in order for the burst phenomenon to occur, small amounts of C or N are essential.[107] The burst phenomenon is closely related to the stabilization of austenite, and will be considered again in Section 5.7.4.

5.2.5 Change in close-packed layer structure induced by stress

It has been described in Section 2.5 that there are numerous close-packed layer structures, based on f.c.c. and h.c.p. lattices. The difference in energy among these structures is very small and slip along layers is apt to take place easily; hence, the transformation from one close-packed structure to another is easily induced by applying a stress.

For example, in a Cu–Al alloy the β_1' martensite has an ordered 9R structure consisting of 18 atomic layers. This martensite changes to a mixture of f.c.c. and h.c.p. structures when subjected to plastic deformation, as described in Section 3.2.4C.[108] This suggests that both f.c.c. and h.c.p. structures have a lower lattice energy than the 9R structure.

In some cases, the metastable f.c.c. structure may change to h.c.p. under plastic deformation. High manganese steels are typical examples (cf. Section 2.3). Similar examples are also found in nonferrous alloys. Barrett[109] has observed that for Cu–(4–5.4)% Si alloys the κ phase (h.c.p.) is precipitated from the α phase (f.c.c.) when specimens are slow cooled from a high temperature; however, a mixture of f.c.c. and h.c.p. phases is obtained when the specimens are rapidly quenched to prevent the occurrence of diffusional transformation. In this case, both phases (f.c.c. and h.c.p.) have the same composition and the newly formed h.c.p. phase has many internal stacking faults; hence, the h.c.p. phase is considered to be produced from the f.c.c. phase by a martensitic transformation. This transformation may be caused by thermal stress during quenching. A similar phenomenon has been observed in a Cu–12.5% Ge alloy.[110]

These phenomena were originally observed in Co alloys, particularly in Co–30% Ni.[111] When the WC–Co hard metal[112,113] is stressed at low temperature, the f.c.c. phase changes to the h.c.p. phase by a martensitic transformation.

5.2.6 Thermoelastic martensite and the shape memory effect[114]

Kurdjumov and Khandros[115] studied the β_1-to-γ_1' martensitic transformation and the reverse γ_1'-to-β_1 transformation in a Cu–14.7% Al–1.5% Ni alloy ($M_s = 70°C$), and found that the γ_1' martensite plate produced last on the initial transformation is the first to undergo reverse transformation.† This phenomenon was attributed[117] to an elastic strain that might have been stored in the martensite during the initial transformation and thus might enhance the reverse transformation. In these transformations, therefore, it can be supposed that the chemical driving force for transformation is balanced by the nonchemical energy. In other words, the growth and shrinkage of the martensite plates occur under a balance between thermal and elastic effects, and thus the transformation can be reversible. Martensites that exhibit such reversibility on cooling and heating are generally called *thermoelastic* martensites. Alternate prerequisites for their occurrence are (1) small lattice deformation for the transformation, (2) martensites containing internal twins that can be easily detwinned, and (3) martensites having an ordered structure that cannot be destroyed by slip.

Martensites in β brass are well known to be induced by stress;[118–121] ‡ they also exhibit thermoelastic behavior.[123] Figure 5.9 shows an electrical resistivity versus temperature curve associated with the martensitic and the reverse transformations in β brass. It is seen that the temperature range of

† There is another report[116] that this transformation is not perfectly reversible.

‡ Stress-induced martensites are also found in the β phase of Ag–Zn alloys.[122]

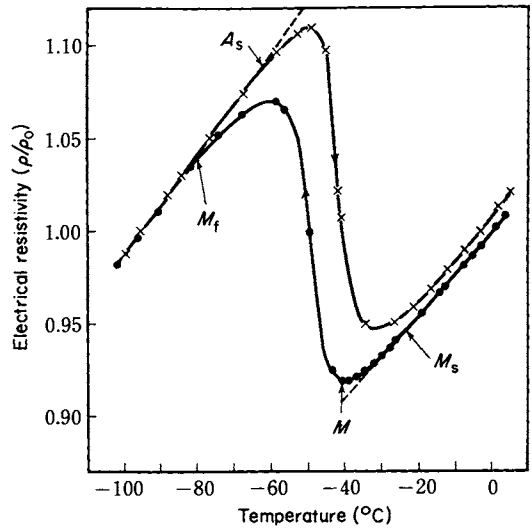

FIG. 5.9 Change in electrical resistivity during the martensitic transformation in Cu–38.8% Zn. (After Hummel and Koger.[125])

the transformation on cooling overlaps that on heating, and the M_s temperature is higher than the A_s temperature.[124–126] Such behavior is not observed in ordinary martensitic transformations in ferrous alloys, and may be attributed to the thermoelastic characteristics. Thermoelasticity of martensites is also found in Ag–Zn[127] and In–Tl[128–130] alloys.

A. *The shape memory effect*

According to an experiment by Arbuzova *et al.*,[131] γ_1' martensites in a Cu–14.44% Al–4.75% Ni alloy can be nucleated and grown by stress even at a constant temperature if the temperature is suitable. All the martensite crystals produced in this case have such orientations that the strain associated with their formation relieves the applied stress. If such a specimen is heated to a temperature somewhat higher than A_s, the γ_1' martensites may revert to the parent phase, producing strain in the inverse direction.[132] Actually, it was found that a plastically deformed specimen of martensite reverted to its original size upon being heated.† This phenomenon is termed the *shape memory effect.*

The phrase "memory effect," in a broad sense, may also be used to mean that martensite crystals partially revert to the original parent phase orientation upon reverse transformation. The memory effect in this sense

† This phenomenon was also examined by electrical resistivity measurements.[133]

was previously known to exist in other alloys exhibiting martensitic transformations (see, e.g., Fig. 3.25). In those cases, however, the effect was not so perfect as in the Cu–Al–Ni alloy, and no attention has been paid to the external shape of the specimen. Recently interest has been concentrated on alloys whose shape memory is perfect or nearly perfect.[134] In this case, Wayman and Shimizu[135] advocated a new term, "marmem," because shape memory is always related to the martensitic transformation.

Alloys having such properties, in addition to the Cu–Al–Ni alloys, are TiNi,[136,137] Au–Cd,[138] Cu_3Al,[139] Fe–Pt,[140] $Cu_{1-x}Au_xZn$[141–143] (near the composition of the Heusler alloy $CuAuZn_2$), and β_1' NiAl.[144–147]

As to the origin of the shape memory effect, the following considerations are presented: One[148] is that, on reverse transformation, internal stress† stored in deformation-induced martensites facilitates shearing in the direction opposite to that of the deformation.‡ This consideration applies also to the imperfect shape memory that is observed in ordinary reverse transformations. However, it is not applicable in the case of martensites that were deformed after transformation by cooling; moreover, there is no guarantee that the internal stresses make the martensites shear along the direction opposite to that of the deformation. Thus, this consideration is not reasonable for the perfect or nearly perfect shape memory effect. In view of these circumstances, Otsuka *et al.* gave a more reasonable interpretation for the shape memory effect on the basis of their experiments on TiNi[150] and Cu–14.2% Al–4.3% Ni[151,152] alloys. According to their explanation, deformation resulting from an applied stress occurs by detwinning of transformation twins (i.e., twin boundary movement) in martensites produced on cooling, and/or by transformation of retained austenite to martensite. On the reverse transformation, the detwinned regions revert to the original orientation of the parent lattice because of the internal stress stored in the martensite. Similarly, deformation-induced martensites also revert to the original orientation of the parent lattice. Moreover, it was emphasized that any irreversible deformation mode, such as slip, should not occur in such a reversible phenomenon. For easy detwinning of transformation twins, a small lattice deformation and easy mobility of transformation dislocations may be necessitated. In addition, a superlattice structure in the parent phase may also promote the shape

† If this consideration were correct, specimens that have undergone a single-interface martensitic transformation would not exhibit the shape memory effect because internal stress is never stored in martensite. However, the effect is actually observed in such specimens.

‡ Apart from martensitic transformations, a similar memory effect was observed in an iron single crystal. According to the reference,[149] under certain conditions an α iron single crystal remained single even when heated above A_3 and cooled to the α region. Conditions were such that the heating and cooling rate were kept constant at 20°C/hr and the heating temperature was 6°C higher than the A_3. The most important factor for this memory effect is a small concentration of carbon or nitrogen atoms.

memory effect, because the superlattice structure would be destroyed by deformation and so the energy would be increased, if the reverse transformation were not performed by shear processes that are perfectly inverse to those involved in the initial martensitic transformation and subsequent deformation. Thus, it is understood why an ordered Fe_3Pt alloy undergoes a thermoelastic martensite transformation and exhibits the shape memory effect,[140,153] whereas the disordered alloy does not.

Enami *et al.*[154] recently reported that in a 304 stainless steel deformed at $-196°C$ the shape of a specimen approaches that of the original when the specimen is heated to room temperature or about 100°C. In this case two martensitic transformations, γ to ε and γ to α', are induced by deformation, but the α' martensites do not contain transformation twins, and the amount of ε martensite is decreased on holding the specimen at room temperature. Therefore, the shape memory effect may be attributed only to the reverse $\varepsilon \rightarrow \gamma$ transformation. A similar shape memory effect is also found in an Fe–21% Cr–14% Mn–0.68% N steel.[155] Such shape memory effects in a broad sense can be found, to a greater or lesser extent, in many other alloys[156] that undergo martensitic transformations. This imperfect effect is rather a shape recovery effect associated with reverse transformations, and should be distinguished from the so-called shape memory effect, by which a deformed specimen reverts completely to its original shape.

As mentioned in Section 3.6, a kind of shape memory effect can be brought about merely by removing an applied stress. This is called rubberlike behavior, or pseudoelasticity, when it occurs below the M_s point and is not associated with the reverse transformation; this behavior is found in Au–Cd and In–Tl alloys. On the other hand, a similar effect such as is found in Cu–Zn and other alloys is called superelasticity when it occurs above the M_s and is associated with the reverse transformation.

5.2.7 High damping during martensitic transformation

When elastic vibrations are applied to thermoelastic martensite, forward and reverse transformations take place alternately, dissipating the vibrational energy.[157,158] Therefore, if the stress-induced martensitic transformation occurs in an alloy, the alloy will have a high damping capacity for vibrations in the temperature range in which the transformation occurs.

Such a phenomenon has been known from early days.[159–162] Scheil and Thiele[161] studied the torsional vibration of a wire of Fe–22.4% Ni resistance-heated to high temperatures. They found remarkably high vibration damping over the temperature range of transformation as shown in Fig. 5.10. The logarithmic decrement is very high at temperatures between M_s (135°C) and 50°C. The apparent elastic modulus is correspondingly low.

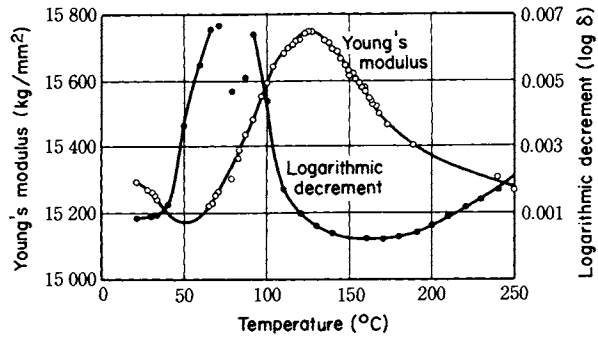

FIG. 5.10 Change in elastic modulus and damping due to martensitic transformation (Fe–22.4% Ni). (After Scheil and Thiele.[161])

The phenomenon of high damping is also observed in alloys exhibiting a second-order transformation, such as Mn–Cu,[163–166] Au–Cd,[164,167] and so on.†

High damping is also observed for ultrasonic waves, for example, in the TiNi alloy.[167]

The diffuse scattering of neutrons by phonons has been studied using $AuCuZn_2$,[171] and anomalous scattering observed at the transition temperature has been explained as due to the instability of the phonons, which are polarized in the $[1\bar{1}0]$ direction and are propagating along the [110] direction.

5.3 Effect of lattice defects existing before transformation

It is expected that lattice defects in the parent phase affect the regular rearrangement of atoms during the martensitic transformation. Usually there are many different kinds of defects in the parent phase. Most investigations have observed the combined effects of these various defects, and it is difficult to separate the effects from one another. Nevertheless, some considerations of the contribution of each kind of defect will be given in the following subsections.

5.3.1 Effect of lattice vacancies

The density of vacancies is higher at higher temperatures.‡ In the conventional quenching process, the high density of vacancies existing in the

† High internal friction values at the transformation temperature are observed even in some cases other than martensitic transformations, such as occur in Fe,[168] Co–Ni,[169] etc. Theories have been proposed for these cases.[170]

‡ For example,[172] in an Fe–29% Ni alloy quenched from 1050°C to 4°K, the concentration of frozen-in vacancies is 0.5 at.%, as estimated from the electrical resistance increase.

parent phase at the austenitizing temperature is brought to the M_s temperature and then martensitic transformation occurs. These vacancies may make it easier for the transformation to occur, because an atom is more mobile in the region of a vacancy. Consequently, the driving force for transformation may become smaller and the formation of nuclei and their growth may become easier. If the quenching temperature is higher, the density of vacancies is higher and the transformation may be further enhanced, giving an increase of the M_s temperature. If an alloying element can affect the vacancy density of the parent phase, the martensitic transformation is influenced this way as well as by the change in chemical free energy due to alloying elements.

In the foregoing discussion, however, the contribution of impurity atoms was not taken into consideration. Usually, a considerable amount of impurities exist, especially in iron alloys. The impurity atoms trap the vacancies, so that the density of free vacancies is generally thought to be considerably decreased before the occurrence of the martensitic transformation. This is why the effect of vacancies on the transformation is not usually taken into account.

Since neutron irradiation produces vacancies and interstitials, it must also have an effect on the martensitic transformation. Reynolds *et al.*[173] found in an austenitic stainless steel that the ferrite content was increased by neutron bombardment during transformation. Porter and Dienes[174] observed a similar effect of neutron irradiation promoting the martensitic transformation in an Fe–25.5 at. % Ni alloy using a neutron flux of 10^{17} nvt. The M_s temperature of the alloy, determined after irradiation, however, was found to be lowered approximately 6°C by the damage produced. This means that the austenite retained after irradiation is stabilized by the lattice defects introduced by the irradiation.

5.3.2 Effect of dislocations

Around an edge dislocation, there are two regions of high and low atomic density, which give rise to compressive and tensile strains. These strains can enhance the nucleation of the transformation and consequently an increase in the M_s temperature is expected. However, there is also a possibility that the growth of nuclei is suppressed by dislocations. It is not known which contribution is dominant.

5.3.3 Effects of stacking faults and twin faults

Both stacking faults and twin faults in the parent phase may have effects similar to dislocations with respect to the martensitic transformation. The twinning dislocation governing these faults in f.c.c. materials has a Burgers vector $a/6\ \langle 112 \rangle$. Upon further splitting into two half dislocations, the atomic arrangement of the lattice between these is nearly b.c.c.[175] This

suggests that martensite nuclei are easily formed in this region. Actually, martensite platelets have been observed at stacking faults by electron microscopy, as described previously (see Section 3.4). Furthermore, it is reported[176] that the schiebung transformation took place at regions about 1 μm wide along twin boundaries at a temperature 20°C higher than usual. This indicates that twin faults can produce transformation nuclei.

5.3.4 Surface effect and M_s temperature of surface martensite

In general, the lattice energy at the surface of a crystal is higher than that in the interior. The energy difference depends on the composition and crystal orientation. Similarly, the boundary energy between the transformed phase and the matrix depends on the composition and crystal orientation of both phases. It follows that the M_s temperature of the surface region may in some cases be higher and in other cases lower than that in the interior.

Honma[176] showed an example of the higher M_s point at the surface. Table 5.1 from his work gives the M_s temperatures at the surface and in the interior for several Fe–Ni alloys. The former were measured from surface relief observations and the latter by dilatometry. The M_s temperature in a surface layer about 0.02 mm thick was higher by 10°–30°C than that in the interior. The different morphology of the surface martensite has been discussed in Section 2.2.

In the investigation by Huizing and Klostermann,[177] austenite single crystal spheres 0.1–0.3 mm in diameter of Fe–(25.7–30.6)% Ni alloys were transformed to martensite. The amount of martensite formed at the surface was larger, and the amount of retained austenite was less, than that in the interior, in agreement with the previous results of Honma.

The surface effect on the M_s temperature is supposed to be very marked in the case of thin foils. Actually, Warlimont[178] found that the M_s temperature of a thin foil 50–1000 Å thick was higher than that of a bulk specimen

TABLE 5.1 M_s **temperatures of surface and interior martensites in Fe–Ni alloys**[a]

	M_s (°C)	
Ni (%)	Interior (by dilatometer)	Surface (by relief)
25	100	110
27.5	50	65
28	32	55
29	5	25
29.5	−10	20

[a] After T. Honma.[176]

of the same material. The difference was 90°C in Fe–5.1% Mn–1.15% C, 40°C in Fe–30.9% Ni, and 54°C in Fe–31.7% Ni. Nagakura *et al.*[179] obtained a higher M_s point using vapor-deposited films of Fe–(14.35–27.1) at.% Ni 500–1500 Å thick. Recently, Warlimont[180] measured the M_s temperature more accurately by using foils of Fe–(30.0–32.6)% Ni 0.4–12 μm thick; the measured values were highly scattered. This finding was interpreted in terms of two surface effects, one raising and the other lowering the M_s temperature.

The lowering of the M_s due to the surface effect, in most cases, often overlaps the effect due to fine grain size, as will be explained in the next paragraph. For example,[181,182] thin cobalt foils vapor deposited below the transformation temperature exhibit abnormal structures. In foils about 130 Å thick, the structure is f.c.c., which is commonly observed as the high-temperature modification, whereas, in 1300-Å foils the h.c.p. phase, the common low-temperature modification, forms. In foils between 130 and 1300 Å thick, mixtures of f.c.c. and h.c.p. phases are found. This abnormality may be due to the surface effect, which lowers the boundary temperature between the stable ranges of f.c.c. and h.c.p. structures.

5.3.5 Effect of parent phase grain size

A grain boundary might be considered a preferential site for martensite nucleation because it is an extensive defect. Actually, however, grain boundaries serve to stabilize the parent phase and thus hinder the martensitic transformation, as will be described next. Grain boundary atoms are relatively stable to martensitic transformation for they are partly free from restriction by neighboring atoms and tend not to take part in the coordinated atom movements of such transformations. Moreover, the lattice defects near the grain boundary can migrate to the boundary and disappear, and thus the number of nucleation sites is expected to decrease.

The growth of a martensite crystal is also stopped at grain boundaries.† From the foregoing facts, it is concluded that a small grain size results in stabilization of the parent phase.‡

The effect of grain size on transformation is important in practical cases. This kind of study is relatively easy to carry out, and consequently many investigations[185–190] have been made.

† Thomas and Vercaemer,[183] using an Fe–20 at.% Ni–19 at.% Cu alloy, measured the size of martensite crystals formed in a matrix consisting of two concentration layers that were formed by the spinodal decomposition, and found that the martensite grain size was larger than the wavelength of the concentration fluctuation.

‡ Neither of the two effects just described holds for large grains. When a specimen is heat treated so as to increase the grain size markedly, the number of lattice defects in the specimen is decreased, and more substitutional elements may go into solution; hence, the M_s temperature is observed to be low in spite of the large grain size.[184]

TABLE 5.2 Stabilization of austenite by fineness of grains in Fe–31.5% Ni–0.02% C alloy[a]

Average austenite grain diameter (μm)	Amount of retained austenite at -195°C (%)
60	5
9.4	12
0.6	74

[a] After Leslie and Miller.[187]

A. *Investigations using specimens that were grain-refined by heat treatment or deformation*

Leslie and Miller[187] used an Fe–31.5% Ni–0.02% C alloy for grain refinement studies. The alloy was first transformed to martensite (95%) by being cooled to -195°C, cold worked, and then subjected to reverse transformation by holding for various times at 300°C. With this treatment, austenitic specimens of different grain sizes were obtained. These specimens were cooled again to -195°C to transform them, but there was still some retained austenite. Table 5.2 shows the retained austenite content as measured by x rays. From the results of Leslie and Miller, it is established that the amount of retained austenite increases as the austenite grain size decreases. This means that the austenite grain boundaries impede formation of martensite.†

An old study by Nishiyama[190] was also concerned with the grain size problem. The surface of an annealed and slow-cooled cobalt specimen was examined by x-ray diffraction; unexpectedly, a large amount of f.c.c. phase was found at the surface region. The f.c.c. phase of cobalt is usually unstable at room temperature. To understand this abnormality, examination was repeated after the surface layer of the specimen was removed little by little by etching. It was then found, as shown in Fig. 5.11, that the f.c.c. phase was observed only in a 0.04-mm surface layer where the grain size was extremely fine compared with that in the inner part of the specimen. This shows that

† Before this study, Izumiyana[188] carried out a similar experiment, using Fe–28.5% Ni specimens that were subjected to reverse transformation at 550°C and then cooled. By dilatation measurement, he found the M_s temperature to be 70°C lower than usual. From electron microscopy he found a refinement of the grains.

Krauss and Cohen[189] studied Fe–(30.5–35.5)% Ni alloys that were back-transformed to austenite at 450°–475°C by slow heating. They also recognized stabilization effects. Since the martensite formed from this austenite was found to be enriched in Ni, according to lattice parameter measurement, they suggested that this austenite was chemically stabilized. It is therefore thought that the stabilization found in these investigations is a chemical effect due to diffusion during heating to cause the reverse transformation, as well as stabilization due to a fine grain size.

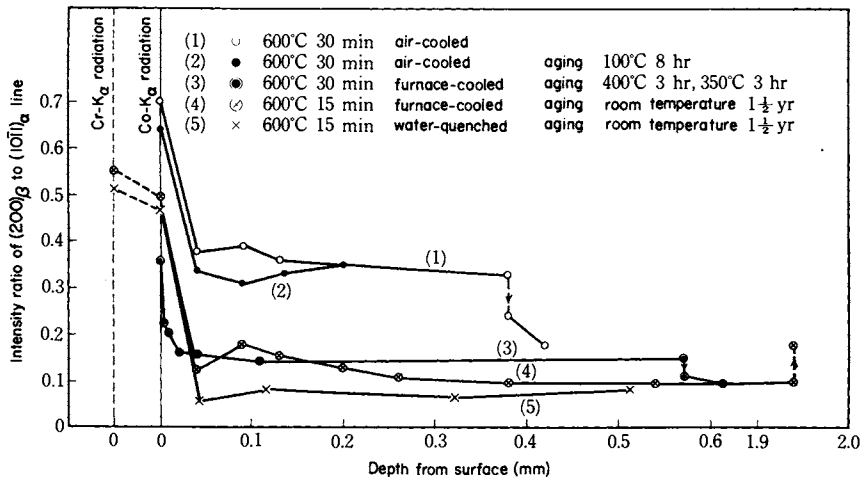
(1) 600°C 30 min air-cooled
(2) 600°C 30 min air-cooled aging 100°C 8 hr
(3) 600°C 30 min furnace-cooled aging 400°C 3 hr, 350°C 3 hr
(4) 600°C 15 min furnace-cooled aging room temperature 1½ yr
(5) 600°C 15 min water-quenched aging room temperature 1½ yr
Cr-Kα radiation
Co-Kα radiation
Intensity ratio of (200)β to (10$\bar{1}$1)α line
Depth from surface (mm)

FIG. 5.11 Residual f.c.c. phase in the surface layer of a cobalt rod. (After Nishiyama.[190])

only the surface layer was not yet coarsened by annealing, since before annealing, the surface layer had been severely deformed by machining. From this experiment it is concluded that a fine grain size decreases the M_s temperature. However, there may also be a surface energy effect to some extent, as explained in the earlier paragraph discussing vapor-deposited cobalt film.

Maksimova and Nemirovskiy[191] reported that a decrease in austenite grain size also lowered the burst transformation temperature M_b. Figure 5.12 shows the M_b in Fe–30% Ni–0.02% C plotted against $d^{-1/2}$ where d is the grain diameter.

A lowering of the M_s temperature with decreasing grain size is also observed in β brass. As described before, β brass can be transformed by stressing. In the investigation of Hummel *et al.*,[192] a β brass specimen was

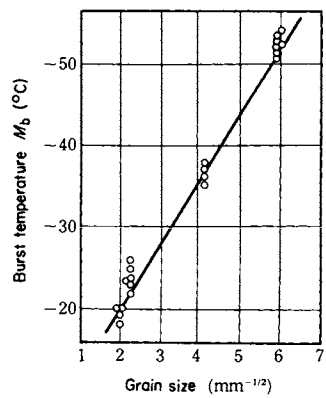

FIG. 5.12 Dependence of burst transformation temperature on grain size (Fe–30% Ni–0.02% C). (After Maksimova and Nemirovskiy.[191])

partially transformed into martensite (α_1)† by rolling and then cooled at a rate of 1°C per minute. On cooling, the residual β_1 was transformed into low-temperature β'' martensite. The M_s temperature of the β_1-to-β'' transition was lowered with reduction by rolling. The M_s was lowered about 30°C by 15% reduction but heavier reductions caused no further change. This can be interpreted as follows: Each β_1 grain was initially partitioned by the α_1 formed during rolling; the increased effect of β_1 boundaries suppressed the formation of β''. The reason the M_s did not change after more than 15% reduction is that α_1 is soft relative to β_1 and hence is deformed preferentially after rolling more than 15%.

B. *Transformation of powder particles*

In the foregoing, we described the effect of grain size on transformation of bulk specimens, in which each grain is restricted by neighboring grains. To avoid the effect of such a restriction, separate particles may be utilized.

Cech and Turnbull[193] used Fe–30.2% Ni powder particles having diameters of 25–100 μm. These particles were made from an oxide by reduction. The powders were subzero cooled and the amount of α' martensite produced‡ was determined by x-ray diffraction from the intensity ratio between the $(110)_{\alpha'}$ and $(111)_{\gamma}$ lines. The amount of α' decreased with a decrease in particle diameter for a constant cooling temperature below 0°C. For ferromagnetic powders selected by magnetic separation, however, the amount of α' did not depend on the particle diameter. These results show that for powders having diameters larger than 25 μm, the particle surface has an effect on the number of particles transformed but not on the amount of transformation. In fact, the burst transformation temperature M_b of powders was much lower than the M_s temperature of bulk specimens. For particles having diameters smaller than 44 μm, about one twentieth of the particles remained untransformed, even after cooling to −196°C. This suggests that heterogeneous nucleation occurred.

Nagashima and Nishiyama[194] examined fine particles (0.01 μm diameter) of 0.9% C and 1.4% C steels made by electric spark machining, and found the retained austenite content to be much larger than that in bulk specimens, according to both x-ray diffraction and electron microscopy.

Kachi *et al.*[195] also studied the size effect, using fine powders of an Fe–27.4% Ni alloy§ made from oxalates by reduction. These powders were

† Since α_1 and β'' have a 9R structure, both of them are denoted by β_1' in Section 2.5.3.

‡ Fe_2O_3 and NiO were mixed according to the alloy composition required, and the mixture was heated for 8 hr at 1350°C, crushed, and reduced by hydrogen to become Fe–Ni alloys.

§ Aqueous solutions of Fe and Ni oxalates were mixed according to the alloy composition required. A 1 *N* solution of oxalic acid was added to the solution to precipitate $Fe_{1-x}Ni_xC_2O_4$. The precipitates were then reduced at 350°–800°C for 25 hr and then rapidly cooled to room temperature. Particle size was controlled by varying the temperature and time of reduction.

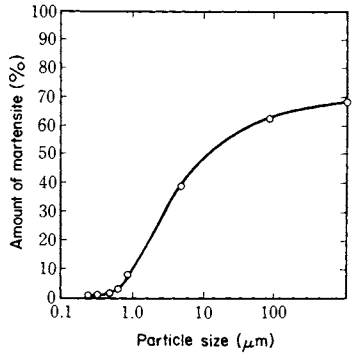

FIG. 5.13 Dependence of the amount of martensite on the particle size of powders (Fe–27.4% Ni alloy powder quenched from a high temperature to room temperature). (After Kachi *et al.*[195])

quenched from a high temperature to room temperature. The amount of martensite in the powders, measured by x-ray diffraction, is plotted in Fig. 5.13, which shows that particles smaller than about 0.8 μm hardly transformed. For larger particles, however, the amount of α' increases with particle size up about 100 μm, and then the effect is saturated. This result means that the austenite in fine particles is highly stabilized. In the same work the authors also used 29.2% and 25.5% Ni powders and obtained essentially the same result.[196]

The foregoing results are also supported by experiments of Klyachko and Baranova,[197] using three kinds of steels: 1.2% C–2% Mn, 1.6% C–3% Mn, and 1.5% C–1% Mn. They first quenched the specimens and then electrolytically separated the austenite into powder particles. Of these powders, particles 5–10 μm in diameter did not transform, even when cooled in liquid nitrogen. On the other hand, rod specimens of the same steels 2.5 mm in diameter were transformed to α' by cooling in liquid nitrogen. The lattice parameter measurement showed that the compositions of both the powder and rod specimens were not different. Therefore the fact that the powders could not be transformed is interpreted as stabilization due to fine particles.

It is frequently observed that the M_f temperature is lowered in powders even when the M_s is scarcely changed. This finding indicates that the particles have different transformation temperatures relative to each other; that is, some particles are stabilized more effectively than others.[198]

C. *Dependency of the nucleation rate of martensite on austenite grain size*

This problem can be studied by the formation rate at an early stage of isothermal martensitic transformation. Raghavan and Entwisle,[199,200] using an Fe–26% Ni–2% Mn alloy, measured the incubation period τ_i, i.e., the time after which the amount of transformation became measurable (0.2%). The values of τ_i are plotted against grain size in Fig. 5.14, which shows that

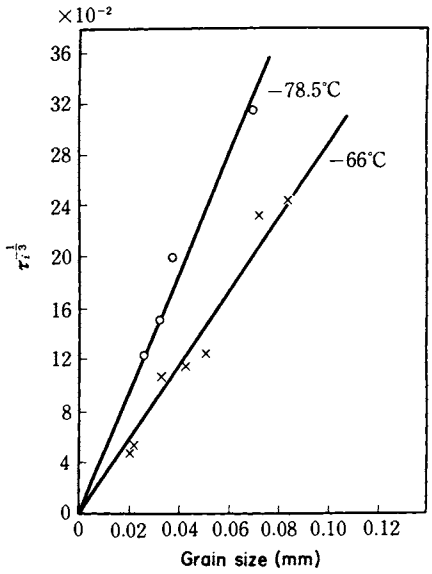

FIG. 5.14 Effect of grain size on incubation period τ_i (in seconds) of martensite nucleation (Fe–26% Ni–2% Mn). (After Raghavan and Entwisle.[199])

$\tau_i^{-1/3}$ is proportional to the grain size, indicating that transformation becomes more difficult with a decrease in grain size.

Pati and Cohen[201] also measured τ_i, using Fe–Ni–Mn alloys,† and derived the nucleation rate‡ from the results. Figure 5.15 shows their results for an

† Three steels in the range of (23–25)% Ni–(2–3)% Mn–(0.015–0.043)% C–(0.001–0.010)% N were used, and the desired grain sizes were obtained by controlling the heat treatment and varying the degree of deformation.

‡ The nucleation rate of isothermal martensite is defined by

$$\dot{N} = \frac{1}{1-f}\frac{dN_v}{dt}, \tag{1}$$

where f is the volume fraction of α', N_v the number of α' crystals per unit volume, and t the reaction time. N_v can be derived from f and the mean volume of an α' crystal ($\bar{v}$):

$$N_v = f/\bar{v}. \tag{2}$$

The value of f can be measured. Although $\bar{v}$ is difficult to measure directly, it can be estimated from Fullman's equation[202]

$$\bar{v} = \pi^2 f / 8\overline{l^{-1}} N_A \tag{3}$$

where N_A is the number of α' crystals per unit area of specimen cross section, and $\overline{l^{-1}}$ is the mean value of the reciprocal of the length of an α' plate. Since both N_A and $\overline{l^{-1}}$ are measurable, $\bar{v}$ and subsequently N_v can be obtained. For N_v crystals formed within a time τ_i during isothermal transformation, Eq. (1) becomes

$$\dot{N} = \frac{1}{1-f}\frac{dN_v}{dt} \doteqdot \frac{N_v}{\tau_i}. \tag{4}$$

Therefore, $\dot{N}$ can be calculated by measuring τ_i (refer to Eq. (3) in Section 4.5).

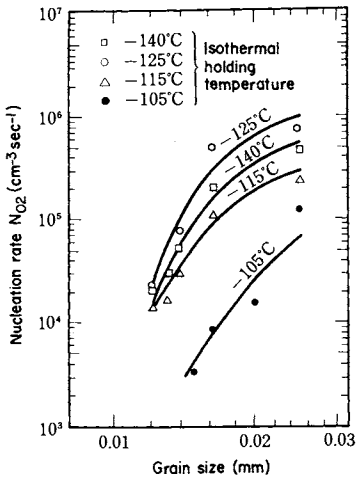

FIG. 5.15 Effect of grain size on nucleation rate (Fe–24% Ni–3% Mn). (After Pati and Cohen.[201])

Fe–24% Ni–3% Mn alloy† for various austenite grain sizes. In this figure, the isothermal transformation temperature‡ is noted for each curve. For any curve, the nucleation rate decreases with decrease in grain size.

5.3.6 Effects of a Cottrell atmosphere and precipitated particles

In a supersaturated solid solution obtained by quenching, interstitial atoms, such as carbon, migrate to the expanded sides of edge dislocations during aging and form Cottrell atmospheres. Such atmospheres obstruct the lattice-invariant shears in martensitic transformation in the same manner as in the case of strain aging, and thus stabilize the austenite.[107] Precipitated particles also suppress the martensitic transformation by the same effect as that due to the increase in the number of grains.

At the beginning of precipitation, there is a stage at which the atomic arrangement of fine precipitates is coherent with the matrix. Such precipitates obstruct the shape change for the martensitic transformation; the initiation of transformation is thus more difficult and the M_s temperature decreases. Hornbogen and Meyer[203] treated this problem, using an Fe–28 at. % Ni–12 at. % Al alloy ($M_s \approx -45°C$). In the aged state of this alloy, precipitated particles of Ni_3Al are highly coherent with the matrix and the matrix is still of a composition capable of undergoing martensitic transformation. Figure 5.16 shows the M_s temperature versus aging time at 600°C and 700°C.

† The exact composition is 24.20% Ni, 2.98% Mn, 0.017% C, and 0.001% N. This steel is one of the three studied.

‡ The transformation rate was greatest at −125°C. This means that −125°C corresponds to the nose temperature of the C curve in the time–temperature diagram for 0.2% transformation (cf. Fig. 4.13).

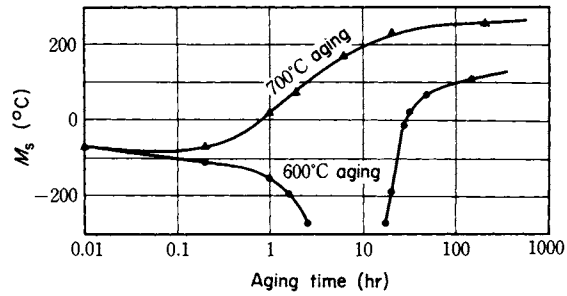

FIG. 5.16 Change of M_s temperature of austenite matrix with precipitation at 600° or 700°C (Fe–28 at.% Ni–12 at.% Al). (After Hornbogen and Meyer.[203])

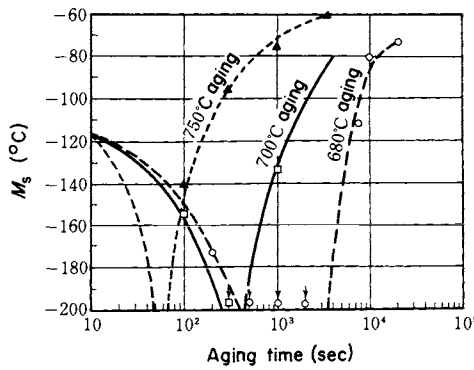

FIG. 5.17 Change of M_s temperature of austenite matrix with precipitation at 680°, 700°, or 750°C (Fe–29.5% Ni–4% Ti). (After Abraham and Pascover.[204])

At the beginning of aging at 600°C, fine precipitates accompanied by coherency strains are observed by transmission electron microscopy. At this stage, the M_s temperature is decreased. Aging for a longer time at 600°C or aging at 700°C, however, causes the M_s to increase because the precipitated particles have grown to a large size and lose coherency. Aging at 400°C lowers the M_s markedly because the precipitates are smaller than those at 600°C.

Another example can also be cited. Figure 5.17[204] † shows the case of an alloy containing Ti rather than Al. This alloy shows clusters in the as-quenched state (refer to Section 2.2.2), and in the early stage of aging, Ni_3Ti (DO_{24} type) precipitates with high coherency,[205] as illustrated in Figure 5.18; the lattice orientation relationships are $(001)_{Ni_3Ti}\|(111)_\gamma$, $[010]_{Ni_3Ti}\|[\bar{1}10]_\gamma$, and the lattice misfit is only 0.65%. Furthermore, the stacking order of the

† See Fig. 2.3.

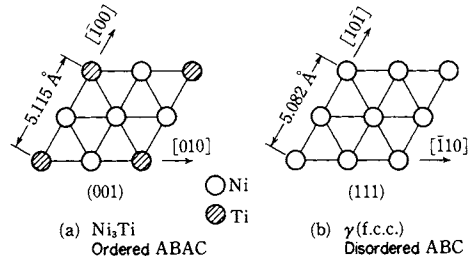

FIG. 5.18 Lattice similarity between Ni_3Ti and γ (f.c.c.).

(001) planes of Ni_3Ti is ABAC, whereas that of the matrix is ABC. Therefore, the f.c.c. phase with a stacking fault is equivalent to the Ni_3Ti structure. The atomic arrangement in Ni_3Ti is thus quite similar to the f.c.c. lattice, so good coherency is expected. This is verified from the fact[206] that in the x-ray diffraction pattern, satellite reflections appear near the austenite spots, and in the electron micrograph, interference rings due to coherency strains are observed around the precipitates.

Malyshev and Butakova[207] carried out similar experiments, using Fe–Ni–Cr and Fe–Ni–Cr–Ti alloys.† Heating them to 450°–800°C resulted in stabilization of the austenite and retention of an abnormal amount of austenite. While the retained austenite is held at 0°–100°C, however, martensite forms isothermally, the amount gradually approaching the normal value. The stabilization in this experiment is also thought to be due to precipitates produced during heating.

Next let us consider the case in which the matrix hinders the martensitic transformation of coherently formed particles. In 1940, Smith[208] found that the paramagnetic γ–Fe particles precipitated in a Cu alloy become ferromagnetic upon plastic deformation. These particles do not transform when cooled to liquid helium temperature without deformation.[209] These observations attracted the attention of many researchers. Easterling *et al.*[210,211] attempted to clarify these observations, using a Cu–1% Fe alloy. This alloy is completely f.c.c. in the as-quenched state, but precipitates 500 Å in diameter are produced by heating it for 20 hr at 700°C. Although these precipitates are essentially pure iron, they are not b.c.c. but remain f.c.c., even at room temperature. The reason for this is as follows. The lattice constant of f.c.c. Fe is nearly equal to that of Cu, and the crystallographic orientation of the Fe precipitates coincide with that of the Cu matrix. Hence, good coherency is maintained. Therefore, the Fe precipitates are stabilized in the f.c.c. condition. When the specimen is deformed under tension, partial transformation to b.c.c. takes place in the precipitates. This transformation is

† Fe–0.01% C–19.84% Ni–4.5% Cr and Fe–0.06% C–20.50% Ni–3.86% Cr–0.68% Ti.

detected by magnetic measurements and electron diffraction. In the electron micrographs, the martensite is lathlike, and the lattice orientation relationship between the f.c.c. phase and the martensites is near the Greninger–Troiano one (see Section 2.2.4), and the longitudinal direction of the martensite laths is $[\bar{1}10]_\gamma$ ($[001]_\alpha$). The occurrence of this transformation is due to the destruction of coherency by deformation. When the size of the precipitates is less than 200 Å, the precipitates are not transformed even by deformation. The foregoing coherency concept is also corroborated by the following electron microscopic observations.[211] Before deformation, interference fringes due to coherent strains are observed in the regions of the matrix near the Fe precipitates. At the first stage of deformation, however, the interference fringes vanish, and small plates of martensite appear in the precipitates.

Further, investigation of Cu–1.5% Fe–(0–5)% Ni alloys by electron microscopy[211] showed that the precipitates of Fe were transformed by separation from the matrix by electrolytic extraction without deformation.

5.4 Effect of ausforming on transformation temperature and mechanical stabilization of austenite

When austenite is plastically deformed, residual stresses and lattice defects are introduced. The residual stresses are principally long-range elastic stresses that raise the start temperature M_s and lower the A_s temperature. The effect increases with increasing degree of deformation and reaches a saturation value. On the other hand, lattice defects (i.e., short-range stresses) lower the martensite finish temperature M_f and raise the A_f temperature. Thus, the temperature range of transformation is widened by plastic deformation.

5.4.1 Ferrous alloys

A. *M_d temperature*

In the Fe–Ni system, the temperature difference between M_d and A_d is small, as illustrated in Fig. 4.7, and both these temperatures appear to approach T_0 upon deformation. Therefore, the value of T_0 can be estimated as $\frac{1}{2}(M_d + A_d)$.

As described before, in the umklapp transformation a large transformation stress is generated locally around the martensite plate and therefore transformation is accelerated by autocatalytic action (refer to Section 5.2.4). In this regard, Honma[57] found an interesting phenomenon. When an Fe–31% Ni specimen in the γ state was cooled in a temperature gradient, the temperature at the tip of an α' crystal formed in the low-temperature por-

tion of the specimen was higher by 85°–90°C than the usual M_s temperature of the alloy: The transformation around the tip was of the schiebung type. It therefore seems that the internal stress due to the formation of α' by umklapp was so large that the temperature was higher than the M_d point and consequently the schiebung transformation occurred.†

Hosoi and Kawakami,[52] using an ultralow carbon Fe–31.72% Ni–0.004% C alloy ($M_s = -50$°C), measured the M_d after rolling at room temperature, and found that the M_d increases with an increasing degree of rolling, the saturation value being -35°C at about 35% rolling. Guimarães *et al.*[213,214] carried out a similar experiment, using 28.25% Ni–0.21% C and 31.15% Ni–0.09% C steels ($M_s <$ room temperature). It was found that the M_d point was higher by ~ 15°C than the M_s point for 50% reduction, but then decreased again for more than 80% reduction. Thus a maximum M_d occurred between the two reductions.‡

For specimens partly transformed by subzero cooling before rolling, the maximum in M_d occurred at lower rolling reductions. This trend increased with lowering of the subzero cooling temperature.

B. *M_f temperature*

Now we turn to the problem of the M_f temperature. It is evident that this temperature is markedly lowered by plastic deformation. If the M_f is lowered well below M_d, the transformation range is well spread out and therefore measurement of the M_f becomes very difficult. But the M_f can be estimated from the amount of martensite produced by cooling to various temperatures. Fiedler *et al.*[215] employed this method for 18–8 stainless steels containing 0.006%–0.127% C. They deformed the steels under tension at 93°C, cooled them for 15 sec at -195°C, and measured the amount of martensite. Figure 5.19 shows the result.§ The amount of martensite first increases with prior deformation due to the rise in the M_s. It then decreases for deformations larger than 10%, indicating that the M_f is lowered by deformation. That is, when the degree of deformation becomes high, stabilization of the austenite occurs. In this investigation, the deformation

† The M_d temperatures of an Fe–27% Ni alloy containing Al, Si, Mn, or Cr as the third element were given by Zhuravlev *et al.*[212]

‡ Such a maximum was also observed in the amount of burst transformation, although the degree of rolling reduction at the maximum point was as low as 10%, probably owing to the difficulty of burst transformation in heavily deformed steel.

§ In Fig. 5.19, the amount of martensite for higher carbon steels is smaller because of the lower M_s temperature. Breedis,[62] also using a stainless steel, obtained a similar result; the maximum was found at 6% strain under tension. Moreover, he examined the distribution of dislocations in the deformed austenite by electron microscopy, and considered their relation to the transformation behavior.

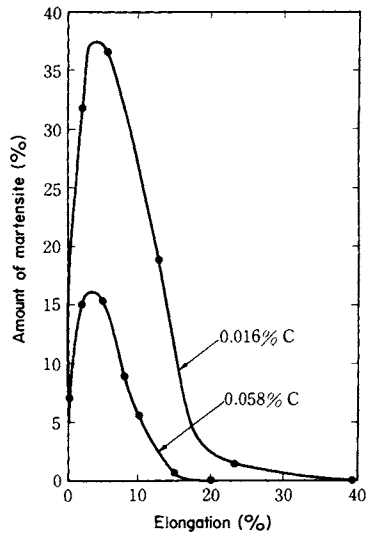

FIG. 5.19 Correlation of the amount of martensite formed by cooling to −195°C (15 sec) with the degree of prior deformation at 93°C (Fe–18.6% Cr–8.4% Ni–0.016% C; Fe–18.5% Cr–8.5% Ni–0.058% C). (After Fiedler *et al.*[215])

temperature was 93°C, so that carbon atoms in solution were able to migrate gradually to form clusters at defects formed by deformation. However, the contribution of such clusters to stabilization will be small, since similar results were obtained even in the case of room-temperature deformation.[216–218] It is, therefore, highly possible that the stabilization just discussed is mainly mechanical.

Hirayama and Kogirima,[219] using austenitic Fe–Cr–Ni spring steels of various chemical compositions, recognized that the amount of martensite decreases with increasing rolling temperature from room temperature to 200°C. The amount of martensite was equal to the sum of the stress-induced martensite and that thermally transformed from mechanically stabilized austenite during cooling to room temperature.

C. *Ausforming*

When the deformation temperature is high, and the material is in the austenite state, the deformation is called *ausforming*. In this case, the effect of precipitation of carbides as well as that of clusters of carbon atoms must be taken into consideration. Gooch and West,[220] using Ni steels, measured the M_s temperatures after rolling at 300°C. Their results are shown in Fig. 5.20, which reveals that the M_s first rises, then falls, and rises again monotonically with increasing degree of rolling. To examine whether or not there was an aging effect during rolling, they measured the M_s change due to aging at 300°C after rolling. They found that the M_s was lowered and the

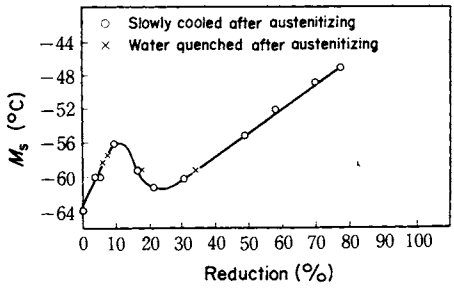

FIG. 5.20 Change of M_s temperature with degree of rolling at 300°C (Fe–26.4% Ni–0.42% C), (After Gooch and West.[220])

hardness was increased with aging time, even by rolling to only 4% reduction. In a specimen rolled 49%, the M_s was further lowered, while the hardness showed a maximum at 1 hr aging. From these results, it is inferred that formation of clusters or precipitates occurred during rolling at 300°C. This would explain the lowering of the M_s at 10–20% rolling, as seen in Fig. 5.20.† That the M_s rises again at heavier deformations is due to the decreased carbon content in the austenite because of extensive precipitation of carbides.

Tamura *et al.*,[222] using an Fe–28.7% Ni–0.26% C alloy, obtained results similar to those shown in Fig. 5.20. They measured the M_s as well as the amount of transformation. At high degrees of rolling, the amount of martensite was not increased, even though the M_s was increased. These observations are consistent with the foregoing interpretations.

Tamura *et al.* made further experiments by rolling another alloy, Fe–15.2% Cr–12.6% Ni–0.002% C at 300°C, in which two kinds of martensite, α' and ε, form. Their results are shown in Fig. 5.21, where the two lower curves indicate the change in the M_s for α' and ε with the degree of rolling. It is seen that for both phases the M_s temperature always decreases with rolling, in contrast with Fig. 5.20. The amount of α' formed at -196°C after rolling is somewhat increased by rolling up to about 4% reduction, but then decreases markedly, as indicated by the upper curve. Such a trend is similar to the previous case, except that the rise in the M_s at low degrees of deformation is not observed. The absence of this rise may be due, first, to the initial formation of ε (which is different from α' in the transformation mechanism), and second, to the relaxation of internal stresses due to rolling temperatures as high as 300°C. That the M_s did not increase again after heavy deformations can be understood by considering that the increase, if any, in M_s caused by precipitation, is slight for the low carbon content.

† Guimarães and Shyne,[221] using electrical resistance measurements, determined the M_s point of a 31.15% Ni–0.09% C steel rolled at room temperature and aged at 250°C. They found that the M_s temperature is decreased by rolling up to 25% and then increased by further rolling.

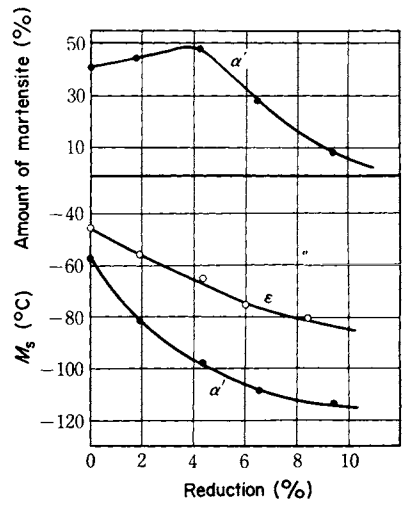

FIG. 5.21 Effect of rolling at 300°C on the M_s temperature for ε and α' and on the amount of martensite formed by cooling to −196°C (Fe–15% Cr–13% Ni). (After Tamura *et al.*[222])

Figure 5.22 shows the results of Georgiyeva *et al.*[223] for high-temperature rolling at 525°C of an Fe–16.7% Ni–1.0% C alloy, one of the three steels they used. In this figure, the upper curve shows the change of M_s with the degree of rolling; the other curves show the change in the amounts of martensite after rolling followed by quenching to various temperatures. These results are, to some extent, similar to those mentioned earlier but there are some important differences.

A major cause of these differences may be fluctuation of the carbon

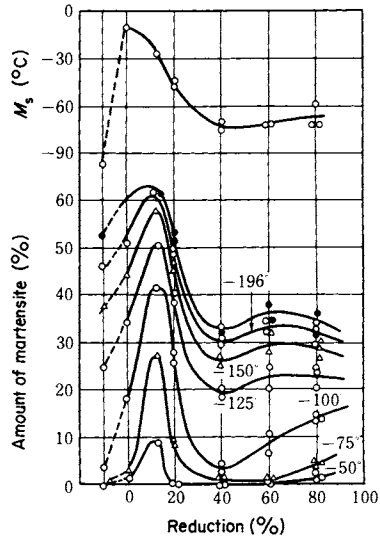

FIG. 5.22 Effect of prior rolling at 525°C on M_s temperature and amount of martensite formed by subzero cooling at temperature indicated on the curve (Fe–16.7% Ni–1.0% C). (After Georgiyeva *et al.*[223])

concentration in the austenite during rolling at 525°C. In the rolled state before subzero cooling, this alloy was austenitic and did not contain carbide precipitates. With an increase in the degree of rolling, and the concomitant increase in duration of rolling, the magnetic Curie point was raised—90°C for 14% deformation and 390°C for 80% deformation. The change in Curie temperature was lessened with decreasing carbon content in the alloy. In an Fe–31% Ni–0.02% C alloy, it was difficult to find any change. The difference is, therefore, thought to be caused by carbon atoms, for example, by the fluctuation of their concentration in the austenite due to the formation of clusters, such as Cottrell atmospheres. From this viewpoint, the abnormality shown in Fig. 5.22 will be considered in further detail.

In this experiment the specimen was step quenched, that is, cooled from 1200°C to 525°C, held for 5 min without rolling, and quenched in water. The M_s of this specimen was higher than that of the specimen directly quenched (the initial point of the upper curve in Fig. 5.22). The rise of the M_s temperature caused by holding at 525°C is probably due to the formation of regions relatively low in carbon, because carbon atoms migrate to lattice defects, such as grain boundaries.

Next, consider ausforming at 525°C. The M_s decreases with the amount of rolling, and shows no maximum, although this is not certain, since there are no data for less than 14% deformation. At temperatures as high as 525°C, internal stresses are relieved; hence, the factors raising the M_s will become lessened. However, there will still remain lattice defects that are not annihilated by heating to 525°C. Some such defects can accelerate the transformation below the M_s. This is why the amount of martensite is increased at a low degree of prior deformation. At deformations between 14% and 40%, lattice defects that stabilize austenite are formed (carbon atoms migrate to them) and lower the M_s and decrease the amount of martensite; that is, the austenite is considerably stabilized. Finally, for more than 40% deformation, only a further fluctuation of the carbon concentration occurs. Consequently, the M_s is raised, the austenite becomes unstable, and the amount of martensite increases, as shown in Fig. 5.22.

Nakamura and Yamanaka,[224] using an 0.8% C steel, found that a specimen quenched after deformation at the austenitizing temperature contains a larger amount of retained austenite than an as-quenched specimen without deformation. Hirayama and Kogirima[219] found some martensite in rolled austenitic stainless steels containing 16.5%–19% Cr and 7%–11.5% Ni. The rise in the rolling temperature (from room temperature to 200°C) lessened the martensite, which consisted of stress-induced martensite and martensite produced during cooling from the rolling temperature in the austenite stabilized by rolling deformation.

D. *Reverse transformation*

A phenomenon similar to the mechanical stabilization of austenite is found in the reverse transformation of deformed martensite. For example, if an Fe–30% Ni alloy transformed to martensite by subzero cooling is rolled, its reverse transformation temperature (A_s) is raised. The amount is about 15°C for 5% rolling.[225] Such a rise in the A_s can be interpreted in terms of the arguments used earlier to explain the lowering of the M_s upon deformation.

5.4.2 Cobalt alloys

In the f.c.c. → h.c.p. transformation of cobalt or its alloys, the differences in the chemical free energy and its temperature coefficient between the two phases are small. Hence, the driving force for transformation due to supercooling is small, and the M_s temperature is affected sensitively by small differences in transformation conditions. Therefore, the transformation temperature range is very wide and both the M_s and A_s are difficult to determine with precision. But if the driving force is assisted by stressing, the transformation takes place easily and the alloy quickly reaches its equilibrium state. Using deformation, the M_d and A_d can be measured without special effort.

Accordingly, Hess and Barrett[226] obtained Fig. 5.23, in which the M_d temperatures for Co–Ni alloys are plotted versus Ni content. In their experiment, the M_d was determined by the following procedure: specimens annealed for 4 hr at 900°C were peened at various temperatures and then

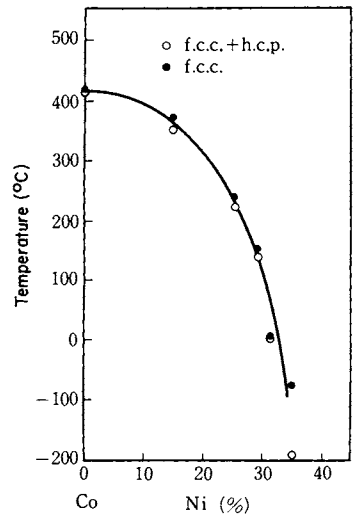

FIG. 5.23 M_d (A_d) temperature versus nickel content in Co–Ni alloys. (After Hess and Barrett[226])

examined by x-ray diffraction. The temperature at which the low-temperature (h.c.p.) phase was first detected was considered to be the M_d. After the specimen was transformed almost entirely to the h.c.p. phase by peening, it was again subjected to peening at various temperatures, and the temperature at which the h.c.p. phase began to decrease (i.e., the f.c.c. phase began to increase) was taken as the A_d temperature. The A_d measured in this way coincides with the M_d, as shown in Fig. 5.23, within experimental error. Therefore, such a temperature is also considered to be T_0.† Cerium[227] and Au–50% Cd[228] are also stabilized by plastic deformation.

5.5 Effect of an intense magnetic field[229]

5.5.1 Static magnetic fields

The martensitic transformation is affected only slightly by a magnetic field of ordinary strength, even in ferromagnetic metals and alloys, but a rather intense field exerts a noticeable effect. A series of investigations concerned with this problem were carried out in recent years, mostly in the Soviet Union.[230–245]

These investigations demonstrate that the M_s temperature of a steel is raised by applying a magnetic field, and the amount of martensite is increased. The effect is roughly proportional to the strength of the field. The rise in M_s is several degrees and the increase in the amount of martensite is a few percent with an increase in field of 10 kOe;[235] however, the magnitude of the effect depends somewhat on the composition of the steel.

This effect is explained as due to the lowering of the free energy of the α' phase in a magnetic field, as shown in Fig. 5.24. The γ phase in steels of ordinary compositions is paramagnetic, whereas the α is ferromagnetic. Without a magnetic field, transformation occurs at the M_s temperature, where the difference in the free energies of the γ and α' phases is equal to the driving force of the transformation ΔF, whereas in a magnetic field the free energy of the α' phase is lowered by the magnetic energy ΔE_m, as indicated by the broken line. Thus the driving force assumes a value that is large enough to induce transformation at a temperature, say M_s', above M_s.

Table 5.3 presents evidence for the agreement between the foregoing explanation and the experimental results in several alloys. (Data for Fe–15% Ni are given by Miroshnichenko *et al.*[246]) The magnetic energy ΔE_m is obtained by the relation

$$\Delta E_m = J_\alpha H$$

† Using this method, the equilibrium temperature between the f.c.c. and h.c.p. phases in pure cobalt was found to be 417° ± 7°C.

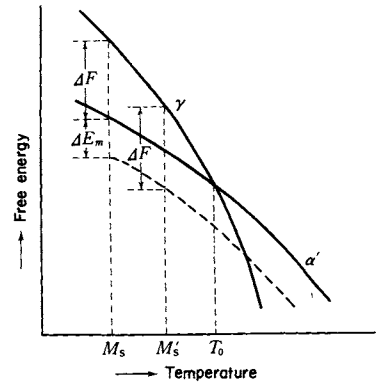

FIG. 5.24 Effect of a magnetic field on the free energy.

where J_α is the intensity of magnetization of the α' phase and H the strength of magnetic field. It is easily seen from Fig. 5.24 that ΔT, the increase in M_s, is given by

$$\Delta T = \frac{\Delta E_m}{\Delta F}(T_0 - M_s).$$

The value of ΔE_m can be obtained by magnetic measurement, while both $T_0 - M_s$ and ΔF are known from other experiments. Therefore, ΔT is readily calculated from the foregoing equation. In Table 5.3, reasonable agreement is seen between the increase in ΔT obtained by calculation and that found by direct measurement. This agreement shows quantitatively the plausibility of the explanation of the increase in M_s in a magnetic field based on the magnetic energy. Another value of the foregoing equation is that it supplies us with ΔF, the driving force of the transformation, provided that ΔT is measured by experiment. The A_s temperature is also raised by an intense magnetic field,[241] which may be understood from similar reasoning.

TABLE 5.3 Rise of M_s temperature in a strong magnetic field[a]

Composition (%)					H	ΔE_m	$T_0 - M_s$	ΔF	Rise of M_s, ΔT (°C)		
C	Ni	Cr	Mo	Si	(kOe)	(cal/mol)	(°C)	(cal/mol)	Calc.	Obs.	Lit.
—	30	—	—	—	350	87	200	330	52	37	234
0.48	18.7	—	—	—	18.7	5.1	220	220	5.1	4	235
0.58	8	3.8	1.1	3	19	4.8	222	360	2.9	3	239
1.0	—	1.5	—	—	16	4.6	260	265	4.5	3.3	242
0.3	2.8	0.6	0.6	—	16	4.5	240	265	4.1	4.6	242

[a] After Satyanarayan *et al.*[242]

An acceleration of the transformation is also observed for the ε (h.c.p.) → α′ (b.c.c.) transformation induced by cooling in a magnetic field. For example,[245] in an Fe–14% Mn–0.05% C steel, the amount of α′ phase is only 12% when the steel is cooled to −196°C after quenching from 1000°C, but increases to 46% when the steel is cooled in a magnetic field of 400 kOe. This increase in α′ is due to the transformation of most of the ε phase, which was produced during quenching, into α′ phase in the course of magnetic field cooling. That such a transformation actually takes place was verified by means of x-ray diffraction and thermal dilatometry. When the manganese content is increased to 16%, the ε → α′ transformation by magnetic field cooling does not occur without prior plastic deformation.

Attempts to produce magnetically anisotropic substances by means of magnetic field cooling were originally made in Japan by Chikazumi. Several such substances were obtained by cooling specimens that undergo martensitic transformation from above to below the M_s point in a strong magnetic field.[247–250] This occurred perhaps mainly because those α′ plates with energetically favorable orientations are produced more abundantly than and preceding those with less favorable orientations, and the transformation strain acts to retain such anisotropy.

Observations were also made on the effect of the application of a magnetic field at constant temperatures, using Fe–28.8 at.% Ni[251] and other alloys. The effect was substantial; in an Fe–20% Ni–2% Mn alloy,[252] the rate of isothermal martensitic transformation is nearly tripled by a 20-kOe field at −60°C. This effect can be predicted from thermodynamic considerations.

5.5.2 Pulsating magnetic fields

A pulsating magnetic field has a more pronounced effect on the martensitic transformation than a static one. Figure 5.25[253] shows an example in which a threshold field obviously exists. The value of the threshold field

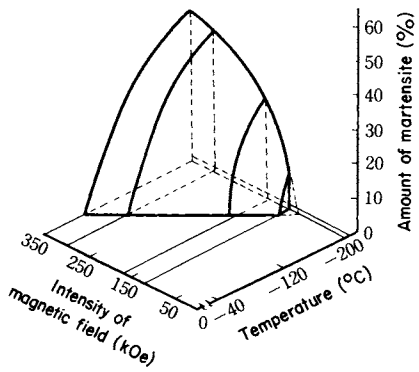

FIG. 5.25 Effect of a pulsating magnetic field on the amount of martensite produced (Fe–2.05% Cr–21.9% Ni–0.49% C quenched from 1200°C). (After Sadovskij *et al.*[253])

is almost independent of the frequency of pulsation, but decreases with decreasing temperature.

The pulsating magnetic effect has been studied in steels with M_s temperatures above room temperature.[254] It was found in commercial carbon steels (1.05%–1.2% C) that a pulsating magnetic field of 300–400 kOe whose frequency is 5000 Hz raises the M_s temperature by 60°–80°C and produces more α' phase than is produced without a field.

The effect of a magnetic field is enhanced by stress.[255] For example, a magnetic field larger than 100 kOe is necessary to induce martensite in the steel referred to in Fig. 5.25, whereas a 70-kOe field is sufficient if a stress of 5 kg/mm^2 is applied concurrently. Another work[256] on Fe–23% Ni–4% Mn reports a similar effect due to an intense magnetic field.

Transformation during austempering is also influenced by an intense magnetic field in a similar manner.[257]

5.6 Effect of superlattice formation on M_s temperature

Ordering of constituent atoms in the parent lattice before martensitic transformation lowers the potential energy of the parent phase. The order in the parent phase is inherited by the martensite, but usually it is not necessarily the most stable atomic arrangement for the martensite. The lowering of potential energy due to ordering is, therefore, not so large as in the parent. Hence, the ordering in the parent phase might lower the M_s temperature. A typical example is found in an iron-rich Fe–Pt alloy. The effect is most conspicuous in the case of an alloy of composition Fe_3Pt. In the γ (f.c.c.) state, this alloy has a Cu_3Au-type superlattice.[258] When the alloy is quenched from a high temperature, it transforms into martensite; but when cooled slowly or quenched after being kept at an appropriate temperature, ordering occurs, and consequently the M_s temperature is lowered so much that no martensitic transformation takes place at all.

Tadaki and Shimizu[259] studied this problem using electron microscopy. The M_s temperature of this alloy is found to be above room temperature from the fact that α' martensite (though only a small amount) is formed when the alloy is quenched from 1000°C in water at room temperature. Examining an electron diffraction pattern of the retained γ phase (Fig. 5.26a), we see some weak and blurred superlattice spots, such as (010), between the incident beam and the fundamental spots, such as (020). This shows the occurrence of ordering, although the degree of order is not very high. At this stage, no fine structure is observed in the electron microscopic images, which means that ordered domains, if any, must be very small. Then, if the specimen is reheated to 650°C for 30 min after being quenched from 1000°C, the superlattice spots become sharpened and intensified, indicating the

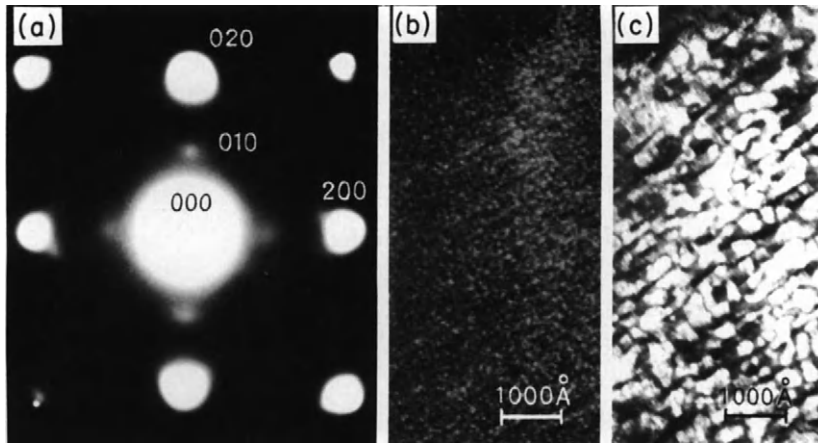

FIG. 5.26 Formation of superlattice Fe_3Pt. (a) Electron diffraction pattern ([001] zone), as quenched from 1000°C. (b), (c) Dark-field images with (100) reflection, heated for 30 min and 24 hr, respectively, at 650°C after quenching. (After Tadaki and Shimizu.[259])

development of ordering. In the dark-field image using a $(100)_\gamma$ spot, ordered domains (< 100 Å) are observed distinctly (Fig. 5.26b). The M_s point of the specimen heat treated as just described is around −50°C. Prolonged heating for up to 24 hr causes the domain size to grow to about 500 Å (Fig. 5.26c). At this stage of heat treatment, the martensitic transformation does not proceed even if the specimen is cooled to −196°C. The phenomenon of the lowering of the M_s point due to ordering is consistent with the lowering of the A_3 point as observed magnetically in an Fe–27.1 at.% Pt alloy by Bertowitz *et al.*[260] Recently, Dunne and Wayman[153] determined the transformation start temperatures of an Fe–24 at.% Pt alloy during both cooling and heating by means of metallographic examination and electrical resistivity measurement; their results are shown in Fig. 5.26A, where it can be

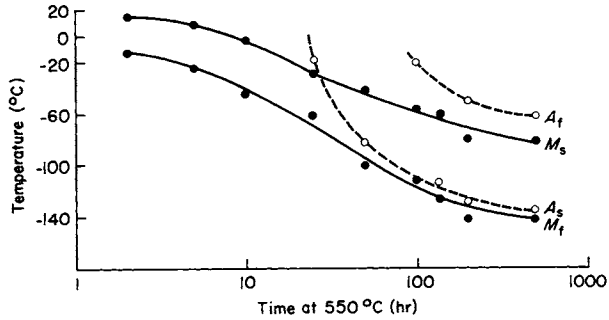

FIG. 5.26A Variation in transformation temperatures as a function of ordering time at 550°C (Fe–24 at.% Pt). (After Dunne and Wayman.[153])

seen that the effect of ordering is not only the lowering of the transformation start temperature in both cases, but also a widening in the difference between the M_s and M_f temperatures, and a lowering of the A_s below the M_s. Such effects cause the martensitic transformation in ordered alloys to be thermoelastic.

5.7 Stabilization (mainly thermal) of austenite

Making the transformation from austenite to martensite difficult is called *stabilization of austenite*, a phenomenon that occurs in many cases. Stabilization is usually classified as follows:

(a) Chemical stabilization (due to a change in chemical composition);
(b) Thermal stabilization (due to thermal treatment); and
(c) Mechanical stabilization (due to plastic deformation).

Of these three, chemical stabilization is, simply put, the lowering of M_s due to a change in chemical composition, as described in Section 4.3. As for the other two, each operating factor has already been discussed in the preceding sections. In actual cases, however, more than a single factor usually operates, and the manner in which these factors cooperate becomes essential. Therefore, an independent section shall be devoted to the illustration of the stabilization of austenite by means of heat treatment. First, all possible causes of stabilization are mentioned; then the effect of individual factors is considered.

5.7.1 Classification of causes of stabilization

Generally speaking, the temperature of initiation of transformation, the progress of transformation, and other features are controlled, as described in the previous chapters, by the chemical and nonchemical free energies of the system. The former depends on three factors. The first is the change in chemical composition and is essentially based on the diffusion of atoms. The second is the variation in the atomic arrangement without a change in the crystal structure, such as the formation of an ordered structure or rearrangement of interstitial atoms. Both of these factors change the enthalpy and the entropy of the system. The third factor is the internal stress (compression and tension), which mainly affects the enthalpy.

The chemical free energy difference $\Delta F^{\gamma \to \alpha'}$ is the driving force of the transformation and is converted to nonchemical free energy. The latter partly goes into the energy of lattice imperfections inevitable upon transformation, including the interface energy between the γ and α' phases, and is partly consumed in the work done, which is afterward changed into heat.

These energies form a part of the activation energy for the nucleation and growth of the transformation products. The increase in vacancies makes the γ phase less stable by increasing the nucleation sites. Grain boundaries and other lattice imperfections also act as nucleation sites and contribute to making the γ phase unstable, whereas on the other hand, they contribute to stabilization of the γ phase by hindering the growth of the transformation product. Which of these various contributions predominates depends on the chemical composition and the nature of the imperfections.

Summarizing the foregoing, we can list the following seven mechanisms of stabilization (a plus sign denotes stabilizing, a minus, unstabilizing).

I. Chemical stabilization
   1. Change in composition (diffusion of atoms) $\pm$;
   2. Atomic rearrangement (e.g., ordering) $+$;
   3. Internal compression and tension $\pm$;

II. Nonchemical stabilization
   4. Internal shear stress (long-range lattice strain) $-$;
   5. Lattice imperfections and short-range lattice strain:
      (a) hindrance of growth $+$;
      (b) nucleation sites $-$;
   6. Cottrell atmospheres and coherent precipitation $+$;
   7. Frozen-in vacancies (nucleation sites) $-$.

5.7.2 Range of transformation temperature[261]

There is a gap between the start temperature M_s and the finish temperature M_f in most martensitic transformations, which means that the transformation temperature is not uniquely defined throughout a specimen. In other words, we can say that the matrix of the region that transformed later was more stable than the region that transformed earlier.

We now discuss how stabilization occurs in the following example. First, consider an Fe–Ni alloy where the Ni content is about 30%; the M_s point is below room temperature, so that we may legitimately neglect the effect of diffusion of atoms during transformation. Moreover, no ordering of the lattice occurs. Therefore, we may exclude mechanisms 1 and 2. Suppose a crystallite of the α' phase is produced, which causes a surrounding internal stress. A region that is exposed to tension is readily induced to transform, whereas the regions exposed to compression suppress the transformation, and the M_s temperature is lowered. Mechanism 3 is therefore working here.†

† By measurement of the lattice constant of the retained γ during cooling, it was found[262] that in the early stage of a martensitic transformation an expansion occurs and in the later stage a compression takes place.

The region left untransformed is poorer in favorable nucleation sites, and a partitioning effect cooperates, which means that mechanism 5+ is working. It is therefore concluded that in a high-nickel Fe–Ni alloy, mechanisms 3 and 5 create a transformation temperature range. Since an alloy with less Ni content has a higher transformation temperature, mechanism 1 might intervene if the cooling is slow enough. It should be noted that in such a case the transformation is no longer martensitic in an exact sense and that the product has a massive structure because of the individual motion of atoms.

Next, a steel with interstitials such as carbon or nitrogen is considered. In this case mechanisms 3 and 5 operate, as in the case of Fe–Ni alloys. During transformation, an ordering of the Fe_4C or Fe_4N type occurs in the retained γ, stabilizing it. But the stabilization cannot be very large, because the ordering is inherited in the α', so that the effect would be partly canceled. A more important effect of stabilization is perhaps due to the diffusion of C (N) atoms into the retained γ from the α' phase that is already transformed, when the C (N) content is low and the transformation temperature high. But in this case the transformation approaches the transformation by which bainite is formed, and will be discussed in detail in the section on stabilization due to aging.

5.7.3 Effect of austenitization temperature (maximum heating temperature) and quenching temperature

In most experiments concerned with the effect of the austenitization temperature, the maximum temperature of heating and the quenching temperatures were taken to be identical. It is desirable that these two temperatures be regarded as two mutually independent factors, because the latter controls the number of vacancies (mechanism 7), whereas the former controls the grain size and other imperfections (mechanism 5). Because of the lack of research on the difference between these two temperatures, we have to be content with discussing work that assumed a common temperature for the two.

A. *Effects on M_s temperature*

Sastri and West[263] reported that the higher the austenitization temperature, the higher the M_s temperature. Figure 5.27 shows an example, in which the broken line indicates that the γ grain size increases as the austenitization temperature increases. Also, the longer the heating time, the higher the M_s temperature (Fig. 5.28). Similar results[264] had been obtained before this work.

As to the interpretation of this fact, mechanism 7 may be suggested, because a higher quenching temperature produces more frozen-in vacancies

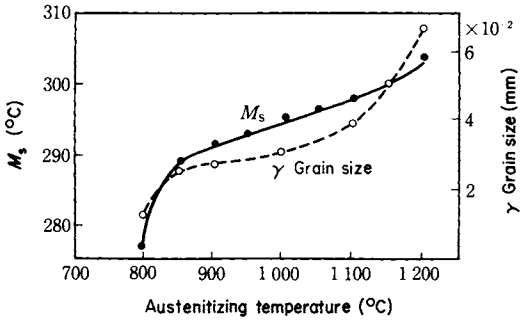

FIG. 5.27 Change of M_s temperature and austenite grain size with austenitizing temperature (Fe–0.33% C–3.26% Ni–0.85% Cr–0.09% Mo; heating time 2 min for 800°–1000°C, 1 min for >1000°C). (After Sastri and West.[263])

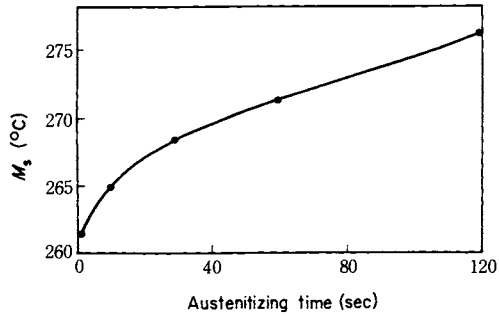

FIG. 5.28 Change of M_s temperature with heating time of austenitization (same alloy as in Fig. 5.27; heating temperature 800°C). (After Sastri and West.[263])

and hence more nucleation sites. But it is uncertain how effective this phenomenon actually is. On the other hand, a higher quenching temperature must produce a larger thermal strain during quenching; hence it is expected to raise the M_s temperature. This effect, however, cannot be very large. A more likely cause of raising the M_s temperature is the reduction of the energy needed for the complementary shear during transformation, which originates in the elimination of lattice imperfections due to heating to a higher temperature. Experimental facts discussed in the following paragraph seem to support this interpretation. Another argument will be given in Section 6.7.5.

Figure 5.29, for high Ni steels, is due to Entwisle and Feeney.[265] In this figure, the transformation start temperature is designated as M_b to show that the martensitic transformation occurs through a burst phenomenon in this alloy. Figure 5.29a shows that the M_b temperature is raised as the austenitization temperature is raised. Figure 5.29b shows the relation between M_b and the

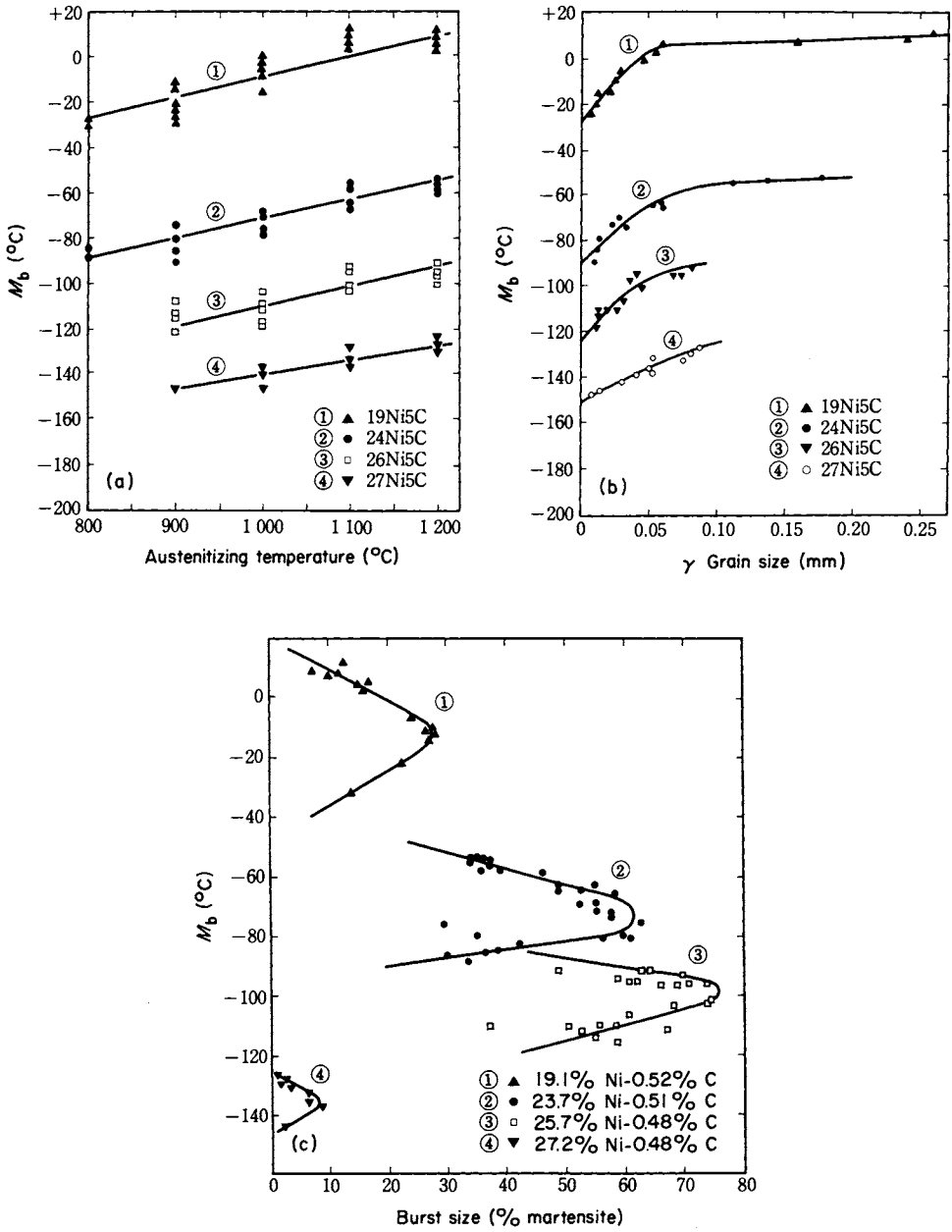

FIG. 5.29 Change of M_b with (a) austenitizing temperature, (b) austenite grain size, and (c) amount of burst martensite. (After Entwisle and Feeney.[265])

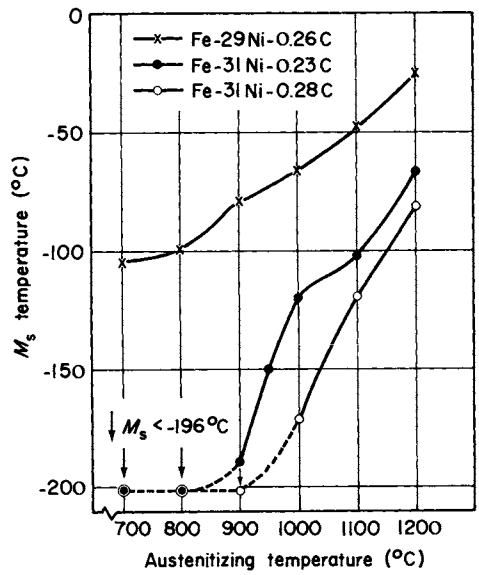

FIG. 5.29A Effect of austenitizing temperature (holding time 1 hr) on M_s temperature (Fe–Ni–C). (After Maki *et al.*[266])

γ grain size. This parallelism, however, should not be interpreted as indicating that the larger γ grain size raises the M_b point, but rather that the growth of γ grains and the increase in M_b take place simultaneously and independently, with increasing austenitization temperature. Figure 5.29c shows a relationship between the burst size (the amount of α' produced by burst transformation) and M_b. For each alloy the curve shows a maximum burst corresponding to an austenitization temperature of $\sim$1050°C.

Ankara[102] studied an Fe–30% Ni alloy, which was austenitized by reheating to various temperatures after quenching to form the α' phase. He observed that the higher the austenitization temperature, the higher the M_s temperature and the lower the yield point of the γ phase. From this observation it was inferred that the decrease in the energy for the complementary shear of the transformation raises the M_s. He also observed that the effect on M_s was exaggerated by cooling immediately after rapid heating (600°C/min), so that as many lattice imperfections as possible would be retained. This observation is well understood by the considerations just presented.

Maki *et al.*[266] studied the effect of austenitizing temperature on high Ni steels, and observed that the higher the austenitization temperature, the higher the M_s point (Fig. 5.29A).† It was recently reported[267] that the M_s

† It was stated that some 20°C increase might be due to the effect of decarburization from the annealing atmosphere when a high austenitization temperature was adopted.

is raised with increasing austenitization temperature up to a certain temperature, beyond which it begins to decrease in some cases. The reason for this, however, is not yet clear.

Bolton *et al.*[268] also reported that the M_s point is raised by increasing the austenitization temperature, using an Fe–10% Mn alloy, though there is the opposite tendency for austenitizing below 800°C, which might be due to an insufficient solution treatment.

B. *Effects on the amount of retained austenite*

In alloys with M_f below room temperature, part of the austenite phase remains untransformed after quenching to room temperature. The amount of retained austenite depends on the conditions of quenching.

In earlier days, Tamaru and Sekito[269] studied the problem using carbon steels and obtained the results shown in Fig. 5.30; their findings reveal that the retained austenite content increases with increasing carbon content.[270] This effect is obviously due to the lowering of M_s and M_f with increasing carbon content and is irrelevant to the present problem.

The first point to note is that the amount of retained austenite is maximum for a certain austenitizing temperature. It is readily concluded, then, that the amount of retained austenite is limited for too low austenitizing temperatures because of insufficient dissolving of iron carbide. On the other hand, that the amount of retained austenite still increases even with aus-

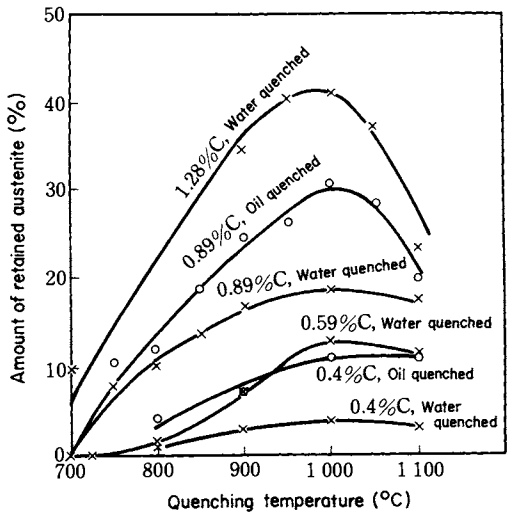

FIG. 5.30 Change in amount of retained austenite with quenching temperature (in carbon steels). (After Tamaru and Sekito.[269])

tenitizing temperatures as high as 900°–1000°C where all of the carbon is in solution is understood as follows: annihilation of lattice imperfections and the decrease in the number of γ grain boundaries caused by heat treatment result in the predominance of mechanism 5− over mechanism 5+. When the quenching temperature is raised further, the retained austenite takes a maximum value and then begins to decrease. The reason for this is not yet clear.†

A second point to be noted is that more austenite is retained with oil quenching than water quenching. The reason for this is related to the quenching rate and will be discussed in Section 5.7.8.

5.7.4 Stabilization by holding above M_s temperature

So far we have discussed the effect of increasing the austenitizing temperature. Alternately expressed, the lower the austenitizing temperature, the more stabilized the austenite and hence the lower the M_s temperature. In order to make this effect most conspicuous, the quenching temperature should be lowered to just above the M_s point, although a long holding time is necessary to obtain a significant effect. Works on thermal stabilization thus achieved are explained in the following.

Okamoto and Odaka[273] studied a ball bearing chromium steel. Figure 5.31 shows how the M_s temperature is affected by the holding time at 250°C, which is above the initial M_s value. At first, the M_s decreases with holding time, indicating stabilization; it then changes to increase from about 2 min on, and no change is observed for a while after that. For a still longer holding time, an abrupt decrease in M_s takes place, which was found by dilatometry to be due to the bainitic transformation, as shown in the same figure by a solid line.‡

Izumiyama[188,278] studied the M_s behavior of a nickel steel that was quenched to 20°C (above the M_s point) and then aged at 150°C. Figure 5.32

† Matsuda *et al.*[271] studied this point recently and concluded that even above 1000°C a decrease in retained austenite barely occurs, which arouses the suspicion that the decrease above 1000°C shown in Fig. 5.30 might be caused by decarburization during heating. Even results opposite to Fig. 5.30 were reported.[201,272] Depending on the heat treatment conditions, the retained austenite content can increase by carburization from the atmosphere.

‡ When a bainitic transformation occurs, supersaturated ferrite is first produced, in which the degree of supersaturation of interstitial atoms is larger than in the parent austenite. Those interstitials, therefore, diffuse into the untransformed austenitic matrix and concentrate. Hence, the M_s temperature after this transformation is lowered remarkably. There are other reports[274,275] indicating such lowering of the M_s temperature. In another paper it was reported[276] that the M_s is lowered in both carbon and silicon steels but is raised in Cr–Mn steels. It was also reported[277] that in some cases the lattice constant was not changed while the M_s point was changed.

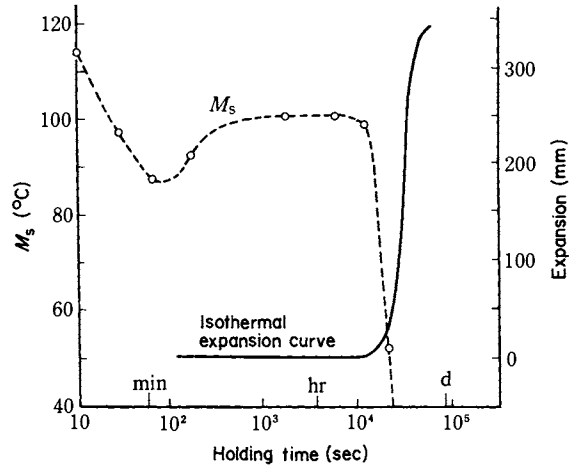

FIG. 5.31 Effect of aging at 250°C ($>M_s$) on M_s temperature (Fe–1.06% C–1.63% Cr). (After Okamoto and Odaka.[273])

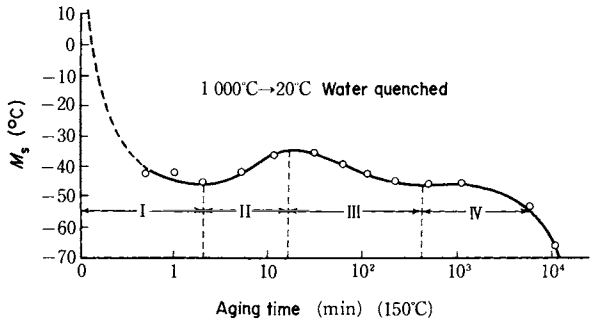

FIG. 5.32 Effect of aging at 150°C ($>M_s$) on M_s temperature (Fe–1.05% C–3.08% Ni). (After Izumiyama.[188])

shows that the M_s point changes with aging time in four stages.† A corresponding behavior is found when the aging time is kept constant while the aging temperature is varied.

The activation energy was determined for each stage by measurement of the change in M_s with aging time at various temperatures and by dilatometry. The results are shown in Table 5.4.[188,279] Stabilization mechanisms based on these values are also listed in the last column of the table. It is

† As determined by dilatometry. If aged at a higher temperature, the curve is shifted to shorter time, although its shape is preserved.

TABLE 5.4 Stabilization of austenite by aging at temperatures above M_s in an Fe–3.08% Ni–1.05% C alloy[a]

Stage	Aging temperature	Activation energy (kcal/mol)	Mechanism of stabilization of austenite
I	Below room temperature	—	Elastic interaction among dislocations in austenite[b]
	Room temperature 60°C	30–21.5	Elastic interaction between dislocation and interstitial atom
	Above 60°C	32.3	Obstruction of dislocation movement by fine precipitates
II	Above 80°C	18.4	Relaxation of stress in α' (rise of transformation temperature)
III	Above 80°C; after stage II	18.7	Increase of energy in γ–α' boundary
IV	Above 100°C	28.1	α' formation due to partial decomposition of retained austenite

[a] After Izumiyama.[188]

[b] Including the case in which strain embryos become inactive as transformation nuclei by trapping interstitial atoms. The existence of a suitable concentration gradient of interstitials seems to make the effect more conspicuous.[279]

worth adding that hindrance of the transformation by coherent precipitates, described in Section 5.3.6, seems to be involved in the later period of the first stage, and that the effect of loss of coherency probably exists in the second stage.

Similar conclusions were derived from studies on nickel steels containing 0.9%–1.3%C[280] or 1.43%C.[281] When the carbon and nitrogen contents are reduced to very low values, to the order of 0.004%, stabilization is also promoted by holding the specimen above M_s. This phenomenon corresponds[282] to the first stage in Fig. 5.32. The stabilization of austenite is also reported in steels containing 10%–14%Ni and 9.4%–9.7%Cr[283] by holding at 300°–500°C.

Hitherto we have considered examples in which the interstitial atoms, carbon or nitrogen, play a main role in the stabilization of austenite. There is a possibility that hydrogen atoms, too, which dissolve interstitially, take part in the stabilization. The role of hydrogen appears, however, unimportant from a practical point of view for two reasons: there is no great difference between solubilities in the f.c.c. and b.c.c. phases; and the diffusion of hydrogen in steels is extraordinarily fast.[284]

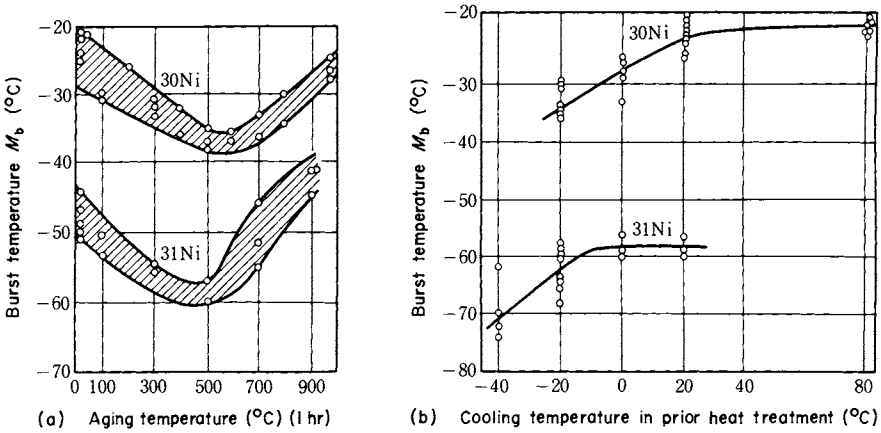

FIG. 5.33 Effect of prior heat treatment on M_b temperature (Fe–Ni alloys). (a) M_b versus aging temperature. (b) M_b versus cooling temperature after aging at 500°C. (After Maksimova and Nemirovskiy.[191])

Stabilization due to aging markedly affects the burst formation of martensite, as reported by Maksimova and Nemirovskiy.[191] They used the following two high nickel alloys with low carbon content.

Notation	Ni	C	Mn	Si	Fe	M_s
30Ni	30.1	0.02	0.25	0.07	Balance	−30°C
31Ni	31.6	0.02	0.28	0.02	Balance	−50°C

Specimens of these alloys drawn to a diameter of 1.5 mm were quenched to room temperature or −20°C from 900°–1000°C (all remained austenitic), then reheated to various temperatures and held for 1 hr† (aging), and finally cooled at 10°C/min. The burst transformation temperature M_b, measured during cooling, is shown versus the aging temperature in Fig. 5.33a. In both alloys the burst temperature first decreases with increasing aging temperature, showing the stabilization effect, which is explained as follows: The ease of nucleation differs from place to place (depending on the state of lattice imperfections), and more nuclei are made ineffective by trapping interstitials at higher aging temperatures, where they diffuse more easily; consequently, the M_b is lowered. If the aging temperature is raised further, however, a countereffect begins to work: the thermal vibrations disperse

† Most effects were revealed within the first 10–20 min and further aging time made little contribution.

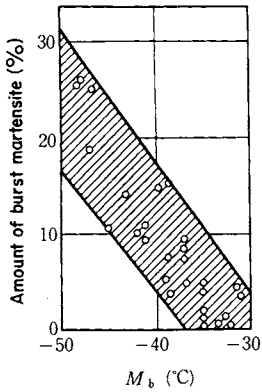

FIG. 5.34 Correlation between M_b temperature and amount of burst martensite (Fe–30% Ni). (After Maksimova and Nemirovskiy.[191])

the suggested interstitials and restore perfect solid solutions. These two mutually opposing actions produce a minimum value in M_b at a particular aging temperature, say, about 500°C in this case.†

The results just described were obtained for specimens that were aged at various temperatures after a heat treatment with a certain cooling temperature. In contrast, it was found that the variation in the cooling temperature in the prior heat treatment affects the stabilization, provided that the cooling temperature is chosen so that no martensitic transformation occurs. Figure 5.33b shows how the cooling temperature in the prior treatment affects the burst transformation temperature M_b after aging at 500°C. It is seen that the effect appears only when the cooling temperature is below a specific temperature (20°C for 30Ni and −10°C for 31Ni), and that the lower the temperature, the lower the M_b. This experiment shows that as the cooling temperature in the prior treatment is lowered, approaching M_s, nuclei are formed that require higher energy to transform.

No definite rule is obtained concerning the amount of burst transformation product occurring at M_b, but there is a tendency‡ for the amount to increase with decreasing M_b temperature (Fig. 5.34). The total amount of transformation, including the burst transformation as well as the transformation that gradually occurs afterward during cooling to −196°C, is, however, independent of the prior treatment. That the amount of burst transformation increases with lowering M_b temperature may be understood by considering that a larger supercooling is advantageous for the absorption of the heat of transformation.

So far experiments with constant austenite grain size (0.17–0.24 mm) have been reviewed. Concerning the grain size effect, it should be recalled that the M_b is lowered with decreasing grain size (Fig. 5.12).

† Furuya *et al.*[285] observed a similar phenomenon in a 17.7% Cr–13.6% Ni–0.02% C steel. In order to eliminate the effect of grain size, they used single crystals.

‡ This tendency is true for specimens aged after deformation.[214]

5.7.5 Stabilization by aging below M_s temperature or by interruption of quenching

A number of works[280–293] over many years have been concerned with the phenomenon that untransformed austenite (designated hereafter as the γ_R phase) is stabilized by interrupting the martensite formation during quenching and holding at that temperature (below the M_s point). Figure 5.35, due to Harris and Cohen,[287] shows how the amount† of α' martensite varies with the holding temperature in a ball bearing chromium steel. When cooled continuously, the transformation starts at M_s and the amount of α' increases according to the top curve. Next, suppose the cooling is interrupted at a temperature T_h and the specimen is held there. The amount of α' remains constant not only during holding but after the resumption of cooling, so that the point indicating the amount of α' deviates from the original curve, as is shown by a horizontal line, indicating that the stabilization of austenite has occurred. Transformation starts again only when a temperature M_s' is reached. The M_s' temperature can in this way be determined for each T_h temperature (holding time 30 min), and a locus for M_s', as shown by the broken line, is obtained. It is understood that stabilization of γ_R occurs

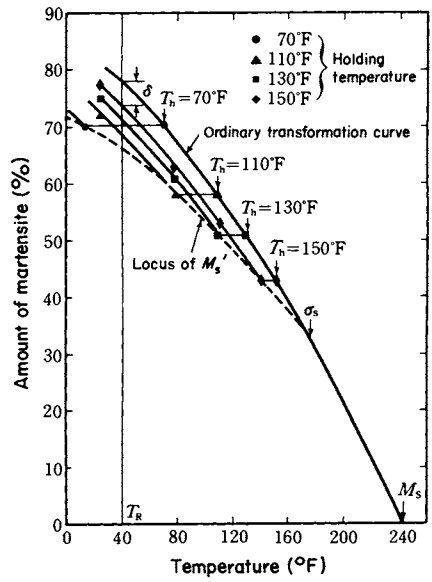

FIG. 5.35 Amount of martensite formed during cooling and after holding for 30 min at temperatures T_h ($< M_s$) (Fe–1.5% Cr–1.1% C). (After Harris and Cohen.[287])

† Determination of the amount of α': After cooling to a certain predetermined temperature, the specimen is reheated to 332°C, held for 10 sec, and quenched in brine at 25°C; the microstructure is then examined. The α' produced during cooling to a predetermined temperature is etched darkly because of tempering, whereas that produced later by the brine quenching is not etched so much. Therefore, they are easily distinguished. The amount of α' is determined by the lineal analysis.

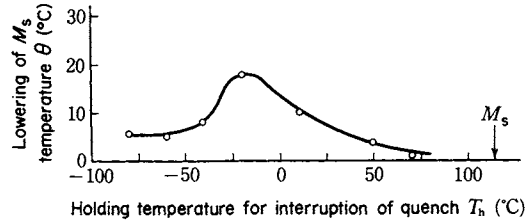

FIG. 5.36 Effect of interruption of quench on lowering of M_s temperature (Fe–1.63% Cr–1.06% C). (After Okamoto and Odaka.[273])

below a temperature corresponding to σ_s, the intersection point of the broken line and the continuous cooling curve designated by the solid line. The decrease in α' due to this stabilization is roughly proportional to $\sigma_s - T_h$.

The quantity $\theta = M_s - M_s'$ is taken as a criterion of stabilization,† which is closely related to the interruption temperature T_h. Okamoto and Odaka[273] studied a steel similar in composition to that of Fig. 5.35, and obtained the results shown in Fig. 5.36, the holding time being 1 hr. With lowering T_h, θ increases initially, then decreases after passing a maximum.

A model[294] based on the assumption that α' nuclei exist in the γ_R phase below the M_s was proposed to explain the stabilization of the γ_R phase. Accordingly, interstitial atoms diffuse to dislocation arrays at boundaries between the nuclei and the γ_R matrix and pin them during aging, so that a larger driving force for the transformation is required. This model assumes, as Knapp and Dehlinger did, the existence of α' nuclei of finite size in the γ_R phase. This assumption is not convincing. Without this assumption, boundaries between the transformed α' region and the untransformed γ_R region and the remaining lattice imperfections in the γ_R phase may be regarded as nucleation sites, and may be enriched by diffusing interstitials during aging. According to this revised model, stabilization is explained by mechanism 5−, a decrease in nucleation sites.‡ In either model, interstitial atoms are considered essential for this kind of stabilization mechanism.

5.7.6 Isothermal martensite formation after partial transformation

As stated in Section 5.2.4, the effect of the presence of the previous martensite on the transformation behavior of retained austenite is most

† A decrease in martensite content is also regarded as a criterion of stabilization. Let us explain it using Fig. 5.35. The amount of decrease in martensite at a certain standard temperature T_R, due to holding at, say, $T_h = 150°F$, is designated as δ, which is taken as the criterion of stabilization.

‡ A report[295] should be mentioned which insists that γ_R is more stabilized when α' is abundant rather than scarce.

prominent in the case when the previous transformation is induced catastrophically, but it should be remembered that the effect is also observed, more or less, in the general case. Here we are discussing phenomena somewhat different from this effect. It is how the presence of some athermal martensite produced affects the subsequent isothermal martensitic transformation.

Maksimova and Éstrin[296–299] studied this problem in a Ni–Mn steel, which undergoes a typical isothermal martensitic transformation. Previously, the steel had been quenched to −196°C to produce a small amount of athermal martensite. An examination of the progress of the subsequent isothermal transformation showed that its amount increases with the amount of the previous athermal martensite, the increasing rate being large at the initial stage of the latter. The initial part of the isothermal transformation is most influenced. Isothermal transformation behavior also depends on the temperature. The solid curve in Fig. 5.37 shows the initial isothermal transformation rate versus temperature for a steel transformed 4.3% at −196°C. The curve shows a peak between −50° and −100°C. Without previous athermal martensite, as is shown by the small peak (broken line) near the lower left-hand corner of the figure, the initial transformation rate is very small and the temperature of the transformation is fairly low and its range is narrow, the behavior showing a conspicuous contrast to that with previous athermal martensite. In other words, the presence of previous athermal martensite accelerates the isothermal transformation of the retained aus-

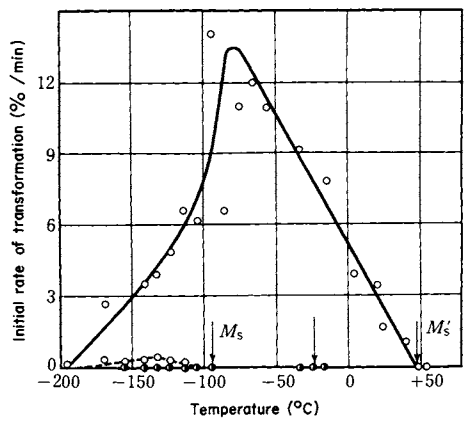

FIG. 5.37 Temperature dependence of the initial rate of isothermal transformation after previous partial transformation in an Fe–22.8% Ni–4.0% Mn–0.02% C alloy:—, after partial transformation of 4.3% at −196°C; – – –, without previous transformation; ◑, after holding at a temperature (center arrow). (After Éstrin.[298])

tenite, increasing the initial transformation rate and extending upward the temperature range of transformation.

Such accelerating action (i.e., enhanced instability) due to athermal transformation prior to isothermal transformation is less effective at higher pretransformation temperatures than at lower ones. Moreover, when the pretreatment temperature is above M_s, the effect is reversed; the isothermal transformation at lower temperatures is suppressed (stabilization), as shown by the solid semicircles in the figure. When the previous transformation is allowed to occur successively at several temperatures, the resultant effect is determined mainly by the last of the previous transformation steps.

A model was proposed[299] to explain the cause of the phenomena, which is principally based on the lattice strain energy developed during the previous transformation.

5.7.7 Effect of temper-aging on the transformation of retained austenite

Okamoto and Odaka[273] studied the effect of aging on the transformation of retained austenite, using the chromium steel as used for Fig. 5.36. The steel was quenched from 1000°C to room temperature to partially transform, and it was then aged. Figure 5.38 shows a decrease (θ) in M_s' temperature of γ_R versus aging time. The aging temperature is noted on each curve in the figure. When aged at 10°C, θ increases steadily with time, indicating a monotonic increase in stabilization, while at 100°C it increases faster and reaches a maximum at 1 hr, and then decreases somewhat for longer aging

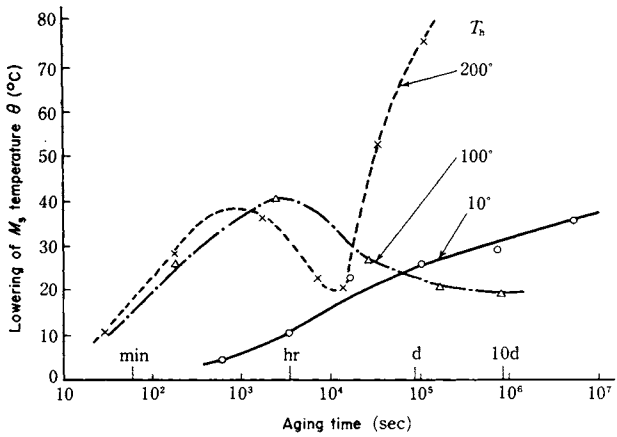

FIG. 5.38 Lowering of M_s temperature of retained austenite through aging (Fe–1.63% Cr–1.06% C, after partial transformation by quenching from 1000°C). (After Okamoto and Odaka.[273])

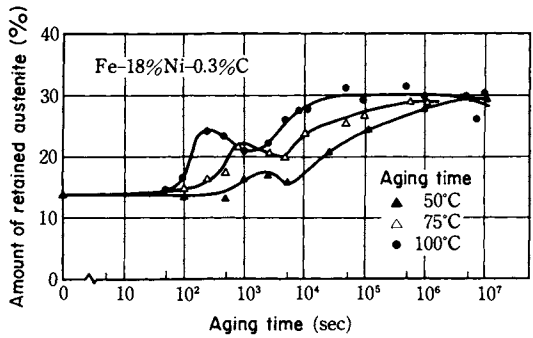

FIG. 5.39 Amount of austenite retained after aging followed by subzero cooling (Fe–18% Ni–0.3% C; 900°C → quenching to 0°C → aging → −78°C). (After Suto and Yamagata.[301])

times. When aged at a still higher temperature, 200°C, behavior similar to that noted at 100°C occurs in a shorter time; in addition, an abnormal increase in θ is observed again in the later period of aging.

Glover[300] obtained a similar result on a 1.4% C steel. A result[281] on an Fe–5% Ni–1.43% C alloy, whose M_s is at room temperature, indicated that aging above 50°C decreases θ after passing a maximum, even making it negative, then increases it again. This negative θ is attributed to overaging.

Suto and Yamagata[301] studied this problem using five kinds of high nickel steels. Figure 5.39 shows the change in the amount of γ_R (as determined by means of x-ray diffraction) versus aging time, which indicates stabilization occurring in two stages, and that the phenomenon is shifted to a shorter time by raising the aging temperature. The activation energies were determined as 16 kcal/mol for the first stage and 28 kcal/mol for the second stage. This stabilization phenomenon does not appear in specimens of extremely low carbon content (decarburized and denitrided by a wet hydrogen process). Recently, Hanada *et al.*[302] studied the effect of aging on the isothermal martensitic transformation in an Fe–23% Ni–3% Mn alloy, and found that the nose of the C curve of isothermal transformation is shifted to shorter times by aging (enhancing instability) at temperatures up to 100°C and is gradually shifted to longer times (stabilization) for aging temperatures above 100°C. This phenomenon disappears if the carbon content is decreased to around 0.009%.

Breedis[303] studied the effect of tempering (reversion) above 500°C. A Ni–Cr stainless steel,† whose M_s is −80°C, was quenched to −196°C to produce 14% α' martensite. It was then reheated to revert the reaction at various temperatures for 2 min or 2 hr, and was quenched again to −196°C to transform. The amount of martensite was determined by means of mag-

† The total of carbon and nitrogen contents is less than 0.005%.

netic measurement; the result are shown in Fig. 5.40. For specimens reverted by heating at 500°C the amount of α' is greater than the amount of α' present before reheating, but heating to a higher temperature has a stabilizing effect. An electron microscopic examination revealed that imperfections, such as internal twins, remained. These lattice imperfections therefore are a probable cause of γ stabilization. Several other works[304,305] concerning this problem were reported, the results of which essentially coincide.

We now consider why stabilization takes place. In Fig. 5.38, the initial increase in θ with aging time is due either to segregation of diffusing interstitial atoms into nucleation sites or to the diffusion of interstitials from α' martensite into the retained austenite. Berdova *et al.*[306] found that on reheating a quenched 7.25% Ni–0.38% C steel, the lattice constant of the retained austenite begins to increase at around 160°C, the amount reaching 0.004 Å (apart from thermal expansion), whereas the intensity and width of x-ray diffraction spots from the retained austenite remain unchanged. They suggested that the increase in the lattice constant affords evidence of the condensation of interstitials into retained austenite.

At a high enough aging temperature, however, the interstitial solute atoms begin to cluster to form preprecipitates after their segregation to nucleation sites. The clustering results in a lowering of the interstitial content in the γ phase and consequently an increase in M_s. This consideration explains

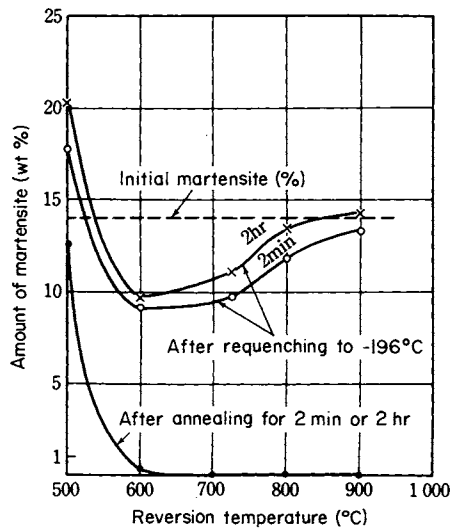

FIG. 5.40 Correlation of the amount of martensite formed with reversion temperature (in an Fe–16% Cr–12% Ni alloy containing 14% α' produced by cooling to −196°C from 900°C). (After Breedis.[303])

why θ decreases after passing a peak for $T_h = 100°C$ or 200°C in Fig. 5.38. It should be noted that θ increases again rather abnormally in the last stage of aging at 200°C. This is understood by considering that a bainitic phase is formed, which is supersaturated with interstitials, which diffuse into the matrix of γ_R to enhance its concentration, and the M_s is therefore lowered.

5.7.8 Stabilization during quenching and the effect of cooling rate

An examination of Fig. 5.30 reveals that the amount of retained austenite in steels is higher when the specimen is oil quenched rather than water quenched. This has been known[307] for some years to be due to the effect of the cooling rate and is observed in the following experiment as well. Figure 5.41, due to Esser and Cornelius,[308] shows the effect of the cooling rate on the amount of retained austenite. Except for cooling rates so slow that extremely small amounts of retained austenite result because of insufficient quenching, the amount of retained austenite decreases with increase in cooling rate. The main reason for this is that when cooled more slowly, frozen-in vacancies in specimens have enough time to migrate and disappear during cooling so that cause 7 works positively, in addition to cause 6 arising from the pinning of lattice imperfections by interstitials, as stated in the last section. It should be added that there is a possibility due to cause 4† that the smaller thermal stress developed by slow cooling also contributes to the stabilization.

The athermal stabilization as just described lowers the M_s for ordinary quenching compared to rapid quenching.[312–315] Figure 5.42, due to Messler *et al.*,[315] shows that with increasing cooling rate,‡ the M_s point of a 0.5%C steel rises sigmoidally, even 160°F higher for an extremely rapid cooling compared to ordinary cooling. Such a rise was also observed[316] for alloys containing nickel.

† This possibility was noticed earlier,[44,309] but from a practical point of view it is difficult to make a sweeping statement, because it depends on the nature of the specimen as well as on other conditions. For example, Hagiwara *et al.*[310] studied how the retained austenite is influenced by suppression of the axial contraction that generally takes place on quenching a rod specimen. For a 5-mm diameter high carbon alloy steel rod, the tensile stress for suppression of the axial contraction took a maximum value of 10 kg/mm^2 at temperatures around M_s, and the suppression increased the retained austenite remarkably. In contrast, the effect was scarcely observed for medium carbon alloy steels, and is even reversed for low carbon steels; that is, the retained austenite was decreased by suppression of contraction. On the other hand, an externally applied compression generally decreased the retained austenite. It is worth mentioning that such a stress effect appears only when the stress is above a threshold value.[311]

‡ Cooling was performed by spraying water on both sides of the surfaces of thin specimens. Variation of the cooling rate was achieved by changing the thickness of the specimen within the range of 0.1–1.5 mm. The temperature was measured by a thermocouple spark-welded to the specimen, and the M_s point was determined by magnetic measurement.

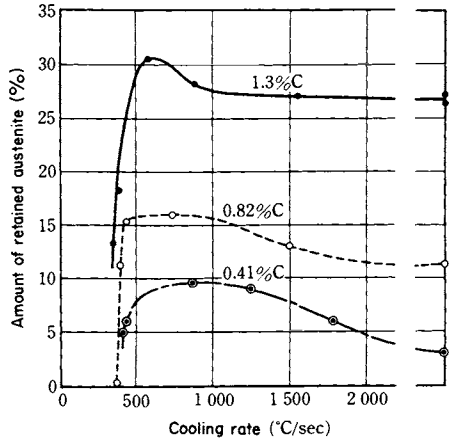

FIG. 5.41 Effect of cooling rate on the amount of retained austenite (carbon steel). (After Esser and Cornelius.[308])

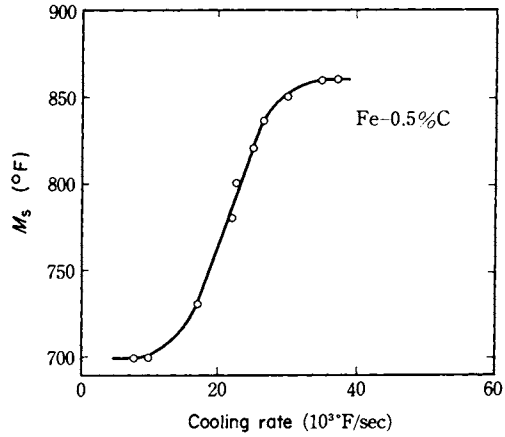

FIG. 5.42 Effect of cooling rate on M_s temperature. (After Messler *et al.*[315])

5.7.9 Stabilization by reverse transformation and by repetition of cyclic transformation

A. *Repetition of $\gamma \rightleftarrows \alpha'$ cycles*

In Fe–Ni alloys, the γ_r phase formed by reheating the martensite above A_f has a higher strength than the original γ phase.† This is perhaps due to the preservation of lattice imperfections developed during the first transformation. (It was shown in Section 3.7 that the γ_r phase forms martensitically

† See Messler *et al.*[315] and Thomas and Krauss[317] for 18–8 stainless steels.

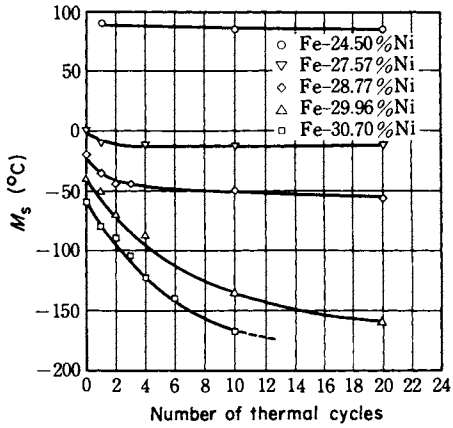

FIG. 5.43 Lowering of M_s temperature after $\gamma \leftrightarrows \alpha'$ thermal cycling. (After Imai *et al.*[323])

on rapid heating.) The α' phase produced by cooling γ_r again is strengthened compared to the former α' phase. It has been well known[307] that repetition of heating and cooling increases the strength with each cycle. Krauss and Cohen[189] studied Fe–(30.5–33.5)% Ni alloys and found that one thermal cycle increased the yield strength 2.5 times and five cycles gave an increase of 2.8 times.† Similar experiments[319,320] were also made on Fe–Ni alloys containing either vanadium or titanium.

In general, repetition of transformation stabilizes the austenite and lowers the M_s. It also prolongs the incubation period[282] of the isothermal martensitic transformation. It was reported[321] that alloys such as Fe–34% Ni, Fe–18% Ni–1% C, or Fe–5% Ni–1.5% C became, after many thermal cycles, incapable of martensitic transformation even if cooled to −189°C. The degree of stabilization seems to depend on the rate of heating and cooling, as well. The maximum stabilization was attained by a rate of 3°–4°C/min for Fe–(30.5–33.5)% Ni.[322]

According to Imai *et al.*,[323] the decrease in M_s of Fe–(24.5–30.7)% Ni alloy due to repetition of the $\gamma \rightleftarrows \alpha'$ transformation by cycling between −196°C and just above A_f is more striking for higher nickel contents, as shown by Fig. 5.43. An electron microscopic examination revealed that the dislocation density in the γ_r phase was increased and the structure became finer after transformation to α' occurred. In addition, it was observed that the internal twins decreased while the dislocation density increased as the repetition went on, leaving only dislocations after more than five cycles.

† According to Kondo and Hachisuka,[318] the hardness of a bearing steel (0.9% Cr–1.0% C) is increased by repeated subzero cooling, even when the heating temperature is not so high for the reverse $\alpha' \rightarrow \gamma$ transformation, but the effect is limited to two cycles and further cycles are scarcely effective.

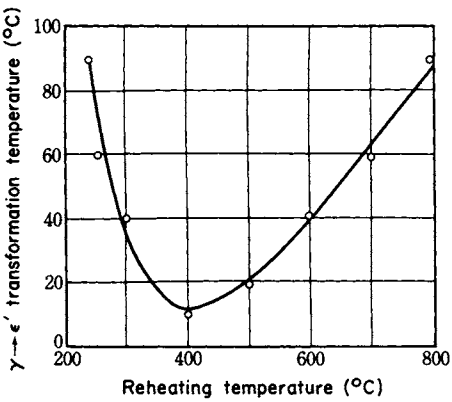

FIG. 5.44 Change of $\gamma \rightarrow \varepsilon$ transformation temperature with reheating temperature (Fe–19.1% Mn–0.05% C). (After Bogachev and Yegolaev.[332])

It was inferred[324] from these experimental findings that the decrease in M_s, that is, the stabilization of γ due to repetition of transformation, occurs mainly because lattice imperfections (such as dislocations) introduced during previous transformations impede subsequent transformations, in the end requiring a larger driving force for the transformation. The smaller stabilization effect for lower nickel content is attributed† to the annihilation of lattice imperfections owing to the higher M_f point.

The effect of repeated transformation has also been studied by measuring the coercive force of an Fe–Ni–Co alloy and correlating the results to the change in the microstructure.[326]

B. *Repetition of* $\gamma \rightleftarrows \varepsilon$ *cycles*

Stabilization by aging and thermal cycling occurs in the γ (f.c.c.) $\rightarrow \varepsilon$ (h.c.p. martensite) transformation, too.[327] Yershova and Bogachev[328] found that when $\gamma \rightarrow \varepsilon$ cycles at 100°–90°C and $\varepsilon \rightarrow \gamma$ cycles at 150°–200°C are repeated on an Fe–19.7% Mn–0.06% C steel, the amount of ε increases, and is accompanied by a hardness increase, up to four cycles. Further repetition stabilizes the austenite and decreases the amount of ε phase, which results in a decrease in hardness. This stabilization is increased by adding either Cr or Ni,[329] or Mo or W.[330] The stabilization effect is largest for thermal cycles around 400°C,[331] whereas too low or too high a temperature is disadvantageous for stabilization. Stabilization was observed even for a single cycle,[332] in which case the maximum stabilization occurs at 400°C, as shown in Fig. 5.44. The effect is more prominent for a longer heat treatment time.

† Also, for higher nickel content, if the heating temperature is high, say 475°C, an increase in M_s, instead of stabilization, occurs.[325] The reason is simply that the M_s is brought above the burst transformation temperature M_b, because the impurity atoms (carbon and nitrogen) precipitate as compounds and the resulting fineness of γ grains suppresses the burst transformation.

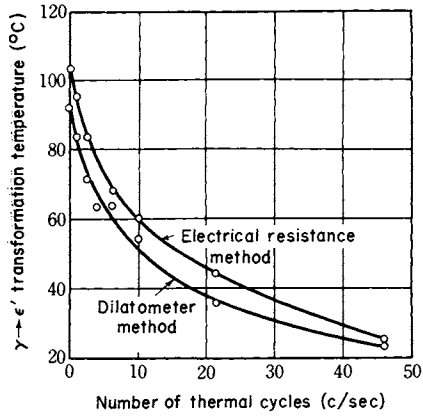

FIG. 5.45 Change of $\gamma \rightarrow \varepsilon$ transformation temperature with $-180°C \leftrightarrows 400°C$ thermal cycling (Fe–16.4% Mn–0.09% C–1.01% Si). (After Schumann and Heider.[333])

Schumann and Heider[333] studied an Fe–16.4% Mn–0.09% C steel and found that the M_s of the $\gamma \rightarrow \varepsilon$ transformation decreased as a result of repetition of cycles between $-180°C$ and $+400°C$ (Fig. 5.45); the amount of transformation increased, as revealed by the thermal expansion hysteresis curve and changes in electrical resistivity and hardness. The situation is changed more or less by reducing the heating and cooling rate in a cycle. For example, after repetition of the cycle

$$20°C, 7\,hr \overset{5\,hr}{\rightarrow} 400°C, 4\,hr \overset{5\,hr}{\rightarrow} 20°C, 7\,hr$$

the M_s point gradually decreases, and finally the γ phase is so stabilized that it does not transform, although it gradually transforms to ε when left for a long time at ambient temperature. The transformation in this case occurs more rapidly for a specimen subjected to a smaller number of cycles.

Austenite stabilization by the $\gamma \rightleftarrows \varepsilon$ cycles described in the foregoing, as well as by $\gamma \rightleftarrows \alpha'$ cycles, owes its origin to interstitial atoms. Lysak and Nikolin[334] † conducted thermal cycle experiments between $-196°C$ and $400°C$ on Fe–16% Mn–(0–0.35)% C steels and obtained the results shown in Fig. 5.46. It is clear that stabilization is enhanced by increasing the carbon content. A steel containing no carbon shows almost no stabilization and there is even a slight tendency toward enhancing the instability.‡ They also made experiments on an Fe–20% Mn steel with no carbon content and obtained a similar result.

† As was stated in Section 3.8, these authors insist on the existence of the ε' phase, which may be regarded as a γ phase containing periodic stacking faults, being formed in a stage preparatory to the formation of the ε phase. They suggest[334] that on repetition of $\gamma \rightleftarrows \varepsilon$ cycles, the ε' phase together with increased irregular stacking faults can be a cause of hardening.

‡ Discussed in Section 2.3 from a crystallographic point of view.

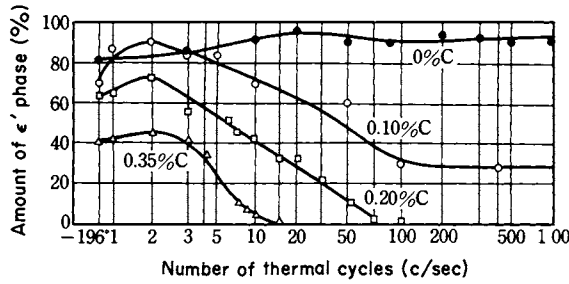

FIG. 5.46 Change in amount of ε phase with $-196°C \rightleftarrows 400°C$ thermal cycling (Fe–16% Mn–(0–0.35)% C). (After Lysak and Nikolin.[334])

Stacking faults developed during thermal cycles also contribute to stabilization. Shklyar *et al.*[335,336] studied stabilization by repeated $\gamma \rightleftarrows \varepsilon$ transformation cycles by means of x-ray diffraction, using an Fe–19.1% Mn–0.05% C steel. In their first report, the changes in x-ray reflections from relatively large grains grown by heating to 1150°C were observed, while in their second paper, the relative amounts of the ε and γ phases were estimated from the ratio of the integrated intensities of $(111)_\gamma$ and $(10.1)_\varepsilon$ reflections, using fine-grained specimens that were obtained by annealing at 800°C after plastic deformation. Figure 5.47a shows this ratio for three different kinds of thermal cycles. In each case the ε phase content increases for a single cycle but decreases with repetition of more than two cycles, indicating stabilization of the γ phase. The cycle involving $400°C \rightleftarrows -196°C$ caused for the most part the largest stabilization among these three kinds of cycles. During the thermal cycling, broadening and shift of the retained austenite lines, due to lattice imperfections that developed, was observed. From measurement of the line broadening and line shift, a stacking fault parameter α was calculated. It is largest for the $400°C \rightleftarrows -196°C$ cycle, as is shown in Fig. 5.47b,

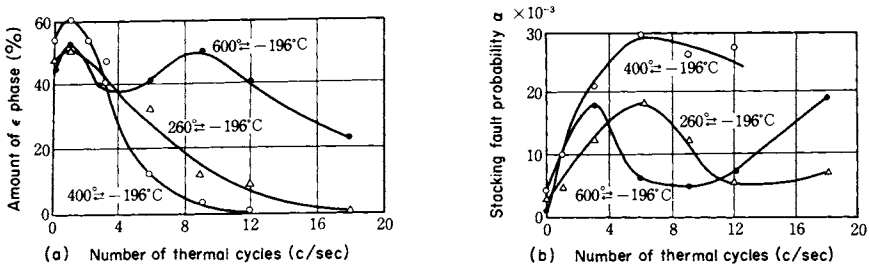

FIG. 5.47 Effect of repeated $\gamma \rightleftarrows \varepsilon$ transformations (Fe–19.1% Mn–0.05% C). (a) Change in amount of ε martensite. (b) Change of stacking fault probabilities in austenite. (After Shklyar *et al.*[336])

reaches a maximum value for six cycles, and remains almost constant for further repetition of the thermal cycling. The stabilization of austenite by thermal $\gamma \rightleftarrows \varepsilon$ cycling in high manganese steels is prominent in cases above 18% Mn.[337] It is mentioned in Section 3.8.1 that a phase with a different structure appears during the $\gamma \rightarrow \varepsilon$ transformation of Mn steels.

A similar phenomenon is observed for cobalt, a typical metal that undergoes the $\gamma \rightarrow \varepsilon$ transformation. In cobalt, a single cycle is effective for stabilization, but further repetitions scarcely strengthen it,[338] because a high heating temperature such as 500°C is necessary for reverse transformation. But it was ascertained[339] on commercial cobalt that stacking faults in the ε phase increase steadily with repetition of transformation cycles. For example, in a specimen that has undergone repetitions of 520°C $\rightleftarrows$ room temperature, after annealing at 650°C, the number of stacking faults increases as shown in the accompanying tabulation, where α and β designate the probabilities of stacking faults and twin faults, respectively, that were determined by means of Fourier analysis of x-ray diffraction profiles of (10.1) and (10.2) lines from the ε phase.

	As annealed at 650°C	Repetition of heat cycles			
		1	2	5	10
$(3\alpha + \beta) \times 10^3$	95	123	149	130	150

A stabilization phenomenon also occurs in TiNi martensite by repetition of transformation; it causes grain refinement and strain development. The M_s temperature, originally 22°C, was lowered to 9°C by repeating the transformation ten times.[340]

References

1. W. Paul and D. M. Warshauer, "Solids Under Pressure" (D. W. Bridgman, ed.). McGraw-Hill, New York, 1962.
2. G. C. Kennedy and P. N. La Mori, "Progress in Very High Pressure Research," p. 304. Wiley, New York, 1961.
3. L. Kaufman, *Acta Metall.* **9**, 896 (1961).
4. Z. S. Basinski, W. Hume-Rothery, and A. L. Sutton, *Proc. Roy. Soc. London* **A229**, 459 (1955).
5. L. Kaufman, E. V. Cloughery, and R. J. Weiss, *Acta Metall.* **11**, 323 (1963).
6. F. B. Bundy, *J. Appl. Phys.* **36**, 616 (1965).
7. P. C. Johnson, B. A. Stein, and R. S. Davis, *J. Appl. Phys.* **33**, 557 (1962).
8. T. Takahashi and W. A. Bassett, *Science* **145**, 483 (1964).
9. S. A. Novikov, I. I. Divnov, and A. G. Ivanov, *Fiz. Met. Metalloved.* **21**, 252 (1966).
10. R. C. Ruhl and M. Cohen, *Trans. AIME* **245**, 241 (1969).

11. D. Bancroft, E. L. Peterson, and S. Minchall, *J. Appl. Phys.* **27**, 291 (1956).
12. P. M. Giles, M. H. Longenbach, and A. R. Marder, *J. Appl. Phys.* **42**, 4290 (1971).
13. V. A. Zil'bershteyn and É. I. Éstrin, *Fiz. Met. Metalloved*, **32**, 463 (1971).
14. J. E. Hilliard and J. W. Cahn, "Progress in Very High Pressure Research," p. 109, Wiley, New York, 1961.
15. S. A. Kulin, M. Cohen, and B. L. Averbach, *J. Met.* **4**, 661 (1952).
16. S. V. Radcliffe, *Nature* (*London*) **200**, 161 (1963).
17. J. S. Pascover and S. V. Radcliffe, *Acta Metall.* **17**, 321 (1969).
18. L. Kaufman, A. Leyenaar, and J. S. Harvey, "Progress in Very High Pressure Research," p. 90. Wiley, New York, 1961; *Acta Metall.* **8**, 270 (1960).
19. L. E. Tanner and S. A. Kulin, *Acta Metall.* **9**, 1038 (1961).
20. R. E. Hanneman, R. E. Ogilvie, and H. C. Gotos, *Trans. AIME* **233**, 685 (1965).
21. L. D. Blackburn, L. Kaufman, and M. Cohen, *Acta Metall.* **13**, 533 (1965).
22. E. Scheil and W. Normann, *Arch. Eisenhüttenwes.* **30**, 751 (1959).
23. W. Jellinghaus and O. Schmidt, *Arch. Eisenhüttenwes.* **36**, 47 (1965).
24. L. Kaufman and A. E. Ringwood, *Acta Metall.* **9**, 941 (1961).
25. R. W. Rohde, *Acta Metall.* **18**, 903 (1970).
26. T. R. Loree, R. H. Warnes, E. G. Zulas, and C. M. Fowler, *Science* **153**, 1277 (1966).
27. R. A. Graham, D. H. Anderson, and J. R. Holland, *J. Appl. Phys.* **38**, 223 (1967).
28. T. P. Yershova and E. G. Ponyatovskij, *Russ. Metall.* **4**, 81 (1967).
29. A. Christou and N. Brown, *J. Appl. Phys.* **42**, 4160 (1971).
30. M. Fujita and Y. Uchiyama, *High Pressure Symp., Jpn., 14th* Oct., 25A12 (1972).
31. W. H. Gust and E. B. Royce, *J. Appl. Phys.* **41**, 2443 (1970).
32. S. V. Radcliffe, M. Schatz, and S. A. Kulin, *J. Iron Steel Inst.* **201**, 143 (1963); *J. Met.* **12**, 731 (1960).
33. J. E. Hilliard, *Trans. AIME* **227**, 429 (1963).
34. S. V. Radcliffe and M. Schatz, *Acta Metall.* **10**, 201 (1962).
35. R. E. Predmore and E. P. Klier, *Trans. ASM* **62**, 768 (1969).
36. A. J. Stregulin and N. P. Chuprakova, *Fiz. Met. Metalloved.* **1**, 368 (1955).
37. A. J. Strengulin and L. A. Nel'Nikov, *Fiz. Met. Metalloved.* **8**, 406 (1959).
38. R. F. Vyhnal and S. V. Radcliffe, *Acta Metall.* **15**, 1475 (1967).
39. M. Suzuki and M. Fujita, *Trans. Nat. Res. Inst. Met.* **10**, 73 (1968).
40. R. E. Hanneman, R. E. Ogilvie, and H. C. Gotos, *Trans. AIME* **233**, 685, 691 (1965).
41. R. W. Rohde and R. A. Graham, *Trans. AIME* **245**, 2441 (1969).
42. L. E. Pope and L. R. Edwards, *Acta Metall.* **21**, 281 (1973).
43. J. Brettschneider and H. Warlimont, *Z. Metallkd.* **59**, 70 (1968).
44. E. C. Bain, *Trans. Am. Soc. Steel Treat.* **8**, 14 (1925).
45. A. W. McReynolds, *J. Appl. Phys.* **20**, 896 (1949).
46. Z. Nishiyama, *Sci. Rep. Tohoku Imp. Univ.* **25**, 94 (1936).
47. S. Takeuchi and H. Suzuki, *Sci. Rep. RITU* (*Tohoku Univ.*) **A2**, 50 (1950).
48. J. C. Fisher and D. Turnbull, *Acta Metall.* **1**, 310 (1953).
49. C. Crussard, *C. R. Acad. Sci. Paris* **237**, 1709 (1953).
50. T. Hirayama and M. Kogirima, *J. Jpn. Inst. Met.* **34**, 507 (1970).
51. F. Fraunberger and E. Klement, *Z. Metallkd.* **53**, 611 (1962).
52. Y. Hosoi and Y. Kawakami, *Tetsu to Hagane* **49**, 1780 (1963).
53. G. F. Bolling and R. H. Richman, *Ser. Metall.* **4**, 539 (1970).
54. J. R. Patel and M. Cohen, *Acta Metall.* **1**, 531 (1953).
55. L. Kaufman and M. Cohen, *Trans. AIME* **206**, 1393 (1956).
56. G. Wassermann, *Arch. Eisenhüttenwes.* **11**, 89 (1937).
57. T. Honma, *J. Jpn Inst. Met.* **21**, 263 (1957).
58. A Kochendörfer and H. G. Müller, *Arch. Eisenhüttenwes.* **26**, 291 (1955).

59. W. Schmiedel and H. Lange, *Arch. Eisenhüttenwes.* **26**, 359 (1955).
60. M. G. H. Wells and D. R. F. West, *J. Iron Steel Inst.* **200**, 710 (1962).
61. J. F. Breedis and W. D. Robertson, *Acta Metall.* **11**, 547 (1963).
62. J. F. Breedis, *Acta Metall.* **13**, 239 (1965).
63. T. Hirayama, *J. Jpn. Inst. Met.* **35**, 447 (1971).
64. J. R. C. Guimarães, *Scr. Metall.* **6**, 795 (1972).
65. I. Hagiwara and S. Kanazawa, *Trans. JIM* **3**, 133 (1963).
66. W. G. Burgers and J. A. Kosterman, *Acta Met.* **13**, 568 (1965).
67. H. P. Sattler, and G. Wassermann, *J. Less-Common Met.* **28**, 119 (1972).
68. Y. Higo, F. Lecroisey, and T. Mori, Private communication (1971).
69. A. Kochendörfer and G. Otto, *Arch. Eisenhüttenwes.* **29**, 709, 775 (1958); **30**, 227 (1959).
70. B. L. Averbach, S. G. Lorris, and M. Cohen, *Trans. ASM* **44**, 746 (1952).
71. L. W. Pateman and H. S. Peiser, *Nature (London)* **171**, 696 (1953).
72. M. B. Reynolds, J. R. Low, Jr., and L. O. Sullivan, *J. Met.* **7**, 555 (1955).
73. I. N. Bogachev and L. S. Malinov, *Fiz. Met. Metalloved.* **15**, 678 (1963).
74. T. Honma, T. Sato, and S. Oizumi, Japan Inst. Metals, Spring Meeting, p. 27 (1972).
75. F. Lacroisey and A. Pineau, *Metall. Trans.* **3**, 387 (1972).
76. C. J. Guntner and R. P. Reed, *Trans. ASM* **55**, 399 (1962).
77. S. A. Kulin and M. Cohen, *Trans. AIME* **188**, 1139 (1950).
78. F. V. Ellis and G. P. Mohanty, *Scr. Metall.* **4**, 929 (1970).
79. K. Otsuka and K. Shimizu, *Phil. Mag.* **24**, 481 (1971).
80. K. Otsuka, T. Nakamura, and K. Shimizu, *Trans. JIM* **15**, 200, 211 (1974).
81. R. V. Krishnan and L. C. Brown, *Metall. Trans.* 1017 (1973).
82. R. V. Krishnan and L. C. Brown, *Scr. Metall.* **6**, 883 (1972).
83. M. Adachi and T. Tsujimoto, *J. Jpn. Inst. Met.* **25**, 568 (1961).
84. D. N. Williams, R. A. Wood, R. I. Jaffee, and H. R. Ogden, *Trans. AIME* **230**, 256 (1964).
85. M. J. Blackburn and J. A. Feeney, *J. Inst. Met.* **97**, 132 (1971).
86. M. K. Koul and J. F. Breedis, *Acta Metall.* **18**, 579 (1970).
87. R. J. Wasilewski, *Scr. Metall.* **5**, 131 (1971).
88. P. W. Bridgman, *J. Appl. Phys.* **30**, 214 (1959).
89. R. D. Nelson and J. C. Shyne, *Trans. AIME* **236**, 1725 (1966).
90. T. A. Read, M. W. Burkart, C. W. Chen, M. S. Wechsler, and D. S. Lieberman, U.S. Atomic Energy Commission, Publ. NYO-3960 (1953).
91. B. Predel, *Z. Metallkd.* **55**, 117 (1964).
92. R. J. Wasilewski, *Metall. Trans.* **2**, 2973 (1971).
93. E. C. Roberts, H. Kellerer, and F. D. Walsh, *Metallography* **3**, 291 (1970).
94. I. Tamura, *Tetsu to Hagane* **56**, 429 (1970).
95. S. Petsche and F. Stangler, *Z. Metallkd.* **62**, 601, 606 (1971).
96. A. Sauveur, *Iron Age* **113**, 581 (1924).
97. M. de Jong and G. W. Rathenau, *Nature (London)* **181**, 1396 (1958).
98. R. H. Bush and J. C. Bokros, *Acta Metall.* **12**, 102 (1964).
99. V. F. Zackay, E. R. Parker, D. Fahr, and R. Busch, *Trans. ASM* **60**, 252 (1967).
100. I. Tamura, T. Maki, and H. Hato, *Trans. ISIJ* **10**, 163 (1970).
101. I. Tamura, T. Maki, H. Hato, and K. Aburai, *J. Jpn. Inst. Met.* **33**, 1383 (1969).
102. A. Ankara *J. Iron Steel Inst.* **208**, 819 (1970).
103. R. A. Kot and V. Weiss, *Metall. Trans.* **1**, 2685 (1970).
104. E. S. Machlin and M. Cohen, *Trans. AIME* **191**, 746 (1951); **194**, 519 (1952).
105. O. P. Maksimova, N. P. Soboleva, and É. I. Éstrin, *Dokl Acad. Nauk SSSR* **134**, 871 (1960).
106. J. C. Bokros and E. R. Parker, *Acta Metall.* **11**, 1291 (1963).
107. J. Philibert and C. Crussard, *Rev. Métall.* **53**, 973 (1956).

108. S. Kajiwara, *Trans. JIM* **9**, Suppl. 543 (1968); *Trans. Nat. Res. Inst. Met.* **10**, 295 (1968); *J. Phys. Soc. Jpn.* **25**, 1741 (1968); **27**, 268 (1969).
109. C. S. Barrett, *Trans. AIME* **188**, 123 (1950).
110. P. S. Kotval and R. W. K. Honeycombe, *Electron Miscrosc. Conf.*, 6th p. 471 (1966); *Acta Metall.* **16**, 597 (1968).
111. E. de Lamotte and C. Altstetter, *Trans. AIME* **245**, 651 (1969); Inst. Met. Monograph. No. 33, p. 189 (1969).
112. H. Suzuki, T. Yamamoto, and K. Hayashi, *J. Jpn. Soc. Powder Metall.* **14**, 262 (1967).
113. H. Suzuki, T. Yamamoto, and H. Sakanoue, *J. Jpn. Inst. Met.* **32**, 993 (1968).
114. C. M. Wayman and K. Shimizu, *Met. Sci. J.* **6**, 175 (1972).
115. G. V. Kurdjumov and L. G. Khandros, *Dokl. Akad. Nauk SSSR* **66**, 211 (1949).
116. C. W. Chen, *Trans. AIME* **209**, 1202 (1957).
117. G. V. Kurdjumov, *Dokl. Akad. Nauk SSSR* **60**, 1543 (1948).
118. A. B. Greninger and V. G. Mooradian, *Trans. AIME* **128**, 337 (1938).
119. E. Hornbogen and G. Wassermann, *Z. Metallkd.* **47**, 427 (1956).
120. E. J. Suoninen, R. M. Genevray, and M. B. Bever, *Trans. AIME* **206**, 283 (1956).
121. E. Hornbogen, A. Segmüller, and G. Wassermann, *Z. Metallkd.* **48**, 379 (1957).
122. L. C. Brown and M. J. Stewart, *Trans. AIME* **242**, 1353 (1968).
123. J. E. Reynolds and M. B. Bever, *Trans. AIME* **194**, 1065 (1952).
124. A. L. Titchener and M. B. Bever, *Trans. AIME* **200**, 303 (1954).
125. R. E. Hummel and J. W. Koger, *Trans. AIME* **239**, 1655 (1967); **242**, 1754 (1968).
126. R. E. Hummel; *Z. Metallkd.* **59**, 153 (1968).
127. J. D. Ayers and C. P. Herring; *J. Mater. Sci.* **6**, 1325 (1971).
128. M. W. Burkart and T. A. Read, *Trans. AIME* **197**, 1516 (1953).
129. Z. S. Basinski and J. W. Christian, *Acta Metall.* **2**, 101 (1954).
130. S. G. Khayutin, *Fiz. Met. Metalloved.* **26**, 742 (1968).
131. I. A. Arbuzova, G. V. Kurdjumov, and L. G. Khandros, *Fiz. Met. Metalloved* **11**, 272 (1961).
132. V. A. Lobodyuk, V. K. Tkachuk, and L. G. Khandros, *Fiz. Met. Metalloved* **33**, 137 (1972).
133. K. Otsuka, K. Shimizu, I. Cornelis, and C. M. Wayman, *Scr. Metall* **6**, 377 (1972).
134. A. Nagasawa, *J. Phys. Soc. Jpn.* **30**, 1200, 1505 (1971); **31**, 136 (1971).
135. C. M. Wayman and K. Shimizu, *Met. Sci. J.* **6**, 175 (1972).
136. W. J. Buchler, J. V. Gilfrich, and R. C. Wiley, *J. Appl. Phys.* **34**, 1475 (1963).
137. R. J. Wasilewski, *Metall. Trans.* **2**, 2973 (1971).
138. L.-C. Chang and T. A. Read, *Trans. AIME* **189**, 47 (1951).
139. A. Nagasawa and K. Kawachi, *J. Phys. Soc. Jpn.* **30**, 296 (1971).
140. C. M. Wayman, *Scr. Metall.* **5**, 489 (1971).
141. Y. Kachi, N. Nakanishi, Y. Murakami, S. Miura: Japan Inst. Metals, Spring Meeting, p. 47 (1971).
142. N. Nakanishi, Y. Murakami, Y. Kachi, T. Mori, and S. Miura, *Phys. Lett.* **37A**, 61 (1971).
143. Y. Murakami, *J. Phys. Soc. Jpn.* **33**, 1350 (1972).
144. K. Enami and S. Nenno, *Metall. Trans.* **2**, 1487 (1971).
145. K. Enami, S. Nenno, and Y. Inagaki, Japan Inst. Metals, Fall Meeting, p. 233 (1972).
146. Y. K. Au and C. M. Wayman, *Scr. Metall.* **6**, 1209 (1972).
147. J. L. Smialek and R. F. Hehemann, *Metall. Trans.* **4**, 1591 (1973).
148. R. C. de Lange and J. A. Zijderveld, *J. Appl. Phys.* **39**, 2195 (1968).
149. G. Donzé and R. Faivre, *C. R. Acad. Sci. Paris* **245**, 2277 (1957).
150. K. Otsuka, T. Sawamura, K. Shimizu, and C. M. Wayman, *Metall. Trans.* **5**, 2583 (1971).
151. K. Otsuka and K. Shimizu, *Scr. Metall.* **4**, 469 (1970).
152. K. Otsuka, *Jpn. J. Appl. Phys.* **10**, 571 (1971).

153. D. P. Dunne and C. M. Wayman, *Metall. Trans.* **4**, 137, 147 (1973).
154. K. Enami, S. Nenno, and Y. Minato, *Scr. Metall.* **5**, 663 (1971).
155. V. V. P. Kutumbarao and P. Rama Rao, *Scr. Metall.* **6**, 1103 (1972).
156. A. Nagasawa, *Phys. Status Solidi (a)* **8**, 531 (1971).
157. V. A. Teplov, V. A. Pavlov, and K. A. Malyshev, *Fiz. Met. Metalloved.* **27**, 339 (1969).
158. I. A. Arbuzova, V. S. Gavrilyuk, and L. G. Khandros, *Fiz. Met. Metalloved.* **27**, 1126 (1969); **30**, 181 (1970).
159. E. Scheil, Unpublished.
160. G. Wassermann, *Arch. Eisenhüttenwes.* **10**, 321 (1936/37).
161. E. Scheil and W. Thiele, *Arch. Eisenhüttenwes.* **12**, 103 (1938).
162. E. Scheil and J. Müller, *Arch. Eisenhüttenwes.* **27**, 801 (1956).
163. T. Aoyagi and K. Sumino, *Phys. Status Solidi* **33**, 317 (1969).
164. K. Sumino, *Phys. Status Solidi* **33**, 327 (1969).
165. K. Sugimoto, Japan Inst. Metals, Fall Meeting, p. 155 (1969); Spring Meeting, p. 36 (1970); Spring Meeting, p. 90 (1971).
166. D. Birchon, *J. Inst. Met.* **93**, 547 (1965).
167. N. G. Pace and G. A. Saunders, *Phil. Mag.* **22**, 73 (1970).
168. R. I. Garber and Zh. F. Kharitonova, *Fiz. Met. Metalloved.* **26**, 888 (1968).
169. V. N. Belko, B. M. Darinskii, and V. S. Postnikov, *Fiz. Met. Metalloved* **27**, 141 (1968).
170. B. M. Darinskii and Yu. N. Levin, *Fiz. Met. Metalloved.* **27**, 1051 (1968).
171. Y. Yamada and M. Mori, *Intern. Congr. Cryst.* **9**, XIII-21, 179 (1972).
172. R. P. Reed, A. F. Clark, and R. E. Schramm, *Scr. Metall.* **5**, 485 (1971).
173. M. B. Reynolds, J. R. Low, Jr., and L. O. Sullivan, *J. Met.* **7**, 555 (1955).
174. L. F. Porter and G. J. Dienes, *Bull. Am. Phys. Soc.* **3**, II, 118 (1958).
175. M. A. Jaswon, *I. U. Cr. Int. Congr. 3rd* (1954).
176. T. Honma, *Bull. Jpn. Inst. Met.* **21**, 122 (1957).
177. R. Huizing and J. A. Klostermann, *Acta Metall.* **14**, 1693 (1966).
178. H. Warlimont, *Trans. AIME* **221**, 1270 (1961).
179. S. Nagakura, M. Kikuchi, Y. Kaneko, and S. Oketani, *Jpn. J. Appl. Phys.* **2**, 201 (1963).
180. H. Warlimont, *Metall. Trans.* **2**, 1847 (1971).
181. E. Grünbaum and G. Kremer, *J. Appl. Phys.* **39**, 347 (1968).
182. T. Kato and S. Ogawa, *Jpn. J. Appl. Phys.* **9**, 875 (1970).
183. G. Thomas and C. Vercaemer, *Metall. Trans.* **3**, 2501 (1972).
184. For example, M. G. Gaidukov and V. D. Sadovskij, *Dokl. Akad. Nauk SSSR* **96**, 67 (1954).
185. W. J. Barrett and A. R. Troiano, *Trans. AIME* **175**, 910 (1948).
186. M. R. Meyerson and S. J. Rosenberg, *J. Res. Nat. Bur. Std.* **55**, 177 (1955).
187. W. C. Leslie and R. L. Miller, *Trans. ASM* **57**, 972 (1964).
188. M. Izumiyama, *Sci. Rep. IRTU (Tohoku Univ.)* **14**, 11 (1962).
189. G. Krauss, Jr. and M. Cohen, *Trans. AIME* **224**, 1212 (1962); **227**, 278 (1963).
190. Z. Nishiyama, *J. Jpn. Inst. Met.* **2**, 202 (1938).
191. O. P. Maksimova and V. V. Nemirovskiy, *Dokl. Acad. Nauk SSSR* **177**, No. 1, p. 81 (1967).
192. R. E. Hummel, J. W. Koger, and W. Pasupathi, *Trans. AIME* **241**, 249 (1968).
193. R. E. Cech and D. Turnbull; *Trans. AIME* **206**, 124 (1956).
194. S. Nagashima and Z. Nishiyama, *J. Jpn. Inst. Met.* **23**, 728 (1959).
195. Y. Kachi, Y. Bando, and S. Higuchi, *Jpn. J. Appl. Phys.* **1**, 307 (1962).
196. Y. Bando, *Trans. JIM* **5**, 135 (1964).
197. Yu. A. Klyachko and G. K. Baranova, *Fiz. Met. Metalloved.* **25**, 569 (1968).
198. R. C. Bowe, L. Muldaver, and F. Chambers, *Scr. Metall.* **4**, 581 (1970).
199. V. Raghavan and A. R. Entwisle, *Iron Steel Inst. Spec. Rep.* **93**, 30 (1965).

200. V. Raghavan, *Acta Metall.* **17**, 1299 (1969).
201. S. R. Pati and M. Cohen, *Acta Metall.* **17**, 189 (1969).
202. R. L. Fullman, *Trans. AIME* **197**, 447 (1953).
203. E. Hornbogen and W. Meyer, *Acta Metall.* **15**, 584 (1967); *Z. Metallkd.* **58**, 445 (1967).
204. J. K. Abraham and J. S. Pascover, *Trans. AIME* **245**, 759 (1969).
205. G. R. Speich, *Trans. AIME* **227**, 754 (1963).
206. Y. Honnorat, G. Henry, and J. Manenc, *Mém. Sci. Métall.* **62**, 429 (1965).
207. K. A. Malyshev and E. D. Butakova, *Fiz. Met. Metalloved.* **30**, 602 (1970).
208. C. S. Smith, "Age Hardening of Metals," p. 186. Am. Soc. Metals, (1940).
209. J. B. Newkirk, *Trans. AIME* **209**, 1214 (1957).
210. K. E. Easterling and G. C. Weatherly, *Acta Metall.* **17**, 845 (1969).
211. K. E. Easterling and P. R. Swann, The Mechanism of Phase Transformations in Crystalline Solids, Inst. Metals, Spec. Rep. No. 33, p. 152 (1969); *Acta Metall.* **19**, 117 (1971).
212. L. G. Zhuravlev, V. V. Golikova, M. M. Shteynberg, and N. V. Partileyenko, *Fiz. Met. Metalloved.* **27**, 478 (1969).
213. J. R. C. Guimarães and J. C. Shyne, *Scr. Metall.* **4**, 1019 (1970).
214. D. R. Wollmann and J. R. C. Guimarães, *Scr. Metall.* **7**, 355 (1973).
215. H. C. Fiedler, B. L. Averbach, and M. Cohen, *Trans. ASM* **47**, 267 (1955).
216. R. P. Reed, *Acta Metall.* **10**, 865 (1962).
217. R. Lagneborg, *Acta Metall.* **12**, 823 (1964).
218. J. F. Breedis, *Acta Metall.* **13**, 239 (1965).
219. T. Hirayama and M. Kogirima, *J. Jpn. Inst. Met.* **34**, 826 (1970).
220. T. G. Gooch and D. R. F. West, *J. Iron Steel Inst.* **205**, 555 (1967).
221. J. R. C. Guimarães and J. C. Shyne, *Metall. Trans.* **2**, 2063 (1971).
222. I. Tamura, T. Maki, M. Nakanishi, and H. Oka, *Suiyokaishi* **17**, 75 (1970).
223. I. Ya. Georgiyeva, G. V. Kurdjumov, O. P. Maksimova, and V. V. Nemirovskiy, *Fiz. Met. Metalloved.* **23**, 1070 (1967).
224. H. Nakamura and H. Yamanaka, Japan Inst. Metals, Fall Meeting, p. 211 (1970).
225. L. E. Pope, *Metall. Trans.* **3**, 2151 (1972).
226. J. B. Hess and C. S. Barrett, *Trans. AIME* **194**, 645 (1952).
227. C. C. Koch and C. J. McHargue, *Acta Metall.* **16**, 1105 (1968).
228. W. Wallace and W. J. Kitchingman, *J. Inst. Met.* **97**, 56 (1969).
229. K. R. Satyanarayan and A. P. Miodownik, The Mechanism of Phase Transformation in Crystalline Solids, Inst. Metals, Spec. Rep. No. 33, p. 162 (1969).
230. V. D. Sadovskij, N. M. Rodizin, L. V. Smirnov, G. M. Filonchik, and I. G. Fakidov, *Fiz. Met. Metalloved.* **12**, 302 (1961).
231. E. A. Zavadskij and I. G. Fakidov, *Fiz. Met. Metalloved.* **12**, 311 (1961).
232. Ye. A. Fokina and E. A. Zavadskij, *Fiz. Met. Metalloved.* **16**, 311 (1963).
233. Ye. A. Fokina, L. V. Smirnov, and V. D. Sadosvkij, *Fiz. Met. Metalloved.* **19**, 592 (1965).
234. M. A. Krivoglaz and V. D. Sadovskij, *Fiz. Met. Metalloved.* **18**, 502 (1964).
235. É. I. Éstrin, *Fiz. Met. Metalloved.* **19**, 929 (1965).
236. Ye. A. Fokina, L. V. Smirnov, V. D. Sadovskij, and A. F. Peikul, *Fiz. Met. Metalloved.* **19**, 932 (1965).
237. I. G. Fakidov, L. D. Voronchikhin, E. A. Zavadskij, and A. M. Burkhanov, *Fiz. Met. Metalloved.* **19**, 852 (1965).
238. M. L. Bernshteyn, G. I. Granik, and P. R. Dolzhanskij, *Fiz. Met. Metalloved.* **19**, 832 (1965).
239. L. D. Voronchikhin and I. G. Fakidov, *Fiz. Met. Metalloved.* **21**, 436 (1966).
240. Ye. A. Fokina, L. V. Smirnov, and V. D. Sadovskij, *Fiz. Met. Metalloved.* **19**, 722 (1965).
241. P. A. Malinen and V. D. Sadovskij, *Fiz. Met. Metalloved.* **21**, 787 (1966).
242. K. R. Satyanarayan, W. Eliasz, and A. P. Miodownik, *Acta Metall.* **16**, 877 (1968).

243. P. A. Malinen, V. D. Sadovskij, L. V. Smirnov, and Ye. A. Fokina, *Fiz. Met. Metalloved.* **23**, 535 (1967).
244. L. D. Voronchikhin and I. G. Fakidov, *Fiz. Met. Metalloved.* **24**, 459 (1967).
245. P. A. Malinen and V. D. Sadovskij, *Fiz. Met. Metalloved.* **28**, 1012 (1969).
246. F. D. Miroshnichenko, V. L. Snezhnoy, and P. A. Malinen, *Fiz. Met. Metalloved.* **25**, 374 (1968).
247. N. Ohashi and S. Chikazumi, *J. Phys. Soc. Jpn.* **21**, 2086 (1966).
248. A. S. Yermolayev, A. Z. Mens'hikov, and P. A. Malinen, *Fiz. Met. Metalloved.* **26**, 76 (1968).
249. L. N. Romashev, I. G. Fakidov, and L. D. Voronchiklin, *Fiz. Met. Metalloved.* **25**, 1128 (1968).
250. A. S. Yermdenko, V. I. Zel'dovich, and Ye. S. Somoylova, *Fiz. Met. Metalloved.* **29**, 256 (1970).
251. H. Saito and Y. Suzuki, Japan Inst. Metals, Spring Meeting, p. 27 (1972).
252. C. T. Peters, P. Bolton, and A. P. Miodownik, *Acta Metall.* **20**, 881 (1972).
253. V. D. Sadkovskij, L. V. Smirnov, Ye. A. Fokina, P. A. Malinen, and I. P. Sorokin, *Fiz. Met. Metalloved.* **24**, 918 (1967).
254. Ye. A. Fokina, L. V. Smirnov, and V. D. Sadovskij, *Fiz. Met. Metalloved.* **27**, 756 (1969).
255. W. J. Bassett, U.S. Patent, RZh Met. 71387 (1966).
256. P. A. Malinen, V. D. Sadovskij, and I. P. Sorokin, *Fiz. Met. Metalloved.* **24**, 305 (1967).
257. G. I. Granik, M. L. Bernshteyn, and O. D. Dolgunovskaya, *Fiz. Met. Metalloved.* **24**, 1133 (1967).
258. A. Kussmann and G. G. V. Rittberg, *Z. Metallkd.* **41**, 470 (1950).
259. T. Tadaki and K. Shimizu, *Trans. JIM* **11**, 44 (1970).
260. A. E. Berkowitz, F. J. Donahoe, A. D. Franklin, and R. P. Steijn, *Acta Metall.* **5**, 1 (1957).
261. S. Takeuchi and H. Suzuki, *Sci. Rep. RITU (Tohoku Univ.)* **A2**, 43 (1950).
262. V. M. Yershov and N. L. Oslon, *Fiz. Met. Metalloved.* **25**, 874 (1968).
263. A. S. Sastri and D. R. F. West, *J. Iron Steel Inst.* **203**, 138 (1965).
264. Y. Imai and M. Izumiyama, *Sci. Rep. RITU (Tohoku Univ.)* **11**, 393 (1959).
265. A. R. Entwisle and J. A. Feeney, Inst. Metals Monogr., Rep. Ser. No. 33, p. 156 (1969).
266. T. Maki, S. Shimooka, M. Umemoto, and I. Tamura, *Metall. Trans.* **2**, 2944 (1971); *Trans. JIM* **13**, 400 (1972).
267. T. Araki and K. Shibata, Iron *and Steel Inst.* Japan, Spring Meeting, p. 153 (1972).
268. J. D. Bolton, E. R. Petty and E. B. Allen, *J. Iron Steel Inst.* **207**, 1314 (1969).
269. K. Tamaru and S. Sekito, *Kinzoku no Kenkyu* **8**, 595 (1931).
270. C. S. Roberts, *Trans. AIME* **697**, 203 (1953).
271. A. Matsuda, M. Kimura, and K. Nakajima, Japan Inst. Metals, Fall Meeting, p. 210 (1970).
272. S. R. Pati and M. Cohen, *Acta Metall.* **14**, 1001 (1966).
273. M. Okamoto and R. Odaka, *J. Jpn. Inst. Met.* **16**, 81 (1952).
274. A. B. Greninger and A. R. Troiano, *Trans. AIME* **140**, 307 (1940).
275. F. Wever and K. Mathiew, *Mitt. K. W. I. Eisenforsch.* **22**, 9 (1940).
276. Y. Imai, Japan Inst. Metals, I, Meeting of Branch 7, p. 9 (1947).
277. T. Lyman and A. R. Troiano, *Trans. AIME* **162**, 196 (1945).
278. M. Izumiyama, *J. Jpn. Inst. Met.* **24**, 58 (1960).
279. E. G. Ramachandran and C. Dasarathy, *Acta Met.* **8**, 274, 666 (1960).
280. E. R. Morgan and T. Ko, *Acta Metall.* **1**, 36 (1953).
281. R. Priester and S. G. Glover, "Physical Properties of Martensite and Bainite," Iron Steel Inst. Spec. Rep. 93, p. 38 (1965).
282. J. Philibert, *C. R. Acad. Sci. Paris* **240**, 529 (1955).

283. K. A. Malyshev, N. A. Borodina, and V. A. Mirmelshtein, *Chem. Abstr.* **50**, 16616 b (1956).
284. E. G. Ramachandran and C. Dasarathy, *Acta Metall.* **8**, 729 (1960); *Nature (London)*, **187**, 684 (1960).
285. K. Furuya, Y. Higo, T. Mori, and M. Nakamura, *Trans. Iron Steel Inst. Jpn.* **13**, 409 (1973).
286. E. Scheil, *Z. Anorg. Chem.* **183**, 98 (1929).
287. W. J. Harris and M. Cohen, *Trans. AIME* **180**, 447 (1949); *Met. Tech.* **15**, T. P. No. 2446, 24 (1948).
288. M. Okamoto and M. Nagakura, *Tetsu to Hagane*, **37** (1951) 19.
289. P. P. Petrosyan, *Dokl. Akad. Nauk SSSR* **59**, 1109 (1948).
290. J. Philibert and C. Crussard, *C. R. Acad. Sci. Paris* **239**, 1493 (1954).
291. B. Edmondson, *Acta Metall.* **5**, 208 (1957).
292. J. Woodilla, P. G. Winchell, and M. Cohen, *Trans. AIME* **215**, 849 (1959).
293. S. G. Glover, *J. Iron Steel Inst.* **200**, 102 (1962).
294. K. R. Kinsman and J. C. Shyne, *Acta Metall.* **14**, 1063 (1966); **15**, 1527 (1967).
295. Y. Imai and M. Izumiyama, *J. Jpn. Inst. Met.* **23**, 156 (1959).
296. O. P. Maksimova and É. I. Éstrin, *Fiz. Met. Metalloved.* **9**, 426 (1960).
297. O. P. Maksimova and É. I. Éstrin, *Sov. Phys.-Dokl.* **7**, 63 (1962).
298. É. I. Éstrin, *Dokl. Akad. Nauk. SSSR* **148**, 818 (1963).
299. É. I. Éstrin, "Solid State Transformations," p. 147 Consultants Bureau, 1966.
300. S. G. Glover, *J. Iron Steel Inst.* **200**, 102 (1962).
301. H. Suto and T. Yamagata, *J. Jpn. Inst. Met.* **34**, 968 (1970).
302. S. Hanada, M. Izumiyama, and Y. Imai, Japan Inst. Metals, Fall Meeting, p. 208 (1970).
303. J. F. Breedis, *Trans. AIME* **236**, 218 (1966).
304. É. I. Éstrin, "Solid State Transformations," p. 165. Consultants Bureau (1966).
305. J. Philibert, *C. R. Acad. Sci. Paris* **240**, 190 (1955).
306. V. S. Berdova, V. M. Yershov, and N. L. Oslon, *Fiz. Met. Metalloved.* **29**, 209 (1970).
307. J. A. Mathews, *Amer. Soc. Steel Treat.* **8**, 565 (1925).
308. H. Esser and H. Cornelius, *Arch. Eisenhüttenwes.* **7**, 693 (1934).
309. K. Honda and K. Iwase, *Kinzoku no Kenkyu* **3**, 326 (1926).
310. I. Hagiwara, S. Kanazawa, and A. Kumada, *J. Jpn. Inst. Met.* **23**, 299, 735 (1959); *Trans. JIM* **1**, 121 (1960); **2**, 71 (1961).
311. L. F. Porter and P. C. Rosenthal, *Acta Metall.* **7**, 504 (1959).
312. E. P. Klier and A. R. Troiano, *Trans. AIME* **162**, 175 (1945).
313. A. P. Gulysev and A. P. Akshentseva, *Zh. Tekh. Fiz.* **25**, 299 (1955).
314. H. R. Woehrle, W. R. Clough, and G. S. Ansell, *Trans. ASM* **59**, 784 (1966).
315. R. W. Messler, Jr., G. S. Ansell, and V. I. Lizunov, *Trans. ASM* **62**, 362 (1969).
316. G. S. Ansell, S. J. Donachic, and R. W. Messler, Jr., *Met. Trans.* **2**, 2443 (1971).
317. S. R. Thomas and G. Krauss, *Trans. AIME* **239**, 1136 (1967).
318. M. Kondo and T. Hachisuka, *J. Jpn. Inst. Met.* **21**, 227 (1957).
319. Ya. M. Golovchiner and Yu. D. Tyapkin, *Dokl. Akad. Nauk SSSR* **93**, 39 (1953).
320. Ya. M. Golovchiner, *Fiz. Met. Metalloved.* **15**, 544 (1963).
321. B. Edmondson and T. Ko, *Acta Metall.* **2**, 235 (1954).
322. G. Krauss and M. Cohen, *MIT Metall. Rep.* **13**, No. 5, 6 (1962).
323. Y. Imai, M. Izumiyama, and S. Hanada, *J. Jpn. Inst. Met.* **31**, 898 (1967).
324. H. Suto and N. Uchida, *J. Jpn. Inst. Met.* **36**, 779 (1972).
325. R. N. Caron and G. Krauss, *Metall. Trans.* **1**, 333 (1970).
326. R. Kossowsky and D. A. Colling, *Metall. Trans.* **4**, 799 (1973).
327. G. Wassermann, *Arch. Eisenhüttenwes.* **6**, 347 (1933).

328. L. S. Yershova and I. N. Bogachev, *Fiz. Met. Metalloved.* **13**, 300 (1962).
329. I. N. Bogachev and L. S. Malinov, *Fiz. Met. Metalloved.* **14**, 828 (1962); **15**, 678 (1963).
330. I. N. Bogachev and V. F. Yegolayev, *Fiz. Met. Metalloved.* **16**, 710 (1963).
331. I. N. Bogachev, V. F. Yegolayev, and L. S. Malinov, *Fiz. Met. Metalloved.* **16**, 544 (1963).
332. I. N. Bogachev and V. F. Yegolayev, *Fiz. Met. Metalloved.* **23**, 678 (1967).
333. H. Schumann and F. Heider, *Z. Metallkd.* **56**, 165 (1965).
334. L. I. Lysak and B. I. Nikolin, *Fiz. Met. Metalloved.* **23**, 93 (1967); **24**, 693 (1967).
335. R. Sh. Shklyar, V. F. Yegolayev, L. D. Chumakova, L. S. Malinov, V. D. Solovey, and V. B. Vykhodets, *Fiz. Met. Metalloved.* **20**, 908 (1965).
336. R. Sh. Shklyar, V. F. Yegolayev, L. D. Chumakova, L. S. Malinov, and V. D. Solovey, *Fiz. Met. Metalloved.* **21**, 235 (1966).
337. Yu. N. Makogon and B. I. Nikolin, *Fiz. Met. Metalloved.* **33**, 1271 (1972).
338. V. F. Yegolayev, L. S. Malinov, L. D. Chumakova, and R. Sh. Shklyar, *Fiz. Met. Metalloved.* **23**, 78 (1967).
339. I. N. Bogachev, V. F. Yegolayev, L. D. Chumakova, and R. Sh. Shklyar, *Fiz. Met. Metalloved.* **26**, 263 (1968).
340. Y. Takashima and T. Horiuchi, Japan Inst. Metals, Spring Meeting, p. 50 (1971).

6

The Crystallographic Theory of Martensitic Transformations

Since the formation of martensites is related to practical heat treatment techniques in many alloys and greatly influences the physical and mechanical properties of the alloys, a number of crystallographic and thermodynamic theories have been proposed to explain the transformation mechanisms. In the current thermodynamic theories on the growth of the martensite nucleus, the interfacial and internal chemical energies are considered to be dominant, as in the case of crystallization in a liquid. In addition, the strain energy of the transformation is also taken into account. These theories, however, assume thermal equilibrium and ignore the microstructural and crystallographic characteristics of the martensitic transformation. Such theories are therefore not reasonable, and will not be described in detail in this chapter. It is desirable to construct a thermodynamic theory that takes microscopic structures into consideration.

For this reason, we will discuss only the phenomenological theories,[1–10] which enable us to predict satisfactorily the crystallographic features of the martensitic transformation such as the habit planes, and the dislocation theory on the formation of martensite. A correlation between the transformation temperature and elastic moduli will also be referred to briefly.

6.1 Early theories on the mechanism of martensitic transformations

6.1.1 Bain correspondence and Bain distortion

Many experimental results mentioned previously suggest that the martensitic transformation does not proceed through long-range diffusion, but

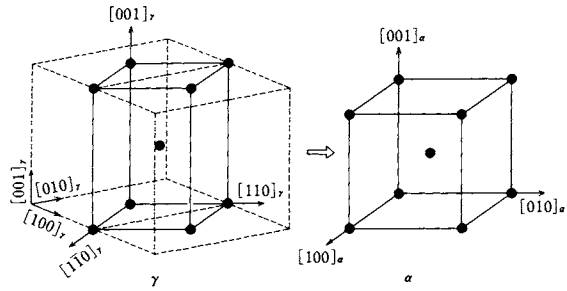

FIG. 6.1 Bain distortion for the $\gamma \rightarrow \alpha'$ martensitic transformation.

rather through a cooperative movement of atoms. Therefore, the transformation mechanism should be such that atomic neighbors are maintained before and after the transformation. One of the possible mechanisms is a deformation of the austenite lattice, although the amount of deformation is extremely large compared with ordinary elastic deformations. Bain[11] proposed such a model for the deformation of the austenite lattice. Figure 6.1 shows his model in which a b.c.c. (α) lattice can be generated from an f.c.c. (γ) lattice by compression along one principal axis, say $[001]_{fcc}$, and a simultaneous uniform expansion along the other two axes perpendicular to it. Such a homogeneous distortion, which makes one lattice change to another, is termed a lattice deformation, and in the special case of the f.c.c.-to-b.c.c. (or b.c.t.) transformation, it is called the *Bain distortion.* Assuming the Bain distortion, a correspondence between lattice points in the initial and final lattices can be determined uniquely, and this is called the *Bain correspondence.*

Let a lattice vector $[x_1, x_2, x_3]_b$† in the b.c.c. lattice correspond to a lattice vector $[x_1, x_2, x_3]_f$ in the f.c.c. lattice. Then, the Bain correspondence gives the following equations between the components of each lattice vector:

$$(x_1)_b \sim (x_1 - x_2)_f, \qquad (x_2)_b \sim (x_1 + x_2)_f, \qquad (x_3)_b \sim (x_3)_f. \tag{1}$$

These equations can be expressed compactly by matrices

$$\begin{bmatrix} x_1 \\ x_2 \\ x_3 \end{bmatrix}_b = \begin{bmatrix} 1 & \bar{1} & 0 \\ 1 & 1 & 0 \\ 0 & 0 & 1 \end{bmatrix} \begin{bmatrix} x_1 \\ x_2 \\ x_3 \end{bmatrix}_f \tag{2}$$

or inversely

$$\begin{bmatrix} x_1 \\ x_2 \\ x_3 \end{bmatrix}_f = \frac{1}{2} \begin{bmatrix} 1 & 1 & 0 \\ \bar{1} & 1 & 0 \\ 0 & 0 & 2 \end{bmatrix} \begin{bmatrix} x_1 \\ x_2 \\ x_3 \end{bmatrix}_b . \tag{2'}$$

† In this chapter, subscripts b and f refer to the b.c.c. (b.c.t.) and f.c.c. lattices, respectively.

The correspondence between the lattice planes is

$$(h_1 \quad h_2 \quad h_3)_b = (h_1 \quad h_2 \quad h_3)_f \frac{1}{2}\begin{bmatrix} 1 & 1 & 0 \\ \bar{1} & 1 & 0 \\ 0 & 0 & 2 \end{bmatrix} \tag{3}$$

or inversely

$$(h_1 \quad h_2 \quad h_3)_f = (h_1 \quad h_2 \quad h_3)_b \begin{bmatrix} 1 & \bar{1} & 0 \\ 1 & 1 & 0 \\ 0 & 0 & 1 \end{bmatrix}. \tag{3'}$$

These square matrices of order 3 are termed the Bain correspondence matrices.

One can find other possible lattice deformations to generate a b.c.c. (b.c.t.) lattice from an f.c.c. lattice. However, the Bain deformation is most reasonable because it involves the smallest relative atomic displacements $\sum_i \eta_i$ (η_i are the diagonal elements in the diagonalized deformation matrix) and thus the smallest strain energy.

The validity of the Bain deformation has also been confirmed experimentally. One of the experiments verified that α' martensite with interstitial atoms has a tetragonality of a specific orientation with respect to the austenite lattice. As explained previously, the tetragonality may be attributed to the fact that the site of the interstitial atoms in α' martensite is inherited from the octahedral sites in austenite through the Bain distortion.

Tetragonal martensites are also found in substitutional solid solutions, for example, in Fe–Ni–Ti alloys, as mentioned in Chapter 2. In the alloys, Ti atoms are arranged at special sites in the austenite lattice (actually forming Ni_3Ti clusters). The special sites after the Bain distortion become lattice sites with tetragonal symmetry. In this way, a tetragonal martensite can be obtained in the Fe–Ni–Ti alloys. In other words, the existence of tetragonal martensite in these alloys is evidence of the Bain distortion.

The validity of the Bain distortion can be proven more clearly by a martensitic transformation that takes place in superlattice alloys. A typical example is an Fe–25 at. % Pt alloy.† This alloy forms a disordered f.c.c. structure above, and an ordered Cu_3Au-type structure below 800°C, and undergoes a martensitic transformation below room temperature.[14] Since the transformation is an f.c.c.-to-b.c.c. one when the ordered arrangement

† Fe–Pd alloys with compositions of 0–20% Pd undergo martensitic transformations, and the martensites are reported to have a cubic structure.[12] According to an x-ray diffraction study[13] of an Fe–32 at.% Pt alloy, the alloy heated at 750°C was initially a homogeneous phase with a tetragonal FePt ordered lattice, although it contained ordered domains 1000 Å in diameter, that subsequently decomposed into FePt and Fe_3Pt phases.

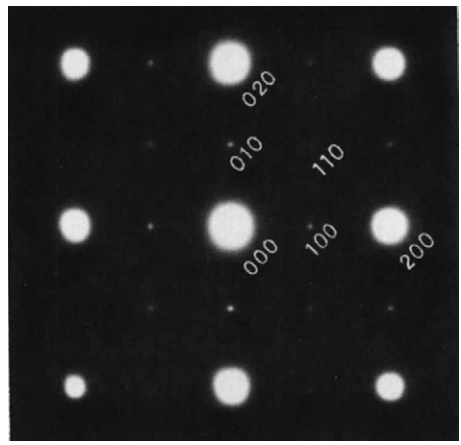

FIG. 6.2 Electron diffraction pattern of austenite in an Fe_3Pt alloy, showing the $[001]_\gamma$ zone. (Taken from an ordered specimen quenched from 1000°C and subsequently heated for 30 min at 650°C. (After Tadaki and Shimizu.[15])

of atoms is disregarded, the alloy is highly suitable for experimental confirmation of the Bain distortion. Thus, Tadaki and Shimizu[15] studied the martensitic transformation in the Fe_3Pt ordered alloy. Figure 6.2 is an electron diffraction pattern taken from a specimen of this alloy heated initially to 1000°C, quenched in water, and subsequently heated to 650°C and held at this temperature for 30 min to induce ordering. The pattern is of the [001] zone of the austenite lattice with the Cu_3Au-type ordered structure. The M_s temperature of the alloy heat treated as just described is about -50°C. Figure 6.3 is an optical micrograph taken from a specimen heat treated like the one in Fig. 6.2 and then cooled to -196°C. Martensite plates accompanied by surface relief effects can be seen. An example of electron diffraction patterns taken from such a martensite is shown in Fig. 6.4. Incidentally, the structure of martensite, which may be derived from the Cu_3Au-type ordered austenite lattice by the Bain deformation, should be, as explained in Fig. 2.4, basically a b.c.c. lattice, but is actually base-centered tetragonal if the atomic ordering is taken into account. Then, the structure factor for superlattice reflections from the lattice can be expressed as

$$F = F_{\text{atom}}\{1 + \exp[2\pi i(2h + 2k)/2]\}$$

where F_{atom} is a term including the atomic scattering factors, and h and k are allowed to be half integers because the Miller indices are referred to the basic b.c.c. lattice. When $h + k =$ half integer, $F = 0$. Therefore, reflections

FIG. 6.3 Optical micrograph of Fe_3Pt martensite, showing surface relief effects associated with the formation of martensite. (Taken from a specimen heat treated like that in Fig. 6.2 and then subzero cooled to $-196°C$ after electropolishing.) (After Tadaki and Shimizu.[15])

that satisfy the condition

$$h + k = \text{integer},$$

that is, reflections when both the k and h are integers or half integers can be observed. The superlattice reflections observed in Fig. 6.4 satisfy the

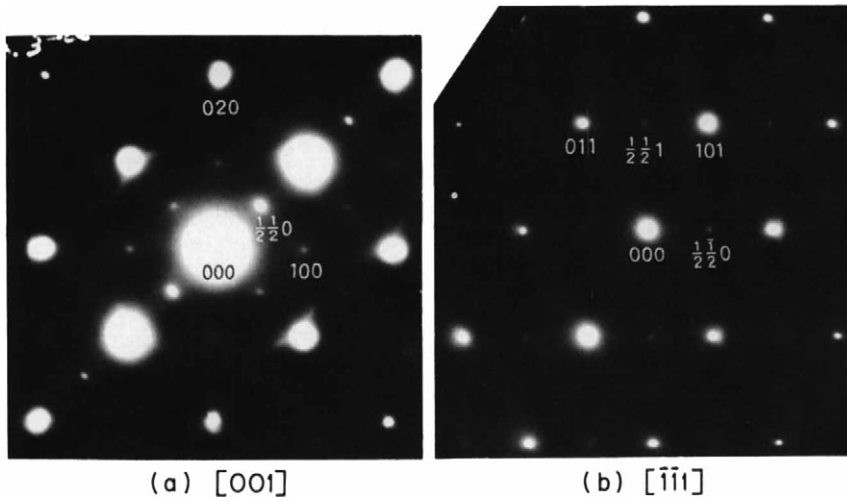

FIG. 6.4 Electron diffraction patterns taken from Fe_3Pt martensite formed in a specimen heat treated like that in Fig. 6.3. (After Tadaki and Shimizu.[15])

foregoing condition completely. It should also be noted that the martensite formed by the Bain distortion is internally twinned on the {112} planes where 2 is the l index (not on {121}- nor {211}-type planes). This fact reflects the physical situation that such twinning does not create nearest-neighbor platinum–platinum bonds (that is, does not change the crystal structure) whereas other twinning modes do. This fact also supports the validity of the Bain distortion.

Another investigation[16] made on a high aluminum steel with a composition of Fe–10%Al–1.50%C also supports the Bain distortion. This composition is nearly Fe:Al = 3:1, so the alloy forms[17] the Cu_3Au-type superlattice at high temperatures, as in the Fe_3Pt alloy. Electron diffraction patterns taken from martensite produced by quenching the alloy from the austenite region are essentially the same as those in Fig. 6.4 except that the intensities of the superlattice as well as the fundamental reflections are altered by the different atoms in this case. The c axis of the martensite is uniquely identified in this case not only from the tetragonal symmetry due to ordering, but also from the tetragonality $c/a = 1.11$ of the martensite lattice itself. Using the unique c axis, planar faults observed in the martensite were verified to occur on the {112} planes of $l = 2$. On making the c axis correspond to the contraction axis of the Bain distortion, all electron micrographs and diffraction patterns are consistent, and this consistency also proves the validity of the Bain distortion.

The Bain distortion was originally proposed for an f.c.c.-to-b.c.c. (b.c.t.) martensitic transformation, but this idea can be applied to other types of martensitic transformations provided that different lattice deformations are taken into account.†

6.1.2 Early shear mechanism models for the martensitic transformation

The Bain distortion is concerned with only the correspondence between initial and final lattices, and does not give the actual crystal orientation relationships between them. Rather, the orientation relationships have been determined experimentally. For example, the Kurdjumov–Sachs (K–S)[19] relationships have been observed for an Fe–1.4%C steel, and the Nishiyama (N)[20] relationships for an Fe–30% Ni alloy, as mentioned in Section 2.2.

Martensite was originally believed to be formed by a shear‡ on the planes and along the directions involved in the descriptions of the orientation relationships. That is, martensite with the K–S relationships was thought to be generated from an austenite parent by shear on $\{111\}_\gamma$ planes along

† See a paper by Kubo and Hirano[18] on the lattice deformation in a martensitic transformation from a b.c.c. to a long-period stacking order structure.

‡ Shear does not necessarily mean a simple shear.

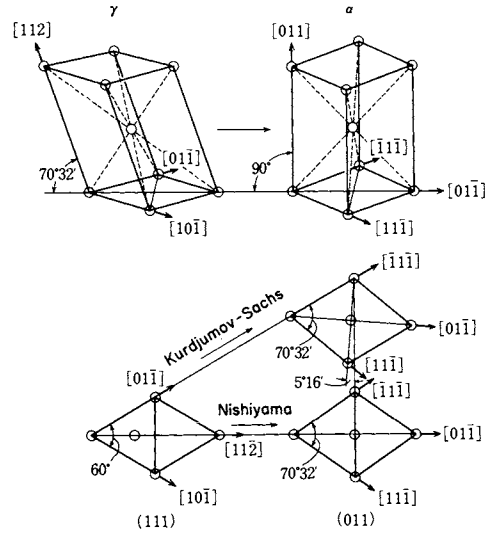

FIG. 6.5 Illustrations of shear mechanism in the $\gamma \rightarrow \alpha'$ transformation proposed by Kurdjumov and Sachs[19] and Nishiyama.[20]

$\langle 110 \rangle_\gamma$ directions lying in the planes, whereas for those with the N relationships a shear on $\{111\}_\gamma$ planes along $\langle 112 \rangle_\gamma$ directions lying in the planes (see Fig. 6.5) was considered responsible. Both these shears are identical to the Bain distortion if the rigid body rotation of the martensite due to the shear is disregarded, and therefore they have been considered reasonable models. However, as experimental information has accumulated, these shear mechanisms have been found to be too simple to be consistent with all the experimental facts.

First, if the shear occurs on the (111) plane of austenite, then the habit plane of the martensite plate should be the $(111)_\gamma$ plane. However, actual habit planes are quite different from $(111)_\gamma$, and depend on the alloy composition and the transformation temperature, as stated in Chapter 2.2. Second, the shear does not necessarily act along the same direction on every parallel atomic plane. For instance, in copper base alloys, shufflings can occur periodically parallel to the shear planes. The shufflings are also cooperative movements and involve the smallest atomic displacement. Thus, shufflings must be included in a transformation shear. In the f.c.c.-to-h.c.p. transformations, shears must occur on every two $(111)_{fcc}$ planes, as indicated in Fig. 2.29. Such shears were previously taken into account by Shoji[21] and Nishiyama.[22] In the b.c.-to-h.c.p. transformation, shufflings on alternate $(110)_{bcc}$ planes were considered by Burgers[23] (see Fig. 6.6).

There is an important additional remark[24] on the relation between the orientation relationships, on which preliminary models of the shear mechanism have been based, and internal twins observed in martensites. When

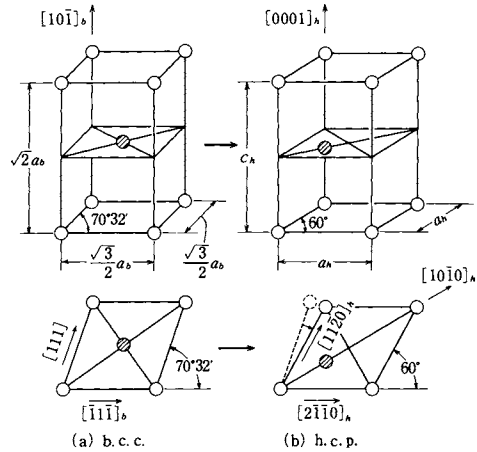

FIG. 6.6 Shear mechanism in the b.c.c. → h.c.p. transformation proposed by Burgers.[23]

the K–S relationships hold, 24 variants of martensite may possibly be formed in an austenite matrix. These variants can be regarded as consisting of 12 twin-related pairs. It is, therefore, likely that a twinned martensite plate consists of two twin-related variants. On the other hand, when the N relationships hold, 12 variants of martensite are formed in an austenite matrix, and no twin-related pair can be chosen from the 12. Then, if a martensite plate with the N relationship contains twin crystals, the twins may not be of another variant but may represent a lattice-invariant shear. Electron microscopy and diffraction studies have revealed the twinned structure of martensite, but thus far no x-ray diffraction study has showed twinned patterns. While the electron diffraction method is not very appropriate for precise determinations of orientation relationships, the x-ray diffraction method might overlook the twinned structure because of the weakness of the twin reflections. Therefore, the orientation relationships between austenite and each martensite matrix and its twin must be determined more precisely, for example, by the microdiffraction method. After such an experiment, the contradiction just indicated will be solved.

6.2 Introduction to the crystallographic phenomenological theory

6.2.1 The Greninger–Troiano experiment and the double shear mechanism

Greninger and Troiano[25] determined the orientation relationship between the martensite and austenite lattices in an Fe–22% Ni–0.8% C alloy (Section 2.2). At that time, they found that the martensite plate exhibited a surface relief whose appearance suggested that the plate had undergone a

uniform shear on a certain plane in the austenite. This fact seemed to have verified the shear mechanism mentioned in the preceding section. However, the observed shear plane was irrational and not the $\{111\}_f$ plane as expected from that shear mechanism. In addition, the shear angle was measured to be 10°45′, which was inconsistent with the 19.5° predicted from the (111) shear mechanism. If the f.c.c. lattice had undergone the macroscopic shear as measured, it would have transformed to a triclinic lattice. Therefore, they suggested[25] that another shear had to be added in order to produce the b.c.t. lattice as determined by x-ray diffraction. This was the first suggestion of the double shear mechanism.

In the double shear mechanism, the martensitic transformation is considered to be accomplished through first a macroscopic shear, which contributes the shape change, and second a microscopic shear, which is undetectable by ordinary optical microscopy. The microscopic shear was assumed to occur on $\{112\}$ planes along $\langle 111 \rangle$ directions in martensite since $\{112\}$ striations were frequently recognized on the etched surface of martensite plates. Then, the magnitude of the shear was estimated to be 12°–13°, corresponding to about one third of the twinning shear magnitude. In the twinning shear of the b.c.c. lattice, points on every sixth (112) layer are common to both the twinned and the untwinned lattice. Hence, it was assumed that the second shear would take place about every 18 atomic planes. Such twins had been thought to be undetectable by means of ordinary optical microscopy because of their extreme fineness. At present, however, the twins are detectable by means of electron microscopy, and the consideration noted earlier on the spacing of twins is not very different from the present electron microscopy results.

Later on, the double shear mechanism theory was supported by Bowles,[26] who (using an Fe–1.35%C alloy) measured the amount of surface relief accompanying the martensitic transformation. The amount of shape deformation can also be determined by using a scratch displacement method; this method utilizes the fact that straight scratches drawn on specimen surfaces prior to transformation are bent at the interfaces between the austenite and martensite crystals after the transformation. Machlin and Cohen[27] measured the shape deformation by this method on each of three perpendicular surfaces of a single crystal of Fe–30% Ni alloy, and obtained a deformation matrix. Subsequently, they found that such a deformation matrix did not generate a b.c.c. lattice from an f.c.c. austenite lattice, and thus they supported the double shear mechanism.

6.2.2 Foundation of the crystallographic phenomenological theory

The double shear mechanism mentioned in the foregoing is open to the criticism that the second shear is hypothetically introduced only to achieve

consistency between experimental results and theoretical considerations. However, the phenomenological theory, described next, introduces the second shear in a logical manner, and thus has been recognized as an appropriate theory. The theory has been developed independently by Bowles and Mackenzie (B–M theory) and by Wechsler, Lieberman, and Read (W–L–R theory); subsequently, almost equivalent theories were developed by Bullough and Bilby and by Bilby and Frank (although the formulation of these theories was a little different from those of the previous ones). In the following, the B–M and W–L–R theories will be described. The main points of the theories are as follows.

A. *An invariant plane is required for the transformation*

Since the martensitic transformation proceeds through a cooperative motion of atoms, the interface between the parent and product crystals must be highly coherent. During the transformation, therefore, the interface should be an undistorted and unrotated plane (unless the parent lattice rotates). A plane satisfying these two conditions is termed an *invariant plane*, and a deformation on the invariant plane is termed an *invariant plane strain*. Accordingly, the crystallographic properties of a martensitic transformation should be described by the invariant plane strain. This is the starting point of the phenomenological theory, and orientation relationships, habit planes, and so forth can be derived from the foregoing restriction.

B. *The Bain distortion has no invariant plane*

As stated previously, the Bain distortion is such that a contraction occurs along one of the principal axes and uniform expansions occur in the directions perpendicular to it. Analogously, it is seen from Fig. 6.7 that due to the Bain distortion a unit sphere representing the parent crystal transforms into an oblate spheroid representing the product crystal, and that cones A′OB′ and C′OD′, defined by intersections of the unit sphere with the spheroid, are composed of vectors unchanged in magnitude during the lattice deformation. Such vectors are termed *unextended lines*. The initial positions

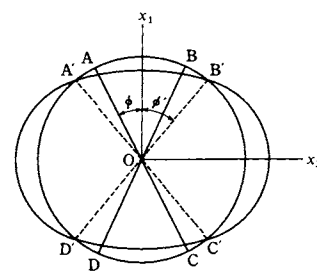

FIG. 6.7 Deformation of a unit sphere into an ellipsoid due to the Bain distortion (x_1 is perpendicular to the plane of the paper). The initial and final cones of unextended lines are AOB and A′OB′, respectively.

of the unextended lines can be represented by the cones AOB and COD. Therefore, all other vectors not involved in the cones would be changed in magnitude, and so the Bain distortion would result in no undistorted plane, that is, no invariant plane. It is thus difficult to obtain a coherent planar interface between the parent and product crystals only by the Bain distortion.

In order to overcome this difficulty, it is necessary for another shear to occur in addition to the Bain distortion. Since the additional shear must not bring about any change in crystal structure, it should be microscopically inhomogeneous, although the whole shear is macroscopically homogeneous. As a mode of inhomogeneous shear, deformation by slip or twinning can be considered, and can be regarded macroscopically as a simple shear. Thus in martensitic transformations such as the f.c.c.-to-b.c.c. transformation deformation by slip or twinning is predicted.

C. *A lattice-invariant shear must accompany the Bain distortion*

Of course, the lattice-invariant shear (the term *complementary shear* is often used instead) must be of such magnitude so as to produce an undistorted plane, when combined with the Bain distortion. Although the lattice-invariant shear has been confirmed to exist experimentally, it was merely hypothetical at the time it was proposed.

6.2.3 Stereographic analysis of the martensitic transformation[6,28,29]

Taking into account the necessary conditions just noted, we can construct the phenomenological theory by using matrix algebra; this theory enables us to predict habit planes, orientation relationships, shape changes, and other transformation characteristics. Before proceeding to the general analysis by matrix algebra, it may be more instructive to show a graphical method with reference to a stereographic projection, because the method may help readers to understand more easily the physical meanings of the matrix formulations. Results obtained from the stereographic method are less precise than those obtained from the direct mathematical method because of errors involved in graphical analysis.

In the graphical method, the Bain distortion and a complementary shear can first be represented stereographically. Next, combining an appropriate rotation with the two, an invariant habit plane can be derived. The rotation determines the orientation relationship. A numerical example will be given, based on the experimental information from the Fe–22% Ni–0.8% C alloy investigated by Greninger and Troiano.[25]

A. *Stereographic representation of the Bain distortion*

The lattice parameters of the austenite and martensite in Fe–22% Ni–0.8% C alloy were determined by the x-ray method to be $a_0 = 3.592$ Å for austenite

and $a = 2.845\,\text{Å}$, $c = 2.973\,\text{Å}$, and $c/a = 1.045$ for martensite. Using these values and referring to Fig. 6.1, the principal strains in the Bain distortion, denoted by η_i, are represented as follows:

$$\begin{aligned} (1/\sqrt{2})a_0 \to a, \quad & \eta_1 = \sqrt{2}a/a_0 = 1.12011 && \text{along } \boldsymbol{x}_1; \\ (1/\sqrt{2})a_0 \to a, \quad & \eta_2 = \sqrt{2}a/a_0 = \eta_1 && \text{along } \boldsymbol{x}_2; \\ a_0 \to c, \quad & \eta_3 = \ c/a_0 \ = 0.82767 && \text{along } \boldsymbol{x}_3. \end{aligned}$$

A unit sphere representing the austenite crystal

$$x_1^2 + x_2^2 + x_3^2 = 1 \tag{1}$$

transforms to an ellipsoid

$$\frac{x_1^2}{\eta_1^2} + \frac{x_2^2}{\eta_2^2} + \frac{x_3^2}{\eta_3^2} = 1 \tag{2}$$

due to the Bain distortion. Then, the cones of unextended lines in Fig. 6.7 are easily found from the equation

$$\left(\frac{1}{\eta_1^2} - 1\right)x_1^2 + \left(\frac{1}{\eta_2^2} - 1\right)x_2^2 + \left(\frac{1}{\eta_3^2} - 1\right)x_3^2 = 0. \tag{3}$$

The semiapex angle ϕ' of the cone is obtained from the value of x_2/x_3 when $x_1 = 0$. That is,

$$\tan\phi' = \left(\frac{x_2}{x_3}\right)_{x_1=0} = \left(\frac{1-\eta_3^2}{\eta_1^2 - 1}\right)^{1/2}\left(\frac{\eta_1}{\eta_3}\right) \tag{4}$$

($\phi' = 56.4°$ for Fe–22% Ni–0.8% C alloy) gives the positions of the unextended lines after transformation.

The initial cone of the unextended lines can be determined by considering a hypothetical inverse transformation, such as the α'-to-γ transformation. That is, a unit sphere representing the martensite crystal transforms to an ellipsoid representing the austenite

$$\eta_1^2 x_1^2 + \eta_2^2 x_2^2 + \eta_3^2 x_3^2 = 1, \tag{5}$$

the semiaxes of which are $1/\eta_1$, $1/\eta_2$, and $1/\eta_3$. Therefore, it is easily seen that the equation

$$(\eta_1^2 - 1)x_1^2 + (\eta_2^2 - 1)x_2^2 + (\eta_3^2 - 1)x_3^2 = 0 \tag{6}$$

represents the locus of all vectors that are unchanged in magnitude due to the hypothetical inverse transformation. The locus is nothing but the initial cone of the unextended lines. The semiapex ϕ of the initial cone is calculated

from

$$\tan \phi = \left(\frac{x_2}{x_3}\right)_{x_1=0} = \left(\frac{1-\eta_3{}^2}{\eta_1{}^2-1}\right)^{1/2} \tag{7}$$

($\phi = 48.0°$ for Fe–22% Ni–0.8% C alloy).

The initial cone of the unextended lines can also be obtained with help of the plane normal concept. A plane normal is defined as a vector whose direction is parallel to the normal of the plane and whose magnitude is proportional to the inverse of the interplanar distance.† Then a unit sphere (formed by the plane normals) in the austenite lattice transforms to an ellipsoid, whose semiaxes are $1/\eta_1$, $1/\eta_2$, and $1/\eta_3$, as represented by Eq. (5). The intersection of the ellipsoid with the unit sphere forms a circle, and a cone passing through the circle gives the final position of plane normals which are unchanged in magnitude. Such a plane normal is termed an unextended normal. Thus, the initial positions of the unextended lines coincide with the final positions of the unextended normals, and in the same way, the final positions of the unextended lines coincide with the initial positions of unextended normals. An unextended normal and an unextended line that are also unchanged in direction are termed an *invariant normal* and an *invariant line*, respectively.

A stereographic representation of the initial and final cones of the unextended lines is given in Fig. 6.8, the projection plane being normal to the $[001]_f$ contraction axis. Any vector lying on the initial cone with a semiapex of ϕ moves radially (in the figure) onto the final cone with a semiapex of ϕ' due to the Bain distortion.

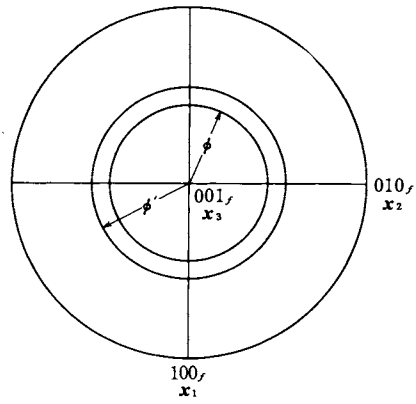

FIG. 6.8 Stereographic representation of the Bain distortion shown in Fig. 6.7.

† This vector is simply a reciprocal lattice vector.

B. *Stereographic representation of the complementary shear*

Figure 6.9 shows schematically the complementary shear acting as a simple shear on a unit sphere. As indicated, K_1 is the shear plane and $\boldsymbol{d}_2$ is the shear direction. The diameter AOB is in the shear plane and is perpendicular to $\boldsymbol{d}_2$, and K_0 is a plane containing AOB and is perpendicular to the shear plane.

Now, let the unit sphere be sheared along $\boldsymbol{d}_2$ by an angle θ. Then, the unit sphere $x_1^2 + x_2^2 + x_3^2 = 1$ is deformed to an ellipsoid expressed by the equation

$$x_1^2 + (x_2 - x_3 \tan\theta)^2 + x_3^2 = 1.$$

The intersection of the ellipsoid with the unit sphere can be obtained from

$$\{x_1^2 + (x_2 - x_3 \tan\theta)^2 + x_3^2\} - (x_1^2 + x_2^2 + x_3^2) = 0,$$

that is,

$$x_2/x_3 = \tfrac{1}{2}\tan\theta.$$

This means that the intersection is a plane satisfying the equation $x_2/x_3 = \frac{1}{2}\tan\theta$. Such a plane is shown as K_2' in Fig. 6.9. If the angle between the K_2' and K_0 planes is α, then the following relation is obtained:

$$\tan\alpha = \tfrac{1}{2}\tan\theta. \tag{8}$$

Therefore, the intersection of the ellipsoid with the unit sphere can be determined by the intersection of the sphere with the K_2' plane, which makes an angle α with K_0. Any vector in the K_2' plane does not change in length due to the shear, and thus a line OC′ in the plane represents the final position of an unextended line. It is easily seen from Fig. 6.9 that the line OC repre-

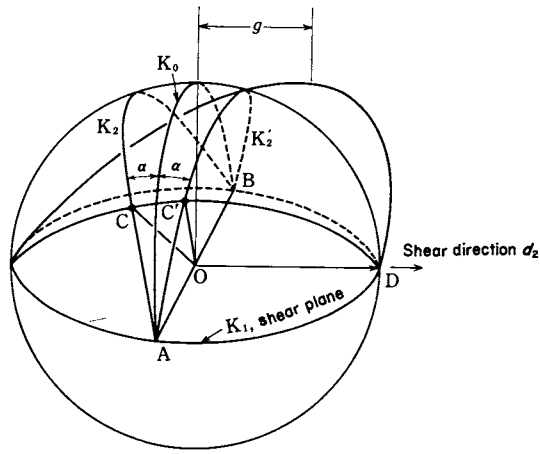

FIG. 6.9 Deformation of a unit sphere by simple shear.

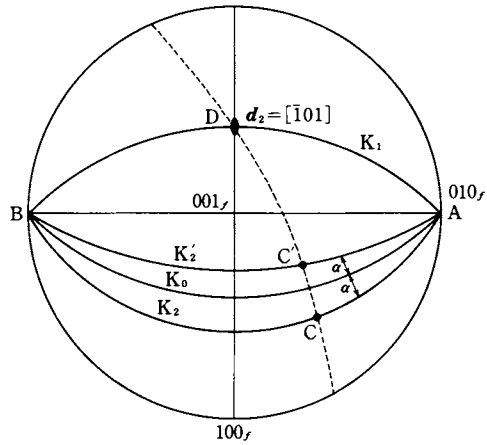

FIG. 6.10 Stereographic representation of the simple shear shown in Fig. 6.9.

senting the initial position of OC′ is in the K_2 plane that makes an angle of α with K_0 in the opposite side of the K_2' plane.

Figure 6.10 is a stereographic illustration of the complementary shear just mentioned. As can be seen from the figure, an unextended line C moves to the final position C′ along the circumference of the great circle defined by $\boldsymbol{d}_2$ and C.

C. *Stereographic analysis of the complete transformation process*

If the Bain distortion (i.e., principal strain) is known and the plane and direction of a complementary shear are assumed, an invariant plane, that is, a habit plane, of the transformation can be obtained stereographically. The method is based on the following principle: If the complementary shear magnitude can be determined so that two arbitrary lines in the shear plane and the angle between them remain unchanged, then the shear plane containing the two lines defines an undistorted plane. The undistorted plane can become an invariant plane if the lattice is subsequently subjected to a rigid body rotation, by which the undistorted plane rotates back to its initial position. The analysis will be performed with reference to the austenite basis. The Bain distortion was shown in Fig. 6.8 referring to the austenite basis.

In Fig. 6.11, $\boldsymbol{d}_2$ and K_1 of the complementary shear, as well as the Bain cones, are shown stereographically. There are two vectors $\boldsymbol{b}$ and $\boldsymbol{c}$, which are defined by intersections of the initial Bain cone with the K_1 plane. These vectors are invariant lines during the complementary shear because they lie in the K_1 plane and thus remain unchanged in both direction and magnitude.

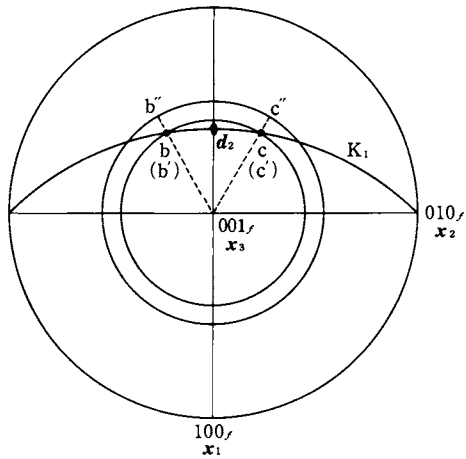

FIG. 6.11 Stereographic illustration of the unextended lines associated with the Bain distortion and complementary shear.

Thus, the final vectors $\boldsymbol{b}'$ and $\boldsymbol{c}'$ after the complementary shear are parallel to the initial vectors $\boldsymbol{b}$ and $\boldsymbol{c}$, respectively. If the Bain distortion is now applied the two vectors $\boldsymbol{b}$ ($\boldsymbol{b}'$) and $\boldsymbol{c}$ ($\boldsymbol{c}'$) become $\boldsymbol{b}''$ and $\boldsymbol{c}''$, lying on the final Bain cone, respectively, without changing their magnitude.† Therefore, if an appropriate rotation can be found in order to return $\boldsymbol{b}''$ and $\boldsymbol{c}''$ to their initial positions, $\boldsymbol{b}$ and $\boldsymbol{c}$ become invariant lines. However, both $\boldsymbol{b}$ and $\boldsymbol{c}$ cannot simultaneously be invariant lines in a certain invariant plane; that is, the plane defined by $\boldsymbol{b}$ and $\boldsymbol{c}$ cannot be an invariant plane, because the angle between $\boldsymbol{b}$ and $\boldsymbol{c}$ is not equal to that between $\boldsymbol{b}''$ and $\boldsymbol{c}''$.

Accordingly, other unextended lines must be found in order to obtain an invariant plane. Let us look for the lines in the K_2' plane of the complementary shear. The shear angle α must be known for such a purpose, but it is not yet known. So, the analysis must be done by trial and error. In Fig. 6.12, the K_0 plane is drawn perpendicular to the K_1 plane, and the K_2 and K_2' planes are drawn for a trial value of α. We define $\boldsymbol{a}'$ and $\boldsymbol{d}'$ as the intersections of the K_2' plane with the initial Bain cone. Then, $\boldsymbol{a}$ and $\boldsymbol{d}$ are obtained from the intersections of the K_2 plane with great circles defined by $\boldsymbol{a}'$ and $\boldsymbol{d}_2$ and by $\boldsymbol{d}'$ and $\boldsymbol{d}_2$, respectively. $\boldsymbol{a}''$ and $\boldsymbol{d}''$ are changed from $\boldsymbol{a}'$ and $\boldsymbol{d}'$, respectively, by the Bain distortion. Thus, the sequences $\boldsymbol{a} \rightarrow \boldsymbol{a}' \rightarrow \boldsymbol{a}''$ and $\boldsymbol{d} \rightarrow \boldsymbol{d}' \rightarrow \boldsymbol{d}''$ are seen to be accompanied by no change in length through the transformation process, consisting of the Bain distortion and a complementary shear. The

† It is assumed here that a complementary shear precedes the Bain distortion. Even if the Bain distortion were to precede the complementary shear, the result would be identical, provided that the plane and direction of the latter are represented in the α' lattice.

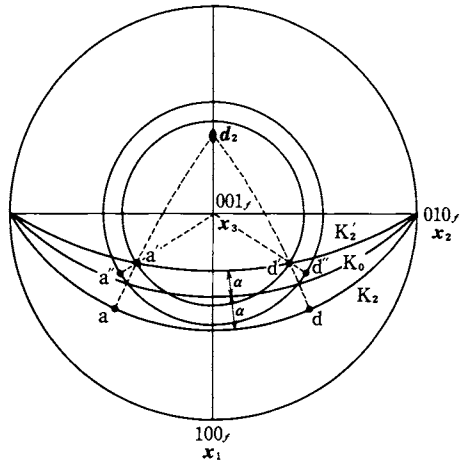

FIG. 6.12 Stereographic method for the determination of unextended lines in the K_2 plane. The shear angle of the complementary shear is assumed for trial calculations.

plane defined by $\boldsymbol{a}$ and $\boldsymbol{d}$, however, cannot be an invariant plane for the reason mentioned earlier for vectors $\boldsymbol{b}$ and $\boldsymbol{c}$.

It is now seen that there are four possible invariant planes (habit planes), depending on the choice of combinations of $\boldsymbol{b}$ or $\boldsymbol{c}$ with $\boldsymbol{a}$ or $\boldsymbol{d}$. For example, the plane defined by $\boldsymbol{a}$ and $\boldsymbol{c}$ can be an invariant one if the angle between $\boldsymbol{a}$ and $\boldsymbol{c}$ is equal to that between $\boldsymbol{a}''$ and $\boldsymbol{c}''$. Thus, the value of α is varied graphically until the angles become equal to each other. In the case of the Fe–22% Ni–0.8% C alloy, when α was chosen to be 11.6°, the angle between $\boldsymbol{a}$ and $\boldsymbol{c}$ was equal to that between $\boldsymbol{a}''$ and $\boldsymbol{c}''$. Of the four possible invariant planes, those defined by ($\boldsymbol{a}$, $\boldsymbol{c}$) and ($\boldsymbol{a}$, $\boldsymbol{b}$) are equivalent to those defined by ($\boldsymbol{b}$, $\boldsymbol{d}$) and ($\boldsymbol{c}$, $\boldsymbol{d}$), respectively, and therefore only two distinct habit planes are obtained.†

The invariant planes defined by ($\boldsymbol{a}$, $\boldsymbol{c}$) and ($\boldsymbol{a}''$, $\boldsymbol{c}''$) are referred to the γ and α' lattices, respectively, in which case they should coincide. Thus, the α' lattice must be rotated. The axis required for the rotation $\boldsymbol{u}$ is shown in Fig. 6.13. It can be determined as the intersection of a great circle bisecting $\boldsymbol{aa}''$ with another great circle bisecting $\boldsymbol{cc}''$, as shown in the figure. The amount of rotation can be determined stereographically so that $\boldsymbol{a}''$ and $\boldsymbol{c}''$ coincide simultaneously with $\boldsymbol{a}$ and $\boldsymbol{c}$, respectively. Such a coincidence is possible because the angle between $\boldsymbol{a}$ and $\boldsymbol{c}$ is equal to that between $\boldsymbol{a}''$ and $\boldsymbol{c}''$. By using such a rotation, an orientation relationship between the γ and α' crystals can be determined for a specific variant of the Bain distortion.

† Four habit planes are obtained in general, but in the present case the high symmetry of the example reduces the number of distinct variants.

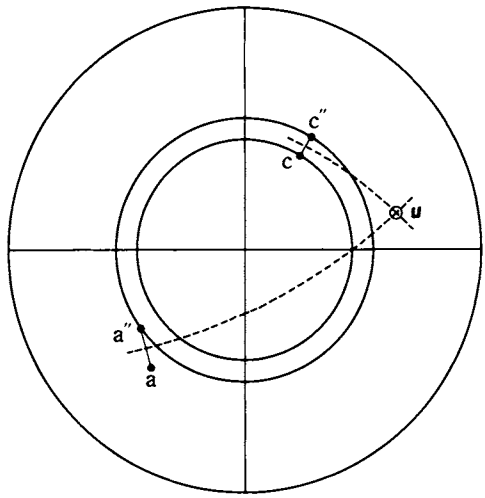

FIG. 6.13 Stereographic method for the determination of an axis of rotation by which a pair of unextended lines become invariant lines.

When only orientation relationships are in question, the graphical method can be simplified as follows: We utilize the fact that, in general, there exist invariant normals as well as an invariant plane upon transformation.† For example, as shown in Fig. 6.15, invariant normals during a complementary shear lie on the K_0 plane. Therefore, two invariant normals $\boldsymbol{n}_2'$ and $\boldsymbol{n}_1'$, which are defined by intersections of the K_0 plane with the initial cone of invariant normals during the Bain distortion, should be the initial positions

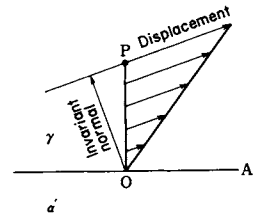

FIG. 6.14 Relation between atomic displacement and an invariant normal in a martensitic transformation.

† In Fig. 6.14, let the plane OA (perpendicular to the paper) be the γ–α' interface, that is, an invariant plane. As the transformation progresses, the interface moves upward, and a certain point P in the γ lattice undergoes a displacement to become a point in the α' lattice. The directions of the displacements for all other points are parallel to each other, although they are generally oblique with respect to the interface. Planes (in the figure a plane perpendicular to the paper is shown for simplicity) containing the directions do not change in orientation and interplanar distance. In other words, the planes have invariant normals.

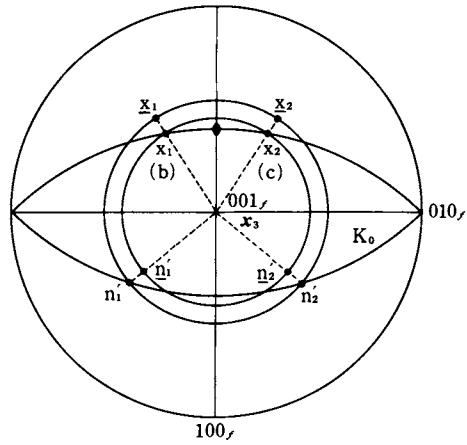

FIG. 6.15 Stereographic method for the determination of lattice orientation relationships using invariant normals.

of invariant normals through the transformation. They, of course, transform to $\boldsymbol{n}_2'$ and $\boldsymbol{n}_1'$, respectively, due to the Bain distortion. Since invariant normals are fixed in the initial γ lattice, $\boldsymbol{n}_2'$ should return to its initial position, $\boldsymbol{n}_2'$, by a rotation that makes $\boldsymbol{a}''$ and $\boldsymbol{c}''$ rotate at the same time into $\boldsymbol{a}$ and $\boldsymbol{c}$, respectively. In this way, the axis and amount of the required rotation are determined, and thus an orientation relationship can be obtained without any knowledge of the shear angle α.

6.3 Fundamentals of analysis of crystallography of martensitic transformation by matrix algebra

The stereographic analysis just discussed is not very accurate, as can easily be understood. It is thus desirable that appropriate methods of numerical analysis be constructed. The deformations and rotations involved in martensitic transformations are mathematically nothing but linear transformations in three-dimensional space. Therefore, they can be described by 3×3 matrices, and so martensitic transformations can be analyzed numerically by matrix algebra.[30] For general information on matrix algebra the reader should refer to other books (e.g., Wayman[6]).

As known from the previous description, a martensitic transformation is essentially considered to consist of a lattice deformation (in the case of the γ-to-α transformation, this is the Bain distortion), a lattice-invariant shear, and a lattice rotation (the last two are essential for the existence of an

invariant plane upon transformation). If $\boldsymbol{B}$, $\boldsymbol{P}$, and $\boldsymbol{R}$ are matrices† representing, respectively, a lattice deformation, lattice-invariant shear, and lattice rotation, then the total shape deformation due to the transformation $\boldsymbol{P}_1$, which can be observed as a surface relief effect, should be described as a product of those matrices, that is, $\boldsymbol{P}_1 = \boldsymbol{RPB}$. The requirement that $\boldsymbol{P}_1$ be an invariant plane strain is a basic point in the phenomenological theory. Therefore, in the matrix algebra analysis, $\boldsymbol{P}$ and $\boldsymbol{R}$ are determined so that $\boldsymbol{P}_1$ becomes an invariant plane strain, and accordingly habit planes and orientation relationships are obtained by using the numerical values of $\boldsymbol{P}$ and $\boldsymbol{R}$. It is convenient for $\boldsymbol{P}$ to be referred to the parent lattice before $\boldsymbol{B}$ operates. To do so, $\boldsymbol{BPB}^{-1}$ must be used instead of $\boldsymbol{P}$, and thus we obtain

$$\boldsymbol{P}_1 = \boldsymbol{R}(\boldsymbol{BPB}^{-1})\boldsymbol{B} = \boldsymbol{RBP}. \tag{1}$$

Then, $\boldsymbol{P}$ can operate in the parent lattice prior to $\boldsymbol{B}$.

In the analysis of martensitic transformations by matrix algebra, only the elements of $\boldsymbol{B}$ are known. For example, in the case of the Bain distortion, the matrix can be expressed as

$$(\mathrm{fBf}) = (\mathrm{diag}: \eta_1\eta_2\eta_3), \qquad \eta_1 = \eta_2 = \sqrt{2}a/a_0, \eta_3 = c/a_0 \tag{2}$$

where (fBf) means explicitly that the matrix $\boldsymbol{B}$ is referred to the initial f.c.c. lattice (this will be abbreviated as the f basis). When it is clear that matrices are referred to the f basis, the notation will be simplified and (fBf) abbreviated as $\boldsymbol{B}$.

The total shape deformation $\boldsymbol{P}_1$ cannot be ascertained unless the matrix elements of the lattice-invariant shear $\boldsymbol{P}$ are known or are assumed. Then, in the case of the f.c.c.-to-b.c.c. (or b.c.t.) transformation, $\boldsymbol{P}$ is assumed to be a simple shear on the $\{112\}_b$ plane in the $\langle 111\rangle_b$ in the martensite, taking into account that this shear system is one of the active deformation modes in the b.c.c. lattice. If a specific variant $(112)_b\ [\bar{1}\bar{1}1]_b$ of those shear systems is assumed for the components of $\boldsymbol{P}$, the shear system referred to the f basis is $(101)_f\ [\bar{1}01]_f$ in the austenite by using Eqs. (2) and (3) in Section 6.1. The magnitude of the shear is still unknown, but will be determined so that an invariant plane results.

The phenomenological analysis of martensitic transformation by matrix algebra was first developed by Bowles and Mackenzie, and by Wechsler, Lieberman, and Read, although their theories have been proved to be identical.[2] On the other hand, a theory based on the concept of a surface dislocation has been proposed by Bullough and Bilby, and a theory based on prism matching between the γ and α lattices has been proposed by Bilby and Frank. The latter two theories, which are also equivalent to each other,

† A bold capital letter such as $\boldsymbol{B}$ represents a 3×3 matrix. On the other hand, a bold lowercase letter, such as $\boldsymbol{d}$, represents a 3×1 matrix, and one with the prime symbol, such as $\boldsymbol{p}'$, is a 1×3 matrix. In general, the prime sign denotes the transposition of a matrix.

will be described in the next section. In the following, the Bowles–Mackenzie theory will be discussed first.

6.3.1 Bowles–Mackenzie theory[31,32,33]

Equation (1) can be rewritten as

$$\boldsymbol{P}_1\boldsymbol{P}_2 = \boldsymbol{R}\boldsymbol{B} = \boldsymbol{S} \tag{3}$$

where $\boldsymbol{P}_2 = \boldsymbol{P}^{-1}$. The $\boldsymbol{P}_2$ defined in this way is termed a complementary shear and it again represents a lattice-invariant shear as $\boldsymbol{P}$ does. Therefore, $\boldsymbol{P}_2$ can be written in the form

$$\boldsymbol{P}_2 = \boldsymbol{I} + \boldsymbol{d}_2\boldsymbol{p}_2' \tag{4}$$

where $\boldsymbol{p}_2'$ and $\boldsymbol{d}_2$ are the unit plane normal and the direction (including the magnitude) of the complementary shear, respectively, and they satisfy an orthogonal condition, $\boldsymbol{p}_2'\boldsymbol{d}_2 = 0$. Since the shape deformation must be an invariant plane strain, $\boldsymbol{P}_1$ can also be represented in a similar form,

$$\boldsymbol{P}_1 = \boldsymbol{I} + \boldsymbol{d}_1\boldsymbol{p}_1'. \tag{5}$$

However, since $\boldsymbol{P}_1$ is not a simple shear, the shear plane normal and the shear direction do not in general satisfy the orthogonal condition.

Both $\boldsymbol{P}_1$ and $\boldsymbol{P}_2$ are invariant plane strains, so the line of intersection of the two invariant planes is not affected by the strains; that is, the product $\boldsymbol{S}$ has an invariant line given by the intersection. Such an intersection, then, is termed an invariant line and the associated strain is termed an invariant line strain. If $\boldsymbol{S}$ is obtained from some other conditions, all unknown elements of $\boldsymbol{P}_1$ and $\boldsymbol{P}_2$ can be calculated.

The method of the analysis may consist of the following four steps: (i) Unextended lines and unextended normals for the deformation $\boldsymbol{B}$ are calculated so that the former lie in the $\boldsymbol{p}_2'$ plane and the latter are along the directions perpendicular to $\boldsymbol{d}_2$. (ii) An invariant line strain $\boldsymbol{S}$ is calculated so that the unextended lines and normals are unrotated, that is, are invariant lines and normals, respectively, following an appropriate rotation. (iii) Elements $\boldsymbol{p}_1'$ and $\boldsymbol{d}_1$ of $\boldsymbol{P}_1$ and the magnitude m_2 of $\boldsymbol{d}_2$ in $\boldsymbol{P}_2$ are calculated. (iv) The orientation relationship is obtained from a calculation of the directional change of the principal axes due to the strain $\boldsymbol{S}$.

In the following analyses will be performed relating to a numerical example for an Fe–31% Ni† alloy after Wayman.[6] The input data used are

$$a_0 = 3.591\,\text{Å} \qquad \text{for } \gamma,$$
$$a = c = 2.875\,\text{Å} \qquad \text{for } \alpha',$$

† Most recent data for the lattice parameters of austenite and martensite in the Fe–Ni alloy was obtained by Reed and Schramm.[34]

from which we find that

$$\eta_1 = \eta_2 = \frac{\sqrt{2}a}{a_0} = 1.132136 \qquad \text{and} \qquad \eta_3 = \frac{c}{a_0} = 0.800541.$$

For the convenience of calculations by computer, a_0 and a are taken as 3.59100 Å and 2.87500 Å, respectively.

A. *Calculation of invariant lines and normals*

Suppose a unit vector $\boldsymbol{x}_i(\boldsymbol{x}_i'\boldsymbol{x}_i = 1)$ is parallel to the invariant line. The Bain distortion makes $\boldsymbol{x}_i$ transform to $\underline{\boldsymbol{x}}_i = \boldsymbol{B}\boldsymbol{x}_i$. Because $\boldsymbol{x}_i$ is unchanged in length, $\underline{\boldsymbol{x}}_i'\underline{\boldsymbol{x}}_i = 1$ holds, and then the equation can be rewritten as $(\boldsymbol{B}\boldsymbol{x}_i)'\boldsymbol{B}\boldsymbol{x}_i = \boldsymbol{x}_i'\boldsymbol{B}'\boldsymbol{B}\boldsymbol{x}_i = \boldsymbol{x}_i'\boldsymbol{B}^2\boldsymbol{x}_i = 1$. In addition, $\boldsymbol{p}_2'\boldsymbol{x}_i = 0$ because the shear plane $\boldsymbol{p}_2'$ of the complementary shear must involve $\boldsymbol{x}_i$. Assuming $\boldsymbol{p}_2' = (1/\sqrt{2})(101)$, we obtain the following three equations for $\boldsymbol{x}_i$.

$$\begin{aligned} \boldsymbol{x}_i'\boldsymbol{x}_i &= 1 \cdots {x_1}^2 + {x_2}^2 + {x_3}^2 = 1, \\ \boldsymbol{x}_i'\boldsymbol{B}^2\boldsymbol{x}_i &= 1 \cdots \eta_1^2 {x_1}^2 + \eta_2^2 {x_2}^2 + \eta_3^2 {x_3}^2 = 1, \\ \boldsymbol{p}_2'\boldsymbol{x}_i &= 0 \cdots x_1 + x_3 = 0. \end{aligned} \tag{6}$$

From these equations, two solutions for $\boldsymbol{x}_i$ can be obtained:

$$\boldsymbol{x}_{i1} = \begin{bmatrix} -0.663032 \\ -0.347528 \\ 0.663032 \end{bmatrix}; \qquad \boldsymbol{x}_{i2} = \begin{bmatrix} -0.663032 \\ 0.347528 \\ 0.663032 \end{bmatrix}. \tag{6'}$$

The first and second equations in (6) are equivalent to Eqs. (1) and (5), respectively, in the preceding section.

Next, let a unit normal $\boldsymbol{n}_i'$ (n_1, n_2, n_3) be the invariant normal. The Bain distortion, then, causes $\boldsymbol{n}_i'$ to transform to $\underline{\boldsymbol{n}}_i' = \boldsymbol{n}_i'\boldsymbol{B}^{-1}$. As the $\underline{\boldsymbol{n}}_i'$ is unchanged in length, $\underline{\boldsymbol{n}}_i'\underline{\boldsymbol{n}}_i = \boldsymbol{n}_i'\boldsymbol{B}^{-2}\boldsymbol{n}_i$. In addition, $\boldsymbol{n}_i'\boldsymbol{d}_2 = 0$ because the plane with normal $\boldsymbol{n}_i'$ does contain the shear direction $\boldsymbol{d}_2$. Assuming that $\boldsymbol{d}_2$ is parallel to $[\bar{1}01]$, we obtain the following three equations for $\boldsymbol{n}_i'$.

$$\begin{aligned} \boldsymbol{n}_i'\boldsymbol{n}_i &= 1 \cdots {n_1}^2 + {n_2}^2 + {n_3}^2 = 1, \\ \boldsymbol{n}_i'\boldsymbol{B}^{-2}\boldsymbol{n}_i &= 1 \cdots \frac{{n_1}^2}{\eta_1^2} + \frac{{n_2}^2}{\eta_2^2} + \frac{{n_3}^2}{\eta_3^2} = 1, \\ \boldsymbol{n}_i'\boldsymbol{d}_2 &= 0 \cdots -n_1 + n_3 = 0. \end{aligned} \tag{7}$$

From these equations two solutions for $\boldsymbol{n}_i'$ are derived:

$$\begin{aligned} \boldsymbol{n}_{i1}' &= (0.530784, 0.660708, 0.530784); \\ \boldsymbol{n}_{i2}' &= (0.530784, -0.660708, 0.530784). \end{aligned} \tag{7'}$$

As explained in the stereographic analysis, four combinations of $\boldsymbol{x}_i$ and $\boldsymbol{n}_i'$ are possible. From these four, one combination of $\boldsymbol{x}_{i1}$ and $\boldsymbol{n}_{i1}'$ will be taken as an example of numerical calculations.

Then, $\boldsymbol{x}_i$ after the Bain distortion is written as

$$\underline{\boldsymbol{x}}_i = \boldsymbol{B}\boldsymbol{x}_i = [-0.750642, -0.393449, 0.530784].^{\dagger} \tag{8}$$

Now $\boldsymbol{p}_2'$ transforms to $\boldsymbol{p}_2'\boldsymbol{B}^{-1} = (0.624578, 0, 0.883286)$ due to the Bain distortion. Considering the normalized $\underline{\boldsymbol{p}}_2'$, we have,

$$\underline{\boldsymbol{p}}_2' = \boldsymbol{p}_2'\boldsymbol{B}^{-1}/(\boldsymbol{p}_2'\boldsymbol{B}^{-2}\boldsymbol{p}_2)^{1/2} = (0.577351, 0, 0.816496). \tag{9}$$

$\underline{\boldsymbol{x}}_i$ is seen to lie in the plane with normal $\underline{\boldsymbol{p}}_2'$, because $\underline{\boldsymbol{p}}_2' \cdot \underline{\boldsymbol{x}}_i = \boldsymbol{p}_2'\boldsymbol{B}^{-1}\boldsymbol{B}\underline{\boldsymbol{x}}_i = \boldsymbol{p}_2' \cdot \boldsymbol{x}_i = 0$.

B. *Calculation of the invariant line strain S*

$\boldsymbol{S}$ can be calculated if a rotation matrix is known, with which both $\underline{\boldsymbol{x}}_i$ and $\underline{\boldsymbol{n}}_i'$ rotate back to the initial positions, $\boldsymbol{x}_i$ and $\boldsymbol{n}_i'$, respectively. Such a rotation matrix $\boldsymbol{R}_0$ can be obtained in principle by solving two equations, $\boldsymbol{R}_0\underline{\boldsymbol{x}}_i = \boldsymbol{x}_i$ and $\underline{\boldsymbol{n}}_i'\boldsymbol{R}_0^{-1} = \boldsymbol{n}_i'$, and by using the properties of an orthogonal matrix. But, in practice, solving these equations is troublesome unless a computer is used. A more convenient method is used to obtain the invariant line strain, as explained next.

The method consists of two steps: The first is to obtain a rotation matrix that makes $\underline{\boldsymbol{x}}_i$ transform to $\boldsymbol{x}_i$, and the second is to obtain a rotation matrix that leaves $\boldsymbol{x}_i$ unchanged and makes $\underline{\boldsymbol{n}}_i'$ transform to $\boldsymbol{n}_i'$. As we will soon prove, the former matrix can be expressed as the product of a rotation matrix $\boldsymbol{R}_1$, whose elements in the first column coincide with the components of $\boldsymbol{x}_i$, by another rotation matrix $\boldsymbol{R}_2'$, whose elements in the first row coincide with the components of $\underline{\boldsymbol{x}}_i$. Though the other elements of the rotation matrices, $\boldsymbol{R}_1$ and $\boldsymbol{R}_2'$, are arbitrary, their three component vectors must satisfy the orthogonal conditions. As a component vector satisfying these conditions, $\boldsymbol{p}_2$ and $\underline{\boldsymbol{p}}_2$ vectors will be chosen for $\boldsymbol{R}_1$ and $\boldsymbol{R}_2$, respectively. Then, we obtain

$$\boldsymbol{R}_1 = (\boldsymbol{x}_i, \boldsymbol{p}_2, \boldsymbol{u}), \tag{10}$$

where $\boldsymbol{u} = \boldsymbol{x}_i \times \boldsymbol{p}_2 = [-0.245739, -0.937669, 0.245739]$, and

$$\boldsymbol{R}_2 = (\underline{\boldsymbol{x}}_i, \underline{\boldsymbol{p}}_2, \boldsymbol{v}), \tag{11}$$

where $\boldsymbol{v} = \boldsymbol{x}_i \times \underline{\boldsymbol{p}}_2 = [-0.321250, 0.919345, 0.227158]$.

† To conserve space, column vectors are represented laterally with square brackets.

Thus, it is seen, as required, that $\boldsymbol{R}_1\boldsymbol{R}_2'\underline{\boldsymbol{x}}_i = \boldsymbol{R}_1[100] = \boldsymbol{x}_i$, and that $\boldsymbol{R}_1\boldsymbol{R}_2'$ is a rotation matrix that makes $\underline{\boldsymbol{x}}_i$ rotate back to $\boldsymbol{x}_i$. In other words, the matrix defined by

$$\boldsymbol{S}_0 \equiv \boldsymbol{R}_1\boldsymbol{R}_2'\boldsymbol{B} \tag{12}$$

has $\boldsymbol{x}_i$ as an invariant line.

In order to obtain a rotation matrix that makes $\underline{\boldsymbol{n}}_i'$ transform to $\boldsymbol{n}_i'$ and $\boldsymbol{x}_i$ remain unchanged, it is convenient to convert the f basis to a new i basis (i_1, i_2, i_3) defined by three orthogonal vectors $\boldsymbol{x}_i$, $\boldsymbol{p}_2$, and $\boldsymbol{u}$. In the i basis, Eq. (12) can be rewritten as

$$(\mathrm{iS_0i}) = \boldsymbol{R}_1'\boldsymbol{S}_0\boldsymbol{R}_1 = \boldsymbol{R}_1'\boldsymbol{R}_1\boldsymbol{R}_2'\boldsymbol{B}\boldsymbol{R}_1 = \boldsymbol{R}_2'\boldsymbol{B}\boldsymbol{R}_1. \tag{13}$$

Then, the invariant line strain $\boldsymbol{S}$ referred to the i basis (iSi) is obtained by adding a rotation of amount β around $\boldsymbol{x}_i$; that is,

$$\begin{bmatrix} 1 & 0 & 0 \\ 0 & \cos\beta & -\sin\beta \\ 0 & \sin\beta & \cos\beta \end{bmatrix} \boldsymbol{R}_2'\boldsymbol{B}\boldsymbol{R}_1 \equiv (\mathrm{iSi}). \tag{14}$$

The value of β must be chosen so that $\boldsymbol{n}_i'$ remains unchanged after it is operated on by (iSi). When $\boldsymbol{n}_i'$ is referred to the i basis, that is,

$$(\boldsymbol{n}_i'; \mathrm{i}) = \boldsymbol{n}_i'\boldsymbol{R}_1 = (-0.229615, 0.750642, 0.619525), \tag{15}$$

the following equation must hold:

$$(\boldsymbol{n}_i'; \mathrm{i})(\mathrm{iSi}) = (\boldsymbol{n}_i'; \mathrm{i}). \tag{16}$$

From these equations, β can be determined. That is, substituting Eqs. (14) and (15) into (16), and equating corresponding elements, we determine β to be

$$\cos\beta = 0.994373, \qquad \sin\beta = 0.105924.$$

By substituting these values into Eq. (14), we can determine the invariant line strain (iSi), and subsequently, by converting the i basis to the f basis, we obtain the final matrix $\boldsymbol{S}$.

$$\boldsymbol{S} = \boldsymbol{R}_1(\mathrm{iSi})\boldsymbol{R}_1' = \begin{bmatrix} 1.122157 & -0.036954 & 0.102787 \\ 0.021153 & 1.125262 & 0.086809 \\ -0.148488 & -0.118969 & 0.789154 \end{bmatrix} \tag{17}$$

C. *Calculation of the elements of* $\boldsymbol{P}_1$ *and* $\boldsymbol{P}_2$

Since the invariant plane normal $\boldsymbol{p}_1'$ in the shape deformation is parallel to $\boldsymbol{p}_2'\boldsymbol{S}^{-1} - \boldsymbol{p}_2' = (0.025377, 0.107452, 0.081697)$,† the normalized vector $\boldsymbol{p}_1'$ should be

$$\boldsymbol{p}_1' = (0.184765, 0.782337, 0.594820). \tag{18}$$

The displacement vector $\boldsymbol{d}_1$ of the shape deformation is equal to‡

$$\frac{\boldsymbol{S}\boldsymbol{d}_2 - \boldsymbol{d}_2}{(\boldsymbol{p}_1'\boldsymbol{d}_2)} = [-0.047235, 0.160116, -0.152072]. \tag{19}$$

Thus, $\boldsymbol{d}_1$ is not a unit vector. From the normalization factor for this vector, the magnitude of the shape deformation can be obtained:

$$m_1 = 0.225820. \tag{20}$$

The direction $\boldsymbol{d}_2'$ of the complementary shear $\boldsymbol{P}_2 = \boldsymbol{P}^{-1}$ can be obtained from the relation $\boldsymbol{d}_2 = (\boldsymbol{y} - \boldsymbol{S}^{-1}\boldsymbol{y})/\boldsymbol{p}_2'\boldsymbol{y}$,§ where $\boldsymbol{y}$ is an arbitrary vector lying in the plane with normal $\boldsymbol{p}_1'$. Then, choosing $\boldsymbol{y}$ to be $[100] \times \boldsymbol{p}_1 = [0.594820, 0, -0.184765]$, we obtain

$$\boldsymbol{d}_2 = [0.181581, 0, -0.181581].$$

From the normalization factor for $\boldsymbol{d}_2$, the magnitude m_2 and the shear angle α of the complementary shear can be obtained:

$$m_2 = 0.256794, \qquad \alpha = \tan^{-1}(0.256794/2) = 7.3°.$$

† From the equation $\boldsymbol{S} = (\boldsymbol{I} + \boldsymbol{d}_1\boldsymbol{p}_1')(\boldsymbol{I} + \boldsymbol{d}_2\boldsymbol{p}_2')$ it follows that

$$\boldsymbol{S}^{-1} = (\boldsymbol{I} + \boldsymbol{d}_2\boldsymbol{p}_2')^{-1}(\boldsymbol{I} + \boldsymbol{d}_1\boldsymbol{p}_1')^{-1} = (\boldsymbol{I} - \boldsymbol{d}_2\boldsymbol{p}_2')\left(\boldsymbol{I} - \frac{\boldsymbol{d}_1\boldsymbol{p}_1'}{k}\right).$$

Using this relation, we obtain

$$\boldsymbol{p}_2'\boldsymbol{S}^{-1} = \boldsymbol{p}_2'(\boldsymbol{I} - \boldsymbol{d}_2\boldsymbol{p}_2')\left(\boldsymbol{I} - \frac{\boldsymbol{d}_1\boldsymbol{p}_1'}{k}\right) = \boldsymbol{p}_2'\left(\boldsymbol{I} - \frac{\boldsymbol{d}_1\boldsymbol{p}_1'}{k}\right)$$

$$= \boldsymbol{p}_2' - \frac{(\boldsymbol{p}_2'\boldsymbol{d}_1)\boldsymbol{p}_1'}{k}.$$

Then, we obtain

$$\boldsymbol{p}_2'\boldsymbol{S}^{-1} - \boldsymbol{p}_2' = -\frac{(\boldsymbol{p}_2'\boldsymbol{d}_1)\boldsymbol{p}_1'}{k} \| \boldsymbol{p}_1' \qquad \text{which is parallel to } \boldsymbol{p}_1$$

‡ $\boldsymbol{S}\boldsymbol{d}_2 = (\boldsymbol{I} + \boldsymbol{d}_1\boldsymbol{p}_1')(\boldsymbol{I} + \boldsymbol{d}_2\boldsymbol{p}_2')\boldsymbol{d}_2 = \boldsymbol{d}_2 + \boldsymbol{d}_1\boldsymbol{p}_1'\boldsymbol{d}_2$.

§ $\boldsymbol{S}^{-1}\boldsymbol{y} = (\boldsymbol{I} - \boldsymbol{d}_2\boldsymbol{p}_2')\left(\boldsymbol{I} - \frac{\boldsymbol{d}_1\boldsymbol{p}_1'}{k}\right)\boldsymbol{y} = (\boldsymbol{I} - \boldsymbol{d}_2\boldsymbol{p}_2')\boldsymbol{y} = \boldsymbol{y} - \boldsymbol{d}_2\boldsymbol{p}_2'\boldsymbol{y}$.

D. *Calculation of the orientation relationship*

The total shape change $\boldsymbol{P}_1$ associated with the transformation is equal to $\boldsymbol{SP}$. Since $\boldsymbol{P}$ is not accompanied by any change of crystal orientation, the orientation relationship is determined only by $\boldsymbol{S}$. According to the Bain correspondence, $(111)_f$ and $[\bar{1}01]_f$ in the austenite lattice correspond to $(011)_b$ and $[\bar{1}\bar{1}1]_b$, respectively, in the martensite lattice. Relations between the corresponding planes and directions will be examined later. The $(111)_f$ plane should be transformed by $\boldsymbol{S}$ to $(1/\sqrt{3})(111)\boldsymbol{S}^{-1} = (0.581425, 0.594602, 0.590467)$. The unit normal, $[0.570063, 0.582983, 0.578923]$, of the transformed $(111)_f$ plane should be a unit vector parallel to the normal of the $(011)_b$ plane. Therefore, the scalar product of the normal of the $(011)_b$ plane and that of the original $(111)_f$ plane,

$$(1/\sqrt{3})(111)[0.570063, 0.582983, 0.578923] = 0.999956,$$

is the cosine of the angle between $(111)_f$ and $(011)_b$, and gives us a value of $0.53°$.

Next, $[\bar{1}01]_f$ is transformed by $\boldsymbol{S}$ to $\boldsymbol{S}[\bar{1}01]_f = [-0.720803, 0.046426, 0.663013]$. By normalizing this, we obtain a unit vector, $[-0.735170, 0.047351, 0.676228]$, parallel to $[\bar{1}\bar{1}1]_b$. From the scalar product of this unit vector with that of $[\bar{1}01]_f$,

$$(1/\sqrt{2})(\bar{1}01)[-0.735170, 0.047351, 0.676228] = 0.998008,$$

the angle between $[\bar{1}01]_f$ and $[\bar{1}\bar{1}1]_b$ is obtained to be $-3.62°$. This value is greater than those attributable to experimental error, and the nonparallelism indicates that the K–S relation does not hold exactly in the Fe–31% Ni alloy. Similar calculations regarding the $[\bar{1}\bar{1}2]_f$ direction showed that the $[\bar{1}\bar{1}2]_f$ direction makes an angle of $1.67°$ with the corresponding $[0\bar{1}1]_b$ direction. Thus, the orientation relationship in the Fe–31% Ni alloy is midway between the K–S and N relations, but is nearer to the N relation.

Although we have so far been concerned with only the f.c.c.-to-b.c.c. (b.c.t.) transformation, the calculations can be performed in the same way for other structural changes. In fact, the b.c.c.-to-orthorhombic (close-packed structures with long-period stacking order) transformations were treated by Bowles and Mackenzie.[33] In it, the lattice correspondence between the b.c.c. and orthorhombic lattices was taken to be†

$$[100]_c \rightarrow [100]_o, \qquad [01\bar{1}]_c \rightarrow [010]_o, \qquad \text{and} \qquad [011]_c \rightarrow [001]_o.$$

In such transformations, some atoms in the unit cell undergo shufflings. It was shown, however, that the shufflings do not affect this calculation.

† Subscripts c and o apply respectively to the cubic and orthorhombic lattices.

6.3.2 Wechsler–Lieberman–Read theory[35,36]

Of the three matrices composing the total shape deformation $\boldsymbol{P}_1 = \boldsymbol{RBP}$, $\boldsymbol{R}$ is a rigid body rotation, as mentioned previously. Then the pure strain associated with the transformation is attributed to the product of $\boldsymbol{B}$ and $\boldsymbol{P}$, that is, to

$$\boldsymbol{BP} \equiv \boldsymbol{F}. \tag{21}$$

Thus, $\boldsymbol{F}$ plays an important role in the shape deformation $\boldsymbol{P}_1$. The W–L–R theory is based on the properties of the pure strain matrix $\boldsymbol{F}$.

Since $\boldsymbol{P}_1$ is rewritten as

$$\boldsymbol{P}_1 = \boldsymbol{RF}, \tag{22}$$

$\boldsymbol{F}$ should also be an invariant plain strain. Therefore, any vector, say $\boldsymbol{v}$, lying in the habit plane remains unchanged in length due to $\boldsymbol{F}$. That is,

$$\boldsymbol{v}'\boldsymbol{F}'\boldsymbol{F}\boldsymbol{v} = \boldsymbol{v}'\boldsymbol{v}. \tag{23}$$

Here the matrix $\boldsymbol{F}'\boldsymbol{F}$ is symmetric, and thus it can be diagonalized by an orthogonal transformation $\boldsymbol{R}_\mathrm{d}$. That is,

$$\boldsymbol{R}_\mathrm{d}'\boldsymbol{F}'\boldsymbol{F}\boldsymbol{R}_\mathrm{d} = \boldsymbol{F}_\mathrm{d}^2 \tag{24}$$

where

$$\boldsymbol{F}_\mathrm{d} = (\mathrm{diag}: \lambda_1, \lambda_2, \lambda_3). \tag{25}$$

The λ_i $(i = 1\text{–}3)$ can be obtained from the equation

$$\det|\boldsymbol{F}'\boldsymbol{F} - \lambda^2\boldsymbol{I}| = 0. \tag{26}$$

$\boldsymbol{F}_\mathrm{d}$ also causes no change in the length of arbitrary vectors, say $\overline{\boldsymbol{v}}\,(=\boldsymbol{R}_\mathrm{d}\boldsymbol{v})$, lying in the habit plane. Then, the equation

$$\overline{\boldsymbol{v}}'\boldsymbol{F}_\mathrm{d}^2\overline{\boldsymbol{v}} = \overline{\boldsymbol{v}}'\overline{\boldsymbol{v}} \tag{27}$$

holds.

For the convenience of calculations, a new basis g is introduced, for which $\boldsymbol{g}_1 = \boldsymbol{d}_2$, $\boldsymbol{g}_2 = \boldsymbol{p}_2$, and $\boldsymbol{g}_3 = \boldsymbol{d}_2 \times \boldsymbol{p}_2$ compose the orthogonal coordinates. The basis change from f to g, thus, is performed by a rotation matrix $\boldsymbol{R}_\mathrm{g}'$ which is defined by

$$\boldsymbol{R}_\mathrm{g} = (\boldsymbol{d}_2, \boldsymbol{p}_2, \boldsymbol{t}) = \begin{bmatrix} d_1 & p_1 & t_1 \\ d_2 & p_2 & t_2 \\ d & p & t \end{bmatrix}, \tag{28}$$

where $\boldsymbol{t} = \boldsymbol{d}_2 \times \boldsymbol{p}_2$ and is a unit vector. With reference to the g basis, $\boldsymbol{P}$ is simply written as

$$(\mathrm{gPg}) = \begin{bmatrix} 1 & g & 0 \\ 0 & 1 & 0 \\ 0 & 0 & 1 \end{bmatrix}, \tag{29}$$

where g is the magnitude of the shear $\boldsymbol{P}$ to be determined. We can determine g from the condition that one of the eigenvalues λ_i must be unity for a plane of zero distortion to exist.

In order to obtain the value of g, it is convenient to express $\boldsymbol{B}$ relative to the g basis. That is,

$$(\mathrm{gBg}) = \boldsymbol{R}_g'(\mathrm{fBf})\boldsymbol{R}_g = \begin{bmatrix} \eta_1 + d^2\Delta & dp\Delta & dt\Delta \\ dp\Delta & \eta_1 + p^2\Delta & pt\Delta \\ dt\Delta & pt\Delta & \eta_1 + t^2\Delta \end{bmatrix}, \tag{30}$$

where $\Delta = \eta_3 - \eta_1$. From Eqs. (29) and (30), it follows that

$$(\mathrm{gFg}) = (\mathrm{gBg})(\mathrm{gPg}) = \begin{bmatrix} \eta_1 + d^2\Delta & \eta_1 g + \gamma d\Delta & dt\Delta \\ dp\Delta & \eta_1 + \gamma p\Delta & pt\Delta \\ dt\Delta & \gamma t\Delta & \eta_1 + t^2\Delta \end{bmatrix}, \tag{31}$$

where $\gamma = dg + p$. The symmetric matrix (gJg), defined by $(\mathrm{gJg}) = (\mathrm{gFg})'(\mathrm{gFg})$, can be obtained directly from Eq. (31), and its matrix elements are written explicitly as

$$\begin{aligned} j_{11} &= \eta_1^2 + d^2(\eta_3^2 - \eta_1^2), \\ j_{22} &= \eta_1^2(g^2 + 1) + \gamma^2(\eta_3^2 - \eta_1^2), \\ j_{33} &= \eta_1^2 + t^2(\eta_3^2 - \eta_1^2), \\ j_{12} &= \eta_1^2 g + d\gamma(\eta_3^2 - \eta_1^2), \\ j_{13} &= dt(\eta_3^2 - \eta_1^2), \\ j_{23} &= t\gamma(\eta_3^2 - \eta_1^2). \end{aligned} \tag{32}$$

The eigenvalues λ^2 of (gJg) can be obtained from $\det\{(\mathrm{gJg}) - \lambda^2\boldsymbol{I}\} = 0$, that is, from

$$\lambda^6 - T\lambda^4 + Q\lambda^2 - D = 0, \tag{33}$$

where

$$\begin{aligned} D &= \det(\mathrm{gJg}) = \eta_1^4\eta_3^2, \\ T &= \mathrm{tr}(\mathrm{gJg}) = \eta_1^2[2 - 2gdp + g^2(1 - d^2)] + \eta_3^2[1 + 2gdp + g^2d^2], \\ Q &= \eta_1^4[1 - 2gdp + g^2p^2] + \eta_1^2\eta_3^2[2 + 2gdp + g^2(1 - p^2)]. \end{aligned} \tag{34}$$

Substituting $\lambda^2 = 1$, which is a necessary condition for having a plane of zero distortion, into Eq. (33), we obtain a quadratic equation for g, from which

$$g = \frac{{\eta_1}^2 - 1}{A}\left[dp({\eta_1}^2 - {\eta_3}^2) + \delta_g\sqrt{H}\right] \qquad (\delta_g = \pm 1) \tag{35}$$

where

$$A = ({\eta_1}^2 - {\eta_3}^2)(d^2 + p^2{\eta_1}^2) - {\eta_1}^2(1 - {\eta_3}^2),$$
$$H = [{\eta_1}^2(1 - {\eta_3}^2) - ({\eta_1}^2 - {\eta_3}^2)d^2][(1 - {\eta_3}^2) - p^2({\eta_1}^2 - {\eta_3}^2)].$$

Thus, two values, g_1 and g_2, can be obtained for g. These two values, however, give a geometrically equivalent result when the complementary shear is a twinning shear. Such a degeneracy of solutions is said to be g type.[2]

The foregoing calculations will be now carried out for the Fe–31% Ni alloy.[6] If we assume for the components of $\boldsymbol{R}_g$ that

$$\boldsymbol{d}_2 = \frac{1}{\sqrt{2}}[\bar{1}01], \qquad \boldsymbol{p}_2 = \frac{1}{\sqrt{2}}[101], \qquad \boldsymbol{t} = [010], \tag{36}$$

then d and p should be $1/\sqrt{2}$ and $1/\sqrt{2}$, respectively. Using these values and then the values of η_1 and η_2, we obtain from Eq. (35) two values of g:

$$g_1 = 0.256794, \qquad g_2 = 0.409872. \tag{37}$$

Next, (gFg) can be obtained by substituting g into Eq. (31). Using the g_1 value for g, we find that (gFg) is

$$(\mathrm{gFg}) = \begin{bmatrix} 0.966338 & 0.082352 & 0 \\ -0.165798 & 0.923763 & 0 \\ 0 & 0 & 1.132136 \end{bmatrix}. \tag{38}$$

The eigenvalues of (gJg) can be obtained from Eq. (33), as mentioned previously. Since one of the values is already known to be ${\lambda_1}^2 = 1$, the other two values, ${\lambda_2}^2$ and ${\lambda_3}^2$, follow from

$$\lambda^4 - (1 - T)\lambda^2 + D = 0, \tag{39}$$

which is obtained by dividing Eq. (33) by $(\lambda^2 - 1)$ and by using the value of g in Eq. (35). Thus, ${\lambda_2}^2$ and ${\lambda_3}^2$ are obtained:

$${\lambda_2}^2 = 1.281732, \qquad {\lambda_3}^2 = 0.821418 \qquad ({\lambda_1}^2 = 1).$$

The eigenvalues of (gJg) are the same as those of ${\boldsymbol{F}_d}^2$, and can be derived from the relation

$$(\mathrm{gJg})\boldsymbol{x} = \lambda^2\boldsymbol{x} \qquad (\lambda = \lambda_1, \lambda_2, \lambda_3). \tag{40}$$

Thus, we obtain

$$\begin{aligned} \boldsymbol{J}_g^{(1)} &= [0.885036, -0.465523, 0] \quad \text{for } \lambda = \lambda_1, \\ \boldsymbol{J}_g^{(2)} &= [001] \quad \text{for } \lambda = \lambda_2, \\ \boldsymbol{J}_g^{(3)} &= [0.465523, \quad 0.885036, 0] \quad \text{for } \lambda = \lambda_3. \end{aligned} \tag{41}$$

Next, these eigenvectors will be referred to the f basis. Doing so requires that they be operated on by the rotation matrix $\boldsymbol{R}_g'$ which is given by the Eqs. (28) and (36). That is, $(\mathrm{fJf}) = \boldsymbol{R}_g(\mathrm{gJg})\boldsymbol{R}_g'$, and then $\boldsymbol{J}_f^{(\lambda)} = \boldsymbol{R}_g'\boldsymbol{J}_g^{(\lambda)}$. These eigenvectors referred to the f basis determine the elements of matrix $\boldsymbol{R}_d$. In this way we obtain

$$\begin{aligned} \boldsymbol{J}_f^{(1)} &= [-0.954989, 0, 0.296640] = \boldsymbol{d}^{(1)} \quad \text{for } \lambda = \lambda_1, \\ \boldsymbol{J}_f^{(2)} &= [0\,1\,0] \quad\quad\quad\quad\quad\quad\quad\quad = \boldsymbol{d}^{(2)} \quad \text{for } \lambda = \lambda_2, \\ \boldsymbol{J}_f^{(3)} &= [0.296640, 0, 0.954989] \quad = \boldsymbol{d}^{(3)} \quad \text{for } \lambda = \lambda_3, \end{aligned}$$

and

$$(\boldsymbol{d}^{(1)}, \boldsymbol{d}^{(2)}, \boldsymbol{d}^{(3)}) = \boldsymbol{R}_d. \tag{42}$$

Substituting Eqs. (28), (36), and (38) into $(\mathrm{fFf}) = \boldsymbol{R}_g(\mathrm{gFg})\boldsymbol{R}_g'$, we finally obtain

$$(\mathrm{fFf}) = \begin{bmatrix} 0.986773 & 0 & -0.145363 \\ 0 & 1.132136 & 0 \\ 0.102788 & 0 & 0.903327 \end{bmatrix}. \tag{43}$$

A. *Determination of habit plane*

Equation (27), which defines an undistorted plane due to $\boldsymbol{F}_d$, takes the form

$$(\lambda_1^2 - 1)\bar{v}_x^2 + (\lambda_2^2 - 1)\bar{v}_y^2 + (\lambda_3^2 - 1)\bar{v}_z^2 = 0$$

where the components $\bar{v}_x$, $\bar{v}_y$, and $\bar{v}_z$ of $\bar{\boldsymbol{v}}$ are referred to the d basis. Since $\lambda_1 = 1$, the foregoing equation becomes

$$(\lambda_2^2 - 1)\bar{v}_y^2 + (\lambda_3^2 - 1)\bar{v}_z^2 = 0, \tag{44}$$

from which it follows that

$$\frac{\bar{v}_y}{\bar{v}_z} = \delta_k K \left[\delta_k = \pm 1, K = \left(\frac{1 - \lambda_3^2}{\lambda_2^2 - 1} \right)^{1/2} = 0.796161 \right].$$

Equation (44) is nothing but an equation of the habit plane referred to the d basis, and then the habit plane is

$$(\boldsymbol{p}_1'; \mathrm{d}) \| (0, 1, \delta_k K). \tag{45}$$

For cubic crystals, the two solutions $(01K)$ and $(01\bar{K})$, corresponding respectively to $\delta_k = +1$ and -1, give two crystallographically equivalent habit planes, and such a degeneracy is said to be of the K type.

Choosing the positive sign for δ_k and substituting the values of $\lambda_2{}^2$ and $\lambda_3{}^2$ into Eq. (45), we obtain, after normalizing, the habit plane

$$(\boldsymbol{p}_1'; \mathrm{d}) = (0, 0.782337, 0.622862).$$

The habit plane referred to the f basis, then, can be obtained from $(\boldsymbol{p}_1'; \mathrm{f}) = (\boldsymbol{p}_1'; \mathrm{d})\boldsymbol{R}_\mathrm{d}'$, and it is

$$(\boldsymbol{p}_1'; \mathrm{f}) = (0.184765, 0.782337, 0.594820). \tag{46}$$

This is identical to the result obtained from the B–M theory, Eq. (18).

B. *Determination of* $\boldsymbol{R}$

$\boldsymbol{R}$ can be determined from the amount of rotation of two arbitrary vectors in the habit plane due to $\boldsymbol{F}$. Two vectors in the habit plane, say $\boldsymbol{v}_1$ and $\boldsymbol{v}_2$, will be chosen as follows:

$$\begin{aligned} \boldsymbol{v}_1 &= [0, 1, 0] \times \boldsymbol{p}_1 = [0.954989, 0, -0.296642], \\ \boldsymbol{v}_2 &= [0, 0, 1] \times \boldsymbol{p}_1 = [-0.973227, 0.229848, 0]. \end{aligned} \tag{47}$$

By applying (fFf) to these vectors, we obtain two undistorted vectors

$$\begin{aligned} \underline{\boldsymbol{v}}_1 &= [0.985478, 0, -0.169803], \\ \boldsymbol{v}_2 &= [-0.960354, 0.260219, -0.100036]. \end{aligned} \tag{48}$$

Then, the axis $\boldsymbol{u}$ and amount of rotation θ due to $\boldsymbol{F}$ are calculated using Euler's theorem,

$$\boldsymbol{u} \tan\frac{\theta}{2} = \frac{[\underline{\boldsymbol{v}}_1 - \boldsymbol{v}_1] \times [\underline{\boldsymbol{v}}_2 - \boldsymbol{v}_2]}{[\underline{\boldsymbol{v}}_2 - \boldsymbol{v}_2] \cdot [\underline{\boldsymbol{v}}_1 + \boldsymbol{v}_1]}.$$

Substituting Eqs. (47) and (48) into this equation, we have

$$\boldsymbol{u} \tan(\theta/2) = [-0.053771, 0.065364, 0.012925].$$

Thus, we obtain

$$\begin{aligned} &\boldsymbol{u} = [u_1, u_2, u_3] = [-0.628018, 0.763415, 0.150960], \\ &\tan(\theta/2) = 0.085621, \qquad \theta = 9°47.25', \\ &\sin\theta = 0.169996, \qquad \text{and} \qquad \cos\theta = 0.985445. \end{aligned}$$

$\boldsymbol{R}$ can be expressed in terms of u_1, u_2, u_3 and θ (see p. 36 of Wayman[6]).

$$\boldsymbol{R} = \begin{bmatrix} u_1{}^2(1-\cos\theta)+\cos\theta & u_1u_2(1-\cos\theta)-u_3\sin\theta & u_1u_3(1-\cos\theta)+u_2\sin\theta \\ u_2u_1(1-\cos\theta)+u_3\sin\theta & u_2{}^2(1-\cos\theta)+\cos\theta & u_2u_3(1-\cos\theta)-u_1\sin\theta \\ u_3u_1(1-\cos\theta)-u_2\sin\theta & u_3u_2(1-\cos\theta)+u_1\sin\theta & u_3{}^2(1-\cos\theta)+\cos\theta \end{bmatrix} \tag{49}$$

and numerically becomes

$$\boldsymbol{R} = \begin{bmatrix} 0.991185 & -0.032641 & 0.128398 \\ 0.018684 & 0.993927 & 0.108438 \\ -0.131157 & -0.105083 & 0.985776 \end{bmatrix}.$$

The orientation relationship between the matrix and product is determined only by $\boldsymbol{R}$ because neither $\boldsymbol{B}$ nor $\boldsymbol{P}$ changes the crystal orientation. $\boldsymbol{R}$ can be calculated in a way similar to that by which $\boldsymbol{S}$ was determined in the B–M theory, and the result obtained is the same.

The magnitude of the shape deformation is calculated to be

$$\boldsymbol{d}_1 = \boldsymbol{R}(\mathrm{fFf})\boldsymbol{p}_1 - \boldsymbol{p}_1 = [-0.047235, 0.160116, -0.152072], \qquad (50)$$

which is identical to that obtained by the B–M theory.

A more general method, applicable to the cubic-to-orthorhombic transformation, has been established.[37]

6.3.3 Application of the Wechsler–Lieberman–Read theory to internally twinned martensites[35,38]

In the preceding sections, a simple slip shear was adopted for the complementary strain. But, as illustrated in Fig. 6.16, a twinning shear can also produce an invariant plane. In the figure, if the EBCF region in the ABCD region after the lattice deformation undergoes a twinning shear on the twinning plane† EF it becomes the EB′C′F region. The ABCD region produced by the lattice deformation can be regarded as transformed to AB′C′D. The thickness ratio between regions 1 and 2, $(1 - x)/x$, must take an appropriate value and the thickness of each region must be small. The twinned regions 1 and 2 can otherwise be considered to be generated from the parent

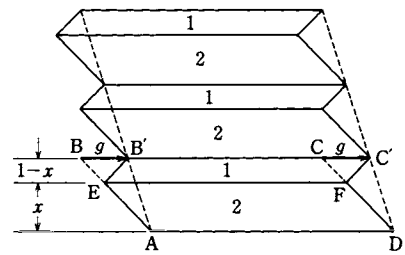

FIG. 6.16 Complementary strain by twinning shears.

† The plane and direction of twinning shear can be determined to some extent from electron microscopic observation of internal twins. However, since there are formally many twinning systems,[39] the one to be adopted for calculations must be carefully determined from electron microscopic and other results.

phase by means of different but crystallographically equivalent Bain distortions. In fact, this is how Wechsler, Lieberman, and Read treated the formation of twinned martensites in their first paper dealing with the f.c.c.-to-b.c.c. transformation, and they showed that an invariant plane can exist only when the volume ratio of regions 1 and 2, $(1 - x)/x$, has a certain value.

The Bain distortions and rotations for regions 1 and 2 will be denoted by $\boldsymbol{B}_1$ and $\boldsymbol{B}_2$ and $\boldsymbol{R}_1$ and $\boldsymbol{R}_2$, respectively. Then, the total shape deformation can be expressed as

$$\boldsymbol{P}_1 = (1 - x)\boldsymbol{R}_1\boldsymbol{B}_1 + x\boldsymbol{R}_2\boldsymbol{B}_2 = \boldsymbol{R}_1\boldsymbol{F}. \tag{51}$$

Here, $\boldsymbol{B}_1$ and $\boldsymbol{B}_2$ are assumed to be

$$\boldsymbol{B}_1 = (\text{diag: } \eta_1\eta_3\eta_1), \qquad \boldsymbol{B}_2 = (\text{diag: } \eta_3\eta_1\eta_1). \tag{52}$$

In addition, the twin relation between regions 1 and 2 should result in the following relation between $\boldsymbol{R}_1$ and $\boldsymbol{R}_2$:

$$\boldsymbol{R}_2 = \boldsymbol{R}_1\boldsymbol{\Phi}$$

(Fig. 6.17). In the case of $(112)_b$ twinning, $\boldsymbol{\Phi}$ is known to be

$$\boldsymbol{\Phi} = \begin{bmatrix} \cos\phi & -\sin\phi & 0 \\ \sin\phi & \cos\phi & 0 \\ 0 & 0 & 1 \end{bmatrix}$$

where

$$\cos\phi = \frac{2\eta_1\eta_3}{\eta_1^2 + \eta_3^2} \quad \text{and} \quad \sin\phi = \frac{\eta_1^2 - \eta_3^2}{\eta_1^2 + \eta_3^2}. \tag{53}$$

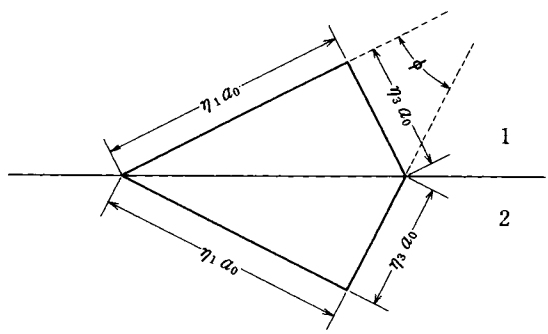

FIG. 6.17 Geometric relation between twins.

Substituting Eqs. (52) and (53) into (51), we obtain

$$\boldsymbol{F} = \begin{bmatrix} \eta_1(1 - x\sin\phi) & -\eta_1 x\sin\phi & 0 \\ \eta_3 x\sin\phi & \eta_3(1 + x\sin\phi) & 0 \\ 0 & 0 & \eta_1 \end{bmatrix}, \tag{54}$$

which corresponds to Eq. (31). However, Eq. (31) involved g as an unknown quantity and was referred to the g basis, whereas Eq. (54) involves x as an unknown quantity and is referred to the f basis.

Equation (54) shows that $\boldsymbol{F}$ is a nonsymmetric matrix and therefore does not represent a pure distortion. However, $\boldsymbol{F}$ can be expressed as the product of a rotation matrix $\boldsymbol{\Psi}$ and a symmetric matrix $\boldsymbol{F}_s$ (representing a pure distortion), and $\boldsymbol{F}_s$ can be transformed to a diagonalized matrix $\boldsymbol{F}_d$ by a rotation matrix $\boldsymbol{\Gamma}$, that is,

$$\boldsymbol{F} = \boldsymbol{\Psi}\boldsymbol{F}_s = \boldsymbol{\Psi}\boldsymbol{\Gamma}\boldsymbol{F}_d\boldsymbol{\Gamma}', \tag{55}$$

from which it follows that $\boldsymbol{F}_d = \boldsymbol{\Gamma}'\boldsymbol{\Psi}'\boldsymbol{F}\boldsymbol{\Gamma}$. Here, $\boldsymbol{F}_d$, $\boldsymbol{\Psi}$, and $\boldsymbol{\Gamma}$ can be put in the form

$$\boldsymbol{F}_d = \begin{bmatrix} \lambda_2 & 0 & 0 \\ 0 & \lambda_3 & 0 \\ 0 & 0 & \lambda_1 \end{bmatrix}, \qquad \boldsymbol{\Psi} = \begin{bmatrix} \cos\psi & -\sin\psi & 0 \\ \sin\psi & \cos\psi & 0 \\ 0 & 0 & 1 \end{bmatrix},$$

and

$$\boldsymbol{\Gamma} = \begin{bmatrix} \cos\gamma & -\sin\gamma & 0 \\ \sin\gamma & \cos\gamma & 0 \\ 0 & 0 & 1 \end{bmatrix} \tag{56}$$

Upon comparison of $\boldsymbol{F}$ with $\boldsymbol{F}_d$, it is immediately seen that

$$\lambda_1 = \eta_1.$$

Since $\boldsymbol{F}_d$ differs from $\boldsymbol{F}$ only by a rotation, it follows that $\det\boldsymbol{F} = \det\boldsymbol{F}_d$. Substituting Eqs. (54) and (56) into this relation, we obtain

$$\lambda_2\lambda_3 = \eta_1\eta_3. \tag{57}$$

If $\boldsymbol{F}_d$ results in a plane of zero distortion, one of the three λ must be unity. Then, either λ_2 or λ_3 must be unity because λ_1 is already known to be η_1. Since the two solutions derived from $\lambda_2 = 1$ and $\lambda_3 = 1$ are crystallographically equivalent, we can set arbitrarily $\lambda_3 = 1$. Then, we obtain $\lambda_2 = \eta_1\eta_3$, and subsequently

$$\begin{aligned} &\boldsymbol{F}_d = (\text{diag: } \eta_1\eta_3, 1, \eta_1) = (\text{diag: } \lambda_2, \lambda_3, \lambda_1), \\ &\lambda_1 = 1.12011, \qquad \lambda_2 = 0.927075, \qquad \lambda_3 = 1. \end{aligned} \tag{58}$$

Numerical calculations will now be made for an Fe–22% Ni–0.8% C alloy, as discussed in Section 6.2.3. Substituting Eq. (58) into Eq. (55) and comparing with Eq. (54), we finally obtain

$$\cos\psi = \frac{\eta_1 + \eta_3}{1 + \eta_1\eta_3}\left[1 - \frac{(\eta_1 - \eta_3)^2}{{\eta_1}^2 + {\eta_3}^2}\,x\right],$$
$$\sin\psi = \frac{\eta_1 + \eta_3}{1 + \eta_1\eta_3} \cdot \frac{{\eta_1}^2 - {\eta_3}^2}{{\eta_1}^2 + {\eta_3}^2} \cdot x, \tag{59}$$

where

$$x = \frac{1}{2} \pm \frac{1}{2}\frac{1 - {\eta_1}^2{\eta_3}^2}{{\eta_1}^2 - {\eta_3}^2}(1 - A^2)^{1/2} = 0.419191 \text{ or } 0.580809,$$
$$A = \frac{({\eta_1}^2 - 1)(1 - {\eta_3}^2)}{1 - {\eta_1}^2{\eta_3}^2} = 0.570781. \tag{60}$$

As seen from the equation for x, this term has two values, and for one value of x the other value becomes $(1 - x)$. Therefore, the two values lead to crystallographically equivalent results.

A. *Determination of the habit plane*

As in the preceding section, the habit plane is referred to the d basis, which is constructed with the principal axes of $\boldsymbol{F}_d$, and is

$$(\boldsymbol{p}_1'; \mathrm{d}) = (1 + K^2)^{-1/2}(K, 0, 1),$$
$$K = \left(\frac{1 - {\eta_1}^2{\eta_3}^2}{{\eta_1}^2 - 1}\right)^{1/2} = 0.742830. \tag{61}$$

The habit planes referred to the f and d bases are related to each other as

$$(\boldsymbol{p}_1'; \mathrm{f}) = (\boldsymbol{p}_1'; \mathrm{d})\boldsymbol{\Gamma}'. \tag{62}$$

Therefore, in order to obtain that referred to the f basis, the rotation matrix $\boldsymbol{\Gamma}$ must be known. It can be determined in the following way.

Since the twinning plane is assumed to come from $(110)_f$,† the vector parallel to the intersection of the twinning plane with the habit plane has the form

$$\boldsymbol{t} = [b, -b, a]. \tag{63}$$

The vector $\boldsymbol{t}$ in both regions 1 and 2 undergoes the same length changes during transformation. The change in region 1 will be taken up in the

† $(1\bar{1}0)$ can also be taken as the twinning plane. In this case, Eq. (63) takes the form $[b, b, a]$, which is equivalent to $[b, -b, a]$.

following calculations. In this case, $\boldsymbol{t}$ becomes $\boldsymbol{R}_1\boldsymbol{B}_1\boldsymbol{t}$ due to the transformation, but is not changed in length. We thus obtain

$$|\boldsymbol{t}|^2 = |\boldsymbol{R}_1\boldsymbol{B}_1\boldsymbol{t}|^2 = (\boldsymbol{B}_1\boldsymbol{t})'\boldsymbol{R}_1'\boldsymbol{R}_1(\boldsymbol{B}_1\boldsymbol{t}) = |\boldsymbol{B}_1\boldsymbol{t}|^2. \tag{64}$$

Substituting Eqs. (52) and (63) into this equation, and taking into account the condition that $a^2 + 2b^2 = 1$ when $\boldsymbol{t}$ is normalized, we obtain

$$a = \left(\frac{2 - \eta_1^2 - \eta_2^2}{\eta_1^2 - \eta_2^2}\right)^{1/2}, \qquad b = \left(\frac{\eta_1^2 - 1}{\eta_1^2 - \eta_2^2}\right)^{1/2}, \tag{65}$$

and thus

$$\boldsymbol{t} = \left[\left(\frac{\eta_1^2 - 1}{\eta_1^2 - \eta_2^2}\right)^{1/2}, -\left(\frac{\eta_1^2 - 1}{\eta_1^2 - \eta_2^2}\right)^{1/2}, \left(\frac{2 - \eta_1^2 - \eta_2^2}{\eta_1^2 - \eta_2^2}\right)^{1/2}\right]. \tag{66}$$

Since the vector $\boldsymbol{t}$ is also unchanged in length due to $\boldsymbol{F}$, $|\boldsymbol{F}\boldsymbol{t}|^2 = |\boldsymbol{t}|^2 = 1$. It follows that

$$\boldsymbol{t}'\boldsymbol{\Gamma}\boldsymbol{F}_d\boldsymbol{\Gamma}'\boldsymbol{\Psi}'\boldsymbol{\Psi}\boldsymbol{\Gamma}\boldsymbol{F}_d\boldsymbol{\Gamma}'\boldsymbol{t} = \boldsymbol{t}'\boldsymbol{\Gamma}\boldsymbol{F}_d^2\boldsymbol{\Gamma}'\boldsymbol{t} = 1.$$

Substituting Eqs. (66) and (56) into the foregoing, we obtain

$$2\sin\gamma\cos\gamma = A \tag{67}$$

$$\begin{aligned}\cos\gamma &= \tfrac{1}{2}(1 + A)^{1/2} + \tfrac{1}{2}(1 - A)^{1/2},\\ \sin\gamma &= \tfrac{1}{2}(1 + A)^{1/2} - \tfrac{1}{2}(1 - A)^{1/2}.\end{aligned} \tag{68}$$

Using Eq. (60), we can calculate the elements of $\boldsymbol{\Gamma}$ from Eq. (68). Substituting these elements in Eq. (62), we have

$$\begin{aligned}(\boldsymbol{p}_1'; \mathrm{f}) = (\boldsymbol{p}_1'; \mathrm{d})\boldsymbol{\Gamma}' &= (1 + K^2)^{-1/2}(K\cos\gamma, K\sin\gamma, 1)\\ &= \left(\frac{1}{2\eta_1}\left[\left(\frac{\eta_1^2 + \eta_3^2 - 2\eta_1^2\eta_3^2}{1 - \eta_3^2}\right)^{1/2} + \left(\frac{2 - \eta_1^2 - \eta_3^2}{1 - \eta_3^2}\right)^{1/2}\right],\right.\\ &\quad \frac{1}{2\eta_1}\left[\left(\frac{\eta_1^2 + \eta_3^2 - 2\eta_1^2\eta_3^2}{1 - \eta_3^2}\right)^{1/2} - \left(\frac{2 - \eta_1^2 - \eta_3^2}{1 - \eta_3^2}\right)^{1/2}\right],\\ &\quad \left.\frac{1}{\eta_1}\left(\frac{\eta_1^2 - 1}{1 - \eta_3^2}\right)^{1/2}\right).\end{aligned} \tag{69}$$

As is easily seen from this expression, the habit planes generally have irrational indices.

B. *Determination of the magnitude and direction of the macroscopic shear*

Figure 6.18 is a schematic illustration of the shape change $\boldsymbol{P}_1$ in reference to the habit plane (AD). In the figure, the axes are orthogonal such that

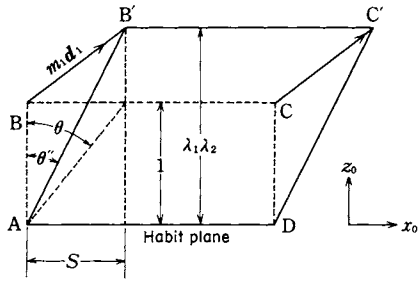

FIG. 6.18 Relations between shape deformation, angle of shear, and habit plane.

z_0 is normal to the habit plane, x_0 is parallel to the projection of the shear direction onto the habit plane, and y_0 is perpendicular to both of them. In this coordinate system, the total deformation can be expressed as

$$\boldsymbol{P}_1 = \begin{bmatrix} 1 & 0 & -S \\ 0 & 1 & 0 \\ 0 & 0 & \lambda_1\lambda_2 \end{bmatrix}, \tag{70}$$

where S is the projection of the displacement $m_1\boldsymbol{d}_1$ onto the habit plane. It is also seen from the figure that

$$|\boldsymbol{P}_1\boldsymbol{p}_1|^2 = (\lambda_1\lambda_2)^2 + S^2. \tag{71}$$

The left-hand term of this equation can be rewritten as

$$\begin{aligned} |\boldsymbol{P}_1\boldsymbol{p}_1|^2 &= |\boldsymbol{F}\boldsymbol{p}_1|^2 = |\boldsymbol{\Psi\Gamma F}_\mathrm{d}\boldsymbol{\Gamma}'\boldsymbol{p}_1|^2 = \boldsymbol{p}_1'\boldsymbol{\Gamma F}_\mathrm{d}'\boldsymbol{\Gamma}'\boldsymbol{\Psi}'\boldsymbol{\Psi\Gamma F}_\mathrm{d}\boldsymbol{\Gamma}'\boldsymbol{p}_1 \\ &= \boldsymbol{p}_1'\boldsymbol{\Gamma F}_\mathrm{d}{}^2\boldsymbol{\Gamma}'\boldsymbol{p}_1 = (\boldsymbol{p}_1';\mathrm{d})\boldsymbol{F}_\mathrm{d}{}^2[\boldsymbol{p}_1;\mathrm{d}] \\ &= \frac{1}{1+K^2}(\lambda_1{}^2 + K^2\lambda_2{}^2) = \lambda_1{}^2 + \lambda_2{}^2 - 1. \end{aligned} \tag{72}$$

This is equal to the right-hand term of Eq. (71), and so we obtain

$$\tan\theta \equiv S = [(\lambda_1{}^2 - 1)(1 - \lambda_2{}^2)]^{1/2} \qquad (\theta = 10.71°). \tag{73}$$

Since the direction of $\boldsymbol{S}$ is perpendicular to $\boldsymbol{p}_1$, $\boldsymbol{S}$ referred to the d basis should be

$$\boldsymbol{S}_\mathrm{d} = (1 + \mathrm{K}^2)^{-1/2}[-1, 0, K], \tag{74}$$

and related to the f basis it should be

$$\boldsymbol{S} \equiv \boldsymbol{\Gamma S}_\mathrm{d} = (1 + K^2)^{-1/2}[-\cos\gamma, -\sin\gamma, K]. \tag{75}$$

The shear angle θ'' is thus obtained to be

$$\tan\theta'' = \frac{S}{\lambda_1\lambda_2} = \frac{[(\lambda_1{}^2 - 1)(1 - \lambda_2{}^2)]^{1/2}}{\lambda_1\lambda_2} \qquad (\theta'' = 10.30°). \tag{76}$$

C. *Determination of the orientation relationship*

The orientation relationship can be determined if $\boldsymbol{R}_1$ is known. $\boldsymbol{R}_1$ can be calculated from the condition that any vector in the habit plane remains unchanged as a result of the total deformation. That is,

$$\boldsymbol{P}_1\boldsymbol{v} = \boldsymbol{R}_1\boldsymbol{F}\boldsymbol{v} = \boldsymbol{v} \qquad \text{or} \qquad \boldsymbol{F}\boldsymbol{v} = \boldsymbol{R}_1'\boldsymbol{v} \tag{77}$$

where $\boldsymbol{v}$ is an arbitrary vector in the habit plane. As three vectors satisfying the foregoing condition, we choose the cross-products of $\boldsymbol{p}_1 \equiv [hkl]$ with unit vectors along the x, y, and z axes. That is,

$$\boldsymbol{v}_1 = [0, l, \bar{k}], \qquad \boldsymbol{v}_2 = [\bar{l}, 0, h], \qquad \boldsymbol{v}_3 = [k, \bar{h}, 0].$$

By substituting these vectors into Eq. (77), nine equations can be obtained for the nine elements of $\boldsymbol{R}_1$. Since only six of those equations are independent, three additional equations are needed to obtain all nine elements. The additional equations, fortunately, can be obtained from the normalization conditions for the elements. Thus, all nine elements of $\boldsymbol{R}_1$ can be determined, and the orientation relationship is given by using $\boldsymbol{R}_1$ as explained previously.

D. *Relation between internal twins and slip*

As can be seen from Fig. 6.16, if slip occurs on the same plane as the twinning shear, the twinned regions 1 can be replaced by slipped regions with the same orientation as regions 2, the shear magnitude being kept equal to that due to the twinning shear. Now, let us examine the relation between the amount of slip shear g and the fraction x of twinning. The slip shear $\boldsymbol{G}$ referred to the f basis can be obtained by a rotation matrix $\boldsymbol{\Omega}'$, and can be expressed as

$$\boldsymbol{G} = \boldsymbol{\Omega}\begin{bmatrix} 1 & -g & 0 \\ 0 & 1 & 0 \\ 0 & 0 & 1 \end{bmatrix}\boldsymbol{\Omega}'. \tag{78}$$

For a slip shear on the $(121)_b$ plane in the $[1\bar{1}1]_b$ direction, we obtain

$$\boldsymbol{\Omega} = \begin{bmatrix} \cos\omega & \sin\omega & 0 \\ -\sin\omega & \cos\omega & 0 \\ 0 & 0 & 1 \end{bmatrix},$$

where

$$\cos\omega = \frac{\eta_1}{(\eta_1^{\,2} + \eta_3^{\,2})^{1/2}}, \qquad \sin\omega = \frac{\eta_3}{(\eta_1^{\,2} + \eta_3^{\,2})^{1/2}}. \tag{79}$$

Substituting (78) and (79) into the relation $\boldsymbol{F} = \boldsymbol{B}_1\boldsymbol{G}$, which is equivalent to $\boldsymbol{F} = \boldsymbol{B}_1\boldsymbol{P}$ in the preceding section, we obtain

$$\boldsymbol{F} = \begin{bmatrix} \eta_1\left(1 - \dfrac{\eta_1\eta_3}{\eta_1^2 + \eta_3^2}g\right) & -\dfrac{\eta_1^2\eta_3}{\eta_1^2 + \eta_3^2}g & 0 \\ \dfrac{\eta_1\eta_3^2}{\eta_1^2 + \eta_3^2}g & \eta_2\left(1 + \dfrac{\eta_1\eta_3}{\eta_1^2 + \eta_3^2}g\right) & 0 \\ 0 & 0 & \eta_1 \end{bmatrix}. \tag{80}$$

A close comparison of this equation with Eq. (54) gives the following relation between the x and g:

$$x = \frac{\eta_1\eta_3}{\eta_1^2 - \eta_3^2}g. \tag{81}$$

Thus, it is seen that twinning and slip can be treated as equivalent as far as the shape change is concerned.

Applying the foregoing argument to the martensitic transformation in an Fe–22% Ni–0.8% C alloy, we find that calculated features are in good agreement with the measured ones, within experimental error, as will be seen in the third column in Table 6.8 (p. 416).

The Wechsler–Lieberman–Read theory has been extended to other types of martensitic transformations (e.g., cubic to orthorhombic[39–43]). Although additional examples will be given later (Section 6.6.4), two examples for In–Tl† and Au–Cd alloys will be discussed briefly here. Since the martensite in In–Tl alloys consists of internal twins about 10 μm wide, the martensite crystallography can be calculated using the W–L–R theory. The calculated features[42] were highly consistent with the measured ones. However, it seems that the very small lattice deformation involved does not permit a critical test of the theory. On the other hand, the martensite in an Au–47.5 at.% Cd alloy contains internal twins at about 1 μm intervals, and the lattice deformation involved in the $\beta_1 \rightarrow \gamma_1'$‡ transformation is not small, like that in the In–Tl alloys just mentioned. Applying the theory to the Au–Cd alloy,[37] we find that the predicted crystallographic features are in good agreement with the experimental ones. For example, the predicted value, 0.28, for x is close to the experimental value, 0.25. It should, however, be noted that a difference of 2.5° exists between the predicted and measured orientation relationships (planar relationship). Whether the difference is within experimental error or not is not clear in the original paper. However, since the

† These alloys undergo an f.c.c.-to-f.c.t. transformation (see Sections 2.5.1 and 3.2.1).

‡ β_1 and γ_1' represent, respectively, the parent phase of the CsCl-type superlattice and the martensite of the 2H-type orthorhombic lattice (see Sections 2.4.2C and 3.2.2).

difference is, generally speaking, beyond experimental error, such a discrepancy may suggest that the theory must be modified somewhat.

In general, applications of the theory to cubic-to-orthrhombic transformations are not so simple, and there have been discussions of the problem whether the plane or direction of shear should be rational.[41,44]

6.4 Improvements in the phenomenological theory

Matrix algebra analysis of the martensitic transformation, as presented in the previous section, represents the first theoretical treatment and so has been applied only to simple and basic cases. In practical cases, however, various factors make the transformation phenomenon very complex. Therefore, the theory requires a number of improvements so that calculated quantities may agree better with experimental results.

In the foregoing analyses, the plane and direction of the complementary shear have been presumed to be known. Although those elements are usually inferred from information on plastic deformation behavior, the shear elements in martensitic transformations may not necessarily be the same as those for plastic deformation. It would, therefore, be preferable to infer those elements from the lattice defects observed by electron microscopy. When no information is available on the shear modes, the elements of the complementary shear must be inferred so that calculated quantities are consistent with measured ones.

6.4.1 Introduction of an isotropic dilatation parameter δ

As noted earlier, the Bowles–Mackenzie theory is equivalent to the Wechsler–Lieberman–Read theory, and both theories are mostly in agreement with experimental data. However, the agreement is not complete. For example, according to the theories, the predicted habit plane normals shift by varying the lattice parameters, but the amount of shift is not substantial. In the case of a steel whose complementary shear system is $\boldsymbol{p}_2' \| (101)_f$ and $\boldsymbol{d}_2 \| [\bar{1}01]_f$, the calculated habit plane normal falls in the neighborhood of $\{3\ 10\ 15\}_f$, irrespective of the variation in lattice constants. However, the observed ones in some steels are well away from the $\{3\ 10\ 15\}_f$ pole. As a main reason for such a scatter, it can be considered[45–47] that the martensite lattice is not perfectly coherent with the parent lattice, so a strain is inevitably caused at the interface. However, since the direction and amount of coherency strain is very complex, depending on not only the crystal structures but also the constraints from the surroundings, it is difficult to incorporate such constraints into the theory.

Thus, in the first approximation, Bowles and Mackenzie assumed the coherency strain to be isotropic. This assumption is based on the following

fact: If the strain were not isotropic, lines in the habit plane would be rotated during the transformation. However, when the surface relief of a large martensite plate was observed, the martensite interface was in focus along the whole length, meaning that the interface was unrotated. Thus, using a scalar parameter δ, the invariant plane strain was represented as $\boldsymbol{P}_1/\delta$. That is,

$$\boldsymbol{P}_1 = \delta \boldsymbol{RBP}$$

where δ is an isotropic dilatation parameter and has a value of about 0.98–1.02. ($\delta = 1$ means that the coherency strain is zero.) No theoretical origin has been given for δ, and its appropriate value has been assumed to provide good agreement with experimental results.

Later, Bowles and Mackenzie[48] calculated the crystallographic features of {225} martensite in steels assuming that δ is isotropic. From a comparison of the predicted shape deformation with the experimental one, it was concluded that the complementary shear determined by the inverse analysis was not a simple one with rational low indices. Thus, they concluded that δ must be anisotropic or that the plane and direction of the complementary shear must have irrational indices.

6.4.2 Introduction of an anisotropic dilatation

The assumption of an isotropic coherency strain was based on observation of surface relief effects by optical microscopy. However, the observation is macroscopic in scale compared with the fine scale of electron microscopy, which does not verify the assumption. The assumption of isotropic δ, therefore, may not be reliable.

Thus, Otte[49] assumed that the coherency strain at the interface was anisotropic and its principal axes coincided with those of the Bain distortion. Under such an assumption, he attempted to determine the elements of the complementary shear by analyzing experimental data such as the habit plane and orientation relationship. However, the experimental data were so highly scattered that the elements could not be determined; thus the value of the anisotropic strain could not be assumed.

Mackenzie[50] attempted to formulate a theory in which two parameters were used to incorporate anisotropy into the coherency strain. However, no result that could be compared with experimental findings was obtained.

Dislocation mechanisms formulated by Suzuki and by Frank for martensitic transformations, which will be explained in Sections 6.5.3 and 6.5.4, correspond to introducing a kind of anisotropy.

6.4.3 Introduction of a composite shear as the complementary shear

Crocker and Bilby[51] computed habit planes, orientation relationships, and shear magnitudes g and angles γ for complementary shears for the

f.c.c.-to-b.c.c. (b.c.t.) transformation in steels. Computations were carried out for each of 13 shear systems with simple indices by changing the plane for a fixed shear direction and vice versa. As a result, many possible solutions were obtained. In addition, the corresponding experimental data, such as habit plane scattered largely, and the selection of a unique solution was not possible. Accordingly, they limited the shear systems to those likely to operate in plastic deformation and considered an isotropic δ in an appropriate range for each shear system. Nevertheless, they could not provide a satisfactory explanation for experimental results.

So far in this book we have described only cases in which one shear system was operative as the complementary shear. However, recent electron microscopic observations have revealed the coexistence† of different kinds of lattice defects or a combination of them in the same field in some martensite crystals. In such cases, a composite shear should be incorporated into the crystallographic theory.‡

(i) Crocker and Bilby[51] suggested that some transformations can be well explained if the complementary shear is assumed to be composed of two shears. For example, when the shear direction is fixed as $[110]_b$ and the shear plane is changed, the $(1\bar{1}0)_b$ plane was found to minimize the magnitude of the shear, and in this case the habit plane was estimated to deviate from $\{111\}_f$ by 3°. This habit plane well agrees with the experimental observation for a pure iron.[54] However, the shear system $(1\bar{1}0)\ [110]_b$ can hardly be recognized as the shear mode, and thus it was considered to be a composite of two shear systems having a common $(1\bar{1}0)$ plane, $(1\bar{1}0)\ [1\bar{1}1]_b$ and $(1\bar{1}0)\ [11\bar{1}]_b$, of identical magnitude. In a similar way, if two shears, $(\bar{1}11)\ [110]_f$ and $(\bar{1}11)\ [101]_f$, are combined in an appropriate ratio, the habit plane is estimated to lie near $\{259\}_f$. On the other hand, the $\{225\}_f$-type habit plane can be predicted by an appropriate combination of $(\bar{1}11)\ [211]_f$ with $(01\bar{1})\ [\bar{2}1\bar{1}]_f$ shears. In the same manner, calculations have been carried out for 350 different shear system combinations.[55]

The composite shear mechanism just mentioned did not give a satisfactory explanation of the experimental results. Thus, Crocker[55,56] extended the component shear systems as follows: In the foregoing calculations, two combined shears involved either a common plane or a common direction. Those two shears are the easiest ones to bring about a simple shear as the resultant of two shears. However, any combination will do, as long as a

† It has also been reported[52] that internal twins on three systems are simultaneously observed in one α' martensite plate.

‡ Some workers[53] call this a double shear theory, but because the terminology is the same as that of the original classical double shear theory (Section 6.2.1), another term, *composite shear theory*, will be used here to avoid confusion.

resultant shear is obtained, and then restrictions are not necessary for the planes and directions of the combined shears, and even a rotation may be included in the description. Taking this into account, one available way of analysis is to consider the case in which all the shear directions and plane normals of the assumed shears are contained together in a single plane. This plane is called the same plane of shear.[57] Moreover, since a rotation is difficult to incorporate in the parent austenite, the product martensite should be considered to undergo such a rotation. Therefore, by referring to the product martensite, analyses are more easily performed.

As deformation modes in b.c.t. crystals, slip occurs in $\langle 111\rangle_b$ directions on $\{110\}_b$, $\{112\}_b$, and $\{123\}_b$ planes, and twinning involves the $\{112\}\langle 111\rangle_b$ shear system. Of these shear modes, a combination of $(112)\,[\bar{1}\bar{1}1]_b$ with $(\bar{1}\bar{1}2)\,[111]_b$ satisfies the condition that the shear directions and shear plane normals have the same plane of shear. A combination of $(1\bar{1}2)\,[\bar{1}11]_b$ with $(\bar{1}12)\,[1\bar{1}1]_b$ is equivalent to the previous one, so the former case will be examined. As can be seen from Fig. 6.19, the same plane of shear in this case is the $(\bar{1}10)_b$ plane. Therefore, the resultant shear system can generally be represented as $(1\,1\,x)\,[\bar{x}\,\bar{x}\,2]_b$. If these shear systems are referred to the parent lattice by using the Bain correspondence, the component shears become $(101)\,[\bar{1}01]_f$ and $(\bar{1}01)\,[101]_f$, and the resultant is $(m_1\,0\,m_3)\,[m_3\,0\,m_1]_f$ where $m_3^2 = 1 - m_1^2$.

Under these conditions, the habit plane $\mathbf{v}$ $(v_1v_2v_3)_f$ was found to be

$$\begin{aligned} v_1^2 &= [-A \pm 2m_1(1-m_1^2)^{1/2}B^{1/2}]/[\eta_1^2(1-\eta_3^2)], \\ v_2^2 &= (\eta_1^2 - 1)/[\eta_1^2(1-\eta_3^2)], \\ v_3^2 &= 1 - v_1^2 - v_3^2 \end{aligned} \tag{1a}$$

where

$$\begin{aligned} A &= (\eta_1^2 - 1)[1 - m_1^2(1-\eta_3^2)] - 2m_1^2(1-m_1^2)(\eta_1^2 - \eta_3^2), \\ B &= [m_1^2(\eta_1^2 - \eta_3^2) - (\eta_1^2 - 1)][\eta_1^2(1-\eta_3^2) - m_1^2(\eta_1^2 - \eta_3^2)]. \end{aligned}$$

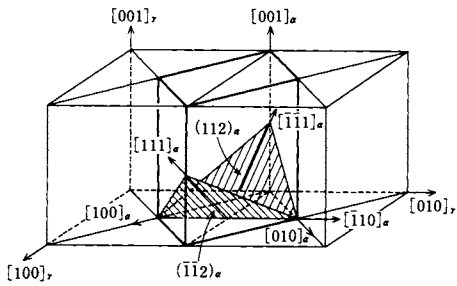

FIG. 6.19 Shear planes and directions in the double shear mechanism. (After Crocker.[56])

In these equations, η_1 and η_3 represent the principal deformations of the Bain distortion.

As can be seen from the foregoing equations, $m_1{}^2$ should have a value such that $v_1{}^2$ is a real number. Values of $m_1{}^2$ for an Fe–22% Ni–0.8% C steel were calculated to be in the range 0.4470–0.6937 by inserting the values of η_1 and η_2 into the equations above. Subsequently, the magnitudes of the resultant shears were calculated for these values.[51] Moreover, from the condition that the resultant magnitude must be divided into two component shears, it is deduced that $m_1{}^2 < 0.50$, and thus the range of admissible values for $m_1{}^2$ was further narrowed.

Figure 6.20 shows a comparison of the **v** calculated from Eq. (1a) with the measured one. The calculated **v** for the range $m_1{}^2 < 0.50$ fall on a curve and are within the range of experimentally determined habit plane normals (denoted by a broken line). At the point where $m_1{}^2 = 0.50$, the curve intersects a curve (denoted by δ) that was calculated on the assumption of a single shear plus the dilatation parameter δ.

In the analysis by composite shears, the required rotation around the $[\bar{1}10]$ axis affects the orientation relationship as shown in Table 6.1. (In the table, the case in which $m_1{}^2 = 0.50$ corresponds to the occurrence of a single shear.)

(ii) Lieberman and Bullough[58,59] attempted to analyze transformations that exhibit the $(225)_f$-type habit plane. The crystallography of this transformation remains unexplained. The experimental facts on steels undergoing this type of transformation are as follows: (a) When internal twins are observed throughout a martensite plate, the martensite does not exhibit the $(225)_f$-type habit plane. (b) The internal twins are always of the $(112)\,[11\bar{1}]_b$ type. (c) The midrib plane, the boundary plane between twinned and dislocated regions, and the interface plane (the habit plane) between the α' martensite and parent austenite are all parallel. On the basis of these facts, Lieberman and Bullough assumed that the total shape deformation $\boldsymbol{F}$ can

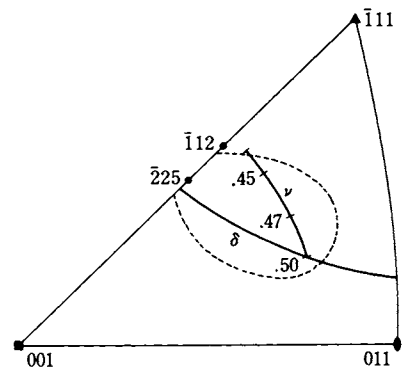

FIG. 6.20 Stereograph of the habit plane. Curve ν: Predicted from the double shear mechanism (added numbers show values of $m_1{}^2$). Curve δ: Predicted from the single shear mechanism using dilatation parameter δ. The habit planes observed in Fe–22% Ni–0.8% C fall into the region enclosed by the broken-line curve. (After Crocker.[56])

TABLE 6.1 Orientation relationships predicted using a composite shear assumption[a]

	$m_1^2 = 0.50$	$m_1^2 = 0.447$ (Minimum)
$(111)_f \wedge (101)_b$	15′	1°51′
$[10\bar{1}]_f \wedge [11\bar{1}]_b$	3°0′	1°19′

[a] After Crocker.[55]

be given by

$$\boldsymbol{F} = \boldsymbol{RBR}_2\boldsymbol{S}_2\boldsymbol{S}_1 \tag{1b}$$

where $\boldsymbol{S}_1$ is the first inhomogeneous shear on the (hll) $[01\bar{1}]_f$ system, the $(hll)_f$ being the habit plane; $\boldsymbol{S}_2$ is the second inhomogeneous shear on the (011) $[01\bar{1}]_f$ system, corresponding to the twinning shear in α'; $\boldsymbol{R}_2$ is a rotation, the axis being in the habit plane $(hll)_f$ and perpendicular to $[01\bar{1}]_f$; and $\boldsymbol{B}$, $\boldsymbol{R}$ are the same as before. That is, the complementary shear is assumed to be composed of two inhomogeneous shears that have a common shear direction. The plane of the first shear is parallel to the habit plane; subsequently, rotation $\boldsymbol{R}_2$ operates. According to this model, when internal twins are observed throughout a martensite plate, $\boldsymbol{S}_1$ and $\boldsymbol{R}_2$ can be taken to be unit matrices. Then the preceding equation is also suitable for cases exhibiting the (259)-type habit plane.

Lieberman *et al.* analyzed transformations of the (225) type according to Eq. (1b). An approximate analysis was made by a self-consistent iteration method with a stereographic net, and a more accurate analysis was carried out using an electronic computer. According to the results for an Fe–7.9% Cr–1.1% C steel, discrepancies between the calculated and experimental values[60] were 0.8° for the habit plane, and 0.4°, 0°, and 2° for the orientation relationship with respect to the three orthogonal axes. Thus, the theory seems to explain some of the experimental results, but it has been criticized as involving some faults.

(iii) Crocker and Ross[61] attempted to explain the habit plane in the transformation of γ (b.c.c.) to α (base-centered orthorhombic) in a U–5 at.% Mo alloy by the phenomenological theory. Although their computation took account of the known atomic correspondences for the γ-to-α transformation, as well as possible twinning planes and directions for the elements of a complementary shear, they failed to obtain a real solution (imaginary numbers appeared). Obtaining a hint from the calculations, they attempted to establish a new theory for the f.c.c.-to-b.c.c. transformation.[62]

This theory is based on the premise that the shear can be of the high-index type relative to both the parent and product lattices, because the shear is not uniquely defined by either lattice if it occurs during the lattice change.

Such a consideration may be especially true for complex crystal structures like uranium. Naturally, a high-index complementary shear system can be regarded as a combination of shears with low-index systems.

In general, a unit sphere changes to an ellipsoid (not necessarily a spheroid) due to a double shear, and the intersection of the ellipsoid with the original sphere forms a cone, although the cone is not circular. The generating lines of the cone are the final positions of the unextended lines as a result of the double shear. Therefore, in case of the f.c.c.-to-b.c.c. transformation, intersections of the double shear cone with the Bain cone are unextended lines as a consequence of the whole process of transformation. Depending on the position and geometry of the double shear cone, the unextended lines take several distinct configurations. When the double shear cone does not intersect the Bain cone, as shown in Fig. 6.21a, there is no unextended line. On the other hand, when the two cones intersect, two (Fig. 6.21b) and four (Fig. 6.21c) generating lines become unextended lines. If the angle between a pair of unextended lines remains unchanged during the transformation, the plane defined by the two lines is an undistorted plane. Such an undistorted plane becomes an invariant plane after receiving a rotation. Crystallographic details of the transformation can, then, be obtained by choosing the elements of the double shear so as to satisfy the foregoing conditions.

Following the treatment just presented, computations have been carried out for habit planes, shape deformations, and so on. In these computations, various systems were assumed for two lattice-invariant shears $\boldsymbol{S}_1$ and $\boldsymbol{S}_2$; that is, a $(1\bar{1}0)\,[111]_b$ slip shear was taken as $\boldsymbol{S}_1$ and a $(112)\,[\bar{1}\bar{1}1]_b$ twinning shear as $\boldsymbol{S}_2$, or the reverse, and a $(112)\,[\bar{1}\bar{1}1]_b$ twinning shear was taken as $\boldsymbol{S}_1$ and the $(hkl)\,[111]_b$ slip shear as $\boldsymbol{S}_2$, where h, k, and l are variable. Of these, the following cases are of particular interest.

$$\left.\begin{array}{ll} \text{I} & \boldsymbol{S}_1: (01\bar{1})\,[1\bar{1}\bar{1}]_b \text{ slip shear} \\ \text{II} & \boldsymbol{S}_1: (\bar{1}12)\,[1\bar{1}1]_b \text{ twinning shear} \end{array}\right\} \boldsymbol{S}_2: (112)\,[\bar{1}\bar{1}1]_b \text{ twinning shear.}$$

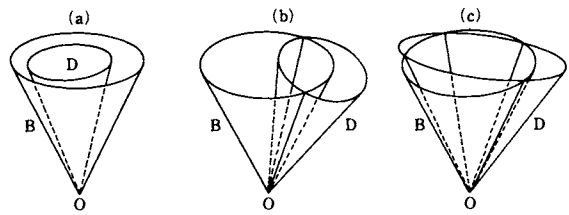

FIG. 6.21 Three cases showing relations between invariant cones and unextended lines in the Bain distortion and the double shear model. (After Ross and Crocker.[62])

In these cases, the habit plane varies with the S_2 shear magnitude. The loci of the habit planes form two smooth curves joining the $(3\,15\,10)_f$ and $(10\,15\,3)_f$ poles, as shown in Fig. 6.22. The two curves for cases I and II (labeled $\mathbf{v}_I$ and $\mathbf{v}_{II}$) are 4.8° and 3.5°, respectively, from the $(252)_f$ pole. For convenience, the shear directions $\boldsymbol{d}_I$ and $\boldsymbol{d}_{II}$ of the shape deformation are shown in the same stereographic triangle as the habit planes $\mathbf{v}$, although $\boldsymbol{d}_I$ and $\boldsymbol{d}_{II}$ are about 75° away from the habit plane normals.

Acton and Bevis[63] proposed independently a theory that is nearly equivalent to the Ross–Crocker theory just detailed. In order for the two shears assumed in both these theories to occur, the dislocations at the interface between the parent and product phases may have to be mobile to permit transformation.[64]

Dunne and Wayman[53] also analyzed the $\{225\}_f$-type martensitic transformations assuming that the complementary shear also consists of two shears. One of the shears was the $(112)\,[\bar{1}\bar{1}1]_b$ twinning shear and the other was a high-index shear that had been considered earlier in the crystallography of an Fe–8% Cr–1.1% C steel.[65] They also found that habit plane normals scatter in two dimensions by doubling the shear systems. However, the habit planes obtained and some other predictions were not satisfactory.

(iv) Kennon and Bowles[66] studied the martensitic transformations in nonferrous alloys, and in particular examined the applicability of the phenomenological theory to the γ_1' (orthorhombic) martensite in a Cu–14.95% Sn alloy. A single crystal specimen, 3 mm thick, of the parent β_1 phase (Fe_3Al type) was quenched from 700°C and subsequently cooled in

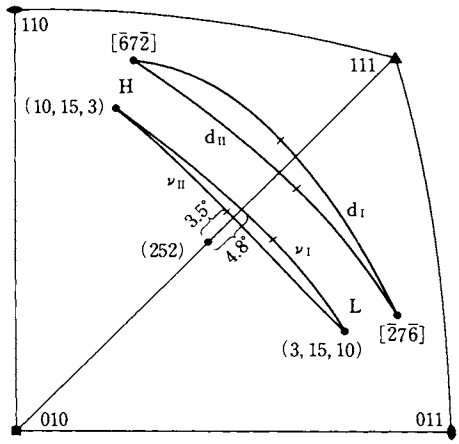

FIG. 6.22 Habit plane normal (v) and direction of total shape change (d) predicted from the double shear mechanism. (After Ross and Crocker.[62])

liquid nitrogen. In this way large γ_1' martensite plates 0.3 mm wide were produced in the specimen, after which the habit plane, orientation relationship, shape deformation, and so on were measured. The crystallographic features were theoretically predicted using the measured lattice constants, an assumed lattice correspondence, and a simple shear as the complementary shear. The predicted orientation relationship agreed within 1° with the measured one, while the predicted habit plane deviated from the measured one by 6.5°. Kennon and Bowles also noticed that the cotangent ratio D,[†] which should be constant, varied in the range of 0.14%–2.40%. Accordingly, they tried to determine the complementary shear by reverse analysis using the measured habit plane. The orientation relationship and shape deformation estimated from the complementary shear were quite consistent with those experimentally observed, but the plane and direction of the complementary shear had irrational indices. It can, therefore, be considered that the complementary simple shear assumed first is composed of two invariant line strains or is more complex yet. In fact, electron microscopic observations of Cu–Sn martensites by Morikawa *et al.*[68] revealed internal twins on the $(10\bar{1}1)$ plane and stacking faults on (0001), as mentioned in Chapter 2. Therefore, it is likely that there are at least two kinds of shear that might leave those internal faults in the martensites.[‡] Kubo and Hirano[18] explained a b.c.c.-to-9R transformation by the phenomenological theory assuming two shears on different systems as a complementary shear.

6.4.4 Accommodation strains in the parent crystal

When martensite is examined by microscopy, slip lines are often observed in the surrounding austenite.[61,70] Although the situation is a little different, McDougall and Bowles[71] observed striations in martensites with the $\{225\}_f$-type habit plane in 1.35%C and 1.19%C steels. The striations were parallel to the original $\{111\}_f$ plane and different from the $\{112\}_b$ twins observed simultaneously in these martensites. Thus, the striations were inferred to be slip lines that were inherited from those in the parent austenite crystal. Similarly, Jana and Wayman[72] obtained a micrograph revealing $\{101\}_b$ planar faults in the α' martensite in an Fe–3%Mn–3%Cr–1%C steel, and found that the faults were connected with $\{111\}_f$ planar faults in the sur-

[†] Suppose two scratches are drawn on the specimen surface in two different directions. One makes an angle ρ with the surface trace of parent and martensite interface and the other makes an angle σ. These angles may change to ρ' and σ', respectively, due to the transformation. In such a case, if a complementary shear is a simple shear, $D \equiv (\cot\sigma' - \cot\rho')/(\cot\sigma - \cot\rho)$ must be constant[67] irrespective of the direction of the scratches.

[‡] According to a subsequent study by Kennon,[69] the experimental data could not be explained satisfactorily even if a double shear were assumed.

rounding austenite. From these facts, it can be supposed that plastic deformation† to accommodate the transformation stress occurs in the austenite crystal ahead of the growing martensite plates, at least for the $\{225\}_f$-type martensite.‡ Thus, the theory must be modified to incorporate such an accommodation strain.

In considering martensite crystallography, including the above consideration of accommodation strains, Bowles and Dunne[77] made the following assumptions concerning the formation of $\{225\}_f$-type martensites (Suzuki and Frank also did, as will be described in Section 6.6).

(i) The habit plane is exactly of the form $(hhl)_{f'}$.

(ii) The direction ($\boldsymbol{d}_2$) of a complementary shear is exactly $[1\bar{1}0]_f$. No dilatation occurs along the line that lies in the habit plane and is perpendicular to the $[1\bar{1}0]_{f'}$.

(iii) The total shape deformation is exactly an invariant plane strain, that is, $\delta = 1$.

(iv) The plastic accommodation strain $\boldsymbol{P}_f$ occurs in the γ matrix ahead of the growing α' martensite, so as to satisfy conditions (i)–(iii); $\boldsymbol{P}_f$ is generally composed of multiple slips.

With the foregoing in mind, we see that the total shape deformation $\boldsymbol{P}_R$ is an invariant plane strain which can be described in the following form:

$$\boldsymbol{P}_R = \boldsymbol{L}\boldsymbol{P}_f, \tag{2a}$$

where

$$\boldsymbol{L} = \boldsymbol{R}\boldsymbol{B}\boldsymbol{P}_2{}^{-1}. \tag{2b}$$

The $\boldsymbol{L}$ takes the place of the earlier $\boldsymbol{P}_1$, although it is different in physical significance; that is, $\boldsymbol{L}$ is not an invariant plane strain, whereas $\boldsymbol{P}_1$ was. The

† An elastic deformation can also be expected to occur in the surrounding austenite crystal due to the formation of martensites. However, its effect on the habit plane of martensite is reported[73] to be small.

‡ Such an accommodation strain can also be expected for the transformation with another habit plane. According to an experiment on an Fe–(31.7–32.8)% Ni alloy by Bell and Bryans,[74] the α' martensites that formed first had the $\{3\,10\,15\}_f$-type habit plane, and were explained by the phenomenological theory with a single complementary shear. On the other hand, martensite that formed later in the same neighborhood exhibited a different habit plane from $\{3\,10\,15\}_f$, which could not be explained even if a composite complementary shear was employed. Such a difference can be attributed to an accommodation strain that might be caused by the formation of the first martensite plates in the surrounding parent austenite. An even more extreme case of the effect of an accommodation strain has been reported.[75,76] That is, an austenite single crystal of 0.7–1.0 mmϕ of an Fe–22% Ni–1.7% C steel was cooled in liquid nitrogen to produce α' martensites. The retained austenite was severely deformed due to the α' formation, to the extent that the martensite crystal structure changed from a tetragonal lattice ($c/a = 1.11$) to a monoclinic lattice ($c/a < 1$ and $\gamma < 86°$).[75,76]

sequence of calculations is first to find $\boldsymbol{P}_2$ and $\boldsymbol{P}_f$, so that $\boldsymbol{P}_R$ may become an invariant plane strain, and then to determine $\boldsymbol{P}_R$.

Since $\boldsymbol{P}_2$ can be considered to be composed of a twinning shear and a slip shear, it is convenient to describe the elements of $\boldsymbol{P}_2$ in the i basis, which is defined by

$$\boldsymbol{i}_1 = \left[\frac{1}{\sqrt{2}}\ \frac{-1}{\sqrt{2}}\ 0\right]_f, \qquad \boldsymbol{i}_2 = \left[\frac{1}{\sqrt{2}}\ \frac{1}{\sqrt{2}}\ 0\right]_f, \qquad \boldsymbol{i}_3 = [001]_f;$$

that is,

twinning shear $(110)\,[1\bar{1}0]_f \rightarrow (010)\,[100]_i$
(the shear magnitude being t),
slip shear $(111)\,[1\bar{1}0]_f \rightarrow (0\ \sqrt{\tfrac{2}{3}}\ \sqrt{\tfrac{1}{3}})\,[100]_i$
(the shear magnitude being s).

Thus, we obtain as the total shear

$$(iP_2i) = \begin{pmatrix} 1 & t + \sqrt{\tfrac{2}{3}}s & \sqrt{\tfrac{1}{3}}s \\ 0 & 1 & 0 \\ 0 & 0 & 1 \end{pmatrix}. \tag{3}$$

The shear plane $\boldsymbol{p}_2'$ is

$$(0\ \cos\sigma\ \sin\sigma)_i \qquad \text{where} \qquad \tan\sigma = s/(\sqrt{3}\,t + \sqrt{2}\,s). \tag{4}$$

Omitting the derivation of other equations, we will compare the computed results with the experimental ones. For an Fe–6.14% Mn–0.95% C steel,[78] the computed habit plane $(0.4028, 0.4028, 0.8219)_f$ deviates by only 0.7° from the mean value of measured ones $(0.3888, 0.3994, 0.8296)_f$. Similarly, for the orientation relationship, the calculated angle, 16′, between the $(101)_b$ and $(111)_f$ planes is in reasonable agreement with the measured ones, 25′[79] and 27′.[65]

For the total shape deformation, the variation of the shear direction $\boldsymbol{d}_1$ with σ is shown in Fig. 6.23. Curves 1 and 2 are those calculated for Fe–6.14% Mn–0.95% C and Fe–1.2% C alloys, respectively, by using their lattice parameters. The experimental values of $\boldsymbol{d}_1$ (○, Fe–Mn–C; ●, Fe–C) fall on the calculated curves very well. Since such agreement cannot be obtained by considering only the dilatation parameter δ, the theory that includes an accommodation strain occurring in the parent crystal seems most reasonable at present. The fact that the experimental values of $\boldsymbol{d}_1$ scatter along the calculated line suggests that the values of σ are different from martensite plate to martensite plate even in the same specimen. However, this is not always the case. According to the result of accurate measurements on an

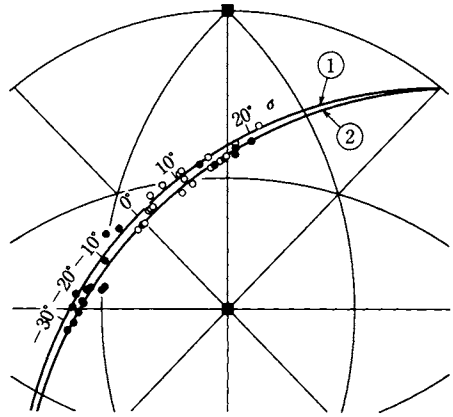

FIG. 6.23 Direction ($\boldsymbol{d}$) of total displacement of shape change (P_K). Curve 1: Calculated, for Fe–6.14% Mn–0.95% C, from $a_\gamma = 3.604$ Å, $a_{\alpha'} = 2.859$ Å, $c_{\alpha'}/a_{\alpha'} = 1.033$; ○, experimental results for this alloy. Curve 2: Calculated, for Fe–1.2% C, from $a_\gamma = 3.601$ Å, $a_{\alpha'} = 2.845$ Å, $c_{\alpha'}/a_{\alpha'} = 1.054$; ●, experimental results for this alloy ($\tan\sigma = s/(\sqrt{3}t + \sqrt{2}s)$, where t is the amount of twinning shear and s the amount of slip shear). (After Bowles and Dunne.[77])

Fe–3% Mn–3% Cr–1% C steel by Jana and Wayman,[72] the direction $\boldsymbol{d}_1$ is unique; although there is some scatter, it is not along a curve. They also suggested that the $\{225\}_f$-type martensitic transformation involves $(112)_b$ internal twins and $(111)_f$ stacking faults, that δ may be unity, and that further theoretical considerations may be indispensable.

Afterward, Dautovich and Bowles[80] measured precisely the habit plane and orientation relationship on $\{225\}_f$-type martensite in an Fe–6% Mn–0.9% C steel, and examined their results in accordance with the plastic accommodation model. They found experimentally that $[1\bar{1}0]_f$ is not perfectly parallel to $[11\bar{1}]_b$, so they could not satisfactorily explain the $\{225\}_f$-type martensite by the model. They concluded that the model must be modified somewhat and that further precise experimental measurements should be made.

Lysak *et al.*[81] also emphasized that deformation should have taken place in the parent phase as a preliminary step for transformation. However, their theoretical treatment is quite different from that of Bowles and Dunne, though an accommodation strain $\boldsymbol{P}_f$ is similarly involved. The treatment by Lysak *et al.* is based on the following experiment. An austenite single crystal of an Fe–1.7% C–2.2% Ni alloy ($M_s = -130$°C) was made, and then cooled in liquid nitrogen to produce α' martensite in about 25% of the specimen. The martensite was analyzed by an x-ray diffraction method with the result that both the habit plane and the amount of α' martensite were found to vary, depending on the shape of the parent γ single crystal. To

explain this result, the researchers hypothesized that a preliminary deformation, dependent on the shape of the parent crystal, occurred in the parent phase prior to the transformation. The α' martensite then formed in the deformed parent crystal, and an exact K–S orientation relationship held between the deformed parent (γ_d) and the martensite crystals. In this way, they accounted for the accommodation strain assumed by Bowles and Dunne. Their work, however, appears to focus on maintaining the K–S relationship rather than the invariability of the habit plane, as in the Bowles–Dunne theory. Lysak *et al.* further emphasized that one more relation, say

$$\{211\}_{\alpha'} \| \{211\}_{\gamma_d}$$

(the index with respect to the c axis of α' being set as 1), must be added as the orientation relationship besides the usual two relations representing the K–S relationship. The additional relation only means that the direction of the c axis in the α' martensite must be compatible with that in the Bain distortion. Though they did not carry out any measurement on the habit plane, they proposed that the habit plane should be indexed relative to the deformed parent lattice γ_d. There remains a question in the studies by Lysak *et al.*, however, in that a complementary shear did not receive proper consideration.

Yershov and Oslon[82] made an x-ray investigation of alloy steels, and observed an expansion of the $(200)_\gamma$ spacing and a contraction of the $(111)_\gamma$ spacing in the retained austenite, which shows the existence of anisotropic strain or stacking faults in the austenite. This experimental fact supports the idea mentioned earlier: the presence of transformation strain in the remaining austenite.

6.5 Dislocation theories on the habit of martensite

In the phenomenological theory of martensitic transformations presented thus far, we have not described the mechanism of lattice deformations, although on first principles such a description should have been made at the outset. The following dislocation theories on martensitic transformation are no better than attempts, but a survey will be made of those offered so far.

As regards the shear process of a martensitic transformation from an atomic point of view, the shear should be thought to occur by the propagation of something like dislocations in plastic deformation, because many atoms in a given volume cannot move together at one time. Thus, a certain defect structure, like an imperfect dislocation, should be introduced; this is called a transformation dislocation. Such a transformation dislocation, of course, must not give rise to an inhomogeneous change in a crystal (as happens

with slip dislocations), and its movement must produce a homogeneous shear for a given volume of crystal. Moreover, if the formation mechanism of a deformation twin is regarded as similar to that of a martensitic transformation, the transformation dislocation must be able to change slip planes, (climb), nucleate successively, or multiply on successive planes. Or, a dense two-dimensional array of transformation dislocations must move in formation to produce homogeneous shear. The movement of such transformation dislocations must be accompanied by the movement of slip dislocations, which produces the complementary shear and relaxes the transformation stress. The lattice defects observed in the martensite are the results of these dislocation movements.

The characteristics of a transformation dislocation are influenced by the crystal structures before and after the transformation. Therefore, classifying the transformations according to the types of crystal structure, their mechanisms will be explained in view of the dislocation theory.

6.5.1 Mechanism of the f.c.c.-to-h.c.p. (ε) transformation

As is known from the measured amount of surface relief and the Shoji–Nishiyama orientation relationship mentioned in Chapter 2, the lattice deformation in this transformation is inferred to be a shear on the $\{111\}_{fcc}$ plane. Although this shear corresponds to the Bain deformation in the $\gamma \rightarrow \alpha'$ transformation, it does not occur homogeneously on every layer but rather on every other layer. Recalling that the displacement of each plane by $(a/6)\ [11\bar{2}]$ (a is the lattice constant) associated with the transformation is the same as the Burgers vector of Heidenreich–Shockley half dislocations in plastic deformation and that a half dislocation can propagate under a rather small shearing stress, we can regard the current transformation shear, too, as a result of the movement of a half dislocation. Then, what becomes important is the mechanism by which the half dislocation can move on every two layers.

Christian[83] applied Frank's surface reflection model[84] of dislocations to the f.c.c.-to-h.c.p. transformation. Thus, he proposed a theory that the h.c.p. martensite can be produced by reflections of a half dislocation on every two $\{111\}$ layers of the parent f.c.c. austenite. However, the theory was retracted later[85] because it was shown to be theoretically impossible.[86,87] Later, Bollmann[88] proposed the alternate theory that a half dislocation can be reflected at a planar fault inclined with respect to the slip plane of the half dislocation.

Seeger[89] applied the Cottrell–Bilby[90] mechanism for deformation twinning in b.c.c. crystals to the f.c.c.-to-h.c.p. transformation. The mechanism is schematically explained in Fig. 6.24. Suppose that a perfect dislocation

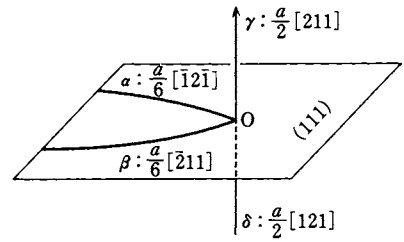

FIG. 6.24 Seeger's pole dislocation mechanism for the f.c.c. → h.c.p. transformation.

$(a/2)\,[\bar{1}10]$ lying in the (111) plane of a parent f.c.c. crystal is dissociated into two partials, α: $(a/6)\,[\bar{1}2\bar{1}]$ and β: $(a/6)\,[\bar{2}11]$. These partials form a node at O and intersect with dislocations γ and δ, which have the following Burgers vectors:

$$\gamma: \quad \tfrac{1}{2}a\,[211] = \tfrac{2}{3}a\,[111] + \tfrac{1}{6}a\,[2\bar{1}\bar{1}],$$
$$\delta: \quad \tfrac{1}{2}a\,[121] = \tfrac{2}{3}a\,[111] + \tfrac{1}{6}a\,[\bar{1}2\bar{1}].$$

In such a case, if the partial dislocation α rotates clockwise about dislocation γ, it can be displaced upward by $\frac{2}{3}a\,[111]$; that is, it climbs two atomic layers. Repeating such a rotation causes the upper part of the (111) plane to be transformed to the h.c.p. structure. Here, γ is called a *pole* dislocation and α a *sweeping* dislocation. If δ and β operate as the pole and sweeping dislocations, respectively, and β rotates counterclockwise about δ, then the lower part changes to the h.c.p. structure. This mechanism for the f.c.c.-to-h.c.p. transformation is called Seeger's pole dislocation mechanism. The transformation, thus, seems to be roughly explained by the pole mechanism. However, since Seeger's theory provides no explanation for the mechanism by which pole dislocations γ and δ are formed, and since no experimental evidence supporting this theory has been found, there is considerable doubt whether this mechanism occurs or not.[91]

6.5.2 α' nucleus and transformation dislocation in the f.c.c.-to-b.c.c. (b.c.t.) transformation

A perfect dislocation in an f.c.c. structure, $(a/2)\,\langle 011\rangle$, dissociates into two partial dislocations, $(a/6)\,\langle 112\rangle$, and a single twin layer is formed between them. If these twinning dislocations further dissociate, as

$$(a/6)\,\langle 112\rangle = (a/12)\,\langle 112\rangle + (a/12)\,\langle 112\rangle,$$

a stacking fault layer is formed between them, as shown in Fig. 6.25. The atomic configuration at the stacking fault is very similar to that of the b.c.c. structure. It can thus be supposed that a stacking fault 2–3 Å wide may become a nucleus of α' martensite. Such a supposition is Jaswon's hypothesis.[92]

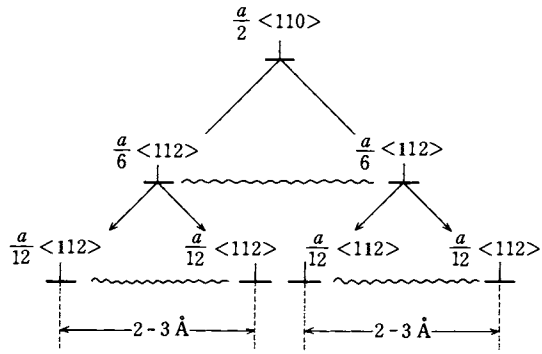

FIG. 6.25 Jaswon's nucleation hypothesis for the f.c.c. → b.c.c. transformation.

Bogers and Burgers[93] considered the Bain deformation to be composed of two shears, each of which has a displacement vector of $(1/18)\, a_\gamma \langle 112 \rangle_\gamma$ on the $\{111\}_\gamma$ plane and of $\frac{1}{8} a_\alpha \langle 110 \rangle_\alpha$ on the $\{110\}_\alpha$ plane, respectively. According to this hypothesis, stress-induced α' formation can be explained[94] through a connection between the nucleation of h.c.p. ε and b.c.c. α' martensites.

6.5.3 H. Suzuki's growth mechanism[95] for α' martensites

As mentioned before, martensites can be considered to grow by the propagation of a transformation dislocation. In such a growth mode, there should accumulate a large stress, which requires plastic deformation to relax it. The basic assumption by Suzuki† is that a perfect dislocation, which gives rise to plastic deformation, controls the propagation of the transformation dislocation. In Suzuki's formulation, the transformation dislocation is characterized by a tensor, and no further physical significance is considered in his treatment. An effort is made, however, to determine the nature of the dislocations required to relax the transformation stress, and to explain various experimental results. The motion of the accommodation dislocation is regarded by Suzuki as nothing but the occurrence of a complementary shear introduced in the phenomenological theory. Therefore, the results computed by Suzuki for habit planes, orientation relationships, and so forth could have been included in the previous section on the phenomenological theory. However, the results are described in this section because Suzuki's theory uses the dislocation concept ingeniously.

† In the present text, some notations and expressions are changed from those of his original paper; the meaning, however, is not changed.

In general, two different processes for shearing by slip or twinning are known to occur during a martensitic transformation. The first is a quasi-static process, like in the schiebung transformation, and the second is a dynamic one, like in the umklapp transformation (see Section 2.2.5).

Whether the process be quasi-static or dynamic, Suzuki's theory must incorporate the Bain correspondence and the Bain deformation, as in all other theories.

A. *Quasi-static process*
(Schiebung transformation)

The quasi-static kind of transformation, is believed to proceed by the motion of dislocations so as to release the transformation stress. Therefore, a number of such dislocations may form an array at the interface between the γ and α' crystals, in which case they surround the α' crystal, forming loops. These loops cannot readily expand (beyond a certain distance) in the direction perpendicular to the Burgers vector, but are easily extended in the direction of the Burgers vector because of the nature of the jogs. If the loops have the same Burgers vector, the habit plane must involve the direction of the Burgers vector. Although partial dislocations may also be available (if they are glissile), we will deal only with perfect dislocations, as in the original paper.

For convenience of computation, we consider one case in which a dislocation with Burgers vector $\boldsymbol{b}$ sweeps once every n layers on the slip planes $\boldsymbol{p}'$ (the interplanar distance being $a/|\boldsymbol{p}|$ where a is the lattice constant of martensite). Such a deformation is simply a shear along the slip plane. The shear magnitude is $d = b/(na/|\boldsymbol{p}|)$, and so the deformation matrix can be represented as

$$\boldsymbol{P} = \boldsymbol{I} + \boldsymbol{d}\frac{\boldsymbol{p}'}{|\boldsymbol{p}|} = \boldsymbol{I} + \frac{\boldsymbol{b}}{na}\boldsymbol{p}'. \tag{1a}$$

Now, the elements in the equation will be referred to a b.c.c. lattice. If we thus assume $\boldsymbol{p}' = (112)_b$ and $\boldsymbol{b} = (a/2)\,[\bar{1}\bar{1}1]_b$, then we have

$$\boldsymbol{P} = \boldsymbol{I} + \frac{1}{2n}\begin{bmatrix}\bar{1}\\ \bar{1}\\ 1\end{bmatrix}(112). \tag{1b}$$

If the lattice undergoes deformation $\boldsymbol{P}$, an atom at the $[x\ y\ z]_b$ position moves to a new coordinate position, expressed as

$$[x'\ y'\ z']_b = \boldsymbol{P}[x\,y\,z]_b. \tag{2}$$

Substituting Eq. (1b) into this equation, and writing the Bain correspondence as

$$\begin{bmatrix} x \\ y \\ z \end{bmatrix}_{\mathrm{b}} \rightleftarrows \begin{bmatrix} 1 & 1 & 0 \\ \bar{1} & 1 & 0 \\ 0 & 0 & 1 \end{bmatrix} \begin{bmatrix} x \\ y \\ z \end{bmatrix}_{\mathrm{f}}$$

in accordance with the original paper, we obtain

$$\begin{bmatrix} x' \\ y' \\ z' \end{bmatrix} \rightleftarrows \begin{bmatrix} 1 & 1-\frac{1}{n} & -\frac{1}{n} \\ -1 & 1-\frac{1}{n} & -\frac{1}{n} \\ 0 & \frac{1}{n} & 1+\frac{1}{n} \end{bmatrix} \begin{bmatrix} x \\ y \\ z \end{bmatrix}_{\mathrm{f}}. \tag{3}$$

For the planes, the following holds.

$$(h'\,k'\,l')_{\mathrm{b}} \rightleftarrows (h\,k\,l)_{\mathrm{f}} \frac{1}{2} \begin{bmatrix} 1 & -1 & 0 \\ 1-\frac{1}{n} & 1-\frac{1}{n} & -\frac{2}{n} \\ \frac{1}{n} & \frac{1}{n} & 2+\frac{2}{n} \end{bmatrix}. \tag{4}$$

(*a*) *Habit plane* As mentioned before, the habit plane must involve the Burgers vector of perfect dislocations, $(a/2)\,[\bar{1}\bar{1}1]_{\mathrm{b}}$. This vector can be converted into $(a/2)\,[01\bar{1}]_{\mathrm{f}}$ by the Bain correspondence. If these vectors are exactly parallel to each other, the habit plane can be expressed as $(1\,X\,X)_{\mathrm{f}}$. One line that lies in this plane and is also perpendicular to $[01\bar{1}]_{\mathrm{f}}$ is found to be $[2\bar{X}, 1, 1]_{\mathrm{f}}$ and, according to Eq. (3), corresponds to the direction

$$\left[1-\frac{2}{n}-2X,\ 1-\frac{2}{n}+2X,\ 1+\frac{2}{n}\right]_{\mathrm{b}}. \tag{5}$$

This direction should remain in the habit plane and remain unrotated even after the transformation, and therefore it must be perpendicular to $[\bar{1}\bar{1}1]_{\mathrm{b}}$. That is,

$$\left[\left(1-\frac{2}{n}-2X\right)a,\ \left(1-\frac{2}{n}+2X\right)a,\ \left(1+\frac{2}{n}\right)c\right][\bar{a}\,\bar{a}\,c] = 0, \tag{6}$$

where a and c are the lattice parameters for tetragonal martensite. Rearranging this equation and eliminating the parameter X, we obtain

$$n = 2\left(\frac{2 + \alpha^2}{2 - \alpha^2}\right) \tag{7}$$

where $\alpha = c/a$.

The next step is to estimate the value of X that determines the habit plane. To do so, the condition that an unextended line exists in the habit plane is used. One line along the Burgers vector may be extended because a stress along it is released by dislocation movements, whereas another line perpendicular to it, $[2\bar{X}, 1, 1]_f$, may not be extended. The length of the lattice vector can be expressed as $(4X^2 + 2)^{1/2}a_f$ (a_f is the lattice constant) of the parent austenite. In the martensite, it should be $[1 - (2/n) - 2X, 1 - (2/n) + 2X, 1 + (2/n)]_b$, according to expression (5). These two are equal, and then we obtain

$$X = \pm\left[\frac{2 + \alpha^2 - 4\alpha^2\eta^2}{(2 + \alpha^2)(4\eta^2 - 2)}\right]^{1/2} \tag{8}$$

where $\eta = a/a_f$.

Inserting lattice parameters into Eqs. (7) and (8) enables us to obtain n, X, and finally, the habit plane. The calculated values for Fe–Ni alloys and plain carbon steels are shown in Table 6.2. The value of n that represents the mean distance between adjacent slip planes is 6 for the b.c.c. structure, and increases with the tetragonality α of b.c.t. structures. The calculated habit plane lies near $(422)_f$ rather than the measured $(522)_f$. This discrepancy is greater

TABLE 6.2 Martensite habit planes in Fe–Ni and Fe–C alloys calculated according to the quasi-static process[a]

Alloy	Martensite a, c (Å)	Austenite a_f (Å)	X	n	Habit plane	$(111)_f \wedge (011)_b$
Fe–20% Ni	a 2.8688	3.589	±0.516	6	$(3.9\,2\,2)_f$	25′
Fe–30% Ni	a 2.8632	3.576	±0.507	6	$(3.9\,2\,2)_f$	23′
Fe–0.8% C	a 2.816 c 2.954	3.584	±0.473	6.67	$(4.2\,2\,2)_f$	22′
Fe–1.4% C	a 2.846 c 3.028	3.610	±0.456	7.22	$(4.4\,2\,2)_f$	22′

[a] After Suzuki.[95]

than the experimental error, which suggests that the assumptions adopted in the calculations are too rough.

(*b*) *Orientation relationships* The habit plane $(1\ X\ X)_f$ becomes $\frac{1}{2}(1 + X, -1 + X, 2X)_b$, according to expression (5). Since the martensite lattice contacts the parent lattice through this plane, the relation

$$(1\ X\ X)_f \| (1 + X, -1 + X, 2X)_b. \tag{9}$$

must hold. The orientation relationships can be obtained from this relation together with the following one, which was assumed earlier:

$$[01\bar{1}]_f \| [\bar{1}\bar{1}1]_b. \tag{10}$$

Thus, the angles between the $(111)_f$ and $(011)_b$ planes were calculated for Fe–Ni alloys and plain carbon steels. All of them were within 1° of each other, as shown in the last column of Table 6.2. This relation, as well as relation (10), satisfies the Kurdjumov–Sachs relations. However, since the Fe–Ni alloys that have low M_s temperatures undergo transformation through a dynamic process (Section 6.5.3B), comparison of the Nishiyama relations with the orientation relationships calculated in the foregoing manner is not meaningful.

(*c*) *Shape deformation associated with the transformation* The shape deformation is observed as a shear along the habit plane, and its magnitude can be estimated by calculating the final direction of an atom row that was originally perpendicular to the habit plane $[1\ X\ X]_f$. According to Eq. (4), the atom row becomes

$$\left[1 + X + \frac{2}{n}X, -1 + X + \frac{2}{n}X, \left(1 - \frac{2}{n}\right)X\right]_b$$

after the transformation. The angle between this direction and $[1\ X\ X]_f$, that is, $[1 + X, -1 + X, 2X]_b$, gives the shear angle. The shear direction and angle were actually calculated for an Fe–1.4%C steel and were found to be $[0.\overline{831}, 0.695, 1.129]_f$ and 10.6°, respectively, for the $(4.37, 2, 2)_f$ habit plane. These values agree with observations.[8]

B. *Dynamic process* (Umklapp transformation)

As the temperature decreases, perfect dislocations find it harder to move because resistance to their dislocation movement increases rapidly; consequently, the schiebung transformation does not occur easily at low temperatures. Such restriction for dislocation movement causes a concentration of stress at the tip of the growing martensite plate, finally giving rise to a twin in the martensite. If the twin grows too thick, an inverse stress will be

induced. To release this inverse stress, an untwinned crystal with the same orientation as the first one can again be produced in the same martensite plate. By repeating such processes, thin internal twins can be produced in martensite, and accordingly the apparent shape deformation may diminish. A necessary condition may be that the stress concentrated at the tip of a growing plate become large enough to supply the formation energy of a twin boundary, γ_T. A value similar to that of the γ_T for deformation twinning in silicon–iron, 200 kg/mm^2,[96] can be thought to apply in the case of martensitic transformations, too. Such a large stress value could be difficult to generate by static means. It may, however, occur as the local stress at a martensite plate's growing tip, which propagates at high speeds. In this way, internal twins in martensites in iron alloys are produced by a dynamic process, and consequently the umklapp transformation can occur.

It should not be assumed that internal twins are produced only by a dynamic process. They can also be produced by a static process when γ_T, and thus the shear stress, is small. For example, deformation twins in some alloys grow slowly, and internally twinned martensites of In–Tl alloys also grow slowly. These cases of slow growth can be attributed to a small γ_T.

Next, habit planes and orientation relationships will be calculated for umklapp transformations accompanied by internal twins.

(*a*) *Habit plane* Let the twinning plane be $(112)_b$ and the shear direction be $[\bar{1}\bar{1}1]_b$, and treat as if the twinning deformation is a slip shear on the same plane. The slip shear is now supposed to occur by $(a/2)[\bar{1}\bar{1}1]_b$ every n planes [this corresponds to the case in which the relative thicknesses of the internal twins have the ratio $1/n$ and $1-(1/n)$]. The atomic positions and planes are transformed according to Eqs. (3) and (4). If the habit plane is $(1\ Y\ Z)_f$ and an arbitrary direction in this plane is $[1\ y\ z]_f$, the following relation holds between them.

$$(1\ Y\ Z)_f[1\ y\ z]_f = 1 + Yy + Zz = 0. \tag{11}$$

Unlike the schiebung transformation, the umklapp transformation does not require that the habit plane have a particular atom row. It is necessary only that the habit plane be undistorted. Thus, the length of $[1\ y\ z]_f$ must be equal to the value obtained for martensite transformed according to Eq. (3), and we obtain

$$(1+y^2+z^2)a_f{}^2 = \left[1+\left(1-\frac{1}{n}\right)y-\frac{z}{n}\right]^2 a^2 + \left[-1+\left(1-\frac{1}{n}\right)y-\frac{z}{n}\right]^2 a^2 + \left[\frac{y}{n}+\left(1+\frac{1}{n}\right)z\right]^2 c^2. \tag{12}$$

Eliminating z from (11) and (12), we obtain an equation containing only one parameter, y. Since the equation should hold for any value of y, each coefficient of the y^2, y, and y^0 terms is independently zero; that is,

$$\begin{aligned}
&\left[\frac{2}{n^2}+\left(1+\frac{1}{n}\right)^2\alpha^2-\eta^2\right]\frac{Y^2}{Z^2}+\frac{2}{n}\left[2\left(1-\frac{1}{n}\right)-\left(1+\frac{1}{n}\right)\alpha^2\right]\frac{Y}{Z}\\
&\qquad\qquad +2\left(1-\frac{1}{n}\right)^2+\frac{\alpha^2}{n^2}-\eta^2=0,\\
&\left[\frac{2}{n^2}+\left(1+\frac{1}{n}\right)^2\alpha^2-\eta^2\right]\frac{Y^2}{Z^2}+\frac{1}{n}\left[2\left(1+\frac{1}{n}\right)-\left(1+\frac{1}{n}\right)\alpha^2\right]=0,\\
&\left[\frac{2}{n^2}+\left(1+\frac{1}{n}\right)^2\alpha^2-\eta^2\right]\frac{1}{Z^2}+2-\eta^2=0.
\end{aligned} \tag{13}$$

From these equations, the values of n, Y, and Z can be obtained.

These values have actually been computed for an Fe–22% Ni–0.8% C alloy that undergoes the umklapp transformation; they are shown in Table 6.3, which lists four different solutions. According to the table, the relative thickness of the twins is either 12:88 or 18:82, corresponding to the two different values of n, while the habit plane is $\{0.2213, 0.7039, 1\}_f \cong \{2, 6.36, 9.04\}_f$ for either value of n. Comparing this habit plane with the $\{259\}_f$ measured by Greninger and Troiano,[25] we see that the discrepancy is only 6°, which indicates fair agreement, since the measured values scatter by more than 6°.

(*b*) *Orientation relationships* The orientation relationships can be obtained from the fact that the position of the habit plane does not change before and after transformation; that is, the habit plane remains unrotated. This means that the habit plane estimated in the preceding subsection must

TABLE 6.3 Martensite habit planes in an Fe–22% Ni–0.8% C alloy calculated according to the dynamic shear process[a]

$1/n$	Y	Z	
0.1168	±0.2213	±0.7039	Double signs
0.1769	±0.7639	±0.2213	in same order

[a] After Suzuki.[95] Input data were $\alpha^2 = 1.092$, $1/\eta^2 = 0.627$.

be parallel to that for martensite transformed according to Eq. (4). That is,

$$(1, 0.2213, 0.7039)_f \| (1.165, -0.8351, 1.2950)_b. \tag{14}$$

The angle between the left-hand side and the $(111)_f$ plane is 26°34′, whereas that between the right-hand side and the $(101)_b$ plane is 26°19′. The 15′ difference between these angles is simply the angle between the $(111)_f$ and $(101)_b$ planes and is very small. Since the $(111)_f$ plane is transformed to the $(101)_b$ plane, these two planes have to meet in the habit plane. Thus, the intersections of these two planes with the habit plane are parallel, that is,

$$[0.4826, 0.2961, -0.7788]_f \| [0.8351, -0.1301, -0.8351]_b. \tag{15}$$

Other parts of the orientation relationships can also be obtained by calculating the angles between the direction in (15) and low-index directions in the $(111)_f$ and $(101)_b$ planes. The calculated angles are in good agreement with the ones measured by Greninger and Troiano,[25] as shown later in the first and third columns of Table 6.8.

The foregoing description represents an outline of the Suzuki theory,[95] but one important comment has to be added. In the theory, the habit plane was first assumed to be an undistorted plane in the calculation, and was then further assumed to be an unrotated plane for estimating the orientation relationships. In this way, the habit plane was assumed to be an invariant plane. This assumption is the same as that in the phenomenological theory. If the habit plane is an invariant plane, then the orientation relationship can be determined exactly, irrespective of the configuration of the atoms in both phases. From the relationship obtained, the two directions of the intersections of the $(111)_f$ and $(101)_b$ planes with the habit plane can be calculated. In general, these two directions do not exactly coincide. The deviation between them is, however, very small for current cases, so there is no problem. However, it is unreasonable to assume, as in Suzuki's theory, that the two directions are perfectly parallel. On the other hand, if we insist on the invariability of the habit plane, we are obliged to adopt a continuum approximation for alloys or steels, thus ignoring their crystalline nature. Therefore, it may physically be more reasonable to relax the requirement for an invariant habit plane and to assume that the $(111)_f$ plane is exactly parallel to the $(101)_b$ plane. Such a modification corresponds to the introduction, in the phenomenological theory, of an anisotropic coherency strain for the habit plane.

C. *Transformation propagation speed*

As mentioned earlier, the propagation of the schiebung transformation is much slower than that of sound waves. For example, for the schiebung transformation caused in an Fe–Ni alloy by pricking the surface of the

supercooled austenite crystal with a needle point, the growth rate of the martensite was only 10^{-4} cm/sec.† The slow propagation rate of the schiebung transformation can be understood as follows: The movement of a perfect screw dislocation is needed for the transformation to progress, as mentioned before. Such a movement of screw dislocations in b.c.c. crystals needs a large stress in order to overcome the Peierls force. Therefore, the growth rate of martensite is related to the dislocation velocity, which is controlled by the formation rate of a pair of kinks and by the propagation rate of the kinks. According to an experiment[97] in which the speed of dislocations in an Fe–Si alloy was measured, the speed of the plastic deformation increases with the external force, but it is slower than 10^{-7} cm/sec until the external stress reaches 10^9 dyn/cm^2. Similarly, the slow growth rate of schiebung-transformed martensite can be understood. If the temperature increases, however, the growth rate becomes faster due to thermal agitation.

For the umklapp transformation to occur, only the migration energy of interface boundaries and the formation energy of internal twin boundaries are required. The former is far smaller than the energy for the movement of perfect screw dislocations, and the latter is also small. Moreover, the heat generated during the transformation does not arrest the transformation, because the specimen is in a highly supercooled state. Thus, the umklapp transformation can proceed at high speed. The speed of 1100 m/sec obtained by Bunshah and Mehl and by Lahteenkorva, as mentioned in Section 4.4, is understandable.

6.5.4 Frank's model of the γ–α' interface[98]

Frank studied the atomic arrangement at the interface between the γ (f.c.c.) and α' (b.c.c. or b.c.t.) phases, and proposed a dislocation model of the interface as follows: He assumed that the close-packed plane and direction of the γ phase transform to those of the α' phase and that they are joined at the interface. However, the interplanar spacings of the $(111)_\gamma$ and $(101)_{\alpha'}$ planes are slightly different from each other. For example, the difference is 1.6% in iron and about 0.2%–2% in steels. It may be allowed, however, if the corresponding (111) and (101) planes in the two phases are not exactly parallel. If they are inclined relative to each other by a small angle ψ, and moreover inclined to the γ–α' interface by a suitable angle φ, as shown in Fig. 6.26, then those two planes may join smoothly despite the difference in interplanar spacings. For case of the $(522)_\gamma$ habit plane, the angle φ is 25° and so the angle ψ is less than 1°. This angle between the $(111)_\gamma$ and $(101)_{\alpha'}$

† However, it is also reported that the speed can be varied to extend beyond 10 cm/sec by a high degree of supercooling.

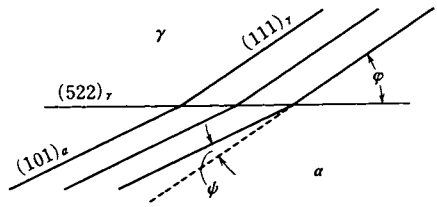

FIG. 6.26 Frank's model for the γ–α' boundary.

planes is not inconsistent with that in the Kurdjumov–Sachs relationships within experimental error.

Next, we must consider the junction of atom rows in the $(111)_\gamma$ and $(101)_\alpha$ planes joined at the interface. Of many atom rows, the close-packed rows $[01\bar{1}]_\gamma$ and $[11\bar{1}]_\alpha$ are of interest. These rows lie in the $(522)_\gamma$ habit plane and are parallel to its intersection with the two close-packed planes; thus they satisfy the Kurdjumov–Sachs relationship. However, the interatomic distance in the $[11\bar{1}]_\alpha$ row is smaller than that in the $[01\bar{1}]_\gamma$ row by about 1%. Although such a discrepancy leads to an imperfect junction of atom rows, there may be no way to avoid the discrepancy except to acommodate it by lattice strain.

A $(111)_\gamma$ plane can be smoothly connected with a $(101)_{\alpha'}$ plane in the way just described. Therefore, the final problem is to examine the relation between successive parallel planes. As can be easily understood from a three-dimensional model, the $[01\bar{1}]_\gamma$ rows are successively shifted, with respect to the $[11\bar{1}]_\alpha$ rows, by one-sixth of an atomic distance in the row direction. If the γ and α' phases were joined with each other without regard for this shift in atom rows, a large stress would accumulate in both the phases, and thus the joining would be impossible. Therefore, Frank suggested that slip occurred to relieve the stress. The $(011)_\gamma$ plane can be chosen as the slip plane because it makes a large angle with the interface plane and has a high density of atoms. This $(011)_\gamma$ plane becomes a $(112)_\alpha$ plane after the transformation. The slip behavior on the $(011)_\gamma$ plane is shown in Fig. 6.27, that is, a unit of slip occurs every six layers.

If so, screw dislocations (indicated by S in the figure) with the Burgers vector $(a/6)[01\bar{1}]_\gamma$ should form a parallel grid at the γ–α' interface, the interdislocation distance corresponding to six layers of $(011)_\gamma$ planes. The obverse and reverse sides of an α' plate may consist completely of parallel screw dislocations of opposite sign. Considering the continuity of dislocation lines, these screw dislocations in the two sides are connected to each other by edge dislocations at the upper and lower regions of the plate in Fig. 6.28, the edge dislocations forming a tilt boundary. At other regions of the plate (right or left regions in Fig. 6.28), new dislocation loops must be created successively as the plate grows. In such a distribution of dislocations, the

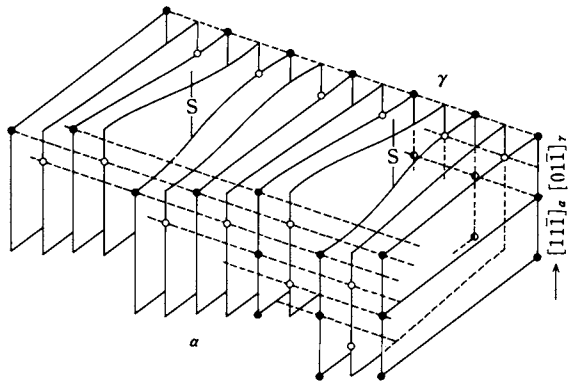

FIG. 6.27 Screw dislocations (S) and atomic arrangement at the γ–α' interface.

plate can easily grow in radial directions (mainly by movement of the edge dislocations), but can grow in the normal direction only with difficulty because parallel movement of the screw dislocations is rather difficult. This may be the reason why martensite phases are platelike.

The foregoing discussion has been restricted to the particular case of the K–S relationships, but a similar analysis can be applied to other cases. For example, in the case of the G–T relationships, similar calculations may be possible by adopting some dislocations that do not lie on the $(111)_\gamma$ plane.

Frank's theory is in principle equivalent to the phenomenological theory, because both theories assume lattice coherency at the γ–α' interface. However, there are some differences. That is, Frank's theory places great emphasis on the junction of two lattices at their interface, and deals with a lattice coherency in which an elastic strain is involved under the condition that the $[01\bar{1}]_\gamma$ and $[111]_{\alpha'}$ atom rows are parallel to each other. Therefore, the interface in Frank's theory is not an undistorted plane, and the distortion is not isotropic. On this account, Frank's theory should be included in the category of Section 6.4.2.

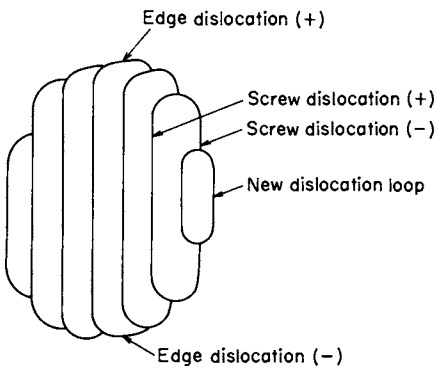

FIG. 6.28 Dislocation loops enclosing a martensite plate.

6.5.5 Analysis by the prism-matching method[99]

The Frank theory dealt with the γ–α' interface as a problem in two-dimensional matching between the two phases. Such lattice matching can be extended to three dimensions; thus a prism-matching theory has been developed. This theory is more intuitive than the phenomenological theory, which uses matrix algebra.

An outline of the prism-matching theory is as follows:

(i) First, an atomic correspondence is assumed to prevail between the two phases both before and after the transformation. This assumption must be made in order that the energy for the lattice deformation be minimized, just as in the Bain correspondence in the f.c.c.-to-b.c.c. transformation.

(ii) Second, consider a smallest triangular prism in each lattice, the edges of which coincide with atom rows of a corresponding direction in each lattice. In this case, any atom row can be adopted for the prism edges, but one that is physically prominent in both phases should be chosen.

(iii) If the two prisms are cut along a plane of each lattice, and if they are joined to each other through the sections, so that the corresponding edges in each phase are matched, then the matching plane can be recognized as an interface between two phases. Many such interfaces can be assumed to exist, and can become invariant planes provided that the atomic arrangements in the sections are ignored. (How such a matched state can be built up will be discussed later.)

(iv) If a matching plane can be found such that the amount of homogeneous deformation† is small, this matching plane may be adopted as a candidate for the habit plane. (At this step, the continuity of atom rows in the vicinity of the habit plane has not yet been taken into consideration.)

(v) Hereupon, the atomic arrangements in the two lattices must be coherently connected to each other at the matching plane, although dislocations may be introduced. Thus, for the first time the matching plane can become a habit plane. The dislocations are selected after considering the plastic deformation modes of both lattices.

Further explanation will be given here of the procedures just listed as they relate to the γ (f.c.c.)-to-α' (b.c.t.) transformation, as in the original paper. Thus, as the first step (i), the Bain correspondence should be assumed. In order to simplify further considerations and calculations, the α' b.c.t. lattice will be regarded as an f.c.t. lattice so that it can be represented by the same indices as the γ f.c.c. lattice, as shown in Fig. 6.29b. This repre-

† The amount of deformation need not be a minimum but is sufficient if it is near the minimum, because the total energy can be lowered by taking advantage of condition (v).

sentation is nothing but an assumption of the Bain correspondence. The indices referred to the f.c.t. lattice will be represented by subscript F, as in $[01\bar{1}]_F$.

As the second step (ii), triangular prisms will be constructed in the γ and α' lattices, the edges of each prism being parallel to $[01\bar{1}]_\gamma$ and $[01\bar{1}]_F$ and passing through the triangles $A_1B_1C_1$ and $A_2B_2C_2$, respectively, as shown in Fig. 6.29. (The $A_1B_1C_1$ plane is perpendicular to the edge of the triangular prism in the γ lattice, whereas the $A_2B_2C_2$ plane is not perpendicular to that in the α' lattice but makes a constant angle.) Figure 6.30 shows the situation where two triangular prisms are matched at plane ABC. In such a case, if the B and C points of the γ triangular prism (i.e., the length x_1) are chosen, then the length x_2 is uniquely fixed. The edges through A_1 and A_2 can be connected at A only when the two prisms are inclined to each other around the fixed axis BC by a suitable angle. The orientation of the

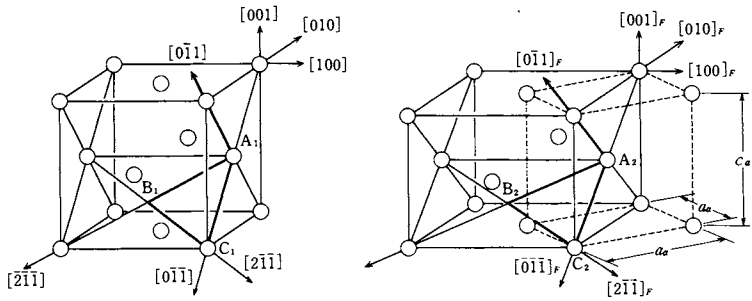

(a) f.c.c. (b) f.c.t. (——), b.c.t. (------)

FIG. 6.29 F.c.c.-to-f.c.t. (b.c.t.) correspondence in the prism-matching theory.

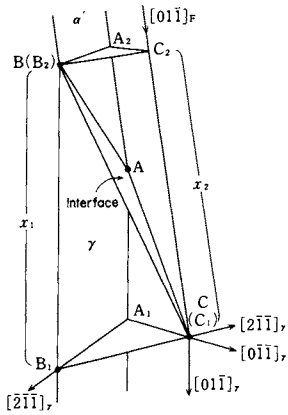

FIG. 6.30 Coherence between γ and α' prisms.

normal of the interface ABC varies with the value of x, which is the average of x_1 and x_2.

In order to compare this theory with experimental results obtained by Greninger and Troiano,[25] the interface normal was calculated for their Fe–Ni–C alloy using the appropriate lattice parameters.

$$\gamma\text{:}\quad a_0 = 3.592\,\text{Å};\qquad \alpha'\text{:}\quad a = 2.845\,\text{Å},\ c/a = 1.045.$$

As shown in the stereogram in Fig. 6.31, the calculated habit plane normal moves along an elliptic orbit depending on the value of x. That is, when $x = 0$, the normal lies at point R, and as x is increased, it moves through point Q along the elliptic orbit. When $x = 8\,\text{Å}$, the habit plane normal reaches the value $(0.8052, 0.1884, 0.5622)_\gamma$, which is approximately equal to the $(15, 3, 10)_\gamma$ habit plane, and when $x = +\infty$, it finally approaches point P, which is in the vicinity of the $(522)_\gamma$ habit plane and corresponds to Frank's γ–α' interface described in the last section. For $x < 0$, the interface normal moves from point P ($x = 0$) to point R ($x = -\infty$) through point S, and this change is equivalent to that for the case in which $x > 0$. The habit plane normal must always lie somewhere on this elliptic orbit.

The α' lattice matched with the γ lattice in the manner described in this section is also produced by a uniform deformation of the γ lattice. The deformation can be expressed as a change in the unit vector $\boldsymbol{k}$ perpendicular to the interface. If $\boldsymbol{k}$ changes to another vector $\boldsymbol{k}'$ due to the deformation, the angle γ_1 between the $\boldsymbol{k}$ and $\boldsymbol{k}'$ vectors, as well as the magnitude of $\boldsymbol{k}'$, represents the amount of deformation. The calculated value of γ_1 varies with

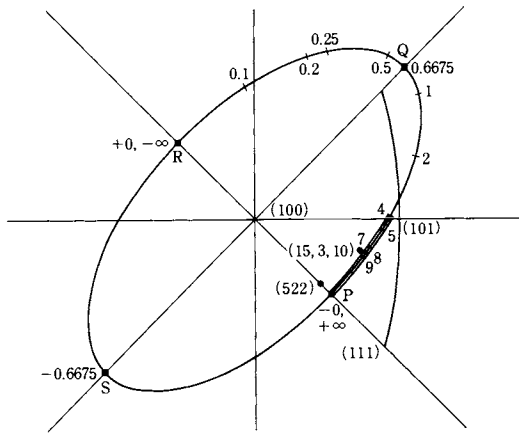

FIG. 6.31 Variation of the habit plane normal predicted by the prism-matching method for γ–α' transformation. (Numbers along the ellipse give the value of x in angstroms.) (After Bilby and Frank.[99])

the parameter x, and it takes a minimum value at $x = 8\,\text{Å}$, as shown in Fig. 6.32. On the other hand, a unit volume of the γ lattice changes to the volume $\boldsymbol{k}' \cdot \boldsymbol{k} = |\boldsymbol{k}'| \cdot \cos\gamma_1$ of the α' lattice due to the deformation. Therefore, $|\boldsymbol{k}'|$ takes a minimum value when γ_1 is minimum since the volume of the α' lattice must be independent of the matching manner, that is, the value of x. Thus, the deformation energy can be minimized when γ_1 is minimum, and $x = 8\,\text{Å}$ gives the habit plane.

In relation to condition (v), it is necessary to examine whether the habit plane obtained earlier is reasonable or not. The Burgers vector of dislocations which need to be introduced is likely to be $\langle 111\rangle_{\alpha'}$ (i.e., $\langle 011\rangle_{\text{F}}$) and specifically will be the direction parallel to the prism edge, namely, $[01\bar{1}]_{\text{F}}$. These dislocations will, moreover, be assumed to be all parallel and to move together with the interface, as suggested by Frank. Their movement, then, causes a simple shear in the direction of the Burgers vector along a slip plane that contains the Burgers vector. Here we will assume that the slip plane suffers a uniaxial deformation along the $[01\bar{1}]_{\text{F}}$ direction of an amount depending on the lattice constants of γ and α' lattices.

The slip plane satisfying this condition should be $(011)_{\text{F}}$ $(=(112)_{\alpha})$, because the $[100]_{\gamma}$ direction, which lies in $(011)_{\gamma}$ and is normal to $[01\bar{1}]_{\gamma}$, remains

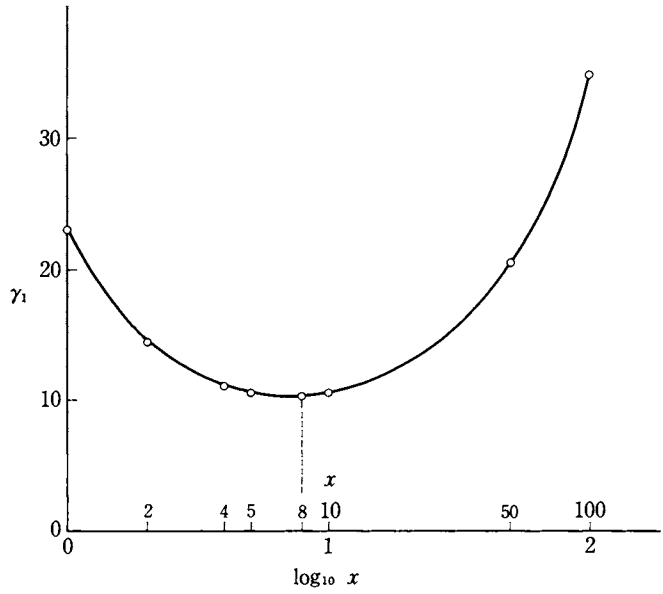

FIG. 6.32 Shear angle of the shape deformation as a function of the parameter x. (After Bilby and Frank.[99])

normal to $[01\bar{1}]_\gamma$ through the Bain deformation, and the $(011)_\gamma$ plane undergoes a uniaxial deformation.

The shape deformation varies with the value of x, as mentioned earlier. Of the various shape deformations, one making the $(011)_\gamma$ plane deform uniaxially can be obtained only when x has a particular value. This value of x is calculated to be 8 Å. This value also satisfies condition (iv), and therefore the matching plane of triangular prisms at $x = 8$ Å is concluded to be the habit plane (cf. Fig. 6.31).

Let us next determine the density of dislocations in the habit plane. For the shape deformation at $x = 8$ Å, the magnitude of the $(011)\,[01\bar{1}]_F$ shear is calculated to be $s_b = 0.062$. However, another shear on the same system should already have occurred due to the Bain deformation. Its amount is $\tan\rho$ where ρ denotes the angle between $[011]_\gamma$ and $[011]_F$. Using the lattice constant, $\tan\rho$ is calculated to be ± 0.3070 where the negative sign means a shear in the opposite direction. Therefore, the complementary shear caused by the passage of the dislocation array should be

$$s_d = \tan\rho - s_b = 0.245 \quad \text{or} \quad -0.369.$$

If one dislocation exists for every n planes of the $(011)_F$ $(=(112)_\alpha)$ type, n can be represented, by the Burgers vector $\boldsymbol{b}$ and the interplanar spacing $d_{(112)_\alpha}$, as $n = b/(s_d d_{(112)_\alpha})$. Substituting the measured values, we obtain

$$n = 5.7 \quad \text{or} \quad 8.5.$$

This number is close to that obtained from Suzuki's theory, $n = 5.653$ or 8.562. A complementary shear equivalent to this can also be brought about by internal twinning.[35] In this case, the thickness ratio of adjacent twins is 18:82 or 12:88.

The orientation relationship between the parent and martensite lattices can be obtained by calculating the angles between the $(111)_\gamma$ and $(111)_F$ planes and between the $[01\bar{1}]_\gamma$ and $[01\bar{1}]_F$ directions for $x = 8$ Å. The calculated values are listed in the last column of Table 6.8 (p. 416), which also presents the experimental values and those predicted by other theories. The agreement among these values is excellent.

We now compare the prism-matching theory with the phenomenological theory described in Section 6.3. The habit plane in the former can be regarded as an invariant plane, as it is in the latter. The former theory is more intuitive than the latter although the computation procedure is complicated because matrix algebra is not used. The prism-matching theory makes it possible to determine the characteristics of dislocations in the interface. Therefore, the physical phenomena, such as the movement of each atom, can be considered in the introduction of an anisotropic strain.

In the prism-matching theory, the value of x was established so as to minimize γ_1 (Fig. 6.32). This seems reasonable because the deformation energy is minimized with respect to γ_1. However, γ_1 may not always be minimum for the minimum total energy if the matching energy in the interface (the energy due to a dislocation array) is predominant. In such a case, therefore, a similarity in the atomic configurations of two lattices in the vicinity of the interface should be important. Many years ago, Doi and Nishiyama[100] tried to determine the interface plane when the K–S or N relationships hold as the orientation relationship. At that time, the interface plane was considered to be such that the atomic configurations in the parent and martensite lattices are as similar and as parallel as possible to each other. According to this simple idea, good matching is obtained when the interface is parallel to $(111)_\gamma$, $(112)_\gamma$, $(113)_\gamma$, or $(123)_\gamma$. If the interface consists of only one of these planes, however, the strain energy may be large. Therefore, the interface may actually be composed of a suitable combination of these planes, and then the strain energy may be lowered substantially. For example, in the case of the $(259)_\gamma$ habit plane, the interface may be regarded as composed of an appropriate microscopic mixture of $(112)_\gamma$ and $(113)_\gamma$ planes. In this case, however, the distribution of dislocations at the interface may become complicated. If the prism-matching theory is developed from this point of view, its application should become widespread.

6.5.6 Analysis by the continuous dislocation theory

By using the continuous dislocation theory,[101–105] Bullough and Bilby[106] analyzed the particular case in which many dislocations exist only in the interface. The basic idea will be described first.†

According to the continuous dislocation theory, the configuration of dislocations in the interface between two phases depends on both the orientation of the interface and the deformation modes in the two phases. If $\boldsymbol{x}_i$ $(i = 1, 2, 3)$ are defined as unit vectors along the axes given by orthogonal Cartesian coordinates, the component along $\boldsymbol{x}_i$ of the resultant Burgers vector of all dislocations that lie in the interface and cut a line segment (unit length) perpendicular to another axis $\boldsymbol{x}_j$ can be expressed as

$$b_{ij} = \sum_{k,l} \varepsilon_{jkl} p_{1k} [E_{il}^{(+)} - E_{il}^{(-)}], \tag{16}$$

† Symbols in the original papers are altered as follows.

Original paper:	$\boldsymbol{P}$	$\boldsymbol{S}$	$\boldsymbol{F}$	$\boldsymbol{v}$	$\boldsymbol{m}$	$\boldsymbol{p}$	$\boldsymbol{l}$	B_{ij}	$\boldsymbol{n}$	e;
Present text:	$\boldsymbol{B}$	$\boldsymbol{P}$	$\boldsymbol{P}_1$	$\boldsymbol{p}_1$	$\boldsymbol{p}_2$	$\boldsymbol{v}$	$\boldsymbol{b}_0$	b_{ij}	$\boldsymbol{l}$	η.

where ε_{jkl} is $+1$ or -1 when j, k, l are an even or odd permutation of numbers 1, 2, 3, and vanishes unless j, k, l are all different. $\boldsymbol{p}_1$ is the interface normal, p_{1k} is its component along the $\boldsymbol{x}_k$ direction, and $E_{il}^{(+)}$ and $E_{il}^{(-)}$ are il components of $\boldsymbol{E}^{(+)}$ and $\boldsymbol{E}^{(-)}$, respectively, which are the reciprocal matrices of the deformation tensors in the two lattices.

The resultant Burgers vector $\boldsymbol{b}$ of dislocations that are cut by an arbitrary unit vector $\boldsymbol{v}$ in the interface is $\sum b_{ij} w_j \boldsymbol{x}_i$, where $\boldsymbol{w}$ is a unit vector that is in the interface and normal to $\boldsymbol{v}$. Since $w_j = \sum_{mn} \varepsilon_{jmn} p_{1m} v_n$, the components of $\boldsymbol{b}$ are

$$b_i = \sum_j b_{ij} w_j = \sum_{iklmn} \varepsilon_{jkl} p_{1k} [E_{il}^{(+)} - E_{il}^{(-)}] \varepsilon_{jmn} p_{1m} v_n. \tag{17}$$

This equation can be simplified by using $\sum_j \varepsilon_{jkl} \varepsilon_{jmn} = (\delta_{km}\delta_{ln} - \delta_{kn}\delta_{lm})^{\dagger}$ and $\sum p_{ln} v_n = 0$, as follows.

$$b_i = \sum_l (E_{il}^{(+)} - E_{il}^{(-)}) v_l. \tag{18}$$

Thus, $\boldsymbol{b}$ can be written as

$$\boldsymbol{b} = \sum_i b_i \boldsymbol{x}_i = \sum_{il} (E_{il}^{(+)} - E_{il}^{(-)}) v_l \boldsymbol{x}_i. \tag{19}$$

Let each of the dislocations move along a slip plane together with the interface as the transformation proceeds. All these dislocations are assumed to have the same Burgers vector $\boldsymbol{b}_0$ (unit vector) and to be arrayed in a parallel manner (this is an assumption for a simple glissile surface dislocation). In this case, the left-hand side of Eq. (19) can be expressed as $t\boldsymbol{b}_0$, since it is proportional to $\boldsymbol{b}_0$. If the parent lattice is undeformed, then $\boldsymbol{E}^{(-)} = \boldsymbol{I}$. On the other hand, the martensite lattice suffers the deformation $\boldsymbol{RB}$, and then $\boldsymbol{E}^{(+)} = (\boldsymbol{RB})^{-1} = \boldsymbol{B}^{-1}\boldsymbol{R}^{-1}$. Thus, Eq. (19) can be written as

$$t\boldsymbol{b}_0 = (\boldsymbol{B}^{-1}\boldsymbol{R}^{-1} - \boldsymbol{I})\boldsymbol{v}. \tag{20}$$

The unit vector $\boldsymbol{v}$ in the parent lattice is changed at the interface due to the passage of the surface dislocations, and the change is given by Eq. (20). In general, a vector $\boldsymbol{u}$ in the parent lattice may be written as $(a\boldsymbol{b}_0 + b\boldsymbol{v})$. The first term is not changed by the passage of the surface dislocations, but $\boldsymbol{v}$ in the second term changes to $\boldsymbol{v} + t\boldsymbol{b}_0$. Then, $\boldsymbol{u}$ becomes $\boldsymbol{u} + bt\boldsymbol{b}_0$. Writing $\boldsymbol{u} + bt\boldsymbol{b}_0$ as $\boldsymbol{Pu}$, we obtain

$$(\boldsymbol{P} - \boldsymbol{I})\boldsymbol{u} = bt\boldsymbol{b}_0. \tag{21}$$

† δ is the Kronecker delta. δ_{ij} is equal to unity when $i = j$ and vanishes when $i \neq j$.

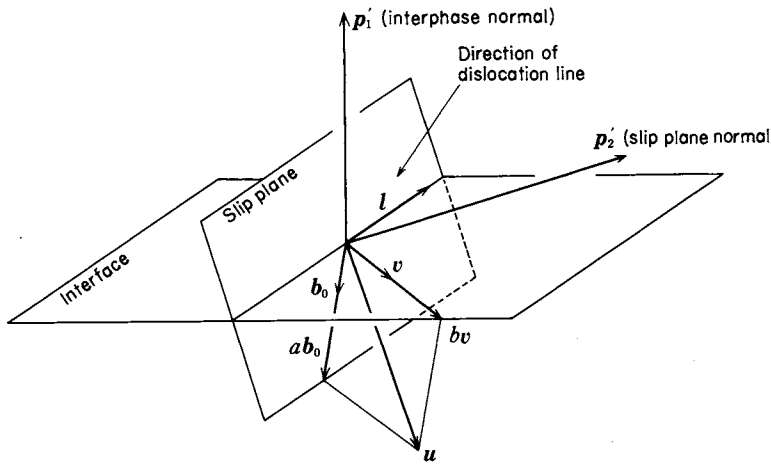

FIG. 6.33 Relations between the interface of two phases, the slip planes, and the surface dislocations in the Bullough–Bilby theory.[106]

Since $\boldsymbol{P}$ must be a deformation matrix that represents a simple shear on the slip plane $\boldsymbol{p}_2$ in the direction $\boldsymbol{b}_0$, the following equation can hold.

$$\boldsymbol{P} - \boldsymbol{I} = g\boldsymbol{b}_0\boldsymbol{p}_2' \tag{22}$$

where g is the amount of the simple shear (Fig. 6.33).

Substituting this equation into Eq. (21), we obtain $bt\boldsymbol{b}_0 = g\boldsymbol{b}_0\boldsymbol{p}_2'\boldsymbol{u} = g(\boldsymbol{p}_2'\boldsymbol{u})\boldsymbol{b}_0$, and then $bt = g\boldsymbol{p}_2'\boldsymbol{u} = g\boldsymbol{p}_2'(a\boldsymbol{b}_0 + b\boldsymbol{v})$. Since $\boldsymbol{p}_2'\boldsymbol{b}_0 = 0$,

$$t = g\boldsymbol{p}_2'\boldsymbol{v} \tag{23}$$

is obtained. If the lattice deformation $\boldsymbol{RB}$ occurs simultaneously with the simple shear $\boldsymbol{P}$, no stress field is produced in either lattice. Therefore, the shape deformation accompanying the martensitic transformation can be expressed as

$$\boldsymbol{P}_1 = \boldsymbol{RBP}. \tag{24}$$

This equation is the same as that obtained in the phenomenological theory. Assuming that $a = 0$ and $b = 1$, replacing $\boldsymbol{u}$ by $\boldsymbol{v}$, and using Eq. (20), we can rewrite Eq. (21) as

$$\boldsymbol{Pv} = \boldsymbol{v} + t\boldsymbol{b}_0 = \boldsymbol{B}^{-1}\boldsymbol{R}^{-1}\boldsymbol{v}. \tag{25}$$

Therefore,

$$\boldsymbol{RBPv} = \boldsymbol{v}, \tag{26}$$

where $\boldsymbol{v}$ lies in the interface. This equation means that all vectors lying in the interface are invariant in spite of the occurrence of the shape change

$\boldsymbol{P}_1 = \boldsymbol{RBP}$. In other words, no long-range stress field will form in either the parent or martensite lattice if the dislocations expressed by Eq. (20) are inserted into the interface between the lattices.

Next, the habit plane will be determined using this theory. For this purpose, the orientation of dislocation lines must first be determined. Since the dislocation lines must lie in the interface as well as in the slip plane, their orientation can be defined by a unit vector $\boldsymbol{l}$, as shown in Fig. 6.33. If $\boldsymbol{v} = \boldsymbol{l}$, the $\boldsymbol{v}$ does not cut $\boldsymbol{l}$. Thus, we can set $t = 0$ in Eq. (25), which consequently becomes

$$\boldsymbol{B}^{-1}\boldsymbol{R}^{-1}\boldsymbol{l} = \boldsymbol{l}, \qquad \text{that is,} \qquad \boldsymbol{l}'\boldsymbol{B}'\boldsymbol{B}\boldsymbol{l} = \boldsymbol{l}'\boldsymbol{l}. \tag{27}$$

Since $\boldsymbol{B}$ is a diagonal matrix, it can be rewritten as

$$\boldsymbol{l}'(\boldsymbol{I} - \boldsymbol{B}^2)\boldsymbol{l} = 0.$$

Substituting $\boldsymbol{B} = (\text{diag}; \eta_1, \eta_2, \eta_3)$ into this equation, we obtain

$$l_1^2(1 - \eta_1^2) + l_2^2(1 - \eta_2^2) + l_3^2(1 - \eta_3^2) = 0. \tag{28}$$

Since $\boldsymbol{l}$ lies on a slip plane, the following holds:

$$l_1(\boldsymbol{p}_2)_1 + l_2(\boldsymbol{p}_2)_2 + l_3(\boldsymbol{p}_2)_3 = 0. \tag{29}$$

Since $\boldsymbol{l}$ is a unit vector,

$$l_1^2 + l_2^2 + l_3^2 = 1 \tag{30}$$

holds. From these three equations, we can obtain components l_1, l_2, l_3 and determine the orientation of the dislocation lines.

We are now ready to determine the interface, that is, the habit plane $\boldsymbol{p}_1$. When the habit plane is calculated, two vectors $\boldsymbol{v}^{(1)}$ and $\boldsymbol{v}^{(2)}$, which lie in the habit plane and are not parallel, must be determined to be invariant. The vectors $\boldsymbol{v}^{(1)}$ and $\boldsymbol{v}^{(2)}$ are arbitrary ones in the habit plane, so they can be chosen so as to simplify the formula, if possible. For this purpose, setting $\boldsymbol{p}_1 = [q_1, q_2, 1]/(q_1^2 + q_2^2 + 1)^{1/2}$, and choosing

$$\begin{aligned} \boldsymbol{v}^{(1)} &= [0, 1, -q_2]/(1 + q_2^2)^{1/2}, \\ \boldsymbol{v}^{(2)} &= [q_2, -q_1, 0]/(q_2^2 + q_1^2)^{1/2}, \end{aligned} \tag{31}$$

we find that these vectors satisfy the condition that they must be normal to $\boldsymbol{p}_1$ and lie in the habit plane. Then, substituting this $\boldsymbol{v}^{(1)}$ into Eq. (26) to make it an invariant line, and multiplying $\boldsymbol{v}^{(1)}$ by its transpose $\boldsymbol{v}^{(1)'}$ and using Eq. (26), we obtain

$$\boldsymbol{v}^{(1)'}\boldsymbol{P}'\boldsymbol{B}^2\boldsymbol{P}\boldsymbol{v}^{(1)} = \boldsymbol{v}^{(1)'}\boldsymbol{v}^{(1)}. \tag{32}$$

Substituting $\boldsymbol{P}$ of Eq. (22) and $\boldsymbol{v}^{(1)}$ of Eq. (31) into Eq. (32), we obtain

$$h^2P + 2h(b_{03}\eta_3{}^2q_2 - b_{02}\eta_2{}^2) + (\eta_3{}^2 - 1)q_2{}^2 + \eta_2{}^2 - 1 = 0, \tag{33}$$

where

$$P = \sum_j b_{0j}{}^2\eta_j{}^2, \qquad h = g\{(p_2)_3q_2 - (p_2)_2\}. \tag{34}$$

Since Eq. (33) involves two unknown quantities, h and q_2, it cannot yet be solved.

However, Eq. (20) can be used to solve Eq. (33). To eliminate $\boldsymbol{R}$, multiplying Eq. (20) by $\boldsymbol{l}'\boldsymbol{B}^2$ and using $\boldsymbol{l}'\boldsymbol{B}'\boldsymbol{R}' = \boldsymbol{l}'$ given by Eq. (27), we obtain

$$t\boldsymbol{l}'\boldsymbol{B}^2\boldsymbol{b}_0 = \boldsymbol{l}'(\boldsymbol{I} - \boldsymbol{B}^2)\boldsymbol{v}. \tag{35}$$

Substituting $\boldsymbol{v} = \boldsymbol{v}^{(2)}$ into this equation, rewriting Eq. (23) in the form

$$t = g\boldsymbol{p}_2{}'\boldsymbol{v}^{(2)} = g\{(\boldsymbol{p}_2)_1q_2 - (\boldsymbol{p}_2)_2q_1\}/(q_1{}^2 + q_2{}^2)^{1/2}, \tag{36}$$

and using the relation that $\boldsymbol{l}$ is normal to $\boldsymbol{p}_1$, that is,

$$l_1q_1 + l_2q_2 + l_3 = 0, \tag{37}$$

we obtain

$$hQ = q_2l_3(1 - \eta_3{}^2) - l_2(1 - \eta_2{}^2) \tag{38a}$$

where

$$Q = \sum_{k=1}^{3} b_{0k}l_k\eta_k{}^2. \tag{38b}$$

Like Eq. (33), this equation involves the unknown quantities h and q_2. Therefore, eliminating h from these two equations, we obtain

$$L_3q_2{}^2 + Mq_2 + L_2 = 0, \tag{39}$$

where

$$\begin{aligned} L_k &= N_k\{N_kP + 2T_kQ - (Q^2/l_k)\}, \qquad (k = 2, 3) \\ -\tfrac{1}{2}M &= N_2N_3P + (N_3T_2 + N_2T_3)Q, \\ N_k &= l_k(1 - \eta_k{}^2), \\ T_k &= b_{0k}\eta_k{}^2. \end{aligned}$$

The value of q_2 can independently be obtained from Eq. (39), and the value of q_1 can be found by substituting q_2 into Eq. (37).

The value of g can be obtained from Eqs. (34) and (38); it is

$$g = \frac{q_2 l_3(1 - \eta_3{}^2) - l_2(1 - \eta_2{}^2)}{Q\{(p_2)_3 q_2 - (p_2)_2\}}. \tag{40}$$

Using this equation, we can determine the value of t from Eq. (36).

Finally, let us reflect on this theory. Simple glissile surface dislocations have been assumed to lie on the interface. However, whether this assumption is adequate or not must be ascertained by experiments. If any discrepancy arises, an alternate assumption should be adopted, so that the theory can be improved.

6.6 Supplementary evidence on the crystallographic phenomenological theory

Although the comparison of the phenomenological theory with experimental results has been carried out in some measure in the preceding sections, the treatment there is not complete.

As described in Chapter 2, crystallographic data such as the habit plane,† shape change, and orientation relationship are obtained by surface relief, scratch bending, x-ray diffraction, and electron diffraction, while theoretical calculations are frequently carried out by electronic computers.

6.6.1 $(259)_f$ habit plane in f.c.c. → b.c.c. (b.c.t.) transformation

Figure 6.34[108‡] shows stereographically the poles of habit planes observed in Fe–Ni alloys with various Ni contents. The habit planes are found to lie near $(259)_f$ or $(3\,10\,15)_f$, although they vary a little with Ni content. The habit planes reported by other investigators[27,109–111] are nearly the same. On the other hand, those predicted by the phenomenological theory for the complementary shear, $\boldsymbol{p}_2' \| (101)_f$, $\boldsymbol{d}_2 \| [10\bar{1}]_f$, vary with δ along a curve as shown in the figure. This curve passes through the mean of the observed habits, where the value of δ is 1.005.

The shape change measured by Machlin and Cohen[27] for an Fe–30% Ni alloy is shown in the second column of Table 6.4. From this table we see that the shape change is not a simple shear but contains a component normal to the habit plane. The values in the third column are those predicted by the phenomenological theory for $\delta = 1.004$. It is seen that there is a fairly good agreement between the experimental and theoretical results.

† Even in the same specimen, the poles of habit planes scatter more than experimental error.[107]

‡ In the Fe–34.8% Ni specimen, the transformation is accomplished under external stress.

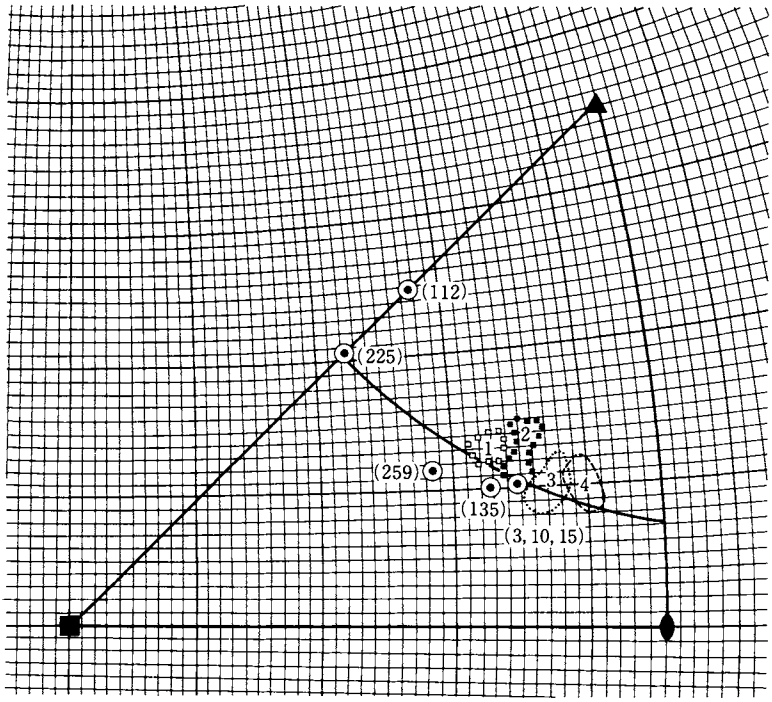

FIG. 6.34 Habit planes of α' martensites in Fe–Ni alloys with various Ni contents: (1) 30.9% Ni; (2) 31.9% Ni; (3) 33.1% Ni; (4) 34.8% Ni. (After Reed.[108])

TABLE 6.4 Shape deformation associated with martensitic transformation in an Fe–30% Ni alloy[a]

Shape change		Exp.	Theor. ($\delta = 1.004$)
d_1	Parallel comp.	0.20	0.291
	Normal comp.	0.05	0.041
Amount m_1		0.206	0.223

[a] After Machlin and Cohen.[27]

The results reported by Breedis and Wayman[110] for Fe–30.9% Ni (Table 6.5) are in good agreement with the theoretical results.

The orientation relationships for Fe–29.90% Ni were first determined by Nishiyama using the x-ray diffraction method; the results were

$$(111)_f \| (011)_b, \qquad [\bar{1}\bar{1}2]_f \| [0\bar{1}1]_b.$$

TABLE 6.5 Crystallographic data on the martensitic transformation in an Fe–30.9% Ni alloy[a,b]

		Theor.	
	Exp.	$\delta = 1.0000$	$\delta = 1.0014$
Habit plane $\boldsymbol{p}_1'$	$\begin{pmatrix}0.1656\\0.7998\\0.5770\end{pmatrix}_f \fallingdotseq \begin{pmatrix}3\\14\\10\end{pmatrix}_f$	$\begin{pmatrix}0.1848\\0.7823\\0.5948\end{pmatrix}_f$ Diff. 1.8°	$\begin{pmatrix}0.1895\\0.7881\\0.5857\end{pmatrix}_f$ Diff. 1.5°
Shape change			
Direction $\boldsymbol{d}_1$		$\begin{bmatrix}-0.0472\\0.1601\\-0.1521\end{bmatrix}_f$	
Angle θ	11°	7.3°	
Orientation relationships			
$(111)_f \wedge (011)_b$	0.3°	0.54°	0.50°
$[\bar{1}\bar{1}2]_f \wedge [0\bar{1}1]_b$	2.2°	1.67°	1.79°
$[\bar{1}01]_f \wedge [\bar{1}\bar{1}1]_b$	−2.4°	−3.62°	−3.49°

[a] After Breedis and Wayman.[110]

[b] Input data are $a_f = 3.591$ Å, $a_b = 2.875$ Å, $\boldsymbol{p}_2' \| (101)_f$ and $\boldsymbol{d}_2 \| [\bar{1}01]_f$

In his experiment, a γ single crystal was transformed into α' martensite by immersing it in liquid nitrogen, and then the orientation relationships were determined by measuring the positions of diffraction spots from α' martensite crystals, the specimen being rotated about a prominent direction of the original γ matrix. He confirmed that all the diffraction spots could be explained as arising from α' variants that satisfy the orientation relationships just given. The experimental error was about 1°.

Later, similar experiments were carried out by many investigators using more refined methods,† and the results are shown in Table 6.6.[33,112–114] According to these results, both experimental and theoretical orientation relationships in Fe–Ni alloys are close to the N relations rather than the K–S relations. However, this statement holds only when the M_s temperature is very low. For alloys with low Ni contents and high M_s temperature, the K–S relationships hold.[115]

According to Efsic and Wayman,[116] Fe–Pt alloys also show characteristics similar to those of Fe–Ni alloys. The α' martensite platelets of this alloy

† Although the accuracy in determining the orientation of one martensite plate by these methods is good, the accuracy for averaged-out values will not be good unless a large number of measurements are made in order to remove the effect of scatter in the orientation of martensite crystals.

TABLE 6.6 Orientation relationships in Fe–Ni alloys[a]

Method of experiment	Ref.	Composition of specimen	$(111)_f \wedge (011)_b$		N $[\bar{1}\bar{1}2]_f \wedge [0\bar{1}1]_b$		K–S $[\bar{1}01]_f \wedge [\bar{1}\bar{1}1]_b$	
			Obs.	Calc.	Obs.	Calc.	Obs.	Calc.
X-ray osci.								
γ: single	[114]	Fe–29.9% Ni	0°		0°			
α: poly	[113]	Fe–30% Ni	2.4°		1.0°			
X-ray back Laue	[33]	Fe–30.9% Ni	0.3°	0.53°	2.2°	1.67°	−2.4°	−3.62°
(microbeam)	[112]	Fe–32% Ni	1°				−4.5°	

[a] Prediction obtained for $\delta = 1$.

are long and have straight boundaries with the γ matrix, and the scatter in habit planes is small. In Fe–24.5 at.% Pt ($M_s = -5°C$), the experimentally determined habit planes lie near $(3\,10\,15)_\gamma$, which is close to that predicted by the theory for $\delta = 0.996$. There is also good agreement between the theory and experiment with regard to the orientation relationships (Table 6.7).† If the alloy is fully ordered, the martensite is expected to have tetragonal symmetry (Section 2.2.2). But data for the ordered state are not available at present, because of the extremely low M_s temperature observed.

As demonstrated as an example in the development of the theory, an Fe–22% Ni–0.8% C alloy also shows the $(259)_f$-type habit plane, and can be explained by the phenomenological theory for $\delta = 1$, as shown in Table 6.8. However, the large discrepancy in the direction of $\boldsymbol{d}_1$ remains unexplained, as in the case of Fe–31% Ni alloys. Alloys of Fe–11% Ni–1.23% C and Fe–1.78% C also show $(259)_f$-type habit planes.[109]

All the examples described above were for alloys with low M_s temperatures. In alloys with low solute content and the associated high M_s temperature, the habit planes may belong to the $(225)_f$ type, as is true for carbon steels, but this point has not been investigated in Fe–Ni and Fe–Pt alloys. In an Fe–7% Al–2.0% C alloy it is reported[117] that the habit plane is within 3° from the $(3\,10\,15)_f$ plane and the orientation relationships are G–T relations. These experimental results can be explained by the theory for $\delta = 1$.

6.6.2 $(225)_f$ habit plane in f.c.c.→b.c.c. (b.c.t.) transformation

As is shown in Fig. 6.35, the orientation of the habit plane of α' martensite in carbon steels lies near $\{259\}_f$ for Fe–1.78% C, whereas the habit plane

† In many of the tables in this book, experimental values are given with many significant figures, as in the original papers. The actual accuracy, however, is probably not as high as these figures indicate.

TABLE 6.7 Crystallographic data on the martensitic transformation in an Fe–24.5 at. % Pt alloy[a,b]

	Exp.	Theor. $\delta = 0.995$	Diff.
Habit plane p_1'	$\begin{pmatrix}0.1910\\0.7599\\0.6214\end{pmatrix}_f \fallingdotseq \begin{pmatrix}3\\12\\10\end{pmatrix}_f$	$\begin{pmatrix}0.1562\\0.7404\\0.6537\end{pmatrix}_f$	2°56′
Shape change			
Direction d_1	$\begin{bmatrix}-0.1275\\0.6723\\-0.7292\end{bmatrix}_f$	$\begin{bmatrix}-0.1738\\0.6579\\-0.7324\end{bmatrix}_f$	3°6′
Angle θ	12.2°	13.1°	0.9°
Amount m_1	0.2157	0.2325	0.0168
Orientation relations			
$(111)_f \wedge (011)_b$	0.86° ± 0.10°	0.83°	0.03°
$[\bar{1}\bar{1}2]_f \wedge [0\bar{1}1]_b$	—	—	—
$[\bar{1}01]_f \wedge [\bar{1}\bar{1}1]_b$	−4.42° ± 0.10°	−4.44°	0.02°

[a] After Efsic and Wayman.[116]

[b] Input data are $a_\gamma = 3.725$ Å, $a_\alpha = 2.967$ Å; $p_2' \| (101)_f$, $d_2 \| [\bar{1}01]_f$.

TABLE 6.8 Crystallographic data on the martensitic transformation in an Fe–22% Ni–0.8% C alloy[a]

	Exp.	Theor.		
	Greninger–Troiano[25]	W–L–R.[35] (Int. tw.)	Suzuki[95] (Dynamic)	Bilby–Frank[99] (Prism match)
Habit plane p_1'	$\begin{pmatrix}0.1642\\0.8208\\0.5472\end{pmatrix}_f = \begin{pmatrix}3\\15\\10\end{pmatrix}_f$	$\begin{pmatrix}0.1783\\0.8027\\0.5691\end{pmatrix}_f$	$\begin{pmatrix}0.1780\\0.8047\\0.5655\end{pmatrix}_f$	$\begin{pmatrix}0.1848\\0.8052\\0.5622\end{pmatrix}_f$
Shape change				
Direction d_1	$\begin{bmatrix}-0.3828\\0.5642\\-0.7315\end{bmatrix}_f$	$\begin{bmatrix}-0.2400\\0.5964\\-0.7660\end{bmatrix}_f$	—	$\begin{bmatrix}-0.2389\\0.5929\\-0.7690\end{bmatrix}_f$
Angle $\theta''(\gamma_1)$	10.66°	10.33°	—	10.28°
$\theta(\gamma_2)$		10.71°	—	10.55°
Orientation relations				
$(111)_f \wedge (011)_b$	<1°	15′	15′	14′
$[\bar{1}\bar{1}2]_f \wedge [0\bar{1}1]_b$	2°	1.9°	—	—
$[\bar{1}01]_f \wedge [\bar{1}\bar{1}1]_b$	−2.5°	−2.7°	−2°56′	3.1°

[a] Input data are $a_\gamma = 3.592$ Å, $a_{\alpha'} = 2.845$, $c_{\alpha'} = 2.973$ Å, $p_2' \| (101)_f$, $d_2 \| [\bar{1}01]_f$.

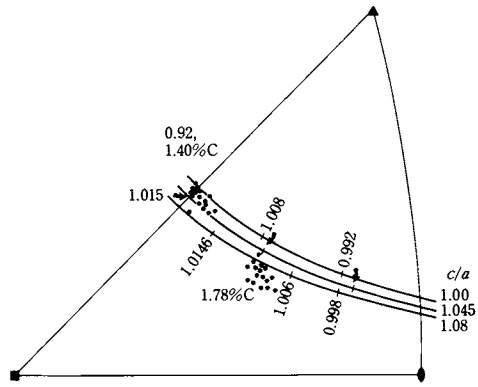

FIG. 6.35 Predicted and experimental habit planes for α′ martensites in steels. The predicted values are obtained with varying δ; the three curves correspond to three c/a values. (Experimental: after Greninger and Troiano;[25] predicted: after Wayman.[9])

lies near $\{225\}_f$ or $\{449\}_f$ for Fe–0.92–1.40%C.† These results seem consistent with the phenomenological theory, in which $\boldsymbol{p}_2' \| (101)_f$, $\boldsymbol{d}_2 \| [\bar{1}01]_f$ are chosen, since the loci of the poles of habit planes pass near the observed habit planes when δ is varied. In this explanation, however, a rather large dilatation parameter, such as $\delta = 1.015$, must be assumed, and the calculated orientation relationship is not consistent with that observed. Data for carbon contents between 1.4% and 1.78% are absent from Fig. 6.35, although there are some experimental data for Cr steels. For example, in Fe–2.8% Cr–1.5% C[119] and Fe–3.09%Cr–1.51%C,[120] the habit planes lie between $\{225\}_f$ and $\{259\}_f$. In general there is a tendency for alloys with high M_s temperatures to exhibit $\{225\}_f$ habit planes, whereas those with low M_s temperatures exhibit $\{259\}_f$ habit planes.[121] However, there are exceptions in certain special steels. Thus the data concerning $\{225\}_f$ habit planes are not well understood, and many investigators have paid attention to the mechanism of this transformation.

Wayman *et al.*[60] investigated a 7.9%Cr–1.1%C steel and obtained the result that the habit plane lies close to $\{449\}_f$ rather than $\{225\}_f$. In repeated investigations[65,122] they observed three types of fine structures in the electron micrographs of α′ martensites. There were thick $(112)_b$ internal twins with low density, $(011)_b$ slip lines, and long dislocations. Table 6.9 shows the experimental results concerning the habit plane and other features. If these are to be explained by a single complementary shear, the plane $\boldsymbol{p}_2'$ must be

† In an experiment by Bowles and Morton,[118] three scratches were drawn on specimen surfaces prior to transformation, and from the bending of those scratches due to transformation, $\boldsymbol{d}_1$ and $\boldsymbol{m}$ were precisely determined.

TABLE 6.9 Crystallographic data on the martensitic transformation in an Fe–7.9% Cr–1.11% C alloy[a]

	Experimental
Habit plane $\boldsymbol{p}_1'$	$\begin{pmatrix}0.3563\\0.8536\\0.3865\end{pmatrix}_f \fallingdotseq \begin{pmatrix}4\\9\\4\end{pmatrix}_f$
Shape change	
Direction $\boldsymbol{d}_1$	$\begin{bmatrix}-0.0025\\0.7419\\-0.6705\end{bmatrix}_f$
Amount m_1	0.2162
Orientation relationship	
$(111)_f \wedge (011)_b$	0.45°
$[\bar{1}01]_f \wedge [\bar{1}\bar{1}1]_b$	0.53°
$[\bar{2}11]_f \wedge [\bar{3}\bar{1}1]_b$	0.24°
$[\bar{1}10]_f \wedge [\bar{1}00]_b$	4.65°
Complementary shear ($\delta = 1.01663$)	
Plane $\boldsymbol{p}_2'$	16.5°–21° from $(101)_f$ to $(1\bar{1}1)_f$
Direction $\boldsymbol{d}_2$	Within 1.5° from $[\bar{1}01]_f$
Amount m_2	0.255 ± 0.007

[a] Input data are $a_f = 3.619$ Å, $a_b = 2.860$ Å, $c_b = 2.983$ Å. After Morton and Wayman.[65]

16.5°–21° away from the $(101)_f$ plane toward $(1\bar{1}1)_f$, although the shear direction is quite close to $[\bar{1}01]_f$. Thus it is considered that the shear consists of two shears along the $(101)_f$ plane and $(1\bar{1}1)_f$ plane. Further, δ must be assumed to be 1.0166.

Bowles and Dunne[78] made an investigation by the scratch method using Fe–6.14% Mn–0.95% C and Fe–1.2% C alloys. They made scratches for shape change measurement at temperatures as high as 1000°C, in order to avoid the effect of strains due to scratches. As a result they found that δ is nearly unity although the habit plane lies close to $(225)_f$.

Then Krauklis and Bowles[123] directly measured the dilatation along the habit plane in an Fe–7.96% Cr–1.08% C alloy, in order to examine whether δ is really greater than unity or not. For that purpose they first made many etch pits† in the specimens, and then measured the change of the distances between two etch pits before and after the transformation. According to

† The etchant consisted of 100 cc of HF, 100 cc of ethanol, 100 cc of water, and 5 g of $CuCl_2$.

the measurement, changes of 0.01%–0.82% were detected in both α' and γ, but the differences between these phases on both sides of the interface were always small and less than 0.2%. Thus, δ was very near unity. Therefore, the introduction of δ different from unity to explain crystallographic data, including the habit plane, is not entirely satisfactory; the theory incorporating plastic accommodation in the parent (Section 6.4.4) is more acceptable.

Although the fact that the habit plane is $\{225\}_f$ or $\{259\}_f$ was regarded only as a quantitative difference in the phenomenological theory, there may be a qualitative difference between the two types of transformations. For example,[124] in an Fe–24% Ni–0.5% C alloy most martensites are the $\{259\}_f$ type and each martensite plate makes an acute angle with the others, whereas in Fe–19% Ni–0.5% C most martensites are the $\{225\}_f$ type and each martensite makes an obtuse angle with the others. Upon transformation, the click sound associated with the burst phenomenon is heard in the former, whereas it is not heard in the latter. Thus the former may correspond to the umklapp transformation and the latter to the schiebung type.

6.6.3 Habit plane in f.c.c.→h.c.p. transformation

In this transformation it is convenient to use a lattice distortion different from the Bain distortion. Starting from the experimentally determined Shoji–Nishiyama relationships, $(111)_{fcc}\|(0001)_{hcp}$, $[11\bar{2}]_{fcc}\|[1\bar{1}00]_{hcp}$, we can obtain the lattice distortion shown in Fig. 6.36 as ***RB***, since the atomic arrangement in the $(111)_{fcc}$ plane is exactly the same as that in the $(0001)_{hcp}$ plane.

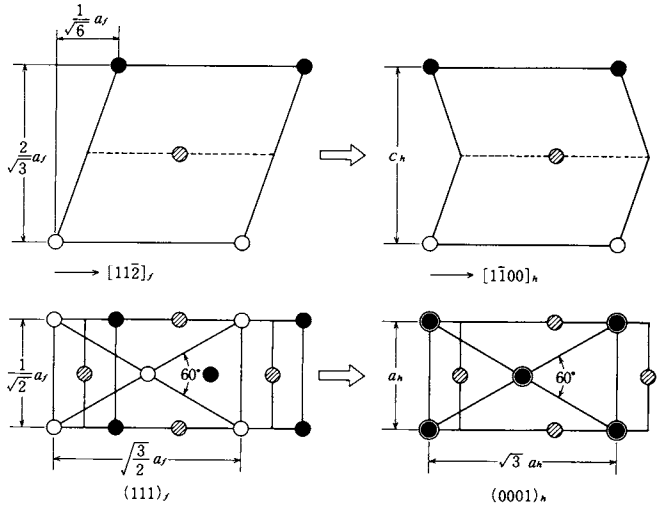

FIG. 6.36 Shear mechanism for the f.c.c.-to-h.c.p. transformation.

This distortion is expressed in matrix form as

$$\begin{bmatrix} \eta_1 & \frac{1}{2\sqrt{2}} & 0 \\ 0 & \eta_1 & 0 \\ 0 & 0 & \eta_3 \end{bmatrix}, \qquad \eta_1 = \sqrt{2}\,\frac{a}{a_0}, \eta_3 = \frac{\sqrt{3}}{2}\,\frac{c}{a_0},$$

where a_0 is the f.c.c. lattice constant and a, c are the h.c.p. lattice constants. This matrix expresses a homogeneous shear. The displacement of atoms in the middle layer of Fig. 6.36 is neglected because the shuffle does not affect the shape change. In the case of cobalt, $a_0 = 3.554\,\text{Å}$, $a = 2.514\,\text{Å}$, $c = 4.105\,\text{Å}$. Using these values, we have

$$\eta_1 = 0.999, \qquad \eta_3 = 1.000.$$

So the distortion is extremely small.† From this and the fact that the atomic arrangements in $(111)_f$ and $(0001)_{hcp}$ are exactly the same, it is obvious that the $(111)_f$ plane can become a possible habit plane. The plane of complementary shear may be the same as the habit plane, but a relatively large shear angle, such as $\tan^{-1}(1/(2\sqrt{2})) = 19°28'$, is required. This is consistent with the observation that the martensites are thin and that many stacking faults exist on the $(0001)_{hcp}$ plane. Thus, in the f.c.c. → h.c.p. transformation, a result can be obtained by simple calculations consistent with the phenomenological theory.

6.6.4 Habit plane in the single interface transformation

A. *Au–47.5 at.% Cd*

An Au–47.5 at.% Cd alloy is typical of the alloys that exhibit single interface transformation behavior when a single crystal is cooled under a temperature gradient. Constraint from the matrix is absent in this transformation, since the interface runs completely across a specimen. Thus the transformation is convenient for measuring the habit plane, orientation relationship, shape change, and so on. As described in Sections 2.4.2C and 3.2.2, the CsCl-type β_1 transforms into the 2H-type (a stacking order structure) γ_1' with an orthorhombic unit cell ($M_s = 60°C$). The lattice parameters are

β_1: $a_0 = 3.3165\,\text{kX}$; γ_1': $a = 3.1476\,\text{kX}$, $b = 4.7549\,\text{kX}$, $c = 4.8546\,\text{kX}$.

† The distortion is also small in Yb, Ce, and La.[125]

So the lattice distortion matrix is

$$\begin{bmatrix} b/(\sqrt{2}a_0) & 0 & 0 \\ 0 & c/(\sqrt{2}a_0) & 0 \\ 0 & 0 & a/a_0 \end{bmatrix} = \begin{bmatrix} 1.0138 & 0 & 0 \\ 0 & 1.0350 & 0 \\ 0 & 0 & 0.9491 \end{bmatrix}.$$

Thus the strains are small compared with the f.c.c. → b.c.c. transformation. This is one reason for the occurrence of the single interface transformation in this alloy. Internal twins run completely across a martensite crystal and their width is as large as 1 μm.

In this transformation, the lattice change is from cubic to orthorhombic, and the lattice-invariant shear is twinning. The habit plane was calculated by using the W–L–R theory described previously. In the original calculation,[37,39] the $\{111\}_{\gamma_1'}$ plane, which corresponds to $\{101\}_{\beta_1}$ in the matrix, was chosen as the twinning plane. Although the twinning direction can be regarded as $\langle 101\rangle_{\beta_1}$, the latter is not a rational direction in the martensite lattice. The results calculated from the foregoing input data are shown in Table 6.10, from which we see that there is fair agreement between the theory and experiment,[39,126] but that the agreement is not quite satisfactory. In order to overcome this difficulty, the combination of a rational twinning direction and an irrational twinning plane was tried[43,44] (since the irrational Burgers

TABLE 6.10 Crystallographic data on the martensitic transformation in an Au–47.5 at. % Cd alloy[a]

	Exp.	Theor.	Diff.
Habit plane p_1'	$\begin{pmatrix} 0.696 \\ -0.686 \\ 0.213 \end{pmatrix}_b$	$\begin{pmatrix} 0.6968 \\ -0.6810 \\ 0.2250 \end{pmatrix}_b$	$<1.5°$
Shape change (shear)			
Direction d_1	$\begin{bmatrix} 0.660 \\ 0.729 \\ 0.183 \end{bmatrix}_b$	$\begin{bmatrix} 0.6510 \\ 0.7322 \\ 0.2001 \end{bmatrix}_b$	$<1.5°$
Angle θ	2.94°	3.25°	0.36°
Twin ratio x	0.25	0.28	0.03
Orientation relationship			
$(001)_c \wedge (001)_0$	0° [123]	2°40′ (twin 1) 2°27′ (twin 2)	2.5°
$[111]_c \wedge [011]_0$	0° [123]	18′ (twin 1) 18′ (twin 2)	0.3°

[a] After Lieberman *et al.*[39]

vector is rare) but the result showed no improvement. Thus, more data are still needed.[41]

B. *In–20.75 at.% Tl*

This alloy also undergoes a single interface transformation, since the distortion is quite small, as described in Section 3.5.1. The complementary strain gives twins 10 μm thick, and the twinning plane is $\{011\}_{fcc}$. The habit plane predicted from the phenomenological theory is $(0.013, 0.993, 1.000)_{fcc}$, and the error from the observed $(011)_{fcc}$ plane is only 0.43°. Although the agreement is good, this case cannot be regarded as proving the general applicability of the theory, since the lattice distortion is too small.

C. *Similar phenomena in Fe*

The following example does not belong to the single interface martensitic transformation, but the behavior is similar and interesting. Zerwekh and Wayman investigated the α–γ transformation in iron whiskers.[127] Various-sized α–Fe whiskers were produced by reducing a halide; those used for analysis had these dimensions: diameter less than 50 μm; length less than 5 mm. The growth axis was $\langle 100 \rangle$, faceted with $\{100\}$ planes that formed a square or rectangular cross section. By using a high-temperature optical microscope, they observed the shape change of specimens heated from one end upon the transformation of α to γ and of α to γ to α. According to their observations, the transformation did not necessarily start at the hottest tip, but rather at a point about one quarter of the specimen length from the tip, and transformation went back toward the tip. This transformation was so rapid that it was not possible to observe the shape change while the specimen was transforming. Then the interface between the two phases moved forward with increased heating, but the movement was jerky. The shape change during the transformation is shown in Fig. 6.37. The α–γ interface is almost straight, and the transformed region is kinked from the untransformed region. Besides, striations parallel to the interface are left behind in the transformed region.

These investigators calculated the habit plane by the Bowles–Mackenzie theory by assuming that the striations are traces of complementary shear during the transformation. Although the plane of the complementary shear was determined, by trace analysis of the striations, to be $(011)_b$, the direction of the complementary shear is not known; they assumed it to be $[12\bar{2}]$ without justification. According to their calculation, the habit plane was located several degrees away from $(011)_b$ and agreed with the experimentally determined habit planes. Also, the shear angle of the shape change $\boldsymbol{P}_1$ was calculated as 8.5°, which agreed with the observed value of 5.6°–8.5° (β in Fig. 6.37). The orientation relationship, however, was not observed.

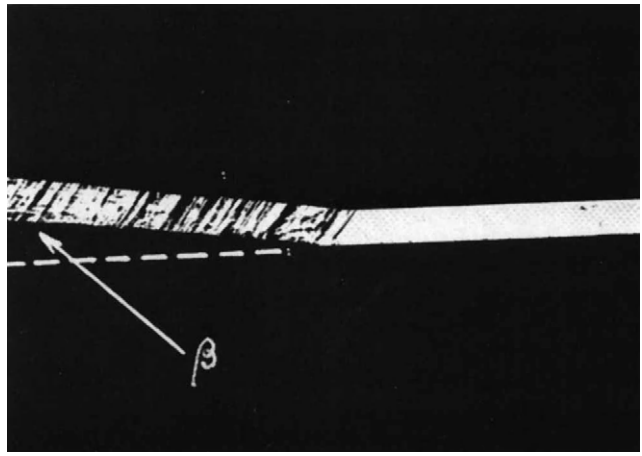

FIG. 6.37 Optical micrograph of Fe whisker after experiencing one $\alpha \rightarrow \gamma \rightarrow \alpha$ transformation cycle ($\times$ 120). (After Zerwekh and Wayman.[127])

From the agreement just noted between theory and experiment, Zerwekh and Wayman concluded that the transformation of iron whiskers at the A_3 temperature is also martensitic. From the observation of the shape change, it may be inferred that the transformation actually does manifest at least a somewhat martensitic nature, but that it may not be perfectly martensitic. Since the thermal vibration of each atom affects the transformation that occurs comparatively slowly at such high temperatures as the A_3 point, the basic assumptions in the phenomenological theory may be violated under these conditions. However, since stiffness diminishes at high temperatures, the cooperative movement of atoms may also occur more easily. Thus, it may also be rationalized in that sense that the transformation in the present case is in some degree martensitic. If these considerations and careful observations are combined, the reason for the choice of $[12\bar{2}]_b$ as the direction of the complementary shear will be clarified.

6.6.5 Relations between adjacent martensite crystals

The foregoing descriptions have been concerned with relations between the habit planes and internal complementary shears in various martensites. That the habit plane is also influenced by the formation of adjacent martensite plates must not be disregarded. The influence of such adjacent formation is substantial, and especially significant, when the two martensite plates form successively or simultaneously and come into contact with each other. When the plates form successively, the transformation stress accompanying the

FIG. 6.38 Optical micrograph of martensite in an Fe–10.3% Al–1.5% C steel (quenched from 1200°C to 0°C). (Arrows indicate lamellar structures.) (After Nishiyama, Shimizu, and Harada.[128])

formation of the first plate is stored in the adjacent region even if a complementary shear has occurred in the martensite. Then, the second martensite plate is a variant with an orientation capable of releasing the stress. Similarly, two martensite plates that form simultaneously have a variant relation to each other so as to relax the transformation stress. In an extreme case, two plates may appear as if they are twin related to each other.

An example of the twinlike morphology of two martensite plates can be found in an aluminum steel,[128] as shown in Fig. 6.38, which is an optical micrograph taken from an Fe–10.38% Al–1.50% C steel quenched from the austenite state. In this micrograph, almost all the plates are wedge-shaped, but lamellar structures resembling repeated twins can be seen at the places indicated by the arrows. An electron micrograph of a region having such a lamellar structure is shown in Fig. 6.39, which reveals that the lamellae are about 0.5 μm thick and have internal fine striations. By selected-area electron diffraction, the striations were found to be parallel to the $\{112\}_{\alpha'}$ traces, and thus they are clearly internal twins or stacking faults. Since all the lamellae have the same striation direction and same crystal orientation, it appears as if the alternate lamellae are twin related to each other. Measurement revealed, however, that their crystal orientations are nearly (but not exactly) in a twin relation, and are two variants such that the contraction axis of the Bain distortion in one variant is nearly perpendicular to that in the other. That is, after the formation of a martensite plate, another martensite plate may be formed in the adjacent region with an orientation such as to compensate for the transformation stress associated with the first plate. The repetition of such a process causes the martensite plate to exhibit a morphology of alternate lamellae that look as if they were twin related. Therefore, it can

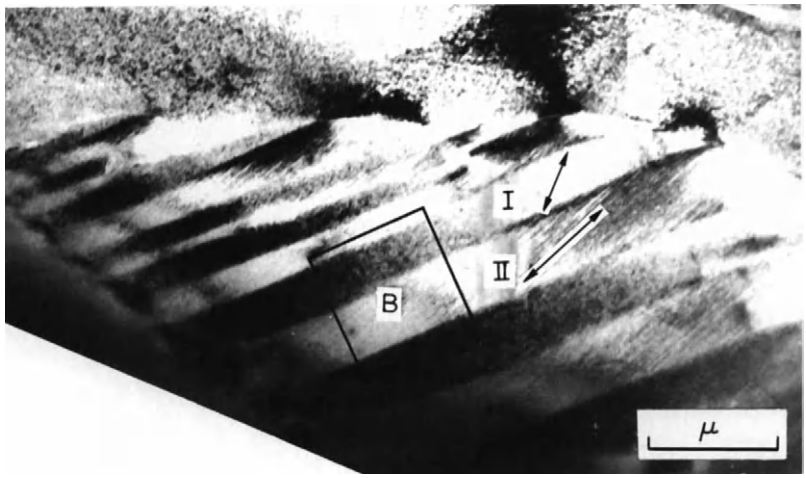

FIG. 6.39 Electron micrograph of martensite in Fe–10.3%Al–1.5%C (same specimens as in Fig. 6.38), showing a lamellar structure due to alternate stacking of two martensite variants and exhibiting striations along the directions shown by the arrows. (After Nishiyama *et al.*[128])

also be understood that the interlamellar boundaries are not as straight as twin boundaries.

A structure similar to the lamellar martensite just discussed had been found earlier,[129] though rarely, in a subzero-cooled Fe–30% Ni alloy, as shown in Fig. 6.40. However, since it was observed only by the replica method of electron microscopy, the origin of the lamellar structure was not explained at the time it was observed.

In very low carbon steels, martensite is well known to form as parallel laths. In some cases, adjoining laths are variants having orientations that compensate for each other's transformation stresses, whereas in certain other cases they nucleate simultaneously with the same variant and grow parallel to each other to form a bundled structure. Oka and Wayman[130] reported

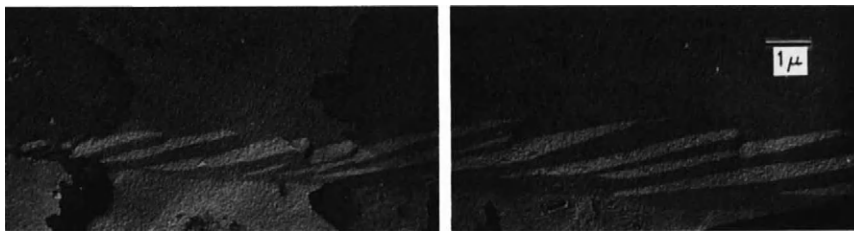

FIG. 6.40 Electron micrograph (replica) showing lamellar martensite in an Fe–30% Ni alloy. (After Nishiyama and Shimizu.[129])

that a peculiar bundled structure was found in α' martensite in an Fe–3% Cr–1.5% C alloy. However, the structure they observed may have been neither twin lamellae nor variant lamellae that compensate for each other's transformation stresses, but may rather have been parallel martensite plates that nucleated with the same orientation and grew simultaneously into each other.

In Fig. 2.72, showing the γ_1' martensite of a Cu–Al–Ni alloy, a spearlike martensite crystal consisting of two variants that mutually relax the transformation stress can be seen. Further, Tas *et al.*[131] observed three such spears nucleating at one point and growing in three directions to form a triangular star. This combination of crystals is also expected from the point of view of the minimum total strain energy of transformation.

6.6.6 Habit plane of surface martensites

The habit plane of surface martensite has a characteristic different from that of inner martensites, as mentioned in Chapter 2. Klostermann[132,133] measured the habit plane of martensites produced on the surface of a single crystal of an Fe–30.2% Ni–0.04% C alloy, and examined whether the measured habit plane can be explained well by the phenomenological theory discussed earlier. According to his study, the habit plane was nearly parallel to a $\{112\}_f$ plane, the scatter being less than 2°. If this habit plane was an invariant plane, an invariant line during the transformation would lie in the plane. However, the invariant lines determined from the measured orientation relationship and the Bain distortion were farther away from the $\{112\}_f$ habit plane than experimental error could account for. This fact suggests that the phenomenological theory, in which the habit plane was assumed to be an invariant plane, is inapplicable to surface martensites. Therefore, the habit plane may instead be defined as in Frank's model, described in Section 6.5.4. That is, the energy in the habit plane should be lowered when the parent and martensite lattices are smoothly connected to each other, and so it is required for the habit plane that the close-packed atomic rows in both lattices be parallel to each other, and that their interatomic distances be equal. If this is so, the $\{112\}_f$ and $\{123\}_f$ planes can be considered the unique habit planes. This is one conclusion from Klostermann's study of surface martensites.

6.7 Correlation of elastic anisotropy with the temperature of martensitic transformation[134]

6.7.1 Elastic moduli of the parent matrix

Much earlier it was explained that martensite occurs as the product of a cooperative movement of atoms in the parent crystal, so that the mode of

lattice distortion in the martensitic transformation is considered to be similar to elastic deformation. Therefore, the transformation start temperature M_s is thought to depend on the elastic moduli of the parent matrix[135] and on the resistance to the lattice-invariant shear that proceeds concurrently with the transformation.

The elastic shear behavior of cubic crystals is most readily expressed by the combination of two moduli, c_{44} and $\frac{1}{2}(c_{11} - c_{12})$, characterizing, respectively, the maximum and the minimum resistance to deformation when a shearing stress is applied across a $\{100\}$ plane in a $\langle 010 \rangle$ direction and across a $\{110\}$ plane in a $\langle 110 \rangle$ direction. In an elastically isotropic material, the two shear moduli are equal and the ratio $c_{44}/\frac{1}{2}(c_{11} - c_{12})$ may thus be used as an elastic anisotropy factor for cubic crystals.

Zener[136] first suggested the possible importance of the elastic anisotropy in the martensitic transformation. Crystals with a small value of the shear moduli, of which β brass is typical, should tend to undergo transformation. The elastic constants of a β phase Cu–48.26 at.% Zn alloy are[137]

$$\begin{aligned} c_{11} &= 1.279 \\ c_{12} &= 1.091 \quad \times 10^{12} \quad \text{dyn/cm}^2 \\ c_{44} &= 0.822 \end{aligned}$$

at room temperature, and the shear moduli for the (001) [100] shear and the (110) $[1\bar{1}0]$ shear are

$$\begin{aligned} c_{44} &= 0.822 \times 10^{12} \quad \text{dyn/cm}^2, \\ \tfrac{1}{2}(c_{11} - c_{12}) &= 0.094 \times 10^{12} \quad \text{dyn/cm}^2, \end{aligned} \tag{1}$$

respectively. It is noteworthy that β brass's elastic anisotropy factor is nearly 10, which is quite high. The elastic anisotropy factors of other metals are listed below for comparison.

	β brass	Na	K	Al	W
$\dfrac{c_{44}}{\frac{1}{2}(c_{11} - c_{12})}$	8.8	7.5	6.3	1.23	1

In general, the occurrence of the martensitic transformation is difficult at low temperatures, since the elastic constants of parent matrices increase with decreasing temperature. On the other hand, the thermal vibration mode of the crystal lattice changes with decreasing temperature in that the low-frequency terms dominate the high-frequency terms and the vibration amplitude is large in the direction of a low elastic constant. Therefore, martensitic transformation will tend to occur even at low temperatures in those alloys (e.g., β brass) in which the elastic anisotropy factor becomes large at low temperatures.

6.7.2 Terms contributing to the elastic anisotropy[138–141]

There are three important terms contributing to the elastic anisotropy of b.c.c. crystals:

(i) Electrostatic interaction between positive ions constituting the crystal lattice (S term).
(ii) Non-Coulomb interaction (repulsion) between ionic shells (R term).
(iii) Fermi energy (F term).

In the following we will review how these terms contribute to the elastic shear moduli.

A. *Electrostatic interaction between ions in crystal lattice* (S term)

An approximate picture of a metallic crystal lattice is a lattice of positive ions held together by a gas of uniformly distributed electrons. The electrostatic energy between positive ions and electrons under shear contributes to the shear moduli. Jones[140] showed, for b.c.c. crystals, that the contributions of the electrostatic terms to the shear moduli are

$$\left.\begin{aligned} c_{44}^{(S)} &= 17.12 \\ \tfrac{1}{2}(c_{11}-c_{12})^{(S)} &= 2.30 \end{aligned}\right\} \times 10^{12} a^{-4} Z_{\text{eff}}^2 \quad \text{dyn/cm}^2 \tag{2}$$

where a is the lattice constant in angstroms, Z_{eff} is the effective charge of the positive ions,† and the superscript (S) indicates the contribution of the S term.‡ The high elastic anisotropy factor suggests a large contribution by the electrostatic interaction term.

B. *Non-Coulomb interaction (repulsion) between ionic shells* (R term)

This effect is very small in the alkali metals, in which the ions are well separated because of the small ionic radii. The non-Coulomb ionic interactions work as repulsive forces arising from closed-shell positive ion overlaps because of large ionic radii and make a negative contribution to the shear moduli. The repulsive force is a central force acting between nearest neighbor ions in the case of ions that have spherical symmetry, as with copper ions; the energy arising from the non-Coulomb interaction between the ionic shells of a pair of ions a distance r apart can be expressed as a function of r, $\varphi(r)$. The contributions this term makes to the shear moduli of b.c.c. crystals have already been calculated.[142] If we take as a first approximation only

† For example, in the β brass of Cu:Zn = $(1-x):x$, $Z_{\text{eff}} = 1 + x$.

‡ Kunze[141] obtained a slightly different expression for the dependency on the alloy composition, though he performed his calculation in a similar way.

the interaction between nearest neighbors, the contributions are given by

$$\begin{aligned} c_{44}^{(R)} &= (4/9)\varphi_0'' r_0^2 + (8/9)\varphi_0' r_0, \\ \tfrac{1}{2}(c_{11} - c_{12})^{(R)} &= (4/3)\varphi_0' r_0 \end{aligned} \tag{3}$$

where r_0 is the interatomic distance in the equilibrium state, $\varphi_0' = (d\varphi/dr)_{r=r_0}$ and $\varphi_0'' = (d^2\varphi/dr^2)_{r=r_0}$. It is known that φ varies very rapidly with r and it is usual to assume that the variation may be represented by

$$\varphi(r) = \varphi_0 e^{-r/\rho} \tag{4}$$

where φ_0 and ρ are constants specifying the atomic species. Substituting (4) into (3), we obtain as the contributions to the two shear moduli

$$c_{44}^{(R)} = -\frac{4}{9}\left(2 - \frac{r_0}{\rho}\right)Q, \qquad \tfrac{1}{2}(c_{11} - c_{12})^{(R)} = -\tfrac{4}{3}Q, \qquad Q = -\varphi_0' r_0 \tag{5}$$

where since φ_0' is always negative, Q has a positive value. So if $[2 - (r_0/\rho)]$ is negative, the contribution to c_{44} is positive. On the other hand, $\frac{1}{2}(c_{11} - c_{12})$ is always negative. Therefore, alloys in which the electrostatic term contributes largely to the shear moduli should undergo transformation easily, since a b.c.c. lattice tends to be unstable because of its very low resistance to shear.

As for the effect of composition, substitution of atoms with large ionic shells makes the magnitude of Q increase whereupon the shear modulus $\frac{1}{2}(c_{11} - c_{12})$ decreases, so that the martensitic transformation occurs readily. For instance, since copper ions Cu^+ have a larger ionic shell than zinc ions Zn^{2+}, an increase in copper content in β brass leads to a smaller shear modulus and a higher M_s temperature (Section 4.3.5).

C. *Fermi energy* (F term)

In b.c.c. phases having an electron–atom ratio of approximately 3/2, of which β brass is typical, the Fermi surface will be in contact with the Brillouin zone boundaries. The Fermi energy changes as the crystal is sheared, since the energy is dependent on the shape of the crystal lattice. Thus the change in the Fermi energy of the conduction electrons under shear can lead to a large contribution to the shear moduli. Calculations of the elastic constants of aluminum and β brass were made by Leigh[138] and Jones,[139] respectively. An outline of the latter calculation will be given next.

The Fermi energy ε has a different value from that of a free electron near the $\{110\}$ Brillouin zone boundaries in $\boldsymbol{k}$ space. The energy of a free electron in terms of the wave vector $\boldsymbol{k}$ is given simply by $\varepsilon = \boldsymbol{k}^2$ where the energies are measured in Rydberg units ($R_y = 21.79 \times 10^{12}$ ergs) and the length in units of the first Bohr orbit (0.529×10^{-8} cm) for hydrogen. The axes in

$\boldsymbol{k}$ space are chosen so that $\boldsymbol{k}_z$ coincides with the normal to a plane of the zone boundary. The effect on the Fermi energy of a single pair of the {110} boundaries of the Brillouin zone was calculated on the assumption that the energy at any point $\boldsymbol{k}$ is given by

$$\varepsilon = \boldsymbol{k}^2 - \boldsymbol{k}_z{}^2 + \boldsymbol{p}^2 f(z), \qquad p = \sqrt{2}\pi/a \tag{6}$$

where a is the lattice constant and p the perpendicular distance from the origin of $\boldsymbol{k}$ space to the Brillouin zone boundary. z is measured in the direction of $\boldsymbol{p}$ as $z = k_z/p$. $f(z)$ is a nondimensional function of z and is defined as behaving like z^2 for small z; at the Fermi surface, $(df/dz)_{z=1} = 0$. In order to satisfy these conditions, the form of the function was assumed to be

$$f(z) = z^2 - \lambda z^{2/\lambda} \qquad (\lambda \ll 1) \tag{7}$$

by introducing a parameter λ to indicate the amount by which the energy at a plane of the Brillouin zone boundary is less than the corresponding energy of a free electron, namely, $f(1) = 1 - \lambda$.

With this form for the Fermi energy, the shear moduli are obtained by calculating the change in the energy under a shear.

$$\begin{aligned} c_{44}^{(\mathrm{F})} &= \kappa(-\tfrac{1}{4}v^2 + Av - 14B), \\ \tfrac{1}{2}(c_{11} - c_{12})^{(\mathrm{F})} &= \kappa(-\tfrac{5}{8}v^2 + Av - 11B), \end{aligned} \tag{8}$$

where

$$\kappa = \frac{p^5}{2\pi^2}\left(\frac{R_y}{a_H{}^3}\right), \quad v = \frac{2\pi^2 n}{P^3}, \quad A = \frac{4}{3}\frac{(1-\lambda)(2+3\lambda)}{(2+\lambda)},$$

$$B = \frac{2}{9}\frac{(1-\lambda)^2(8+38\lambda+27\lambda^2)}{(2+\lambda)^2(2+3\lambda)(4+\lambda)},$$

and n is the number of conduction electrons per unit volume. According to these expressions, the two shear constants depend on the number of electrons for a given crystal lattice. The foregoing calculation should lead to inaccuracies when the assumption that the Fermi surface touches the Brillouin zone boundaries over only a small fraction of the whole surface becomes invalid for a large number of electrons.

6.7.3 Transformation from b.c.c. structure

A. *β brass*

The elastic anisotropy of b.c.c. metals has theoretically been studied most thoroughly for β brass.[139–141] Jones[139] obtained a satisfactory account of the observed values of the elastic shear moduli. To determine the electrostatic contribution according to Eq. (2), the value of Z_{eff} must be known.

The value is very difficult to estimate accurately but it must lie between 1 and 2. For the sake of obtaining approximate numerical results it was assumed simply that $Z_{\text{eff}}^2 = 2.0$, and the contribution of the electrostatic term to the two moduli c_{44} and $\frac{1}{2}(c_{11} - c_{12})$ was estimated to be 0.455 and 0.061 (in units of 10^{12} dyn/cm^2), respectively. The respective Fermi energy contributions according to (8) are 0.18 and 0.12 if we assume that $\lambda = 0.15$, which would correspond to what is believed to be a likely Brillouin zone energy gap of about 3.0 eV. Adding the three contributions together and equating to the observed values in the case of Cu–48.26 at.% Zn,[137] we obtain the following equations.

$$0.18^{(F)} + 0.455^{(S)} - (4/9)(2 - r_0/\rho)Q^{(R)} = 0.824 \quad \text{(observed)},$$
$$0.12^{(F)} + 0.061^{(S)} - (4/3)Q^{(R)} = 0.097 \quad \text{(observed)},$$

from which are obtained $Q = 0.063 \times 10^{12}$ ergs/cm^2 = 1.33 kcal/mol, and $\rho = 0.29$ Å putting $r = 2.549$ Å. These values appear quite reasonable, so that the foregoing theory seems valid.

It is suggested[139] in this theory that the elastic constants change with variations in the alloy composition.[143] McManus[144] found a drastic variation of the elastic anisotropy factor with composition in that the elastic anisotropy factor changes from about 10 in the 45–48 at.% range of zinc content to about 5 at 50 at.% because of a decrease in c_{44} and increase in $\frac{1}{2}(c_{11} - c_{12})$, as shown in Fig. 6.41. This change may arise from contributions to the R and F terms due to the increased degree of order of the CsCl-type superlattice in alloys of about 50 at.% Zn, the R term being affected by variation in the interaction between second-neighbor ions, and the F term by the formation of new Brillouin zone boundaries.[144,145] The decrease in the elastic anisotropy makes the occurrence of a martensitic transformation difficult, which is the case for β brass with about 50 at.% Zn which does not transform spontaneously.[146] If its superlattice is destroyed

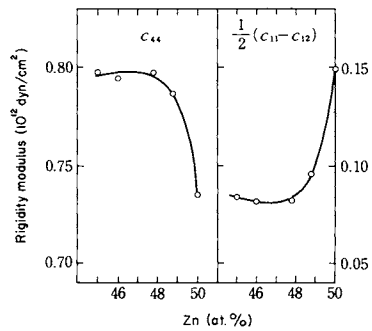

FIG. 6.41 Anisotropy of rigidity modulus for β brass. (After McManus.[144])

by deformation, such β brass is able to transform. Therefore, the difference between the M_s and M_d temperatures is large.

In their study of alloys where gold was substituted for copper in the β phase Cu–Zn, Nakanishi *et al.*[147–150] found that alloys of compositions near the Heusler-type $CuAuZn_2$ transform in three steps, the third step being the martensitic transformation (Section 2.5.3). The curve of M_s temperatures versus gold content in $Au_xCu_{53-x}Zn_{47}$ alloys has a very sharp maximum at 26 at. % Au (Fig. 6.42a).[148,151] The A_s temperature also behaves

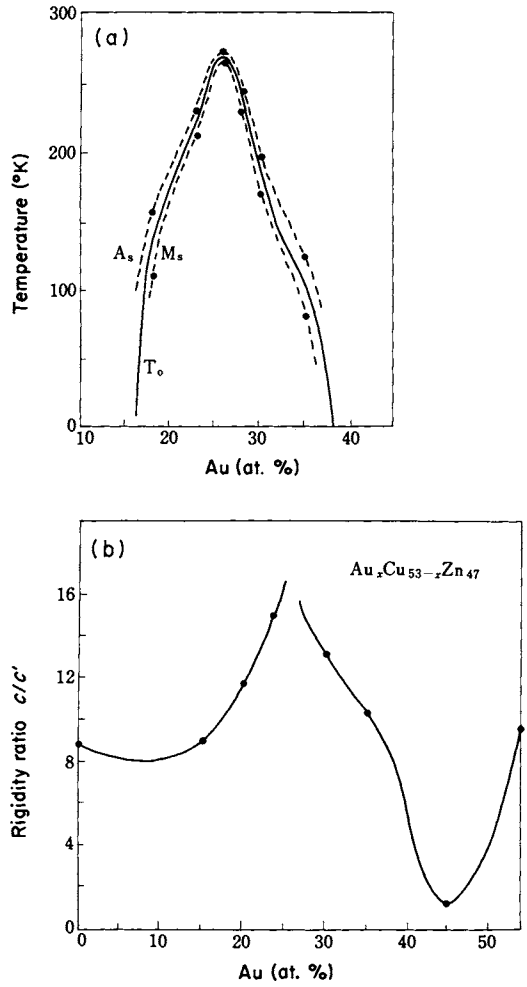

FIG. 6.42 Change in the properties of $Au_xCu_{53-x}Zn_{47}$ along with Au content. (a) Transformation temperatures; (b) rigidity ratio. (After Murakami, Asano, Nakanishi, and Kachi.[148,151])

like the M_s and the difference between A_s and M_s is very small in the composition range of about 26 at.% Au. From measurements of elastic constants using an ultrasonic technique, it was found that the elastic anisotropy factor has a very sharp maximum at the gold content corresponding to the maximum transformation temperature.[151] This fact was also confirmed by neutron scattering.[152] These results suggest certain interrelations between elastic anisotropy and martensitic transformation. In principle, however, the elastic anisotropy must be related more directly to $T_0 - M_s$ and $A_s - T_0$, which are measures of the difficulty of deforming for transformation, than to the transformation temperatures M_s, A_s, and T_0. (T_0 is the temperature at which the chemical free energies of austenite and martensite are equal.) Nakanishi[153] reported recently that the magnitude of the shear modulus $\frac{1}{2}(c_{11} - c_{12}) \equiv C'$ becomes very small with decreasing temperature in composition ranges with high elastic anisotropy, which may suggest that the composition dependence of the transformation temperature and the elastic anisotropy should become significant with decreasing temperature. Nakanishi also found a minimum in Debye temperatures obtained by measuring the heat of transformation and a maximum of the elastic anisotropy factor at 26 at.% Au (Fig. 6.42b, where $C \equiv c_{44}$). The energy of deformation on transformation $-(\frac{1}{2})C'(\Delta\varepsilon)^2$ ($\Delta\varepsilon$ denoting the magnitude of deformation in transformation), derived from the minimum value of C', is 5–10 cal/mol, which is remarkably small as compared to the 300 cal/mol characteristic of steels. This small energy gives a satisfactory explanation of the fact that the transformation occurs at a low degree of supercooling.

B. *Au–Cd alloys*

The β phase in Au–Cd alloys has the CsCl-type structure, as described in Section 2.5.4. The temperature dependence of the elastic anisotropy has been determined by Zirinsky[154] and is shown in Fig. 6.43. The abnormally high elastic shear anisotropy increases with decreasing temperature. The anisotropy for 47.5 at.% Cd is larger than that for 50.0 at.% Cd, which suggests that the former is easier to transform if the T_0 temperatures for both alloys are equal. Actually, the M_s temperature of 47.5 at.% Cd is 50°C, which is 30°C higher than that of 50.0 at.% Cd. A similar result has been obtained for Ag–Cd alloys.[155]

Nakanishi[145] calculated the elastic constants of the Au–Cd alloys that he studied and showed that the shear modulus $\frac{1}{2}(c_{11} - c_{12})$ is smaller than c_{44} by a factor of 10 and depends largely on the composition variation, which suggests that the M_s temperature is composition dependent.

Nakanishi and Wayman[156] studied the effect of the addition of a small amount of copper on martensitic transformation behavior in an Au–47.5 at.% Cd. The M_s temperature was lowered by approximately 70°C per

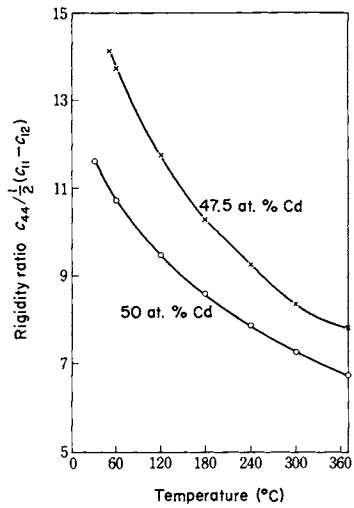

FIG. 6.43 Rigidity ratio of the β phase in Au–Cd alloys. (After Zirinsky.[154])

atomic percent of Cu, and the $A_s - M_s$ difference also decreased. Therefore, the lowering of the M_s temperature may be due to the lowering of T_0, and there are some difficulties in the explanation that it is due to the change in non-Coulomb ionic interactions arising from the substitution of copper atoms, which are smaller than the matrix gold atoms.

In this alloy, martensite forms on slow cooling as well as on rapid cooling, and the M_s temperature is lower in the rapid cooling situation,[157] in which case the elastic anisotropy factor is also small.[146] Rapid cooling introduces vacancies in the crystal lattice and the electron-to-atom ratio changes as if the Cd content had decreased. Therefore, if the contribution of the Fermi energy term is dominant, the elastic anisotropy factor should increase, which is contrary to the experimental result mentioned earlier. Thus in Au–47.5 at.% Cd the contribution of ionic size effects might largely influence its elastic anisotropy.[154]

C. *Li–Mg alloys*

Barrett[158] found that although lithium (b.c.c.) does not transform spontaneously at liquid nitrogen temperature, a transformation can be induced by cold working near this temperature. This transformation may result from lithium's low resistance to a (110) $[1\bar{1}0]$ shear. At lower temperatures a different transformation, into h.c.p., occurs spontaneously. Transformations were also found in a solid solution of magnesium in lithium. The transformation temperature rises with magnesium content, as shown in Fig. 6.44.[159] The elastic anisotropy factors of the alloys derived by Trivisonno and Smith[160] are high and increase with magnesium content from 8.55 for pure

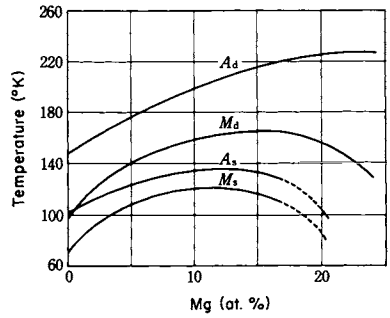

FIG. 6.44 Change of transformation temperatures of β phase in Li–Mg alloys with Mg content. M_d, A_d curves: rolled 60%; M_s, A_s curves: no cold working. (After Barrett and Trautz.[159])

lithium to 8.73 at 4.28 at.% Mg, correlating with the rise in the M_s temperature, thus indicating the important contribution of the elastic anisotropy to the M_s temperature. The curves of M_s and M_d versus Mg content exhibit a maximum at about 12 at.% Mg and then decrease rapidly with Mg content. Further increase in Mg content stops the transformation completely. If this composition dependence of the transformation is caused by a change in elastic properties, the observation may serve as a good example of where the contribution of the Fermi energy[161] to the martensitic transformation is dominant.

Sodium is reported to behave like lithium[162] in undergoing martensitic transformation.

6.7.4 Transformation from h.c.p. structure

The h.c.p.-to-b.c.c. transformation occurs typically on the heating of titanium and zirconium. The orientation relationship in the transformation is that of Burgers, namely

$$(110)_{bcc} \| (0001)_{hcp}, \qquad [1\bar{1}1]_{bcc} \| [11\bar{2}0]_{hcp}.$$

In this orientation relationship, the plane parallelism can also be expressed in the following way:

$$(1\bar{1}2)_{bcc} \| (1\bar{1}00)_{hcp}.$$

The mechanisms of this transformation are believed to be a combination of a shear on a $(1\bar{1}00)_{hcp}$ plane in the $[11\bar{2}0]_{hcp}$ direction and shuffles on a $(0001)_{hep}$ plane. The shear occurs easily when the shear modulus c_{66} is small. The atom shuffles are different from an elastic deformation and hence no correlation with elastic constants can be found.

According to Bullough and Bilby,[163] screw dislocations with the Burgers vector $\frac{1}{2}\langle 11\bar{2}0\rangle$ have different widths, depending on the planes in which they lie:

$$\text{Basal plane} \qquad w_{0001} = \frac{c_0}{2}\Big/\sqrt{A};$$

$$\text{Prismatic plane} \qquad w_{1\bar{1}00} = \frac{4}{3}a_0\sqrt{A};$$

where $A = c_{44}/c_{66}$ is the elastic anisotropy factor for h.c.p. materials. Since a dislocation with a large width can move easily, these equations show that slip on the prismatic plane occurs readily in crystals with a small axial ratio c_0/a_0 and a high elastic anisotropy factor A. The small axial ratio implies a weak bonding of atoms in the basal plane, so that in such a crystal slip on the prismatic planes may occur easily. It can be seen in Table 6.11,[164,165]

TABLE 6.11 Axial ratios, rigidity ratios, and transformation temperatures of various h.c.p. metals[a]

h.c.p. metal	c_0/a_0 (300°K)	$A = c_{44}/c_{66}$ (4°K)	(300°K)	(923°K)	(1123°K)	h.c.p. → b.c.c. transformation temperature (°K)
Cd	1.88	0.542	0.536	—	—	—
Zn	1.86	0.649	0.610	—	—	—
Co	1.623	1.074	1.066	—	—	—
Mg	1.623	0.981	0.971	—	—	—
Re	1.615	0.917	0.937	0.974	0.976	—
Tc	1.60	—	—	—	—	?
Tl	1.590	2.581	2.688	—	—	507
Sc	1.594	—	—	—	—	1608
Zr	1.593	0.829	0.907	1.480	2.000	1135
Gd	1.590	—	—	—	—	1535
Ti	1.587	1.139	1.327	2.103	2.776	1155
Lu	1.583	—	—	—	—	1600
Tb	1.583	—	—	—	—	1583
Ru	1.582	0.972	0.964	0.923	—	—
Hf	1.581	1.034	1.072	—	—	2000
Os	1.579	—	—	—	—	—
Dy	1.574	—	1.000	1.126	—	1670
Y	1.572	1.009	1.018	1.129	—	1760
Tm	1.572	—	—	—	—	1600
Er	1.571	—	1.006	—	—	1600
Ho	1.571	—	—	—	—	1715
Be	1.568	—	—	—	—	1523
Li	1.564	—	—	—	—	70

[a] After Fisher and Renkin[164] and Fisher and Dever.[165]

which lists h.c.p. metals in the order of their axial ratio, that the transformation from h.c.p. to b.c.c. occurs easily in metals whose axial ratio is below 1.60. The elastic anisotropy factors are also high in metals that tend to transform. In zirconium and titanium, transformation occurs at high temperatures, where the elastic anisotropy factor also becomes high.

6.7.5 Role of mechanical properties in the transformation from f.c.c. structure

The martensites of ferrous alloys are mainly produced from f.c.c. structures. The elastic anisotropy is not very remarkable in f.c.c. crystals,† so interrelations between the transformation and the elastic anisotropy are not yet known. The elastic constants, however, have been thought to influence the transformation.

Christian[167] pointed out that the elastic strain energy induced by the nucleation of martensite is proportional to the shear modulus μ. Knapp and Dehlinger[168] also showed the proportionality of the strain energy to μ in their discussion of the transformation in terms of Frank's dislocation model of the γ–α' interface. Fisher[169] derived the proportionality of the interface energy in the transformation to μ on the assumption that the interface energy is mainly due to the energy of screw dislocation cores.

Goldman and Robertson[170] found interrelations between M_s temperatures and elastic constants that were measured in Fe–Ni alloys with additions of Cr, Co, and C. Part of their results are shown in Table 6.12. Although the elastic anisotropy could not be determined for their polycrystalline samples, it is recognized that Young's modulus and the shear moduli are large for materials with low M_s temperatures.

TABLE 6.12 Elastic properties of various iron alloys at the M_s temperature[a]

	M_s (°C)	E (at M_s) (dyn/cm^2)	$\frac{1}{E}\frac{dE}{dT}$ (%/°C)	μ (at M_s) (dyn/cm^2)	$\frac{1}{\mu}\frac{d\mu}{dT}$ (%/°C)
Fe–31.3% Ni–5.7% Co	−15	1.30×10^{12}	+0.06	0.52×10^{12}	+0.18
Fe–30% Ni	−30	1.67×10^{12}	+0.03	0.65×10^{12}	+0.08
Fe–25.1% Ni–0.26% C	−56	1.83×10^{12}	−0.03	0.75×10^{12}	−0.05
Fe–11.7% Ni–15.1% Cr	−58	2.10×10^{12}	−0.03	0.84×10^{12}	−0.06

[a] After Goldman and Robertson.[170]

† Although f.c.c. metals have no appreciable elastic anisotropy, they tend to be easily transformed due to the increase in the amplitude of thermal vibration at temperatures near their M_s point. This is suggested by the experimental fact[166] that, in an Fe–27% Ni alloy, the peak intensity in the Mössbauer absorption spectrum of the austenite increases abnormally upon approaching the alloy's M_s temperature.

Since the magnitudes of tensile and yield stresses have a correlation with the magnitude of the elastic modulus, they can serve as a reference to the present problem. Breinan and Ansell[171] found a linear dependence of M_s temperatures on tensile and yield stresses for a wide variety of compositions in eight kinds of steel, and concluded that M_s temperatures are low and transformations difficult for high-strength materials. The changes in M_s temperatures they noted may reflect in some measure the changes in T_0 temperatures. As described in Section 5.7.3, Ankara[172] showed, in an Fe–30% Ni alloy, that a higher austenitizing temperature results in a high M_s temperature and low yield stress. In this case a low yield stress contributes to a rise in the M_s temperature by lowering the energy necessary for introduction of the complementary shear during transformation.

Also, in In–Tl alloys that are f.c.c. but quite different in character from iron alloys, $\frac{1}{2}(c_{11} - c_{12})$ becomes abnormally small near the transformation temperature. This was found by measurement of the elastic constants[173] and the absorption of supersonic waves.[174] At those temperatures mechanical softening occurs, too.

6.8 Conclusions—Problems for study

As discussed throughout this book, the martensitic transformation is the product of a rearrangement of atoms by cooperative movement, which implies a change in the shape of the crystal lattice. The phenomenological theory originates from the view that plastic deformations are necessary for the martensitic transformation in order to maintain the interface between martensite and the parent matrix, the habit plane, as an invariant plane. Although some problems remain to be solved by the theory, it has fulfilled its role as a tool with which to explain a number of experimental results after some modifications have been made.

The phenomenological theory, however, should not be overestimated. The orientation relationships in the transformation are very important. Since these relationships are believed to have greater influence than an invariant plane at the beginning of transformation, they should also maintain their effects during the growth stage of martensite plates. In the particular case of crystals that grow in rod shape, the direction of the rod should be a rational direction in the parent crystals. Therefore, a more satisfactory theory will be established on the basis of orientation relationships by introducing the invariant-plane hypothesis, after care is taken to select relationships that have good theoretical justification.

Another problem involves the detailed structure of the interface between the martensite and the parent matrix. A part of the interface may be com-

posed of configurations, such as Frank dislocations, but there may remain some unknown structures. If the source of embrittlement in martensite lies in such an unknown region, the problem is serious and of practical importance. Besides theoretical studies to solve this problem, further experimental work may make a significant contribution if the highest resolution of the electron and field ion microscopes are used.

Intimate correlations between the transformation start temperature M_s and elastic anisotropy were discussed in Section 6.7. However, since the lattice deformation accompanying the transformation greatly exceeds ordinary elastic deformation, a completely satisfactory explanation cannot be obtained by a consideration of only the correlation with the elastic shear moduli. There remains the question how to include the effect of deformation beyond Hooke's law. On the other hand, complementary shears can occur with dislocation motions, so they must depend on the Peierls force. How does the Peierls force influence the transformation behavior if the motion of perfect dislocations accompanies the motion of transformation dislocations? Progress in understanding the origin of the M_s temperature is expected through studies of the problems just presented.

Particular structures, such as the close-packed layer structures described in Chapters 2 and 3, arise from the cooperative motion of atoms in the martensitic transformation. The layer structures are usually metastable. Although the raison d'être for such structures has been examined by electron theory in a way similar to the studies of ordered lattices and long-period structures, consideration of the evolved relations relative to transformation mechanisms is yet to appear. Therefore a review of such studies is not included in this book, but the further development of electron theory is definitely expected to include transformation mechanisms.

The martensitic transformation in nonmetallic substances has not been reviewed in this book.

Although the martensitic transformation occurs by the rearrangement of atoms by cooperative motion, some atoms involved in the transformation may move independently. There remains the question how to combine the cooperative motions with the independent movements of atoms in the theoretical treatment of the transformation. If we succeed in answering this question and in including more detailed crystallographic observations in the thermomechanical and kinematic treatment, a more complete theory of martensitic transformations will have been established.

References

1. B. A. Bilby and J. W. Christian, Inst. Metals Monograph and Rep. No. 18, p. 121 (1955).
2. J. W. Christian, *J. Inst. Met.* **84**, 386 (1955/56).

3. J. K. Mackenzie, *J. Aust. Inst. Met.* **5**, 90 (1960).
4. B. A. Bilby and J. W. Christian, *J. Iron Steel Inst.* **197**, 122 (1961).
5. P. M. Kelly, Iron Steel Inst. Spec. Rep. 86, p. 146 (1964).
6. C. M. Wayman, "Introduction to the Crystallography of Martensitic Transformations." Macmillan Series in Material Science, New York, 1964.
7. J. W. Christian, Iron Steel Inst. Spec. Rep. 93, p. 1 (1965).
8. J. W. Christian, "The Theory of Transformations in Metals and Alloys," Pergamon, Oxford, 1965.
9. C. M. Wayman, The crystallography of martensitic transformations in alloys of iron *Adv. Mater. Res.* **3**, 147 (1968).
10. J. W. Christian, Inst. Metals Monograph and Rep. No. 33, p. 129 (1969).
11. E. C. Bain, *Trans. AIME* **70**, 25 (1924).
12. R. Hultgren and C. A. Zapffe, *Nature (London)* **142**, 395 (1938).
13. Ye. N. Vlasova and T. P. Sapozhkova, *Fiz. Met. Metalloved.* **30**, 980 (1970).
14. A. Kussmann and G. G. v. Rittberg, *Z. Mettallkd.* **41**, 470 (1950).
15. T. Tadaki and K. Shimizu, *Trans. JIM* **11**, 44 (1970).
16. Z. Nishiyama, K. Shimizu, and M. Harada, *Trans. JIM* **11**, 152 (1970).
17. T. Tadaki, K. Shimizu, and T. Watanabe, *Trans, JIM* **12**, 386 (1971).
18. H. Kubo and K. Hirano, *J. Jpn. Inst. Met.* **37**, 400, 516 (1973).
19. G. V. Kurdjumov and G. Sachs, *Z. Phys.* **64**, 325 (1930).
20. Z. Nishiyama, *Sci. Rep. Tohoku Univ.* **23**, 637 (1934); **25**, 79 (1936).
21. H. Shoji, *Z. Kristallogr.* **77**, 381 (1931).
22. Z. Nishiyama, *Sci. Rep. Tohoku Univ.* **25**, 79 (1936).
23. W. G. Burgers, *Physica* **1**, 561 (1934).
24. L. I. Lysak and B. I. Nikolin, *Fiz. Met. Metalloved.* **21**, 873 (1966).
25. A. B. Greninger and A. R. Troiano, *Trans. AIME* **145**, 289 (1941); **185**, 590 (1949).
26. J. S. Bowles, *Acta Crystallogr.* **4**, 162 (1951).
27. E. S. Machlin and M. Cohen, *Trans. AIME* **191**, 1019 (1951).
28. D. S. Lieberman, *Acta Met.* **6**, 680 (1958).
29. M. S. Wechsler, T. A. Read, and D. S. Lieberman, *Trans. AIME* **218**, 202 (1960).
30. M. A. Jaswon and J. A. Wheeler, *Acta Crystallogr.* **1**, 216 (1948).
31. J. S. Bowles and J. K. Mackenzie, *Acta Metall.* **2**, 129, 224 (1954).
32. J. K. Mackenzie and J. S. Bowles, *Acta Metall.* **2**, 138 (1954).
33. J. K. Mackenzie and J. S. Bowles, *Acta Metall.* **5**, 137 (1957).
34. R. P. Reed and R. E. Schramm, *J. Appl. Phys.* **40**, 3453 (1969).
35. M. S. Wechsler, D. S. Lieberman, and T. A. Read, *Trans. AIME* **197**, 1503 (1953).
36. M. S. Wechsler and H. M. Otte, *Acta Metall.* **7**, 793 (1959).
37. M. S. Wechsler and H. M. Otte, *Acta Metall.* **9**, 117 (1961).
38. A. G. Crocker, *Acta Metall.* **10**, 113 (1962).
39. D. S. Lieberman, M. S. Wechsler, and T. A. Read, *J. Appl. Phys.* **26**, 473 (1955).
40. D. S. Lieberman, T. A. Read, and M. S. Wechsler, *J. Appl. Phys.* **28**, 532 (1957).
41. H. M. Ledbetter, *Scr. Metall.* **4**, 931 (1970).
42. M. W. Burkart and T. A. Read, *Trans. AIME* **197**, 1516 (1953).
43. H. M. Otte, *Scr. Metall.* **2**, 365 (1968).
44. H. M. Otte, *Trans. AIME* **218**, 342 (1960).
45. J. W. Christian, *Acta Metall.* **6**, 377 (1958); **7**, 218 (1959).
46. B. Ia. Liubov and A. L. Roitburd, *Sov. Phys.—Tech. Phys.* **3**, 659 (1958).
47. L. Kaufman, *Acta Metall.* **7**, 216 (1959).
48. J. S. Bowles and J. K. Mackenzie, *Acta Metall.* **10**, 625 (1962).
49. H. M. Otte, *Acta Crystallogr.* **16**, 8 (1963).

50. J. K. Mackenzie, Unpublished.
51. A. G. Crocker and B. A. Bilby, *Acta Metall.* **9**, 678, 992 (1961).
52. R. P. Reed, *Acta Metall.* **15**, 1287 (1967).
53. D. P. Dunne and C. M. Wayman, *Acta Metall.* **19**, 425 (1971).
54. A. R. Entwisle, "The Mechanism of Phase Transformations in Metals," p. 315. Inst. Metals, 1956.
55. A. G. Crocker, "Numerical Results on Martensite Crystallography," Vol. 1. Deposited at Sheffield Univ. Library, 1961.
56. A. G. Crocker, *Acta Metall.* **13**, 815 (1965).
57. E. O. Hall, "Twinning and Diffusionless Transformations in Metals." Butterworths, London, 1954.
58. D. S. Lieberman and R. Bullough, *Phys. Status Solidi* **12**, 657 (1965).
59. D. S. Lieberman, *Acta Metall.* **14**, 1723 (1966).
60. C. M. Wayman, J. E. Hanafee, and T. A. Read, *Acta Metall.* **9**, 391 (1961).
61. A. G. Crocker and N. D. H. Ross, Inst. Metals Monograph No. 33, p. 176 (1969).
62. N. D. H. Ross and A. G. Corcker, *Scr. Metall.* **3**, 37 (1969); *Acta Metall.* **18**, 405 (1970).
63. A. F. Acton and M. Bevis, *Mater. Sci. Eng.* **5**, 19 (1969).
64. F. J. Schoen and W. S. Owen, *Scr. Metall.* **5**, 351 (1971).
65. A. J. Morton and C. M. Wayman, *Acta Metall.* **14**, 1567 (1966).
66. N. F. Kennon and J. S. Bowles, *Acta Metall.* **17**, 373 (1969).
67. E. J. Efsic and C. M. Wayman, *Trans. AIME* **239**, 873 (1967).
68. H. Morikawa, K. Shimizu, and Z. Nishiyama, *Trans. JIM* **9**, 317 (1968).
69. N. F. Kennon, *Acta Metall.* **20**, 5 (1972).
70. G. Krauss and W. Pitsch, *Arch. Eisenhüttenwes.* **35**, 667 (1964).
71. P. G. McDougall and J. S. Bowles, *Acta Metall.* **12**, 779 (1964).
72. S. Jana and C. M. Wayman, *Metall. Trans.* **1**, 2815, 2825 (1970).
73. E. Scheil and E. Saftig, *Arch. Eisenhüttenwes.* **28**, 49 (1957).
74. T. Bell and R. G. Bryans, *Met. Sci. J.* **5**, 135 (1971).
75. L. I. Lysak and S.A. Artemyuk, *Fiz. Met. Metalloved.* **31**, 70 (1971).
76. L. I. Lysak and E. A. Rybakova, *Fiz. Met. Metalloved.* **32**, 334 (1971).
77. J. S. Bowles and D. P. Dunne, *Acta Metall.* **17**, 677 (1969).
78. J. S. Bowles and D. P. Dunne, *Acta Metall.* **17**, 201 (1969).
79. C. M. Wayman, *Acta Metall.* **9**, 912 (1961).
80. D. P. Dautovich and J. S. Bowles, *Acta Metall.* **20**, 1137 (1972).
81. L. I. Lysak, S. A. Artemyak, and E. A. Rybakova, Ordena Lenina Akademiya Nauk USSR, Inst. Metallofiziki, 70.3 (1970).
82. V. M. Yershov and N. L. Oslon, *Fiz. Met. Metalloved.* **33**, 215 (1972).
83. J. W. Christian, *Proc. Roy. Soc.* **206**, 51 (1951).
84. F. C. Frank, *Rep. Conf. Strength of Solids, Bristol* p. 46 (1948).
85. T. R. Anantharaman and J. W. Christian, *Phil Mag.* **43**, 1338 (1952).
86. G. Leibfried, *Z. Phys.* **126**, 790 (1950).
87. F. R. N. Nabarro, *Proc. Roy. Soc.* **A209**, 278 (1951).
88. W. Bollmann, *Acta Metall.* **9**, 972 (1961).
89. A. Seeger, *Z. Metallkd.* **44**. 247 (1953).
90. A. H. Cottrell and B. A. Bilby, *Phil. Mag.* **42**, 573 (1951).
91. H. Bibring, F. Sebilleau, and C. Bückle, *J. Inst. Met.* **87**, 71 (1958/59).
92. M. A. Jaswon, *Int. Un. Crystallogr. Congr. 3rd* (1954); Inst. Metals Monograph and Rep. Series No. 18, p. 173 (1955).
93. A. J. Bogers and W. G. Burgers, *Acta Metall.* **12**, 255 (1964).
94. G. B. Olsen and M. Cohen, *J. Less-Common Met.* **28**, 107 (1972).

95. H. Suzuki, *Sci. Rep. Tohoku Univ.* **A6**, 30 (1954).
96. C. G. Dunn, F. W. Daniels, and M. J. Bolton, *Trans. AIME* **188**, 368 (1950).
97. D. G. Stein and J. R. Low, Jr. *J. Appl. Phys.* **31**, 362 (1960).
98. F. C. Frank, *Acta Metall.* **1**, 15 (1953).
99. B. A. Bilby and F. C. Frank, *Acta Metall.* **8**, 239 (1960).
100. M. Doi and Z. Nishiyama, *Mem. Inst. Sci. Ind. Res. Osaka Univ.* **11**, 153 (1954).
101. J. N. Nye, *Acta Metall.* **1**, 153 (1953).
102. B. A. Bilby, Defect in crystalline solids, *Phys. Soc. Bristol Conf.* p. 123 (1954).
103. B. A. Bilby, R. Bullough, and E. Smith, *Proc. Roy. Soc.* **A231**, 263 (1955).
104. B. A. Bilby and E. Smith, *Proc. Roy. Soc.* **A236**, 481 (1956).
105. B. A. Bilby, R. Bullough, L. R. T. Gardner, and S. Smith, *Proc. Roy. Soc.* **A244**, 538 (1958).
106. R. Bullough and B. A. Bilby, *Proc. Phys. Soc.* **B69**, 1276 (1956).
107. H. M. Otte and T. A. Read, *J. Met.* **9**, 412 (1957).
108. R. P. Reed, U. S. Dept. of Commerce, Nat. Bur. of Std. Rep. No. 9256 (1966); *Acta Metall.* **14**, 1392 (1966); **15**, 1082 (1967).
109. A. B. Greninger and A. R. Troiano, *Trans. AIME* **140**, 307 (1940).
110. J. F. Breedis and C. M. Wayman, *Trans. AIME* **224**, 1128 (1962).
111. G. Krauss and W. Pitsch, *Trans. AIME* **233**, 919 (1965).
112. H. M. Otte, *Acta Metall.* **8**, 892 (1960).
113. A. Kochendörfer and G. Otto, *Arch. Eisenhüttenwes.* **30**, 227 (1957).
114. G. Wassermann, *Mitt. K-W-I Eisenforsch.* **17**, 149 (1935).
115. R. F. Mehl and G. Derge, *Trans. AIME* **125**, 482 (1937).
116. E. J. Efsic and C. M. Wayman, *Trans. AIME* **239**, 873 (1967).
117. M. Watanabe and C. M. Wayman, *Metall. Trans.* **2**, 2229 (1971).
118. J. S. Bowles and A. J. Morton, *Acta Metall.* **12**, 629 (1964).
119. H. M. Otte and T. A. Read, *Trans. AIME* **209**, 412 (1957).
120. K. A. Johnson and C. M. Wayman, *Acta Crystallogr.* **16**, 480 (1963).
121. R. F. Mehl and D. M. van Winkle, *Rev. Métall.* **50**, 465 (1953).
122. K. Shimizu, M. Oka, and C. M. Wayman, *Acta Metall.* **9**, 1 (1971).
123. P. Krauklis and J. S. Bowles, *Acta Metall.* **17**, 997 (1969).
124. R. Brook and A. R. Entwisle, *J. Iron Steel Inst.* **203**, 905 (1965).
125. F. X. Kayser, *Scr.* Metall. **5**, 1105 (1971).
126. L.-C. Chang and T. A. Read, *Trans. AIME* **191**, 47 (1951).
127. R. P. Zerwekh and C. M. Wayman, *Acta Metall.* **13**, 99 (1965).
128. Z. Nishiyama, K. Shimizu, and M. Harada, *Trans. JIM* **11**, 152 (1970).
129. Z. Nishiyama and K. Shimizu, *Kinzoku Butsuri* **2**, 71 (1956).
130. M. Oka and C. M. Wayman, *Trans. ASM* **62**, 820 (1969).
131. H. Tas, R. V. Krishnan, and L. Delaey, *Scr. Metall.* **7**, 183 (1973).
132. J. A. Klostermann, Inst. Metals Monograph Rep. No. 33, p. 143 (1969).
133. J. A. Klostermann, *J. Less-Common Met.* **28**, 75 (1972).
134. N. Nakanishi, Mem. Kōnan Univ., Sci. Ser. No. 15, Art. 77 (1972).
135. W. D. Robertson, *Iron Steel Inst. Spec. Rep.* **93**, 26 (1965).
136. C. Zener, *Phys. Rev.* **71**, 846 (1947); "Elasticity and Anelasticity of Metals," p. 37 *Univ. of Chicago Press*, 1943.
137. D. Lazarus, *Phys. Rev.* **74**, 1726 (1948); **76**, 545 (1949).
138. R. S. Leigh, *Phil. Mag.* **42**, 139 (1951).
139. H. Jones, *Phil. Mag.* **43**, 105 (1952).
140. H. Jones, *J. Appl. Phys.* **23**, 697 (1952).
141. G. Kunze, *Z. Metallkd.* **55**, 277, 307, 405, (1964).

142. G. Leibfried, "Handbuch d. Physik," Vol. VII/1, Kristallphysik, p. 231. Springer-Verlag, Berlin and New York, 1955.
143. R. A. Artman and D. O. Thompson, *J. Appl. Phys.* **22**, 358 (1951).
144. G. M. McManus, *Phys. Rev.* **129**, 2004 (1963).
145. N. Nakanishi, *Trans. JIM* **6**, 222 (1965).
146. H. Pops and T. B. Massalski, *Acta Metall.* **15**, 1770 (1967).
147. N. Nakanishi, Y. Murakami, and Y. Kachi, *Jpn. J. Appl. Phys.* **4**, 544 (1965).
148. Y. Murakami, H. Asano, N. Nakanishi, and Y. Kachi, *Jpn. J. Appl. Phys.* **6**, 1265 (1967).
149. N. Nakanishi, H. Takehara, Y. Murakami, Y. Senda, and Y. Kachi, *Jpn. J. Appl. Phys.* **6**, 1341 (1967).
150. N. Nakanishi, Y. Murakami, H. Takehara, Y. Senda, H. Sugiyama, and Y. Kachi, *Jpn. J. Appl. Phys.* **7**, 302 (1968).
151. N. Nakanishi, Y. Murakami, and Y. Kachi, *Scr. Metall.* **2**, 673 (1968).
152. M. Mori and Y. Yamada, Phys. Soc. Japan, Spring Meeting (1972).
153. N. Nakanishi, Y. Murakami, and Y. Kachi, *Scr. Metall.* **5**, 433 (1971).
154. S. Zirinsky, *Acta Metall.* **4**, 164 (1956).
155. D. B. Masson, *Trans. AIME* **218**, 94 (1960).
156. N. Nakanishi and C. M. Wayman, *Trans. AIME* **227**, 500 (1963).
157. M. S. Wechsler and T. A. Read, *J. Appl. Phys.* **27**, 194 (1956).
158. C. S. Barrett, *Phys. Rev.* **72**, 245 (1947).
159. C. S. Barrett and O. R. Trautz, *Trans. AIME* **175**, 579 (1948).
160. J. Trivisonno and C. S. Smith, *Acta Metall.* **9**, 1064 (1961).
161. D. B. Masson, *Acta Metall.* **10**, 986 (1962).
162. C. S. Barrett, *Am. Mineral.* **33**, 749 (1948).
163. R. Bullough and B. A. Bilby, *Proc. Phys. Soc.* **67**, 615 (1954).
164. E. S. Fisher and C. J. Renken, *Phys. Rev.* **135**, 482 (1964).
165. E. S. Fisher and D. Dever, *Trans. AIME* **239**, 48 (1967).
166. Ye. Ye. Yurchikov and A. Z. Men'shikov, *Fiz. Met. Metalloved.* **32**, 168 (1971).
167. J. W. Christian, *Acta. Metall.* **6**, 377 (1958).
168. H. Knapp and U. Dehlinger, *Acta Metall.* **4**, 289 (1956).
169. J. C. Fisher, *Trans. ASM* **47**, 457 (1955).
170. A. J. Goldman and W. D. Robertson, *Acta Metall.* **12**, 1265 (1964).
171. E. M. Breinan and G. S. Ansell, *Metall. Trans.* **1**, 1513 (1970).
172. A. Ankara, *J. Iron Steel Inst.* **208**, 819 (1970).
173. D. B. Novotny and J. F. Smith, *Acta. Metall.* **13**, 881 (1965).
174. N. G. Pace and G. A. Saunders, *Proc. Roy. Soc.* **A326**, 521 (1972).

Author Index

Numbers in parentheses are reference numbers and indicate that an author's work is referred to although his name is not cited in the text. Numbers in italics show the page on which the complete reference is listed.

A

Abdykulova, S. M., 31(83), *125*
Abell, J. S., 123(471), *134*
Abraham, J. K., 18(24), 19, 29(24), 33(91), 115(24), *124*, *126*, 290(204), *333*
Aburai, K., 273(101), 274(101), *330*
Acton, A. F., 383, *441*
Adachi, M., 273(83), *330*
Adams, R., 218(*33*), *258*
Agarwala, R. P., 189, *209*
Ahlers, M., 119(425, 427), *133*
Akshentseva, A. P., 322(313), *335*
Albutt, K. J., 40(124), 115(124), *126*
Allen, E. B., 310(268), *334*
Alperin, H. A., 104(319), *131*
Al'Shevskiy, Yu. L., 163, 200, 201(181), *208*, *210*
Altstetter, C. J., 28(68), 110(347), 115(68), 116(372), *125*, *131*, *132*, 223(54), 218(33), *258*, *259*, 276(111), *331*
Anagnostidis, M., 123(458), *133*
Anandaswaroof, A. V., 243(161), *261*
Anantharaman, T. R., 74(240), 120(437), *129*, *133*, 389(85), *441*
Anderson, D. H., 266(27), *329*
Andrushchik, L. O., 201(183), 202, 203(188), 204(189), 205(193, 194, 195), *210*
Ankara, A., 275(102), 309, *330*, 438, *443*
Ansell, G. S., 38(114), *126*, 322(314, 315, 316), 323(315), *335*, 438, *443*
Aoki, K., 47(143), *127*
Aoyagi, T., 280(163), *332*
Apple, C. A., 187, *209*
Arakawa, K., 221(52), *259*
Araki, T., 309(267), *334*
Arata, Y., 27, *125*, 237(117), *260*
Arbuzov, M. P., 144(22, 23), 154, *206*, *207*
Arbuzova, I. A., 277, 279(158), *331*, *332*
Arima, H., 57, 116(172), *127*
Arimoto, T., 41(133), 42(133), *126*
Armitage, W. K., 73(232), 117(232), *129*
Artemyuk, S. A., 204(190), 205(195), *210*, 385(75), 387(81), *441*
Artman, R. A., 431(143), *443*
Asano, H., 97, 120(293), *130*, 432(148), *443*
Au, Y. K., 278(146), *331*
Averbach, B. L., 17(12), 51(155), 60(193), 115(12), 116(155, 193), *124*, *127*, *128*, 137(9), 139(9), *206*, 239(137), 240(142, 154), 241(154), *261*, 266(15), 272(70), 293(215), 294(215), *329*, *330*, *333*
Ayers, J. D., 119(426), *133*, 232(99), *260*, 277(127), *331*

B

Backofen, W. A., 68(221), *128*
Bacon. G. E., 111(355), 112, *131*
Bain, E. C., 269(44), 322(44), *329*, 338, *440*
Baker, C., 117(404), *132*
Balasubramanian, V., 90(271), 119(271), *129*
Ball, A., 120(438), *133*

Bancroft, D., 265, *329*
Bando, Y., 286(195), 287(196), *332*
Banerjee, B. R., 226(66), *259*
Banerjee, S., 74(236), 118(236), *129*
Banks, E., 74(237), *129*
Baranova, G. K., 287, *332*
Barantserva, I. G., 144(23), *207*
Barrett, C. S., 66(217), 67(217), 97(290), 108(343), 109(343), 117(375), 118(396, 398, 400), 120(431), 122(343), 123(466, 472, 473), *128*, *130*, *131*, *132*, *133*, *134*, 232(95), *260*, 276, 298, *331*, *333*, 396, 434(159), 435(162), *443*
Barrett, W. J., 283(185), *332*
Barton, C. J., 29(77), 115(77), *125*
Barton, J. W., 117(387), *132*
Baschwitz, R., 123(458), *133*
Basinski, Z. S., 110(344), 111(349), 118(395), *131*, *132*, 172, 173(103), 177, *208*, 238(123), *261*, 264(4), 277(129), *328*, *331*
Bassett, J. B., 228(74), *259*
Bassett, W. A., 265(8), *328*
Bassett, W. J., 302(255), *334*
Bassi, G., 119(424), *133*
Bastien, P., 60(194), 116(194), *128*, 237(118), *260*
Batterman, B. W., 123(461, 466), *133*, *134*
Beaudier, Mlle J., 122(457), *133*
Beisswenger, H., 235, *260*
Belko, V. N., 280(169), *332*
Bell, T., 18(19), 19(19), 32(86), 115(19), *124*, *125*, 160, *208*, 226(64), *259*, 385(74), *441*
Benedicks, C., 175, *208*
Berdova, V. S., 321, *335*
Berkowitz, A. E., 303, *334*
Berman, H. A., 104(332), *131*
Bernshteyn, M. L., 299(238), 302(257), *333*, *334*
Bertaut, F., 60(199), 116(199), *128*
Beshers, D. N., 206(201), *210*
Betteridge, W., 177(119), *209*
Bever, M. B., 276(120, 123), 277(124), *331*
Bevis, M., 36(103), 38(112), 115(103), *126*, 383, *441*
Bibby, M. J., 219, 220(49), 221, 225(49), *259*
Bibring, H., 48(151), 49(150), 116(150, 151), *127*, 231(93), 238(122), *260*, *261*, 390(91), *441*
Bickerstaffe, J., 33(94), *126*
Bilby, B. A., 29(79), 116(79), *125*, 337(1, 4, 5), 377, 378, 380(51), 389, 402(99), 404, 405, 407(102, 103, 104), 409(106), 416, 436, *439*, *440*, *441*, *442*, *443*
Birchon, D., 280(166), *332*
Birnbaum, H. K., 120(443, 444), *133*, 177(110), *208*
Biswas, M. G. A., 40(123), 115(123), *126*
Blackburn, L. D., 66(215), *128*, 266(21), *329*
Blackburn, M. J., 73(234), *129*, 273(85), *330*
Bogachev, I. N., 33(90), 57(180, 181), 60(190, 191), 115(90), 116(180, 181, 189), 126, *128*, 229(88), 247(171), *260*, *262*, 272(73), 325(329, 330, 331, 332), 328(339), *330*, *336*
Bogers, A. J., 23(47), 115(47), *125*, 391, *441*
Bollmann, W., 389, *441*
Bokros, J. C., 25, *125*, 273(98), 275(106), *330*
Boku, R., 121(451), *133*
Bolling, G. F., 270(53), 293, *329*
Bolton, J. D., 310, *334*
Bolton, M. J., 396(96), *442*
Bolton, P., 301(252), *334*
Borodina, N. A., 313(283), 316(283), *335*
Bose, B. N., 18(17), 19(17), 115(17), *124*
Bover, M. B., 232(96), *260*
Bowden, H. G., 27, *125*, 192, *209*
Bowe, R. C., 287(198), *332*
Bowles, J. S., 28(74), 39(121), 68(222), 95(282), 108(343), 109, 117(222), 118(392), 119(282), 122(343), *125*, *126*, *128*, *130*, *131*, *132*, 345, 357(31, 32, 33), 362, 377, 383, 384, 385, 386(78), 387, 414(33), 417, 418, *440*, *441*, *442*
Bowman, F. E., 123(469), *134*
Bradley, A. J., 119(409), *132*
Bragg, W. L., 161, *208*
Braun, M., 212(9), *258*
Breedis, J. F., 23(43), 65(208), 115(43), 116(207, 208), *124*, *128*, 271(61, 62), 272, 273(86), 293, 294(218), 320, 321, *330*, *333*, *335*, 412(110), 413, *442*
Breinan, E. M., 438, *443*
Brettschneider, J., 85(256), *129*, 268(43), *329*
Bridgman, P. W., 273(88), *330*
Brook, R., 25(54), 47(54), *125*, 241(159), *261*, 419(124), *442*
Brookes, M. E., 121(445, 447), *133*, 232(100, 101), *260*
Brown, A. R. G., 117(402), *132*
Brown, L. C., 101(302), 120(302, 433), *130*, *133*, 273(81, 82), 276(122), *330*, *331*
Brown, N., 169, *208*, 266(29), *329*

Bryans, R. G., 385, *441*
Buchler, W. J., 101, 102(314), 104(326, 333), *130*, *131*, 278(136), *331*
Buckley, J. I., 120(436), *133*
Bückle, C., 390(91), *441*
Bühler, H. E., 182(137), *209*
Bullough, R., 380, 407(103, 105), 409(106), 436, *441*, *442*, *443*
Bundy, F. B., 264(6), *328*
Bunshah, R. F., 234, 235, 237, *260*
Burgers, W. G., 27, 67(219), 117(219) *125*, *128*, 237(119), *260*, 272(66), *330*, 343, 344, 391, *440*, *441*
Burkart, M. W., 110(345), *131*, 176, *208*, 273(90), 277(128), *330*, *331*, 375(42), *440*
Burkhanov, A. M., 299(237), *333*
Bush, R. H., 273(98), *330*
Butakova, E. D., 180(130), *209*, 240(149), 244(149), *261*, 289(207), 291, *333*
Butcher, B. R., 122(455), *133*
Butler, E. P., 111(350), 123(350), *131*
Butler, S. R., 101(305), 104(325, 330, 334), *130*, *131*
Bywater, K. A., 117(379), *132*

C

Cabane, G., 122(457), *133*
Cahn, J. W., 21(34), 115(34), *124*, 265(14), 266(14), 267, *329*
Cahn, R. W., 117(375), *132*
Campbell, E., 17, *124*
Capus, J. M., 161(67), *208*
Carapella, L. A., 229(86), *260*
Carlile, S. J., 177(118), *209*
Carnahan, D. E., 21(35), 115(35), *124*
Caron, R. N., 325(325), *335*
Castleman, L. S., 97, *130*
Cech, R. E., 239(131), 240(145), 242, *261*, 286, *332*
Chambers, F., 287(198), *332*
Chandra, K., 101(307), *130*
Chang, L.-C., 98(300), 120(300, 441), *130*, *133*, 174, 175, 176, *208*, 239(126), *261*, 278(138), *331*, 421(126), *442*
Chaudhuri, D. K., 149(32), *207*
Chen, C. W., 90(274), 119(274, 416), *130*, *133*, 273(90), 276(116), *330*, *331*
Chevenard, P., 226, *259*
Chikazumi, S., 301(247), *334*
Chilton, J. M., 29(77), 115(77), *125*
Chipman, J., 212(11), *258*
Chiswik, H. H., 228(72), *259*
Chormonov, A. B., 236(114), *260*
Chou, C. H., 220, *259*
Christian, A. L., 143(20), *206*
Christian, J. W., 15(3), 51(152), 110(344), 111(349), 117(379, 384), 118(384), *124*, *127*, *131*, *132*, 172, 173(103), 177(118), *208*, *209*, 238(123), *261*, 277(129), *331*, 337(1, 2, 4, 7, 8, 10), 365(2), 376(45), 389(85), 395(8), 414, 437, *439*, *440*, *441*, *443*
Christou, A., 192, *209*, 266(29), *329*
Chumakova, L. D., 327(335, 336), 328(338, 339), *336*
Chuprakova, N. P., 267(36), *329*
Cina, B., 57(171), 64, 116(171, 192, 203), *127*, *128*
Clark, A. F., 280(172), *332*
Clark, C. A., 228(68), *259*
Clark, D., 117(402), *132*
Clifton, D. F., 118(398), *132*
Clough, W. R., 322(314), *335*
Clougherty, E. V., 212(10), *258*, 264(5), *328*
Cocks, F. H., 123(462), *134*
Cohen, M., 17(12, 13), 20, 31, 51(155), 60(193), 66(215), 115(12, 13, 29, 81), 116(155, 193), *124*, *125*, *127*, *128*, 162(78), 169(95), 180(131), 189(154), 190, 191, *208*, *209*, 211(1), 212(6), 213(6), 214(24), 216(24), 218(37), 225(6), 227(6), 235, 239(128, 129, 130, 132, 133, 134, 135, 137), 240(129, 142, 154), 241(154, 156), 243, 256(24), 257(6), *258*, *259*, *260*, *261*, 265(10), 266(15, 21), 270, 271, 272(70), 273(77), 275(104), 283(189), 284, 288, 289, 293, 294, 311(272), 316(287, 292), 324(322), *328*, *329*, *330*, *332*, *333*, *334*, 345, 391, 412(27), 413, *440*, *441*
Collette, G., 57(174), 116(174), *127*
Colling, D. A., 325(326), *335*
Colombie, M., 123(458), *133*
Cood, I., 40(123), 115(123), *126*
Cornelis, I., 103, *130*, 149, *207*, 277(133), *331*
Cornelius, H., 322, 323, *335*
Cottrell, A. H., 389, *441*
Cottrell, C. L. M., 219(38), *259*
Coutsouradis, D., 229(89), *260*
Crocker, A. G., 29(79), 116(79), 123(471), *125*, *134*, 368(38), 377, 378(55), 379, 380(51), 381(62), 382, 383, 384(61), 417, *440*, *441*

Crussart, C., 57(174), 116(174), *127*, 240, 256, *261*, *262*, 270(49), 275(107), 316(290), *329*, *330*, *335*

D

Dahlgren, S. D., 67(218), *128*
Damask, A. C., 164(86), 165, *208*
Daniels, F. W., 396(96), *442*
Danil'yenko, V. Ye., 204(191), *210*
Darinskii, B. M., 280(169, 170), *332*
Darken, L. S., 212(4), 213(4, 15), *258*
Das, B. K., 113, 114(360), 123(359), *131*
Das, S. K., 33, 37(88), 38(88), 115(88), *125*, *126*
Dasarathy, C., 312(279), 313(279, 284), 316(284), *334*, *335*
Das Gupta, S. C., 240(143), *261*
Dash, J., 65, 66, 116(209, 210), *128*
Dash, S., 169, *208*
Dautovich, D. P., 104(331, 336), *131*, 387, *441*
Davies, R. G., 25, *125*
Davis, R. S., 265(7), *328*
Debrunner, P., 158(59), *207*
Dedieu, J. M. B., 60(194), 116(194), *128*
Dehlinger, U., 217, 243, *258*, 437, *443*
de Jong, M., 273(97), *330*
Delaey, L., 85(257, 258, 259), 86(262), 102, 115(262), 119(258, 259), 120(257), *129*, *130*, 149, *207*, 426, *442*
de Lamotte, E., 276(111), *331*
deLange, R. C., 278(148), *331*
Della Gatta, G., 21(30), 115(30), *124*
DePasquali, G., 158(59), *207*
Derge, G., 23(40), 24(40), 115(40), *124*, 414(115), *442*
De Savage, B. F., 102(314), 104(326, 333), *130*, *131*
Desch, C. H., 43, *127*
Dever, D., 436(165), *443*
Dienes, G. J., 164(86), 165, *208*, 281, *332*
Dieter, G. E., 188, *209*
Digges, T. G., 225(59), *259*
Dijkstra, D. J., 160, *208*
Divnon, I. I., 265(9), *328*
Dörnen, P., 22(37), 28(37), 115(37), *124*
Doi, M., 44(139), 45(139), *127*, 153(45), 154, *207*, 407, *441*
Dolgunovskaya, O. D., 302(257), *304*
Dolzhanskij, P. R., 299(238), *333*
Donachic, S. J., 322(316), *335*
Donahoe, F. J., 303, *334*
Donzé, G., 278(149), *331*
Douglass, D. L., 123(459), *133*
Drachinskaya, A. G., 199, 200(175), 206, *210*
Dragsdorf, R. D., 52(161), 116(151), *127*
Drickamer, H. G., 158(59), *207*
Dührkop, J., 53(166), *127*
Duggin, M. J., 89(267), 119(415), 120(267, 430), *129*, *133*
Dunn, C. G., 396(96), *442*
Dunne, D. P., 31(82), 115(365), *125*, *132*, 279(153), *332*, 378(53), 383, 385, 386(78), 387, 418, *441*
Duwez, P., 219(39), 221, 231(39), *259*

E

Eastabrook, J., 117(402), *132*
Easterling, K. E., 291, 292(211), *333*
Edge, C. K., 158(59), *207*
Edmondson, B., 316(291), 324(321), *335*
Edwards, L. R., 268, *329*
Edwards, O. S., 51(153, 154), 116(153, 154), *127*
Efsic, E. J., 116(362), *131*, 384(67), 414, 416, *441*, *442*
Eichelman, G. H. Jr., 229(80, 87), 231(80), *260*
Eilender, W., 220(46), *259*
Eliasz, W., 241(157), *261*, 299(242), 300, *334*
Ellis, F. V., 273(78), *330*
Ellis, W. C., 49(148), *127*
Enami, K., 121(449), *133*, 177(121, 122), *209*, 278(144, 145), 279, *331*, *332*
Engel, N., 220(45), 221, *259*
Entin, R. I., 224(56), 228(75), *259*
Entwisle, A. R., 25(54), 28(69), 47(54), 115(69), *125*, 239(127), 240(151, 153), 241(159), 247, 248(177), *261*, *262*, 287(199), 288, 307, 308, *332*, *334*, 378(54), 419(124), *441*, *442*
Erikson, R. H., 71(225), 73(233), 117(225, 233, 380), *128*, *129*, *132*
Ernst, D. W., 104(320), *131*
Eshelby, J. D., 164(82), *208*
Esser, H., 220(46), *259*, 322, 323, *335*
Éstrin, É. I., 265(13), 275(105), 299(235), 318(296, 297, 298, 299), 319(299) 321(304), *329*, *330*, *333*, *335*

F

Faber, V. M., 33(90), 115(90), *126*
Fahr, D., 273(99), *330*
Faivre, R., 278(149), *331*
Fakidov, I. G., 299(230, 231, 237, 239, 244), 301(249), *333*, *334*
Fallot, M., 66(214), 67, *128*
Fearon, E. O., 36(103), 38, 115(103), *126*
Feeney, J. A., 248(177), *262*, 273(85), 307, 308, *330*, *334*
Ferraglio, P., 97, *130*
Fiedler, H. C., 60(193), 116(193), *128*, 293, 294, *333*
Filonchik, G. M., 299(230), *333*
Finbow, D., 113(356), *131*
Fink, W., 17, 115(7), *124*
Fisher, E. S., 436(164, 165), *443*
Fisher, J. C., 165, *208*, 212(3), 214(18, 25), 217, *258*, 270(48), *329*, 437, *443*
Fisher, R. M., 220(50), 221, *259*
Flanagan, W. F., 67(218), *128*
Fletcher, S. C., 239(137), 240(142), *261*
Flinn, P. A., 155(58), 158, 159, *207*
Förster, F., 25, *125*, 233(106), 234, 249(178), *260*, *262*
Fokina, Ye. A., 299(232, 233, 236, 240, 243), 301(253), 302(253, 254), *333*, *334*
Fowler, C. M., 266(26), *329*
Frank, F. C., 15(2), *124*, 216, *258*, 389(84), 399, 402(99), 404, 405, 406, *441*, *442*
Franklin, A. D., 303, *334*
Frauenfelder, H., 158(59), *207*
Fraunberger, F., 270(51), *329*
Fujime, S., 51(158), 52(158), 116(158), *127*
Fujishiro, S., 71, 117(226), *129*
Fujita, F. E., 155(54, 55, 56, 57), 156(57), 157(54, 55, 56, 57), 158(54, 55, 56, 57), 159, 205, *207*, *210*
Fujita, H., 149(33), 150, 167, 168, *207*, *208*
Fujita, M., 266(30), 267(39), *329*
Fukai, S., 231(92), *260*
Fullman, R. L., 288(202), *333*
Funabashi, M., 205, *210*
Furrer, P., 74(240), 120(437), *129*, *133*
Furuya, K., 315, 316(285), *335*

G

Gaggero, J., 169(98), *208*
Gaidukov, M. G., 283(184), *332*
Garber, R. I., 280(168), *332*
Garber, S., 40(124), 115(124), *126*
Gardner, L. R. T., 407(105), *442*
Garwood, R. D., 90(273), 119(273, 399), *130*, *132*
Gaunt, P., 51(152), 111(354), 112, 113(356), 117(384), 118(384), 123(354), *127*, *131*, *132*
Gavrilyuk, V. S., 279(158), *332*
Gawranek, V., 80(248), *129*
Gefen, Y., 97(298), *130*
Gegel, H. L., 71, 117(226), *129*
Geisler, A. H., 117(374), *132*
Geneste, J., 60(199), 116(199), *128*
Genevray, R. M., 276(120), *331*
Genin, J.-M. R., 155(58), 158, 159, *207*
Georgiyeva, I. Ya., 245(165), 246(168), *261*, *262*, 296, *333*
Gielen, P. M., 155(52), 159, *207*
Gilbert, A., 212(7, 8), 220(7, 47), 224, *258*, *259*
Gilbert, R. W., 74(238), *129*
Giles, P. M., 265, *329*
Gilfrich, J. V., 278(136), *331*
Glover, S. G., 313 (281), 316(281, 293), 320(281), *334*, *335*
Goebel, J. A., 121(448), *133*
Goland, A. N., 164(84), 165, *208*
Goldman, A. J., 65, 116(211), *128*, 140(12), 142(17), *206*, 218(34), *259*, 437, *443*
Golikova, V. V., 41, *126*, 229(83), 230(83), *260*, *293*, *333*
Golovchiner, Ya. M., 324(319, 320), *335*
Gomersall, D. W., 228(76), *259*
Gonchar, V. N., 229(83), 230(83), *260*
Goncharenko, I. B., 197(169), *210*
Gooch, T. G., 294, 295, *333*
Goodtzow, N., 17, 115(8), *124*
Gorbach, V. G., 31(83), *125*, 180(126, 130), *209*
Goringe, M. J., 123(467), *134*
Gotos, H. C., 266(20), 267(40), *329*
Goux, C., 180, 181, *209*
Govila, R. K., 119(422), 420(428, 429), *133*
Goykhenberg, Yu. N., 28(64), *125*, 214(21), 229(85), *258*, *260*
Graham, R. A., 192(160), *209*, 266(27), 267(41), *329*
Grange, R. A., 163(79), *208*, 225(61), *259*
Granik, G. I., 299(238), 302(257), *333*

Greiner, E. S., 49(148), *127*
Grenga, H. E., 39(117), *126*
Greninger, A. B., 16, 24, 28(66), 29(48), 91(277), 115(48, 66), 119(407), *124*, *125*, *130*, *132*, 150(36), *207*, 225(60), 228(72), 239(125, 136), *259*, *261*, 276(118), 311(274), *331*, *334*, 344, 345(25), 347, 397, 398, 404, 412(109), 415(109), 416, 417, *440*, *442*
Grewen, J., 180(129), *209*
Gridnev, V. N., 226, *259*
Grünbaum, E., 283(181), *332*
Guentert, O. J., 140(13), 141, 144(13), *206*
Guimarães, J. R. C., 271(64), 293(214), 295, 315(214), *330*, *333*
Gulysev, A. P., 322(313), *335*
Guntner, C. J., 272, *330*
Gupta, S. P., 102(310), 105, *130*
Gust, W. H., 266(31), *329*
Guttman, L., 108(343), 109(343), 110(340), 122(340, 343), *131*
Guy, A. G., 15(5), *124*

H

Habraken, L., 51(159), 116(159), *127*, 229(89), *260*
Habrovec, F., 184, *209*
Hachisuka, T., 324, *335*
Hälbig, H., 183(138), *209*
Härter, D., 97(299), 119(299), *130*
Hagen, J., 108(341), 122(341), *131*
Hagiwara, H., 92(281), 119(281), *130*
Hagiwara, I., 272(65), 322, *330*, *335*
Haines, H. R., 248(173), *262*
Hall, E. O., 379(57), *441*
Hammond, C., 70(224), 73(224), 117(224, 403), *128*, *132*
Hanada, S., 320, 324(323), *335*
Hanafee, J. E., 24, 115(49), *125*, 381(60), *441*
Hanak, J. J., 123(461, 465), *133*, *134*
Hanemann, H., 225(58), *259*
Hanneman, R. E., 266(20), 267(40), *329*
Hanlon, J. E., 101(305), 104(325, 330, 334), *130*, *131*
Hans v. Klitzing, K., 57(179), 116(179), *127*
Harada, M., 40(126), *126*, 342(16), 424(128), 425, *440*, *442*
Harris, W. J., Jr., 241(156), *261*, 316(287), *335*
Harvey, J. S., 266(18), *329*
Hashiguchi, R., 104(324, 328), *131*
Hato, H., 273, 274, *330*
Hauser, J. J., 226(66), *259*
Hawkes, M. F., 18(17), 19(17), 115(17), *124*
Haworth, W. L., 226(63), *259*
Hayashi, K., 276(112), *331*
Hayes, A. G., 229(81), *260*
Hedley, J. A., 111(348), *131*
Hehemann, R. F., 102(313), 104(321, 322), *130*, *131*, 278(147), *331*
Heider, F., 326, *336*
Henry, G., 18(22, 23), 19, 115(22, 23), *124*, 291(206), *333*
Herring, C. P., 119(426), *133*, 232(99), *260*, 277(127), *331*
Hess, J. B., 298, *333*
Heumann, T., 110(346), 123(346), *131*
Higgins, G. T., 74(237), *129*
Higo, Y., 272(68), 315, 316(285), *330*, *335*
Higuchi, S., 286, 287, *332*
Hillert, M., 214(23), 256, *258*, *262*
Hilliard, J. E., 265(14), 266(14, 33), 267, *329*
Hirano, K., 342, 384, *440*
Hirayama, T., 270(50), 271(63), 294, 297, *329*, *330*, *333*
Hirone, T., 233, *260*
Hirose, H., 159, *207*
Hirsch, P. B., 37(108), *126*
Hoff, W. D., 120(435, 442), *133*
Hofman, W., 22(37), 28(37), 115(37), *124*
Holden, A. N., 248(172), *262*
Holland, J. R., 192(160), *209*, 266(27), *329*
Hollomon, J. H., 214(18), 240(145), 242, 243(160), *261*
Honda, K., 17(10), 115(10), *124*, 322(309), *335*
Honeycombe, R. W. K., 56, 57(175, 176), 116(175, 176), *127*, 276(110), *331*
Honjo, G., 77, 78(246), 86(265), 87(265), 115(265), 119(265), *129*
Honma, T., 25(51, 52), 29(51), 33, 50, 51(149), 104, 107(339), 116(149, 368), *125*, *126*, *127*, *131*, *132*, 232(102), 236, 237, 238, 249(104), *260*, 271(57), 272(57, 74), 282(176), 292, *329*, *330*, *331*
Honnorat, Y., 18(22, 23), 19, 115(22, 23), *124*, 291(206), *333*
Hopkins, E. N., 116(370), *132*
Hori, T., 111(352, 353), 123(353), *131*

Horiuchi, T., 102(315), 107(315), *130*, 328(340), *336*
Hornbogen, E., 21(32), 115(32), *124*, 188, *209*, 276(119, 121), 289, 290, *331*, *333*
Hosler, W. R., 102(314), 104(326, 333), *130*, *131*
Hosoi, Y., 270(52), *329*
Houdremont, E., 256(182), *262*
Houska, C. R., 51(155), 116(155), *127*
Hovi, V., 118(393), *132*
Howie, A., 37(108), *126*
Hu, H., 180(124), *209*
Huang, Y.-C., 231(91, 92), *260*
Huizing, R., 282, *332*
Hull, D., 90(273), 96(288), 119(273, 288, 399, 421), *130*, *132*, *133*, 169(98), *208*
Hull, F. C., 229(80, 87), 231(80), *260*
Hultgren, R., 339(12), *440*
Hume-Rothery, W., 177(118), *209*, 264(4), *328*
Hummel, R. E., 277(125, 126), 285, *331*, *332*

I

Ibaragi, M., 40, 41, 115(128), *126*
Ibrahim, E. F., 241(159), *261*
Ichijima, I., 220(43), *259*
Iguchi, N., 184, *209*
Il'ina, V. A., 154(48, 49), *207*
Imai, Y., 18(16), 19(16), 40(122), 56, 57(177, 178), 60, 115(16, 122), 116(173, 177, 178, 200), *124*, *126*, *127*, *128*, 214, 220(51), 221, 222, 223, 224, 225, 227, 228, 229, 240(148, 150), 243, 244(148), 245, 247, *258*, *259*, *261*, 306(264), 311(276), 317(295), 320, 324, *334*, *335*
Inagaki, Y., 177(122), *209*, 278(145), *331*
Ino, H., 155(54, 55, 56), 156(57), 157(54, 55, 56), 158(54, 56), 159, 160, 205, *207*, *210*
Inokuti, Y., 160, *208*
Inoue, T., 8(1), 12, *13*
Irie, T., 205, *210*
Isaitschev, I., 86(264), 115(264), 119(264, 419), *129*, *133*, 150(35), *207*
Ishida, K., 229(84), 230(84), *260*
Ishiwara, T., 52(162), 116(162), *127*
Ivanov, A. G., 265(9), *328*
Iwasaki, H., 120(440), *133*
Iwasaki, K., 104(324, 328), *131*
Iwase, K., 322(309), *335*
Iyer, K. J. L., 229(79), *260*
Izmaylov, Ye. A., 31(83), *125*, 180(126), *209*
Izotov, V. I., 39(120), 41, 48, 115(144), *126*, *127*, 236(114), 245, *260*, *262*
Izumiyama, M., 18(16), 19(16), 40(122), 60, 115(16, 122), 116(200), *124*, *126*, *128*, 214, 220(51), 221, 222, 223, 224, 225, 227, 228, 229, 240(148, 150), 243, 244(148), 245, 247, *258*, *259*, *261*, 283(188), 284, 306(264), 311, 312(188), 313, 317(295), 320, 324, *332*, *334*, *335*

J

Jack, K. H., 18(14), 19(14), *124*
Jaffee, R. I., 273(84), *330*
Jana, S., 186, *209*, 384, 387, *441*
Jaswon, M. A., 137(3, 6), *206*, 281(175), *332*, 355(30), 390(92), *440*, *441*
Jellinghaus, W., 266(23), *329*
Jellison, J., 80(251), *129*
Jepson, K. S., 117(402), *132*
Jepson, M. D., 240(141), *261*
Johannson, C. H., 212(2), 213(2), *258*
Johari, O., 37(109), 115(109), 117(388), *126*, *132*
Johnson, A. A., 102(310), 105, *130*
Johnson, K. A., 417(120), *442*
Johnson, P. C., 265(7), *328*
Johnson, R. A., 159(60), 164(86), 165, *207*, *208*
Johnson, R. T., 52(161), 116(161), *127*
Jolley, W., 119(421), *133*
Jones, F. W., 214(17), *258*
Jones, H., 428(139, 140), 429, 430(139, 140), 431(139), *442*
Jones, K. C., 239(127), *261*
Jones, P., 119(409), *132*
Jones, W. K. C., 247, *262*
Jovanović, M., 232(101), *260*

K

Kachi, Y., 97(294), 120(293, 294), *130*, 278(141, 142), 286, 287, *331*, *332*, 432(147, 149, 150), 433(151, 153), *443*
Kajiwara, S., 78(247), 80(252), 82, 83, 84, 86(261), 97, 116(369), 119(252, 260), *129*, *130*, *132*, 147(28), 148(28, 29, 30), 149(30,

Kajiwara (*cont.*)
33, 34), 150(37, 38, 39), 151(40, 41, 42), *207*, 275(108), *331*
Kakinoki, J., 85(254), 104(338), 121(338), *129*, *131*, 145, 147(28), 148(28), *207*
Kamada, A., 47(142), *127*
Kamenetskaya, D. S., 225, *259*
Kaminsky, E., 80(248), 86(264), 115(264), 119(264), *129*, 150(35), *207*
Kanazawa, S., 272(65), 322, *330*, *335*
Kaneko, H., 231(91), *260*
Kaneko, Y., 283, *332*
Kanibolotskij, V. G., 216(28), *258*
Kaplow, R., 155(52), *207*
Kasper, J. S., 76(244), 86(244), 87(244), *129*
Katagiri, S., 37(107), *126*
Kato, T., 283(182), *332*
Kaufman, L., 66(215), *128*, 211(1), 212(6, 10), 213(6), 214(19), 218(37), 219(41), 225(6), 227(6), 239(130), 257(6), *258*, *259*, *261*, 264(3, 5), 266(18, 21, 24), 271, *328*, *329*, 376(47), *440*
Kawachi, K., 278(139), *331*
Kawakami, Y., 270(52), *329*
Kawanaka, R., 33(99), *126*
Kayser, F. X., 420(125), *442*
Keating, D. T., 164(84), 165, *208*
Keller, K. R., 123(465), *134*
Kellerer, H., 273(93), *330*
Kelly, P. M., 27, 28(73, 75), 38(73, 113), 56(169), 65, 70(224), 73(224), 111(350), 115(75, 113), 116(75, 169, 367), 117(224), 123(350), *125*, *127*, *128*, *130*, *131*, *132*, 192, *209*, 337(5), *440*
Kennedy, G. C., 264(2), *328*
Kennon, N. F., 95(282), 96(285), *130*, 383, 384, *441*
Kessler, H., 182, 183(138), 184(136, 141, 145), 185, *209*
Khachaturyan, A. G., 151, 162(77), 205, *207*, *208*, *210*
Khandarov, P. A., 236(114), 245(166, 167), *260*, *261*, *262*
Khandros, E. L., 200(173), *210*
Khandros, L. G., 90(272), 91(279), 119(272, 418, 420), *130*, *133*, 177(112), 203, 204, *208*, *210*, 276, 277(132), 279(158), *331*, *332*
Kharitonova, Zh. F., 280(168), *332*
Khayutin, S. G., 177(114, 115), *208*, 277(130), *331*
Kidin, I. N., 181, *209*
Kidron, A., 155(53), *207*
Kikuchi, M., 283, *332*
Kimmich, H., 235, *260*
Kimura, M., 311, *334*
King, H. W., 74(239), 108, 120(434), 122(342), 123(460, 462), *129*, *131*, *133*, *134*
Kingery, W. D., 15(4), *124*
Kinsman, K. R., 317(294), *335*
Kiseleva, K. V., 123(463), *134*
Kitchingman, W. J., 120(435, 436, 442), *133*, 299(228), *333*
Kittl, J. E., 119(413, 414), *133*
Klement, E., 270(51), *329*
Klier, E. P., 80(251), *129*, 267(35), 322(312), *329*, *335*
Klostermann, J. A., 27, *125*, 237(119, 120), *260*, 282, *332*, 426, *442*
Klyachko, Yu. A., 287, *332*
Knapp, H., 217, 243, *258*, 437, *443*
Ko, T., 313(280), 316(280), 324(321), *334*, *335*
Koch, C. C., 116(371), *132*, 299(227), *333*
Kochendörfer, A., 23(42), 115(42), *124*, 271(58), 272(58, 69), *329*, *330*, 414(113), *442*
Kogan, L. 1., 224(56), 228(75), *259*
Koger, J. W., 277(125), 285(192), *331*, *332*
Kogirima, M., 270(50), 294, 297, *329*, *333*
Kohlhaas, R., 212(9), *258*
Kohn, A., 57(174), 116(174), *127*
Koistinen, D. P., 241(158), *261*
Komar, A. P., 117(389), *132*
Komissarova, M. L., 142(14), *206*
Komura, Y., 145, *207*
Kondo, M., 324, *335*
Kondrat'yev, S. P., 201(182), 205, *210*
Kononenko, V. L., 193(165), *210*
Koskimaki, D., 101(304), 104(337), *130*, *131*
Koss. D. A., 65, 116(211), *128*
Kossowsky, R., 325(326), *335*
Kosterman, J. A., 272(66), *330*
Kot, R. A., 275(103), *330*
Kotval, P. S., 276(110), *331*
Koul, M. K., 273(86), *330*
Kounicý, J., 184, *209*
Koval', Yu. M., 203, 204, *210*
Kozlovskaya, V. J., 187(152), *209*
Krauklis, P., 418, *442*
Krauss, G., 28(70), 31(84), 37(110), 115(70, 84, 110), *125*, *126*, 180(131), 183, 184(140), 187, *209*, 323, 324(322),

325(325), *335*, 384(70), 412(111), *441*, *442*
Krauss, G. Jr., 180(127), *209*, 283(189), 284, 324, *332*
Kremer, G., 283(181), *332*
Krên, E., 113(357), 123(357), *131*
Krisement, O., 256(182), *262*
Krishnan, R., 74(236), 118(236), *129*
Krishnan, R. V., 101(302), 120(302), *130*, 273(81, 82), *330*, 426, *442*
Kritskaya, V. K., 154(48, 49), *207*
Krivoglaz, M. A., 164(87), 165, *208*, 299(234), *333*
Krovobok, V. N., 52(164), 116(164), *127*
Kubo, H., 342, 384, *440*
Kulin, S. A., 235, 240(144), *260*, *261*, 266(19, 32), 273(77), *329*, *330*
Kumada, A., 322, *335*
Kumar, R., 90(271), 119(271), *129*, 229(78), *259*
Kunze, G., 96(284), 97(284), 119(284), *130*, 428(141), 430(141), *442*
Kuporev, A. L., 177(112), *208*
Kurdjumov, G. V., 22(36), 80(248), 86(263, 264, 266), 115(36, 263, 264, 266), 119(264, 266), 120(263), *124*, *129*, 145, 150(35), 154(48, 49), 163, 200, *207*, *208*, *210*, 240(138, 139, 140), 242, *261*, 276(117), 277, 296, *331*, *333*, 342, 343, *440*
Kurdumoff, J., 17, 115(8), *124*
Kurumchina, S. Kh., 66(212), 115(212), *128*
Kussmann, A., 302(258), *334*, 339(14), *440*
Kutumbarao, V. V. P., 279(155), *332*

L

Lacoude, M., 180, 181, *209*
Lacroisey, F., 272(75), *330*
Lähteenkorva, E. E., 28(67), 115(67), *125*, 235, *260*
Lagneborg, R., 65, 116(204), *128*, 294(217), *333*
La Mori, P. N., 264(2), *328*
Lange, H., 271(59), *330*
Langeron, J. P., 117(390, 391), *132*
Larikov, L. N., 193(165), *210*
Lazarus, D., 427(137), 431(137), *442*
Lebedinskiy, V. S., 101(306), 104(306), *130*
Lecroisey, F., 272(68), *330*
Ledbetter, H. M., 36(105), 97(296), 115(105), 121(446), *126*, *130*, *133*, 375(41), 376(41), 422(41), *440*
Lee, C. S., 73(231), 117(231), *129*
Lee, E. D., 117(388), *132*
Lefever, I., 86(262), 115(262), *129*
Lehmann, J., 122(454), *133*
Lehr, P., 117(390, 391), *132*
Leibfried, G., 389(86), 428(142), *441*, *443*
Leigh, R. S., 428(138), 429, *442*
Lement, B. S., 240(143), *261*
Lenoir, G., 48(151), 116(151), *127*, 231(93), 238, *260*
Leslie, W. C., 188, 189(154), 190, 191, *209*, 283(187), 284, *332*
Lesoille, M., 159, *207*
Levin, Yu. N., 280(170), *332*
Leyenaar, A., 266(18), *329*
Lieberman, D. S., 113, 114(360), 123(359), *131*, 175(108), *208*, 220, *259*, 273(90), *330*, 347(28, 29), 363(35), 368(35, 39), 375(39, 40), 380, 406(35), 416(35), 421(39), *440*, *441*
Lipson, H., 51(153, 154), 116(153), *127*, 154, *207*
Litvinov, V. S., 121(450), *133*
Liu, Y. C., 117(381, 385), *132*
Liu, Y. H., 214(22), *258*
Liubov, B. Ia., 376(46), *440*
Lizunov, V. I., 38(114), *126*, 181, *209*, 322(315), 323, *335*
L'nianoi, V. N., 187(150), *209*
Lobodyuk, V. A., 90(272), 91(279), 119(272, 420), *130*, *133*, 277(132), *331*
Löhberg, K., 153(46), *207*
Lomer, W. M., 122(456), *133*
Longenbach, M. H., 265, *329*
Loree, T. R., 266(26), *329*
Lorris, S. G., 272(70), *330*
Low, J. R. Jr., 272(72), 281, *330*, *332*, 399(97), *442*
Lucas, F. F., 43, *134*
Lucci, A., 21(30), 115(30), *124*
Luo, H. L., 108, 122(341), *131*
Lyman, T., 311(277), *334*
Lysak, L. I., 57, 58, 116(170, 184), *127*, *128*, 144, 154, 193(162, 165), 194, 195, 196(163, 164), 197(167, 169), 199, 200(175, 176, 179), 201(182, 183), 202(184, 185), 203(186, 188), 204(190, 191), 205(193, 194, 195), 206, *206*, *207*, *210*, 326(334),

Lysak (*cont.*)
327, *336*, 343(24), 385(75, 76), 387, *440*, *441*
Lyubov, B. Ya., 217, 252, *258*, *262*

M

McDougall, P. G., 28(73), 39(121), *125*, *126*, 384, *441*
McHargue, C. J., 116(371), 117(373), 123(470), *132*, *134*, 299(227), *333*
Machlin, E. S., 31, 115(81), 117(383), *125*, *132*, 214(24), 216(24, 30), 239(128, 129), 240(129), 256(24), *258*, *261*, 275(104), *330*, 345(27), 412(27), 413, *440*
Mackenzie, J. K., 68(222), 117(222), *128*, 337(3), 357(31, 32, 33), 362, 377, 414(33), *440*, *441*
McManus, G. M., 431(144), *443*
McMillan, J. C., 73(230), 117(230, 377), *129*, *132*
McReynolds, A. W., 269(45), *329*
Maeda, Y., 155(54, 57), 156(57), 157(54, 57), 156(57), 157(54, 57), 158(54, 57), *207*
Mäntysalo, E., 118(393), *132*
Magee, C. L., 25, *125*, 238(124), *261*
Mailfert, R., 123(461), *133*
Maki, T., 41(130, 131, 133), 42, 49, 104 (338), 121(338), *126*, *131*, 273, 274, 295, 296, 309, *330*, *333*, *334*
Makogon, Yu, N., 196(166), 197(167), *210*, 328(337), *336*
Maksimova, O. P., 240(138, 139, 140), 242, 246(168), *261*, *262*, 275(105), 285, 296 (223), 314, 315, 318(296, 297), *330*, *332*, *333*, *335*
Malinen, P. A., 299(241, 243, 245, 246), 300(241), 301(245, 248, 253), 302(256), 303, *333*, *334*
Malinov, L. S., 60(190), *128*, 247(171), *262*, 272(73), 325(329, 331),), 327(335, 336), 328(338), *330*, *336*
Malyshev, K. A., 240(149), 244(149), *261*, 279(157), 289(207), 291, 313(283), 316(283), *332*, *333*, *335*
Mance, A., 248(175), *262*
Manenc, J., 18(22, 23), 19, 115(22, 23), *124*, 291(206), *333*
Mangonon, L., Jr., 65, 116(205), *128*
Marcinkowski, M. J., 101(304), 104(327, 337), 116(370), *130*, *131*, *132*
Marder, A. R., 28(70), 31(84), 115(70, 84), *125*, 265, *329*
Margolin, H., 117(385), *132*
Martburger, R. E., 241(158), *261*
Martin, D. L., 118(394, 401), *132*
Massalski, T. B., 74(239), 97(290), 119(413, 423), 120(434, 439), *129*, *130*, *133*, 232(97), *260*, 431(146), 434(146), *443*
Masson, D. B., 118(397), 119(422), 120(429, 431, 432), *132*, *133*, 433(155), 435(161), *443*
Masumoto, H., 48, *127*
Mathews, J. A., 322(307), 324(307), *335*
Mathias, B., 177(120), *209*
Mathiew, K., 311(275), *334*
Matsuda, A., 311, *334*
Matsuda, S., 8(1), 12, *13*
Matsumoto, M., 104, 107(339), *131*, 232(102), *260*
May, G. H., 122(453), *133*
Mazur, J., 137(4, 5, 7), *206*
Medvedev, S. A., 123(463), *134*
Mehl, R. F., 23(40), 24(40), 28(65), 115(40, 65), *124*, *125*, 234, 235, 237, *260*, 414(115), 417(121), *442*
Melandri, B. A., 20(28), 115(28), *124*
Melkui, Z., 104(331), *131*
Ménard, J., 60(196), 116(196), *128*
Men'shikov, A. Z., 244(163), *261*, 301(248), *334*, 437(166), *443*
Merriam, M. F., 108, 122(341), *131*
Messler, R. W., Jr., 38(114), *126*, 322(315, 316), 323, *335*
Meyer, L., 123(472), *134*
Meyer, W., 289, 290, *333*
Meyerson, M. R., 283(186), *332*
Mihajlovic, A., 248(175, 176), *262*
Miller, R. L., 283(187), 284, *332*
Miller, T. M., 96(285), *130*
Milshailov, V. V., 123(463), *134*
Minato, Y., 279, *332*
Minchall, S., 265, *329*
Miner, R. E., 20(25), 115(25), *124*
Minervina, Z. V., 76, *129*
Miodownik, A. P., 241(157), *261*, 299(229, 242), 300(242), 301(252), *333*, *334*
Miretskii, V., 86(266), 115(266), 119(266), *129*
Mirmelshtein, V. A., 313(283), 316(283), *335*
Miroshnichenko, F. D., 216(28), *258*, 299, *334*
Mirzayev, D. A., 28(64), *125*, 197(170), *210*, 214(21), 223, 229(85), *258*, *259*, *260*

Mitani, H., 80(249), 119(417), *129*, *133*
Miura, S., 278(141, 142), *331*
Miwa, Y., 184, *209*
Miyagi, M., 66(213), 67, 115(366), *128*, *132*
Miyahara, S., 233, *260*
Mizushima, S., 220(43), *259*
Mohanty, G. P., 273(78), *330*
Mooradian, V. G., 91(277), *130*, 239(125), *261*, 276(118), *331*
Morgan, E. R., 313(280), 316(280), *334*
Mori, M., 280(171), *332*, 433(152), *443*
Mori, N., 182, *209*
Mori, T., 272(68), 278(142), 315, 316(285), *330*, *331*, *335*
Morikawa, H., 91(276, 278, 280), 92, 93, 94(276), 96, 119(276), *130*, 384, *441*
Morikawa, S., 62, 63, 64, 116(202), *128*
Moriya, T., 155(54, 55, 56), 156(57), 157(54, 55, 56), 158(54, 55, 56), 159(61, 62), 205(196, 197), *207*, *210*
Morozov, O. P., 28(64), *125*, 223, *259*
Morton, A. J., 383(65), 417(65), 418, *441*, 417, *442*
Moss, S. C., 166, *208*
Mott, B. W., 248(173), *262*
Mouturat, P., 122(457), *133*
Müller, H. G., 271(58), 272(58), *329*
Müller, J., 279(162), *332*
Mukherjee, K., 97, 102(310), 105, *130*
Muldaver, L., 287(198), *332*
Murakami, Y., 72, 97(294), 117(228), 120(293, 294), *129*, *130*, 278(141, 142, 143), *331*, 432(147, 149, 150), 433, *443*
Murayama, A., 96, 119(287), *130*
Murry, G., 18(23), 19, 115(23), *124*

N

Nabarro, F. R. N., 389(87), *441*
Nagakura, M., 316(288), *335*
Nagakura, S., 283, *332*
Nagasawa, A., 101(303), 102, 104, 105(309), 120(303), 121(309, 338), *130*, *131*, 278(134, 139), 279(156), *331*, *332*
Nagashima, S., 286, *332*
Nagy, E., 113(357), 123(357), *131*
Nagy, I., 113(357), 123(357), *131*
Nakagawa, H., 59(187), 68(220), 69, 70, 71, 72(229), 73, 116(187), 117(220, 229, 386), *128*, *129*, *132*
Nakagawa, Y., 111(352, 353), 123(353), *131*
Nakajima, K., 311, *334*
Nakamura, H., 297, *333*
Nakamura, M., 315, 316(285), *335*
Nakamura, T., 273(80), *330*
Nakanishi, M., 295, 296, *333*
Nakanishi, N., 80(249, 250), 92(281), 97(293, 294), 119(281, 410, 417), 120(293, 294), *129*, *130*, *132*, *133*, 278(141, 142), *331*, 426(134), 431(145), 432(148, 151), 433(151), *442*, *443*
Naklimov, D. M., 143(19), *206*
Nel'Nikov, L. A., 267(37), *329*
Nelson, R. D., 123(469), *134*, 273(89), *330*
Nembach, E., 123(468), *134*
Nemirovskiy, V. V., 28(71), 115(71), *125*, 285, 296(223), 314, 315, *332*, *333*
Nenno, S., 121(449, 451), *133*, 177(121, 122), *209*, 278(144, 145), 279, *331*, *332*
Nesterenko, Ye. G., 145, 154(50), *207*
Neuhäuser, H. J., 46, 47, *127*
Newkirk, J. B., 117(374), *132*, 291(209), *333*
Nicolaides, P., 229(89), *260*
Niedzwiedz, S., 155(53), *207*
Nikitina, I. I., 245(165, 166), *261*
Nikolin, B. I., 57(170), 58, 116(170, 184), *127*, *128*, 193(165), 194, 195, 196(163, 164, 166), 197(167), 202(184), *210*, 326(334), 327, 328(337), *336*, 343(24), *440*
Nilles, J. L., 28(72), *125*
Nishiyama, Z., 17(10), 18(20), 22, 23(38, 46), 25(57), 26, 32(85), 33(96, 97, 99, 100), 37(107), 40(126), 43(138), 44(97, 139), 45(139), 47(142), 49(147), 57, 58, 59(185, 186, 187), 62, 63, 64, 68(220), 69, 70, 71, 72(229), 73, 80(252), 82, 83, 84, 86, 91(278, 280), 92, 93, 94(276), 96(280), 115(10, 38, 46, 100), 116(147, 172, 185, 186, 187, 202), 117(220, 229, 386), 119(252, 260, 276, 287), *124*, *125*, *126*, *127*, *128*, *129*, *130*, *132*, 142(18), 147(28), 148(28), 153(45), 154, 169(96, 97), 178(123), 179, *207*, *208*, *209*, 249, 251(179), 253(181), *262*, 269(46), 283(190), 284, 285, 286, *329*, *332*, 342(16, 20), 343, 384(68), 407, 424(128), 425(129), *440*, *441*, *442*
Nishizawa, T., 229(84), 230(84), *260*
Norman, W., 214, *258*, 266(22), *329*
Novikov, S. A., 265(9), *328*
Novotny, D. B., 438(173), *443*

Nutting, J., 28(75), 38(75, 113), 115(75, 113), 116(75), *125*, *126*
Nye, J. N., 407(101), *442*

O

Odaka, R., 311, 312, 317, 319, *334*
Ogawa, S., 51(158), 52(158), 116(157, 158), *127*, 283(182), *332*
Ogden, H. R., 273(84), *330*
Ogilvie, R. E., 266(20), 267(40), *329*
Ohashi, N., 301(247), *334*
Oizumi, S., 272(74), *330*
Oka, H., 295(222), 296(222), *333*
Oka, M., 39(118, 119), 40(125), 43(125), 55, 59(185, 187), 68(220), 69(220), 70(220), 71(220), 72(229), 73(231), 115(119, 125, 361), 116(168, 185, 187), 117(220, 229, 231, 382, 386), *126*, *127*, *128*, *129*, *131*, *132*, 170(100), 197, 198, *208*, *210*, 417(122), 425, *442*
Okada, M., 27, *125*, 237(117), *260*
Okamoto, H., 32(87), *125*
Okamoto, M., 240(146), *261*, 311, 312(288) 316(288), 317, 319, *334*, *335*
Okamura, T., 233, *260*
Oketani, S., 283(179), *332*
Ölander, A., 175, *208*
Olsen, G. B., 391(94), *441*
Ono, K., 57(182), 116(182), *128*
Onuma, Y., 51(157), 116(157), *127*
Ooka, K., 59, 116(188), *128*
Orr, R. L., 212(11), *258*
Oshima, R., 20(26), 115(26), *124*
Oslon, N. L., 248, *262*, 305(262), 321(306), *334*, *335*, *388*, *441*
Otani, T., 97(291), 119(291), *130*
Otsuka, K., 36(106), 90(270), 91(275), 102, 103, 104, 105, 106, 107(312), 119(268, 269, 270, 275), 121(311, 312), *126*, *130*, 177(111), *208*, 273(79, 80), 277(133), 278(150, 151, 152), *330*, *331*
Otte, H. M., 23(41), 24(41), 60(195), 65, 66, 115(41), 116(195, 209, 210), *124*, *128*, 142(16), 169, *206*, *208*, 368(37), 375(37, 43), 376(44), 377, 412(107), 414(112), 417(119), 421(37, 43, 44), *440*, *442*
Otto, G., 23(42), 24(42), 115(42), *124*, 272(69), *330*, 414(113), *442*
Owen, E. A., 214(22), *258*
Owen, W. S., 18(19), 19(19), 28(72), 32(86), 115(19), *124*, *125*, 160(73), *208*, 212(7, 8), 220(7, 47), 224, *258*, *259*, 383(64), *441*

P

Pace, N. G., 280(167), *332*, 438(174), *443*
Pál, L., 113(357), 123(357), *131*
Pankova, M. N., 245, *262*
Paranjpe, V. G., 214(24), 216(24), 239(128), 256(24), *258*, *261*
Parker, A. M. B., 154, *207*
Parker, E. R., 25(53), *125*, 273(99), 275(106), *330*
Parr, J. Gordon, 104(335), 117(387), *131*, *132*, 218(33), 219, 220(48, 49), 221, 225(49), 226(63), 227(67), 228(70, 76, 77), *259*
Partileyenko, N. V., 293(212), *333*
Pascover, J. S., 18(24), 19(24), 29(24), 33(91), 115(24), *124*, *126*, 266(17), 290(204), *329*, *333*
Pasupathi, W., 285(192), *332*
Patel, J. R., 270, *329*
Pateman, L. W., 272(71), *330*
Pati, S. R., 243, *261*, 288, 289, 311(272), *333*, *334*
Paton, N. E., 68(221), *128*
Patrician, T. J., 36(105), 115(105), *126*
Patterson, A. L., 76(244), 86(244), 87(244), *129*
Patterson, R. L., 26(58), 29, 30, 38, 40, 41, 115(58, 129), *125*, *126*
Patterson, W. R., 111(351), 123(351), *131*
Paul, W., 263(1), *328*
Pavlov, V. A., 279(157), *332*
Payson, P., 228(73), *259*
Pearson, W. B., 17(9), 18(9), 19(9), 115(9), *124*
Peikul, A. F., 299(236), *333*
Peiser, H. S., 272(71), *330*
Pepperhoff, W., 182(137), *209*
Perkins, A. J., 102(313), *130*
Pesin, M. S., 101(306), 104(306), *130*
Petch, N. J., 152, *207*
Peters, C. T., 301(252), *334*
Peterson, E. L., 265(11), *329*
Petrosyan, P. P., 316(289), *335*
Petsche, S., 273(95), *330*
Petty, E. R., 310(268), *334*
Philibert, J., 240, *261*, 275(107), 313(282),

316(282, 290), 321(305), 324(282), *330*, *335*
Pickert, S. J., 101(308), 104(319), *130*, *131*
Piletskaya, T. B., 225(57), *259*
Pineau, A., 272(75), *330*
Pipkorn, D. N., 158(59), *207*
Pitsch, W., 18(18), 19(18), 23(45), 37(110), 46, 47, 115(19, 45, 110), *124*, *125*, *126*, *127*, 182, 183(138, 139), 184(136, 141, 145), 185, 186(139), *209*, 384(70), 412(111), *441*, *442*
Plateau, J., 57(174), 116(174), *127*
Plekhanova, E. A., 66(212), 115(212), *128*
Polishchuk, Yu. M., 199(174), 200(176, 178, 179), 204(189), *210*
Pollock, J. T. A., 108(342), 122(342), 123(462), *131*, *134*
Polonis, D. H., 67(218), 71(225), 73(230, 233), 117(225, 227, 230, 233, 377, 380), *128*, *129*, *132*
Pomey, G., 57(174), 116(174), *127*
Ponyatovskij, E. G., 266(28), 267, *329*
Pope, L. E., 268, 298(225), *329*, *333*
Pops, H., 85(259), 96(286), 119(259, 423, 425, 427), 120(439), *129*, *130*, *133*, 232(97, 98), *260*, 431(146), 434(146), *443*
Porter, L. F., 281, 322(311), *332*, *335*
Postnikov, V. S., 101(306), 104(306), *130*, 280(169), *332*
Potter, D. I., 110(347), *131*
Predel, B., 110(346), 123(346), *131*, 273(91), *330*
Predmore, R. E., 267(35), *329*
Priester, R., 313(281), 316(281), 320(281), *334*
Prokopenko, V. G., 203(188), *210*
Pumphrey, W. I., 214(17), *258*
Purdy, G. R., 101(307), 104(331, 335, 336), 117(387), *130*, *131*, *132*

Q

Quarrell, A. G., 229(78), *259*

R

Rachinger, W. A., 119(415), 120(430), *133*
Radcliffe, S. V., 218(37), *259*, 266(16, 17, 32), 267(34, 38), 268, *329*
Raghavan, V., 239(133, 135), 240(151), 243(161), *261*, 287(199, 200), 288, *332*, *333*
Ramachandran, E. G., 312(279), 313(279, 284), 316(284), *334*, *335*
Rama Rao, P., 279(155), *332*
Ramsdell, L. C., 75, *129*
Ranganathan, B. N., 39(117), *126*
Rashid, M. S., 116(372), *132*
Rathenau, G. W., 273(97), *330*
Ravindran, P. A., 149(32), *207*
Read, T. A., 24(49), 110(345), 115(49), 120(441), *125*, *131*, *133*, 175, 176, 177(110), *208*, 239(126), *261*, 273(90), 277(128), 278(138), *330*, *331*, 347(29), 363(35), 368(35, 39), 375(39, 40, 42), 381(60), 406(35), 412(107), 416(35), 417(119), 421(40, 126), 434(157), *440*, *441*, *442*, *443*
Reed, R. P., 27(61), 28(76), 33(102), 36(105), 60(197), 115(105), 116(76, 197), *125*, *126*, *128*, 272, 280(172), 294(216), *330*, *332*, *333*, 357, 378(52), 412(108), *440*, *441*, *442*
Renken, C. J., 436(164), *443*
Reynolds, J. E., 276(123), *331*
Reynolds, M. B., 272(72), 281, *330*, *332*
Richman, M. H., 39(115, 116), *126*, 169(95), *208*
Richman, R. H., 270(53), 293, *329*
Ridley, N., 236(98), *260*
Ringwood, A. E., 266(24), *329*
Rittberg, G. G. V., 302(258), *334*, 339(14), *440*
Roberts, C. S., 17(11, 12), 115(11, 12), *124*, 160, *208*, 310(270), *334*
Roberts, E. C., 273(93), *330*
Robertson, W. D., 65, 116(207, 211), *128*, 218(34), *259*, 271(61), *330*, 427(135), 437, *442*, *443*
Rodizin, N. M., 299(230), *333*
Rodriguez, C., 119(414), *133*
Roesler, U., 212(13), *258*
Rohde, R. W., 192(160), *209*, 266(25), 267(41), *329*
Roitburd, A. L., 205, *210*, 217, 252, *258*, *262*, 376(46), *440*
Romashev, L. N., 301(249), *334*
Ron, M., 155(53), *207*
Rosen, M., 97(298), *130*
Rosen, S., 121(448), *133*
Rosenberg, S. J., 283(186), *332*
Rosenberg, W., 21(34), 115(34), *124*
Rosenthal, P. C., 322(311), *335*

Roshchina, I. N., 187(152), *209*
Ross, N. D. H., 381(62), 382, 383, 384(61), *441*
Rowe, A. H., 122(455), *133*
Rowland, E. S., 143(20), *206*, 228(74), *259*
Rowlands, P. C., 36(103), 38, 115(103), *126*
Royce, E. B., 266(31), *329*
Rozner, A. G., 104(332), *131*
Ruhl, R. C., 20, 115(29), *124*, 265(10), *328*
Rushchits, S. V., 197(170), *210*
Russel, R. J., 193(161), *209*
Rybakova, E. A., 385(76), 387(81), *441*
Ryš, P., 184(143), *209*

S

Saburi, T., 119(412), 121(451), *133*
Sachs, G., 22(36), 115(36), *124*, 342, 343, *440*
Sadovskij, V. D., 187(149), *209*, 283(184), 299(230, 233, 234, 236, 240, 241, 243, 245), 300(241), 301(245, 253), 302(254, 256), *332*, *333*, *334*
Saftig, E., 228(69), *259*, 385(73), *441*
Sahara, T., 45(140), *127*
Saito, H., 236(113), *260*, 301(251), *334*
Saito, T., 56, 57(177, 178, 183), 116(173, 177, 178, 183), *127*, *128*
Sakamoto, M., 161(68), *208*
Sakanoue, H., 276(113), *331*
Salli, I. V., 187(150), *209*
Sanderson, G. P., 56, 57(176), 116(176), *127*
Sandrock, G. D., 102, 104(321, 322), *130*, *131*
Sapozhkova, T. P., 339(13), *440*
Sarma, D. S., 33(95), *126*
Sasaki, K., 60(200), 116(200), *128*, 240(150), 247, *261*
Sastri, A. S., 101(304), 104(327, 337), *130*, *131*, 306, 307, *334*
Sato, H., 76, 77, 78(246), 85, 86(265), 87, 98(301), 99(100), 115(265), 119(255, 265), 120(301), *129*, *130*, 161, 162, *208*, 212(13), 214(26), 215(26), *258*
Sato, S., 33(97), 44(139), 45(139), 96(287), 97, 117(386), 119(287, 289, 291), *127*, *130*, *131*, 137, 138, 140, 141, 142(15, 18), 143, *206*
Sato, T., 231(92), *260*, 272(74), *330*
Sattler, H. P., 272(67), *330*
Satyanarayan, K. R., 241(157), *261*, 299(229, 242), 300, *333*, *334*
Saunders, G. A., 280(167), *332*, 438(174), *443*
Sauveur, A., 14(1), 43, *124*, *127*, 220, *259*, 273, *330*
Savage, C. H., 228(73), *259*
Sawamura, T., 102(311), 103(311), 104(311), 105(312), 106(311), 107(312), 121(311, 312), *130*, 278(150), *331*
Schastlivtsev, V. M., 29(80), *125*
Schatz, M., 266(32), 267(34), 268, *329*
Schechter, H., 155(53), *207*
Scheil, E., 25, 43, *125*, *127*, 214, 228(69), 233(106), 234, 235, 249(178), *258*, *259*, *260*, *262*, 266(22), 279(159, 161, 162), 280, 316(286), *329*, *332*, *335*, 385(73), *441*
Schenck, H., 240(152), 244(152), *261*
Scherrer, P., 136(1), *206*
Schmerling, M. A., 113, 114(360), 123(359), *131*
Schmidt, O., 266(23), *329*
Schmidt, W., 52(163), 116(163), *127*, 153(46), *207*
Schmidtmann, E., 240(152), 244(152), *261*
Schmiedel, W., 271(59), *330*
Schoen, F. J., 28(72), *125*, 383(64), *441*
Schramm, R. E., 280(172), *332*, 357, *440*
Schreiner, M. E., 39(115), *126*
Schüller, H. J., 182(137), *209*
Schumann, H., 53, 54, 55(167), 56, 57(165), 60(165), 61, 66(216), 116(165, 198, 201), *127*, *128*, 231(90), *260*, 326, *336*
Schwartzkoff, K., 68(223), *128*
Schwoeble, A. J., 160(70), *208*
Sebilleau, F., 48(151), 116(151), *127*, 231(93), 238(122), *260*, *261*, 390(91), *441*
Seeger, A., 389, *441*
Segmüller, A., 21(32), 115(32), *124*, 276(121), *331*
Seith, W., 18(15), 19(15), *124*
Sekhar, P. C., 39(115, 116), *126*
Sekino, S., 182, *209*
Sekito, S., 137(2), *206*, 310, *334*
Seljakov, N., 17, 115(8), *124*
Senda, Y., 432(149, 150), *443*
Shapiro, S., 183, 184(140), *209*
Sharshakov, I. M., 101(306), 104(306), *130*
Shatalov, G. A., 151, *207*
Shevelev, A. K., 20(27), 115(27), *124*
Shibata, K., 309(267), *334*
Shih, C. H., 240(154), 241, *261*
Shilling, J. W., 160(70), *208*
Shimizu, K., 23(46), 25(57), 26, 32(85, 87), 33(97, 99, 100, 101), 34, 35, 36(106), 37(101, 107, 111), 40(125, 126), 43(125,

138), 44(97, 139), 45(139, 140), 47(142), 55(168), 58, 59(185, 186), 62(202), 63(202), 64(202), 73(231), 90(270), 91(275, 276, 278, 280), 92(276, 278), 93(276), 94(276), 102(311, 312), 103(311), 104(311), 105(312), 106(311), 107(312), 115(46, 100, 111, 125), 116(168, 185, 186, 202, 361, 363), 117(231), 119(268, 269, 270, 275, 276), 121(311, 312, 449), *125*, *126*, *128*, *129*, *130*, *131*, *133*, 169(96, 97, 99), 170, 197(171), 198(171), *208*, *210*, 231(94), *260*, 273(79, 80), 276(114), 277(133), 278(150, 151), 302, 303, *330*, *331*, *334*, 340, 341, 342(16, 17), 384(68), 417(122), 424(128), 425(129), *440*, *441*, *442*

Shimomura, Y., 253(181), *262*

Shimooka, S., 41(130, 131, 133), 42(133) 49(131), *126*, 309(266), *334*

Shiraishi, K., 51(157), 116(157), *127*

Shiryaev, V. I., 225(57), *259*

Shklyar, R. Sh., 57(180), 116(180), 121(450), *128*, *133*, 327, 328(338, 339), *336*

Shoji, H., 49(146), 116(146), *127*, 343(21), *440*

Shpichinetskij, Ye. S., 177(114), *208*

Shrednik, V. N., 117(389), *132*

Shteynberg, M. M., 28(64), *125*, 214(21), 223(55), 229(83, 85), 230(83), *258*, *259*, *260*, 293, *333*

Shtremel', M. A., 181(134), *209*

Shugo, Y., 104(318), 107(339), *131*, 232(102), *260*

Shyne, J. C., 273(89), 293(213), 295, 317(294), *330*, *333*, *335*

Singh, K. P., 218, *259*

Skarek, J., 184(143), *209*

Smallman, R. E., 120(438), *133*

Smialek, J. L., 278(147), *331*

Smirnov, L. V., 299(230, 233, 236, 240, 243), 301(253), 302(254), *333*, *334*

Smith, C. S., 291, *333*, 434, 443

Smith, E., 407(103, 104, 105), *442*

Smith, J. F., 438(173), *443*

Smith, J. H., 111(354), 112, 123(354), *131*

Smith, R. A., 140(10), *206*

Smith, R. P., 212(4), 213(4), *258*

Smith, R. W., 121(445, 447), *133*, 232(100, 101), *260*

Snezhnoy, V. L., 216(28), *258*, 299(246), *334*

Snoek, J. L., 160(65, 66), *207*

Soboleva, N. P., 275(105), *330*

Soejima, T., 92(281), 119(281), *130*

Sokolov, B. K., 187(149), *209*

Solovey, V. D., 327(335, 336), *336*

Somoylova, Ye. S., 301(250), *334*

Sorel, M., 117(376), *132*

Sorokin, I. P., 23(44), 115(44), *124*, 301(253), 302(256), *334*

Speich, G. R., 21(33, 35), 29(77), 115(33, 35, 77), *124*, *125*, 163, *208*, 220(50), 221, 240(144), *259*, *261*, 290(205), *333*

Spenlé, E., 220(46), *259*

Srivastava, L. P., 220(48), *259*

Stager, C. V., 104(331), *131*

Stangler, F., 273(95), *330*

Steijn, R. P., 303(260), *334*

Stein, B. A., 265(7), *328*

Stein, D. G., 399(97), *442*

Stelletskaya, T., 86(263, 266), 115(263, 266), 120(263), *129*

Steven, W., 229(81), *260*

Stevens, D. W., 189(154), 190(154), 191(154), *209*

Stewart, H. M., 163(79), *208*, 225(61), *259*

Stewart, M. J., 120(433), *133*, 276(122), *331*

Stora, G., 237(118), *260*

Storchak, N. A., 203(188), 205(193, 195), 206(200), *210*

Stregulin, A. J., 267(36, 37), *329*

Strocchi, P. M., 20(28), 115(28), *124*

Ström, B., 119(424), *133*

Struyve. T., 102(316), *130*

Suemune, K., 59, 116(188), *128*

Sugeno, N., 97(291), 119(291), *130*

Sugimoto, K., 280(165), *332*

Sugino, K., 23(46), 115(46), *125*, 169(97), *208*

Sugino, S., 119(417), *133*

Sugiyama, H., 432(150), *443*

Sullivan, L. O., 272(72), 281(173), *330*, *332*

Sumino, K., 280(163, 164), *332*

Suoninen, E. J., 276(120), *331*

Suto, H., 320, 325(324), *335*

Sutton, A. L., 264(4), *328*

Suzuki, Hideji, 25(51), 29(51), *125*, 236(115), 237(115), *260*, 270(47), 305(261), *329*, *334*, 391, 394, 397, 398, 416, *442*

Suzuki, Hideo, 249(179), 251(179), *262*

Suzuki, Hiroo, 47(143), *127*

Suzuki, Hisashi, 276(112, 113), *331*

Suzuki, M., 267(39), *329*

Suzuki, S., 231(92), *260*

Suzuki, T., 104(329), *131*

Suzuki, Y., 236, 301(251), *334*

Swann, P. R., 76(245), 80, 83, 85(245), 88, 89, 119(245), *129*, 291(211), 292(211), *333*
Swanson, W. D., 228(70), *259*
Swartz, J. C., 160, *208*
Swisher, J. L., 21(31), 115(31), *124*
Szabo, P., 113(357), 123(357), *131*
Szirmae, A., 220(50), 221(50), *259*

T

Tachikawa, K., 123(468), *134*
Tadaki, T., 45(140), 116(363), *127*, *131*, 231(94), *260*, 302, 303, *334*, 340, 341, 342(17), *440*
Tagaya, M., 40(128), 41(128), 115(128), *126*
Taggart, R., 71(225), 73(230, 233), 117(225, 227, 230, 233, 377, 380, 387), *128*, *129*, *132*
Takahashi, T., 265(8), *328*
Takano, S., 123(468), *134*
Takashima, Y., 102(315), 107(315), *130*, 328(340), *336*
Takehara, H., 432(149, 150), *443*
Takeuchi, S., 25(51), 29(51), 33, 49(149), 50, 51(149), 116(149, 368), *125*, *126*, *127*, *132*, 236, 237, 238, *260*, 270(47), 305(261), *329*, *334*
Takezaea, K., 96(289), 97(289), 119(289), *130*
Tamaru, K., 310, *334*
Tamba, A., 20(28), 115(28), *124*
Tamura, I., 40, 41(130, 131, 133), 42(133), 49(131), 115(128), *126*, 273(94), 274, 295, 296, 309(266), *330*, *333*, *334*
Tanaka, R., 240(146), *261*
Tanaka, Y., 55(168), 116(168), *127*, 197(171), 198(171), *210*
Tanino, M., 47(143), *127*
Tanner, L. E., 266(19), *329*
Tarora, I., 119(408), *132*
Tas, H., 426, *442*
Tauer, K. J., 212(5), 225(5), *258*
Teplov, V. A., 279(157), *332*
Tetelman, A. S., 142(16), *206*
Thiele, W., 279(161), 280, *332*
Thomas, G., 33, 37(88, 109), 65, 115(88, 109), *125*, *126*, *128*, 283, *332*
Thomas, S. R., 323, *335*
Thompson, D. O., 431(143), *443*
Thompson, F. C., 240(141), *261*
Tikhonova, E. A., 164(87), 165, *208*
Tinsanen, K., 118(393), *132*
Titchener, A. L., 232(96), *260*, 277(124), *331*
Titov, P. V., 203(187), 204(187), *210*
Tkachuk, V. K., 91(279), 119(420), *130*, *133*, 277(132), *331*
Toner, D. F., 119(405), *132*
Toth, R. S., 77(246), 78(246), 85, 86(265), 87(265), 98(301), 99, 100, 115(265), 119(255, 265), 120(301), *129*, *130*
Townsend, J. R., 164(83), *208*
Trautz, O. R., 118(400), *132*, 434(159), 435, *443*
Trefilov, V. I., 226, *259*
Trivisonno, J., 434(160), *443*
Troiano, A. R., 24, 28(66), 29(48), 115(48, 66), *125*, 225(60), 239(136), *259*, *261*, 283(185), 311(274, 277), 322(312), *332*, *334*, *335*, 344, 345(25), 347, 397, 398, 404, 412(109), 415(109), 416, 417, *440*, *442*
Tsubaki, A., 249(179), 251(179), *262*
Tsuchiya, M., 18(16), 19(16), 40(122), 115(16, 122), *124*, *126*, 214, 220(51), 221(51), 222(51), 223, 224, 225, 227, 228, 229, *258*, *259*
Tsujimoto, T., 273(83), *330*
Turkdogang, E. T., 21(31), 115(31), *124*
Turnbull, D., 214(18), 239(131), 243(160), *261*, 270(48), 286(193), *329*, *332*
Tyapkin, Yu. D., 324(319), *335*

U

Uchida, N., 325(324), *335*
Uchishiba, H., 111(352, 353), 123(353), *131*
Uchiyama, Y., 266(30), *329*
Ueda, J., 117(378), *132*
Ueda, S., 167, 168, *208*
Uhlig, H. H., 218(36), *259*
Umemoto, M., 41(131), 49(131), *126*, 309(266), *334*
Underwood, E. E., 117(388), *132*
Usikov, M. P., 206, *210*
Utevskiy, L. M., 39(120), 48, 115(144), *126* *127*, 245(167), *262*

V

Valdré, U., 123(467), *134*
Van Paemel, J., 102(316), *130*
Van Winkle, D. M., 28(65), 115(65), *125*, 417(121), *442*

Vaynshteyn, A. A., 142(14), *206*
Venables, J. A., 29(78), 65, 116(78, 206), *125*, *128*, 167, 169, *208*
Venturello, G., 21(30), 115(30), *124*
Vercaemer, C., 283(188), *332*
Verdini, L., 118(395), *132*
Vieland, L. J., 123(464), *134*
Vlasova, Ye. N., 339(13), *440*
Vogt, K., 240(152), 244(152), *261*
Volkov, S. V., 142(14), *206*
von Fircks, H. J., 60, 61, 116(198), *128*
von Hippel, A., 177(120), *209*
Voronchikhin, L. D., 299(237, 239, 244), 301(249), *333*, *334*
Votava, E., 52(160), 116(160), *127*
Vovk, Ya. N., 144, 199(172–174), 200(178, 179), 202(174), 203(186), *206*, *210*
Voyer, R., 60(199), 116(199), *128*
Vyhnal, R. F., 267(38), *329*
Vykhodets, V. B., 327(335), *336*

W

Wachtel, E., 235, *260*
Wada, H., 214(23), *258*
Wada, T., 214(20, 23), 216, 226, *258*
Wagner, C. N. J., 140(11, 12), 142(16, 17), *206*
Wallace, W., 120(442), *133*, 299(228), *333*
Wallbridge, J. M., 228(77), *259*
Walsh, F. D., 273(93), *330*
Wang, F. E., 101, 102(314), 104(320, 326, 333), *130*, *131*
Ward, R., 161(67), *208*
Warlimont, H., 74(240), 76(245), 80, 83, 85(245, 253, 256, 257), 88, 89, 96(283), 97(299), 119(245, 299, 411), 120(257, 437), *129*, *130*, *132*, *133*, 171, *208*, 268(43), 282, 283, *329*, *332*
Warnes, R. H., 266(26), *329*
Warren, B. E., 137(9), 139(9), 140(13), 141, 144(13), 147(27), *206*, *207*
Warshauer, D. M., 263(1), *328*
Wasilewski, R. J., 101(305), 104(323, 325, 330, 334), *130*, *131*, 177(116), *209*, 273(87, 92), 278(137), *330*, *331*
Wassermann, G., 21(32), 23, 115(32, 39), 119(406), *124*, *132*, 180(128, 129), *209*, 271(56), 272(56, 67), 276(119, 121), 279(160), 325(327), *329*, *330*, *331*, *332*, *336*, 414(114), *442*
Watanabe, D., 51(158), 52(158), 116(157, 158), *127*
Watanabe, G., 187, *209*
Watanabe, M., 18(21), 40(21, 127), 115(21), *124*, *126*, 187, *209*, 417(117), *442*
Watanabe, T., 342(17), *440*
Wayman, C. M., 18(21), 20(26), 23(43), 28(68), 26(58), 27, 28(68), 29, 30, 31(82), 33(89), 37(111), 38, 39(118, 119), 40(21, 125, 127), 41, 43(125), 66(213), 67, 97(296), 102(311, 312), 103(311), 105(312), 107(312), 115(21, 26, 43, 49, 58, 68, 111, 119, 125, 129, 364, 365, 366), 116(361, 362), 119(412), 121(312, 446), *124*, *125*, *126*, *128*, *130*, *131*, *132*, *133*, 169(99), 170(100), 186, 192(157), *208*, *209*, 223(54), *259*, 276(114), 277(133), 278(140, 146, 150), 279(140, 153), *331*, *332*, 337(6, 9), 347(6), 355, 357, 365(6), 367, 378(53), 381(60), 383(65), 384(67), 386(79), 387, 412(110), 413, 414, 416, 417(65, 117, 120, 122), 418, 422(127), 423, 425, 433, *440*, *441*, *442*
Weatherly, G. C., 291(210), *333*
Wechsler, M. S., 273(90), *330*, 347(29), 363(35, 36), 368(35, 37, 39), 375(37, 39, 40), 406(35), 416(35), 421(37), 434(157), *440*, *443*
Weil, L., 60(196), 116(196), *128*
Weinig, S., 117(383), *132*
Weiss, R. J., 212(5, 10), 225(5), *258*, 264(5), *328*
Weiss, V., 275(103), *330*
Weisz, M., 57(174), 116(174), *127*
Wells, M. G. H., 36(104), *126*, 271(60), *330*
Wert, J. J., 149(32), *207*
Wesselhöft, W., 57(179), 116(179), *127*
West, D. R. F., 271(60), 294, 295, 306, 307, *330*, *333*, *334*
West, E. D., 104(332), *131*
Wever, F., 220(45), 221, 256(182), *259*, *262*, 311(275), *334*
Wheeler, J. A., 137(3), *206*, 355(30), *440*
Whelan, M. J., 37(108), *126*
White, C. H., 57(175), 116(175), *127*
Whiteman, J. A., 33(95), *126*
Whitwham, D., 73(235), 117(235), *129*
Wiester, H. J., 225(58), 232, *259*, *260*
Wiley, R. C., 278(136), *331*
Wilkens, M., 85(253), 119(411), *129*, *132*
Williams, A. J., 117(375), *132*

Williams, C. D., 74(238), *129*
Williams, D. N., 273(84), *330*
Williams, H. J., 161, *208*
Williams, J. C., 71, 117(227), *129*
Wilman, H., 189, *209*
Wilsdorf, H. G. F., 169(95), *208*
Wilson, A. J. C., 51(156), 116(156), *127*
Wilson, E. A., 32(86), *125*, 222, *259*
Winchell, P. G., 17(13), 21(33), 115(13, 33), *124*, 162(78), 193(161), *208*, *209*, 316(292), *335*
Wirth, W., 33(94), *126*
Woehrle, H. R., 322(314), *335*
Wollmann, D. R., 293(214), 315(214), *333*
Wood, R. A., 273(84), *330*
Woodilla, J., 316(292), *335*
Worden, D., 104(334), *131*
Worrell, F. T., 122(452), *133*, 177(117), *209*

Y

Yakel, H. L., 123(470), *134*
Yakhontov, A. G., 180(125), *209*
Yamada, Y., 249(179), 251(179), *262*, 280(171), *332*, 433(152), *443*
Yamagata, T., 320, *335*
Yamamoto, S., 72(228), 117(228), *129*
Yamamoto, T., 276(112, 113), *331*
Yamanaka, H., 184(142), *209*, 297, *333*
Yamane, T., 117(378), *132*
Yegolayev, V. F., 60(191), 66(212), 115(212), 116(189), *128*, 229(88), 247(171), *260*, *262*, 325(330, 331, 332), 327(335, 336), 328(338, 339), *336*
Yeo, R. B. G., 229(82), 230(82), 237, 240(147), 244(164), *260*, *261*
Yermdenko, A. S., 301(250), *334*
Yermolayev, A. S., 301(248), *334*
Yershov, V. M., 248, *262*, 305(262), 321(306), *334*, *335*, 388, *441*
Yershova, L. S., 57(180, 181), 116(180, 181), *128*, 247(170), *262*, 325, *336*
Yershova, T. P., 266(28), 267, *329*
Yevsyakov, V. A., 101(306), 104(306), 115(128), *126*, *130*
Yoshimura, H., 40(128), *126*
Yoshino, Y., 187(148), *209*
Yurchenko, Yu. F., 193(165), *210*
Yurchikov, Ye. Ye., 244(163), *261*, 437(166), *443*

Z

Zackay, V. F., 273(99), *330*
Zakharov, A. I., 113(358), *131*
Zangvil, A., 72, 117(228), *129*
Zapffe, C. A., 339(12), *440*
Zavadskij, E. A., 299(231, 232, 237), *333*
Zel'dovich, V. I., 301(250), *334*
Zelenin, L. P., 121(450), *133*
Zener, C., 161, 162, *208*, 212(12, 13), 213, 214(14), *258*, 427, *442*
Zerwekh, R. P., 27, *125*, 192(157), *209*, 422(127), 423, *442*
Zhdanov, G. S., 76, *129*
Zhuravel, L. V., 60(189), 116(189), *128*
Zhuravlev, L. G., 229(83), 230(83) *260*, 293, *333*
Zijderveld, J. A., 278(148), *331*
Zil'bershteyn, V. A., 265(13), *329*
Zirinsky, S., 433, 434(154), *443*
Zulas, E. G., 266(26), *329*
Zvigintsev, N. V., 33(90), 115(90), *126*
Zvigintseva, G. Ye., 229(88), *260*
Zwell, L., 21(35), 115(35), *124*

Subject Index

Data in Tables 2.4–2.9 are not indexed here.

A

Accommodation region, 172
Accommodation strain, 384
A_d, 227, 257, 271
Adiabatic transformation, 248
Ag–Zn, 232
α_m Martensite, 199
Anisotropic dilatation, 377
Athermal martensite, 239, 248
Athermal stabilization, 322
A_s, 226, 227
Au–Cd
  crystalline structure, 97
  elastic anisotropy, 433
  high damping, 280
  phenomenological theory, 420
  single interface transformation, 173
Au–Cd–Cu, 434
Au–Cu–Zn, 89, 260, 432
Audible click, 233
Ausforming, 294
Austenization temperature, effect of, 306
Autocatalytic effect, 275
  nucleation, 243

B

Bain correspondence, 5
Bain distortion, 347
β Brass, 96, 430
Body-centered cubic (b.c.c.) lattice, 2
Body-centered tetragonal (b.c.t.) lattice, 4, 16
Bowles–Mackenzie theory, 357
Burgers relationship, 68
Burst effect, 275
  transformation temperature (M_b), 285
Butterfly-like martensite, 27

C

Carbon, 18, 151
Chemical free energy, 211
Close-packed layer structure, 74, 145
Cobalt alloy
  crystallography, 48
  M_d (A_d) of Co–Ni, 298
  schiebung transformation, 237
  surface effect, 285
Coherent domain size, 139
Complementary deformation, 10
Complementary shear, 11, 347, 350
Composite shear, 377
Continuous dislocation theory, 407
Cooling rate, effect of, 219, 322
Cooperative movement of atom, 9, 235
Cottrell atmosphere, effect of, 289
Cr–Mn, 177
Cu–Al, 79, 145
Cu–Al–Ni, 80, 89, 276
Cubic martensite, 21
Cu–Fe, 291
Cu–Fe–Ni, 292
Cu–Ge, 276
Cu–Mn, 177
Cu–Si, 66, 276
Cu–Sn, 75, 91
Cu–Zn, 96, 149, 232

Cu–Zn–Al, 85
Cu–Zn–Ca, 85
Cu–Zn–Ga, 149
Cu–Zn–Si, 85, 149

D

Deformation fault, 135
  probability, 141
Diffusionless transformation, 14
Dilatation parameter, 376
Dipole strain (dipole defect), 152, 160, 164
Dislocation, effect of, 281
Displacive transformation, 15
Domain size, 141
Domino effect, 15
Double shear theory, 344, 378

E

Eigentherm, 220
18–8 Stainless steel, 167, 247
Elastic anisotropy, 426
ε Martensite, 66, 193
Explosion wave, 268
Explosive loading, 188

F

Face-centered cubic (f.c.c.) lattice, 2
f.c.c. Martensite, 73, 178
Fe, 211, 220, 264
Fe–Al–C
  dipole strain, 153
  lamellar structure, 424
  O-site → T-site, 206
  tetragonality, 20, 342
Fe–B, 20
Fe–C
  amount of retained austenite, 310
  dipole strain, 160
  effect of pressure on diagram, 267
  lattice constant, 19
  martensite in, 2
  morphology, 28
  M_s, 220
  substructure, 38
Fe–Cr, 181
Fe–Cr–C
  effect of temper-aging, 319
  initial stage of $\gamma \rightarrow \alpha'$, 170
  interruption of quenching, 316
  isothermal martensite, 240
  stabilization above M_s, 312
  substructure, 40
Fe–Cr–Mn–N, 279
Fe–Cr–Ni, 60, 167, 271
Fe–Cr–Ni–C, 293
Fe–Ir, 66
Fe–Mn, 53, 214, 267
Fe–Mn–C
  effect of repeated $\gamma \rightleftharpoons \varepsilon$, 327
  ε' martensite, 193
  h.c.p. martensite, 52
  initial stage of $\gamma \rightarrow \varepsilon$, 167
  isothermal $\gamma \rightarrow \varepsilon$, 247
Fe–N
  dipole strain, 160
  lattice constants, 19
  morphology, 28
  M_s, 220
  substructure, 38
Fe–Ni
  orientation relation, 7, 22
  phenomenological theory, 413
  M_b, 285, 314
  morphology, 25
  M_s and A_s of, 227
  reverse transformation, 179
  schiebung transformation, 236
  substructure, 32
  surface martensite, 282
  transformation by explosive loading, 189
Fe–Ni–Al, 289
Fe–Ni–B, 20
Fe–Ni–C
  change of M_s due to ausforming, 295
  effect of austenizing temperature, 307
  isothermal martensite, 246
  κ' martensite, 204
  orientation relation, 24
  phenomenological theory, 416
  transformation-induced plasticity, 274
Fe–Ni–Co, 437
Fe–Ni–Cr, 167, 245, 247, 291
Fe–Ni–Cr–C, 301
Fe–Ni–Cr–Ti, 291
Fe–Ni–Cu, 283

Fe–Ni–Mn, 240, 242, 301
Fe–Ni–Mo, 245
Fe–Ni–P, 46
Fe–Ni–Ti, 19, 290, 339
Fe–O, 21
Fe–Pd, 339
Fe–Pt, 302, 339, 416
Fe–Re–C, 201, 204
Fe–Ru, 66
Fourier analysis, 137
Frank's interface, 216, 399

G

Grain size, effect of parent phase, 283, 307
Greninger–Troiano relation, 9, 344
Growth fault, 135

H

Habit plane, 7, 24, 27
Hadfield steel, 57
Heat of transformation, 212
Heterogeneous nucleation, 286
Hexagonal close-packed (h.c.p.) martensite, 48
Hf, 67
High damping, 279
High pressure loading, 187

I

In–Cd, 110, 177
Incubation period, 287, 324
Induction period, 241
Interfacial energy, 216
Internal friction, 159
Internal twin, 10, 16, 33
Interruption of quenching (stabilization), 316
In–Tl, 108, 172, 422
Invariant line, 349
Invariant normal, 349, 354
Invariant plane, 346
Isothermal martensite, 235, 238
  formation after partial transformation, 317

J

Junction plane, 26, 47

K

κ Martensite, 200
κ' Martensite, 200
Kinetics, 211
Köster peak, 161
Kovar, 45
Kurdjumov–Sachs relation, 7, 22, 342

L

Lath martensite, 12, 28, 29
Lattice deformation, 338
Lattice invariant shear, 347
Lattice orientation relationship, 7, 21
Lens-shaped martensite, 12
Li, 67
Li–Mg, 232, 434
Line broadening, 136

M

Magnetic domain, 48
Magnetic field, effect of, 299
Maraging steel, 32
Martensite, definition, 11
Martensite nucleus, 238
Martensite starting temperature, *see* M_s
Massive martensite, 32
M_b (burst transformation temperature), 285
M_d
  definition, 271
  of ferrous alloys, 227, 292
Memory effect, 180, 277
M_f
  definition, 305
  of ferrous alloys, 293
Midrib, 7, 26, 43
Military transformation, 15
Mn–Au, 111
Mn–Cu, 111, 260
Mn–Ni, 111, 113
Mn–Zn, 111
Mössbauer effect, 155
Morphology, 24
M_s
  of carbon steel, 2, 225
  definition, 213
  of Fe-based ternary alloys, 229
  of pure iron, 220

M_s (*cont.*)
of substitutional binary alloy, 226, 227, 229
of Ti-based binary alloys, 231

N

Nb–Ru, 114
Neutron irradiation, 281
Ni–Al, 121
9R structure, 81
Nishiyama relationship, 7, 22, 142, 342
Ni–Ti, 75, 106, 121
Nitrogen, 18, 151
Noble-metal-based alloy, 74
Nonchemical free energy, 216

O

Octahedral site (O-site), 151
Orientation relationship, 7, 21

P

Peak shift, 136
Phenomenological theory, 344
Plane normal, 349
Pole mechanism, 390
Powder particle, transformation of, 286
Precipitated particle, effect of, 289
Pressure, effect of, 263
Prism-matching method, 402
Propagation speed, 398
Pseudoelasticity, 279

R

Ramsdell notation, 75
Rb, 263
Reconstructive transformation, 15
Repetition of cyclic transformation, 323
Retained austenite, 46, 310
Reverse transformation, 178, 182, 187
effect on stabilization, 298, 323
Rubberlike elasticity, 175, 279

S

Scherrer formula, 136
Schiebungsumwandlung, 25, 233, 236, 392
Scratch line bending, 31
Second order transition, 106
Shape change, 9, 29
Shape memory effect, 173, 276
Shear mechanism, 342
Shōgidaoshi, 15
Shoji–Nishiyama relationship, 49, 194
Shuffling, 75, 343
Single interface growth, 420
Size effect on diffraction, 139
Snoek peak, 160
Splat cooling, 265
Stabilization by reverse transformation, 323
Stabilization (thermal) of austenite, 304
Stacking disorder, 145
Stacking fault, 10, 135
cubic and hexagonal type, 146
effect on stabilization, 281
parameter, 148
Stainless invar, 269
Strain embryo, 239, 313
Strain-induced plasticity
definition, 273
morphology, 275
Stress-induced martensite, 57, 269
Substitutional atom, 18
Substructure, 31
Superelasticity, 279
Superlattice formation, effect of, 302
Surface effect, 282
Surface martensite, 27, 282, 426
Surface relief, 9, 29
Suzuki's growth mechanism, 391

T

T_0, 6, 225, 227
Ta–Ru, 113
Temper-aging, effect of, 319
Tetragonal doublet, 154, 166
Tetragonality, 4, 18
Tetragonal martensite, 16
Tetrahedral site (T-site), 151
Thermal stabilization, 304
Thermoelastic martensite, 89, 276
304-Type stainless steel, 62, 279
Ti, 67, 68, 219
Ti–Al, 73
Ti–Al–Mo–V, 73
Ti–Cr, 73

Ti–Cu, 71
Ti–Fe, 72
Ti–Mn, 70
Ti–V, 73
Tl, 219
Transformation induced plasticity (TRIP), 273
Transformation range, 305
Transformation temperature, 219
Transformation twin, 16
Transformation unit, 251
Transformation velocity, 232
Twin fault, 16, 135
  effect on stabilization, 281
  probability of, 141

U

Umklappumwandlung, 25, 232, 395
U–Mo, 248
Undistorted plane, 346
Unextended line, 348
Unextended normal, 349
Unrotated plane, 346
Upheaval, 29

V

Vacancy, effect of, 280
Variant, 23
Velocity of transformation, 211
V–N, 110

W

Wechsler–Lieberman–Read theory, 363

Z

Zener ordering, 161
Zhdanov notation, 76
Zr, 67, 74, 219

A
B
C 8
D 9
E 0
F 1
G 2
H 3
I 4
J 5